THE TECTONO-MAGMATIC EVOLUTION OF THE SOUTH-EASTERN CARIBBEAN PLATE: INSIGHTS FROM LA DÉSIRADE, TRINIDAD AND TOBAGO AND THE AVES RIDGE

Iain Neill

Submitted in partial fulfilment of the requirements for the degree of Ph.D.

2011

ProQuest LLC
789 East Eisenhower Parkway
P.O. Box 1346
Ann Arbor, MI 48106-1346

DECLARATION

This work has not previously been accepted in substance for any degree and is not concurrently submitted in candidature for any degree.

Signed ..... (candidate)
Date 27-6-11

STATEMENT 1

This thesis is being submitted in partial fulfilment of the requirements for the degree of PhD.

Signed ..... (candidate)
Date 27-6-11

STATEMENT 2

This thesis is the result of my own independent work/investigation, except where otherwise stated.

Other sources are acknowledged by explicit references.

Signed ..... (candidate)
Date 27-6-11

STATEMENT 3

I hereby give consent for my thesis, if accepted, to be available for photocopying and for inter-library loan, and for the title and summary to be made available to outside organisations.

Signed ..... (candidate)
Date 27-6-11

STATEMENT 4

I hereby give consent for my thesis, if accepted, to be available for photocopying and for inter-library loans **after expiry of a bar on access previously approved by the Graduate Development Committee**.

Signed ..... (candidate)
Date .....

ABSTRACT

The Caribbean Plate formed in the eastern Pacific; and moved between the Americas by means of a SW-dipping Greater Antilles subduction zone, consuming proto-Caribbean crust which had formed by the rifting of the Americas as part of the break-up of Pangaea. The timing of inception of SW-dipping subduction remains controversial (~135-125 Ma vs. ~90 Ma) and the tectonic implications of the origin of many igneous rock units around the region are unknown.

At four locations in the SE Caribbean, U-Pb zircon dating, major and trace element and radiogenic isotope whole rock analyses were used, as appropriate, on igneous rocks to understand the age, tectonic setting, mantle sources and/or crustal sources of magmatism. The four locations studied were: (a) the Late Jurassic-Early Cretaceous back-arc basin rocks of La Désirade (Lesser Antilles); (b) the Early Cretaceous island-arc rocks of Tobago Island; (c) the suspected Late Cretaceous plume-related San Souci Formation, Trinidad and (d) the Late Cretaceous SE Aves Ridge which is of island arc origin.

The results reveal that: (a) the Late Jurassic eastern Pacific region consisted of an E-dipping Andean/Cordilleran arc-back-arc system which rifted prior to inception of the Greater Antilles arc; (b) the end of E-dipping subduction and the initiation of the SW-dipping Greater Antilles island arc took place at ~135-125 Ma and involved the transform motion of suites of Andean/Cordilleran arc rocks into the N and S ends of the Antillean arc; (c) rocks of the present-day Dutch-Venezuelan Antilles and Aves Ridge record a different tectonic story involving a separate long-lived E-dipping Andean arc system with a polarity reversal event related to the collision of the ~90 Ma Caribbean-Colombian Oceanic Plateau (CCOP) and (d) at ~90 Ma, plume-related rocks were also formed on the proto-Caribbean plate between the Americas as part of an oceanic plateau distinct from the CCOP.

ACKNOWLEDGEMENTS

Thanks must go first and foremost to Dr. Andrew Kerr, my primary supervisor, who has overseen this project and my learning process completely throughout my time in Cardiff, and supplied withering cynicism, enthusiasm and Caribbean conversations in equal measure. Dr. James Pindell of Tectonic Analysis Ltd. helped with connections, fieldwork, funding and of course many stimulating discussions on the Caribbean. Dr. Alan Hastie has been a fantastic source of ideas and geochemical know-how, along with contributions from Professor Julian Pearce.

The attendees of the 2009 workshop on circum-Caribbean tectonic evolution in Cardiff provided many great insights into Caribbean evolutionary models with mention going in no particular order to Esteban Gazel, Claude Herzberg, Roelant van der Lelij and Jim Wright. I am also indebted to Art Snoke of the University of Wyoming for many discussions on the geology of Tobago first conducted during a visit to Laramie in 2008. Jenny Gibbs helped me by cheerfully passing on her undergraduate thesis, rock samples and maps which contributed towards the Lithos paper on La Désirade. The pressure of an interview situation with Mark Allen, Jon Davidson and Jeroen van Hunen of Durham University allowed me to consider my work more fundamentally and helped me to firm up my ideas for my final chapters.

The majority of my funding came from NERC studentship NE/F00219X/1, NIGL grant-in-kind IP/1064/1108 and Tectonic Analysis Ltd. through CASE. A Mineralogical Society travel bursary helped my trip to the AGU Fall Meeting in 2009. Funding for the circum-Caribbean workshop came from BP and Shell. Shell part-funded the San Souci U-Pb dating project. Andrew Kerr, Geoff Steed, Tony Harris, Paul Pearson, Iain McDonald, Johan Lissenberg, Chris Macleod and Richard Lisle gave me opportunities to supplement my income with laboratory demonstrating and field supervision.

Nothing would have been analysed without the excellent work of Iain McDonald at Cardiff University on the ICP-MS. Ian Millar, with help from Neil Boulton, ran the radiogenic isotope analyses at NIGL, Nottingham. Dan Condon and Nicola Atkinson ran the U-Pb zircon analyses in Nottingham. Klaus-Peter Stanek separated zircons from Tobago and the Aves Ridge in Freiberg and dated the Aves Ridge sample in St. Petersburg. Kevin Chamberlain arranged thin sectioning and U-Pb dating of the San Souci sample. Kevin Chamberlain and Art Snoke provided the all-important zircons from the North Coast Schist of Tobago. Laboratory assistance in Cardiff came from Ley Woolley (ICP-OES and flux-fusion lab), Lawrence Badham (thin sections) and Tony Oldroyd (HF acid work).

The citizens of Trinidad and Tobago made my stay a peaceful and insightful one. Laura Cotton assisted in the field particularly in La Désirade and Trinidad. Homer Montgomery and Jennifer Gibbs shared their thoughts on the rocks of La Désirade and their logistical know-how. In Trinidad and Tobago, thanks goes to Rajindra Maraj and his brother Ravi, the latter who helped enormously with all manner of logistics and hired me a truck for two months, just about coping when the engine died. The rest of my fieldwork on Trinidad and Tobago was aided by Krishna Persad and family, Greta Robertson, David Rooks, and last but certainly not least Ingrid Gomes who kept me from going insane at Footprints on Tobago. Rusty Lotti and George Losefski at Lamont

Doherty helped me to obtain samples of the Aves Ridge from their core store during a visit in 2008.

Tony Prave, Ed Stephens and Colin Donaldson, amongst others, in St. Andrews were great mentors who encouraged me to apply for this project. Thank you to Keith James for getting me wound up enough to write to *Geoscientist* Magazine about the Caribbean, and to Ted Nield for facilitating my popular science piece (tongue firmly in cheek).

Thank you to Laura Cotton for everything over the past couple of years. Office-mates in strict alphabetical order: Chris Brough, Jake Ciborowski, Kerry Howard, Caroline Johnson, Rhian Jones and of course, Matthew Minifie - I am so grateful to you all for putting up with me. There are many other people in Cardiff to thank, in both the university and the house in Flora Street - you know who you are and I won't forget you.

This thesis is dedicated to my first geology teacher, George Strachan. His enthusiasm and encouragement to keep going with this wonderful subject is appreciated by a generation of Dingwall Academy leavers. I for one could not be more grateful for it.

CONTENTS

LIST OF FIGURES

LIST OF TABLES

CHAPTER ONE: INTRODUCTION

A rationale for the study, its aims, structure and methodology; followed by an introduction to the key components of Caribbean Plate and the debate over their tectonic evolution

1.1. Opening remarks

This thesis is a study of four poorly-documented occurrences of Jurassic to Cretaceous igneous and meta-igneous rocks in the SE Caribbean and Lesser Antilles basement. Geochronological, major and trace element analyses and radiogenic isotope data will be used to resolve the ages and detailed tectonic settings of these rocks. This new high-resolution data will be combined with existing data from across the Caribbean, to help discuss and improve models of the origin and tectonic evolution of the region.

The opening chapter continues with a very brief introduction to the nature, origin and evolution of the Caribbean Plate (Section 1.2). In this section, the problems associated with studying the tectonic history of the plate are outlined, and the four studied sites are introduced. Section 1.3 is a brief list of the aims of this project. This is followed by an outline of the structure of the remaining chapters of this thesis, along with a list of publications associated with the study. The introductory chapter concludes with Section 1.5 which is a literature review of the key components of the Caribbean Plate. Here, the two most prominent plate tectonic models for the evolution of the Caribbean region will be reviewed and some of their relative merits discussed.

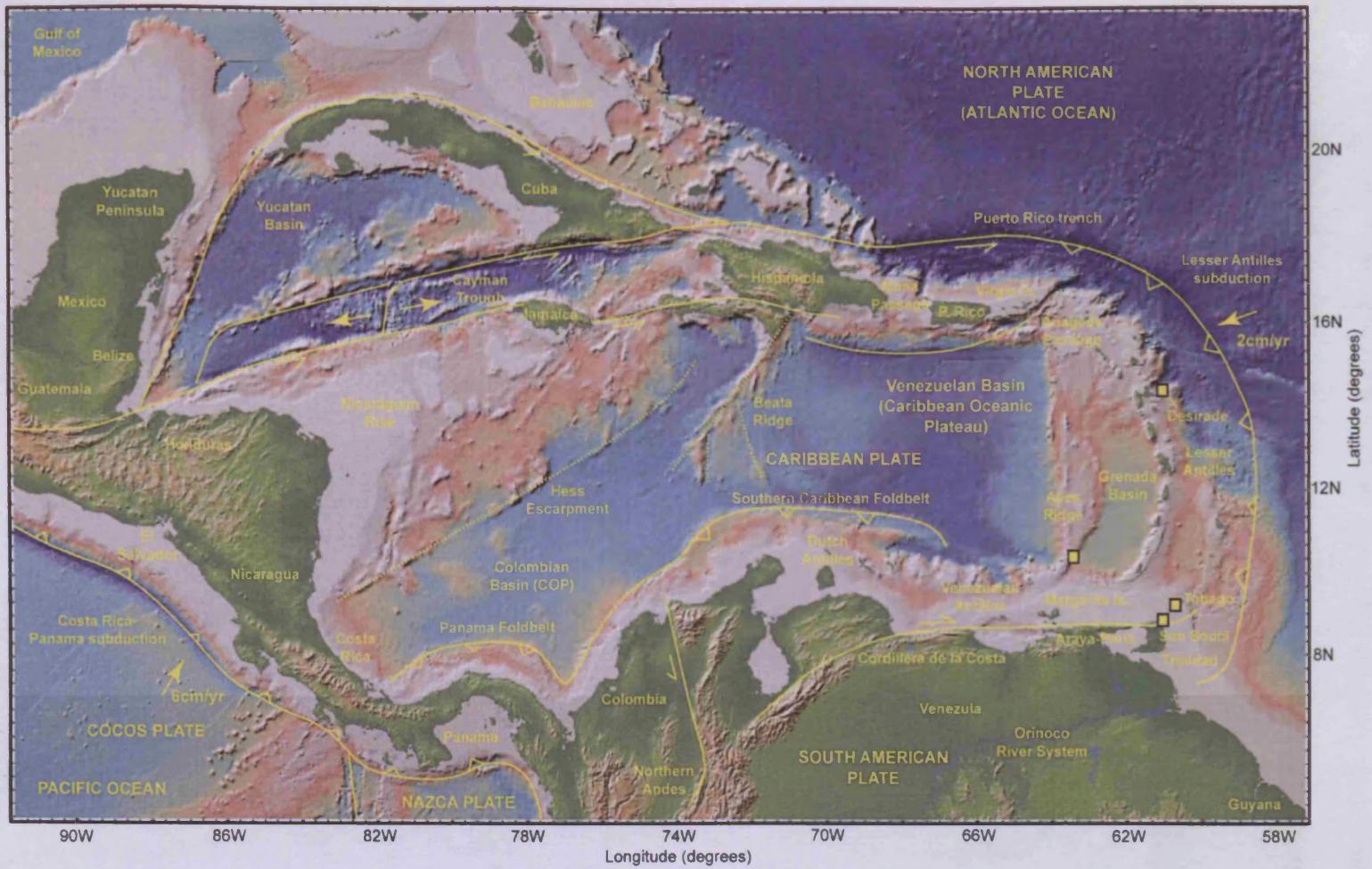

Figure 1.1. A simplified map of the Caribbean region showing principal geological boundaries as sharp and dotted lines. Strike-slip belts are arrowed in the direction of transport; subduction zones/under-thrust belts are saw-toothed. Map downloaded from GeoMapApp (Haxby et al., 2009) by C.J. Macleod and adapted by the author.

1.2 Rationale

The extant Caribbean Plate (Fig. 1.1) is a region of Mesozoic oceanic crust and Cretaceous oceanic plateau material bounded by subduction and transform margins (Kerr et al., 2003). The plate is considered to be an allochthonous part of the Farallon Plate that has moved into the region between North and South America from Cretaceous to recent times (e.g. Kerr et al., 2003; Pindell et al., 2006 and references therein). North and South America drifted apart in the Middle Jurassic with oceanic crust forming between the Americas during the Late Jurassic in the Gulf of Mexico and the **proto-Caribbean seaway** which has since been largely subducted (reviewed in Pindell & Kennan, 2009). On the Pacific margin of the proto-Caribbean, an island arc system initiated during the Early Cretaceous, the '**Great Arc of the Caribbean**' (Burke et al., 1978; Burke, 1988), which superseded Andean/Cordilleran subduction processes at the eastern margin of the Pacific Plate. The Great Arc is composed of the Greater Antilles [Cuba, Hispaniola, Jamaica, Puerto Rico and the Virgin Islands on Fig. 1.1], the Aves Ridge, Lesser Antilles, Dutch-Venezuelan Antilles and arc rocks in Venezuela, Colombia and Ecuador but the actual number of arcs involved and their subduction polarities are uncertain (Fig. 1.1). The Farallon plate was thickened by eruption of plume-related lavas to the west of the Great Arc system at ~94-88 Ma (Sinton et al., 1998; Kerr et al., 2003) forming the **Caribbean-Colombian Oceanic Plateau** (CCOP) (e.g. Kerr et al., 2003). After the CCOP formed, a second arc system, the Costa Rica-Panama arc developed behind the CCOP, leading to the isolation of the Caribbean as a separate plate (Pindell & Dewey, 1982).

To facilitate eastward motion of the Caribbean, subduction on the Greater Antilles portion of the Andean/Cordilleran arc system had to reverse from an E-dipping polarity to SW-dipping Greater Antilles arc subduction (Mattson, 1979). The timing and cause of this subduction polarity reversal is arguably the most controversial aspect of Caribbean geology. One prominent model proposes that E-dipping Andean/Cordilleran subduction continued until ~85 Ma when the CCOP choked the trench, forcing initiation of SW-dipping subduction (e.g. Burke, 1988; Kerr et al., 2003; Hastie & Kerr, 2010). Another model suggests that E-dipping subduction on the Andean/Cordilleran system ceased in the Caribbean region at ~135-125 Ma, resulting in the initiation of SW-dipping subduction of proto-Caribbean crust and therefore the

generation of much of the Great Arc in a SW-dipping subduction setting (e.g. Pindell & Barrett, 1990; Pindell & Kennan, 2009; Stanek et al., 2009; Escuder Viruete et al., 2010).

Magmatism largely ceased on the Caribbean Great Arc system during the Palaeocene to Early Eocene as the Grenada Basin opened (Pindell & Barrett, 1990; Speed & Walker, 1991; Bird et al., 1999). Roll-back of the west-dipping proto-Caribbean subduction zone then initiated the active Lesser Antilles subduction zone (Aitken et al., 2011). Components of the Great Arc accreted to the Caribbean margins whilst the Lesser Antilles subduction zone continues to facilitate the eastwards movement of the Caribbean Plate relative to the Americas.

The tectonic history of the region is more complex than this short description suggests and will be further described in Section 1.4. The key problem hindering a better understanding of Caribbean geology is that the ages and tectonomagmatic settings of individual magmatic units are not known in enough detail to allow definitive tectonic reconstructions and resolution of the subduction polarity debate. Efforts have been hindered because much of the Caribbean is under water; outcrops are scattered, poorly-exposed and contain altered or metamorphosed rocks which affect major, trace element and isotopic systems. Formerly complete crustal units have been tectonically dismembered and so their significance is difficult to ascertain. Early research relied on imprecise laboratory techniques not suited to altered Caribbean rocks, such as K-Ar geochronology, major element analyses and minor element discrimination diagrams. Also there is a limited active research base within the Caribbean region and so many studies have been undertaken by outsiders constrained by funding issues or political problems, leaving some regions of the Caribbean relatively poorly understood.

In this thesis an attempt is made to improve knowledge of potentially important locations using U-Pb geochronology and immobile trace element and radiogenic isotope analyses of mostly mafic island arc and within-plate rocks. The focus is on the SE Caribbean (Fig. 1.2), which is a complex suture zone between the Caribbean and South American Plates, where eastward motion of the Caribbean continues at approximately 2 cm/yr along transpressive boundaries (Weber et al., 2001). The boundary zone contains para-autochthonous Palaeozoic and older South American

crustal units, Mesozoic to Cenozoic extension- and passive margin-related sedimentary and minor volcanic rocks; also allochthonous mostly Mesozoic rocks of the Caribbean Plate including Jurassic-recent island arc and Cretaceous oceanic plateau blocks. Study of these rocks can therefore go a long way to elucidating the evolution of the Caribbean Plate.

Four separate localities in the SE Caribbean have been selected for further study of their allochthonous igneous and meta-igneous rocks in order to help resolve Caribbean tectonic evolution (Fig. 1.2). They are: La Désirade Island, Guadeloupe (Lesser Antilles); Tobago Island; the Souci Formation, Trinidad and the south-eastern Aves Ridge in the Caribbean Sea. These locations: (a) contain mafic rocks amenable to petrogenetic study; (b) have not been hitherto been subjected to sufficient geochemical studies to completely resolve their origin; (c) formed at different times through Caribbean tectonic history and (d) have, with the exception of the Aves Ridge, established field relationships and petrological and structural datasets which will allow for the rapid interpretation of the geochemical results.

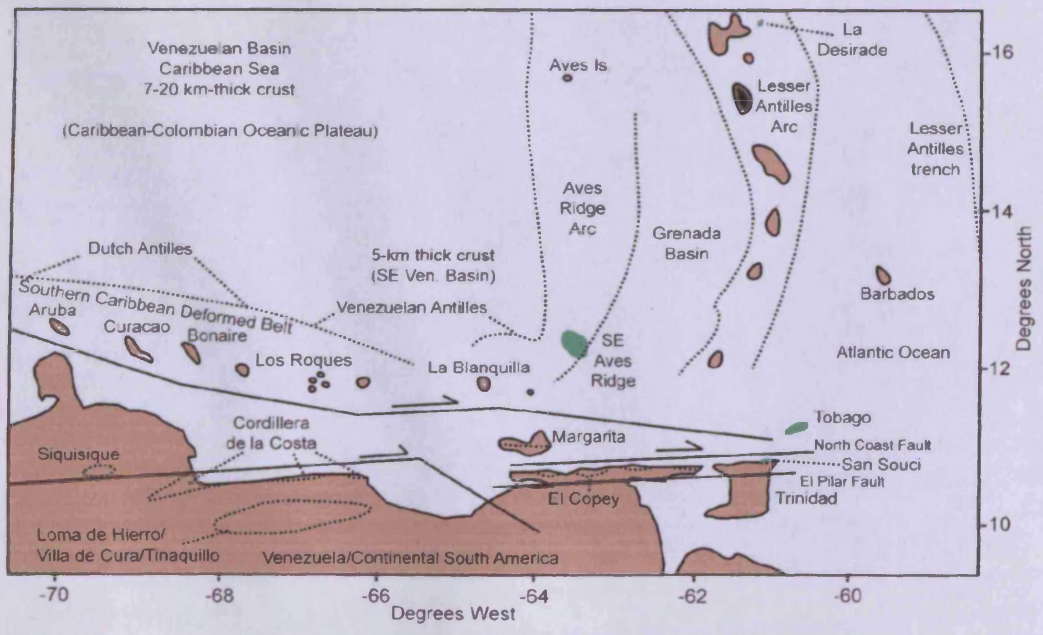

Figure 1.2. A map of the SE Caribbean showing sample locations (green), major islands and rock units mentioned in the text. The area marked continental South America is mostly authochthonous or para-autochthonous, with the exception of the dotted areas which are allochthonous Caribbean-related units. With the exception of Margarita Island, the offshore rocks mostly contain mostly exposed or underlying units of island-arc- or oceanic plateau-related material. The Grenada Basin and the thin crust of the SE Venezuelan Basin are thought to contain oceanic crust, whereas the thick crust of the Venezuelan Basin is considered to contain oceanic crust overlain by thick crust of oceanic plateau affinity.

1.3. Aims, Structure and Methodology

1.3.1. Aims of the project

This aims of this project are to:

- review the geological components of the Caribbean region and the debate over their geological evolution
- introduce the four chosen localities for this study and the previous work undertaken
- describe the geology of the four localities using field evidence, hand specimens and thin sections
- use U-Pb zircon dating, where appropriate, to resolve the age of some critical geological units
- use whole rock major and trace element analyses and whole rock radiogenic isotope analyses to further characterise the studied rocks and assess the links between different units at a given locality
- interpret the new geochemical data to help better understand the tectonic setting and petrogenesis of each individual magmatic unit
- combine the available data with information from nearby localities of a similar age to link each location to regional tectonic scenarios
- provide a critique of problems in Caribbean geology including an assessment of existing Caribbean plate tectonic models and suggesting a new model

1.3.2. Structure and methodology of the project

After this introductory chapter, Chapter 2 will introduce the geological settings of the four chosen localities, giving details of previous studies, an outline of sample collection methods, and the rationale for applying geochemical techniques to each location. Chapter 3 is a review of the field geology and petrography of each unit as studied at each locality.

Chapter 4 contains the geochemical results from each locality in turn. For each locality, the first topic covered in Chapter 4 is the result of any U-Pb zircon dating undertaken. Next in Chapter 4 come the results of major and trace element geochemical studies and radiogenic isotope analysis, with discussion on which elements have been mobilised due to sub-solidus processes and investigation of petrogenetic links between the units studied. Finally, the results of radiogenic isotope analysis are presented (where undertaken) in order to further characterise the units.

Chapter 5 is the first part of the discussion. The chapter begins with a section on how trace element and isotopic data is used to classify mantle sources and identify the 'subduction component' in mafic island arc rocks. This chapter then almost exclusively relates to the data generated during the study and covers the necessary steps to elucidate the petrogenesis of the various units. Each section ends with a summary of magmatic activity at each site which may be quickly referred to when reading the subsequent discussion chapter.

Chapter 6 is the second part of the discussion, which begins with a consideration of the wider context of the studied units. For each locality, this consideration normally includes the correlation of the studied units with other formations in the wider Caribbean region, moving on to a discussion of which, if any, of the tectonic models of the Caribbean are appropriate for the formation of the correlated units. The concluding part of the chapter takes the form of a revised model of Caribbean tectonic evolution based on the findings from this project. Chapter 7 summarises the key outcomes of the study, and finally lists some remaining problems in Caribbean geology and suggestions for further research.

Aspects of this thesis have been incorporated into peer-reviewed articles, published abstracts and public discussion as listed below. Unreferenced written work in this thesis may be attributed solely to the author. Reprints of the underlined publications are presented in Appendix 7.

(1) Neill, I. 2009. Pacific Rising. *Geoscientist Magazine* **19**(11), 12-14

(2) Neill, I., Kerr, A.C., Snoke, A.W., Hastie, A.R., Pindell, J.L., Chamberlain, K., & Millar, I.L. 2009. Geochemistry and geochronology of Tobago Island: A preliminary re-appraisal. *AGU Fall Meeting Abstracts* T51D-06

(3) Kerr, A.C., Neill, I., Urbani, F., Spikings, R., Barry, T. & Tarney, J. 2009. The Siquisique basalts and gabbros, Los Algodones, Venezuela: late Cretaceous oceanic plateau formed within the proto-Caribbean plate? *AGU Fall Meeting Abstracts* V41C-2193

(4) Neill, I., Gibbs, J.A., Hastie, A.R. & Kerr, A.C. 2010. Origin of the volcanic complexes of La Désirade, Lesser Antilles: implications for tectonic reconstruction of the Late Jurassic-Cretaceous Pacific – proto-Caribbean margin. *Lithos* **120**, 407-420

(5) Neill, I., Kerr, A.C., Hastie, A.R., Stanek, K.-P. & Millar, I.L. 2011. Origin of the Aves Ridge and Dutch-Venezuelan Antilles: interaction of the Cretaceous 'Great Arc' and Caribbean-Colombian Oceanic Plateau? *Journal of the Geological Society of London* **168**, 333-347.

Several further papers are planned or are in preparation for international journals relating to the geology of Tobago, San Souci and the evolution of the Caribbean Plate.

1.4. The origin and evolution of the Caribbean Plate

1.4.1. Pacific Origin of the Caribbean Plate

Although some workers (e.g. Meschede & Frisch, 1995; Meschede, 1998; James, 2006; 2009) argue that the Caribbean Plate formed "in-situ" between the Americas, most Caribbean geologists accept that the Caribbean Plate is an allochthonous region of crust formed in the Pacific Ocean which has migrated eastwards, bounded by supra-subduction and transform plate margins. The Pacific origin of the Caribbean Plate has been established for many decades (e.g. Wilson, 1966; Pindell & Dewey, 1982; Pindell, 1985; Burke, 1988; Pindell & Barrett, 1990; Montgomery et al., 1992; Pindell, 1993; Kerr et al., 2003; Pindell et al., 2006). The main findings in favour of a Pacific origin for the Caribbean Plate are listed below.

Firstly, many of these authors point out E-W displacement of over 1100 km on the Cayman Trough. Secondly, as discussed in Sections 1.4.6 and 1.4.7, Aptian or Santonian to Eocene SW-directed subduction beneath the 'Great Arc' indicates substantial relative eastward displacement of the Caribbean Plate. Plate motion vectors for N. and S. America (e.g. Pindell & Dewey, 1982; Müller et al., 1999) show the Caribbean Plate could not have fitted between the Americas during the early Cretaceous. In-situ Cretaceous sedimentary blocks (e.g. in the Bahamas, Yucatan and northern South America) do not contain arc-related tuffs which indicates that the Caribbean arc systems did not evolve close to the eastern parts of the proto-Caribbean where there are found today (Pindell et al., 2006). Fossils of Pacific provenance found in the eastern Caribbean and elsewhere (e.g. Jurassic of La Désirade, Puerto Rico and Hispaniola) pre-date the presence of a significant seaway between the Americas and there is no known mechanism to derive these fossils from the Atlantic (Montgomery et al., 1992). Seismic tomography (e.g. van der Hilst, 1990; van der Meer et al., 2010) shows subducting plates beneath the Caribbean region. The presence of passive margins in eastern North and South America means only relative eastward motion of the Caribbean Plate is possible given the presence of the Lesser Antilles subduction zone [over 1500 km of subduction since ~55 Ma] (van der Hilst, 1990). The Costa Rica-Panama arc has behaved non-compressively from the Late Cretaceous to the present in spite of the rise of the Andes and American Cordillera indicating motion of

the Caribbean during that time relative to the Americas (after Dewey, 1980). In other words, the Caribbean Plate has to have moved eastwards relative to the Americas otherwise an in-situ Caribbean would have undergone the same compressional tectonism that the western seaboard of the Americas has suffered during the Cenozoic. Finally, igneous rocks dredged or sampled from across the Caribbean Plate have oceanic character and bear little relationship to the geology of continental North and South America (e.g. Kerr et al., 2003; Kerr et al., 2009a).

The Caribbean region therefore consists of a Pacific-derived plate which has moved eastwards during the Cretaceous and Cenozoic to over-ride the pre-existing proto-Caribbean crust. The region is thus made up of many different crustal components: (1) N. and S. American crust with remnants of the proto-Caribbean seaway and former passive margins which existed before the arrival of the Caribbean Plate; (2) island arc rocks generated by subduction processes at the eastern edge of the Farallon (Pacific) Plate and latterly the Caribbean Plate; (3) fossil high pressure/low temperature (HPLT) metamorphic belts which accompanied subduction processes in the Caribbean arc system and (4) the pre-existing Pacific Ocean crust overlain by the Caribbean-Colombian Oceanic Plateau. The nature of these components is introduced in turn in the following sections.

1.4.2. Divergence of the Americas and the formation of the proto-Caribbean seaway

The Americas were a part of the supercontinent Pangaea from the Late Palaeozoic to Early Mesozoic. The western seaboard of the Americas had been a site of Farallon (Pacific) subduction since the mid-Early Triassic (Dickinson & Lawton, 2001; Dickinson, 2004). This thesis will refer to components of east-dipping subduction in the Central American/Caribbean region as the "***Andean/Cordilleran arc system***". Rifting of Pangea in the Atlantic and inter-American region began in the Early Jurassic (~200 Ma) and is considered to have been largely intra-cratonic until the Mid-Jurassic (~165 Ma) (Pindell & Kennan, 2009 and references therein). Around the latter time Yucatan detached from the Americas, rotating in an anticlockwise motion, and the inter-American rift developed into organised spreading in the Gulf of Mexico, in a back-arc position relative to the Andean/Cordilleran arc (Pindell & Kennan, 2009; Stern & Dickinson, 2011). This was followed by the opening of a second oceanic basin to the

south known as the ***proto-Caribbean seaway***. Like the Gulf of Mexico in the Middle Jurassic, the westernmost proto-Caribbean through the Late Jurassic was in a back-arc position with respect to the Andean/Cordilleran system and this specific part of the proto-Caribbean is known as the ***Colombian Marginal seaway*** (Pindell & Kennan, 2009). Both fragments of the proto-Caribbean seaway and subduction-related rocks from this period, which may be fragments of the Andean/Cordilleran system, are rare in the present-day Caribbean (see Table 1.1 and Fig. 1.3). The proto-Caribbean seaway continued to open until as late as ~71 Ma (Pindell et al., 1988; Müller et al., 1999). After this time, plate motion calculations indicate that the Americas began to slowly converge (Müller et al., 1999; Pindell et al., 2006). The scarcity of proto-Caribbean and Andean/Cordilleran arc crust is due to later island arc activity within the Caribbean region, as a result of which much of the proto-Caribbean has been subducted or under-thrust beneath the Americas.

Table 1.1. Locations, ages and sources of selected likely proto-Caribbean oceanic rocks or pre-Great Arc subduction-related fragments within the offshore eastern Caribbean and Venezuela.

Location	Unit	Age (Ma)	Type/Source/Comments	References
La Désirade, Guadeloupe	Volcanic-Plutonic complexes	~155-143 (radiolarians and U-Pb zircon CA-TIMS)	Mafic-felsic back-arc tholeiites derived from a depleted mantle source, forming in eastern Pacific or Colombian Marginal Seaway	Mattinson et al., 2008; Cordey & Corneé, 2009; Neill et al., 2010; this study
Margarita Island, offshore Venezuela	La Rinconada formation inc. HP metabasalts	Unknown but metamorphism suspected to be 116-109 Ma	Long suspected to be a slice of proto-Caribbean crust but alternative interpretations as an island arc or oceanic plateau exist. Underwent HPLT metamorphism during mid-Cretaceous	Stöckhert et al., 1995; Giunta et al., 2002; Ostos & Sisson, 2005; Maresch et al., 2009
Puerto Rico	Sierra Bermeja complex	Radiolarians range from Kimmeridgian through to mid-Cretaceous	Mixed serpentinite, basalt and chert; interpreted as proto-Caribbean or Pacific oceanic crust with some cherts containing island arc tuffs indicating a proximal arc	Montgomery et al., 1992, 1994; Schellekens, 1998
Hispaniola	Duarte Complex	Mostly Cretaceous but parts of complex may be Jurassic based on radiolarian assemblages	Serpentinised peridotites, basalts and interbedded cherts, picrites and basalts, amphibolites. Jurassic basalts and cherts appear to have an N-MORB chemistry	Montgomery et al., 1994; Lapierre et al., 1999
	Loma la Monja and Loma Caribe	Upper Jurassic (U-Pb zircon and Ar-Ar hornblende)	Dolerites and gabbros of the Loma la Monja overlie tectonically the peridotites and tectonic slivers of gabbro and dolerite of the Loma Caribe peridotite. N-MORB	Escuder Viruete et al., 2007a; Escuder Viruete et al., 2010
Cuba	Mabujina Unit, Las Villas syncline	~133 (U-Pb zircon on granitoids)	Amphibolites and gneissic granitoids of possible island arc origin which, owing to their structural position, may predate the Greater Antilles arc. Exact origin uncertain	Kerr et al., 1999; Blein et al., 2003; Rojas-Agramonte et al., 2006

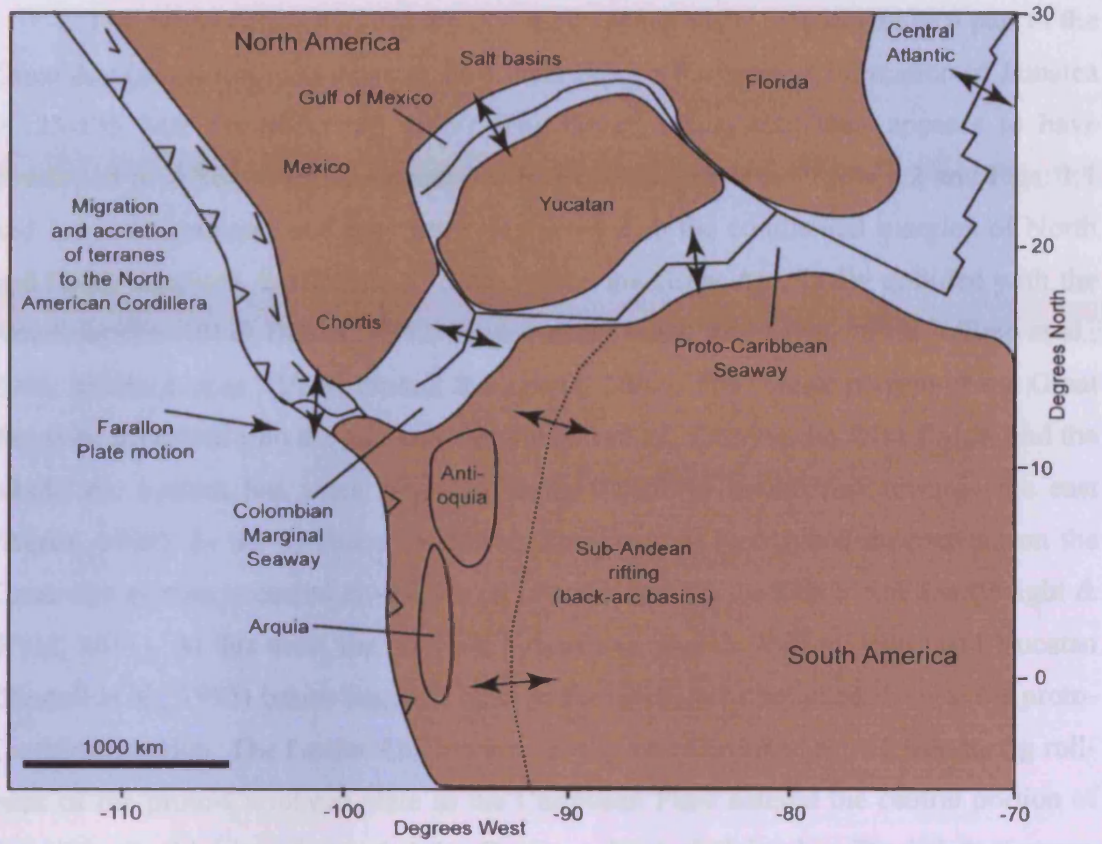

Figure 1.3. Reconstruction of the Caribbean region at ~160 Ma, simplified from Pindell & Kennan (2009), showing the growth of the Gulf of Mexico, proto-Caribbean and Colombian Marginal seaways; with a continuous Andean/Cordilleran subduction zone (saw-teeth) along the west coast of the Americas.

1.4.3. The Great Arc of the Caribbean

By the middle of the Early Cretaceous (~125-120 Ma), island arc rocks were widespread along the boundary between the proto-Caribbean seaway and the Pacific Ocean (Kerr et al., 2003; Pindell et al., 2005), generating what has become known as the ***Great Arc of the Caribbean*** (*sensu* Burke, 1978; 1988), or 'Great Arc system' for short. Fragments of this arc or series of island arc systems are now preserved in the island arc rocks of Venezuela, the Dutch Antilles, Tobago, the Aves Ridge and Greater Antilles (Fig. 1.4). The precise fate of the preceding Andean/Cordilleran system within the Caribbean region is uncertain, and it is not clear how many separate subduction systems made up the Great Arc or their subduction polarities (see Chapter 6 for discussion).

The earliest known island arc axis rocks which many consider to be a part of the Great Arc (*sensu lato*) are those of the Lower Devil's Racecourse Formation of Jamaica (~125-135 Ma; Hastie et al., 2009). The Great Arc system then appears to have developed in different locations more-or-less continuously (see Table 1.2 and Figs. 1.1 and 1.4 for locations), and may have interacted with the continental margins of North and South America, until around 75 Ma, when the Great Arc finally collided with the Americas (Pindell & Dewey, 1982; Pindell et al., 1988; Rosenfeld, 1993; Vallejo et al., 2006; Maresch et al., 2009; Pindell & Kennan, 2009). The central portion of the Great Arc then expanded into the gap between the Americas, forming the Aves Ridge, and the whole arc system has since migrated along transform boundaries towards the east (Burke, 1988). In the southern Caribbean, the youngest recognised magmatism on the Great Arc system occurred at ~57 Ma on Grand Roque in the Dutch Antilles (Wright & Wyld, 2011). At this time, the inter-arc Grenada (Speed & Walker, 1991) and Yucatan (Pindell et al., 1995) basins began to open as the Great Arc continued to enter the proto-Caribbean region. The Lesser Antilles arc subsequently initiated at ~55 Ma during roll-back of the proto-Caribbean plate as the Caribbean Plate entered the central portion of the proto-Caribbean and rounded the Guajira salient of Colombia (Pindell & Kennan, 2009).

At the same time as collision of parts of the Great Arc with the Americas, the Costa Rica-Panama island arc formed to the west behind the trailing edge of the Caribbean-Colombian Oceanic Plateau (see Chapter 2.5) during the Campanian (~75-80 Ma). This new subduction zone led to both the formation of the Caribbean Plate and its anchoring in the mantle reference frame (e.g. Pindell & Barrett, 1990; Luzieux, 2007; Baumgartner et al., 2008; Pindell & Kennan, 2009) but will not be discussed further.

Table 1.2. Locations, ages and sources of selected generally accepted magmatic components of the Cretaceous 'Great Arc' within Venezuela and the Caribbean.

Location	Unit	Age (Ma)	Type/Source/Comments	References
Venezuela	Villa de Cura nappe	Protolith age unknown	Metamorphosed interbedded lavas, tuff, chert, volcaniclastics, graphitic schists, breccia, conglomerates with igneous rocks having an island arc chemistry	Smith et al., 1999; Unger et al., 2005
Margarita Island	Guayacán gneiss, Matasiete metatrondhjemite, El Salado granite	116-106 Ma, 114 Ma, 85-86 Ma (U-Pb zircon)	Felsic island arc plutons emplaced into a high pressure metamorphic complex during the latter stages of deformation	Maresch et al., 2009
Tobago	North Coast Schist, Tobago pluton, Tobago Volcanic Group and Tobago mafic dykes	~130, 112-91, (U-Pb zircon TIMS, Ar-Ar hornblende, ammonites, radiolarians)	Mostly tuffs of the North Coast Schist – mafic to felsic island arc and/or back-arc tholeiites with possible mantle plume and depleted mantle sources. Later mafic island arc tuffs, plutonics, dykes and lavas of tholeiitic composition from a depleted mantle source	Sharp & Snoke, 1988; Frost & Snoke, 1989; Oliver, 1991 unpublished data; Snoke et al., 2001a, Snoke & Noble, 2001; this study
Venezuelan Antilles	Gran Roque and La Blanquilla	76-59 (U-Pb zircon SIMS)	Range of intrusive rocks from quartz diorite to aplite and tonalite, all arc-related, some cutting the Caribbean Oceanic Plateau	Wright & Wyld, 2011
Dutch Antilles	Aruba and Curaçao dykes	89-86 (U-Pb zircon SIMS)	Diorite-tonalite arc-related dykes and intrusions cutting the Caribbean Oceanic Plateau	Wright & Wyld, 2011
Aves Ridge	SE portion is the only part sampled and described in detail	75.9±0.7 (U-Pb zircon SHRIMP)	Mafic calc-alkaline island arc from plume mantle source; felsic calc-alkaline granites from crustal source	Fox et al., 1971; Neill et al., 2011; this study
Virgin Islands	Water Island Fm.	115-110 (radiolarians) at the top of the formation	Mafic and lesser felsic island arc tholeiites with little input from subducted sediments	Donnelly et al., 1971; Donnelly et al., 1990
Puerto Rico	4 main volcanic phases	124-65 (variety of methods)	Mafic to felsic tholeiites, calc-alkaline and shoshonitic rocks of island arc affinity with variable input from subducted sediments	Frost et al., 1998; Schellekens, 1998; Jolly et al., 1998; 2001
Hispaniola	Total of 11 subduction-related blocks	~120 to ~50 (variety of methods, mostly U-Pb zircon)	Boninitic and mafic to intermediate and felsic mostly tholeiitic island arc rocks with variable input from subducted sediments. Associated volcanics, volcaniclastics, tonalites, felsic intrusive etc. Variably metamorphosed. Some adakites and high-Nb basalt at ~90 Ma.	Lebron & Perfit, 1994; Kerr et al., 2003; Kesler et al., 2005; Good summaries in Escuder Viruete et al., 2006; 2007b; 2008; 2010
Jamaica	Exposures in 6 separate inliers. Key is the Devil's Racecourse Formation, others not studied in detail.	>~136 to >~125 Ma (rudists), younger units not related to Great Arc *per se* or not studied in detail	Devil's Racecourse Fm. is best studied and consists of tholeiitic island arc rocks overlain by limestones and calc-alkaline island arc rocks. May correlate to the Great Arc or to pre-polarity reversal Great Arc subduction	Skelton & Masse, 1988; Kerr et al., 2003; Hastie et al., 2009
Cuba	Exposures across the island; Bahia Honda, La Habana-Matanzas, Batabano (covered), Las Villas, Camagüey, Holguin, Oriente	Oldest arc-related unit is ~133 Ma or greater (U-Pb zircon), 120-75 Ma (U-Pb zircon)	Boninites, tholeiites, calc-alkaline island arc rocks, mafic to felsic, arc granitoid intrusions. Uncertain how may island arc systems are preserved	Kerr et al., 1999; Blein et al., 2003; Stanek et al., 2009

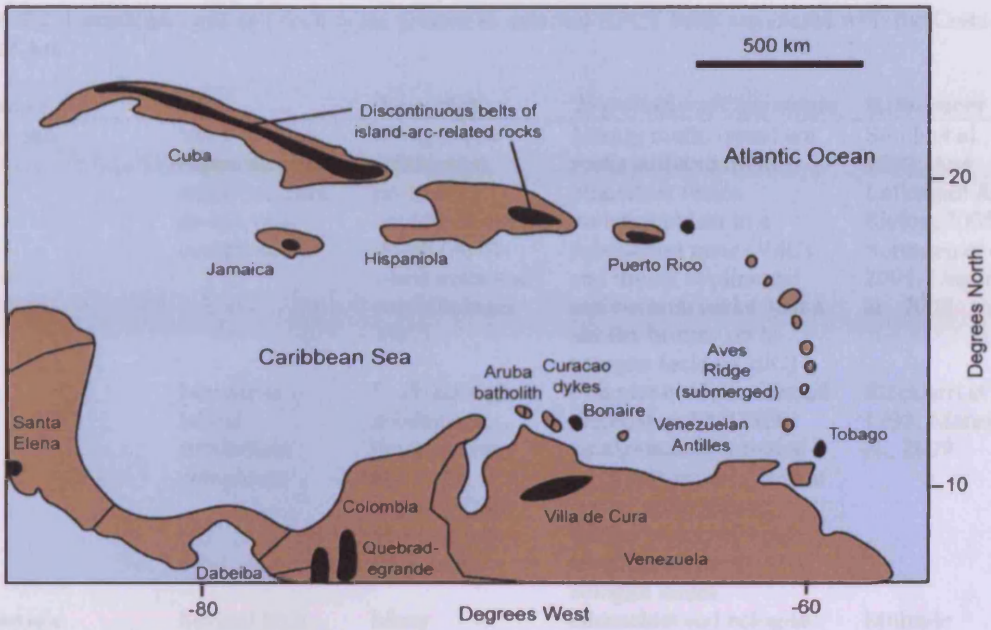

Figure 1.4. Map of the locations of the major components of the Cretaceous island arc systems of the Caribbean region (the Great Arc, for short). Figure adapted from Kerr et al. (2003).

1.4.4. Caribbean subduction zone metamorphism

The magmatic activity preserved in volcanic and plutonic rocks of the Great Arc is accompanied by high pressure-low temperature (HPLT) metamorphic belts which represent the fossilised subduction channels of the Great Arc systems (see Table 1.3 and references therein). In a subduction zone, oceanic crust and the sedimentary veneer gets dragged into the subduction channel and can be later exhumed during terminal collision, ongoing subduction return flow or slab roll-back (e.g. Brun & Faccenna, 2008). Those rocks undergo characteristic pressure and temperature-related changes which can be tracked by radiometric age analysis of minerals such as jadeite, zircon, garnet, phengite, amphiboles, titanite and micas to generate pressure-temperature-time plots (e.g. Hodges, 1991) which may aid the reconstruction of Caribbean subduction history. The locations of HPLT metamorphic belts in the Caribbean are on Figure 1.5 and some of these belts are documented in Table 1.3.

Table 1.3. Locations, ages and rock types present in selected HPLT belts associated with the Cretaceous 'Great Arc'.

Location	Unit	Age (Ma)	Type/Source/Comments	References
Venezuela	Villa de Cura nappe structure and Cordillera de la Costa complexes	No ages pre-subduction; protracted cooling history; 96-80 (Ar-Ar white mica and amphibole on VdC)	Mostly mafic island arc rocks suffered up to blueschist facies metamorphism in a subduction zone (VdC) and mixed continental and oceanic rocks had a similar history up to eclogite facies (CdlC)	Smith et al., 1999; Avé Lallemant & Sisson, 2005; Sorensen et al., 2005; Unger et al., 2005
	Margarita Island subduction complexes	U-Pb ages give subduction, deformation and uplift ongoing from 116 into the Oligocene	Fragments of continental material and MORB amalgamated, intruded by trondhjemites, before end of deformation. Earlier rocks suffered metamorphism to eclogite facies	Stöckhert et al., 1995; Maresch et al., 2009
Hispaniola	Several high pressure and even ultra-high pressure metamorphic belts: Rio San Juan, Puerto Plata, Samaná	Many radiometric ages (U-Pb, Lu-Hf, Ar-Ar) on a variety of minerals. Numerical models show subduction history from ~125/120	Blueschist and eclogite-facies metamorphism of oceanic rocks and ocean crust. Interpreted to represent the combined effect of Aptian to mid-Eocene SW-dipping proto-Caribbean subduction at approximately 2 cm/annum	Multiple references. UHP metamorphism in Abbott et al., 2005; summary and models in Krebs et al., 2008
Jamaica	Blue Mountains	no reliable ages, overlain by Eocene strata	Greenschist, blueschist, amphibolite, serpentinite assumed proto-Caribbean MORB protolith	Draper et al., 1986
Cuba	Several high pressure metamorphic belts: Cangre, Pinos, Escambray, Las Villas, La Suncia, Holguín, La Corea, Purial, Sierra del Convento, Asunción	Many radiometric ages (U-Pb, Lu-Hf, Ar-Ar) on a variety of minerals. Combined geotectonic and numerical models suggest subduction ongoing from ~120	Slices of MORB, continental and island arc protoliths which have been caught up in a subduction zone and stacked in a series of nappe structures. Greenschist, amphibolite and eclogite facies metamorphism at different localities	Multiple references. Excellent summary in Stanek et al., 2009

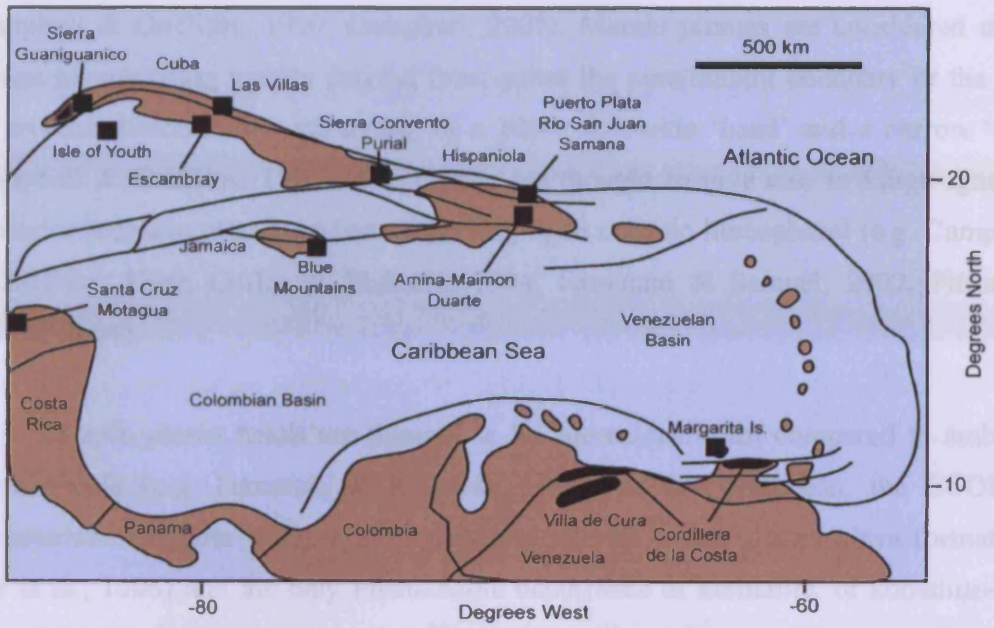

Figure 1.5. Map of locations of the high-pressure/low-temperature rocks of the Caribbean, with strike-slip and other deformational boundaries marked as dark lines. Simplified from Pindell et al. (2005).

1.4.5. The Caribbean-Colombian Oceanic Plateau (CCOP)

Large parts of the Colombian and Venezuelan Basins in the Caribbean Sea are ~10-20 km thick and clearly do not represent normal oceanic floor; as revealed by seismic refraction studies and deductions from thermal subsidence curves (Officer et al., 1959; Edgar et al., 1971; Houtz & Ludwig, 1977; Burke et al., 1978). Magnetic anomalies indicate the basement to this thickened crust is approximately of Middle to Late Jurassic age (Ghosh et al., 1984). The basement is overlain by ~1-2.5 km of basaltic flows and sills (drilled during DSDP Leg 15) thought to be the B" seismic reflector seen across the central Caribbean (Donnelly et al., 1973). Burke et al. (1978) proposed that the Caribbean is an oceanic plateau and that the B" layer represents the oceanic equivalent of a continental flood basalt episode. The **Caribbean-Colombian Oceanic Plateau (CCOP)** thus represents a crustal volume of up to 16 million km^3 (Case et al., 1990; Mauffrey & Leroy, 1997) and includes oceanic plateau-related rocks accreted to the South American margin in Colombia and Ecuador as well as the Caribbean (see Table 1.4 and Fig. 1.6).

Oceanic plateaus are linked to the arrival of a mantle plume head at the base of the oceanic lithosphere and subsequent high-degree partial melting of the plume mantle

(Campbell & Griffiths, 1990; Campbell, 2007). Mantle plumes are considered to be regions of upwelling mantle derived from either the core/mantle boundary or the 660 km seismic discontinuity, consisting of a 1000+ km-wide 'head' and a narrow 'tail' (Campbell & Griffiths, 1990). The former are thought to give rise to Large Igneous Provinces [oceanic plateaus where impacting upon oceanic lithosphere] (e.g. Campbell & Griffiths, 1990; Coffin & Eldholm, 1994; Farnetani & Samuel, 2002; Fitton & Godard, 2004).

Mantle plume heads are thought to be anomalously hot compared to ambient upper mantle (e.g. Farnetani & Richards, 1994). In the Caribbean, the CCOP is characterised by quite widespread high-Mg picrites (e.g. the Curaçao lava formation, Kerr et al., 1996) and the only Phanerozoic occurrence of komatiite, or komatiite-like rocks (Aitken & Etcheverría, 1984; Donnelly, 1994; Alvarado et al., 1997). Both picrites and komatiites require high degrees of melting compared to MORB [picrites can form in island arc settings, but the CCOP is not subduction-related] which requires a higher mantle potential temperature compared to 'ambient' upper mantle in the Phanerozoic (Kerr et al., 1996; Kerr, 2005; Herzberg & Gazel, 2009). Calculated potential temperatures from parts of the plateau range from 1500-1620°C, up to 270°C higher than ambient upper mantle (Herzberg & Gazel, 2009).

Furthermore, none of the rocks collected from the plateau have either subduction-influenced or continental geochemistry rendering a tectonic origin of the thick crust of the Venezuelan and Colombian basins highly improbable (Kerr et al., 2003). Nd and Hf isotope ratios and Nb/Y vs. Zr/Y systematics indicate at least some parts of the plateau have isotopically depleted, Nb-enriched mantle sources with respect to Atlantic or Pacific MORB (Kerr et al., 2003), similar to the geochemical signature of basalts and picrites derived from the Iceland mantle plume and those found in other oceanic plateau settings such as the Kerguelen Plateau (e.g. Fitton et al., 1997; Ingle et al., 2002). Finally, the majority of basalts and picrites in the CCOP were erupted rapidly at ~95-88 Ma which is linked to the rapid melting of the plume head as it rose to meet the lithosphere (Sinton et al., 1998; Kerr et al., 2003). For these reasons, impingement of a mantle plume on the Caribbean lithosphere was the most likely cause of the CCOP magmatism.

The hotspot source of the CCOP is debated, but most likely to be the present-day Galapagos plume (Duncan & Hargraves, 1984; Hauff et al., 2004; Herzberg & Gazel, 2009). Hauff et al. (2004) point to the age range of accreted hotspot tracks in Central America as a 'bridge' between the 'young' Galapagos hotspot track and the 95-88 Ma CCOP. The study of Herzberg & Gazel (2009) including Curaçao and other examples from the Caribbean plateau and hotspot tracks, Gorgona Island (komatiites), Carnegie and Cocos Ridges and the Galapagos Islands, reveals a pattern of secular cooling of mantle potential temperature from ~90 Ma to the present day which tightens the link between the CCOP and Galapagos. The same isotopic domains present in Galapagos today are recognised in the CCOP (E. Gazel, 2009, pers. comm.).

Table 1.4. Locations, ages and rock types present in selected on- and off-shore components of the Caribbean-Colombian Oceanic Plateau.

Location	Unit	Age (Ma)	Type/Comments	References
Siquisique (Los Algadones, Venezuela), El Copey (Araya, Venezuela) and San Souci (Trinidad)	Fragments within allochthonous units strung out between the interior of Venezuela and the North Coast of Trinidad	Approximately 95-90 (plagioclase Ar-Ar)	Some felsic rocks, mostly basalts, gabbros and serpentinites; isotopically and chemically distinct from MORB. Possible proto-Caribbean extension of the CCOP	Wadge & McDonald, 1985; Kerr et al., 2009, this study
Dutch Antilles	Aruba Lava Formation	Turonian (94-89) (ammonite imprints)	Mafic flows, dolerite, volcanic sediment of oceanic plateau affinity	McDonald, 1968; White et al., 1999
	Curaçao Lava Formation	88.9 ± 0.8 (plagioclase Ar-Ar)	Picritic to basaltic pillow lavas of oceanic plateau affinity	Kerr et al., 1996; Sinton et al., 1998
Venezuelan Antilles	Gran Roque basement	Uncertain	Gabbros and dolerites of possible oceanic plateau affinity	Giunta et al., 2002; A.C. Kerr unpublished data
Hispaniola	Duarte Complex	86-87 (amphibole Ar-Ar)	Picrites, ankaramites and amphibolites suspected to be of oceanic plateau affinity	Lapierre et al., 1999
	Dumisseau	92-89 (whole rock Ar-Ar)	Pillowed and flow basalts, picrites and sediments	Sinton et al., 1998
Jamaica	Bath-Dunrobin Formation	92-86 (radiolarians)	Basaltic lavas of oceanic plateau affinity	Montgomery & Pessagno, 1999; Hastie et al., 2008
Caribbean Sea	Smooth B'' seismic reflection layer	94-81 (whole rock Ar-Ar)	Repeated basaltic flows of oceanic plateau affinity; the varying ages relate to long-term supply of plume magmas during later extensional tectonism	e.g. Sinton et al., 1998; Sinton et al., 2000; Kerr et al., 2003; 2009

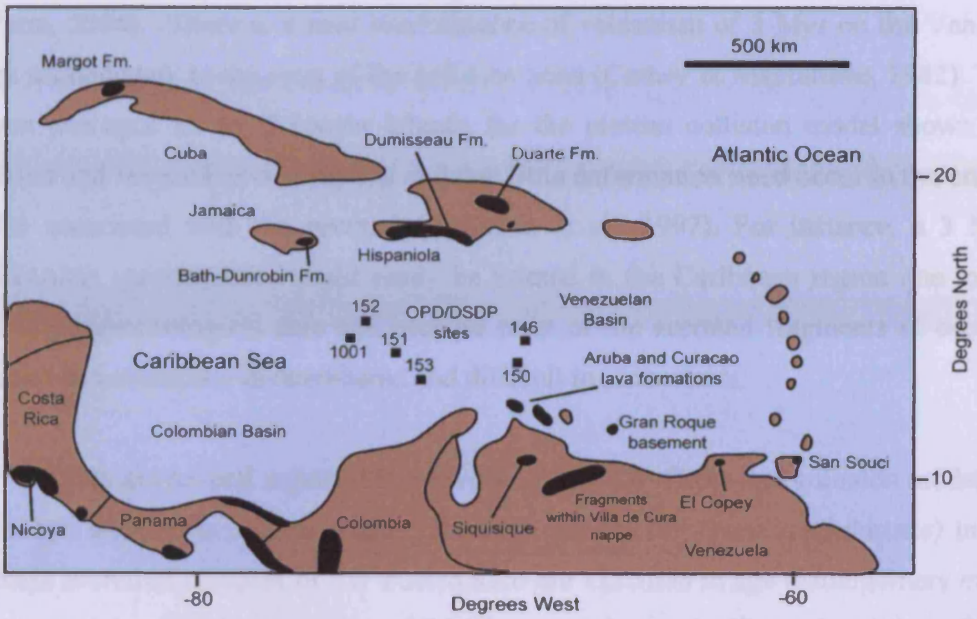

Figure 1.6. Map adapted from Kerr et al. (2003) showing the location of studied plume-related fragments preserved around the Caribbean Plate or drilled/dredged from the floor of the Caribbean Sea during Ocean Drilling Program/Deep Sea Drilling Project voyages.

1.4.6. Great Arc-CCOP collision model of Caribbean tectonic evolution

This section deals with one model that has been developed in order to explain the combined tectonic evolution of the components of the Caribbean Plate listed above. In this model, summarised in Figure 1.7, it is proposed that subduction on the Great Arc system (specifically the Greater Antilles arc) was E-dipping throughout the Early- to Mid-Cretaceous before attempted subduction of the newly-formed CCOP forced a subduction polarity reversal at ~90-85 Ma leading to a phase of SW-dipping Great Arc subduction (Burke, 1978; 1988; Duncan & Hargraves, 1984; Montgomery et al., 1994; White et al., 1999; Giunta et al., 2002; Kerr et al., 2003; Vallejo et al., 2006; Liu et al., 2008; Hastie et al., 2008, 2009, 2010a,b,c; Hastie & Kerr, 2010; van der Lelij et al., 2010).

Young oceanic plateaus may be too thick, hot and buoyant to be entirely subducted at collisional margins (Saunders et al., 1996). In the Solomon Islands, the Ontong-Java plateau clogged the Solomon Islands arc trench, forcing subduction polarity to switch to the other side of the arc system (Hughes & Turner, 1977; Cooper & Taylor 1985; Auzende et al., 1995; Miura et al., 2004). Work on the Ontong-Java collision suggests that collision and polarity reversal took a total of just 2-7 Myr (Mann

& Taira, 2004). There is a very brief absence of volcanism of 3 Myr on the Vanuatu block immediately to the west of the collision zone (Carney & Macfarlane, 1982). This proven analogue in the Solomon Islands for the plateau collision model shows that collision and reversal occurs rapidly and that little deformation need occur in the crustal blocks associated with the reversal (Petterson et al., 1997). For instance, a 3 Myr, diachronous unconformity could easily be missed in the Caribbean region due to the lack of geochronological data and because most of the accreted fragments of oceanic plateau are tectonically dismembered and difficult to reconstruct.

There are several arguments in favour of a CCOP-Great Arc collision model for Caribbean tectonic evolution. Firstly, the youngest Pacific fauna (radiolarians) in the Bermeja accretion complex of SW Puerto Rico are Turonian in age (Montgomery et al., 1994) which implies that accretion of Pacific material onto the Great Arc did not finish until ~90 Ma. This may, however, be a chance occurrence related to the age of material accreted during later crustal shortening. There is also the occurrence of high-Mg andesites and Nb-enriched basalts in the Tireo Formation of the Cordillera Central of Hispaniola, which are said to record possible mid-ocean ridge subduction at ~90 Ma (Escuder Viruete et al., 2007b), the ridge being the still-active proto-Caribbean spreading centre. No such rocks have been recorded prior to ~90 Ma in the eastern Caribbean implying that either there was no ridge subduction prior to this date or that the Tireo Formation is the first to be formed following a ~90 Ma initiation of subduction beneath the Great Arc from the NE. Another similar argument in favour of the plateau collision model is that if there was a pre-existing SW-dipping Great Arc subduction zone, the plateau would have to erupt close to an active island arc, possibly through a slab-gap due to proto-Caribbean ridge subduction (Pindell & Kennan, 2009). This situation would result in contamination of arc- with plateau-related mantle sources and vice versa (Hastie & Kerr, 2010). There is a discussion on this point in Chapter 7.

The primary argument against the collision model is that there is a continuous record of arc magmatism, high pressure metamorphism and subduction return flow in subduction complexes from 125-<80 Ma in the Greater Antilles indicating that subduction with a singular polarity was ongoing throughout the Cretaceous (Pindell & Kennan, 2009; Pindell et al., 2011). Another argument is that there is no widespread unconformity or metamorphic event dated to <95 Ma. These arguments will be

discussed in Section 1.5.7. However, recent geochemical and chronological work on the Dutch Antilles has linked uplift to polarity reversal and/or inception of NW-dipping subduction beneath the CCOP at ~89 Ma (van der Lelij et al., 2010; Wright & Wyld, 2011). In the model of Wright & Wyld, subduction initiated at the NE margin of the CCOP without the presence of a prior subduction zone (e.g. Stern, 2004).

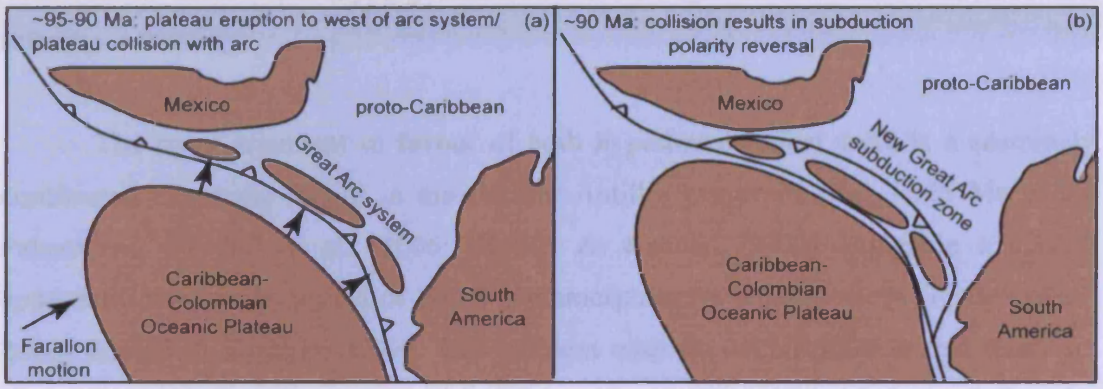

Figure 1.7. Simplified version of the Great Arc/CCOP collision model of the Caribbean showing: (a) the formation of the CCOP, its arrival at the Great Arc trench and (b) the subsequent subduction polarity reversal at around 90 Ma. Adapted from Hastie & Kerr (2010).

1.4.7. Long-lived SW-dipping Great Arc model of Caribbean tectonic evolution

A second set of hypotheses developed to explain the tectonic evolution of the Caribbean Plate are based on the idea that SW-dipping subduction on the Great Arc system occurred uninterrupted from the Early Cretaceous to the Palaeocene and began due to the westward acceleration of the Americas at ~135-125 Ma, with no role for the CCOP (summarised in Fig. 1.8). The two related hypotheses are that: (a) SW-dipping subduction initiated to the east of an early east-dipping Andean/Cordilleran system during a subduction polarity reversal event, or (b) initiation occurred at an intra-oceanic transform far to the east of the Andean/Cordilleran system with the entire of the Great Arc being generated in a SW-dipping subduction setting. Supporters of either model include, but are not limited to: Mattson, 1979; Pindell & Barrett, 1990; Lebron & Perfit, 1993; Draper et al., 1996; Marchesi et al., 2007; Jolly et al., 2008 and references therein; Lázaro & García-Casco, 2009; Pindell et al., 2006 and references therein; Maresch et al., 2009; Pindell & Kennan, 2009; Escuder Viruete et al., 2010 and references therein and Pindell et al., 2011. The two hypotheses both generally reflect an Early Cretaceous change from E-dipping to SW-dipping Caribbean subduction, pre-dating the formation of the CCOP.

Pindell et al. (1988) have proposed that North America began to accelerate west over the mantle at a faster rate than South America at ~135 Ma, compressing the arcs of the North American cordillera. In the proto-Caribbean region, it is suggested that the westward acceleration generated an intra-oceanic transform, which then foundered at ~125 Ma to form a SW-dipping subduction zone (e.g. Pindell & Kennan, 2009 and references therein).

The main argument in favour of both hypotheses is that there is a seemingly continuous magmatic record in the Greater Antilles preserved from ~125 Ma to the Palaeocene (Pindell et al., 2006; Pindell & Kennan, 2009) alongside a similar apparently continuous record of HPLT metamorphism in adjacent belts (Pindell et al., 2006; Pindell & Kennan, 2009). The problem with the HPLT belts is that many lie close to major fault systems which have undergone large translations during the Cenozoic (e.g. Pindell et al., 2005). Nevertheless, the long history of island arc magmatism and HPLT metamorphism is at present in favour of the long-lived SW-dipping subduction model.

In closer detail, hypothesis (a) above is problematic, because arguments for a pre-existing E-dipping subduction zone and polarity reversal in the Greater Antilles have recently been refuted: for example, a widespread change in subduction-related volcanism from tholeiitic to calc-alkaline composition during the Aptian-Albian was proposed to mark the polarity reversal (Pindell et al., 2005; 2006). However, it is now clear from many localities in the Greater Antilles that tholeiitic arc magmatism continues beyond the Aptian-Albian, and elsewhere calc-alkaline magmatism predates this time (e.g. Kerr et al., 2003; Hastie et al., 2009). Changes in arc chemistry can be easily induced by changing the nature of the fluid flux from the slab (e.g. Hastie et al., 2009 for a Caribbean example), the degree of partial melting and the thickness of the arc crust (e.g. Plank & Langmuir, 1988). Therefore the distinction between tholeiitic and calc-alkaline compositions is arbitrary and not necessarily caused by a subduction polarity reversal. A second refuted argument is that an Albian unconformity exists on Hispaniola (Lebron & Perfit, 1993; 1994; Pindell et al., 2006) indicative of a reversal event. Recent investigations have discovered a continuum of arc magmatism through this period on Puerto Rico (Schellekens, 1998; Jolly et al., 2006) and the unconformity

there is only locally developed. Therefore, a local, not regional solution for the unconformity on Hispaniola is possible.

Recent publications have begun to favour hypothesis (b), that the site of inception of the Great Arc lay quite far to the east of the Andean/Cordilleran system and that the entire Great Arc was formed by a singular southwest-dipping subduction zone from ~135-125 Ma onwards (Pindell & Kennan, 2009; Pindell et al., 2011). This hypothesis raises questions over the origin of any fragments of subduction-related material which pre-date the westwards acceleration of the Americas (Table 1.1).

One key point mentioned in Section 1.4.6 is that no geochemical evidence of interaction between the mantle plume source of the CCOP and a SW-dipping Caribbean arc system has been found which dates from the formation of the plateau. As mentioned, the youngest magmatism linked to proto-Caribbean ridge subduction is ~90 Ma (Escuder Viruete et al., 2007) and as yet, no outcrop of the CCOP shows evidence of contamination from subduction-related fluids (Hastie & Kerr, 2010).

Until recently the Great Arc was treated as a singular entity with a single polarity at any given time (Kerr et al. 1996; Giunta et al., 2002; Ostos et al., 2005; Neill et al., 2011; Wright & Wyld, 2011). It is however noticeable that recent studies arguing for the plateau collision model have focussed on the Dutch-Venezuelan Antilles and Jamaica (e.g. Hastie et al., 2008; 2009; $2010_{a,b,c}$; van der Lelij et al., 2010) which may well have been at the extreme north and south of the Caribbean region at ~90 Ma, respectively, whereas the models described above in favour of long-lived SW-dipping subduction concentrate on the rest of the Greater Antillean islands of Cuba, Puerto Rico and Hispaniola. This geographical bias of recent studies may be no coincidence, and may suggest that the so-called Great Arc was made up of different subduction systems which formed in different locations and had different polarities to one another.

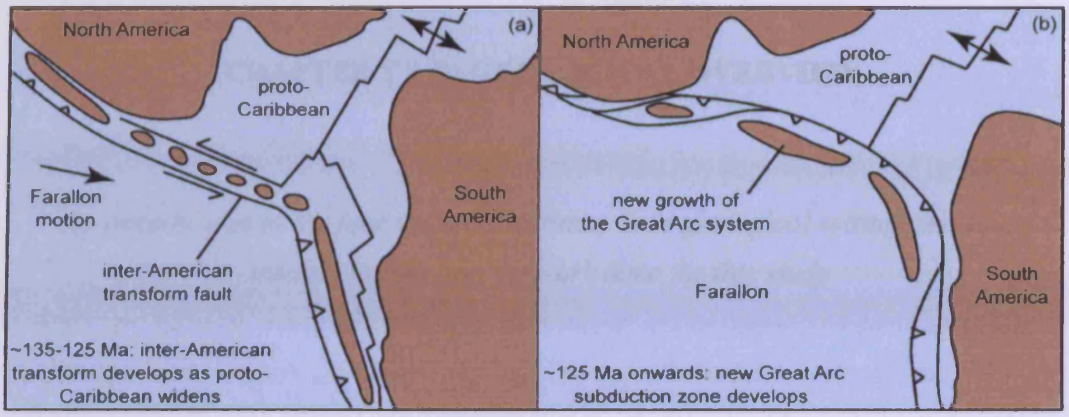

Figure 1.8. Simplified model of the long-lived SW-dipping Great Arc subduction zone model of Caribbean Plate evolution, adapted from Pindell et al. (2006). Part (a) shows the splitting of the Americas and the development of an inter-American transform fault which breaks up the Andean/Cordilleran subduction system. Part (b) shows the subsequent initiation of proto-Caribbean subduction at ~125 Ma as North America pushes westward over the mantle.

1.4.8 How will studying the rocks in this thesis help resolve the tectonic evolution of the Caribbean?

The Late Jurassic to Early Cretaceous basement of La Désirade Island (see Section 2.1) pre-dates any of the accepted rocks of the Great Arc and appears to be of back-arc origin (Section 5.2). Therefore, study of these rocks and correlation with other 'old' fragments preserved within the Caribbean region may help to refine the plate tectonic configuration of the proto-Caribbean and eastern Pacific prior to inception of the Great Arc systems. Both Tobago (Section 5.3) and the Aves Ridge (Section 5.5) represent island arc systems which are a part of the wider Great Arc system. Study of the type of arc magmatism involved in forming the rocks in these localities may help indicate subduction polarity in their respective parts of the Caribbean during the Cretaceous. Finally, the rocks of the San Souci Formation on Trinidad were formed to the east of the Great Arc system (Section 5.4) so their origin can help elucidate the proximity of the Great Arc to the South American continent and the nature of mantle sources present in the proto-Caribbean during the Late Cretaceous.

CHAPTER TWO: GEOLOGICAL OVERVIEW

An introduction to the four studied localities; their geological setting, previous interpretations and the work done for this study

2.1. La Désirade Island, Guadeloupe

2.1.1. Geological Setting

La Désirade (22 km^2) lies 10 km east of Grande Terre, Guadeloupe, on the hanging wall of the active Lesser Antilles subduction zone (Fig. 2.1). The island is capped by Neogene limestone (Baumgartner-Mora et al., 2004) and has been uplifted on a fault scarp revealing the only confirmed suite of Mesozoic volcanic and plutonic rocks in the Lesser Antilles. Trondhjemites and basalts similar to those found on La Désirade have also been dredged from the Falmouth Spur between La Désirade and Antigua and from the Désirade sea trough but have not been dated (Johnston et al., 1971; Fink, 1972; Bouysse, 1984). The presence of Late Jurassic radiolarian assemblages of Pacific origin on La Désirade which pre-date much of the proto-Caribbean seaway demonstrate that La Désirade has travelled eastwards relative to the Americas at the leading edge of the Caribbean Plate (Montgomery et al., 1992, 1994).

Approximately 10 km^2 of Mesozoic igneous rocks are exposed on the island, chiefly around the coasts and particularly in the northeast from Baie Mahault to Baie du Grand Abaque (Fig. 2.1). Recent geochronology and fieldwork (Mattinson et al., 2008) reveal a subaqueous eruptive and intrusive sequence. The first event was eruption of mafic pillow lavas and massive flows, inter-bedded with chert and subordinate limestone. These are referred to here as the ***NE mafic volcanic complex***, and are the main focus of this study. Magmatism then evolved to felsic compositions (Mattinson et al., 2008) forming the ***NE felsic volcanic complex*** near Grand Abaque, the central ***trondhjemite pluton*** and the ***SW felsic complex*** which consists of dykes and flows around Morne Frégule. Finally a suite of ***intermediate-felsic*** *dykes* which cuts both the pluton and the NE complexes was emplaced (Fig. 2.1).

Radiolarians in inter-lava flow chert at Pointe Doublé (NE mafic complex) and Pointe Frégule (SW felsic complex) are from bio-chronostratigraphic zone 4, upper subzone 4β [mid-Upper Tithonian (~150-145 Ma)] (Montgomery et al., 1992; Mattinson et al., 2008). Work by Cordey & Corneé (2009) on the northeast mafic complex has revealed radiolarians dating to the Late Kimmeridgian (~153-150 Ma),

indicating a maximum eruption time of ~8 Ma for the northeast mafic complex (timescale of Ogg et al., 2008). Zircons separated from the trondhjemite pluton have been dated by U-Pb chemical abrasion-thermal ionisation mass spectrometry to 143.74±0.33 Ma (Mattinson et al., 2008), i.e. mid-Berriasian of the Lower Cretaceous. The oldest radiolarian age and the U-Pb age indicate igneous activity on La Désirade lasted up to 10 Ma.

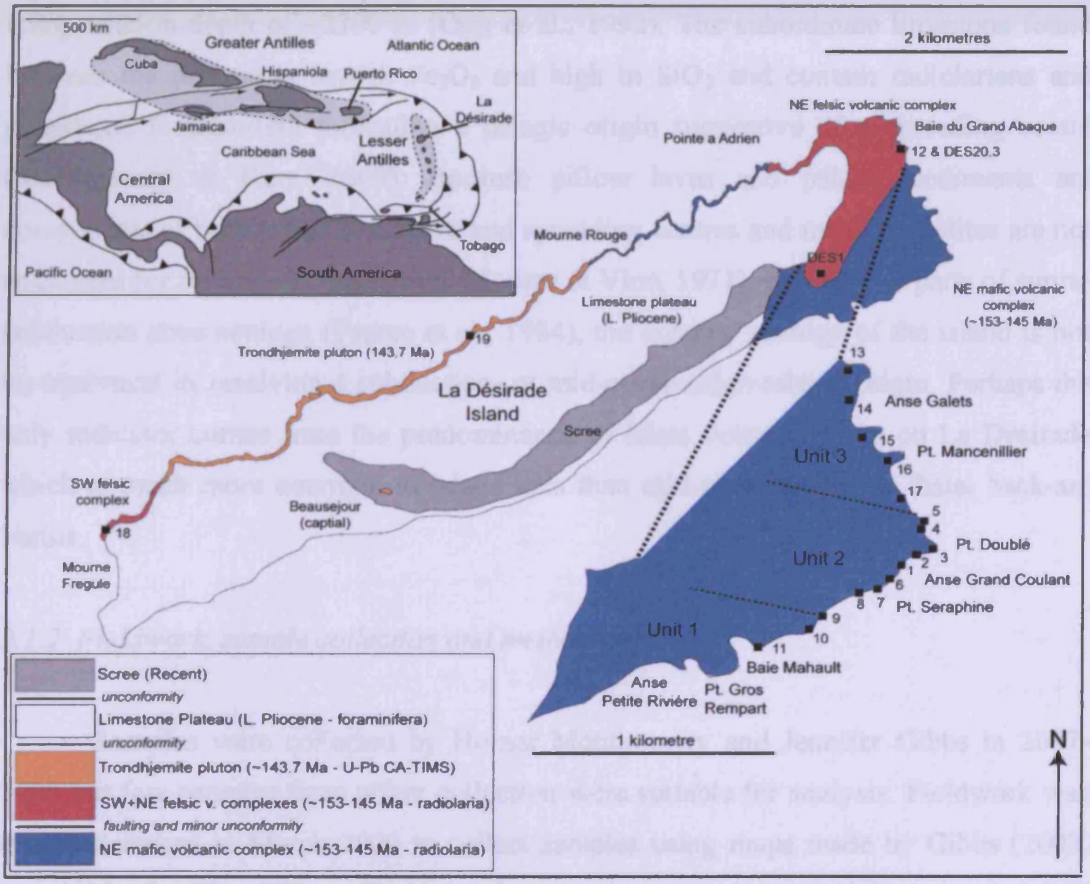

Figure 2.1. Simplified geological map for La Désirade showing the studied units. Sampled locations are numbered; not marked are the mafic-intermediate dykes. References for ages are given in the text and the map was prepared based on field maps from unpublished work of Gibbs (2008).

The occurrence of pillow basalts and what was originally interpreted as pelagic chert lead Mattinson et al. (1980, 2008) to conclude that the mafic rocks were the upper part of an ophiolitic sequence probably formed at a mid-ocean ridge. Bouysse et al. (1983) favoured a subduction-related setting based in part on the lack of components of an ophiolite such as sheeted dykes, gabbros and ultramafic rocks, and a similar model has also been proposed by Baumgartner et al. (2008) and Cordey & Corneé (2009).

A recent re-investigation of the chert of the northeast mafic volcanic complex by Montgomery & Kerr (2009) and Cordey & Corneé (2009) has shown that radiolarites are sparse and that the chert has high levels of MgO and Fe_2O_3, inferring rapid formation in a hydrothermal regime. However there were periods of quiescence during which time pelagic chert and limestone deposition occurred. The occurrence of pelagic limestone demonstrates deposition of material above the postulated carbonate compensation depth of ~2700 m (Ogg et al., 1992). The subordinate limestone found between the pillows is low in Fe_2O_3 and high in SiO_2 and contain radiolarians and planktonic foraminifera indicating a pelagic origin suggestive of a spreading centre (Montgomery & Kerr, 2009). Because pillow lavas and pelagic sediments are components of both subaqueous arcs and spreading centres and many ophiolites are not analogues for mid-ocean ridges (e.g. Moores & Vine, 1971), but integral parts of supra-subduction zone settings (Pearce et al., 1984), the outcrop geology of the island is not un-equivocal in resolving a subduction- or mid-ocean ridge-related origin. Perhaps the only indicator comes from the predominance of felsic volcanic rocks on La Désirade which is much more common in island arcs than mid ocean ridges or distal back-arc basins.

2.1.2. Fieldwork, sample collection and method employed

Samples were collected by Homer Montgomery and Jennifer Gibbs in 2007-2008 but few samples from either collection were suitable for analysis. Fieldwork was thus undertaken in March 2009 to collect samples using maps made by Gibbs (2008, unpublished). The NE mafic volcanic complex was preferentially sampled (25 samples), whilst 18 samples from other units were also collected. Outcrop is excellent in the NE of the island, including a complete coastal section through the mafic stratigraphy. Much of the remaining area is covered by scrub, younger limestone and inaccessible cliffs, limiting collection of most felsic volcanics and trondhjemites to a cliff at Mourne Frégule and a single shore and river gully section near L'Emballage. As the geochronological record of the island is well-defined (Mattinson et al., 2008; Cordey & Corneé, 2009), further dating was deemed unnecessary. In order to determine the tectonic setting and identify mantle and crustal inputs, only whole rock major and trace element analysis was undertaken. Analysis of major elements and Sc was by inductively-coupled plasma optical emission spectrometry (ICP-OES) by Ley Woolley,

and for trace elements by inductively-coupled plasma mass spectrometry (ICP-MS) by Iain McDonald, both at Cardiff University using solutions prepared by the author with methodology in Appendix 3.

2.2. Tobago Island, Trinidad and Tobago

2.2.1. Geological Setting

Tobago lies on a NE-SW trending fault scarp north of the boundary between the South American and Caribbean Plates (Robertson & Burke, 1989) and south of the Lesser Antilles arc (Fig. 2.2). The 400 km^2 island of Tobago has been described as a partial cross-section through a Mesozoic island arc (Snoke et al., 2001a and references therein). Available geochemistry and geochronology point to a history of magmatic activity from the Albian-Turonian (Sharp & Snoke, 1988; Frost & Snoke, 1989) which has led to the inclusion of Tobago as part of the 'Great Arc' (Snoke et al. 2001a; Kerr et al., 2003; Pindell et al., 2005). Following early studies by Cunningham-Craig (1907) and Maxwell (1948), detailed mapping by A.W. Snoke and University of Wyoming colleagues led to the publication of a new map (Snoke et al. 2001b), in which the rock units described below were defined.

The **North Coast Schist (NCS)** (Fig. 2.2) is a deformed lower greenschist facies meta-volcanic suite covering the portion of the island to the N of the prominent Main Ridge rainforest, consisting of the ***Parlatuvier***, ***Karv*** and ***Mount Dillon*** Formations. A thin, discontinuous **amphibolite**-facies belt of deformed plagioclase-phyric volcanic rocks lies approximately between the NCS and the younger Volcano-Plutonic Suite, and is argued to be a metamorphic aureole at the contact between the two suites (see below) (Snoke et al., 2001b). The stratigraphic order is uncertain due to deformation and folding.

The Parlatuvier Formation includes intermediate and mafic meta-tuff, meta-tuff breccia and rare mafic and intermediate lavas and dykes and stocks. The Karv Formation is exposed as a series of bands along the Main Ridge, completely within the Parlatuvier Formation. Karv contains argillaceous graphitic rocks inter-layered with silicic meta-tuffs. The Mount Dillon Formation contains silicic and rare more mafic meta-tuffs, argillaceous schists, phyllites and cherts.

A hornblende ^{40}Ar-^{39}Ar isochron of 115.9±3.2 Ma was considered unreliable as a protolith age for the Parlatuvier Formation (Sharp & Snoke, 1988). Precambrian ages

were obtained from zircons separated from andesitic breccia of the Parlatuvier Formation in 1995 at the University of Wyoming which may represent either an analytical relict or an analysis of an old, detrital zircon (A.W. Snoke & K.R. Chamberlain, 2008 pers. comm.). Analysis of zircons in the same sample by in-situ U-Pb secondary ion mass spectrometry (Schmitt et al., 2010) gave an age of 89±9.5 Ma, which is presently being interpreted, but is not considered of primary magmatic origin (K.R. Chamberlain, 2010 pers. comm.). Finally, regional metamorphism of greenschist grade, coupled with wrench shearing has left a series of steep, south-east-plunging antiforms and synforms in the North Coast Schist argued to relate to deformation within an island arc setting (Snoke et al. 2001a and references therein). Further discussion on the deformation of the NCS and its relationship to the other rocks of the island is in Sections 5.3.1 and 6.3.

The rest of the igneous rocks of Tobago are known as the **Volcano-Plutonic Suite (VPS)** and are split into the **Tobago Volcanic Group (TVG)**, the **Tobago Plutonic Suite (TPS)** (Snoke et al., 2001a,b) and a suite of **mafic dykes** (Fig. 2.2). In the TVG, stratigraphic formations (Fig 2.2) have been identified based on phenocryst assemblages although contacts and volcanic stratigraphy are uncertain (Maxwell, 1948; Snoke et al., 2001a and references therein). Maxwell (1948) defined the Hawk's Bill and Merchison Formations which make up part of a large area of the S and NE of the island and consist of pillow lavas and reworked volcanogenic sediments. These formations are now known as the ***TVG (undifferentiated)*** (Snoke et al., 2001a,b). The ***Argyle Formation*** of the NE of the island contains mostly tuff breccias with hornblende-bearing phenocrysts assemblages. The ***Bacolet Formation*** of the SE of Tobago includes clinopyroxene and plagioclase-phyric tuff breccia, lapilli tuff, scarce lava flows and occasional volcanogenic sediments. The ***Goldsborough Formation*** of the eastern part of Tobago contains plagioclase-phyric tuff breccias and pillow lavas both of intermediate composition.

The **TPS** (Fig. 2.2) consists of three main components. Close to the boundary with the North Coast Schist, ***deformed mafic volcanic and plutonic rocks*** are found in three separate locations (Snoke et al., 2001b). Snoke et al. (2001a) interpreted these as fragments of the volcanic carapace which collapsed into the TPS. A variety of ***ultramafic*** rocks are chiefly exposed on the northern margin of the pluton.

Approximately two-thirds of the TPS comprises a compositionally and texturally heterogeneous ***gabbro-diorite***.

Cutting the pluton is a 7 km-long, 500 m-wide dyke-like intrusion of ***biotite tonalite*** running from Arnos Bay to Mason Hall (Fig. 2.2) which will be dealt with separately along with a small body of ***granitoid*** exposed on the Kendal Road (inland from Carapuse Bay on Fig. 2.2), which will be grouped with several other ***Nb- and LREE-enriched intrusions***.

Radiolarians and ammonites found near Scarborough date from Early-Mid Albian and radiolarians in chert from the Bacolet Formation have an Early-Late Albian age (112-106 Ma) (Snoke & Noble, 2001). Hornblende in tuff breccia in the TVG (Undifferentiated) on Little Tobago yielded a ^{40}Ar-^{39}Ar plateau of 104.2 ± 1.3 Ma (Sharp & Snoke, 1988). A hornblende gabbro pegmatite has been dated (^{40}Ar-^{39}Ar plateau) at 102.9 ± 1.5 Ma (isochron = 103.6 ± 1.4 Ma) whilst a hornblende-quartz diorite yielded an isochron age of 104.7 ± 1.6 Ma (Sharp & Snoke, 1988; Snoke et al., 1990b; Sharp & Snoke, unpublished data). Zircon fission track dates from the gabbro-diorite showed cooling through 250-200°C at ~103 Ma (Cerveny & Snoke, 1993). A previously unreported U-Pb thermal ionisation mass spectrometry (TIMS) date of 104 ± 1 Ma (G.J.H. Oliver 1990, unpublished data) was obtained from 3 whole, un-zoned, fresh zircon crystals in the gabbro-diorite at Culloden Bay. The TPS therefore appears to be broadly contemporaneous or slightly post-dating the volcanics.

Mafic dykes, composed of hornblende micro-diorite, porphyritic gabbros and dolerites, cut the VPS. Dykes cutting the biotite tonalite unit yielded ^{40}Ar-^{39}Ar hornblende ages of 102.8 ± 1.2 Ma (isochron = 103.5 ± 1.1 Ma) and 91.4 ± 2.2 Ma (isochron 92.7 ± 1.1 Ma) (Sharp & Snoke, 1988; unpublished data). If the ~103 Ma age is robust, then the tonalite is also contemporaneous with the VPS. The Turonian age for the other dyke suggests a long history of dyke intrusion after the main phase of island arc magmatism.

Geochemical study has hitherto been restricted to major, minor and some trace elements, along with Nd and Sr isotope analyses (Frost & Snoke, 1989). Despite the

island arc origin of the rocks, little is known about the mantle source of the magmatism, the precise tectonic setting or any crustal inputs. Also, it is unknown if the dyke swarm is part of the VPS or if it is a separate magmatic event. Tobago's nearest arc-related neighbours of a similar age are on Margarita Island offshore Venezuela (300 km to the west) and on Bonaire in the Dutch Antilles (600 km away), so the relationship of Tobago to the rest of Great Arc system also requires investigation (Thompson et al., 2004; Wright & Wyld, 2011). The juxtaposition of the potentially differently-aged NCS and TVG *may* prove important in relation to models of subduction polarity reversal. Therefore, a study of the geochronology and geochemistry of the magmatic rocks of Tobago Island is both necessary and relevant in terms of wider Caribbean tectonic evolution, to help solve these problems.

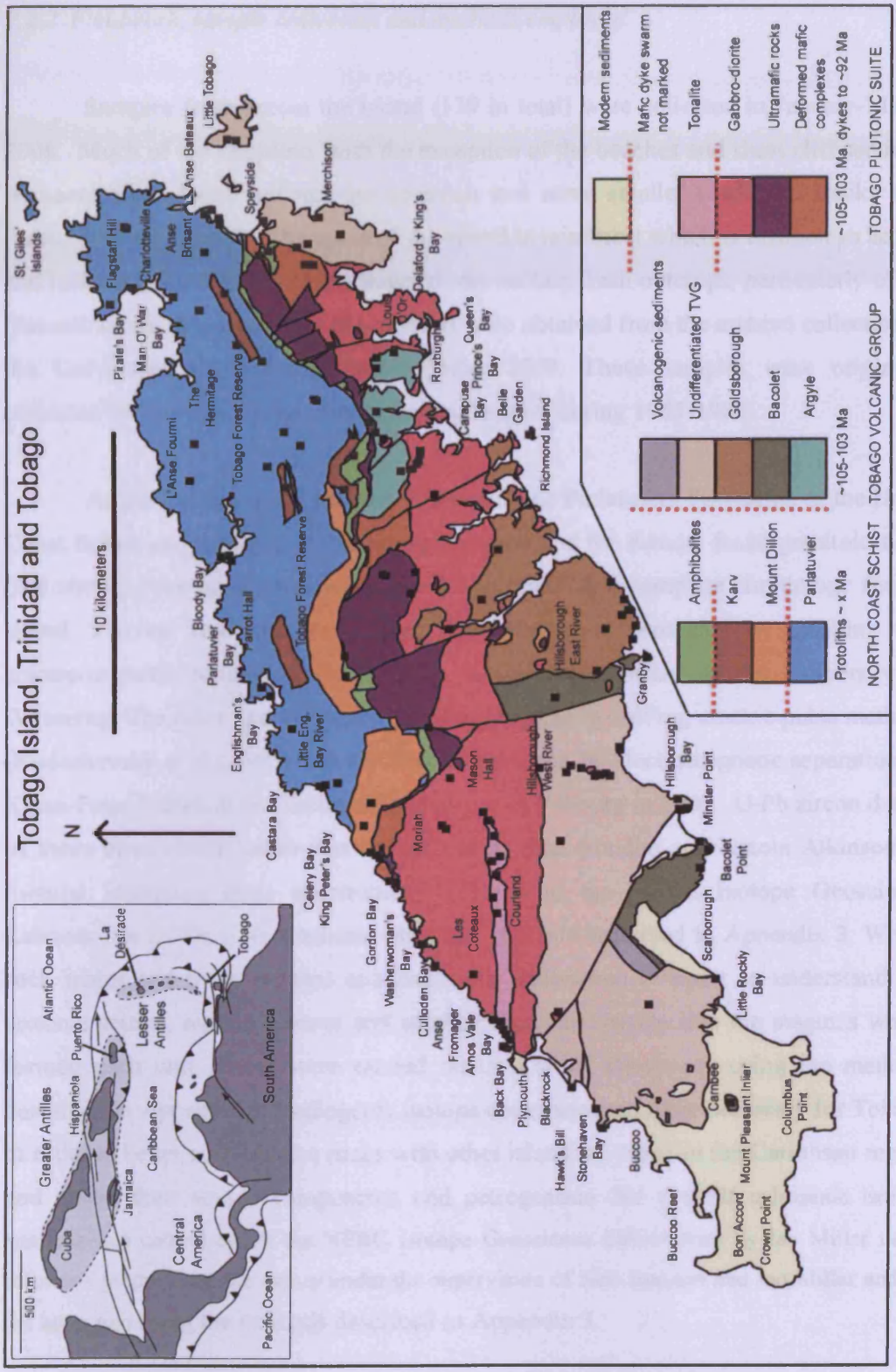

Figure 2.2. Geological map of Tobago adapted from Snoke et al. (2001b). The sample locations are expanded in Appendix 1 and are black squares here. The red dashes in the legend represent unconformities of varying or unknown length.

2.2.2. Fieldwork, sample collection and methods employed

Samples from across the island (139 in total) were collected in January-March 2008. Much of the coastline, with the exception of the beaches and short cliff sections, is inaccessible. Road cuttings are common and some smaller roads and tracks lead further into the interior. The spine of the island is rainforest which is difficult to access and lacks exposure. Many of the larger rivers contain fresh outcrops, particularly of the plutonic facies. More samples (83 in total) were obtained from the archive collection of the University of Wyoming in November 2009. These samples were originally collected by Professor Arthur Snoke and colleagues during 1985-1988.

As part of this study, the protolith age of the Parlatuvier Formation of the North Coast Schist and the ages of the Tobago tonalite and the Kendal Road granitoid body (see above) have been determined in order to establish a complete chronology for the island. Zircons from the Parlatuvier Formation were separated by crushing and electromagnetic separation in 1995 by Kevin Chamberlain at the University of Wyoming. The other two samples were disaggregated by selFrag electric pulse methods (Rudashevsky et al., 1995) and the zircons separated by electromagnetic separation by Klaus-Peter Stanek at the Technical University of Freiburg in 2009. U-Pb zircon dating of these three zircon suites was carried out by Dan Condon and Nicola Atkinson by thermal ionisation mass spectrometry (TIMS) at the NERC Isotope Geoscience Laboratories (NIGL), Nottingham, using the methods described in Appendix 3. Whole rock major and trace element analyses were undertaken in order to understand the tectonic setting, mantle sources and subduction-related inputs into the magmas which formed each unit. These were carried out at Cardiff University using the methods described in Appendix 3. Radiogenic isotope determinations were necessary for Tobago in order to better correlate the rocks with other island arc suites in the Caribbean region and assess their source components and petrogenesis. Nd and Hf radiogenic isotope analysis was carried out at the NERC Isotope Geoscience Laboratories by Ian Millar using solutions prepared by the author under the supervision of Neil Boulton and Ian Millar and by the latter two using the methods described in Appendix 3.

2.3. The San Souci Volcanic Formation, Trinidad

2.3.1. Geological setting

The **San Souci Group** (Cunningham-Craig, 1907; Barr, 1963; Wadge & Macdonald, 1985; Algar & Pindell, 1991, 1993) lies adjacent to meta-sedimentary rocks of the Northern Range between Toco and Grand Riviere on the north coast of Trinidad (Fig. 2.3). The San Souci Group consists of the volcano-plutonic ***San Souci Formation*** and a sequence of turbidites, the ***Toco Formation***, (Wadge & Macdonald, 1985). The San Souci Formation appears to intrude or crudely overly the Toco Formation but the contact is not exposed at the present day, so this conclusion is equivocal (Wadge & Macdonald, 1985; Algar, 1993). The San Souci Group is isolated from the Northern Range by the Toco-Grand Riviere fault system which is a diffuse zone of deformation splayed from the North Coast fault zone (NCFZ). The NCFZ is interpreted to be just offshore from the north coast of Trinidad and is considered the effective boundary between the Caribbean and South American plates (Robertson & Burke, 1991; Algar & Pindell, 1991). The Northern Range has undergone Oligocene to Miocene greenschist-facies metamorphism and penetrative deformation (Frey et al. 1988; Speed & Foland, 1990; Algar, 1993) whereas the San Souci Group is not significantly deformed and has only reached prehnite-pumpellyite facies. Therefore the San Souci Group is allochthonous with respect to Trinidad.

The turbidites of the Toco Formation - black shales inter-digitated with channels of coarser quartzo-feldspathic sandstone - contain micro-fossils of Barremian – Lower Aptian age (~130-120 Ma) (Barr, 1963). Fission track ages from zircons preserved in the Toco Formation cluster at ~108 and ~200 Ma with some Permian ages (Algar et al., 1998). These ages indicate a separate origin for the San Souci Group from the Jurassic protoliths of the Northern Range sediments (Pindell, 1985). Igneous rocks of a similar age to the zircons are found in western Venezuela and Colombia (Algar et al., 1998). Therefore, it seems likely that the San Souci Group has been transported a considerable distance eastwards along the South American-Caribbean plate boundary. The ~108 Ma ages may relate to a proximal Caribbean arc system (Algar et al., 1998). Basaltic lava from the San Souci Volcanic Formation was dated using whole-rock K-Ar methods to

87 ± 4.4 Ma (Wadge and Macdonald, 1985). It is likely that the K-Ar results were affected by alteration processes.

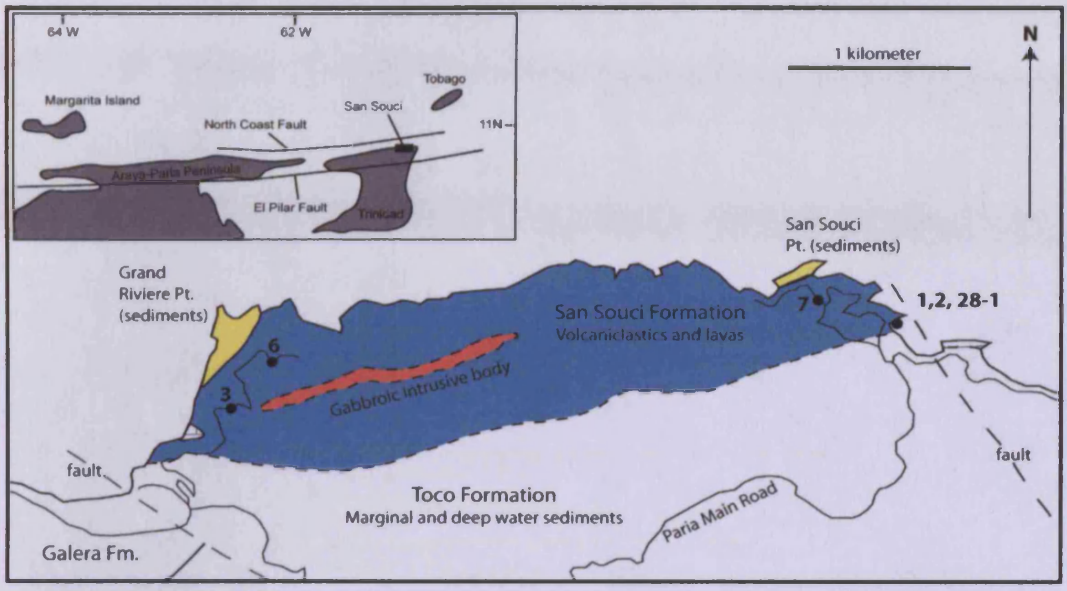

Figure 2.3. Geology of the San Souci Volcanic Formation; adapted from Wadge and Macdonald (1985). Sample locations are numbered; the exact boundary between the San Souci and Toco Formations is uncertain due to rainforest cover.

The majority of exposures of the San Souci Formation (Fig. 2.3, 5 km^2) consist of non-vesicular submarine mafic lavas, auto-brecciated by the intrusion of further magmas (Wadge & Macdonald, 1985). There are also intact mafic and felsic lavas and some dolerites. Two dyke-like dolerite bodies, not exposed at the present day, extend for 2 km in the centre of the San Souci Formation (Fig. 2.3), and for 100 m, 6 km to the south-east along Basin Galap Trace in a fault-bounded sliver (Wadge & Macdonald, 1985).

One previous geochemical study of the San Souci Formation relied on major and trace element discrimination and could not distinguish between MORB, OIB and mantle plume origins (Wadge & Macdonald, 1985). The Formation has been interpreted in terms of a mid-ocean ridge-type setting (Algar & Pindell, 1993), although Wadge & Macdonald (1985) argued that there was little evidence for rifting during the mid-late Cretaceous on the South American margin. Therefore, there is no definite age or tectonic setting for the San Souci Formation. Clarification of the age of the volcanics is required in order to correlate other outcrops on the Venezuelan margin and interior (Kerr et al., 2009b) and with the CCOP. Wadge & Macdonald (1985) tentatively

correlated San Souci with the CCOP but fission-track data and the structural position of the group to the south of any accreted Caribbean island arc terranes points to a proto-Caribbean eruption site. A mantle plume origin for these rocks would suggest that plume activity occurred both to the east and west of the Great Arc system, implying that the volume of material erupted around the Turonian-Coniacian boundary was higher than currently accepted if such an age can be proven for the San Souci Formation (e.g. Kerr & Tarney, 2005). In order to make the distinction between a plume- or MOR-related origin of the San Souci Formation, trace element and isotope studies of the rocks are required. The aims of this part of the study are therefore: (1) to identify the age, tectono-magmatic setting and mantle sources of the San Souci Formation and (2) compare the geochemistry and age of the formation with analyses from the CCOP and other basaltic rocks from the Venezuelan Margin and interior in order to understand its significance for Caribbean tectonic models.

2.3.2. Fieldwork, sample collection and methods employed

Samples collected by Kevin Barr in the 1960s were destroyed following a recent fire at the Seismic Research Institute of St. Augustine, Trinidad. The samples of Wadge & Macdonald (1985) from Lancaster University are thought to be lost (R. Macdonald, 2008 pers. comm.). San Souci is covered by dense rainforest, with few stream sections, only two short access roads and impassable coastal cliffs. Many tracks through the rainforest between San Souci and Grand Riviere meet small private farms and cannabis plantations but no exposures. During March 2009, 18 samples of the least brecciated and altered basalts, dolerites and felsic rocks were collected from cuttings in paved tracks and coastal sections near San Souci Point and from cuttings in a dirt track to the east of Grand Riviere. A single quartzo-feldspathic sedimentary sample was also collected from the Toco Formation.

As the majority of the San Souci rocks are mafic, they do not contain 40+ μm-scale zircons required for traditional U-Pb zircon dating. It was decided to use a new technique of in-situ SIMS dating of micro-zircon and baddeleyite (ZrO_2) (Schmitt et al., 2010) using the methods outlined in Appendix 3, at the University of California, Los Angeles. To understand the likely tectonic setting, whole rock samples were analysed for major and trace element contents at Cardiff University using the methods outlined

in Appendix 3. Six samples were analysed for radiogenic Nd and Hf isotope ratios at NERC Isotope Geosciences Laboratory, Nottingham, as outlined in Appendix 3.

2.4. SE Aves Ridge, Caribbean Sea

2.4.1. Geological Setting

The Aves Ridge lies between the Dutch-Venezuelan Antilles and the Greater Antilles. The Aves Ridge is a broadly north-south trending arcuate structure ~500 km in length running between its sole emergent point at Aves Island in the Caribbean Sea, and Margarita to the north of the Venezuelan coast (Fig. 2.4). The ridge has a topographic profile of up to 1500 m above the surrounding ocean basins and seismic studies reveal the ridge has little sedimentary cover and a crustal thickness of ~26 km (Christeson et al., 2008). Seismic velocities are >6.0 km/s in the mid-crust and ~7.3 km/s at the base of the crust, consistent with an interpretation as an extinct island arc of intermediate composition (Clark et al., 1978; Christeson et al., 2008).

Glassy, brecciated basalts and andesites dredged or drilled from the northern end of the ridge and the Saba Bank between Aves Island and the Greater Antilles (Fig. 2.4) also suggest a volcanic arc origin (Marlowe, 1968; Church & Allison, 2004) (Fig. 2.4). Dredge samples collected by Duke University's R/V "Eastward" in 1968 are the only samples available from the southern part of the ridge. Three dredges from the eastern scarp of the ridge (Fig. 2.4) contained igneous rocks described and dated using K-Ar methods by Fox et al. (1971). Dredge 11317 (12.30°N) contained 1500 kg of granitic boulders and pebbles. Four whole-rock K-Ar ages ranged from 57 to 89 Ma. Dredge 11318 (12.25°N) consisted of 40 kg of mostly doleritic cobbles and pebbles with lesser amounts of porphyritic and/or metamorphosed basalt with two K-Ar ages of 57 and 60 Ma. Dredge 11319 (12.35°N) contained 2000 kg of granitoid material seemingly identical to dredge 11317, but with four K-Ar ages ranging from 18.5 to 67 Ma. No methodology or errors were given for these K-Ar dates by Fox et al. (1971), however the ages are unlikely to be reliable due to significant sub-solidus alteration, and this is evidenced by the wide spread of ages obtained.

Walker et al. (1972) showed the granitoids had some quite primitive $^{87}Sr/^{86}Sr$ ratios which ranged from 0.7038 to 0.7080. Nonetheless, these ratios are likely to have been modified by interaction with Cretaceous seawater ($^{87}Sr/^{86}Sr$ ~0.7075; Veizer,

1989) and hydrothermal alteration. No mafic rocks were found in the granitic dredges and vice versa.

Although the Aves Ridge is an extensive region of crust in the eastern Caribbean, the geochemistry of basement samples has not been studied in any detail. Most workers have argued that the Aves Ridge originated as a Late Cretaceous to Early Palaeocene island arc (Bouysse, 1984; Christeson et al., 2008; Pindell & Kennan, 2009). However, the age, magmatic source(s) and subduction polarity of this arc are unclear. Given its significant spatial extent and because it is likely to represent some of the last island arc magmatism in the south-eastern Caribbean prior to the opening of the Grenada Basin; a better understanding of the origin of the Aves Ridge could help to constrain Caribbean Plate tectonic evolution.

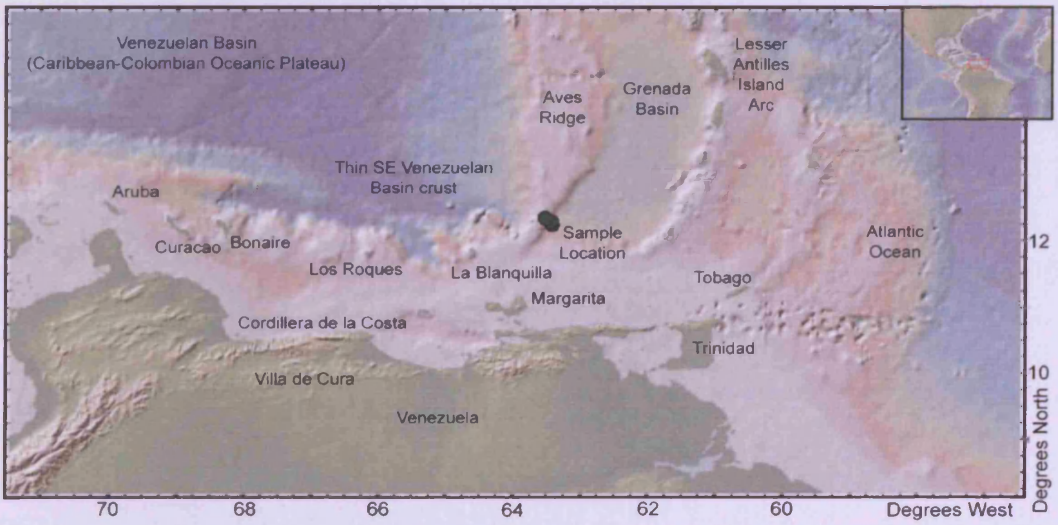

Figure 2.4. Map of the SE Caribbean adapted from a plot generated by GeoMapApp (Haxby et al., 2009) with the sample location in the SE Aves Ridge marked along with major islands and geological features.

2.4.2. Sample collection and methods employed

The only igneous samples from the southern portion of the Aves Ridge remain those obtained in 1968 by R/V "Eastward". These samples are stored at the Lamont Doherty Earth Observatory Deep Sea Sample Repository. For this study, the largest, freshest blocks remaining from each dredge (tens of kilograms) were selected from the repository in November 2008 (34 separate whole rock samples). As no accurate dating has been previously undertaken, the largest felsic sample was sent to the Technical University of Freiberg for sample disintegration by selFrag and zircon separation (see

Appendix 3). Separated zircons were analysed by Sensitive High Resolution Ion Micro-Probe (SHRIMP-II) at the Centre for Isotopic Research, (VSEGEI) in St. Petersburg (Appendix 3). This sample and the rest of the rocks were analysed for major and trace element contents at Cardiff University using the methods in Appendix 3, in order to understand their tectonic setting and mantle and crustal inputs. Two samples were analysed for their Nd and Hf radiogenic isotope ratios at NIGL, Nottingham (Appendix 3), so that more detailed information could be obtained on their mantle and crustal sources and to identify if the mafic and felsic samples have a common source.

CHAPTER THREE: GEOLOGY AND PETROGRAPHY

Further observations of the field geology, rock types and petrology of the units studied at each locality

3.1. Geology and petrography of La Désirade Island

3.1.1. NE mafic volcanic complex

The NE mafic volcanic complex outcrops from Baie Mahault to Anse Galets (Figs. 2.1, 3.1a,b) where it is overlain by the NE felsic volcanic complex. The dominant rock type is a vesicular black to grey-green, often reddened, basalt-basaltic andesite lava, which typically forms pillows up to 1m across (Fig. 3.1b). Voluminous red cherts (jasper) and minor limestone pinch-ups occur between the pillows (Montgomery & Kerr, 2009), which exhibit right-way-up 'teardrop' structures and glassy rinds. Individual packages of pillow lavas define a crude layering which dips at 10° or more to the north exposing ~300 m of volcanic rocks in stratigraphic order. Additionally, volumetrically rare massive mafic lava flows and 1-2 m thick banded hyaloclastites of <1-3 mm grain size are also found. Some minor faulting occurs with displacements of only a few centimetres to several metres, which may be related to emplacement of the intermediate dyke suite; however, the entire mafic complex appears continuous with no recognisable unconformities. The contact with the overlying northeast felsic volcanic complex is faulted (Fig. 3.1c), but chert and basalt clasts are found within the felsic breccias of the overlying unit indicating eruption through the pre-existing mafic complex and an unconformity between the two complexes of unknown length.

In the lower part of the mafic complex, (Loc. 10-11; Fig. 2.1) the lavas can be divided into two petrographic facies. The first type is fine-grained with 0.5 to 1 mm clinopyroxene phenocrysts set in a groundmass consisting of randomly aligned acicular plagioclase, squat clinopyroxene and Fe-Ti oxides. There are brown/green clays, oxides/haematite patches and in some cases, abundant calcite replacing the original textures. The second type of lava has a grain size of up to 2 mm with plagioclase phenocrysts up to 4 mm. Interstitial plagioclase is more tabular, with clinopyroxene and Fe-Ti oxides that have needle-like patterns. Replacement minerals in this second type are brown/green clays, oxides/haematite, chlorite, prehnite and pumpellyite.

Overlying these rocks, some of the pillows at Locality 8 (Fig. 2.1) are quite distinct, consisting of 1 mm grains of hopper-shaped or acicular to elongate splays of clinopyroxene and lesser acicular plagioclase which might indicate rapid quenching of

the lava (Fig. 3.2a). Replacement minerals are quartz, prehnite, pumpellyite and oxides. Vesicles are in-filled by quartz and Fe-Ti oxides. The remaining samples from Localities 8 and 9 (Fig. 2.1) are largely aphyric, ranging from 0.25 mm to 1 mm grain sizes and consisting of acicular plagioclase, squat clinopyroxene, and Fe-Ti oxides, sometimes comb-like or acicular. Replacement minerals include calcite patches and veins, prehnite and oxides including haematite.

The youngest lavas in the complex (Localities 1-7 and 14-17; Fig. 2.1) vary in grain size from <0.25 mm to 0.5 mm. Acicular plagioclase dominates the groundmass with elongate to squat clinopyroxene present. Some samples are clinopyroxene-phyric, often with glomeroporphyritic blebs reaching 1 mm (Fig. 3.2b) whilst others appear glassy with abundant calcite replacement. Other replacement minerals include chlorite, prehnite, pumpellyite, green/brown clays and oxides. The replacement minerals found across the complex are diagnostic of a low-grade prehnite-pumpellyite facies metamorphic assemblage.

3.1.2. Felsic volcanics and the trondhjemite pluton

The NE felsic volcanic complex outcrops around Grand Abaque and contains orange-weathered massive rhyolitic flows, volcanic breccia and scoria (Figs. 2.1, 3.1c). Breccias are darker in colour than the flows and are vesicular with abundant geodes containing quartz and epidote. Other breccias look similar to basalts and cherts of the NE mafic volcanic complex. The rhyolitic flows and breccias consist mostly of plagioclase and quartz with minor haematite crystals and veins. Some chlorite, clays and epidote are present replacement minerals (Fig. 3.2c).

The SW felsic complex occurs at the coast near Mourne Frégule (Fig. 2.1) and is regarded as temporally equivalent to the NE felsic complex (Bouysse et al., 1983; Mattinson et al., 2008), containing similar rhyolitic flows. These flows contain plagioclase and quartz phenocrysts up to 1 mm across, with a fine groundmass dominated by plagioclase with minor quartz and oxides. Clays, haematite and epidote are replacement minerals (Fig. 3.2d).

A trondhjemite pluton is exposed for 4 kilometres along the north coast of the island (Fig. 2.1; 3.1d). There are a variety of igneous facies, with the majority comprising plagioclase-rich trondhjemite with minor amounts of diorite and albite granite (Fig. 3.2e), which are cut by abundant intermediate dykes. The trondhjemite is characterised by 2-3 mm sized grains of tabular plagioclase (~60%), hornblende, quartz, Fe-Ti oxides, titanite and zircon. Alkali feldspar and biotite are absent. The most common replacement minerals are chlorite and epidote.

Although not dated by U-Pb methods, the felsic complexes appear of similar age to the pluton (Mattinson et al., 2008). Mattinson et al. (2008) proposed that the pluton intruded lavas of its own volcanic carapace. These lavas are of the same composition and age as those which formed the NE and SW felsic complexes.

3.1.3. Intermediate-felsic dykes

As shown in Figures 3.1e and 3.2f, clinopyroxene dolerite, microdiorite, granodiorite and granophyre dykes cut the trondhjemite and NE mafic and felsic complexes (Mattinson et al., 1980). Mattinson et al. (2008) contend that the less evolved dykes represent the last magmatism on the island whilst the most felsic dykes are related to the earlier felsic magmatism. The more mafic dykes are yellow-green tinged, 2-3m thick, trend roughly NE-SW within the NE mafic volcanic complex and show chilled margins with the surrounding pillow basalts. Minor faults within the NE mafic complex occur at angles parallel or sub-parallel to the dykes suggesting a structural control upon dyke emplacement. These dykes have a grain size of around 0.25 mm and contain clinopyroxene phenocrysts (~10 %) in a groundmass of elongate plagioclase and minor clinopyroxene and quartz with alteration to chlorite and pumpellyite (Fig. 3.2f). Epidote, albite and prehnite have also been reported (Mattinson et al., 1980). Dykes cutting the trondhjemite pluton are dark green, up to 1 metre across and have a grain size of 0.25 to 0.5 mm. They are dominated by a groundmass of elongate plagioclase, clinopyroxene and Fe-Ti oxides with rare clinopyroxene phenocrysts. Replacement of the clinopyroxenes by clays and chlorite is very common.

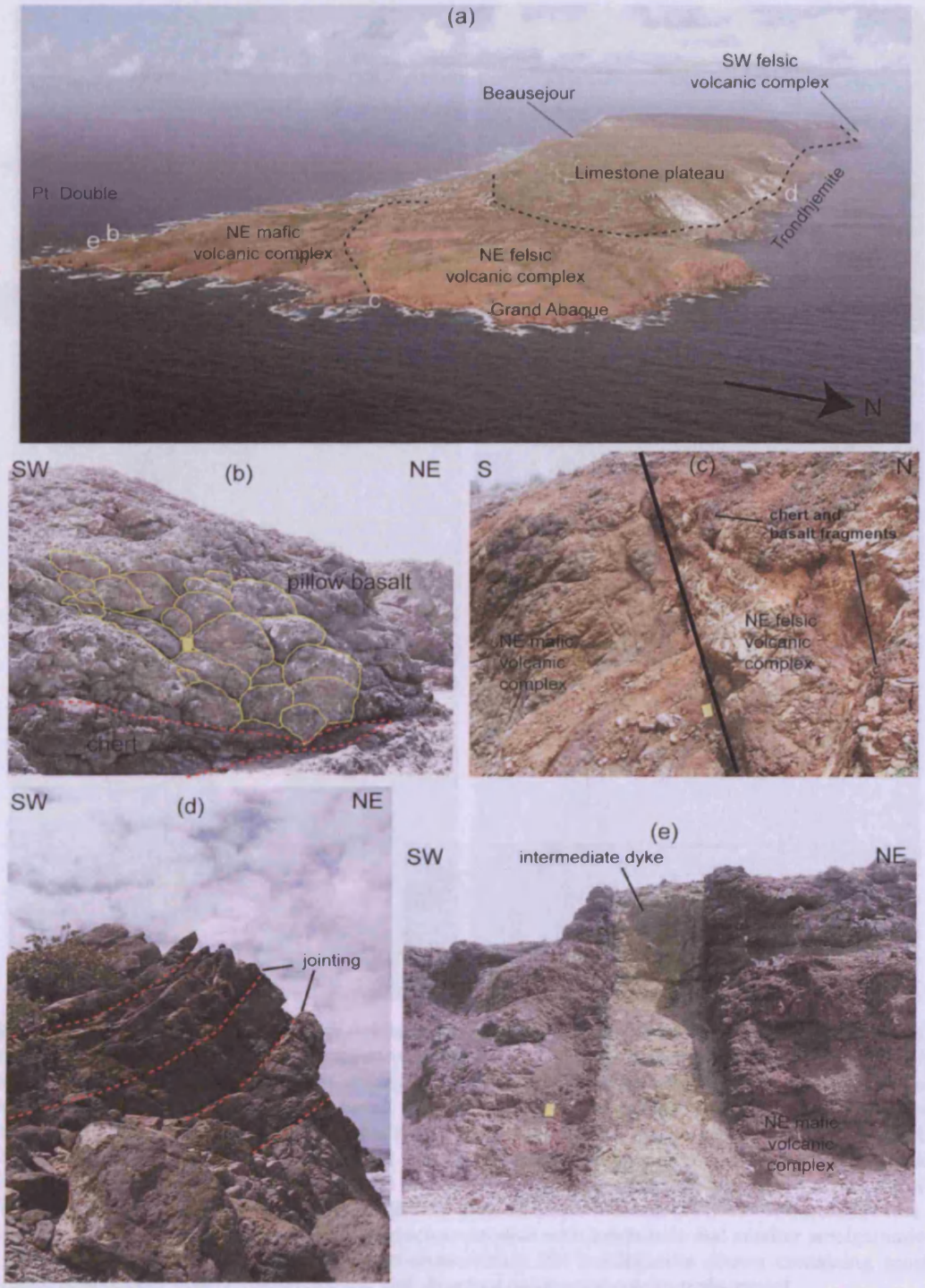

Figure 3.1. Field photographs from La Désirade. (a) Geological overview of La Désirade showing location of field photographs. Photograph supplied to Jennifer Gibbs by Luc Legendre, Minister of the Environment, Guadeloupe. (b) Pillow basalts and chert (NE mafic complex) at Pointe Seraphine with notebook for scale. (c) Faulted contact between pillow basalts of the NE mafic complex and rhyolites of the NE felsic volcanic complex at Grand Abaque (notebook for scale). (d) Example of jointing in the trondhjemite pluton at L'Emballage (author for scale). (e) Intermediate dyke cutting the NE mafic complex at Pointe Seraphine (notebook for scale).

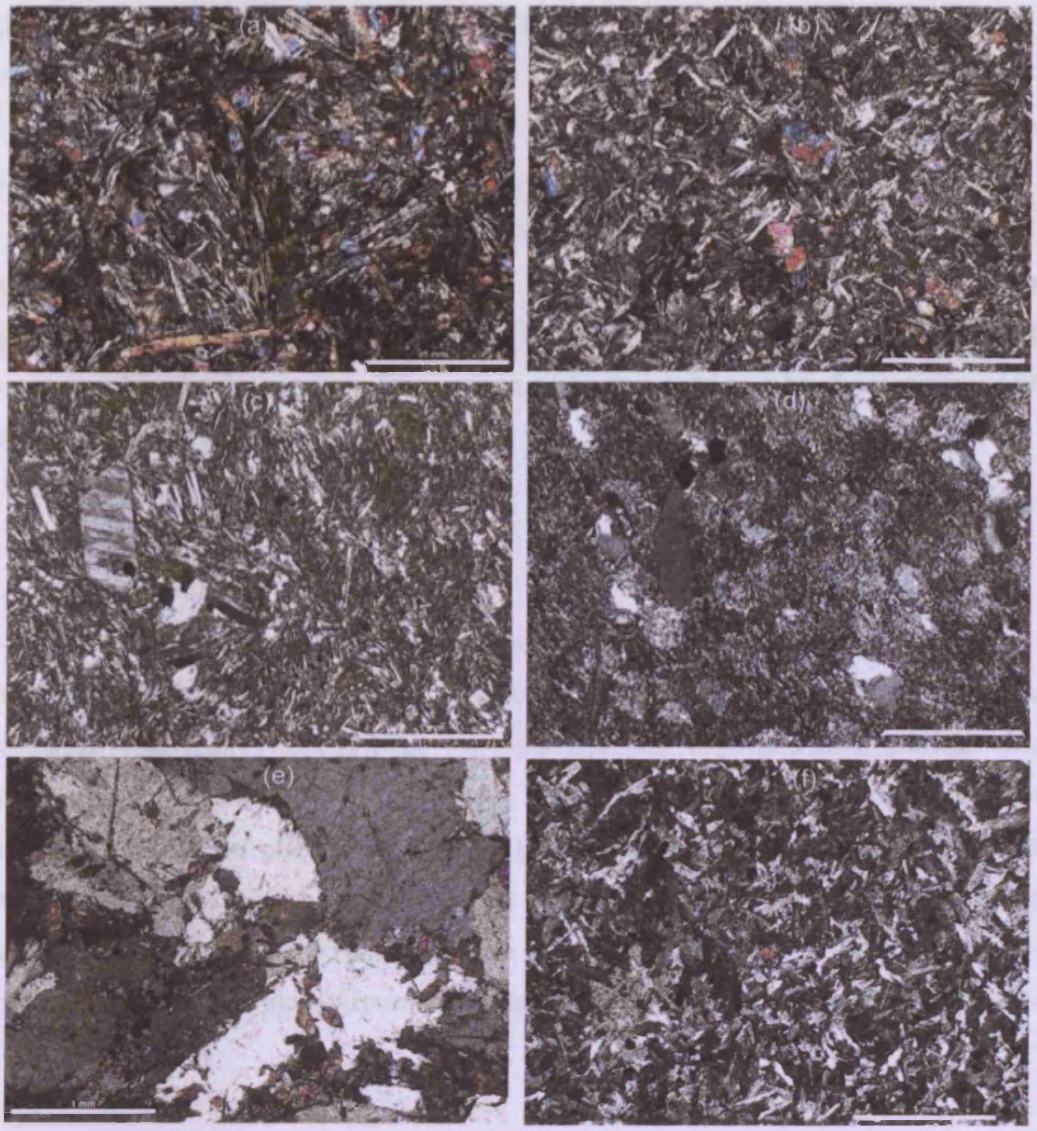

Figure 3.2. Photomicrographs from the volcanic and plutonic complexes of La Désirade. All sections in cross-polarised light with the scale bar representing 1 mm. (a) IND/8.1, fresh pillow basalt of the NE mafic volcanic complex dominated by a combination of clinopyroxene laths, equant clinopyroxene and plagioclase. (b) IND/6.2, fresh pillow basalt (NE mafic volcanic complex) containing plagioclase laths with small glomero-porphyritic patches of clinopyroxene. (c) IND/2.1, altered plagioclase-phyric rhyolite (NE felsic volcanic complex) with aligned plagioclase laths and larger phenocrysts; quartz, oxides, chlorite, clays and epidote also present. (d) IND/18.1, quartz-plagioclase-phyric flow-banded rhyolite (SW felsic volcanic complex) with oxides and clay alteration also present. (e) IND/19.9, trondhjemite of felsic composition with large quartz and plagioclase crystals with amphibole and smaller amalgamations of titanite. (f) IND/19.5, intermediate dyke cross-cutting the trondhjemite pluton containing mostly elongate plagioclase, quartz, clinopyroxene and abundant oxides and calcite replacement.

3.2. Geology and petrography of Tobago Island

3.2.1. Introductory remark

The geology of Tobago is considerably more complex and varied than that of the other localities. A very detailed set of field and petrographical observations have already been published, culminating in the monograph of Snoke et al. (2001a) and the reader should refer to this text. This section will serve only as a brief description of the field geology and sampled rocks.

3.2.2 North Coast Schist

Parlatuvier Formation: The greenschist-facies Parlatuvier Formation makes up around three-quarters of the NCS and covers approximately 75 km^2 of coast and rainforest (Fig. 2.2). There is little exposure save for bays and road cuttings. Most streams are not navigable at the present day. This lack of exposure coupled with abundant evidence of plastic deformation [Snoke et al. (2001a) report two foliations, four fold styles, and four lineations] means that mapping of individual units within the formation is impossible. Structurally, the polyphase deformation of the Parlatuvier Formation occurred in an environment of dextral wrench shearing (Snoke et al., 2001a).

The entire formation is comprised of metamorphosed and deformed mafic to intermediate volcanics and rarer flows and intrusive rocks (Figs. 3.3a,b). The protoliths of the majority of these rocks were mafic to intermediate fine-grained tuffs and coarser tuff breccias with clasts up to 50 cm across, most of which are homogeneous in colour and mineralogy. In thin section, some fragments of primary plagioclase, hornblende and clinopyroxene remain. The greenschist-facies metamorphism has resulted in widespread growth of chlorite and actinolite, giving the rocks a grey-green to dark green colour when fresh, and weathering to bright orange due to the high content of ferro-magnesian minerals (Figs. 3.3c,d).

Another sampled facies in the Parlatuvier Formation is a type of porphyry which occurs most commonly towards the eastern end of the NCS to the north of Speyside (Fig. 2.2). This mafic-intermediate facies is a similar green colour to the tuff

breccias and appears to be a form of this rock type. The rocks however contain abundant relict plagioclase phenocrysts (Fig. 3.3e). This rock type was thought by Yule (1988) to represent the protolith for the most distinctive of the amphibolite-facies metamorphic rocks found on the boundary between the NCS and the Tobago pluton. A final unusual sampled rock type only occurs around Anse Bateaux near Speyside (Fig. 2.2). These are mafic-intermediate tuff breccias with a fine-grained groundmass which have conspicuous fragmental hornblende crystals up to 5 cm in length (Fig. 3.3f). Snoke et al. (2001) have interpreted the hornblendes as representing a relict phenocryst phase, much the same as the plagioclase-phyric rocks discussed above.

Two further facies have not been sampled as they were not observed in the field. Yule (1988) reports rare massive, dense dark grey layers with abundant amygdales which were interpreted to be lavas inter-layered with chlorite-epidote-actinolite schist which may be representative of mafic tuffs which took up the strain during deformation. The meta-lavas are up to 50 cm thick and the amygdales are filled with calcite and epidote (Yule, 1988). Sparse intrusive rocks (massive un-deformed mafic bodies or small deformed dykes) also occur. These plutonic mafic rocks were originally hornblende-phyric gabbros which acted as rigid bodies during deformation. Nonetheless, the original mineralogy of these rocks been partially replaced with a lower greenschist facies assemblage including actinolite, epidote, chlorite and muscovite (Yule, 1988).

Critically, from the point of view of geochemical analysis, there is no evidence within the Parlatuvier Formation of metamorphism above lower greenschist facies, nor is there any widespread evidence of calcification or influx of fluids. This observation implies that the 'immobile' trace element geochemistry of the formation should be representative of the original igneous composition of the rocks.

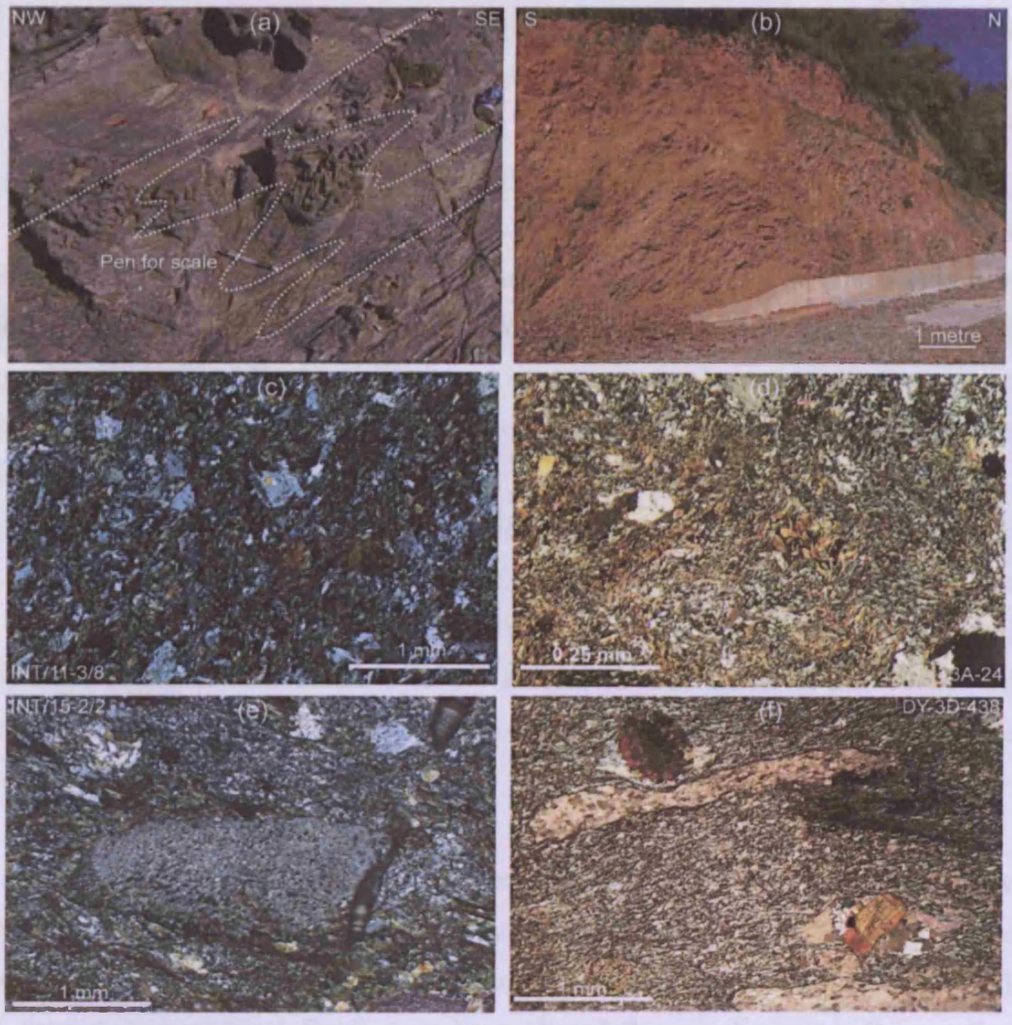

Figure 3.3. Field and thin section photographs of the Parlatuvier Formation (cross-polarised light). (a) Z-folded bedding in coarse mafic tuffs of the Parlatuvier Formation on the shore at Bloody Bay. (b) Orange-weathered outcrop of bedded mafic tuffs above Englishman's Bay. (c) INT/11-3/8 fine mafic tuff with relict clinopyroxene crystals and plagioclase. (d) 3A-24 metamorphosed andesitic crystal tuff containing relict plagioclase phenocrysts. (e) Large relict plagioclase crystal in sample INT/15-2/2, replaced by clays. (f) DY-3D-438, fine-grained mafic tuff with large relict hornblende phenocryst bottom right and patches of calcite replacement.

Mount Dillon Formation: The Mount Dillon Formation makes up under a quarter of the North Coast Schist. The formation is found in two bands about 1-2 km wide (thickening towards the SW) and several kilometres long, chiefly along a stretch of rain forest around and to the south of the Main Ridge (Fig. 2.2). The Mount Dillon Formation is almost entirely enclosed by the outcrop of the Parlatuvier Formation but the contact between the two is invariably faulted or not exposed (Snoke et al., 2001b). Coastal exposures of the Mount Dillon Formation are present for a kilometre near Celery Bay and there is little exposure inland except for road cuttings around the Mount

Dillon lookout point and isolated streams (Fig. 2.2). As with the Parlatuvier Formation, widespread deformation and lack of exposure renders the stratigraphy of the Mount Dillon Formation un-interpretable.

The rock types present are mostly felsic and comprise fine-grained tuffs and chert-like beds (Fig. 3.4a). The tuff is dark grey when fresh, weathering to a very distinctive buff colour. The quartz-rich nature of many of the tuffs makes them resistant to erosion (Fig. 3.4a). In thin section most of these rocks almost entirely comprise very fine-grained strained quartz with some Fe-Ti oxides (Fig. 3.4b). Many samples contain quartz veins (often parallel to any fabric present) and are occasionally cross-cut by calcite veins. Some of the rocks of the Mount Dillon Formation are more mafic (Fig. 3.4c) and resemble those of the Parlatuvier Formation only with grey colouration due to a significant argillaceous component. These contain similar mineral assemblages (epidote, actinolite and chlorite) to the Parlatuvier Formation (Yule, 1988). Other samples are crystal tuffs with relict phenocrysts of quartz and plagioclase up to several mm across (Fig. 3.4d).

The widespread abundance of chert and high-silica rocks is of concern with regard to whole rock geochemistry. If these are simply greenschist-facies meta-igneous rocks then the 'immobile' trace element geochemistry should be intact. However, influx of foreign hydrothermal fluids may have altered the geochemistry. One particular problem is the likely dilution effect of silica on the trace and rare earth elements, which may result in trace and rare earth element patterns unrepresentative of the primary or fractionated melts. Also, if these rocks are derived from felsic volcanic protoliths there has to be a concern that accumulation or fractionation of zircon and other minerals such as apatite will affect trace element ratios normally considered indicative of the melt source in mafic rocks.

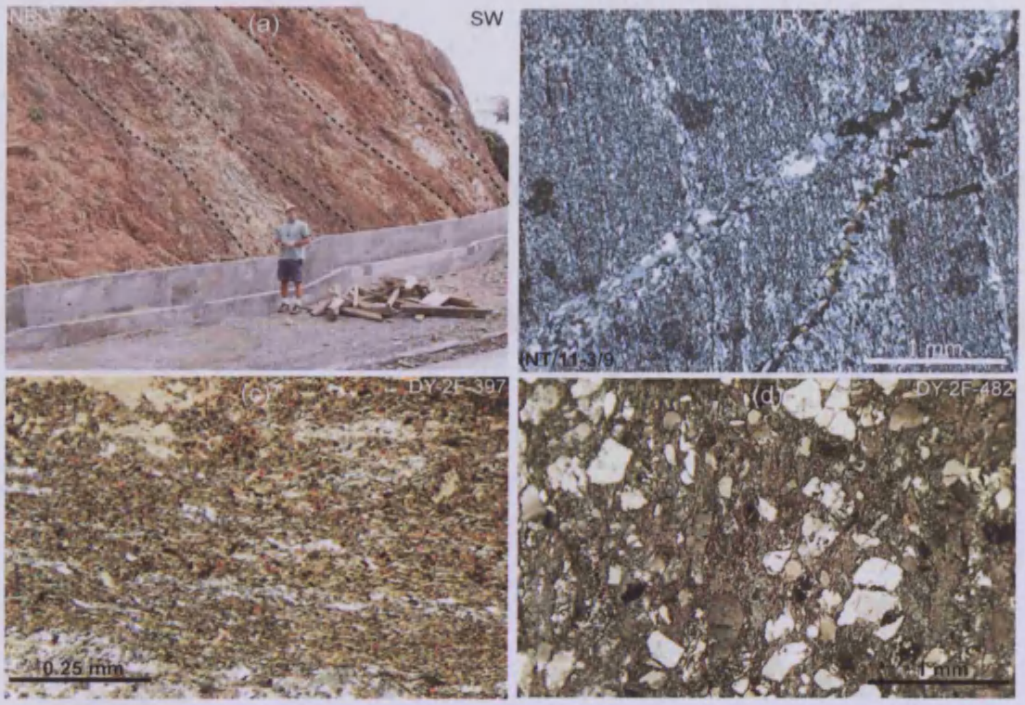

Figure 3.4. Field and thin section photographs from the Mount Dillon Formation in cross polarised light. (a) Type locality at Mount Dillon with silicified tuffs, bedded and inclined at a high angle. James Pindell for scale. (b) INT/11-3/9 a fine-grained, quartz-dominated silicic tuff. (c) DY-2F-397 a relatively mafic fine meta-tuff with calcite patches at top and a fine groundmass of quartz and chlorite, micas, epidote and oxides. (d) DY-2F-482 a felsic metamorphosed crystal tuff with large relict quartz and plagioclase phenocrysts in a fine-grained groundmass.

Karv: Yule (1988) mapped a suite of rocks (see Snoke et al., 2001b) as components of the Mount Dillon Formation which did not appear to contain primary volcanic rocks. Later, in the map of Snoke et al. (2001b), this unit was given its own name, *Karv*, standing for Cretaceous argillaceous volcaniclastics. This formation is located deep within the Tobago Forest Reserve in the hillside above Englishman's Bay (Fig. 2.2, 3.5a). Karv comprises ~300 m-wide, 1-3 km-long bands of severely weathered meta-argillites and inter-layered graphitic schist along with some more mafic tuff-like rocks which were badly altered (Fig. 3.5b). Only four samples were obtained from the University of Wyoming and none were collected from the field during this study.

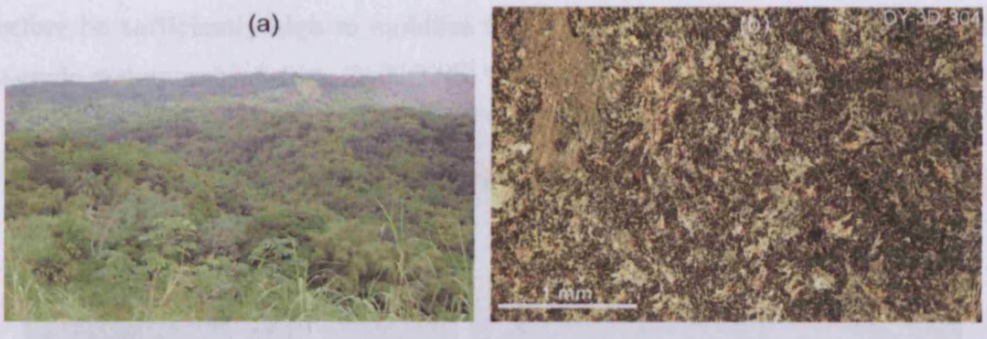

Figure 3.5. (a) A typical view over the Main Ridge of Tobago, showing the lack of exposure and largely impenetrable forest. From http://panoramio.com. (b) DY-3D-304, a mafic tuff-like component of the Karv unit from the Main Ridge.

Amphibolite-facies rocks: These rocks occur in discontinuous bands, often fault-bounded, between the mafic and ultramafic rocks of the Tobago Pluton and the North Coast Schist (Fig. 2.2). In rare locations it is reported to be possible to walk 'down-grade' into the greenschist-facies Parlatuvier Formation (Snoke et al., 2001a,b). Thus, critical to the structure and tectonic evolution of Tobago, the amphibolites are interpreted as a dynamo-thermal aureole resulting from emplacement and later subsidence of the pluton (Snoke et al. 2001a). The formation is marked by rocks of a higher metamorphic grade than the rest of the North Coast Schist, ranging from upper greenschist facies close to the rest of the North Coast Schist to upper amphibolite facies within 20 m of the pluton contact (Apted & Liou, 1983; Snoke et al., 2001a).

The rocks sampled are meta-basic, with a range of weak to strong ductile deformation features (foliation, lineation, development of shear bands and mylonites). Samples range from dense, grey equigranular examples to inequigranular rocks with a fine groundmass and large, flattened plagioclase crystals up to 1 cm long (Fig. 3.6a), to mylonites (Fig. 3.6b). In thin section, at the highest metamorphic grade, the samples contain hornblende, andesine and diopside (Snoke et al. 2001a). Prehnite-pumpellyite grade retrogression is common close to faulted contacts (Snoke et al., 2001) and many of the sampled rocks are characterised by the widespread occurrence of chlorite. Rowe (1987) records thin leucocratic segregations in the Louis D'Or River which may indicate the beginning of partial melting of this host rock. The plagioclase-phyric samples are those thought by Yule (1988) to be directly-related to the plagioclase-phyric rocks of the greenschist-facies Parlatuvier Formation. Many of the rocks are quite badly fractured and the amphibolite-facies metamorphism and deformation may

therefore be sufficiently high to mobilise those elements considered immobile during low-grade metamorphism (e.g. Zr, Hf, Nb, Yb).

Figure 3.6. Thin section photographs of the amphibolite facies 'auerole' in cross-polarised light. (a) INT/8-3/4, amphibolite-facies plagioclase-phyric meta-tuff. (b) DY-3D-557, mafic ultramylonite from the aureole zone containing small amphibole crystals.

3.2.3. Tobago Volcanic Group

Argyle Formation: The Argyle formation lies inland from Roxburgh (Fig. 2.2), covers approximately 5 km^2 and consists of tuff breccia and lapilli tuff, with some mafic-intermediate lavas and volcanogenic sediments (Snoke et al., 2001a and references therein) (Fig. 3.7a). This unit is unique in the TVG in containing hornblende as part of the phenocryst assemblage; which in decreasing order of abundance includes: plagioclase, hornblende and clinopyroxene (Snoke et al., 2001a). Many samples are described as containing conspicuous tabular plagioclase (5-15 mm) with smaller plagioclase, hornblende and clinopyroxene (1-2 mm). In this study, the rocks sampled are a mixture of grey lavas and tuff breccias which are either aphyric or clinopyroxene- or plagioclase-phyric (Fig. 3.8a).

Bacolet Formation: This formation outcrops in two locations, from Scarborough to Bacolet (3 km^2) and inland from Barbados Bay (3 km^2) (Figs. 2.2, 3.7b). According to Snoke et al. (2001a), the formation consists entirely of mafic clinopyroxene-phyric lithic volcaniclastic breccia with lesser plagioclase-phyric facies. The samples collected for this study are uniformly clinopyroxene-phyric with clinopyroxenes to 5 mm and lesser plagioclase reaching 2 mm (Fig. 3.8b). Most samples have a very fine-grained groundmass of plagioclase and oxides and the phenocrysts and groundmass are commonly partially replaced by chlorite, micas, epidote, oxides, occasional prehnite/pumpellyite, and rare patches of calcite in the more

altered samples. Snoke et al. (2001a) report possible chlorite, calcite and epidote pseudomorphs which may be replacing olivine; the only volcanic rocks on Tobago to do so.

Goldsborough Formation: The formation covers approximately 16 km^2 in a 1-4 km-wide coastal strip from Pinfold Bay to Glamorgan (Fig. 2.2). The rock types present are tuffs and tuff breccias, pillow lavas and some volcanogenic sedimentary rocks (Snoke et al., 2001a). These rocks are commonly quite evolved with interstitial quartz present in some specimens. The most common phenocryst phase is plagioclase (Fig. 3.8c) with lesser clinopyroxene (Fig. 3.8d) (Snoke et al., 2001a). Most rocks sampled for this study are either plagioclase or clinopyroxene-phyric with one containing abundant accumulated clinopyroxene. Some rocks contain amygdales invariably filled with calcite and others contain some calcite veining. The igneous mineralogy of plagioclase, clinopyroxene, oxides and rare quartz has been partially replaced by clays, micas, chlorite and epidote.

Undifferentiated TVG: This unit includes the Hawk's Bill and Merchison Formations of Maxwell (1948). The Undifferentiated unit was defined by Snoke et al. (2001a and references therein) because of poor exposure and the lack of obvious boundaries between different formations. The rock types present are varied, from pillow basalts to re-worked volcaniclastic breccias. In the Merchison Formation which occurs to the east of the Merchison River (Maxwell, 1948) (Fig. 2.2), clinopyroxene and plagioclase phenocryst assemblages dominate with rock types similar to those described from the Bacolet Formation (Snoke et al., 2001a). Only one quite badly altered, calcified sample was collected from this part of the TVG. The rocks of the Hawk's Bill Formation outcrop between Rocky Point and Hawk's Bill (Maxwell, 1948), and are mostly mafic to intermediate pillow lavas which have been silicified and now contain quartz-filled amygdales (Frost and Snoke, 1989; Snoke et al., 2001a) (Fig. 3.7d). In thin section these rocks contain both plagioclase and clinopyroxene phenocrysts and are altered with patches of clays, micas and chlorite. Snoke et al. (2001a) considers the Hawk's Bill Formation to be equivalent to the Goldsborough Formation.

The remaining parts of the undifferentiated unit contain plagioclase and clinopyroxene-phyric lavas (Fig. 3.8d), breccias and crystal tuffs; with associated re-worked volcaniclastic breccias and hard-weathering crystal-rich 'grits' made up of large volumes of angular clinopyroxene crystals (Fig. 3.7c). In this study, the lavas, tuffs and large breccia clasts, from which solidified magmas may be sampled, are classed as "Undifferentiated Tobago volcanics" along with those from the Hawk's Bill and Merchison areas. The reworked samples are classed as "Undifferentiated volcanogenic sediments." Some of the re-worked breccias contain slightly rounded clasts which have been reddened, possibly by periodic exposure, together with dark, rounded clasts in a matrix of comparatively fresh material (Fig. 3.8e).

Figure 3.7. Field photographs from the Tobago Volcanic Group. (a) Argyle Formation in roadside at the type locality with poorly defined bedding in volcanogenic sand and mudstones. (b) Bacolet Formation at Granby Point composed of crumbly basaltic volcanic breccias. (c) Undifferentiated TVG from a road cutting on the Hillsborough River with layering in mafic volcanogenic sediments which are rich in relict clinopyroxene crystals. (d) Undifferentiated TVG [Hawk's Bill Formation of Maxwell (1948)] comprising plagioclase-phyric lavas (occasionally pillowed) at Blackrock.

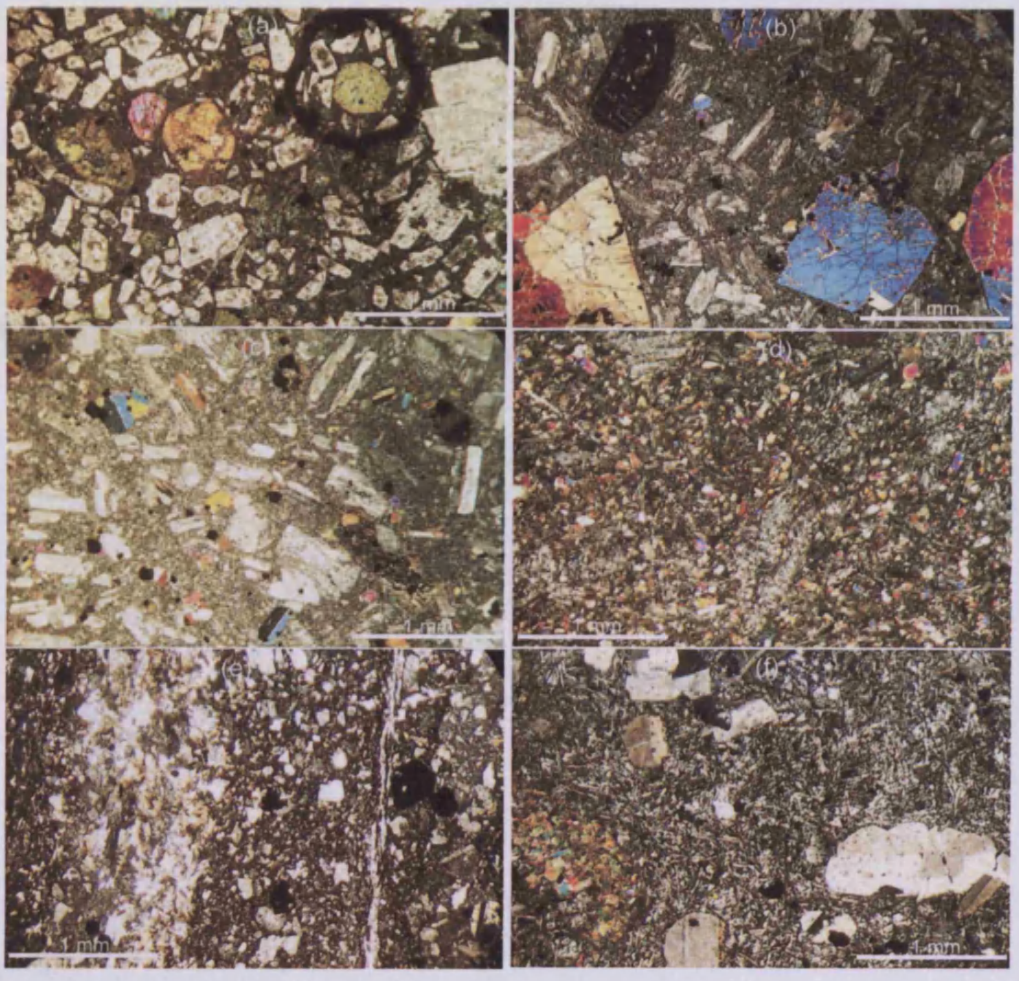

Figure 3.8. Photomicrographs from the Tobago Volcanic Group, all in cross-polarised light and with scales marked. (a) DR-128 (Argyle Formation), basaltic lava from the Louis D'Or area, with equant clinopyroxene and squat plagioclase phenocrysts in a glassy groundmass. (b) DY-2H-282 (Bacolet Formation), basaltic lava from the Hillsborough River, with large clinopyroxene and smaller plagioclase phenocrysts in a fine groundmass. (c) DY-2H-298 (Goldsborough Formation), fine-grained basaltic lava from Studley Park, dominated by elongate plagioclase phenocrysts and rarer clinopyroxene in a fine groundmass. (d) DY-2J-262 (Goldsborough Formation), groundmass detail from basaltic lava from Granby Hill, dominated by rounded clinopyroxene crystals and oxides. (e) DR-818 (Undifferentiated TVG) from Little Tobago Island, volcanogenic sediment consisting of a fine groundmass with relict plagioclase crystals and pyrite growth. (f) IC-53 (Undifferentiated TVG) brecciated basaltic lava from Stonehaven with large plagioclase phenocrysts.

3.2.4. Tobago Plutonic Suite (TPS)

Deformed mafic volcanic-plutonic complexes: These are three distinct highly metamorphosed complexes of which two were sampled; the Anse Flamengo Complex (1 km^2) which lies between and inland from King Peter's Bay and Celery Bay, and the Merchison River Complex (2 km^2) which lies between Speyside and the watershed on the Speyside-King's Bay road. The other is the Richmond River Complex (2 km^2)

which lies in the centre of the island (Fig. 2.2). These units are interpreted as early phases of extrusive and intrusive activity within the Tobago Volcanic Group which have been deformed and metamorphosed by the later intrusion of the Tobago Pluton (Snoke et al., 2001a). These complexes are very hard-weathering and have a mafic fragmental meta-volcanic or hypabyssal origin, with textures frequently overprinted by hornblende- to pyroxene-hornfels metamorphic mineral assemblages. Deformation takes the form of large-scale flattening of breccia clasts, but no larger-scale structural patterns have been identified. The rocks are clearly distinct from the upper greenschist- to upper amphibolite-facies metamorphism of tuffaceous rocks in the amphibolites of the North Coast Schist (Snoke et al., 2001a).

The Anse Flamengo Complex (Fig. 3.9a) consists of fragmented meta-volcanics and hypabyssal intrusive rocks which have been intruded by various components of the TPS (clinopyroxenites, gabbros, diorites and mafic dykes) (Snoke et al., 2001a). The single sectioned sample from the complex consists of a deformed, slightly calcified meta-volcanic rock containing 2-3 mm relict clinopyroxene crystals with plagioclases which have been altered to clays and micas alongside hornblende and oxides. The Merchison River Complex is dominated by deformed plagioclase-megacrystic gabbroic rocks and a few fragmented mafic volcanics; with the samples obtained from this unit containing relict clinopyroxene, hornblende and plagioclase with actinolite, chlorite, clays, quartz and oxides forming replacement textures (Figs. 3.9b, 3.10a).

Ultramafic rocks: Few samples have been obtained from the ultramafic facies of the TPS. Nevertheless they form a volumetrically important part of the TPS (10 km^2) and are found in discontinuous bands of variable thickness close to the contact between the pluton and the North Coast Schist, with magnetic and gravity data suggesting a considerable sub-surface mass (Wadge & Snoke, 1991) (Fig. 2.2, 3.9c). Numerous altered peridotite xenoliths are found within the gabbro-diorite facies of the TPS (Fig. 3.9d). The two largest outcrops of the ultramafic rocks are in the Louis D'Or region of the NE of the island, and the central area around Menna Hill. Samples were mostly taken as blocks from the Louis D'Or River. 'Anhydrous' rock types include dunite, wehrlite and olivine clinopyroxenite (Fig. 3.10b). There is also abundant evidence for a late-stage fluid rich magmatic phase with the occurrence of plagioclase-hornblende clinopyroxenite, hornblendite and abundant veins and dykelets of very distinctive

hornblende/plagioclase pegmatites which look similar to those described by Kerr et al. (2004) from the Bolívar ultramafic complex of the Western Cordillera of Colombia (hydrated oceanic plateau root) and the Smartville complex of Sierra Nevada (island arc root) (Beard & Day, 1986). The sampled ultramafic rock types are: serpentinised dunite; wehrlite with hornblende replacement textures; (olivine) clinopyroxenite (Fig. 3.10b) with hornblende, chlorite and clays; and finally hornblendite, dominated by hornblendes which have been partially altered to chlorite and clays. The ultramafic facies are considered to represent the accumulation of crystals on the floor or sidewalls of the pluton. Interestingly, olivine appears as small anhedral inter-granular aggregates as opposed to an obvious cumulus phase.

Gabbro-diorite: The most voluminous phase of the pluton is represented by a broad range of gabbroic to dioritic rocks which occur across the whole island from near Plymouth to King's Bay (up to 100 km^2) (Fig. 2.2, 3.9d). There is some evidence for igneous layering [for example mafic and felsic banding at Washerwoman's Bay; Snoke et al., (2001b)] but much of this facies is massive in texture. Crystal sizes range from coarse-grained gabbros (Fig. 3.10c) through to slightly finer grained diorites and all rocks are characterised by varying abundances of plagioclase, hornblende, clinopyroxene and oxides. Orthopyroxene is also present in some samples (norites or two-pyroxene gabbros). The sampled rocks show clear evidence of hornblende replacing pyroxene indicating that fluids in the magma reacted with the pre-existing crystal assemblage late in the crystallisation history. Chlorite, clays, micas and oxides form a typical alteration assemblage. Apatite, along with lesser zircon and titanite are the most common accessory minerals. It is also common to find xenoliths of hornblende-rich peridotites within the gabbro-diorites, for example at Arnos Bay (Fig. 3.9d).

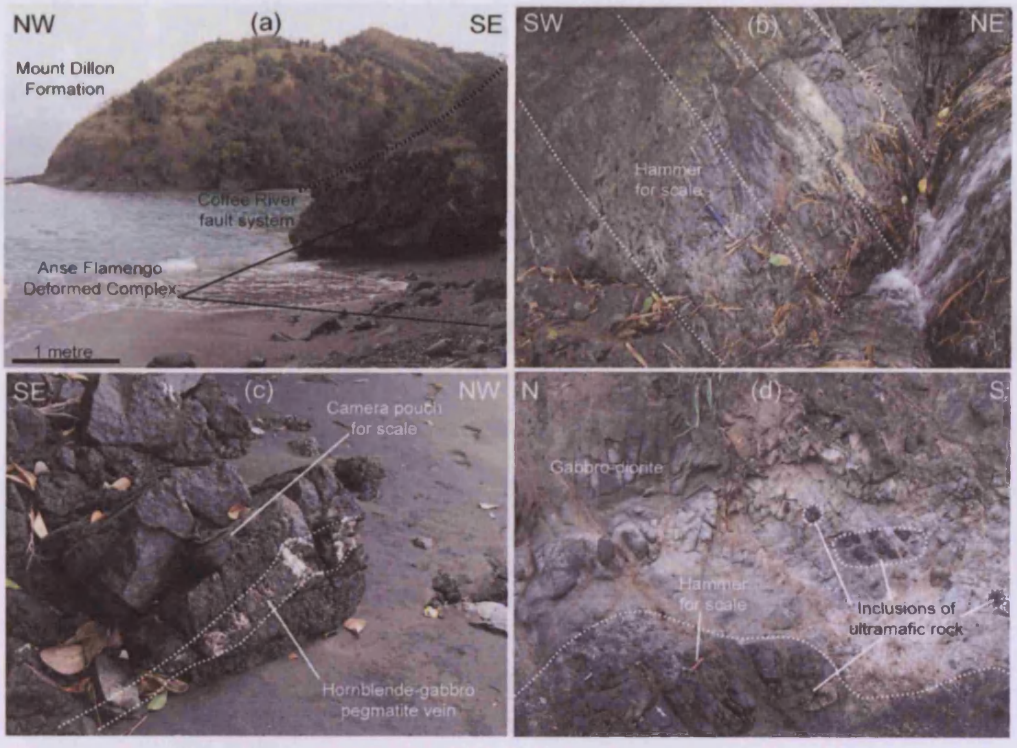

Figure 3.9. Field photographs from the plutonic rocks of Tobago. (a) Boundary between the North Coast Schist (Mount Dillon Formation) and the younger plutonic and volcanic suites marked by the Coffee River fault and a patch of deformed mafic volcanic/plutonic rocks (Anse Flamengo Complex), at Celery Bay. (b) Example of the deformed mafic volcanic/plutonic complexes (Merchison River Complex) showing steeply dipping foliation (dotted), hard splintery texture (dynamothermal metamorphism) and segregations of plagioclase and mafic minerals. Location: road cutting on hillside SW of Speyside. (c) Massive ultramafic rocks exposed in King Peter's Bay, intruded by a small vein of hornblende-gabbro pegmatite. (d) Exposure of the gabbro-diorite pluton with inclusions of ultramafic rock at Arnos Bay.

3.2.5. Mafic dyke swarm

Dykes cutting the NCS: The only post-metamorphic rock type present is a distinctive grey, medium-grained non-metamorphosed diorite dyke facies with 2-3 mm flow-aligned hornblende needles. This variety of dyke is also found cutting the VPS. Assuming that these dykes are of a similar age to the rest of the mafic dyke swarm (~103-92 Ma), this is confirmation that the NCS and the VPS were brought together, or 'stitched' at or before 103 Ma, however further dating work would be needed to verify this hypothesis. In thin section, the dykes are characterised by the acicular hornblendes in a matrix of plagioclase, oxides and some quartz. Calcite veining is common.

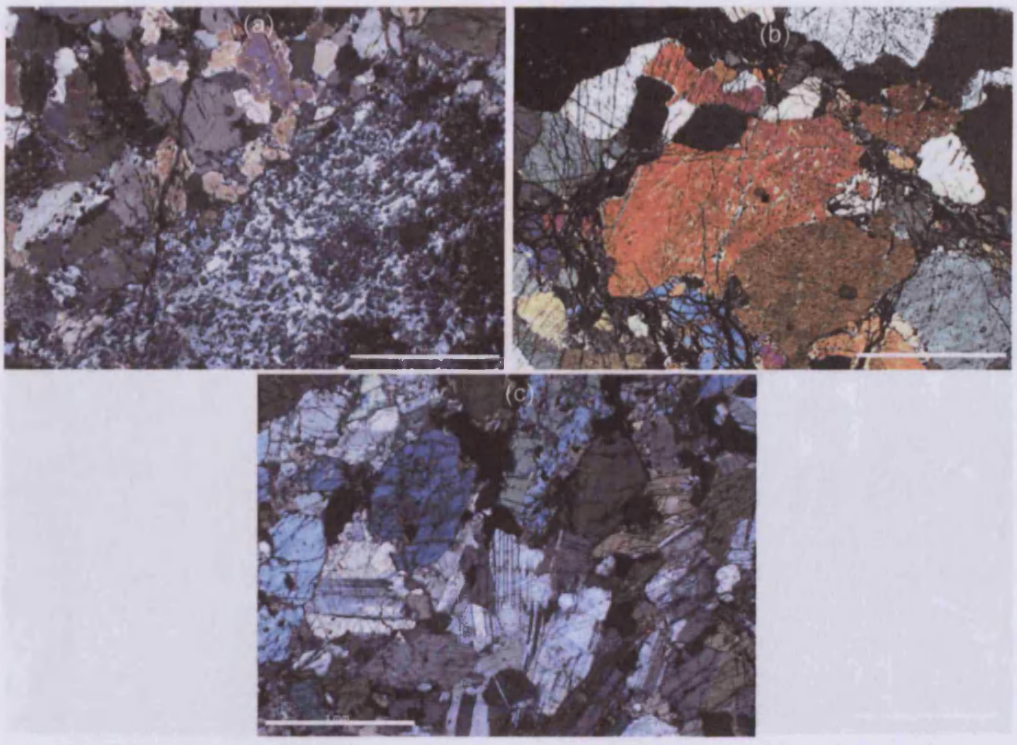

Figure 3.10. Photomicrographs from the Tobago Plutonic Suite, all cross-polarised light with scale bar = 1 mm. (a) INT/6-3/13, altered and deformed plagioclase phenocryst in a groundmass consisting of plagioclase and hornblende, from the deformed mafic volcanic complex at location (b) in Figure 5.5 (Speyside). (b) INT/21-2/4, olivine clinopyroxenite from the Louis D'Or River. (c) INT/3-3/2, gabbro-diorite with plagioclase, clinopyroxene and oxides from the trail between Arnos Vale and Culloden.

Dykes cutting the VPS: The rest of the mafic dyke swarm, which cuts all units of the VPS, is highly variable in character. It is clear that some locations within the biotite tonalite and the gabbro-diorite have been a focus of dyke intrusion (e.g. Arnos Bay, Fig. 2.2, 3.11a) whereas other localities contain only scattered occurrences with much less intense intrusion in the TVG than the TPS. As described above, some dykes are fine-grained diorites with acicular, flow-aligned hornblende. These are found around Courland, Arnos Bay and Back Bay in close proximity to the biotite tonalite unit (Fig. 2.2). Also present are hornblende and/or clinopyroxene dolerites (Fig. 3.11b) and gabbros (Fig. 3.11c); some aphyric and some containing a hornblende phenocryst phase. These mostly coarse-grained dykes have been sampled at the same localities as the other dyke facies along with examples from the Kendal Road (Fig. 2.2). As with the plutonic rocks, clinopyroxene is observed in some cases breaking down to form hornblende. A few dykes are quite glassy and carry large (up to 1 cm) plagioclase phenocrysts (Fig. 3.11d). Clays, oxides and chlorite are ubiquitous replacement minerals.

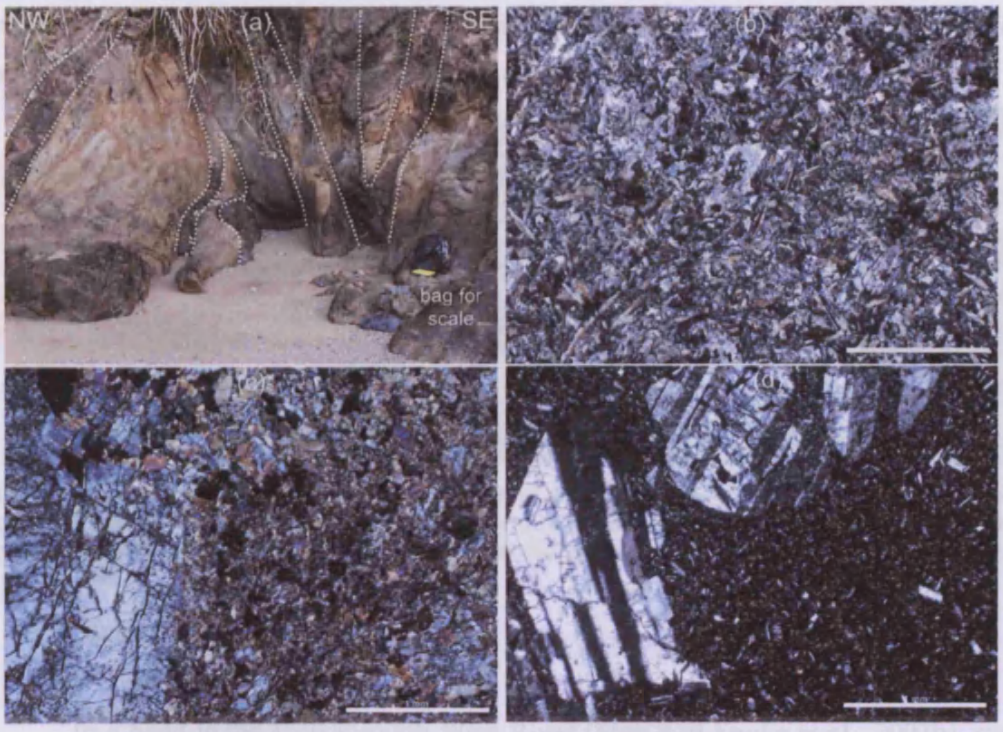

Figure 3.11. Field and thin section photographs of Tobago dykes. All sections in cross-polarised light with scale bar 1 mm. (a) Multiple anastamosing mafic dykes intruding gabbro-diorite of the Tobago pluton at Arnos Bay. b) 2D-14 a mafic dyke comprising elongate plagioclase, hornblende and clinopyroxene crystals, dated to 91.4±2.2 Ma (Sharp & Snoke, 1988). (c) INT/25-1/4 a coarse-grained mafic dyke cutting biotite tonalite in the Courland River, comprising a fine-grained groundmass of hornblende, clinopyroxene, plagioclase and oxides with much larger clinopyroxene crystals. (d) INT/23-2/5 a glassy intermediate dyke with very fine needle-like plagioclase crystals in the groundmass and large plagioclase phenocrysts.

3.2.6. Dyke-like tonalite of Arnos Vale-Mason Hall

Tonalitic rocks are exposed as a single body approximately 500 m wide which may be traced for 7 kilometres from the shoreline at Arnos Vale along the Courland River to Mason Hall (Fig. 2.2) with a possible continuation for 3 km in the sub-surface to the east indicated by aeromagnetic data (Wadge & Snoke, 1991). The tonalite sharply cross-cuts the gabbro-diorite pluton and is composed almost entirely of a uniform medium-grained felsic rock comprising plagioclase, quartz, biotite, ± hornblende, oxides, apatite and zircon (Figs. 3.12a,b). Much of the tonalite body is altered, with chlorite, calcite and sericite common. Rarely, small veins of grey, fine-grained plagioclase-phyric tonalite can be found which cross-cut the main tonalite body, hinting at a minor second stage of intrusion. There is no evidence of gradation from the most felsic plutonic facies (plagioclase and hornblende-bearing diorites) to

these quartz, plagioclase and biotite-bearing tonalites so it is likely that the tonalites represent a separate intrusive event from the VPS.

Figure 3.12. Field photograph and photomicrograph of the Arnos Vale-Mason Hall tonalite. (a) Typical exposure of biotite-tonalite in the Courland River. (b) INT/4-2/3, (cross-polarised light, scale bar 1mm) hornblende-biotite tonalite with abundant plagioclase and subordinate quartz from the Courland River.

3.2.7. Tonalitic partial melts of the TVG

In a bend in the Hillsborough West River (Stop 8 of Snoke et al., 2001b), small tonalitic veins can be observed cross-cutting hardened volcanic breccias of the Tobago Volcanic Group (Figs. 2.2, 3.13). These veins are petrologically similar to the Arnos Vale-Mason Hall tonalite (Fig. 3.12) but are not particularly extensive and only occur within a few tens of metres of the contact with gabbroic-dioritic rocks of the Tobago pluton. Snoke et al. (2001b) interpreted these as partial melts of the TVG formed during emplacement of the Tobago Pluton. It is one of the aims of this thesis to identify if these tonalites differ geochemically from the larger Arnos Vale-Mason Hall body.

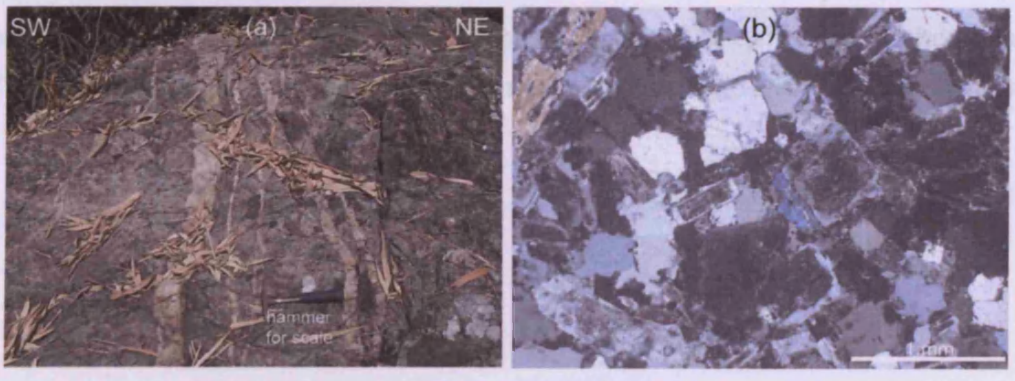

Figure 3.13. Field photograph and photomicrograph of the tonalitic partial melts of the TVG. (a) Exposure of small tonalitic veins cross-cutting the TVG in the Hillsborough River. (b) INT/20-2/2, (cross-polarised light) biotite tonalite with plagioclase and quartz from the Hillsborough River.

3.2.8. Nb- and LREE-enriched mafic and felsic intrusions

These rocks have never been described before from Tobago. In the field, three samples were collected which were presumed to be examples of the mafic dyke swarm (INT/6-3/14 and INT/29-2/2) or the Argyle Formation (DY-3D-103), all from the land between Speyside and the Argyll River (Fig. 2.2) and were later defined on the basis of their geochemistry. These rocks were found to contain high concentrations (~7-28 ppm) of Nb. These three samples all differ slightly in appearance: 29-2/2 is dark-grey/green and aphyric with a sub-0.5 mm grain size and occasional circular patches of calcite. 3D-103 is of similar groundmass grain size but contains conspicuous ~1 mm phenocrysts of either clinopyroxene or hornblende. No thin section was made of these samples. 6-3/14 (Fig. 3.14c) is aphyric but slightly coarser grained than the other samples. The thin section contains only elongate 1 mm grains of equigranular hornblende and plagioclase with moderate alteration of the hornblende to chlorite and the plagioclase to sericite and clays.

A fourth example of these unusual intrusions, this time containing 49 ppm Nb, was a felsic mass intruding the Argyle Formation on Kendal Road inland from Carapuse Bay (Fig. 2.2). The mass is distinct from any other rock type found on Tobago because it consists of medium-grained granite (Fig. 3.14a). The mineralogy is dominated by 1-2 mm grains of optically zoned plagioclase and alkali feldspar with interstitial quartz. The mafic component comprises ~5 % ragged subhedral grains of hornblende (no biotite) and 1-2% anhedral Fe-Ti oxides. Accessory minerals are, in apparent order of abundance; apatite, titanite and zircon. The only obvious alteration is of the feldspars, which are dusty and partly replaced by sericite and clays (Fig. 3.14b).

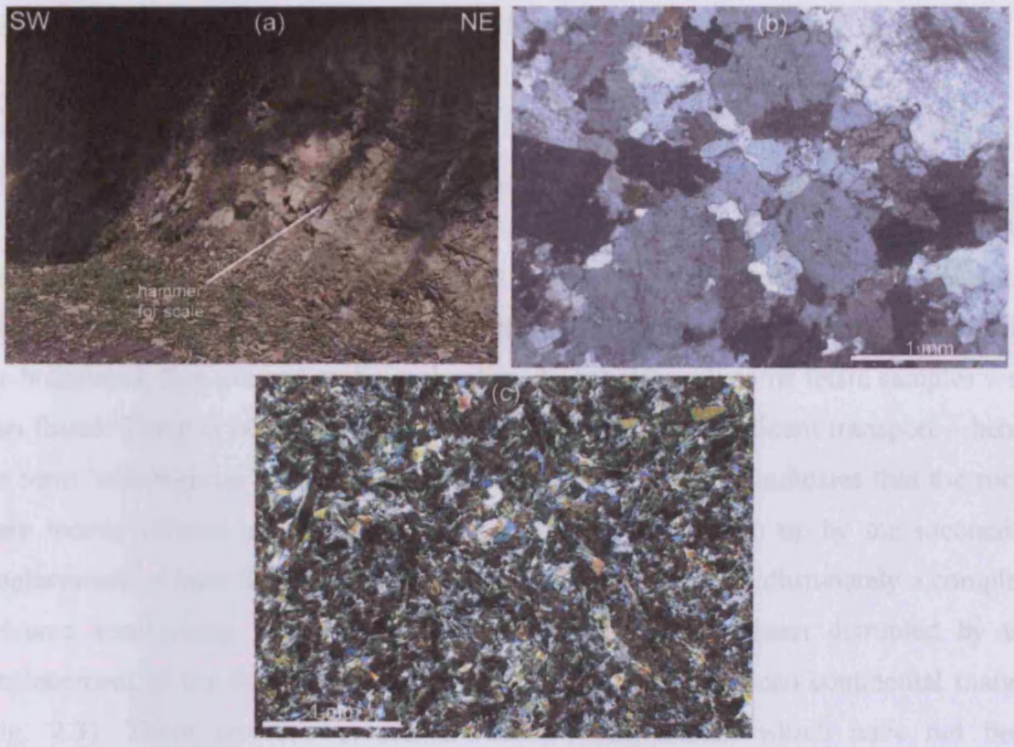

Figure 3.14. Field and thin section photographs of the Nb- and LREE-enriched intrusions in cross-polarised light. (a) Granite outcrop on the Kendal Road. (b) INT/1-3/4 the same granite in thin section showing quartz, plagioclase, alkali feldspar and hornblende. (c) INT/6-3/14 a Nb-enriched basalt dominated by plagioclase, clinopyroxene and oxides.

3.3. Geology and petrography of the San Souci Volcanic Formation

3.1.1. Geology

The strike of the volcanic rocks of the San Souci Formation is parallel to the Caribbean coast of Trinidad and much of it is covered by dense forest. In the field, the rocks are mostly dark with iron oxide staining and considerable alteration. The majority are brecciated, fine-grained mafic rocks (Fig. 3.15a) although some felsic samples were also found. There is no evidence of rounding of clasts or significant transport – hence the term 'autobreccias' of Wadge & Macdonald (1985) which indicates that the rocks were mostly formed as lavas within flows which were broken up by the successive emplacement of later flows probably in the presence of water. Unfortunately a complete volcanic stratigraphy is not exposed and in any case has been disrupted by the emplacement of the San Souci Group against the South American continental margin (Fig. 2.3). There are also coarser intrusive rocks present which have not been brecciated. Although these intrusive mafic rocks are rarer, they have been preferentially sampled because they are more resistant to weathering.

3.3.2. Petrography

The finer lavas and breccias are aphyric and their mineralogy consists of elongate, randomly aligned plagioclase, stubby clinopyroxene and oxides which reach a maximum of 1 mm in grain size (Fig. 3.15b). The plagioclases are altered to clays whilst the clinopyroxene has been replaced with green-brown amphibole particularly at the edges of crystals. Prehnite, pumpellyite, chlorite, clays and calcite are present in varying quantities as replacement minerals and in veins. Olivine or olivine pseudomorphs were not found in any of the thin sections. Some of the brecciated samples contain occasional veins of pyrite. This observation may indicate the development of a hydrothermal fluid-flow regime. The coarser rocks are mostly aphyric dolerites with a primary mineralogy of elongate plagioclase, clinopyroxene which is occasionally twinned, and oxides arranged in an interlocking randomly-aligned texture. The grain size extends to 2-3 mm (Fig. 3.15c). A similar suite of replacement and alteration minerals are present compared to the fine-grained mafic rocks. Occasionally,

there are also fine-grained bands, a few millimetres wide, which contain both fine-grained primary and replacement minerals; these may be small crush zones.

Two felsic plagioclase-phyric auto-breccias have a primary mineralogy dominated by squat plagioclase (with occasional phenocrysts 1-3 mm across), set against a groundmass with grain size of <0.25 mm containing elongate plagioclase, quartz, squat altered clinopyroxene and oxides (Fig. 3.15d). There is some quartz and calcite veining.

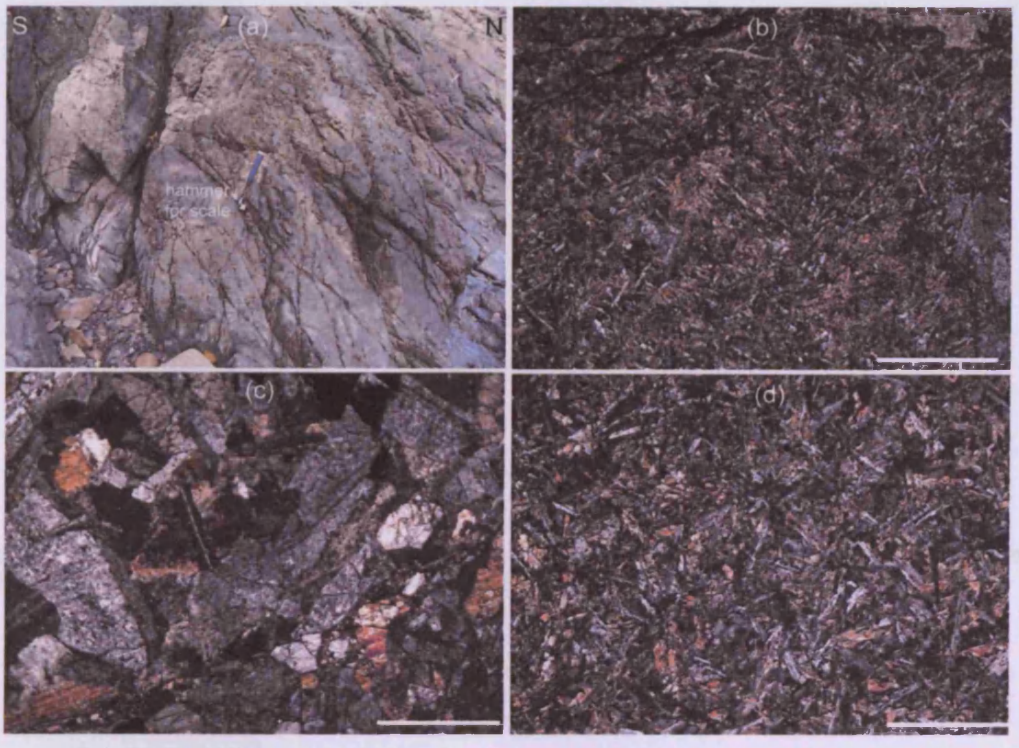

Figure 3.15. Field photograph and photomicrographs of the San Souci Formation (thin sections in cross-polarised light with scale bar 0.25 mm). (a) Altered and fractured basaltic breccias at San Souci beach. (b) INSS3d, fine-grained aphyric basalt with needles of plagioclase and groundmass clinopyroxene. (c) INSS6.3, medium-grained aphyric dolerite with plagioclase, clinopyroxene and oxides. (d) INSS7.3, fine-grained aphyric relatively felsic lava with needles of plagioclase and groundmass clinopyroxene.

3.4. Geology and Petrography of the SE Aves Ridge

3.4.1. Dredge outcrops

In lieu of any surface geology upon which to report, Fox et al. (1971) presented a series of cross-sections which showed the depth of the dredge hauls in relationship to their position on the eastern scarp of the Aves Ridge (Fig. 2.4). The relative positions of the three hauls on their separate portions of the ridge are shown in Figure 3.16.

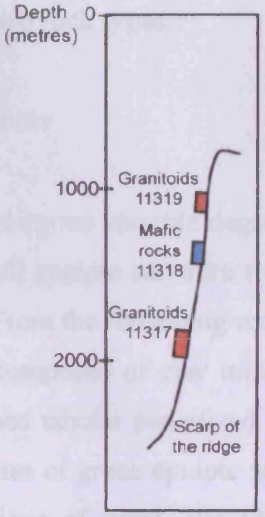

Figure 3.16. Schematic diagram showing the location of the three Aves Ridge dredges relative to each other in depth profile along the eastern scarp of the ridge (adapted from Fox et al., 1971).

3.4.2. Granitoid petrography

The felsic rocks are coated in thick layers of manganese oxides, sometimes over 1 cm thick. The rocks are typically pink to pale green and slightly hydrothermally altered. Two facies have been identified within the granitoid samples. The most dominant facies (~75 %) is of a coarse, granitic nature and the other is fine-grained and more intermediate in composition. The primary mineralogy of the granitic rocks comprises plagioclase, quartz, alkali feldspar, hornblende and opaques (Fig. 3.17b). The feldspars are sericitized and epidote is a common secondary mineral along with clays and chlorite. Zircon and titanite are the most common accessory minerals. Texturally, the rock has a coarse interlocking nature, with grain sizes up to 2 mm and abundant interstitial quartz. Plagioclase is sometimes optically zoned and alkali feldspar is perthitic. Hornblende is squat or slightly elongate.

The intermediate facies occurs as isolated masses or clots distinct from the surrounding granitic material (Fig. 3.17c,d). The boundary between the two facies is, however, indistinct and gradational in thin section suggesting the darker clots may be restitic in nature. This second facies is dioritic and has a grain size ranging from 0.5 to 1 mm. The primary mineralogy is dominated by interlocking sericitized plagioclase, amphiboles, titanite and oxides. Only the dominant coarse granitic facies was selected for geochemical analysis in order to avoid the generation of mixing trends from the artificial homogenisation of the two rock types.

3.4.2. Petrography of the mafic rocks

The mafic rocks have undergone variable degrees of penetrative alteration. The freshest specimens from the small sample set were reserved for geochemical analysis and so little solid rock remains. From the remaining rocks it can be seen that many have a fine grained matrix which is composed of clay minerals with a small proportion of calcite (3.17a). Outlines of aligned tabular sericitized plagioclase feldspar can be seen which are up 2 mm across. Patches of green epidote and oxides up to 1 mm across are present and there are small regions of squat, altered clinopyroxene. The rocks with obvious plagioclase crystals may be porphyritic basalts or basaltic andesites of an extrusive or hypabyssal nature.

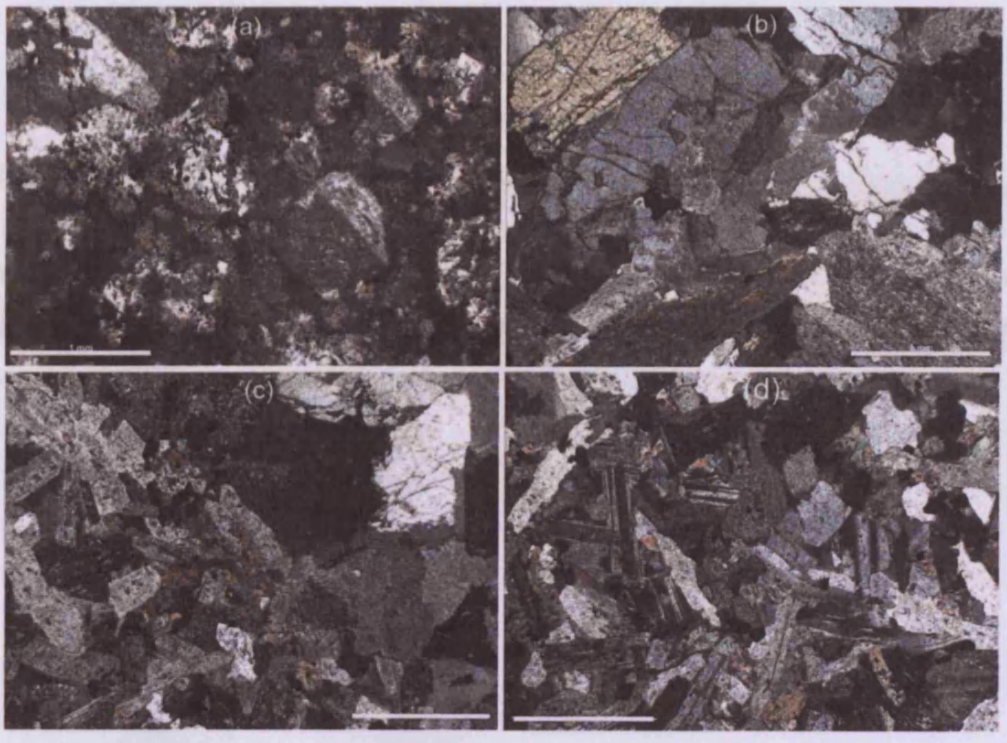

Figure 3.17. Thin section photographs of rocks from the Aves Ridge, cross-polarised light and scale bar 1 mm in all cases. (a) 318f, mafic facies with relict plagioclase phenocrysts and clay groundmass. (b) 317k, granitoid facies with quartz, plagioclase, alkali feldspar and hornblende. (c) 317k, boundary between the granitoid facies and the intermediate facies. (d) 317k, intermediate facies containing mostly plagioclase, amphibole and titanite.

CHAPTER FOUR: GEOCHRONOLOGY AND WHOLE ROCK GEOCHEMISTRY

Results for each locality of: U-Pb zircon analyses, whole-rock ICP-OES and ICP-MS major and trace element geochemistry, and Nd-Hf radiogenic isotope geochemistry where undertaken

4.1. Introduction

In this chapter, the geochronology, major element, trace element and isotopic data are described for each location, where analysed. For reference, the location and descriptions of each sample are presented in Appendices 1-2. Analytical methods, followed by error analysis for the major and trace element geochemistry are in Appendices 3-4. The full major and trace element data are in Appendix 5 and radiogenic isotope data are in Appendix 6.

Included with the description of the major and trace element data for each unit is an assessment of which elements are likely to be reliable petrogenetic indicators, and which have been mobilised by sub-solidus processes such as hydrothermal or seawater-related alteration, calcification, silicification or weathering (e.g. Seewald & Seyfreid, 1990). These features will be investigated using petrology, loss-on-ignition (LOI) values and plots of elemental concentrations within magmatic suites against the known 'immobile' element Nb (e.g. Cann, 1970).

In a magmatic suite linked by fractional crystallisation, where a given element has not been mobilised, it should show a clear trend when plotted against Nb passing through the origin. Conversely, where an element has been mobilised, the data will be scattered with little discernable trend. Trends which do not pass through the origin or deviate from the main trend may indicate multiple melt sources, magma mixing or contamination processes. All major elements plotted against Nb are presented on an anhydrous basin in order to negate the effects of weathering processes and calcification which result in high LOI values (>5 wt.%). The question of whether individual units can be combined into magmatic suites with the same source region will be addressed here in order to guide the main discussion on the petrogenesis of each unit in Chapter 5. Thereafter, the full results of major and trace element analyses will be presented in order to classify the rock types. A single section for each location will contain the radiogenic isotope results.

Traditional whole rock classification methods, such as the SiO_2 vs. K_2O diagram of Peccarillo & Taylor (1976) or the total alkalis vs. silica (TAS) diagram are not suitable for use in this study due to the likely mobilisation of SiO_2, K_2O and Na_2O.

For this reason, a new diagram was selected to classify the rocks in this study which has already been tried and tested on Caribbean samples – the Th vs. Co plot of Hastie et al. (2007). This diagram uses Th and Co as immobile, incompatible proxies for K_2O and SiO_2 and classifies lavas and dykes into their rock type based on Co concentrations (basalt, basaltic andesite, andesite, rhyolites, or dacite) and series based on Th concentrations (tholeiitic, calc-alkaline, shoshonitic).

4.2. Whole rock geochemical results from La Désirade

4.2.1. Major and trace element geochemistry of the igneous complexes of La Désirade

Element mobility and geochemical trends: High loss-on-ignition values of 1-9 wt.% in the NE mafic volcanic complex (Appendix 5) are likely to be due to sub-solidus alteration processes including some calcification. Mobilisation of many major and trace elements such as Si, Mg, Na, K, Ba and Sr is therefore to be expected, as has been noted for other Cretaceous Caribbean igneous rocks (e.g. Hastie et al., 2007).

The NE mafic volcanic complex can be split into three units based on their geochemistry (see below). Unit 1 consists of the lowermost clinopyroxene and plagioclase-phyric lavas (Localities 10 and 11) whereas Unit 2 covers Localities 1 to 9 and Unit 3 is found at Localities 14 to 17 (Fig. 3.1). Representative major and trace element analyses from the rocks in the three units are plotted against Nb in Fig. 4.1 to assess elemental mobility. None of the recognised units display coherent intra-differentiation trends for the major elements (except weak trends for Al_2O_3 and TiO_2) or large ion lithophile elements (LILE) (Ba and Sr). Conversely, immobile trace elements (e.g. Zr, Th and Yb) display coherent intra-magmatic differentiation trends against Nb within each unit. On this basis, Al_2O_3, TiO_2, the Rare Earth Elements (REE, light REE [LREE], middle REE [MREE] and heavy REE [HREE], and the high-field-strength-elements (HFSE) along with Co, Cr, Ni, Sc, V and Y have not been significantly mobilised and may be used in petrogenetic interpretation. Interestingly, on the Zr vs. Nb diagram, two sub-groups can be seen which both display divergent trends against Nb, with 8 samples from Units 1 and 2 following a lower Zr/Nb trend.

As noted above, the Th vs. Co diagram of Hastie et al. (2007) for island arc rocks is used to classify the lavas (Fig. 4.1). The plot shows that the majority of La Désirade lavas range from tholeiitic basalts to tholeiitic rhyolites with a few more calc-alkaline compositions in Unit 2 of the NE mafic volcanic complex.

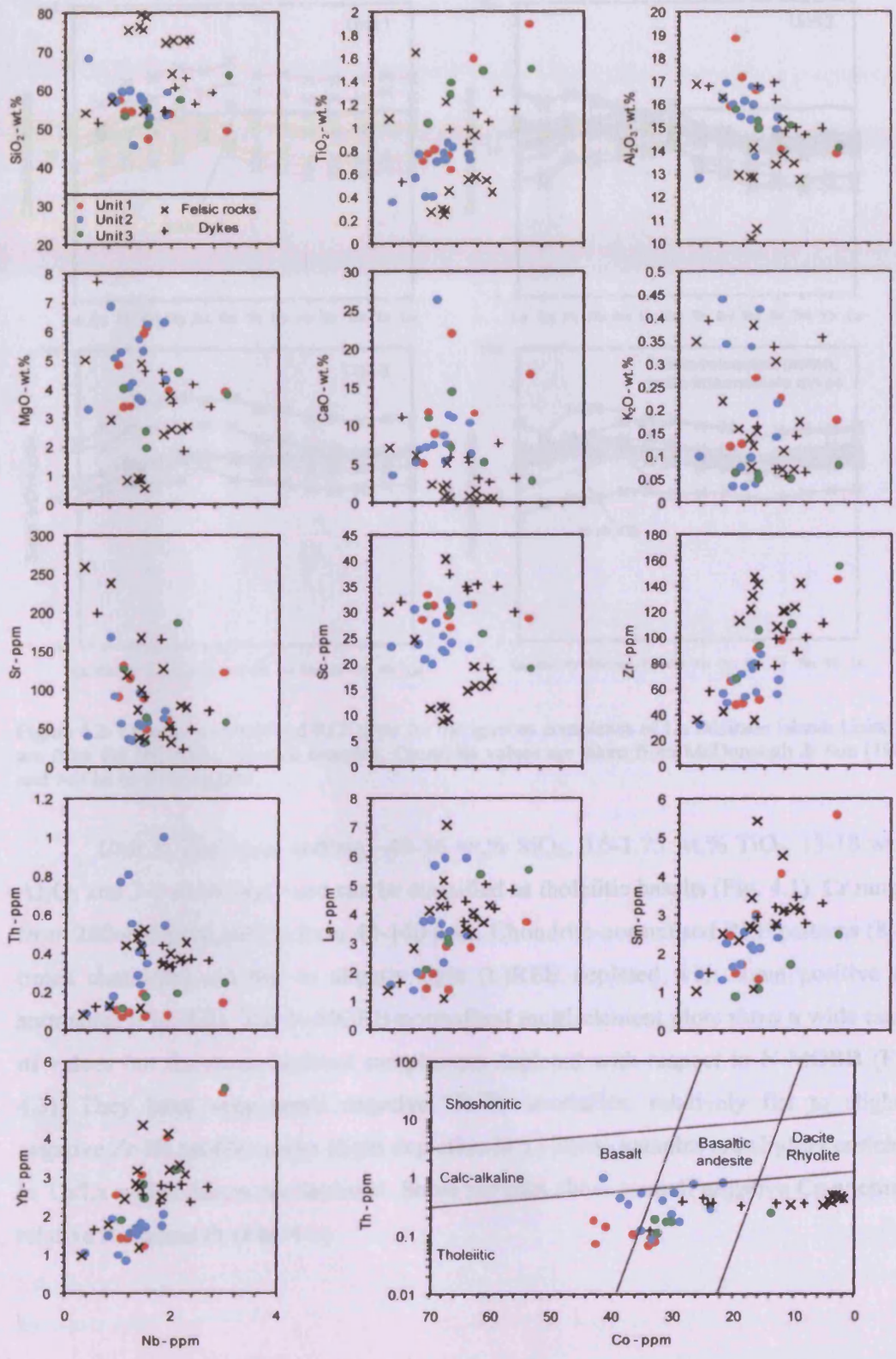

Figure 4.1. Element vs. Nb (after Cann, 1970) and Th-Co plots (after Hastie et al., 2007) for the volcano-plutonic complexes of La Désirade Island.

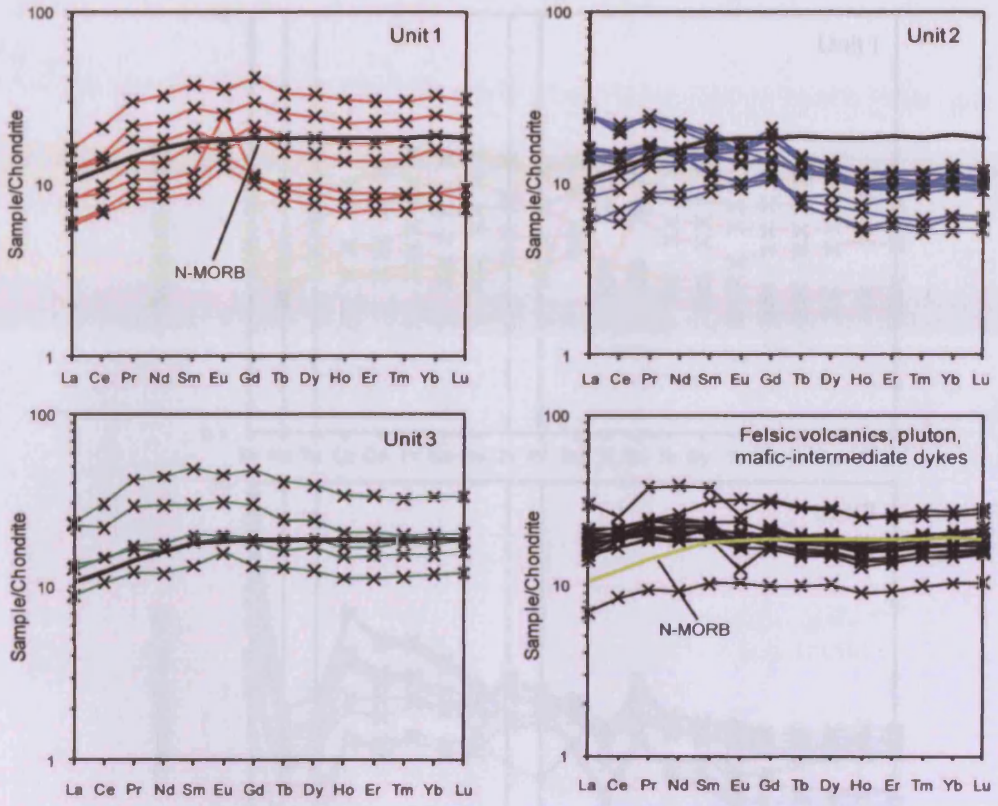

Figure 4.2. Chondrite-normalised REE plots for the igneous complexes of La Désirade Island; Units 1-3 are from the NE mafic volcanic complex. Chondrite values are taken from McDonough & Sun (1989) and will be used throughout.

Unit 1: The lavas contain ~45-56 wt.% SiO_2, 0.6-1.75 wt.% TiO_2, 13-18 wt.% Al_2O_3 and 3-6 wt.% MgO and can be classified as tholeiitic basalts (Fig. 4.1). Cr ranges from 280-450 ppm and Ni from 40-140 ppm. Chondrite-normalised REE patterns (8-30 times chondrite) are flat to slightly light (L)REE depleted with some positive Eu anomalies (Fig. 4.2). The N-MORB-normalised multi-element plots show a wide range of values but the most depleted samples are depleted with respect to N-MORB (Fig. 4.3). They have very small negative Nb-Ta anomalies, relatively flat to slightly negative Zr-Hf profiles and a slight depletion in Ti. Some samples are slightly enriched in Th/La whilst others are depleted. Some samples show a small negative Ce anomaly relative to La and Pr (Fig. 4.3).

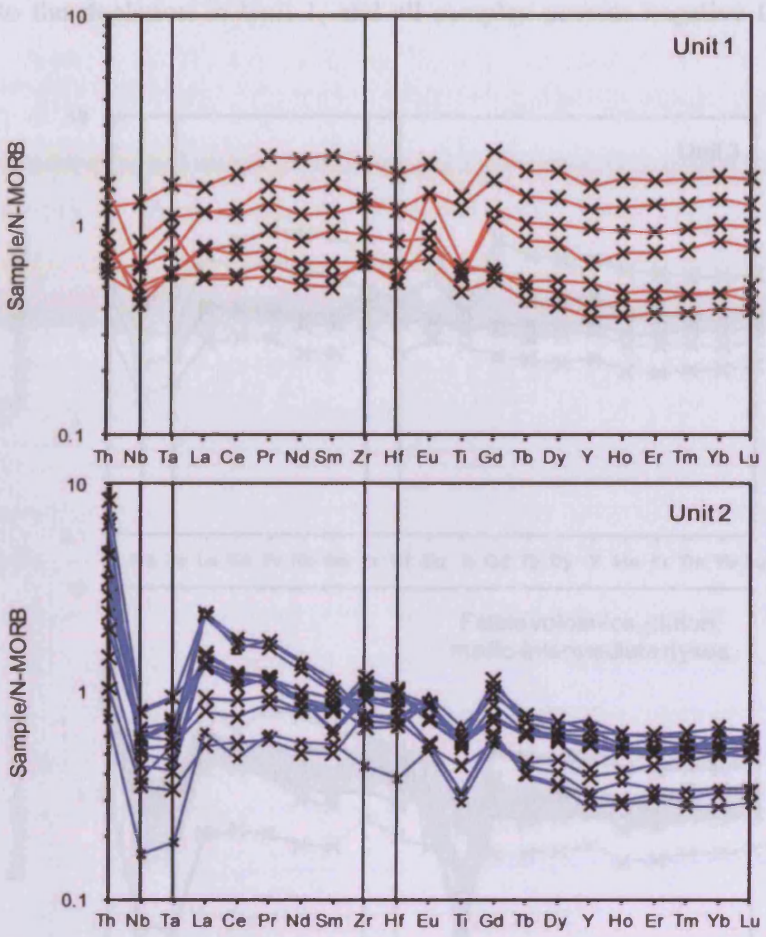

Figure 4.3. N-MORB-normalised trace element plots for Units 1 and 2 of the NE mafic complex of La Désirade Island. N-MORB normalising values are taken from Sun & McDonough (1995) and will be used throughout.

Unit 2: These rocks have 43-58 wt.% SiO_2, 0.4-0.8 wt.% TiO_2, 13-16 wt.% Al_2O_3 and 3.4-6.6 wt.% MgO and are mostly tholeiitic and calc-alkaline basaltic andesites (Fig. 4.1). Compared to Unit 1, Unit 2 lavas are more siliceous and have lower TiO_2 concentrations. They contain high abundances of Cr and Ni - 190-990 ppm and 80-210 ppm respectively. The chondrite-normalised REE patterns for Unit 2 vary from flat to slightly LREE enriched and are generally more depleted in the middle (M)REE and heavy (H)REE than the rocks of Unit 1 (Fig. 4.2). Overall the HREE concentrations are around 5-15 times chondrite with some small positive Eu anomalies. The N-MORB-normalised multi-element plot shows that Unit 2 lavas are quite depleted in the MREE and HREE relative to N-MORB. Unit 2 lavas also have negative Nb-Ta anomalies (Fig. 4.3) along with both positive and negative Zr-Hf anomalies. Ti is also depleted relative to the MREE. Th is strongly enriched over the LREE in all samples,

compared to the depletion in Unit 1, and all samples possess negative Ce anomalies (Fig. 4.3).

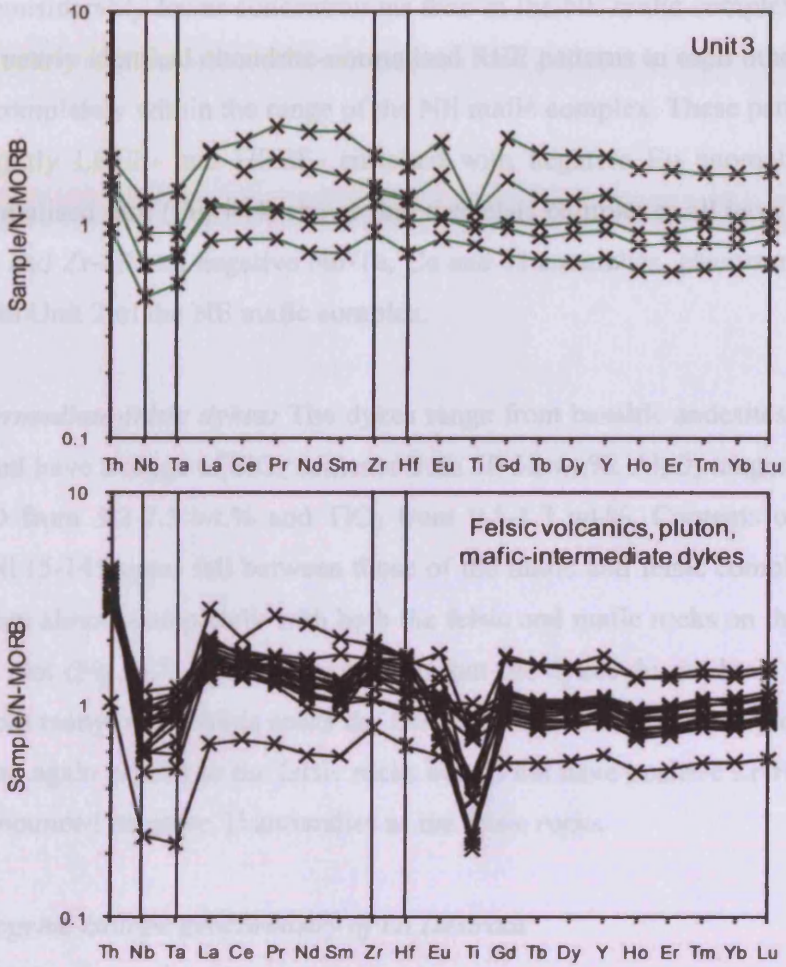

Figure 4.4. N-MORB-normalised trace element plots for Unit 3 of the NE mafic complex of La Désirade Island, the felsic rocks and intermediate dykes.

Unit 3: The lavas are mostly tholeiitic basaltic andesites (Fig. 4.1). SiO_2 varies from 47-61 wt.% and MgO from 1.7-3.8 wt% whilst TiO_2 is consistently above 1 wt.%, much higher than in Unit 2. These rocks contain much less Cr (10-130 ppm) and Ni (5-65 ppm) compared to the other units. The chondrite-normalised REE patterns of Unit 3 are flat to slightly LREE-depleted which is similar to the rocks of Unit 1 (Fig. 4.2). However, on the N-MORB-normalised plot (Fig. 4.4), Nb-Ta depletions are present, unlike Unit 1. Zr and Hf are only very slightly enriched or depleted relative to the REE, Ti is depleted relative to the REE and there are some marked Ce depletions relative to La and Pr, similar to Unit 2 (Fig. 4.4).

Felsic volcanic and plutonic rocks: SiO_2 ranges from 62-79 wt.%, Al_2O_3 from 10-15 wt.%, MgO from 0.3-3.6 wt.% and TiO_2 from 0.3-0.9 wt.%. Ni and Cr are present in considerably lower concentrations than in the NE mafic complex. The felsic rocks have nearly identical chondrite-normalised REE patterns to each other (Fig. 4.2), which fall completely within the range of the NE mafic complex. These patterns are flat to very slightly LREE- and HREE- enriched with negative Eu anomalies. The N-MORB-normalised plot (Fig. 4.4) shows that the felsic complexes all have pronounced positive Th and Zr-Hf and negative Nb-Ta, Ce and Ti anomalies, characteristics which are similar to Unit 2 of the NE mafic complex.

Intermediate-felsic dykes: The dykes range from basaltic andesites to rhyolites (Fig. 4.1) and have a range of SiO_2 contents from 50-58 wt.%. Al_2O_3 ranges from 13-16 wt.%, MgO from 3.2-7.5 wt.% and TiO_2 from 0.5-1.3 wt.%. Contents of Cr (5-145 ppm) and Ni (5-145 ppm) fall between those of the mafic and felsic complexes. These dykes overlap almost completely with both the felsic and mafic rocks on the chondrite-normalised plot (Fig. 4.2), with the exception that the dykes do not have negative Eu anomalies but many of the felsic rocks do. On the N-MORB normalised plot (Fig. 4.4), the dykes are again similar to the felsic rocks but do not have positive Zr-Hf anomalies or such pronounced negative Ti anomalies as the felsic rocks.

4.2.2. Radiogenic isotope geochemistry of La Désirade

Mattinson et al. (1980) and Gaucaht (2004) reported Nd, Pb and Sr radiogenic isotope ratios from all magmatic complexes. Given the level of alteration it is unlikely that Sr and Pb isotopic values can be used to assess petrogenetic processes (e.g. Thompson et al., 2003; Hastie, 2009), hence the non-inclusion of such work in this project. $^{144}Nd/^{143}Nd$ ratios are more resistant to sub-solidus alteration processes so are likely to represent the primary lava composition (e.g. White and Patchett, 1984). The measured $^{144}Nd/^{143}Nd$ ratios of Gauchat (2004) are depleted relative to bulk earth, spanning a narrow range from 0.512786 to 0.512914. Insufficient data are available to calculate initial ratios or compare values with trace element ratios. However, these ratios overlap between the different complexes, suggesting that the mantle source region and/or crustal input for all the igneous complexes was relatively uniform whilst

the depleted values indicate that old continental material was not involved in the petrogenesis of these rocks.

4.3. Geochronology and whole rock geochemical results from Tobago

4.3.1. New geochronological results from Tobago Island

For full details of the separation and analysis methods, see Appendix 3. For all chemical abrasion-isotope dilution-thermal ionisation mass spectrometry (CA-ID-TIMS) analyses, procedural blanks were very low, at mostly <1 pg of Pb, enabling analysis of zircons containing particularly low concentrations of radiogenic Pb, as appears to be the case for Tobago (Table 4.1). All errors are quoted at the 2σ (95 % confidence) level.

Sample 3A-24 from the Parlatuvier Formation, North Coast Schist: Four single grains from basaltic andesite sample 3A-24 were analysed, providing $^{206}Pb/^{238}U$ ages ranging from 128.66±0.23 to 135.03±1.46 Ma (Table 4.1, Fig. 4.5). A conventional concordia plot for this data gives an unacceptable scatter (not shown) so, according to the preferred method of the NERC Isotope Geoscience Laboratories who analysed the sample, the data was regressed using a Tera-Wasserberg plot without correction for common Pb (Fig. 4.5). This method reveals an acceptable concordant model age of 130.4 ± 4.5 Ma for the 4 grains (mean square weighted deviation [MSWD] = 8). We take this to represent the crystallisation and/or eruption age of the mafic-intermediate tuffs of the Parlatuvier Formation. The other formations remain undated.

As stated in the introduction (Section 2.2.1), there is a hornblende Ar-Ar isochron generated from the same unit of 115.9 ± 3.2 Ma (Sharp & Snoke, 1988) and a suspect in-situ U-Pb zircon secondary ion mass spectrometry (SIMS) age from the sample analysed for this project (3A-24) of 89.9 ± 9.5 Ma obtained from micro-zircons of <10 μm diameter (Schmitt et al., 2010; K.R. Chamberlain, pers. comm., 2010). The former age is considered inaccurate due to: (a) the emplacement of the Tobago plutonic suite approximately 500 m from the sample site, which might partially reset the Ar-Ar system and (b) the evidence for dynamic lower greenschist-facies metamorphism of the North Coast Schist which might also affect the ability of the hornblende crystal lattices to retain their magmatic Ar concentrations. The second age has a large error of 10.6 % and there is clear field evidence for a thermal aureole generated by emplacement of the

Tobago plutonic suite (Snoke et al., 2001a,b) which indicates that the North Coast Schist as a whole must be older than the Albian Volcano-Plutonic Suite. The meaning of this young age remains the subject of discussion with K.R. Chamberlain and A.W. Snoke, but it is unlikely to represent a true protolith age. It is possible to both grow new zircon and alter pre-existing zircons at relatively low temperatures in the greenschist facies so the apparent age generated by the SIMS analysis may be somewhat misleading (Hay & Dempster, 2009).

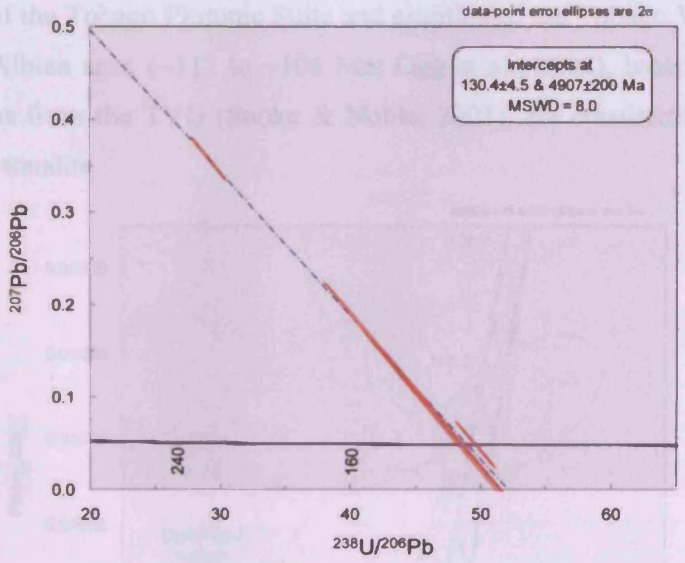

Figure 4.5. Tera-Wasserberg plot for sample 3A-24 (basaltic andesite), Parlatuvier Formation, North Coast Schist, Tobago.

Sample 2D-50 from the Arnos Vale-Mason Hall tonalite: In this sample, the zircon with the lowest radiogenic to common Pb ratio gave a slightly discordant age (Table 4.1; see the concordia plot - Fig. 4.6) which was rejected on the grounds of possible Pb loss. Therefore an age was calculated using four remaining analysed zircons which were concordant (Fig. 4.6), giving a weighted mean of $^{206}Pb/^{238}U$ age models of 105.83 ± 0.17 Ma (MSWD = 2.0).

No other geochronological data is available for the tonalite body. However, there are ages for the gabbro-diorite pluton which the tonalite cross-cuts (Section 2.2.1; Sharp & Snoke, 1988; G.J.H. Oliver, 1990, unpublished data). The previously-obtained zircon U-Pb age for the pluton is 104 ± 1 Ma (G.J.H. Oliver, 1990, unpublished data) and the hornblende Ar-Ar ages are 102.9 ± 1.5 Ma and 104.7 ± 1.6 Ma (Sharp & Snoke, 1988), all slightly younger than the new age for the tonalite. As: (a) there is a

clear cross-cutting relationship demonstrated for the tonalite against the Tobago Plutonic Suite; (b) the new CA-ID-TIMS date uses the most up-to date methodology; (c) previous Ar-Ar dating may be subject to Ar loss and protracted cooling of the pluton and (d) the previous U-Pb age is based on an older methodology which was likely to have contained different calibrations; the newly obtained age of 105.83 ± 0.17 Ma for the tonalite is accepted as the most reliable age of crystallisation. The tonalite is therefore roughly contemporaneous with, but should slightly post-date, the emplacement of the Tobago Plutonic Suite and eruption of the Tobago Volcanic Group. Early to Mid-Albian ages (~112 to ~106 Ma; Ogg et al., 2008), based on ammonites and radiolarians from the TVG (Snoke & Noble, 2001), are consistent with the ~106 Ma age for the tonalite.

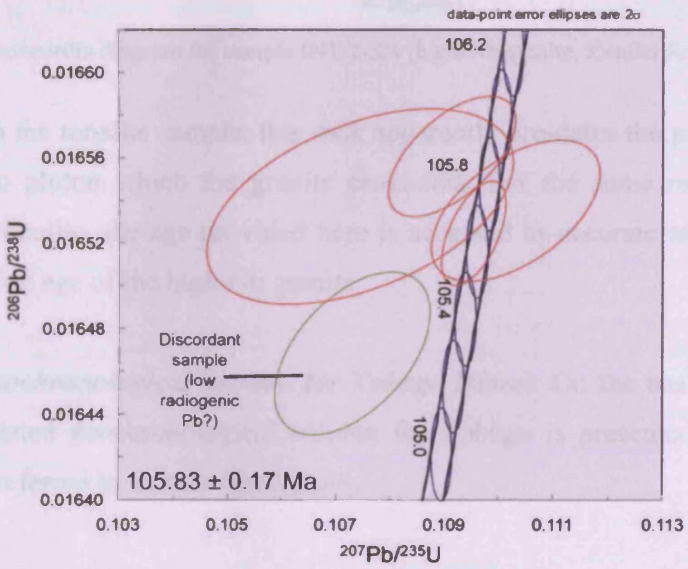

Figure 4.6. U-Pb concordia diagram for sample 2D-50 (Arnos Vale-Mason Hall tonalite body).

Sample INT/1-3/4 from the high-Nb granite body of Kendal Road: Two zircon grains gave $^{206}Pb/^{238}U$ model ages of approximately 620 Ma (Table 4.1). These were rejected as possible inherited grains, for which the geological significance is uncertain. Alternatively these grains are the result of laboratory contamination, either from the selFrag electronic disaggregation or electromagnetic separation in Freiberg, or the CA-ID-TIMS dating process at NIGL (Appendix 3). The remaining three analysed grains were concordant and gave a weighted mean of $^{206}Pb/^{238}U$ age models of 106.24 ± 0.16 Ma with MSWD = 1.7 (Table 4.1, Fig. 4.7).

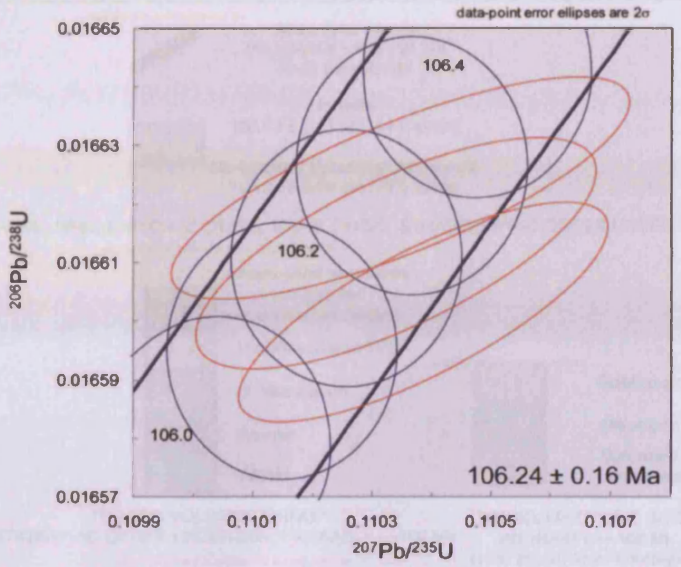

Figure 4.7. U-Pb concordia diagram for sample INT/1-3/4 (high-Nb granite, Kendal Road, Tobago).

As with the tonalite sample, this rock apparently pre-dates the pre-existing ages for the Tobago pluton which the granite cross-cuts. For the same reasons as given above for the tonalite, the age provided here is accepted as accurate and indicative of the crystallisation age of the high-Nb granite.

New geochronological column for Tobago Island: On the basis of these new results, an updated geochronological column for Tobago is presented in Figure 4.8 which may be referred to in later discussions.

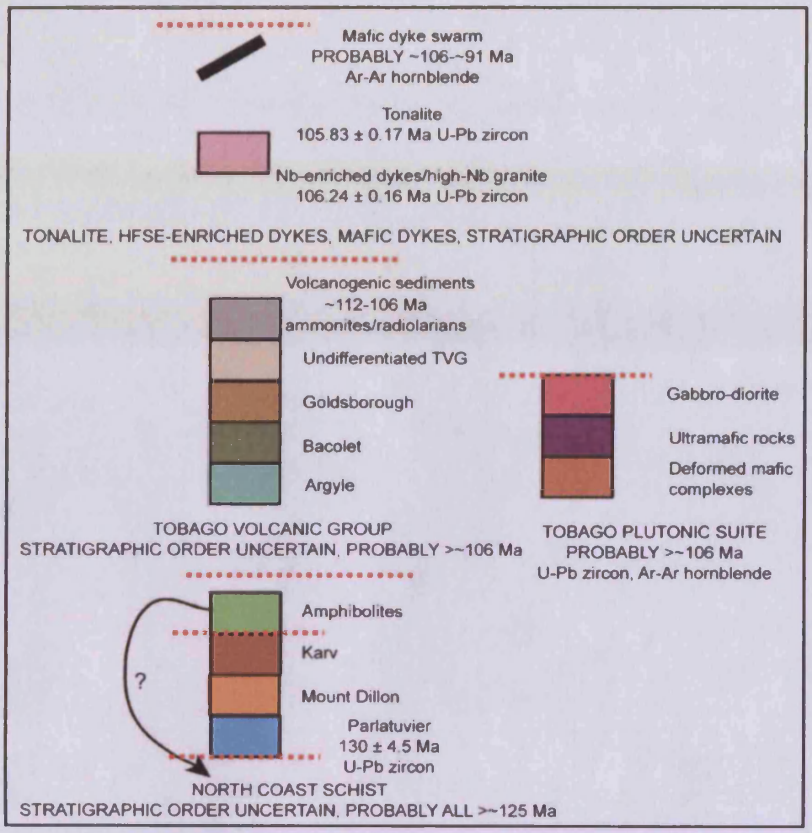

Figure 4.8. A new geochronological column for Tobago Island based on the new U-Pb ages provided by this study and the previous results outlined in Section 2.2.1 and references therein. There is uncertainty over the age of the amphibolite facies rocks as some of these rocks have an N-MORB-like chemical signature. The map of Snoke et al. (2001b) suggests these are the youngest rocks of the North Coast Schist, but the MORB-like chemistry would be more consistent with them pre-dating the more arc-like Parlatuvier and Mount Dillon Formations. See Section 5.3 for a discussion of the geochemical features of the North Coast Schist.

Table 4.1. CA-ID-TIMS U-Pb results for 3 zircon fractions from the NCS (3A-24), Arnos Vale-Mason Hall tonalite (2D-50) and high-Nb granite (INT/1-3/4), Tobago.

		Compositional Parameters						**Radiogenic Isotope Ratios**								**Isotopic Age**	
Sample	Wt. mg	$\frac{Th}{U}$	$^{206}Pb^*$ x10^{-13} mol	mol % $^{206}Pb^*$	$\frac{Pb^*}{Pb_c}$	Pb_c (pg)	$\frac{^{206}Pb}{^{204}Pb}$	$\frac{^{208}Pb}{^{206}Pb}$	$\frac{^{207}Pb}{^{206}Pb}$	% err	$\frac{^{207}Pb}{^{235}U}$	% err	$\frac{^{206}Pb}{^{238}U}$	% err	corr. coef.	$\frac{^{206}Pb}{^{238}U}$	±
(a)	(b)	(c)	(d)	(d)	(d)	(d)	(e)	(f)	(f)	(g)	(f)	(g)	(f)	(g)		(h)	(g)
3A-24																	
z1	0.100	0.510	0.0226	79.26%	1	0.49	89	0.160	0.047787	14.160	0.136045	14.341	0.020648	0.456	0.409	131.84	0.59
z2	0.100	0.493	0.0214	74.19%	1	0.61	72	0.173	0.053980	17.199	0.154119	17.386	0.020707	0.561	0.347	132.21	0.73
z3	0.100	0.562	0.0658	95.26%	6	0.27	390	0.179	0.048533	1.563	0.134803	1.659	0.020144	0.179	0.578	128.66	0.23
z5	0.100	0.950	0.0490	57.02%	0	3.04	43	0.317	0.051126	7.220	0.149136	7.362	0.021156	1.090	0.203	135.03	1.46
2D-50																	
z1	0.100	0.579	0.0727	93.97%	5	0.38	307	0.181	0.047122	2.060	0.107445	2.153	0.016537	0.225	0.458	105.82	0.24
z2	0.100	0.443	0.1727	93.03%	4	1.06	266	0.139	0.047254	1.000	0.107299	1.082	0.016469	0.189	0.505	105.39	0.20
z3	0.100	0.431	0.2296	97.57%	12	0.47	763	0.137	0.047796	0.806	0.109137	0.881	0.016561	0.138	0.599	105.97	0.14
z4	0.100	0.484	0.2256	98.69%	23	0.25	1415	0.154	0.048079	0.389	0.109543	0.445	0.016525	0.121	0.570	105.74	0.13
z5	0.100	0.280	0.0737	96.08%	7	0.25	472	0.090	0.048384	1.071	0.110309	1.149	0.016535	0.163	0.534	105.82	0.17
INT/1-3/4																	
z1	0.100	1.096	1.1755	99.69%	112	0.30	5882	0.341	0.060316	0.113	0.833799	0.202	0.100261	0.111	0.898	616.00	0.65
z2	0.100	2.282	0.5265	99.07%	47	0.41	1981	0.729	0.048145	0.220	0.110346	0.284	0.016623	0.093	0.776	106.30	0.10
z3	0.100	2.082	1.0019	99.64%	120	0.30	5152	0.666	0.048223	0.168	0.110385	0.229	0.016602	0.092	0.774	106.18	0.10
z4	0.100	2.177	0.9070	99.56%	99	0.33	4208	0.696	0.048175	0.192	0.110339	0.249	0.016612	0.097	0.713	106.23	0.10
z5	0.100	0.889	0.5569	99.36%	52	0.30	2874	0.278	0.061082	0.196	0.855980	0.268	0.101637	0.126	0.728	624.06	0.75

(a) z1, z2 etc. are labels for fractions composed of single zircon grains or fragments; all fractions annealed and chemically abraded after Mattinson (2005).

(b) Nominal fraction weights estimated from photomicrographic grain dimensions, adjusted for partial dissolution during chemical abrasion.

(c) Model Th/U ratio calculated from radiogenic $^{208}Pb/^{206}Pb$ ratio and $^{207}Pb/^{235}U$ age.

(d) Pb* and Pbc represent radiogenic and common Pb, respectively; mol % $^{206}Pb^*$ with respect to radiogenic, blank and initial common Pb.

(e) Measured ratio corrected for spike and fractionation only. Daly analyses, based on analysis of NBS-981 and NBS-982.

(f) Corrected for fractionation, spike, and common Pb; up to 1 pg of common Pb was assumed to be procedural blank: $^{206}Pb/^{204}Pb = 18.60 \pm 0.80\%$; $^{207}Pb/^{204}Pb = 15.69 \pm 0.32\%$; $^{208}Pb/^{204}Pb = 38.51 \pm 0.74\%$ (all uncertainties 1-sigma). Excess over blank was assigned to initial common Pb.

(g) Errors are 2-sigma, propagated using the algorithms of Schmitz & Schoene (2007) and Crowley et al. (2007).

(h) Calculations are based on the decay constants of Jaffey et al. (1971). $^{206}Pb/^{238}U$ and $^{207}Pb/^{206}Pb$ ages corrected for initial disequilibrium in $^{230}Th/^{238}U$ using Th/U [magma] = 3.

4.3.2. Major and trace element geochemistry of the North Coast Schist

Element mobility and geochemical trends: Samples from the Parlatuvier, Amphibolite and Karv units have LOI values of between 1 and 6 wt.% implying that there has been some alteration of these rocks, possibly involving slight calcification (Appendix 5). The very quartz-rich Mount Dillon Formation has LOI values of <1 wt.% showing that although these rocks may have been silicified, they do not contain significant proportions of clay or calcite.

A variety of elements from each formation are plotted against Nb to test elemental mobility in the same manner as the mafic volcanic complex on La Désirade (Fig. 4.9). All units show significant scatter for SiO_2, MgO, CaO, Na_2O, K_2O, Sr and Ba vs. Nb, implying that these elements have been mobilised to varying degrees. Sc, TiO_2 and Al_2O_3 show reasonably coherent trends within individual formations, with different formations showing different trends. This observation points to limited mobility of Sc, Ti and Al. The REE, Th and Zr have different gradients of positive slope against Nb for the different units. The trends for the Mount Dillon and Karv formations are similar to each other but distinct from the trends shown for the Parlatuvier Formation and most of the amphibolites. One sample from the amphibolite-facies rocks plots consistently within the field of the Mount Dillon and Karv formations on the REE and Th plots. This may indicate that some of the amphibolites have a different source compared to the other units as well as a higher grade of metamorphism, whereas others are similar geochemically to the North Coast Schist. The fact that there are largely formation-dependent trends shown for the REE, Th and Zr indicates immobility of the elements in question and also that there may be different magmatic sources for some of these units. The possible exceptions are shown on the Yb and Zr vs. Nb plots (Fig. 9) where there is no obvious trend for the Parlatuvier Formation. Given the coherent trends shown for the subduction-mobile LREE and MREE (La and Sm), the lack of a trend against Nb for Zr and Yb may be related to variations in source chemistry. The incompatible trace element trends are very similar for Karv and the Mount Dillon Formation which lends weight to the observations of Yule (1988) that the two may be genetically related but have been structurally separated.

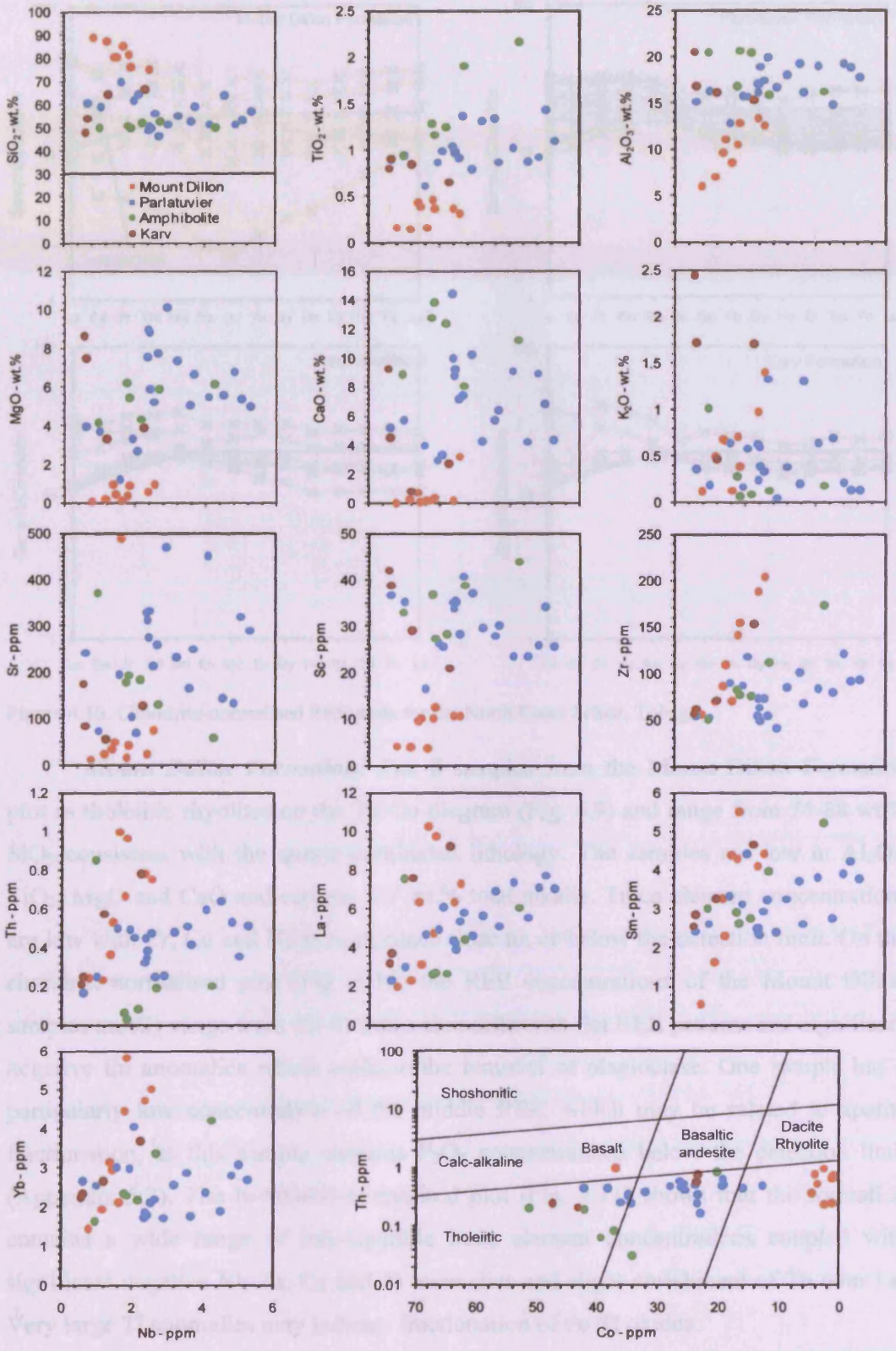

Figure 4.9. Element vs. Nb and Th-Co plots for the North Coast Schist of Tobago.

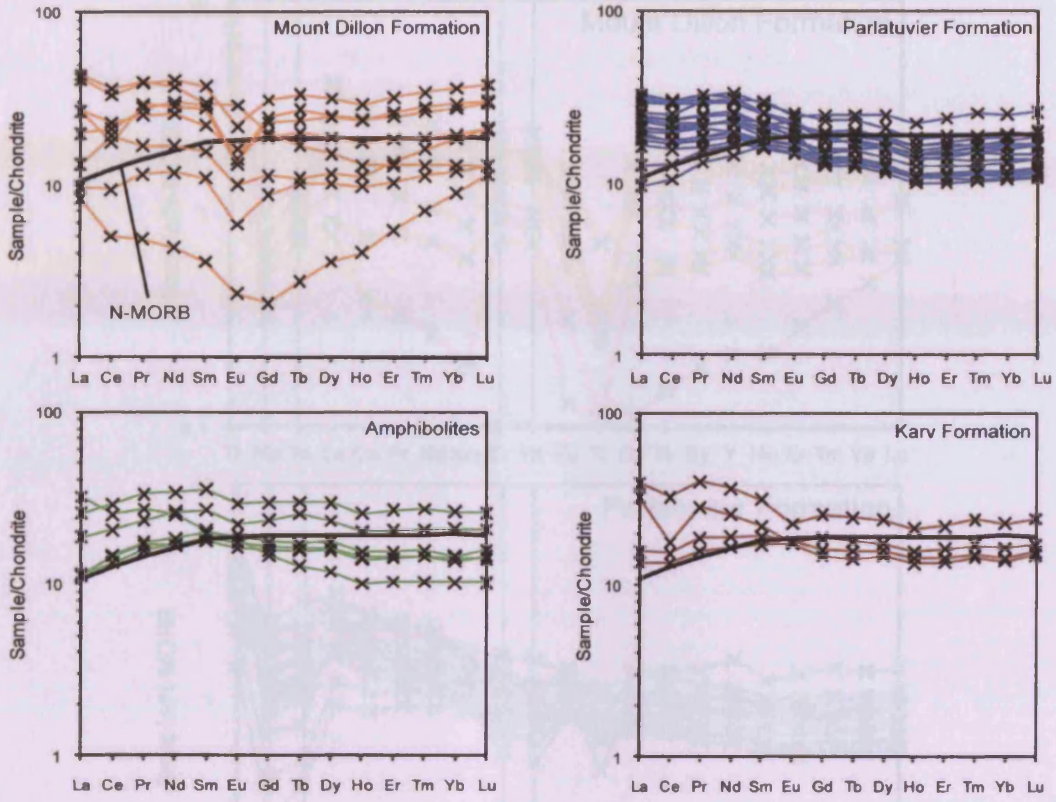

Figure 4.10. Chondrite-normalised REE plots for the North Coast Schist, Tobago.

Mount Dillon Formation: The 8 samples from the Mount Dillon Formation plot as tholeiitic rhyolites on the Th-Co diagram (Fig. 4.9) and range from 74-88 wt.% SiO_2 consistent with the quartz-dominated lithology. The samples are low in Al_2O_3, TiO_2, MgO and CaO and contain 3-7 wt.% total alkalis. Trace element concentrations are low with Cr, Co and Ni in most cases close to, or below the detection limit. On the chondrite-normalised plot (Fig. 4.10) the REE concentrations of the Mount Dillon samples mostly range from 10-40 times chondrite with flat REE patterns and significant negative Eu anomalies which indicate the removal of plagioclase. One sample has a particularly low concentration of the middle REE, which may be related to apatite fractionation, as this sample contains P_2O_5 concentrations below the detection limit (Appendix 5.2). The N-MORB-normalised plot (Fig. 4.11) shows that the formation contains a wide range of incompatible trace element concentrations coupled with significant negative Nb-Ta, Ce and Ti anomalies and slight enrichment of Th over La. Very large Ti anomalies may indicate fractionation of Fe-Ti oxides.

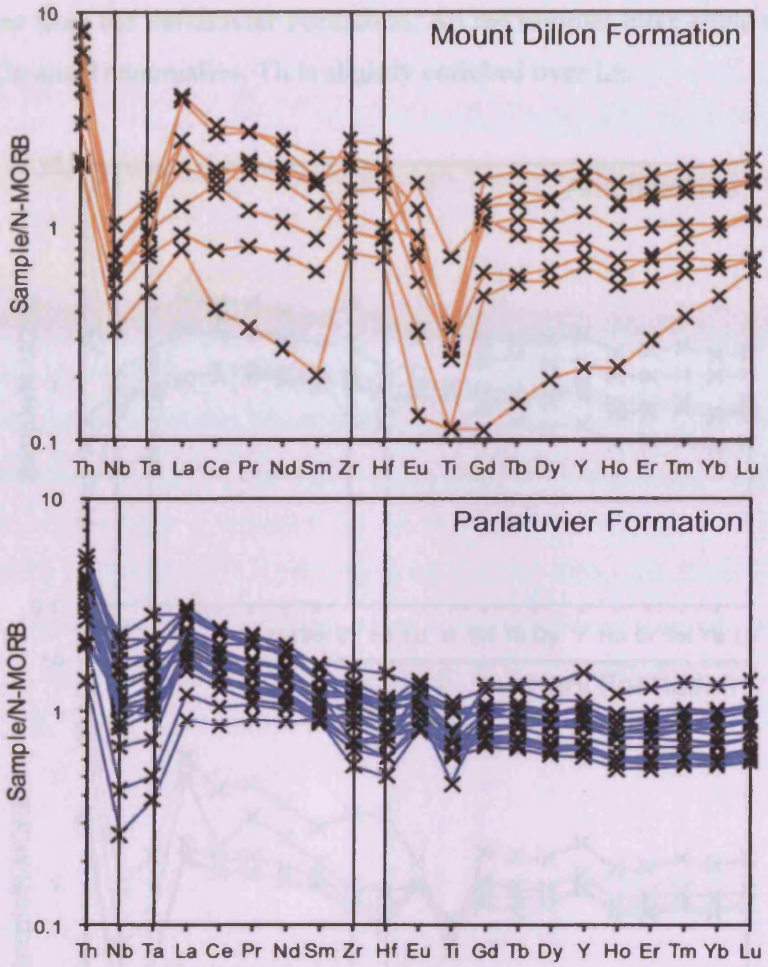

Figure 4.11. N-MORB-normalised trace element plots for the Mount Dillon and Parlatuvier Formations, North Coast Schist, Tobago.

Parlatuvier Formation: Nineteen samples were analysed from the Parlatuvier Formation and they range from tholeiitic basalts to tholeiitic basaltic andesites on the Th-Co diagram (Fig. 4.9). Major element concentrations are variable, with SiO_2 = 44-69 wt.%, Al_2O_3 = 13-19 wt.%, TiO_2 = 0.6-1.4 wt.%, 1-10 wt.% MgO and 3-6 wt.% total alkalis. These results are indicative of the degree of major element alteration suggested by the element vs. Nb plots (Fig. 4.9). Trace element concentrations are also quite variable with 13-446 ppm Cr, 12-222 ppm Ni, 0-900 ppm Ba and 100-500 ppm Sr. The Parlatuvier Formation shows a very uniform chondrite-normalised pattern which lies at 10-30 times chondrite with no Eu anomalies (Fig. 4.10). Although several samples are slightly depleted in the LREE, most have slightly LREE-enriched patterns. The N-MORB normalised plot (Fig. 4.11) also displays the slight LREE-enrichment for

most samples from the Parlatuvier Formation. All the samples have slight negative Nb-Ta, Zr-Hf, Ce and Ti anomalies. Th is slightly enriched over La.

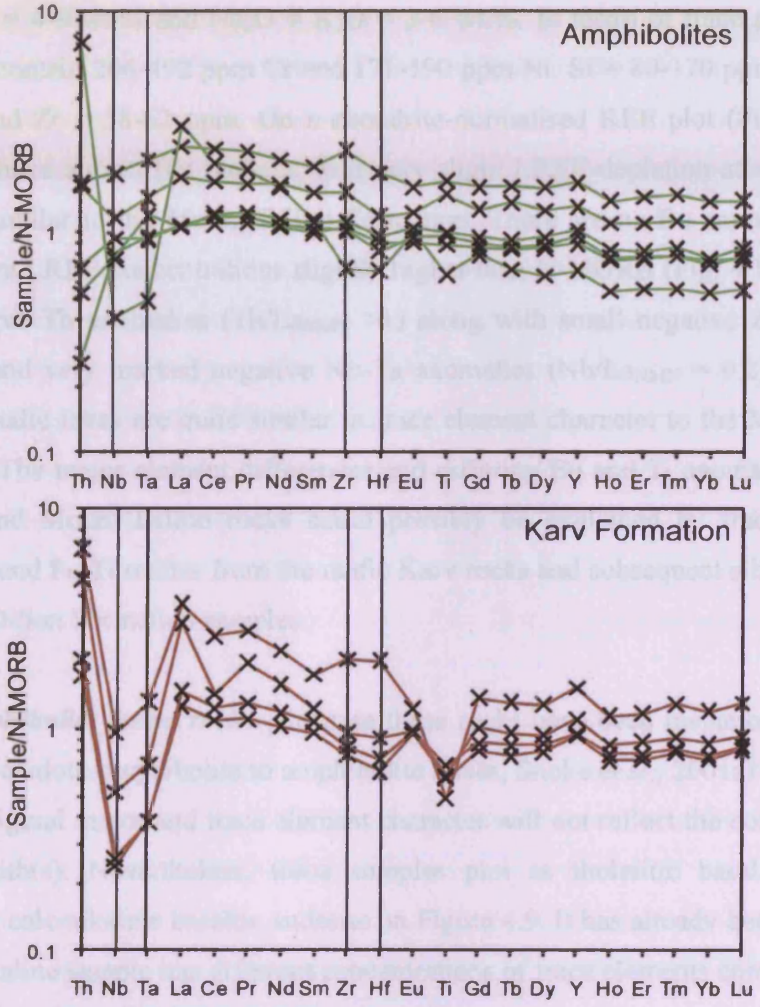

Figure 4.12. N-MORB-normalised trace element plots for the amphibolite unit and the Karv Formation, North Coast Schist, Tobago.

Karv: The rocks of the Karv unit are defined as "argillite with interlayered silicic metatuff... ...[and] includes rock types... similar to... ...the Mount Dillon Formation" (Snoke et al., 1995). Four samples were analysed, two of which (DY-3D-304 and 305) appear to be metamorphosed plagioclase-phyric lavas, whereas the other two (DY-3D-693 and 448) are dark, slaty or crenulated pyrite-rich rocks which are more like metamorphosed argillites. According to the Th-Co diagram the two meta-lavas are tholeiitic basalts (Fig. 4.9). The argillaceous rocks plot as tholeiitic basaltic andesites, indicating their relatively mafic character, but will not be considered further.

Compared to the Mount Dillon Formation, the collected lavas are quite mafic and no silicic meta-tuff was analysed. The mafic lavas have major element concentrations as follows: SiO_2 = 46-52 wt.%, TiO_2 = 0.8-0.9 wt.%, Al_2O_3 = 16-20 wt.%, MgO = 7-8 wt.%, CaO = 4-9 wt.% and $Na_2O + K_2O$ = 3-6 wt.%. In terms of trace elements, the meta-lavas contain 206-492 ppm Cr and 171-190 ppm Ni. Sr = 80-170 ppm, Ba = 700-900 ppm and Zr = 58-62 ppm. On a chondrite-normalised REE plot (Fig. 4.10), the meta-lavas have almost flat patterns with very slight LREE-depletion at ~13-19 times chondrite, similar to the Mount Dillon Formation. There are no Eu anomalies. These samples have LREE concentrations slightly higher than N-MORB (Fig. 4.12) and show slight positive Th anomalies (Th/La_{NMN} >1) along with small negative Zr-Hf and Ti anomalies and very marked negative Nb-Ta anomalies (Nb/La_{NMN} = 0.2). Therefore, these two mafic lavas are quite similar in trace element character to the Mount Dillon Formation. The major element differences and differing Eu and Ti anomalies between the Karv and Mount Dillon rocks could possibly be explained by fractionation of plagioclase and Fe-Ti oxides from the mafic Karv rocks and subsequent silicification of the Mount Dillon Formation samples.

Amphibolite facies rocks: Because these rocks have been metamorphosed to a high grade (epidote-amphibolite to amphibolite facies, Snoke et al., 2001a) it is possible that their original major and trace element character will not reflect the composition of their protolith(s). Nevertheless, these samples plot as tholeiitic basalts with one exception, a calc-alkaline basaltic andesite on Figure 4.9. It has already been noted that this calc-alkaline sample has different concentrations of trace elements compared to the other samples. The tholeiites contain relatively consistent concentrations of major elements: SiO_2 = 48-52 wt.%, TiO_2 = 0.9-2.1 wt.%, Al_2O_3 = 16-20 wt.%, MgO = 4-6 wt.%, CaO = 9-13 wt.%, $Na_2O + K_2O$ = 2-5 wt.%. These amphibolites have 66-138 ppm Ni and 43-322 ppm Cr, as high as the Parlatuvier and Karv formations. The samples also have mostly low concentrations of Ba (30-410 ppm) and Sr (60-370 ppm) and variable amounts of Zr (51-174 ppm). On a chondrite-normalised plot (Fig. 4.10), the meta-basaltic samples have flat to very slightly LREE-depleted patterns at 10-30 times chondrite; the more calc-alkaline rock has a sloping REE pattern with LREE enrichment which looks unlike any other rock from the North Coast Schist with the possible exception of the mafic lavas from the Karv formation. The N-MORB-normalised plot (Fig. 4.12) shows that, with the exception of the more calc-alkaline

rock the samples have flat patterns with compositions similar to N-MORB, no significant anomalies, and very slight depletion in Th, Nb-Ta and La compared to the other elements. The calc-alkaline sample has a very large negative Nb-Ta anomaly, enrichment in Th/La and slight negative Zr-Hf and Ti anomalies on the N-MORB-normalised plot (Fig. 4.12). Texturally, the one calc-alkaline sample is still an amphibolite with large (relict) plagioclase crystals like some of the other amphibolites, despite its very different chemistry. This finding may be significant; because it suggests that the thermal aureole, between the greenschist-facies country rocks of the NCS and the ultramafic pluton of the Tobago Plutonic Suite, overprinted at least two different types of protolith. Firstly, some of the amphibolites may be tholeiitic MORB-like basalts and secondly, some may be calc-alkaline rocks with a similar trace element geochemistry to the Mount Dillon or Karv formations. Sampling of further localities might have yielded amphibolites of a similar bulk composition to the Parlatuvier Formation but this is not apparent in the analysed rocks.

4.3.3. Major and trace element geochemistry of the Tobago Volcanic Group

Elemental mobility and geochemical trends: All 5 formations overlap compositionally on each element vs. Nb plot and where trends are seen, the formations all define the same trend (Fig. 4.13). Some of the major elements, for example CaO, K_2O and Na_2O have very scattered patterns when plotted against Nb which indicate that those elements are likely to have mobilised during alteration. Some broad trends can be distinguished within the major elements, for example a tendency to decreasing CaO, Al_2O_3 and MgO with increasing Nb, most likely relating to fractional crystallisation of such phases as clinopyroxene and plagioclase. Of the trace elements, Ba and Sr both define positive slopes against Nb which are scattered, indicating some mobility of those elements. The HFSE such as Th and Zr have tightly clustered positive correlations against Nb which pass through the origin, as do the REE (e.g. La, Sm and Yb). Sc has a very steep, well-defined negative slope when plotted against Nb.

The compositional overlap between the samples from different formations along similar element vs. Nb trends supports the hypothesis that all the formations in the Tobago Volcanic Group formed by magmatic differentiation of a consistent parental magma source composition. The incompatible element vs. Nb trends (e.g. La vs. Nb,

Fig. 4.13) all pass through the origin, and no other trends are obvious for any given element, so contamination of the TVG magmas with other magma types is unlikely to have occurred. The samples may therefore all be representative of a constantly replenished source with within-formation trends linked by fractional crystallisation processes. The falling Al_2O_3, MgO, CaO and Sc vs. Nb trends probably relate to fractional crystallisation of clinopyroxene and plagioclase. The samples which contain very low concentrations of Al_2O_3 and Nb and very high concentrations of MgO (as high as 21 wt.%) appear to be those carrying plagioclase-free clinopyroxene cumulate loads. Therefore, this study has confirmed the initial suggestion of Frost & Snoke (1989) that the TVG represents a suite of rocks formed by the fractional crystallisation of plagioclase and clinopyroxene. As there is little evidence in any basaltic TVG samples for the presence of olivine, none of these rocks are likely to represent primary magmas.

Argyle Formation: The lavas of the Argyle Formation (5 samples) plot mostly as tholeiitic basaltic andesites on the Th-Co diagram (Fig. 4.13). Most of the samples contain 51-59 wt.% SiO_2, 0.6-0.9 wt.% TiO_2, 15-19 wt.% Al_2O_3, 3-6 wt.% MgO, 8-10 wt.% CaO and 4-5 wt.% $Na_2O + K_2O$. They have 18-800 ppm Ni, 12-120 ppm Cr, 58-71 ppm Zr, 300-800 ppm Ba and 350-400 ppm Sr. On a chondrite-normalised plot (Fig. 4.14) most rocks of the Argyle Formation have gently sloping, LREE-enriched patterns at 10-30 times chondrite, with a slightly concave HREE pattern ($Ho/Lu_{CN} < 1$) and no Eu anomalies. The N-MORB-normalised plot (Fig. 4.15) shows that these samples are quite enriched in Th ($Th/La_{NMN} > 1$) and have negative Nb-Ta, Ce, Zr-Hf and Ti anomalies, with the Nb-Ta anomalies particularly pronounced ($Nb/La_{NMN} = 0.1\text{-}0.2$).

One other sample is part of the Argyle Formation, but is very different compositionally. INT/8-3/7 has a very similar pattern on the normalised plots to the other samples, but is extremely depleted (1-2 times chondrite on Fig. 4.14) and has large Nb-Ta and Zr-Hf anomalies on the N-MORB-normalised plot (Fig. 4.15). It contains much less TiO_2 (0.1 wt.%), Al_2O_3 (1 wt.%) and total alkalis compared to the other samples, with SiO_2 (50 wt.%) similar to the other samples. However, INT/8-3/7 also contains 21 wt.% MgO, 19 wt.% CaO, 2334 ppm Cr (at just 260 ppm Ni) and very low concentrations of other trace elements including Ba and Sr. The sample has not been thin sectioned, but the geochemical analysis and the hand specimen appears to be consistent with an origin as a clinopyroxene cumulate.

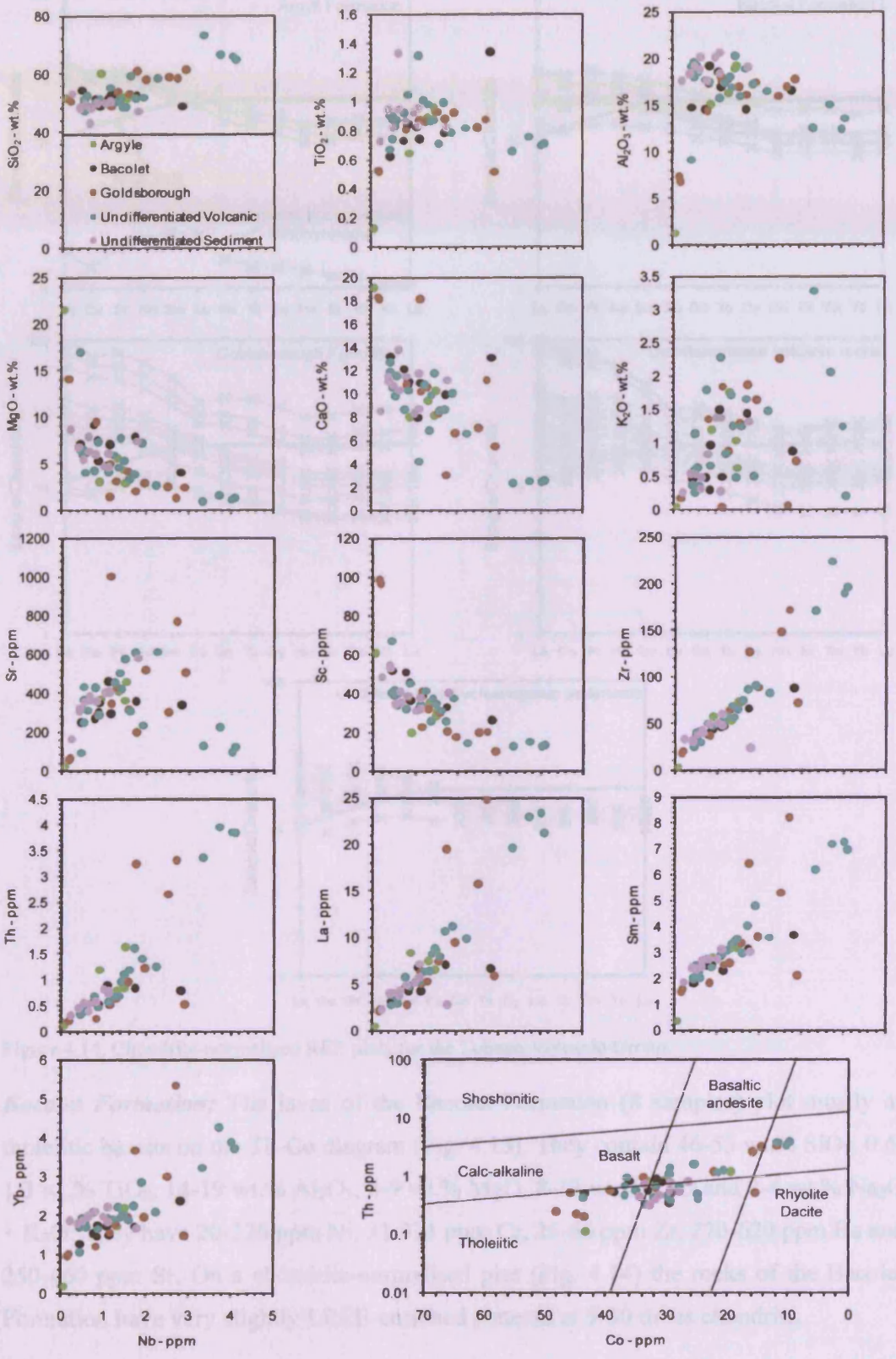

Figure 4.13. Element vs. Nb and Th-Co plots for the Tobago Volcanic Group.

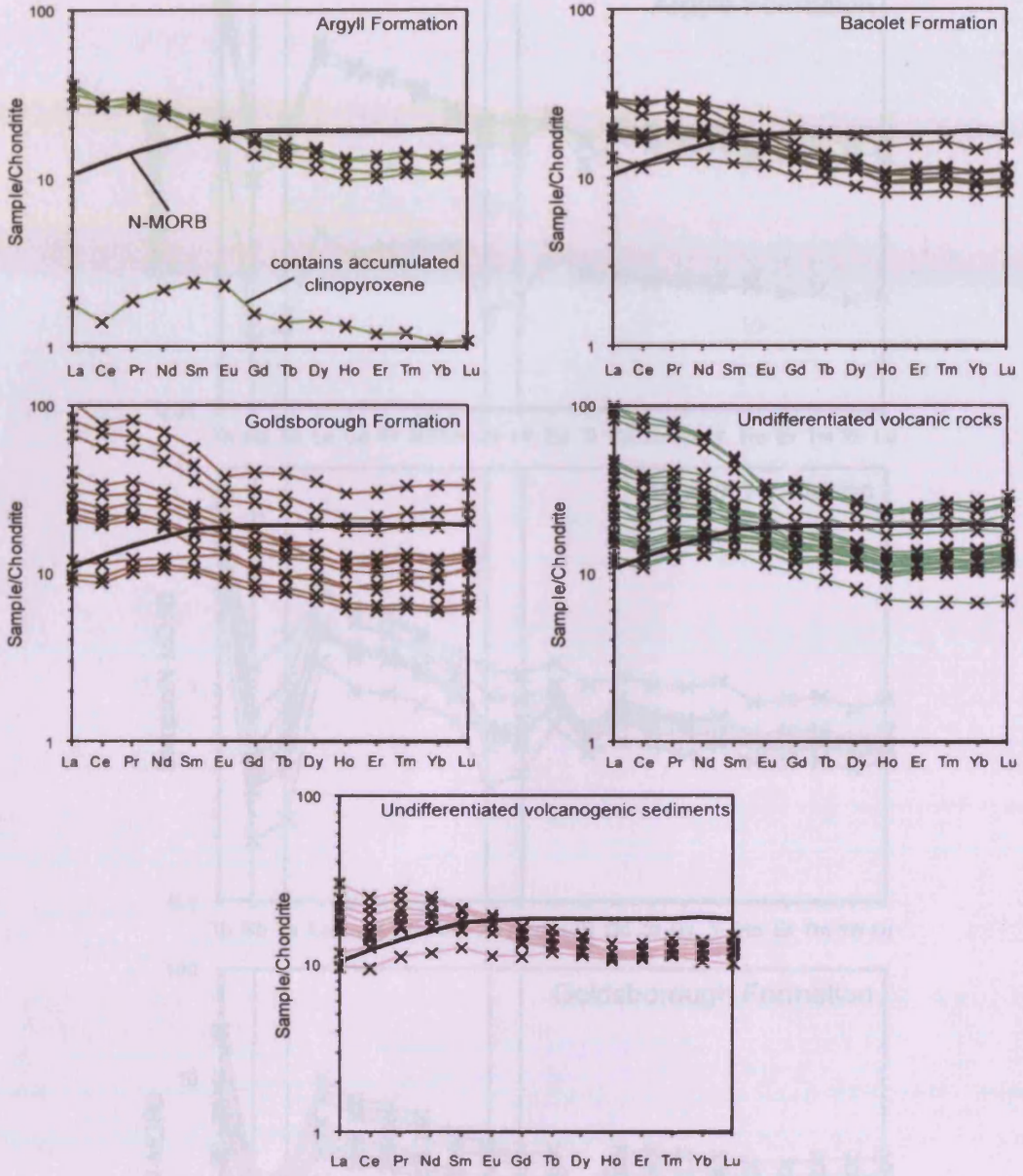

Figure 4.14. Chondrite-normalised REE plots for the Tobago Volcanic Group.

Bacolet Formation: The lavas of the Bacolet Formation (8 samples) plot mostly as tholeiitic basalts on the Th-Co diagram (Fig. 4.13). They contain 46-53 wt.% SiO_2, 0.6-1.3 wt.% TiO_2, 14-19 wt.% Al_2O_3, 4-9 wt.% MgO, 8-13 wt.% CaO and 2-4 wt.% Na_2O + K_2O. They have 20-320 ppm Ni, 31-371 ppm Cr, 25-66 ppm Zr, 270-620 ppm Ba and 250-460 ppm Sr. On a chondrite-normalised plot (Fig. 4.14) the rocks of the Bacolet Formation have very slightly LREE-enriched patterns at 9-30 times chondrite,

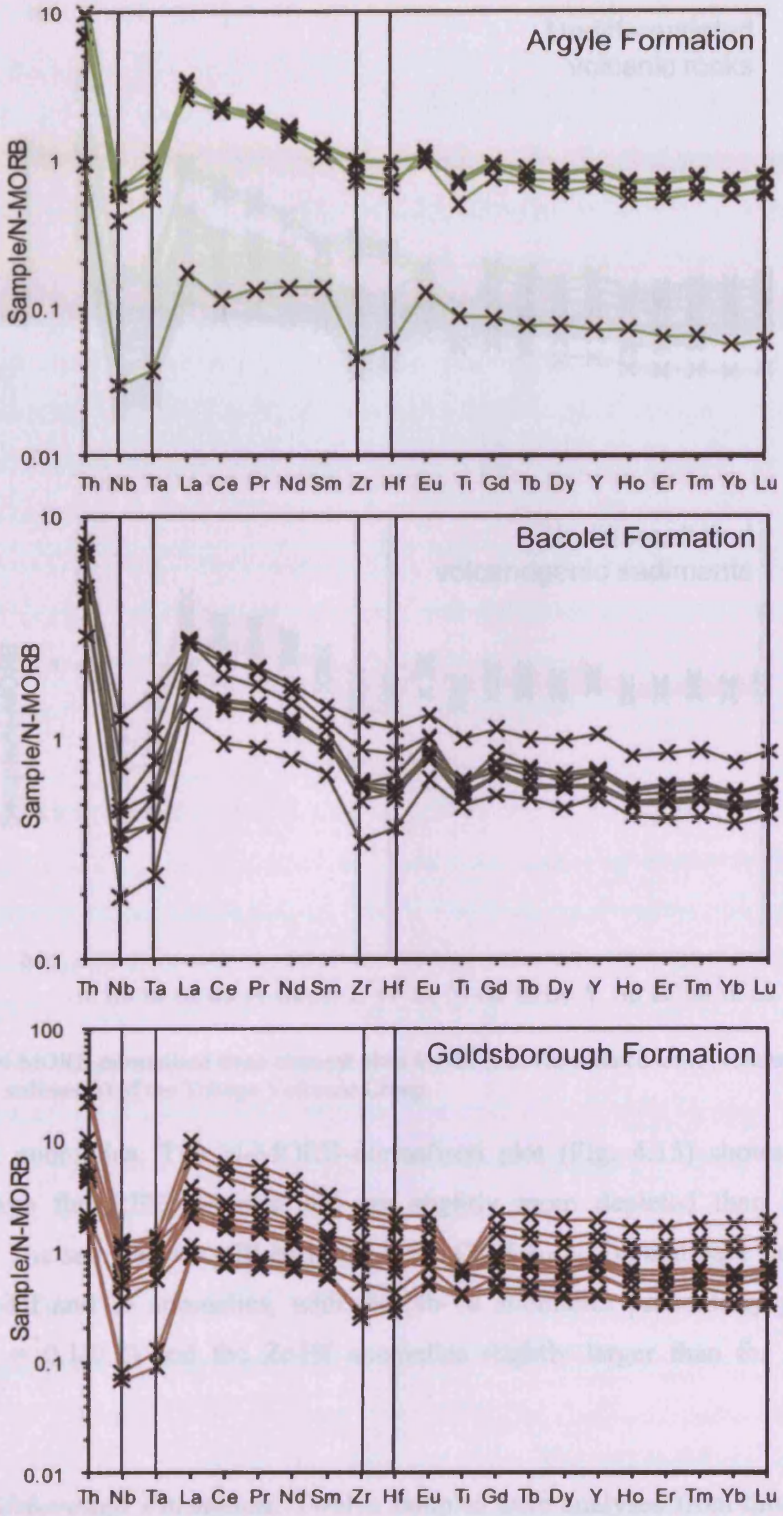

Figure 4.15. N-MORB-normalised trace element plots for the Argyll, Bacolet and Goldsborough Formations of the Tobago Volcanic Group.

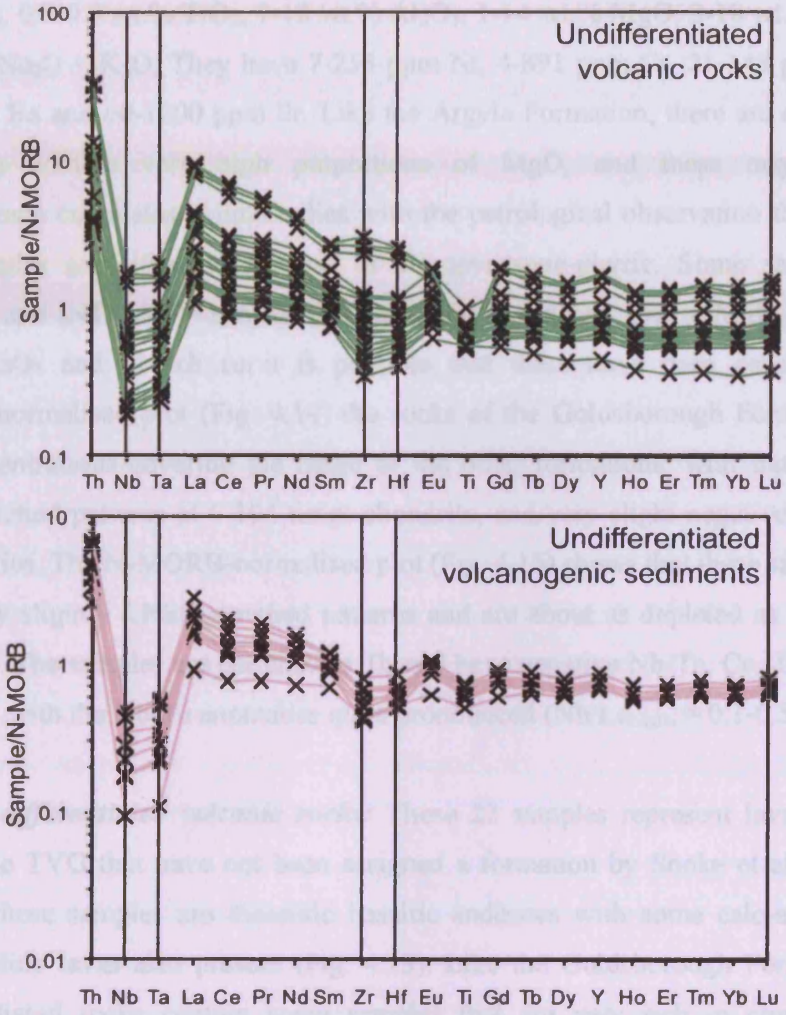

Figure 4.16. N-MORB-normalised trace element plots for the Undifferentiated units (volcanic rocks and volcanogenic sediments) of the Tobago Volcanic Group.

and no Eu anomalies. The N-MORB-normalised plot (Fig. 4.15) shows that these samples have flat REE patterns and are slightly more depleted than the Argyle Formation. The samples are still enriched in Th (Th/La_{NMN} >1) and have negative Nb-Ta, Ce, Zr-Hf and Ti anomalies, with the Nb-Ta anomalies particularly pronounced (Nb/La_{NMN} = 0.1-0.2) and the Zr-Hf anomalies slightly larger than for the Argyle Formation.

Goldsborough Formation: Twelve samples were analysed from this formation. These rocks are quite differentiated, ranging from tholeiitic basalts to more rhyolitic and calc-alkaline rocks on the Th-Co diagram, and completely encompassing compositions of the other formations of the TVG (Fig. 4.13). The lavas contain 49-60

wt.% SiO_2, 0.5-0.9 wt.% TiO_2, 7-18 wt.% Al_2O_3, 1-14 wt.% MgO, 3-18 wt.% CaO and 1-7 wt.% Na_2O + K_2O. They have 7-255 ppm Ni, 4-891 ppm Cr, 21-148 ppm Zr, 10-1000 ppm Ba and 60-1000 ppm Sr. Like the Argyle Formation, there are examples of rocks that contain very high proportions of MgO, and these may represent clinopyroxene cumulates, which tallies with the petrological observation that many of these samples are either plagioclase or clinopyroxene-phyric. Some samples (e.g. INT/8-3/1 and INT/4-3/1 – see Appendices 2 and 5) are very low in MgO but are also Fe_2O_3-, CaO- and Sr-rich so it is possible that these have been calcified. On a chondrite-normalised plot (Fig. 4.14) the rocks of the Goldsborough Formation have REE concentrations covering the range of the other formations, with flat to slightly LREE-enriched patterns at 6-104 times chondrite, and very slight negative or positive Eu anomalies. The N-MORB-normalised plot (Fig. 4.15) shows that these samples have flat to very slightly LREE-enriched patterns and are about as depleted as the Bacolet Formation. The samples are enriched in Th and have negative Nb-Ta, Ce, Zr-Hf and Ti anomalies, with the Nb-Ta anomalies quite pronounced (Nb/La_{NMN} = 0.1-0.5).

Undifferentiated volcanic rocks: These 22 samples represent lavas from the parts of the TVG that have not been assigned a formation by Snoke et al (2001a,b). Many of these samples are tholeiitic basaltic andesites with some calc-alkaline and more rhyolitic lavas also present (Fig. 4.13). Like the Goldsborough Formation, the undifferentiated rocks contain some samples that are very rich in clinopyroxene, leading to high MgO concentrations. Others have low MgO but high CaO, suggesting some degree of calcification. Nonetheless, the major element concentrations are as follows: 46-66 wt.% SiO_2, 0.7-1.3 wt.% TiO_2, 9-20 wt.% Al_2O_3, 2-17 wt.% MgO, 4-13 wt.% CaO and 2-7 wt.% Na_2O + K_2O. They also contain 14-440 ppm Ni, 6-963 ppm Cr, 25-224 ppm Zr, 60-1750 ppm Ba and 90-610 ppm Sr. On a chondrite-normalised plot (Fig. 4.14) the undifferentiated rocks have flat to very slightly LREE-enriched or depleted patterns at 11-50 times chondrite, and only very slight negative or positive Eu anomalies. Four samples, which were quite felsic in character, have more LREE-enriched patterns with La at 80-100 times chondrite. The N-MORB-normalised plot (Fig. 4.16) shows that most samples have flat to very slightly LREE-enriched patterns and have a similar level of depletion to the Bacolet and Goldsborough Formations. The four samples that are more LREE-enriched have small positive Zr-Hf anomalies. The majority of the Undifferentiated samples are enriched in Th and have negative Nb-Ta,

Ce, Zr-Hf and Ti anomalies, with the Nb-Ta anomalies particularly pronounced (Nb/La_{NMN} = 0.1-0.2).

Volcaniclastic sediments: The volcaniclastic rocks which form part of the undifferentiated part of the TVG include 11 samples mostly consisting of volcaniclastic breccias. Despite the features indicative of sedimentary re-working described in Section 3.2, many have relatively low LOI values (<5 wt.%) and coherent immobile trace element geochemical signatures (e.g. REE patterns, Fig. 4.14) despite obvious oxidation and weathering. These samples contain 42-50 wt.% SiO_2, 0.7-1.3 wt.% TiO_2, 17-20 wt.% Al_2O_3, 10-11 wt.% Fe_2O_3(t), 5-8 wt.% MgO, 8-12 wt.% CaO and 3-5 wt.% $Na_2O + K_2O$. They have 10-85 ppm Ni, 15-200 ppm Cr, 24-60 ppm Zr, 70-570 ppm Ba and 160-580 ppm Sr. The volcanogenic rocks have REE patterns that are mostly flat or very slightly LREE-enriched at 11-24 times chondrite (Fig. 4.14). On the N-MORB-normalised plot (Fig. 4.6) the volcaniclastic sediments show enrichment in Th and negative Nb-Ta, Ce, Zr-Hf and Ti anomalies like the other formations. The negative Nb-Ta anomalies in the volcaniclastic sediments are also very similar to the other formations (Nb/La_{NMN} = 0.1-0.2).

4.3.4. Major and trace element geochemistry of the Tobago Pluton

Elemental mobility and geochemical trends: Relatively few samples were analysed from the plutonic rocks as existing field and geochemical evidence indicates fractional crystallisation processes dominate the magmatic history of the pluton. This becomes a problem for understanding petrogenetic processes as, unlike in the TVG, many samples are cumulates of olivine or pyroxene so it was difficult to collect representative samples in the field. Also, as can be seen from the analytical error (Appendix 4) and results tables (Appendix 5), the ultramafic and mafic cumulate rocks are particularly depleted in some trace elements such as the REE and HFSE. Many elements are present in concentrations which approach or fall below the limit of detection rendering petrogenetic interpretation of the plutonic rocks difficult. Nevertheless, a representative suite of major and trace elements are plotted against Nb in order to discern the degree of sub-solidus element mobilisation and the possible nature of magmatic differentiation processes in the plutonic rocks. In this case, Ni and Cr are also plotted to assess potential trends relating in particular to olivine and

clinopyroxene differentiation in the ultramafic rocks. The Th-Co diagram was not designed with for plutonic rocks, so is omitted (Hastie et al., 2007).

On Figure 4.17 it can be seen that the ultramafic rocks contain generally lower concentrations of Nb than the gabbro-diorite, and the deformed mafic volcanic-plutonic complexes contain similar compatible and incompatible element concentrations to the gabbro-diorite. The ultramafic rocks have low concentrations of Al_2O_3 and Sr and high MgO, Sc, Ni and Cr which form trends with a similar slope to the least-differentiated gabbro-diorites and deformed mafic rocks. In accordance with the petrological information (Snoke et al., 2001a and references therein) it is therefore considered that the ultramafic rocks are related to the gabbro-diorites by accumulation of clinopyroxene and olivine (particularly high MgO, Sc, Ni and Cr) and the removal of plagioclase (low Al_2O_3 and Sr). There is a single trend for Zr, Th and the REE (Fig. 4.17) with slight overlap for the ultramafic rocks, gabbro-diorites and deformed mafic rocks indicating that all three rock suites may be derived from a similar source.

It was noted in Chapter 3.2 that the Arnos Vale-Mason Hall tonalite body had sharp contacts with the surrounding gabbro-diorite and did not appear to contain any gabbroic enclaves or transitional facies of an intermediate composition between diorite and tonalite. This feature was interpreted as meaning that the tonalite was not necessarily genetically related to the rest of the pluton. Tonalite analyses are also added to Figure 4.17. If the tonalite formed by differentiation of the gabbro-diorites, the diorite might be expected to continue fractionating hornblende and clinopyroxene, leaving quartz, plagioclase, biotite and hornblende to make up the tonalite. The element vs. Nb plots show that the tonalites have no trends which link with the gabbro-diorites. Incompatible REE, Th and Zr trends for the gabbro-diorite and the tonalite have different slopes indicative of different magmatic sources. Therefore, the tonalite was not formed from the gabbro-diorite by fractional crystallisation and the two rock types do not appear to have a common source.

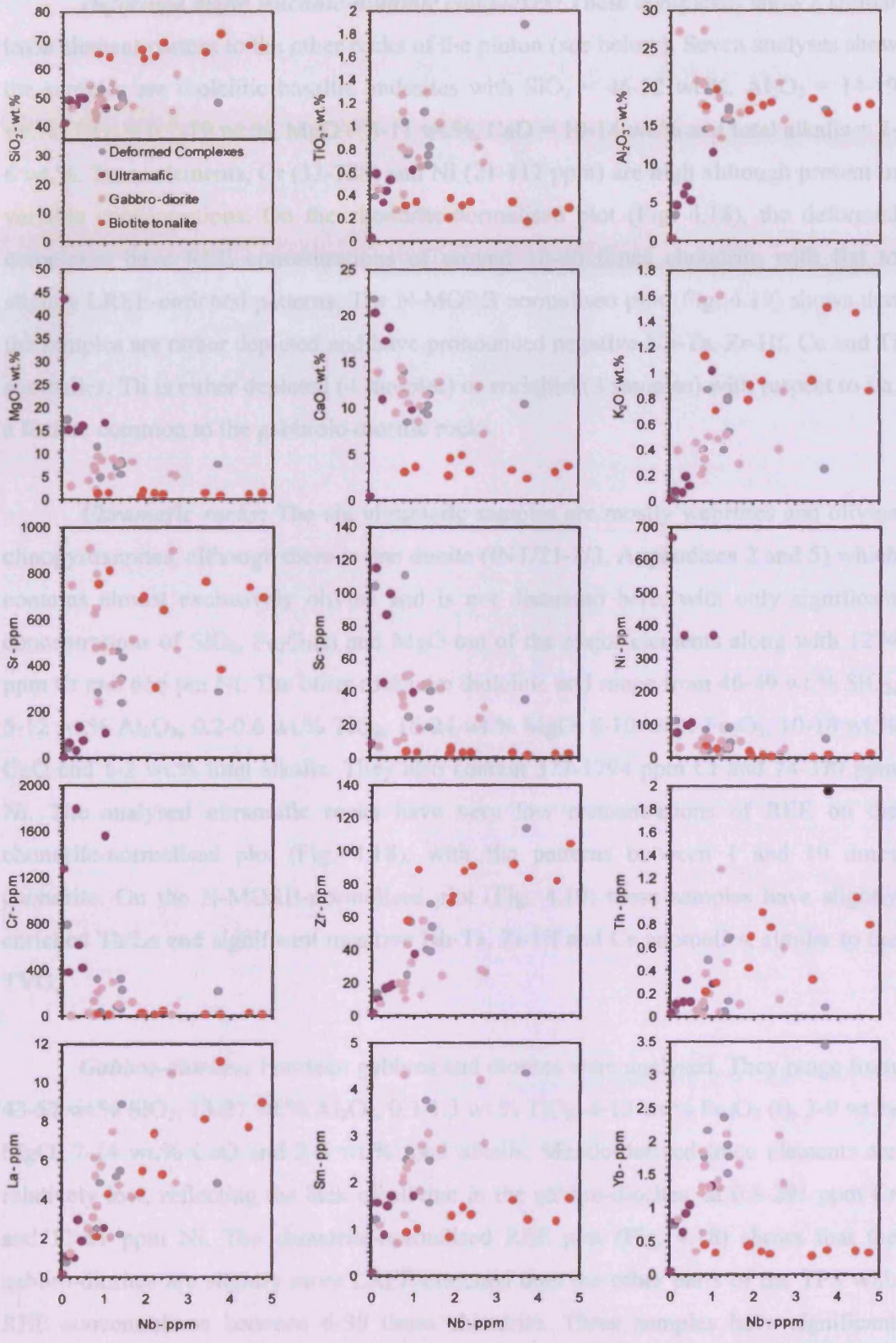

Figure 4.17. Element vs. Nb plots for the plutonic rocks of Tobago.

Deformed mafic volcanic-plutonic complexes: These complexes show a similar trace element pattern to the other rocks of the pluton (see below). Seven analyses show the samples are tholeiitic basaltic andesites with SiO_2 = 46-52 wt.%, Al_2O_3 = 14-19 wt.%, TiO_2 = 0.7-19 wt.%, MgO = 5-11 wt.%, CaO = 10-14 wt.% and total alkalis = 2-6 wt.%. Trace elements, Cr (33-788) and Ni (21-112 ppm) are high although present in variable concentrations. On the chondrite-normalised plot (Fig. 4.18), the deformed complexes have REE concentrations of around 10-40 times chondrite with flat to slightly LREE-enriched patterns. The N-MORB normalised plot (Fig. 4.19) shows that the samples are rather depleted and have pronounced negative Nb-Ta, Zr-Hf, Ce and Ti anomalies. Th is either depleted (4 samples) or enriched (3 samples) with respect to La, a feature common to the gabbroic-dioritic rocks.

Ultramafic rocks: The six ultramafic samples are mostly wehrlites and olivine clinopyroxenites, although there is one dunite (INT/21-2/3, Appendices 2 and 5) which contains almost exclusively olivine and is not discussed here, with only significant concentrations of SiO_2, Fe_2O_3(t) and MgO out of the major elements along with 1274 ppm Cr and 666 pm Ni. The other rocks are tholeiitic and range from 46-49 wt.% SiO_2, 5-12 wt.% Al_2O_3, 0.2-0.6 wt.% TiO_2, 16-24 wt.% MgO, 8-10 wt.% Fe_2O_3, 10-18 wt.% CaO and 1-2 wt.% total alkalis. They also contain 377-1794 ppm Cr and 74-370 ppm Ni. The analysed ultramafic rocks have very low concentrations of REE on the chondrite-normalised plot (Fig. 4.18), with flat patterns between 1 and 10 times chondrite. On the N-MORB-normalised plot (Fig. 4.19) these samples have slightly enriched Th/La and significant negative Nb-Ta, Zr-Hf and Ce anomalies, similar to the TVG.

Gabbro-diorites: Fourteen gabbros and diorites were analysed. They range from 43-57 wt.% SiO_2, 13-27 wt.% Al_2O_3, 0.3-1.3 wt.% TiO_2, 4-13 wt.% Fe_2O_3 (t), 3-9 wt.% MgO, 7-14 wt.% CaO and 2-6 wt.% total alkalis. Mantle-derived trace elements are relatively low, reflecting the lack of olivine in the gabbro-diorites, at 0.8-291 ppm Cr and 12-61 ppm Ni. The chondrite-normalised REE plot (Fig. 4.18) shows that the gabbro-diorites are slightly more LREE-enriched than the other parts of the TPS with REE concentrations between 6-30 times chondrite. Three samples have significant positive Eu anomalies which may be due to the accumulation of plagioclase. The N-MORB-normalised plot for these rocks (Fig. 4.19) is almost identical to the deformed

complexes and to the Goldsborough Formation of the TVG, with negative Nb-Ta, Zr-Hf and Ce anomalies and five samples with depleted Th/La and the rest with enriched Th/La.

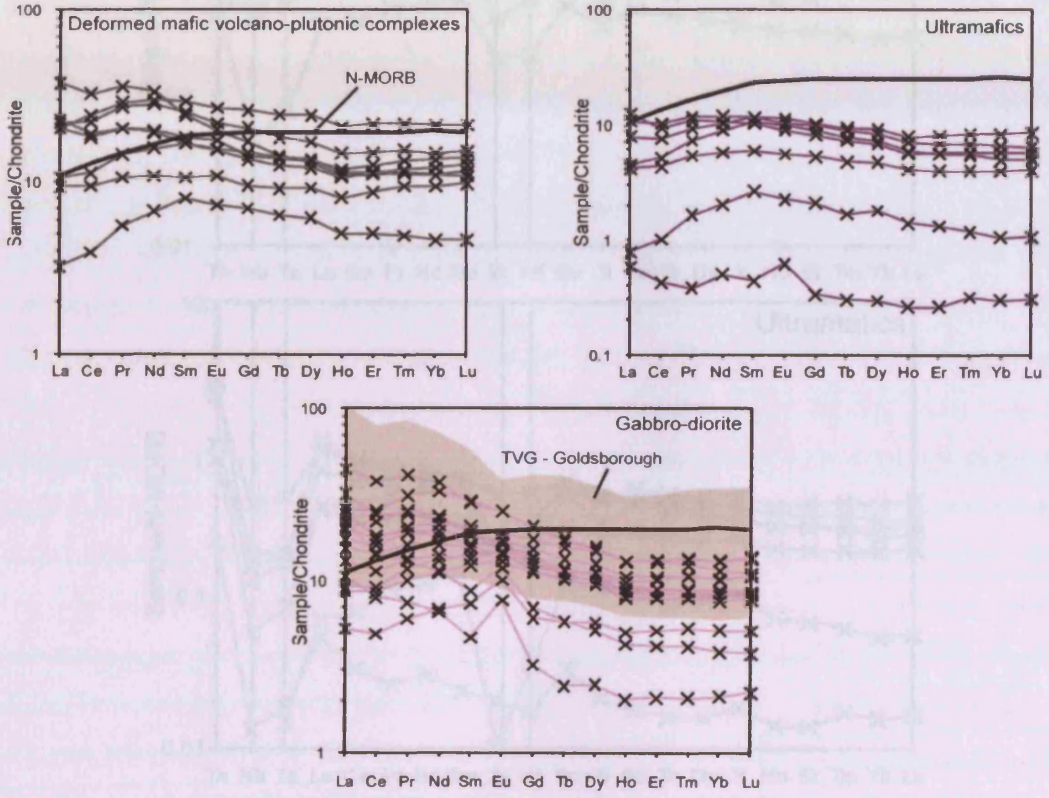

Figure 4.18. Chondrite-normalised REE plots for the Tobago Plutonic Suite. The Goldsborough Formation of the TVG is underlain on the gabbro-diorite field to demonstrate the similarity between the two relatively evolved units.

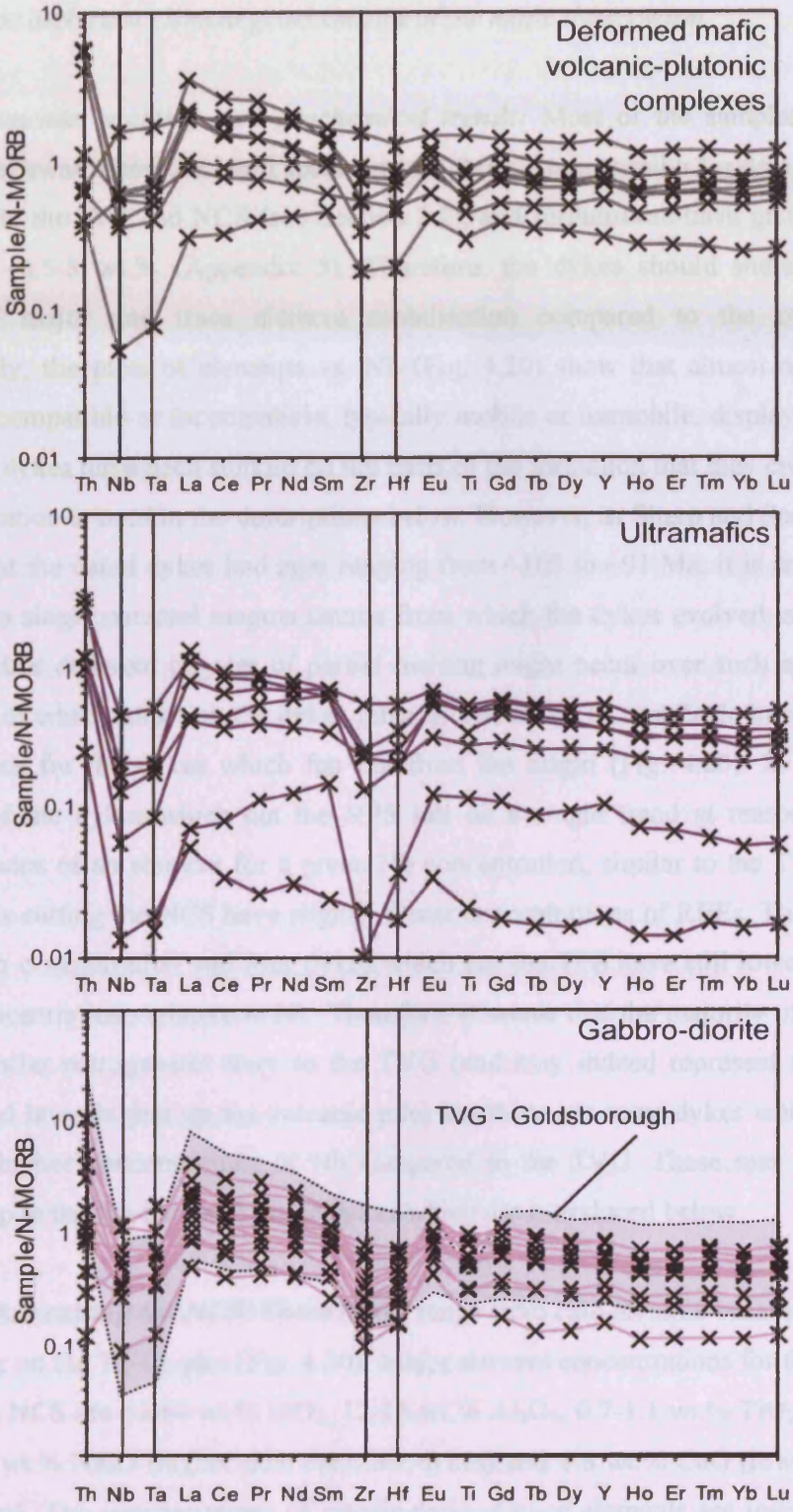

Figure 4.19. N-MORB-normalised trace element plots for the Tobago Plutonic Suite. Field for the TVG Goldsborough Formation is for comparison.

4.3.5. Major and trace element geochemistry of the mafic dyke swarm

Elemental mobility and geochemical trends: Most of the samples from the mafic dykes swarm have, in hand specimen and thin section, similar levels of alteration compared to the TPS and NCS (see Section 3.2), and furthermore have quite low LOI values of ~0.5-3 wt.% (Appendix 5). Therefore, the dykes should share the same pattern of major and trace element mobilisation compared to the other units. Interestingly, the plots of elements vs. Nb (Fig. 4.20) show that almost none of the elements, compatible or incompatible, typically mobile or immobile, display a singular trend. The dykes have been split up on the basis of the formation that they cross-cut and this designation is used in the descriptions below. However, as Sharp and Snoke (1988) showed that the dated dykes had ages ranging from ~103 to ~91 Ma, it is unlikely that there was a single parental magma source from which the dykes evolved, and magma mixing and/or different degrees of partial melting might occur over such a timescale, regardless of which rock unit the dykes intrude. The REE, Th and Zr do however show broad trends for the dykes which fan out from the origin (Fig. 4.20). In detail, the majority of the dykes which cut the VPS fall on a single trend at reasonably high concentrations of an element for a given Nb concentration, similar to the TVG. Those dykes cross-cutting the NCS have slightly lower concentrations of REEs, Th and Zr for a given Nb concentration and four dykes which cut the TPS have still lower REE, Th and Zr concentrations relative to Nb. Therefore, it seems that the majority of the dykes have a similar petrogenetic story to the TVG (and may indeed represent feeders for now-eroded lavas higher up the volcanic pile) but there are some dykes which contain relatively higher concentrations of Nb compared to the TVG. These may bear some relationship to the Nb-enriched mafic dykes which are introduced below.

Dykes cutting the NCS: These dykes range from calc-alkaline basaltic andesites to rhyolites on the Th-Co plot (Fig. 4.20). Major element concentrations for those dykes cutting the NCS are 54-64 wt.% SiO_2, 12-16 wt.% Al_2O_3, 0.7-1.1 wt.% TiO_2, 2-6 wt.% MgO, 4-5 wt.% Na_2O (higher than the other dykes) and 4-8 wt.% CaO (lower than the other dykes). The concentrations of mantle-derived trace elements are lower than the other dykes with 40-349 ppm Cr and 39-123 ppm Ni. Ba (100-200 ppm) and Sr (100-400 ppm) are also lower than the other dykes. Despite these differences the dykes that

cut the NCS show almost identical REE (Fig. 4.21) and trace element profiles (Fig. 4.22) to the other dykes on the normalised plots, with Th, Nb-Ta and Ti anomalies.

Dykes cutting the VPS: These tholeiitic-calc-alkaline dykes display a wide range of compositions, from basalts to basaltic andesites to dacites (Fig. 4.20). Major element concentrations for these dykes are: 48-55 wt.% SiO_2, 13-18 wt.% Al_2O_3, 0.7-1.7 wt.% TiO_2, 4-15 wt.% MgO. The dykes contain similar levels of alkalis to the TVG. Trace element concentrations for these dykes include 0-1349 ppm Cr, 10-328 ppm Ni, 100-1100 ppm Ba and 200-600 ppm Sr. On the chondrite-normalised REE plots (Fig. 4.21), the dykes cutting the TPS and TVG have patterns ranging from slightly LREE-enriched to LREE-depleted at 10-60 times chondrite. The N-MORB-normalised trace element plot (Fig. 4.22) shows that the dykes have slight Th/La enrichment, large negative Nb-Ta and Ti anomalies and mostly negative Zr-Hf anomalies with some positive anomalies. The HREE patterns are flat and there is a range of LREE concentrations from LREE-enriched to flat patterns.

4.3.6. Major and trace element geochemistry of the dyke-like tonalite of Arnos Vale-Mason Hall

The 105.83 ± 0.17 Ma tonalite body is distinct from the other plutonic units in having a wholly siliceous character (Section 3.2, Appendices 2 and 5). Plots of major and trace elements against Nb show scatter for Na_2O and K_2O and to a lesser extent for SiO_2, Sr and Ba (Fig. 4.17). This indicates that these elements may have been mobilised during sub-solidus alteration and/or weathering. Nevertheless, clear trends for MgO, the REE, Zr, Th and Y on Figure 4.17, along with LOI values of <2 wt.% indicate that these rocks are not badly altered and that the elements commonly considered to be immobile, (along with SiO_2, MgO, Al_2O_3, Ba and Sr which do not show badly scattered trends on Fig. 4.17), may be used to assess the petrogenesis of the tonalite. Furthermore, the consistent trends vs. Nb which pass through the origin indicate that the rocks of the tonalite are representative of a single magmatic suite and may be linked by differentiation processes (Fig. 4.17 above). There is no clear evidence for magma mixing or contamination from other sources either geochemically or in the field. As discussed above, the tonalite does not have the same slope of incompatible trace

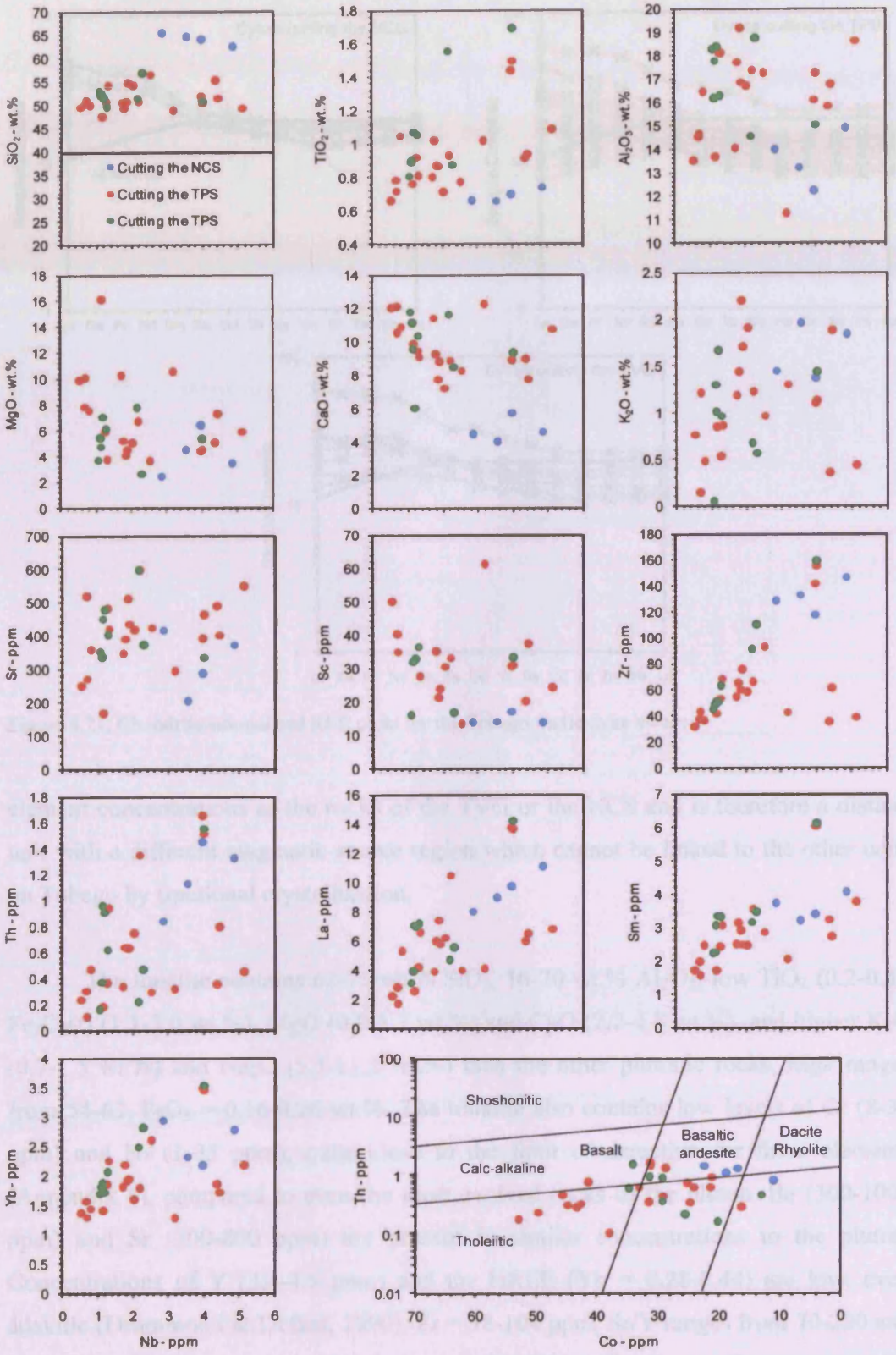

Figure 4.20. Element vs. Nb and Th-Co plots for the mafic dyke swarm of Tobago.

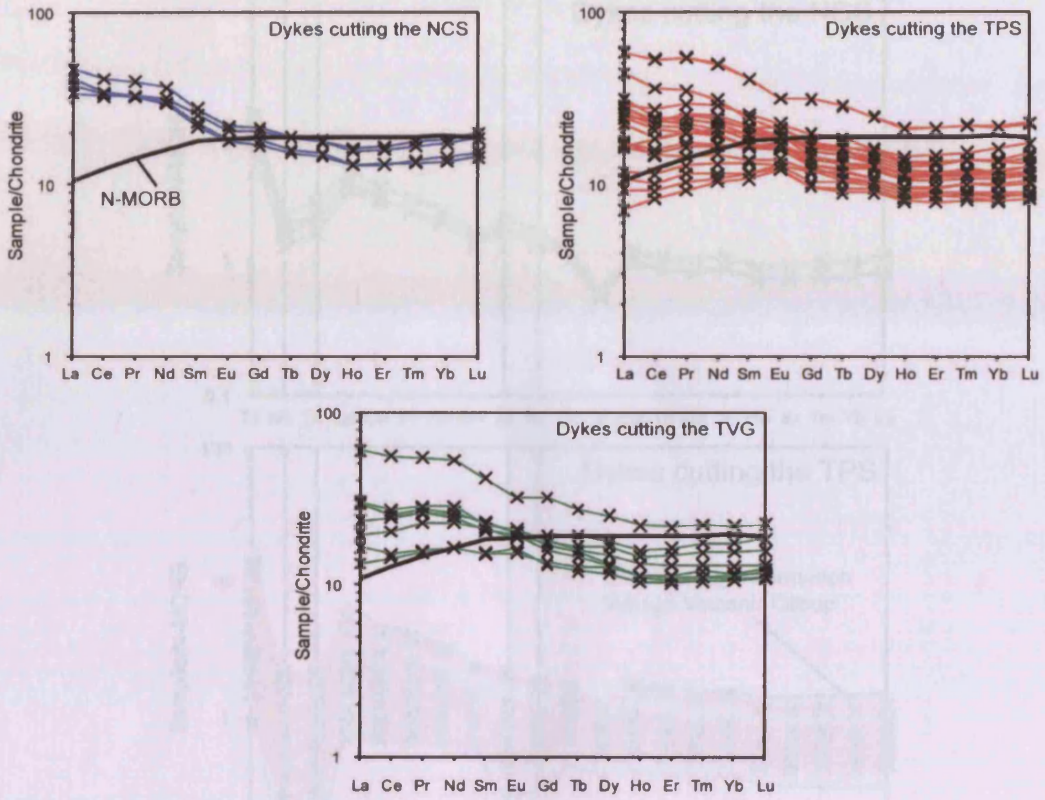

Figure 4.21. Chondrite-normalised REE plots for the Tobago mafic dyke swarm.

element concentrations as the rocks of the TVG or the NCS and is therefore a distinct unit with a different magmatic source region which cannot be linked to the other units on Tobago by fractional crystallisation.

The tonalite contains 62-71 wt.% SiO_2, 16-20 wt.% Al_2O_3, low TiO_2 (0.2-0.4), Fe_2O_3(t) (1.1-3.0 wt.%), MgO (0.8-1.7 wt.%) and CaO (2.2-4.8 wt.%), and higher K_2O (0.7-1.5 wt.%) and Na_2O (5.5-11.2 wt.%) than the other plutonic rocks. Mg# ranges from 54-63. P_2O_5 = 0.16-0.26 wt.%. The tonalite also contains low levels of Cr (8-39 ppm) and Ni (1-35 ppm), quite close to the limit of detection for these elements (Appendix 4), compared to even the most evolved rocks of the pluton. Ba (300-1000 ppm) and Sr (300-800 ppm) are present in similar concentrations to the pluton. Concentrations of Y (3.4-4.5 ppm) and the HREE (Yb = 0.28-0.44) are low, even adakitic (Drummond & Defant, 1990). Zr = 58-104 ppm, Sr/Y ranges from 70-220 and La/Yb from 5-30. On a chondrite-normalised plot (Fig. 4.23), the tonalites

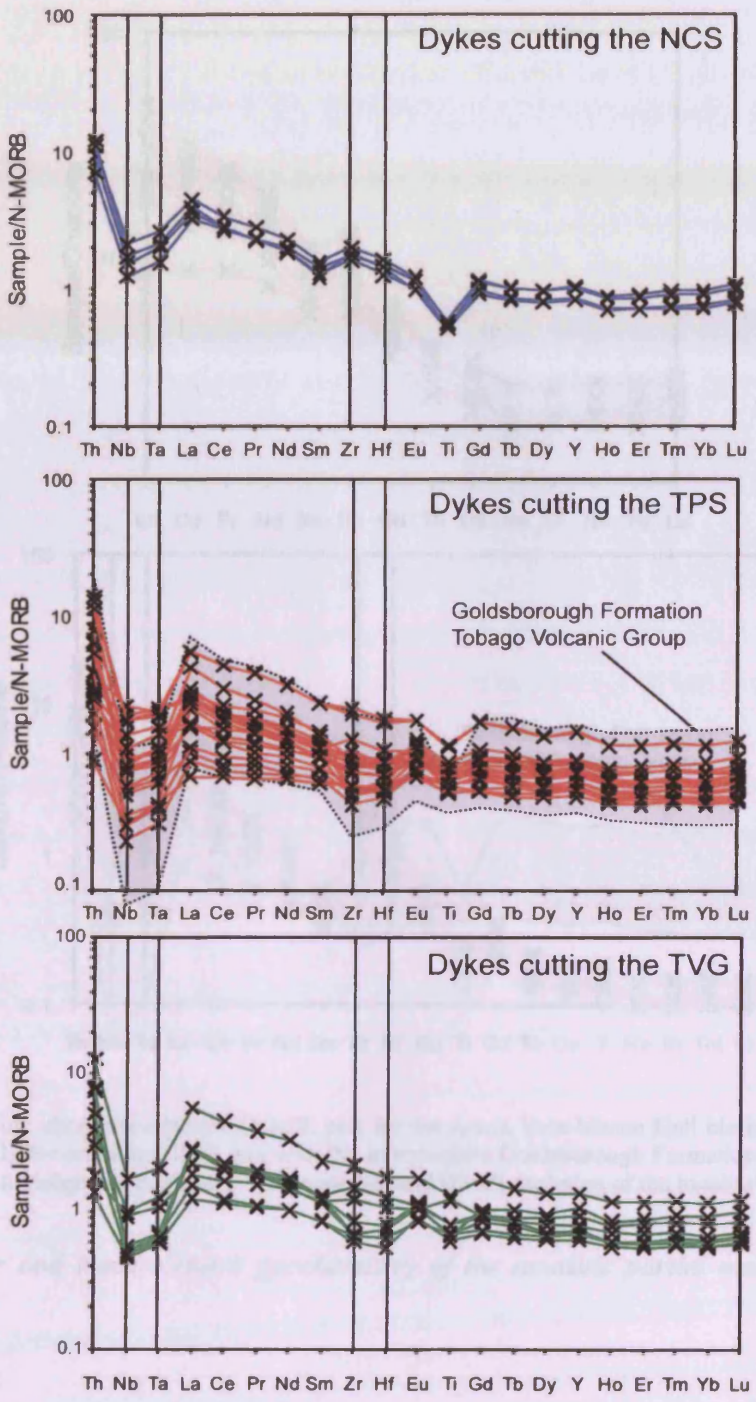

Figure 4.22. N-MORB-normalised trace element plots for the Tobago mafic dyke swarm. The Goldsborough Formation (TVG) is added for comparison.

show marked LREE/HREE fractionation, low HREE contents around 2-3 times chondrite and a slight concave-up profile with Lu/Ho_{CN} >1 and slight positive Eu anomalies. On the N-MORB-normalised plot (Fig. 4.23), there is a slight enrichment in Th over the LREE and conspicuous negative Nb-Ta and positive Zr-Hf anomalies.

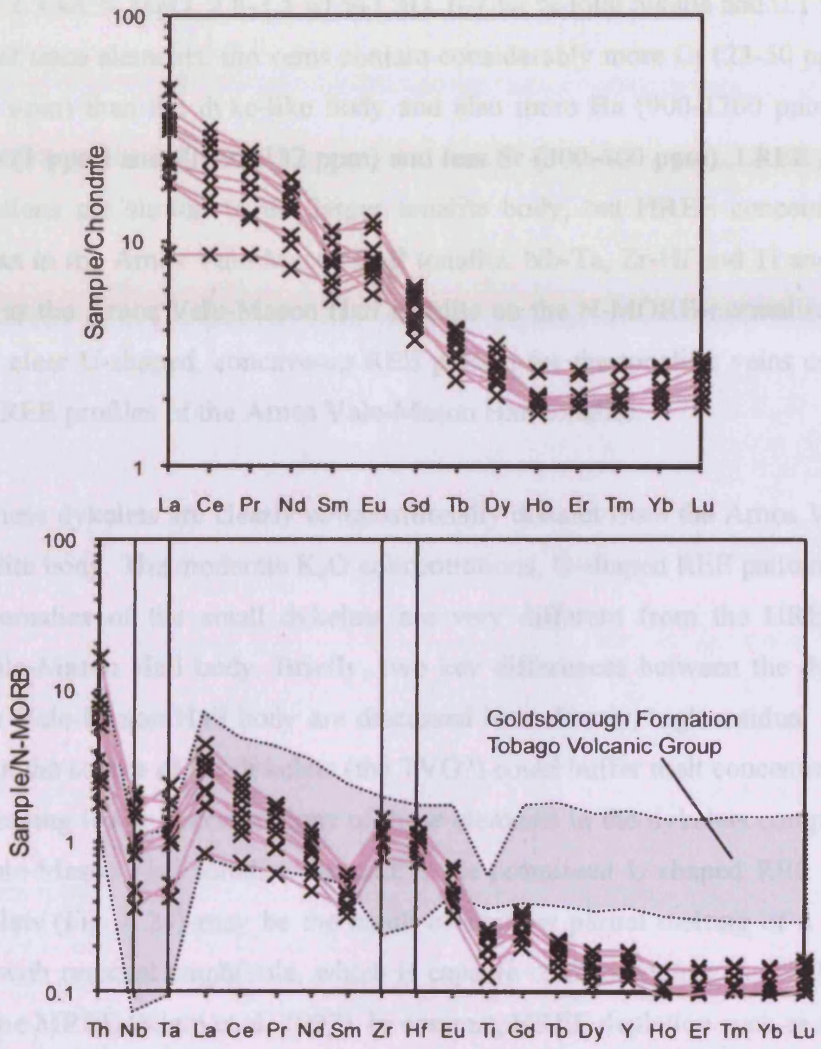

Figure 4.23. Top: chondrite-normalised REE plot for the Arnos Vale-Mason Hall biotite tonalite body. Bottom: N-MORB-normalised REE plot with the intermediate Goldsborough Formation of the TVG for comparison to highlight the positive Zr-Hf anomalies and HREE depletion of the tonalite body.

4.3.7. Major and trace element geochemistry of the tonalitic partial melts within the TVG

These are tonalite veins thought to be generated by partial melting of the Tobago Volcanic Group at its contact with the gabbro-diorite unit on the Hillsborough West River (Snoke et al., 2001a,b). The two samples from here are slightly different in major element contents to the dyke-like tonalite body of the main pluton, the main difference being that the sampled vein contains more K_2O (2.0 wt.%) and less Al_2O_3 (15.2-15.7 wt.%). The tonalite veins also contain 68-70 wt.% SiO_2, 0.28-0.32 wt.%

TiO_2, 1.1-1.3 wt.% MgO, 2.8-3.5 wt.% CaO, 6-7 wt.% total alkalis and 0.1 wt.% P_2O_5. In terms of trace elements, the veins contain considerably more Cr (23-50 ppm) and Ni (109-135 ppm) than the dyke-like body and also more Ba (900-1200 ppm), Y (8-10 ppm), Yb (1 ppm) and Zr (93-132 ppm) and less Sr (300-400 ppm). LREE and MREE concentrations are similar to the larger tonalite body, but HREE concentrations are higher than in the Arnos Vale-Mason Hall tonalite. Nb-Ta, Zr-Hf and Ti anomalies are the same as the Arnos Vale-Mason Hall tonalite on the N-MORB-normalised plot, but there is a clear U-shaped, concave-up REE pattern for the tonalitic veins compared to the flat HREE profiles of the Arnos Vale-Mason Hall tonalite.

These dykelets are clearly compositionally distinct from the Arnos Vale-Mason Hall tonalite body. The moderate K_2O concentrations, U-shaped REE patterns and large Zr-Hf anomalies of the small dykelets are very different from the HREE-depleted Arnos Vale-Mason Hall body. Briefly, two key differences between the dykelets and the Arnos Vale-Mason Hall body are discussed here. Firstly, high residual plagioclase contents in the source of the dykelets (the TVG?) could buffer melt concentrations of Sr and Al, leaving lower concentrations of these elements in the dykelets compared to the Arnos Vale-Mason Hall tonalite. Secondly, the prominent U-shaped REE patterns in the dyke-lets (Fig. 4.24) may be the result of shallow partial melting of a garnet-free protolith with residual amphibole, which is capable of fractionating the HREE and Zr-Hf from the MREE (Klein et al. 1997). In contrast, HREE depletion such as that seen in the Arnos Vale-Mason Hall tonalite is a ubiquitous sign of garnet in the residual or fractionating mineral assemblage. In summary the Arnos Vale-Mason Hall tonalite and the dykelets are petrogenetically unrelated, and the latter are argued to represent a minor local melting event of little significance for the geological evolution of Tobago (Snoke et al., 2001a). A more extensive discussion on the origin of the Arnos Vale-Mason Hall tonalite is in Section 5.3.5.

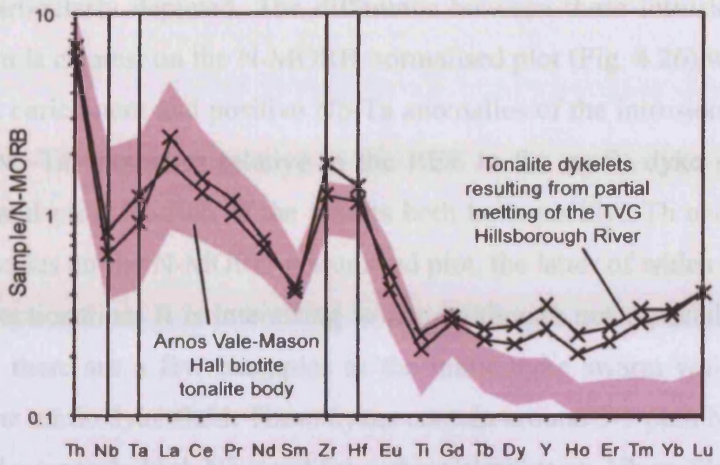

Figure 4.24. N-MORB-normalised trace element plot comparing the geochemistry of the partial melts of the TVG from the Hillsborough West River with the biotite tonalite of Arnos Vale-Mason Hall.

4.3.8. Major and trace element geochemistry of the Nb- and LREE-enriched mafic and felsic intrusions

Four minor intrusions sampled from the TVG between the Kendal Road and Merchison contained unusual levels of incompatible trace elements compared to the mafic dyke swarm. One felsic sample, the granitoid intruding gabbro-diorite on the Kendal Road, consisted of 62 wt.% SiO_2, 19 wt.% Al_2O_3, 0.8 wt.% MgO and high levels of Na_2O (5.2 wt.%) and K_2O (3.8 wt.%). The felsic intrusion also had 260 ppm Zr, 49 ppm Nb and 4 ppm Th, and these levels are considerably higher than other rocks on the island. This felsic sample shall be referred to as ***high-Nb granite***.

The three mafic samples contained 47-50 wt.% SiO_2, 14-18 wt.% Al_2O_3, 6-11 wt.% MgO, 2.0-3.8 wt.% NaO and 0.3-3.4 wt.% K_2O. These rocks plot as either tholeiitic or calc-alkaline basalts on the Th-Co diagram (Fig. 4.25). The mafic dykes also contained high levels of Cr and Ni similar to the rest of the mafic dykes, along with 59-130 ppm Zr, 7-28 ppm Nb (much higher than the mafic dyke swarm) and 0.2-1.9 ppm Th. These samples with 7-28 ppm Nb are referred to as ***Nb-enriched basalts***, in line with the definitions of Nb-enriched basalt (~9-30 ppm Nb) and high-Nb basalt (>~30 ppm Nb) for lavas from Baja California (Castillo, 2008). On a chondrite-normalised plot (Fig. 4.26), all four samples show LREE/HREE enrichment greater than the trend for the mafic dyke swarm, and also have relatively flat HREE patterns

which are not particularly depleted. The difference between these intrusions and the mafic dyke swarm is clearest on the N-MORB-normalised plot (Fig. 4.26) which shows the LREE/HREE enrichment and positive Nb-Ta anomalies of the intrusions compared to the negative Nb-Ta anomalies relative to the REE in the mafic dyke swarm. The high-Nb granite and most Nb-rich of the basalts both have positive Th anomalies and negative Ti anomalies on the N-MORB-normalised plot, the latter of which may be due to Fe-Ti oxide fractionation. It is interesting to note, although not especially clear, on Figure 4.25, that there are a few examples of the mafic dyke swarm which define a small 'kink' on the mafic dyke field. These dykes contain around 3-5 ppm Nb and were those that defined a separate high Nb trend for a given element vs. Nb on Figure 4.20.

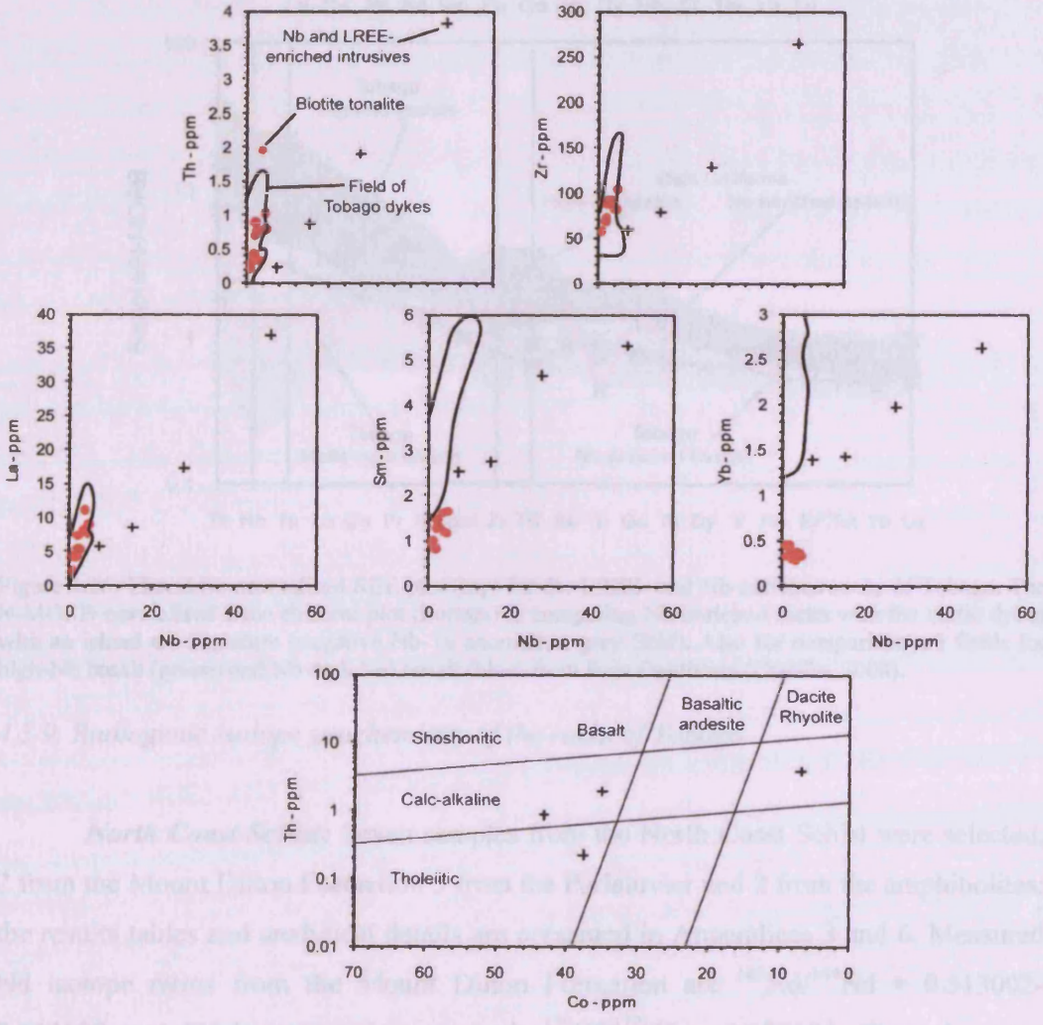

Figure 4.25. Element vs. Nb plots and Th-Co diagram for the LREE- and Nb-enriched intrusions. The Arnos Vale-Mason Hall tonalite is plotted for comparison. Also, the mafic dyke swarm is plotted as some mafic dykes trend towards higher Nb concentrations for a given incompatible element concentration; mirroring the trend of the LREE- and Nb-enriched intrusions.

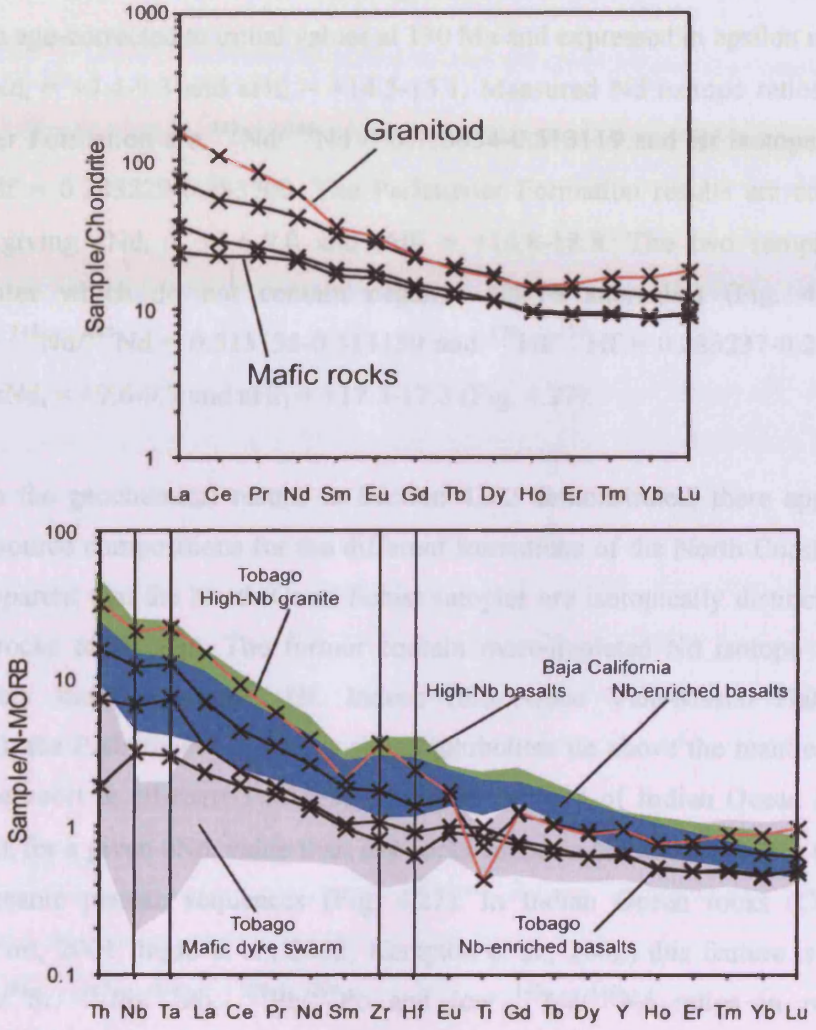

Figure 4.26. Chondrite-normalised REE plot (top) for the LREE- and Nb-enriched rocks of Tobago. The N-MORB-normalised trace element plot (bottom) is comparing Nb-enriched rocks with the mafic dykes with an island arc signature (negative Nb-Ta anomalies, grey field). Also for comparison are fields for high-Nb basalt (green) and Nb-enriched basalt (blue) from Baja California (Castillo, 2008).

4.3.9. Radiogenic isotope geochemistry of the rocks of Tobago

North Coast Schist: Seven samples from the North Coast Schist were selected, 2 from the Mount Dillon Formation 3 from the Parlatuvier and 2 from the amphibolites; the results tables and analytical details are presented in Appendices 3 and 6. Measured Nd isotope ratios from the Mount Dillon Formation are $^{143}Nd/^{144}Nd$ = 0.513002-0.513109 and Hf isotope ratios are both $^{176}Hf/^{177}Hf$ = 0.283184. There is some uncertainty over the age of the Mount Dillon Formation as it has not been directly

dated; however, based on the new U-Pb age for the Parlatuvier Formation, these ratios have been age-corrected to initial values at 130 Ma and expressed in epsilon units giving εNd_i = +7.4-9.3 and εHf_i = +14.5-15.1. Measured Nd isotope ratios from the Parlatuvier Formation are $^{143}Nd/^{144}Nd$ = 0.513054-0.513119 and Hf isotope ratios are $^{176}Hf/^{177}Hf$ = 0.283229-0.283300. The Parlatuvier Formation results are corrected to 130 Ma giving εNd_i = +8.6-9.0 and εHf_i = +16.8-18.8. The two samples of the amphibolites which do not contain negative Nb-Ta anomalies (Fig. 4.12) have measured $^{143}Nd/^{144}Nd$ = 0.513138-0.513139 and $^{176}Hf/^{177}Hf$ = 0.283237-0.283249. At 130 Ma, εNd_i = +9.6-9.7 and εHf_i = +17.3-17.3 (Fig. 4.27).

As the geochemical results in Section 4.3.2 demonstrated, there appear to be different source compositions for the different formations of the North Coast Schist. It is now apparent that the North Coast Schist samples are isotopically distinct from the younger rocks of Tobago. The former contain more-depleted Nd isotope ratios and considerably more radiogenic Hf. Indeed (the Arnos Vale-Mason Hall tonalite excepting), the Parlatuvier Formation and amphibolites lie above the mantle reference line of Vervoort & Blichert-Toft (1999) within the field of Indian Ocean MORB at higher εHf_i for a given εNd_i value than any rocks found in the allochthonous Caribbean arc or oceanic plateau sequences (Fig. 4.27). In Indian Ocean rocks (Chauvel & Blichert-Toft, 2001; Ingle et al., 2002; Kempton et al., 2002) this feature is linked to high $^{87}Sr/^{86}Sr$, $^{207}Pb/^{204}Pb$, $^{208}Pb/^{204}Pb$ and low $^{143}Nd/^{144}Nd$ ratios in relation to $^{206}Pb/^{204}Pb$ compared with Pacific and Atlantic basalts (Hart, 1984). Hart (1984) called this feature the Dupal Anomaly. Suggestions for the origin of the anomaly have ranged from incorporation of recycled oceanic pelagic sediments and crust, to delaminated sub-continental mantle lithosphere (SCLM), to a depleted mantle wedge composition affected by multiple ancient subduction-related melting events (see Ingle et al., 2002). This issue will be discussed further in Section 5.2. Finally, it is interesting to note that the isotopic composition of the amphibolites lies close to that of the Parlatuvier Formation; and that the Mount Dillon Formation does not appear to contain a significant Dupal anomaly.

Tobago Volcanic Group and Pluton: Five samples from the TVG were selected, one from each identified formation (Argyle, Bacolet, Goldsborough) and two

from undifferentiated lavas at opposite sides of the island; the results are presented in Appendix 6 and on Figure 4.27. Measured Nd isotope ratios span a very narrow range from $^{143}Nd/^{144}Nd$ = 0.512957-0.513022 and Hf isotope ratios from $^{176}Hf/^{177}Hf$ = 0.283139-0.283221. These ratios have been age-corrected to initial values at 110 Ma, (faunal ages; Snoke & Noble, 2001) and expressed in epsilon units giving εNd_i = +6.8-7.6 and εHf_i = +14.0-16.5. On the εHf_i vs. εNd_i diagram (Fig. 4.27), the samples from the TVG are quite depleted, with lower εNd_i values with respect to the North Coast Schist. The TVG rocks plot on or slightly above the mantle reference line. Just one sample lies within the field of Indian Ocean MORB. Otherwise, the rocks of the TVG have less radiogenic Hf isotopes than much of the NCS; however, these four TVG samples with low εHf_i are isotopically identical to one sample from the Mount Dillon Formation. Two samples of gabbro-diorite were analysed for comparison with the TVG. The measured Nd isotope ratios range from $^{143}Nd/^{144}Nd$ = 0.512967-0.513009 and Hf isotope ratios range from $^{176}Hf/^{177}Hf$ = 0.283125-0.283155. The age-corrected ratios, corrected to 106 Ma in light of the U-Pb results from the cross-cutting tonalite and Nb-enriched rocks, are εNd_i = +6.9-8.0 and εHf_i = +13.9-14.4. These values are almost identical to the range of the TVG on Figure 4.27.

The TVG and the Tobago pluton are very similar isotopically to the ~96 Ma Washikemba Formation of Bonaire (Thompson et al., 2004) and contain only slightly lower εNd_i values compared to the Lower Cretaceous Devils Racecourse Formation, Jamaica (Hastie et al., 2009) (Fig. 4.27). Unfortunately, despite extensive studies using Nd-Sr-Pb isotope systems, other Middle to Lower Cretaceous Caribbean island arc localities have not been analysed for Hf isotopes. Given the susceptibility of the Sr and Pb isotope systems to weathering and sub-solidus alteration processes, this omission is a major failing in our understanding the geochemical evolution of the Caribbean.

Mafic dyke swarm: One sample of the mafic dyke swarm (2D-14) was analysed for its radiogenic isotope signatures. This sample was a depleted island-arc-like dyke cutting the Arnos Vale-Mason Hall tonalite, dated by Sharp & Snoke (1988) to ~91.4 Ma (see Chapter 2.1). Measured isotope ratios of $^{143}Nd/^{144}Nd$ = 0.513124 and $^{176}Hf/^{177}Hf$ = 0.283123 equate to age-corrected epsilon values of: εNd_i = +9.4 and εHf_i = +12.9. This sample has relatively low Th/Yb, Th/La and Ce/Ce* indicating that it

contains little evidence for involvement of fluid flux derived from subducted sediments (see Chapter 5.3). On the εHf_i vs. εNd_i diagram (Fig. 4.27) this sample has a more depleted Nd isotope signature compared to the TVG and a much less radiogenic Hf isotopic signature, placing it below the mantle array in the field of Atlantic/Pacific MORBs.

Arnos Vale-Mason Hall tonalite: One radiogenic isotope analysis from the Arnos Vale-Mason Hall tonalite shows that the body has measured $^{143}Nd/^{144}Nd$ of 0.513007 and $^{176}Hf/^{177}Hf$ of 0.283292, translating to $\varepsilon Nd_i = +8.27$ and $\varepsilon Hf_i = +20.45$ at 106 Ma. The Nd isotope result is similar to the NCS, but the εHf_i value is the most radiogenic sample found, reflecting a significant decoupling of Nd and Hf isotope systems in excess of that observed in the Parlatuvier Formation. It can now be seen on Figure 4.27 that there are crude trends running from the TVG and TPS, and the Parlatuvier Formation and amphibolites towards extremely high Hf isotopic ratios including the tonalite. This observation may indicate mixing or derivation of some of the Tobago magmas with material derived from a source that has been allowed to develop a radiogenic Hf isotope signature through time. Alternatively, as there have been very few analyses undertaken, these may be false trends with no geological meaning.

Partial melts of the TVG: One isotope analysis of a dykelet suspected to be a partial melt of the TVG, collected from the Hillsborough River (Snoke et al., 2001a,b) has a $^{143}Nd/^{144}Nd$ ratio of 0.513047, slightly higher than the 5 analyses from the TVG, and a $^{176}Hf/^{177}Hf$ ratio of 0.283167, similar to the TVG. Corrected to 106 Ma, the epsilon values for this sample are $\varepsilon Nd_i = +9.04$ and $\varepsilon Hf_i = +15.63$. As the TVG at the site of partial melting was not analysed, it is difficult to ascertain whether the more depleted εNd_i value for the tonalite is reflective of a local difference in composition of the TVG or a non-TVG source for these tonalite dykelets. On Figure 4.27, the dykelet plots on the mantle array between the most depleted member of the Mount Dillon Formation and the Parlatuvier Formation. Realistically, these small veins (5-10 cm across) could not have travelled a significant difference from their partially molten source but this isotopic evidence supports an origin by partial melting, not of the host TVG, but perhaps the NCS at depth.

Nb- and LREE-enriched intrusions: Two of these samples were analysed for their radiogenic isotope ratios. INT/29-2/2 (high-Nb basalt) has measured $^{143}Nd/^{144}Nd$ = 0.512997 and $^{176}Hf/^{177}Hf$ = 0.283041. The high-Nb granite has measured $^{143}Nd/^{144}Nd$ = 0.512953 and $^{176}Hf/^{177}Hf$ = 0.283154. The age-corrected isotopic ratios for 106 Ma are: εNd_i = +7.67 (basalt) and +7.34 (granite) and εHf_i = +10.80 (basalt) and +14.93 (granite). Clearly there is a significant difference in isotopic ratios between the samples. The granitic rock contains the more radiogenic Hf, a signature identical to the rocks of the TVG and Tobago pluton (Fig. 4.27). The high-Nb basalt is the most isotopically enriched of all the analysed Tobago samples, and falls within the East Pacific Rise MORB field on the εHf_i vs. εNd_i diagram (Fig. 4.27).

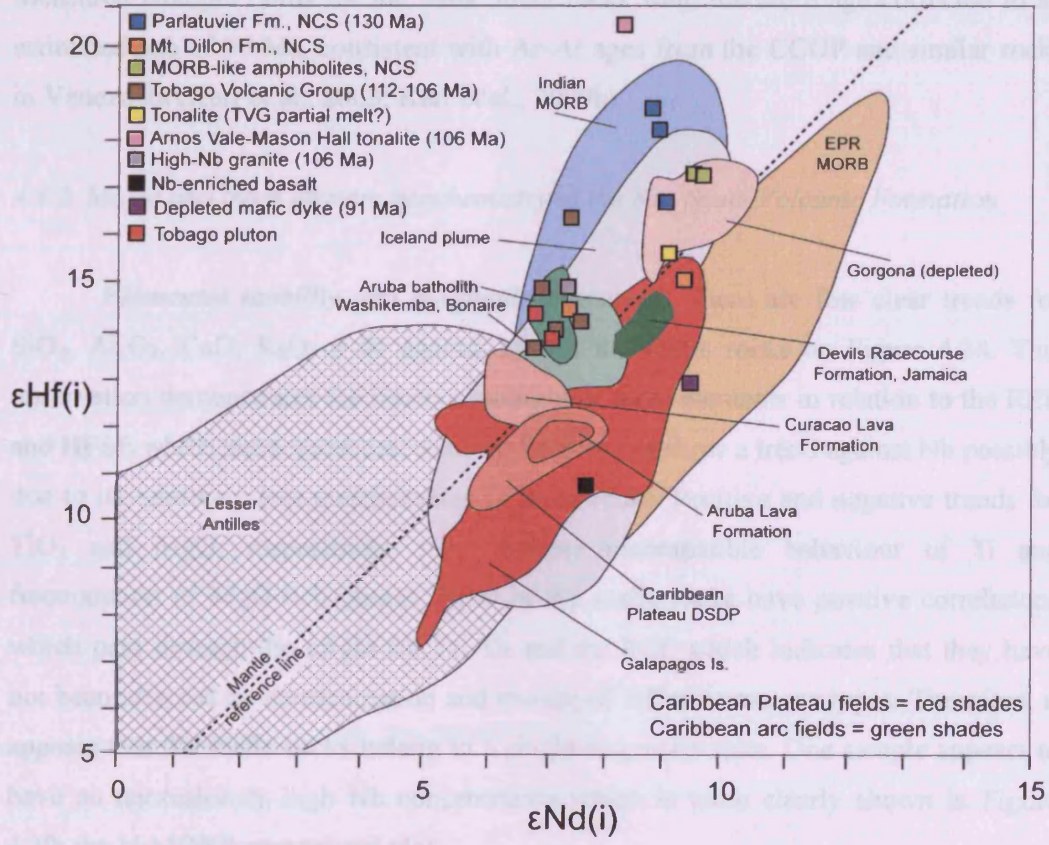

Figure 4.27. Hf-Nd isotope results for Tobago. All the fields are from Thompson et al. (2003, 2004) apart from the Devils Racecourse Formation and Lesser Antilles (Hastie et al., 2009 and references therein), and Indian MORB (Chauvel & Blichert-Toft, 2001 and references therein). The mantle reference line is from Vervoort & Blichert-Toft (1999). The field for present-day Pacific and Indian MORB has not been age-corrected as Thompson et al. (2003) demonstrated that present-day and Jurassic Pacific MORB were isotopically very similar and predicted that the Hf isotope composition within a uniform chondritic reservoir would change by <0.5 epsilon units in 90 Ma. This finding applies to all subsequent isotope diagrams.

4.4. Geochronology and whole rock geochemical results from San Souci

4.4.1. Age of the San Souci Volcanic Formation

It was anticipated that a U-Pb zircon secondary ion mass spectrometry age would be available from the San Souci Formation well in advance of the submission of this thesis. However, due to illness and lab availability, the dating was not carried out at the University of California, Los Angeles in time. Given the constraints of the youngest detrital zircon age from the Toco Formation of ~108 Ma (Algar et al., 1998) and the whole-rock K-Ar age of approximately 87 Ma (Wadge & Macdonald, 1985), it has been assumed that the San Souci Formation dates from between 87 and 108 Ma. Measured isotopic ratios for the Sans Souci rocks were therefore age corrected to an estimated age of 90 Ma, consistent with Ar-Ar ages from the CCOP and similar rocks in Venezuela (Kerr et al., 2003; Kerr et al., 2009b).

4.4.2. Major and trace element geochemistry of the San Souci Volcanic Formation

Elemental mobility and magmatic processes: There are few clear trends for SiO_2, Al_2O_3, CaO, K_2O or Sr against Nb for the mafic rocks on Figure 4.28. This observation demonstrates the relative mobility of these elements in relation to the REE and HFSE which show good correlations. Sc does not show a trend against Nb possibly due to its relatively low concentration in these rocks. Positive and negative trends for TiO_2 and MgO, respectively, may indicate incompatible behaviour of Ti and fractionation of MgO-rich phases. Most of the mafic rocks have positive correlations which pass through the origin for Zr, Th and the REE which indicates that they have not been affected by contamination and mixing of different magma types. Therefore, it appears that the mafic rocks belong to a single magmatic suite. One sample appears to have an anomalously high Nb concentration which is more clearly shown in Figure 4.29, the N-MORB-normalised plot.

Given the patterns described above, the major elements will not be used to study the origin and evolution of the San Souci formation as they appear to have been mobilised during sub-solidus alteration processes. Instead, the HFSE and REE will be utilised.

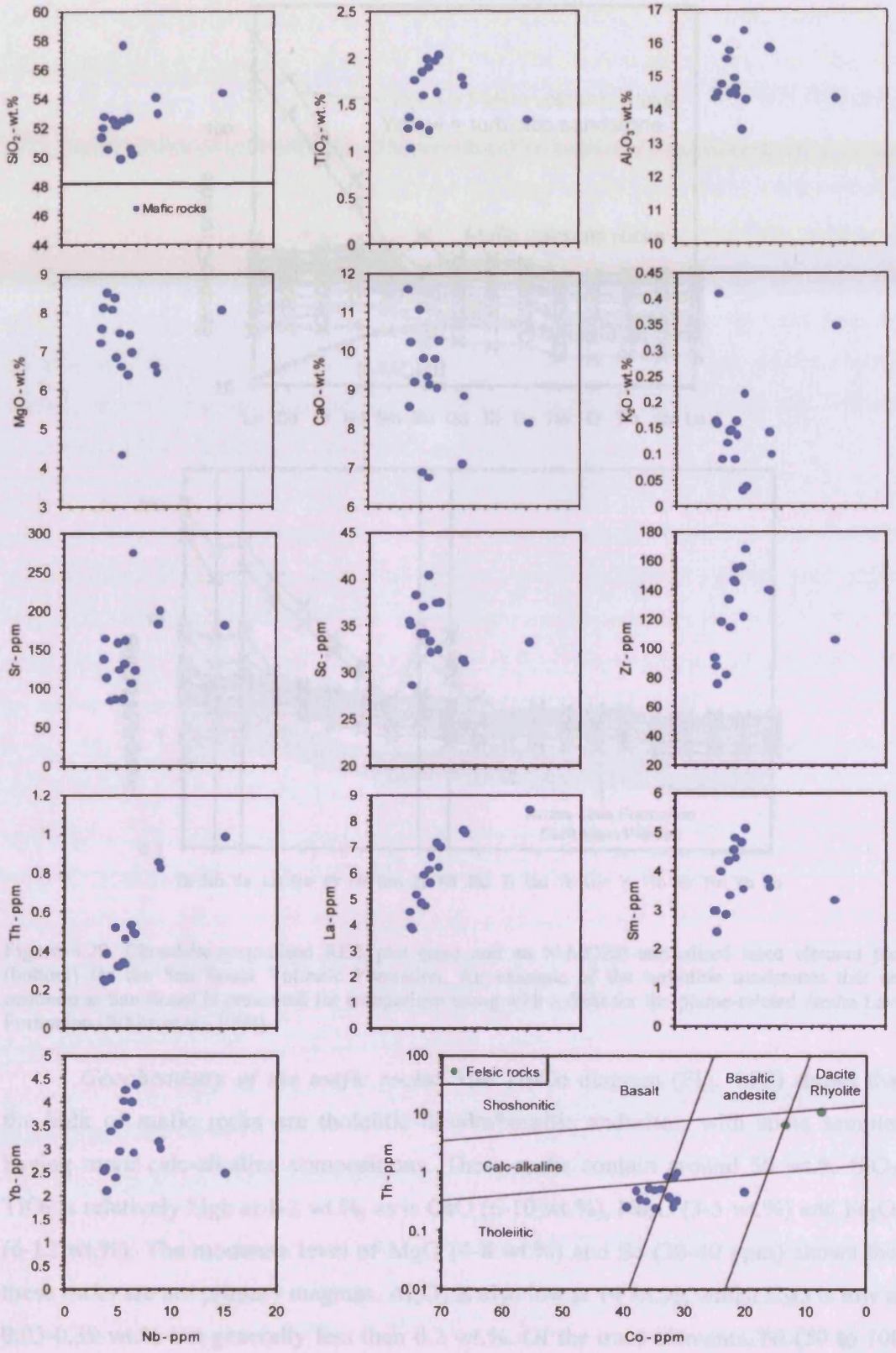

Figure 4.28. Element vs. Nb plots for the mafic rocks of the San Souci Volcanic Formation. Bottom right: Th-Co discrimination diagram with the two felsic volcanic samples marked in green.

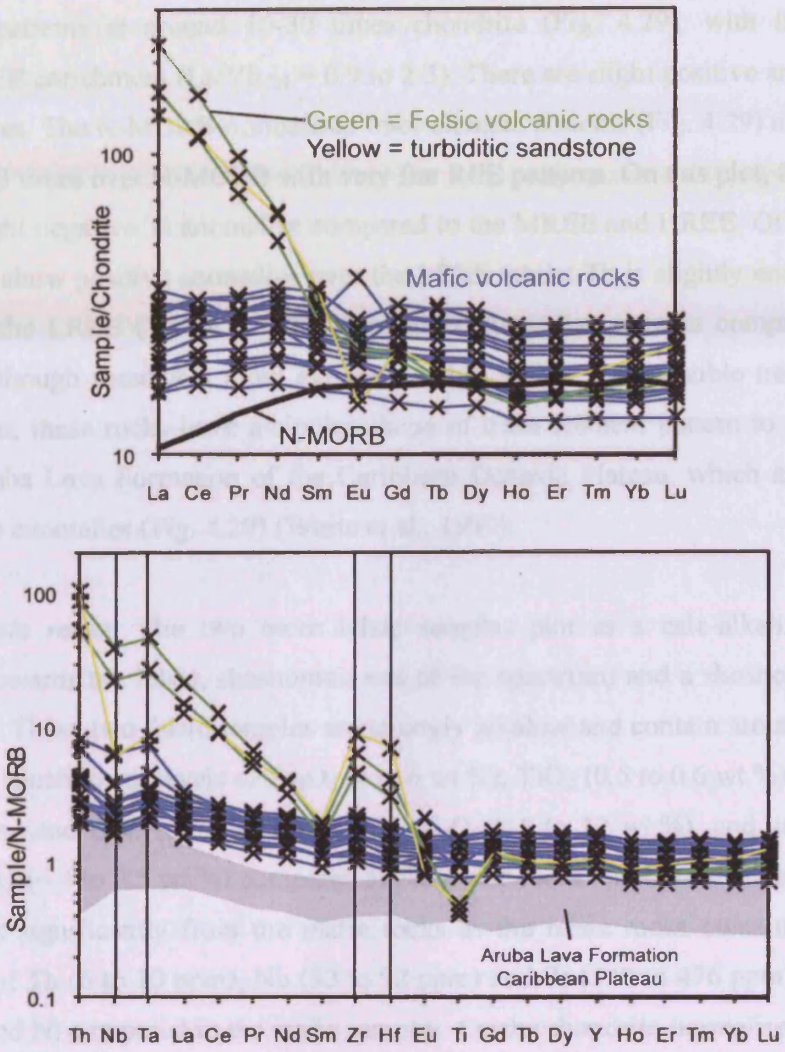

Figure 4.29. Chondrite-normalised REE plot (top) and an N-MORB-normalised trace element plot (bottom) for the San Souci Volcanic Formation. An example of the turbiditic sandstones that are common at San Souci is presented for comparison along with a field for the plume-related Aruba Lava Formation (White et al., 1999).

Geochemistry of the mafic rocks: The Th-Co diagram (Fig. 4.28) shows that the bulk of mafic rocks are tholeiitic basalts/basaltic andesites, with some samples having more calc-alkaline compositions. These rocks contain around 50 wt.% SiO_2. TiO_2 is relatively high at 1-2 wt.%, as is CaO (6-10 wt.%), Na_2O (3-5 wt.%) and Fe_2O_3 (6-12 wt.%). The moderate level of MgO (4-8 wt.%) and Sc (30-40 ppm) shows that these rocks are not primary magmas. Al_2O_3 is also low at 14 wt.%, whilst K_2O is low at 0.03-0.39 wt.% but generally less than 0.2 wt.%. Of the trace elements, Ni (50 to 100 ppm) and Cr (100 to 350) ppm are quite high. Y ranges from 20 to 46 ppm and Zr from 75 to 156 ppm. The chondrite-normalised REE plot for the mafic rocks shows that they

have flat patterns at around 10-30 times chondrite (Fig. 4.29), with little or no LREE/HREE enrichment (La/Yb_{CN} = 0.9 to 2.3). There are slight positive and negative Eu anomalies. The N-MORB-normalised trace element patterns (Fig. 4.29) are enriched between 1-3 times over N-MORB with very flat REE patterns. On this plot, there are no or very slight negative Ti anomalies compared to the MREE and HREE. Of the HFSE, Nb and Ta show positive anomalies over the LREE whilst Th is slightly enriched with respect to the LREE (Th/La = 0.08). Zr and Hf have flat patterns compared to the MREE. Although somewhat more evolved, with a higher incompatible trace element composition, these rocks have a similar shape of trace element pattern to the plume-related Aruba Lava Formation of the Caribbean Oceanic Plateau, which also contain positive Nb anomalies (Fig. 4.29) (White et al., 1999).

Felsic rocks: The two more felsic samples plot as a calc-alkaline basaltic andesite (towards the felsic, shoshonitic end of the spectrum) and a shoshonitic dacite (Fig. 4.28). These two felsic samples are strongly alkaline and contain around 65 wt.% silica, with much lower levels of Fe_2O_3 (4 to 6 wt.%), TiO_2 (0.5 to 0.6 wt.%), MgO (2.0 to 2.4 wt.%) and CaO (2.54 wt.%); higher Al_2O_3 (15 to 17 wt.%), and considerably higher Na_2O (6.4 to 7.5 wt.%) compared to the mafic rocks. The trace element content also differs significantly from the mafic rocks as the felsic rocks contain very high quantities of Th (6 to 10 ppm), Nb (53 to 92 ppm) and Zr (340 to 476 ppm) and much lower Cr and Ni compared to the mafic samples. On the chondrite-normalised REE plot (Fig. 4.29), the felsic samples are markedly enriched in the LREE/MREE but have nearly flat MREE and HREE patterns identical to the mafic samples. La/Yb_{CN} ranges from 10-13, with LREE of 160-230 times chondrite. On the N-MORB-normalised trace element plot (Fig. 4.29), the felsic rocks have negative Ti anomalies and, in contrast to the mafic rocks, they also have very strong positive Zr-Hf and Nb-Ta anomalies. Th is slightly enriched over the LREE, but there is not a particularly high Th/La signature in these felsic rocks as their Th/La ratios are <0.2 (Plank, 2005).

Sandstone: The single analysis of a sedimentary rock from Grand Riviere (Toco Formation) was undertaken in order to compare the local crustal geochemistry with that of the San Souci Formation. The analysis shows that the quartzo-feldspathic sandstone is very siliceous, with around 80 wt.% SiO_2, and contains low concentrations of other major elements. Concentrations of Cr and Ni are similar to the felsic volcanic rocks.

However, the sandstone has high Th (12 ppm), moderate Nb (15 ppm) and extremely high Zr (660 ppm). On the chondrite and N-MORB-normalised trace element plots (Fig. 4.29) the sandstone has enriched LREE/MREE and HREE, a negative Ti anomaly and strongly positive Zr-Hf anomalies, similar to the felsic volcanic rocks. However, the sandstone has enriched Th/La of 0.39 (c.f. <0.2 in the felsic volcanics) consistent with its terrigenous origin, and also conspicuous negative Nb-Ta anomalies which are not present in the mafic or felsic volcanics.

4.4.3. Radiogenic isotope geochemistry of the San Souci Volcanic Formation

Three mafic rocks and the two felsic rocks from San Souci were analysed for radiogenic isotopes. The mafic rocks span a very narrow range of measured isotopic compositions with $^{143}Nd/^{144}Nd$ = 0.513065-0.513089 and $^{176}Hf/^{177}Hf$ = 0.283139-0.283156. These figures translate to initial values at 90 Ma of εNd_i = 8.5-9.0 and εHf_i = 13.3-14.1. On Figure 4.30, the rocks of San Souci plot within the field of the Galapagos hotspot at more depleted Nd isotope ratios than the TVG of Tobago or the CCOP-related Curaçao and Aruba Lava Formations. The two felsic rocks have distinct, enriched isotopic compositions compared to the mafic rocks. These have measured $^{143}Nd/^{144}Nd$ = 0.512856-0.512876 and $^{176}Hf/^{177}Hf$ = 0.282956-0.283013, with calculated initial values (90 Ma) of εNd_i = 5.40-5.72 and εHf_i = 8.02-9.92. These samples are on the fringes of the enriched end of the Galapagos the field of Figure 4.30, and also close to the most enriched values obtained for the Iceland plume.

On Figure 4.30, the Toco Formation sandstone would plot at εNd_i = -15 and εHf_i = -23. As the sandstone contains conspicuous negative Nb-Ta anomalies (Fig. 4.29) it is unlikely that contamination of the mafic rocks by the local crust could generate the felsic volcanics of San Souci with their large positive Nb-Ta anomalies (Fig. 4.29). The isotope results back up this conclusion as any significant contamination from the extremely isotopically enriched upper crust would cause the felsic volcanics to have significantly more enriched isotopic signatures than they do. Nonetheless, the two sets of values for the mafic and felsic rocks are very different and it is concluded that the two suites are not derived from the same mantle source region. The felsic rocks are probably derived from the partial melting of an isotopically enriched mantle source

whereas the San Souci mafic rocks were probably formed by partial melting of more depleted mantle. The San Souci mafic rocks are isotopically similar to mafic rocks sampled from allochthonous units in Venezuela; at El Copey on the Araya peninsula and Siquisique in the Los Algadones region (see Section 5.4) (Kerr et al., 2009b).

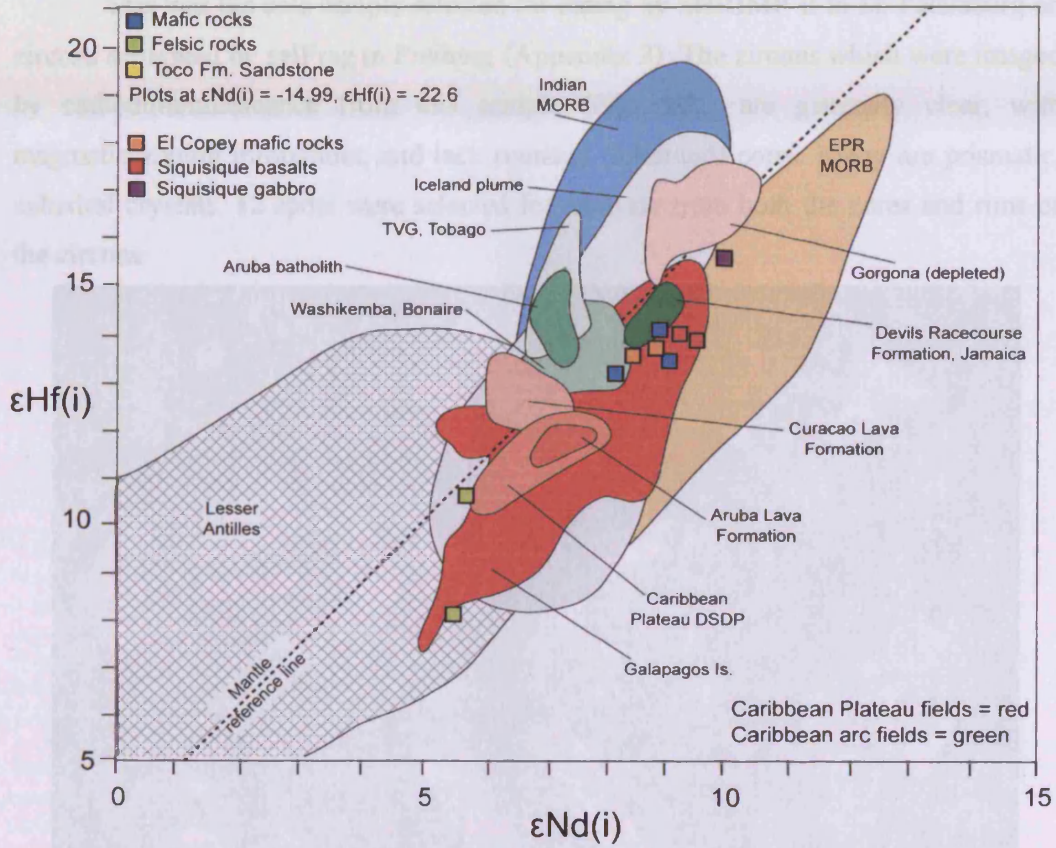

Figure 4.30. Hf-Nd isotope results for San Souci. The fields are from Thompson et al. (2003, 2004), apart from the Devils Racecourse Formation and Lesser Antilles (Hastie et al., 2009 and references therein), Indian MORB (Chauvel & Blichert-Toft, 2001 and references therein), and the TVG (this study). The mantle reference line is from Vervoort & Blichert-Toft (1999). Analyses from Siquisique and El Copey are from Kerr et al. (2009b).

4.5. Geochronological and whole-rock geochemical results from the Aves Ridge

4.5.1. Geochronology of granitoid EA68-11317UPb

This was the sole sample selected for dating by SHRIMP-II in St. Petersburg on zircons separated by selFrag in Freiberg (Appendix 3). The zircons which were imaged by cathodoluminescence from this sample (Fig. 4.31) are generally clear, with magmatic zoning throughout, and lack rounded (inherited) cores. Many are prismatic, euhedral crystals. 12 spots were selected for analysis from both the cores and rims of the zircons.

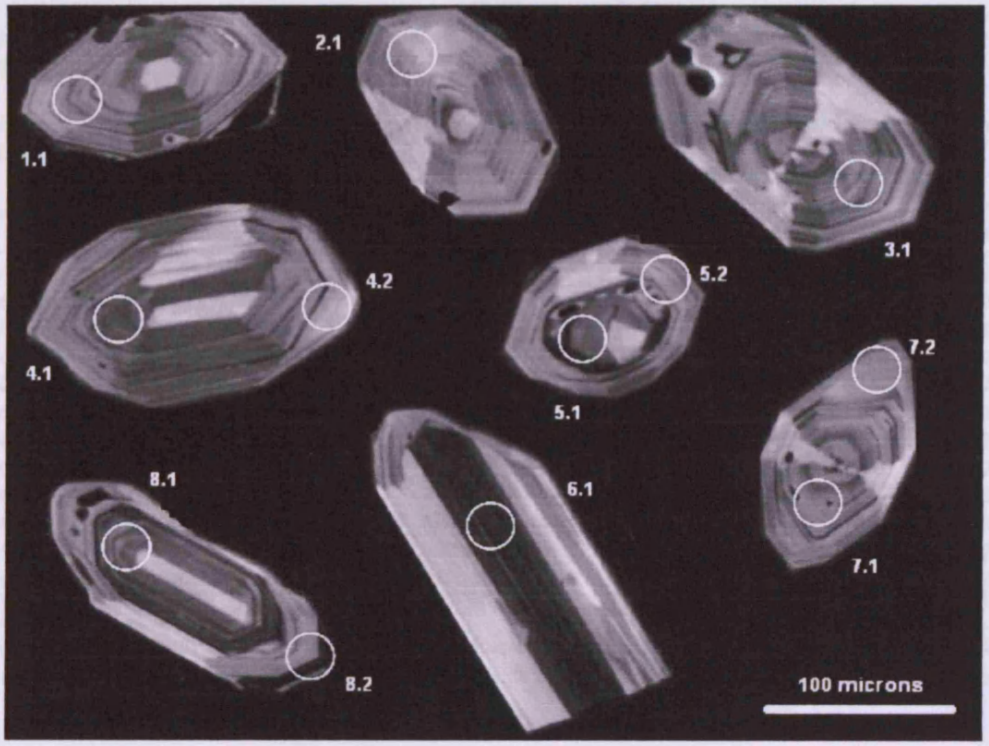

Figure 4.31. Cathodoluminesence images of the zircons selected for analysis from sample 317UPb.

All 12 SHRIMP analyses from 8 zircon grains yield a concordant age with no sign of discordance or inheritance on the $^{207}Pb/^{206}Pb$ vs. $^{238}U/^{206}Pb$ inverse concordia plot (Fig. 4.32). Assuming $^{206}Pb/^{238}U$-$^{207}Pb/^{235}U$ age-concordance, the weighted mean of $^{206}Pb/^{238}U$ ages (Table 4.2) is 75.9 ± 0.7 Ma (MSWD = 0.73), which is thus interpreted as the crystallisation age of the granitoid.

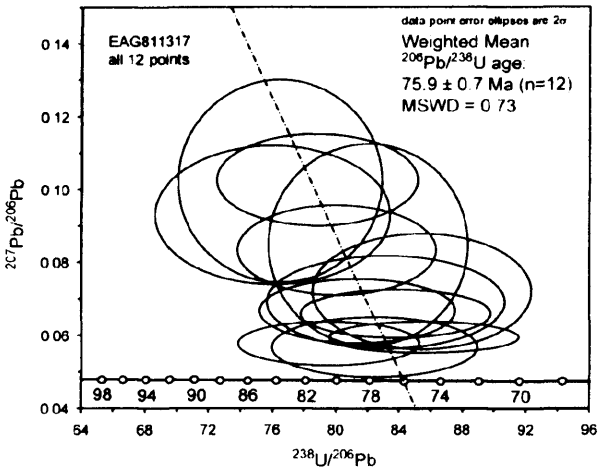

Figure 4.32. Inverse concordia plot for sample 317UPb showing that all 12 zircon analyses match a single concordia.

Table 4.2. U-Pb SHRIMP-II zircon results for sample EA68 11317UPb with a calculated weighted mean $^{206}Pb/^{238}U$ age of 75.9 ± 0.7 Ma.

Spot	*^{206}Pb (%)	U ppm	Th ppm	$^{232}Th/^{238}U$	†^{206}Pb ppm	Total $^{238}U/^{206}Pb$	±%	Total $^{207}Pb/^{206}Pb$	± %	‡$^{206}Pb/^{238}U$ Age (Ma)
EA6811317UPb.1.1	3.86	64	21	0.33	0.724	76	4	0.093	8.3	79.4 ± 3.2
EA6811317UPb.2.1	15.63	84	30	0.37	0.877	82.5	3.2	0.0568	5.9	76.8 ± 2.5
EA6811317UPb.4.1	5.96	106	35	0.35	1.11	82.1	3.1	0.085	13	74.4 ± 2.6
EA6811317UPb.4.2	13.71	73	27	0.38	0.794	78.9	3.3	0.1026	5	75.6 ± 2.5
EA6811317UPb.3.1	7.37	119	47	0.41	1.23	83.2	3.7	0.0692	7.5	74.9 ± 2.8
EA6811317UPb.5.1	6.99	123	47	0.40	1.3	81.4	3.1	0.0667	5.3	76.8 ± 2.4
EA6811317UPb.5.2	2.81	427	287	0.69	4.28	85.6	2.8	0.0595	3	73.8 ± 2.1
EA6811317UPb.7.1	14.03	79	29	0.38	0.79	85.4	3.3	0.0721	9	72.7 ± 2.5
EA6811317UPb.7.2	29.44	56	15	0.27	0.629	76.5	3.4	0.102	11	77.9 ± 2.9
EA6811317UPb.6.1	20.28	200	120	0.62	2.05	83.8	2.9	0.0659	4.1	74.7 ± 2.2
EA6811317UPb.8.1	15.69	94	40	0.44	1	80.1	3.2	0.0835	6	76.4 ± 2.5
EA6811317UPb.8.2	10.71	197	80	0.42	2.13	79.5	2.9	0.0578	4.3	79.5 ± 2.3

Errors in the age calculation are at 1σ

Error in standard calibration was 0.90 % (not included in above errors but required when comparing data from different mounts)

* – Common proportion; † – Radiogenic proportion; ‡ - Common Pb corrected assuming $^{206}Pb/^{238}U$-$^{207}Pb/^{235}U$ age-concordance

4.5.2. Major and trace element geochemistry of the Aves Ridge

Alteration and elemental mobility: To test element mobility, as with the previous units studied, elements are plotted against Nb (Fig. 4.33). For the Aves Ridge samples the high-field-strength-elements (HFSE) and the rare-earth-elements (REE) in the mafic rocks display good correlations with Nb. The correlations indicate that: (a) these elements have been relatively immobile during sub-solidus alteration, despite LOI values of ~3-15 % (Appendix 5), so may be used to investigate the origin of the mafic rocks and (b) the mafic rocks are part of a single co-genetic suite. As the granitoids are

evolved and fairly uniform in composition they do not show liquid lines of descent on Figure 4.33. Nevertheless, the granitoids can be investigated using the immobile HFSE and REE since, despite some epidotisation, the rocks are relatively fresh and are not silicified or calcified, with LOI values of ~1 %. The Mn-oxide coating on many granitoid samples may have acted as a protective layer.

Granitoid major and trace element geochemistry: SiO_2 spans a narrow range from 67 to 72 wt.%. The granitoids have low abundances of TiO_2 (0.4 wt.%), Fe_2O_3 (3.5 wt.%) and MgO (<1.5 wt.%). These rocks have elevated Ba (up to 1095 ppm) and Sr (up to 444 ppm) contents and low Cr (<24 ppm), Co (<7.5 ppm) and Ni (<46 ppm). Compared to the mafic rocks, the granitoids have lower contents of Sm and Sc and higher abundances of Sr and Zr (Fig. 4.33). There is no clear magmatic differentiation trend between the most evolved mafic rocks and the least evolved felsic rocks for any immobile elements shown. Both granitic dredges show identical, slightly concave-up, chondrite-normalised REE patterns (Fig. 4.34). The samples are LREE-enriched with an average La/Yb_{CN} of 4.5 consistent with a calc-alkaline affinity and there is slight HREE/MREE enrichment. On an N-MORB-normalised plot (Fig. 4.34) the granitoids are LREE/HREE enriched and have positive Zr-Hf and Th anomalies along with negative Nb-Ta and Ti anomalies.

Mafic rock major and trace element geochemistry: SiO_2 ranges from 34 to 57 wt.%, MgO from 1 to 6 wt.%, Al_2O_3 from 11 to 22 wt.% and $Na_2O + K_2O$ from 3 to 11 wt.%. TiO_2 has a much narrower range of concentrations than other major elements, from 0.5 to 0.8 wt.%. When plotted against Nb, MgO and Al_2O_3 show a weak positive correlation (Fig. 4.33). As these samples are altered, the Th-Co plot of Hastie et al. (2007) is used again to classify the mafic rocks (Fig. 4.33). Figure 4.33 shows that the rocks mostly classify as basaltic andesites of calc-alkaline affinity, although two samples plot in the tholeiite field.

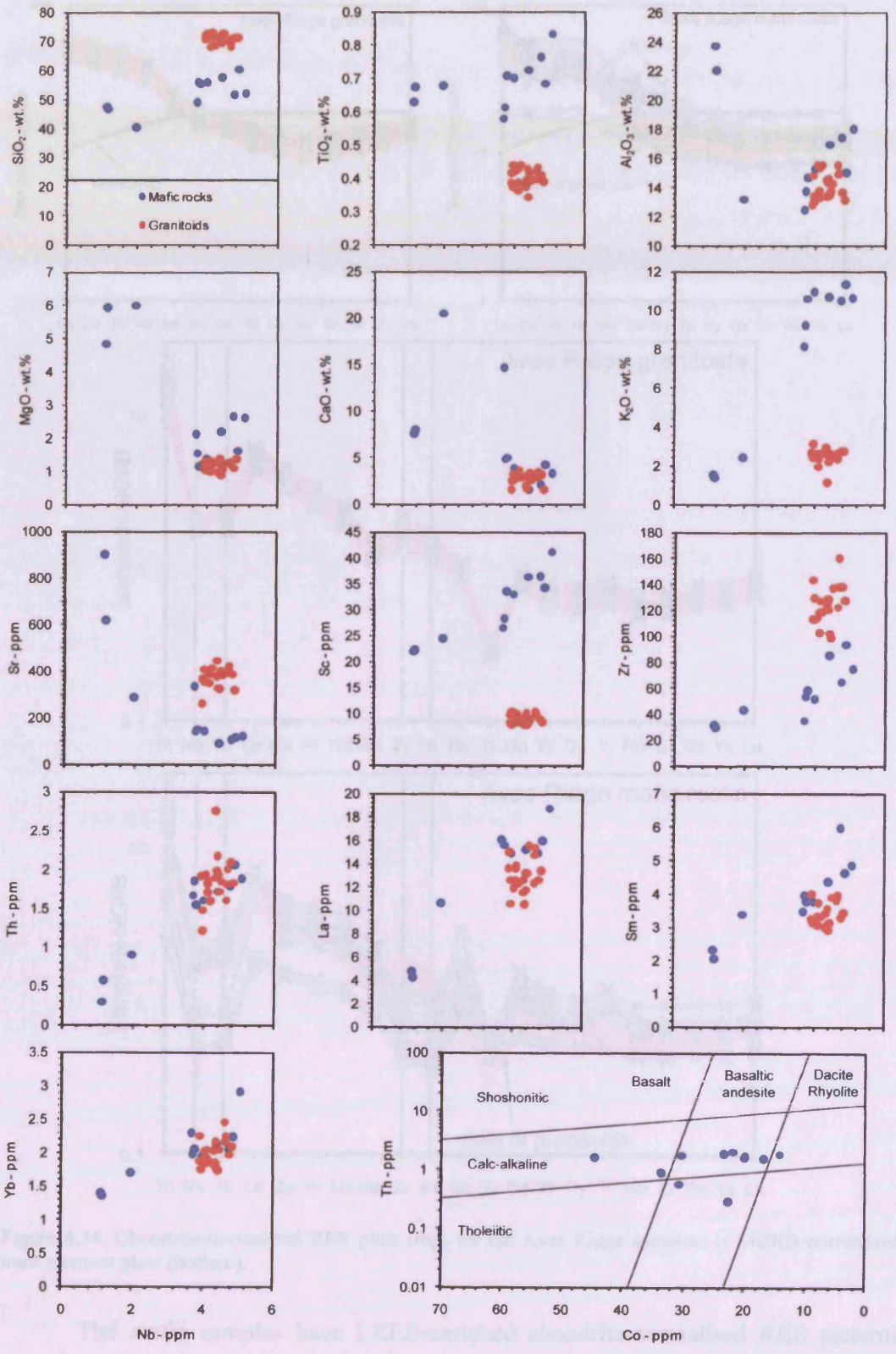

Figure 4.33. Element vs. Nb plots for the Aves Ridge mafic and granitoid rocks. Bottom right – Th-Co classification diagram.

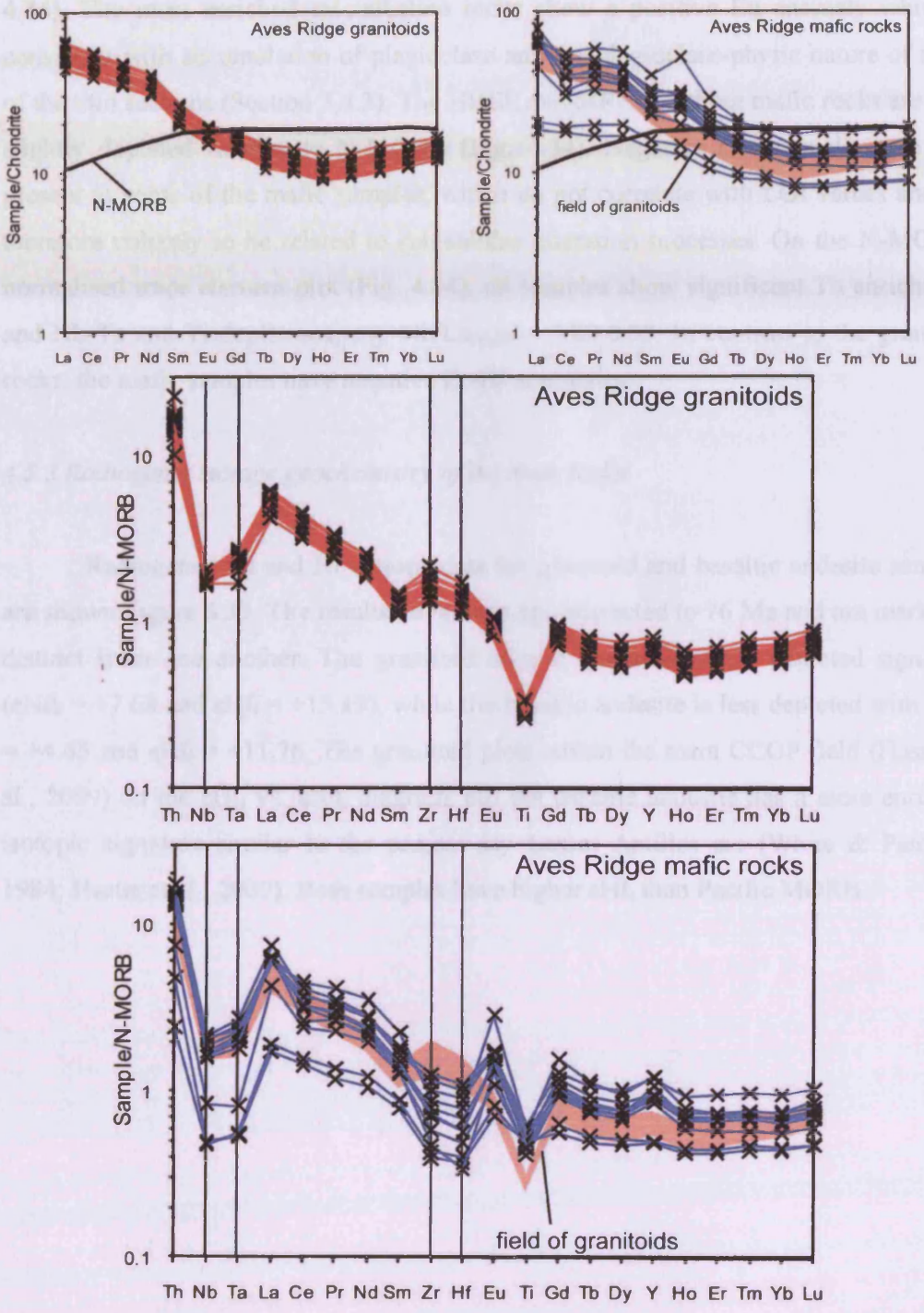

Figure 4.34. Chondrite-normalised REE plots (top) for the Aves Ridge samples; N-MORB-normalised trace element plots (bottom).

The mafic samples have LREE-enriched chondrite-normalised REE patterns (Fig. 4.34). Nine samples have La/Yb_{CN} ratios of ~5 (calc-alkaline), whilst two are less LREE-enriched and have La/Yb_{CN} ~2 (tholeiitic), in line with the Th-Co diagram (Fig.

4.34). The most enriched calc-alkaline rocks show a positive Eu anomaly which is consistent with accumulation of plagioclase and the plagioclase-phyric nature of some of the thin sections (Section 3.4.3). The HREE and MREE in these mafic rocks are both slightly depleted relative to N-MORB (Fig. 4.34). Negative Ce anomalies are also present in some of the mafic samples, which do not correlate with LOI values and are therefore unlikely to be related to sub-solidus alteration processes. On the N-MORB-normalised trace element plot (Fig. 4.34), all samples show significant Th enrichment and Nb-Ta and Ti depletions, e.g. Nb/La_{NMN} = 0.20-0.33. In contrast to the granitoid rocks, the mafic samples have negative Zr-Hf anomalies.

4.5.3 Radiogenic isotope geochemistry of the Aves Ridge

Radiogenic Nd and Hf isotope data for granitoid and basaltic andesite samples are shown Figure 4.35. The results have been age-corrected to 76 Ma and are markedly distinct from one another. The granitoid sample has a relatively depleted signature (εNd_i = +7.68 and εHf_i = +15.19), while the basaltic andesite is less depleted with εNd_i = +4.65 and εHf_i = +11.76. The granitoid plots within the main CCOP field (Hastie et al., 2009) on the εHf_i vs. εNd_i diagram, but the basaltic andesite has a more enriched isotopic signature similar to the present-day Lesser Antilles arc (White & Patchett, 1984; Hastie et al., 2009). Both samples have higher εHf_i than Pacific MORB.

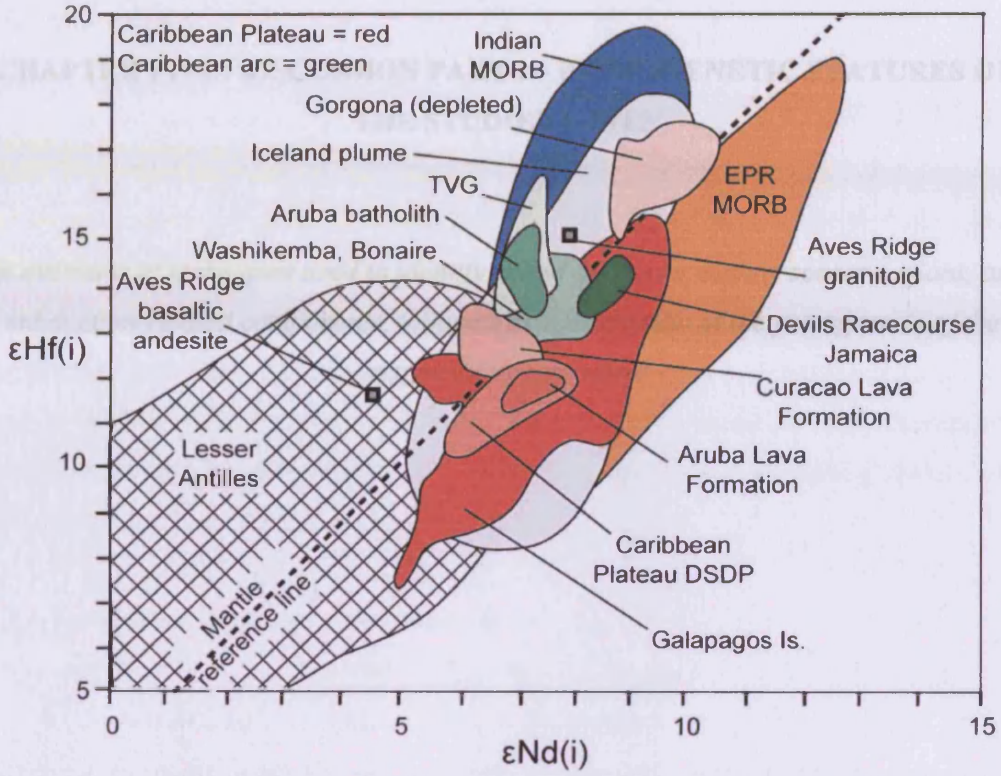

Figure 4.35. Hf-Nd radiogenic isotope plot for the Aves Ridge rocks. All fields from Thompson et al. (2003, 2004) apart from the Lesser Antilles (Hastie et al., 2009 and references therein) and Indian MORB (Chauvel & Blichert-Toft, 2001 and references therein). The analysed rocks from the Aves Ridge are isotopically distinct from one another. The basaltic andesite is more enriched than the CCOP, the granitoid is quite depleted and lies slightly above the mantle reference line of Vervoort & Blichert-Toft (1999).

CHAPTER FIVE: DISCUSSION PART I – PETROGENETIC FEATURES OF THE STUDIED UNITS

An overview of techniques used to identify island arc rocks, mantle source regions, and subduction-related components, followed by a discussion of the petrogenesis of the magmatic units studied

5.1. Introduction

In this chapter, the geochemistry of the studied units is investigated in more detail using the trace element and radiogenic isotope results from Chapter 4. Although the points covered for each individual rock unit will differ, some common themes will be explored as many of the rocks studied are mafic subduction-related rocks. Features such as the tectonic setting, mantle and/or crustal sources and subduction-related signature of each unit will be identified. This first section of the chapter will deal with how to identify subduction-related rocks, their mantle sources and slab-fluid-related components using geochemical data. In the remaining sections (5.2-5.5), the petrogenesis of each location is discussed in turn.

5.1.1. Identification of rocks from island arcs

Ancient subduction zone settings and processes leave field evidence of their past occurrence; for example, the geophysical character of the crust, the presence of tectonic mélanges and high-pressure/low-temperature metamorphic belts in older terranes, and the occurrence of a variety of intrusive or extrusive igneous rocks. The intrusive and extrusive igneous rocks formed in island arc settings also have distinctive geochemical signatures which can be used to identify their supra-subduction zone origin and, more specifically, the type of mantle source and the slab-related component involved in their petrogenesis. However, in tectonically deconstructed regions such as the Caribbean where geophysical or geological data may be limited, or unable to provide definitive conclusions as to the precise origin of a given terrane, the identification of geochemical signatures is crucial in elucidating subduction-related processes and their tectonic significance.

Island arc rocks found either in the oceanic realm, or now accreted to the continental margins, are widely considered to be formed from partial melting of a supra-subduction zone mantle wedge fluxed by fluids dewatering from the down-going oceanic slab, with possible contributions in certain environments from the melting of subducted sediments and/or the slab itself (e.g. Plank & Langmuir, 1988; Hawkesworth et al., 1993; Pearce et al., 1999; Woodhead et al., 2001). Island arc rocks are compositionally diverse. They can range from basaltic through to rhyolitic

compositions and may comprise volcanic, sub-volcanic or plutonic rocks. The key magmatic processes that occur in island arcs include partial melting of compositionally variable mantle sources, fluid or melt metasomatism of the mantle source, fractional crystallisation, and magma mixing (e.g. Wilson, 1989; Stern, 2002). In order to negate the effect of fractional crystallisation on parental melts, it is mafic rocks which are most commonly studied for their petrogenetic signatures. These rocks typically have flat to LREE-enriched normalised trace element patterns which have significant positive Th and negative Nb-Ta, Ce, Zr-Hf and Ti anomalies in relation to the surrounding REE (e.g. Pearce & Peate, 1995). Th and Ce anomalies may relate to the variable contribution of fluids to the mantle wedge derived from terrigenous and oxidised pelagic sediments (Hole et al., 1984; McCulloch & Gamble, 1991; Plank, 2005). Nb-Ta and Zr-Hf, which show negative anomalies on normalised plots, are largely retained in stable mineral phases in the slab and sedimentary veneer ('conservative' behaviour) and so their concentrations are mostly reflective of the mantle wedge composition (e.g. Pearce & Peate, 1995).

A good diagram to distinguish subduction-related rocks from those generated at mid-ocean ridges and from mantle plumes is the Th/Yb vs. Ta/Yb plot (Fig. 5.1a), where the slab-derived excess Th concentration in arc rocks can be plotted (Th/Yb) against the enrichment of the mantle source (Ta/Yb) (Pearce, 1983). This will be the first diagram considered for each location discussed, along with the normalised trace element plots.

It is widely recognised that where the slab and its sedimentary veneer do not partially melt, Nb, Ta, Zr, Hf, Ti and HREE are largely retained in subducting plate, so their concentrations in arc rocks are related to the variable mantle wedge source composition and subsequent melting processes. In contrast, Th, the LREE and the MREE are variably released from the slab and their concentrations reflect the nature and volume of slab-fluid release during subduction (e.g. McCulloch & Gamble, 1991; Pearce & Parkinson, 1993; Pearce & Peate, 1995; Elliott, 2003; Plank, 2005). Ratio-ratio plots such as Zr/Yb vs. Nb/Yb (Fig. 5.1b), can be used to demonstrate if a typically 'conservative' element (in this case Zr) has stayed in the down-going slab, or behaved 'non-conservatively' and been transported from the slab via a melt phase to the mantle wedge (Pearce & Peate, 1995). Therefore, in this thesis, the second diagram

discussed will be the Zr/Yb vs. Nb/Yb plot, which will be used to validate the conservative behaviour of Zr so that the mantle source can subsequently be investigated using ratios of Zr, Nb and the HREE (see below). In mafic rocks, when Zr has been retained in the subducting plate, the related island arc rocks will usually plot within the array of conservative Zr behaviour, which also serves as a MORB array (Pearce & Peate, 1995) (Fig. 5.1b).

5.1.2. Identification of the mantle wedge component

As described above, the HREE, Zr-Hf and Nb-Ta in many cases behave conservatively during island arc magma-genesis. Furthermore, the ratios between these elements are little affected by fractional crystallisation of olivine, Fe-Ti oxides, clinopyroxene and plagioclase in mafic lavas. The concentrations of these elements in arc magmas are therefore largely a reflection of the degree of partial melting and the initial composition of the mantle source (e.g. Thirlwall et al., 1994). In this thesis, the important distinction is between depleted sources similar to depleted MORB mantle (DMM) (Workman & Hart, 2005) and incompatible trace element-enriched sources (possibly plume-related). This information can help to understand the time at which plume-related sources enter the Caribbean island arc system. This distinction can also be applied to non-subduction settings, such as the rocks of San Souci, where conservative behaviour of the elements noted above can be assumed (Section 5.4).

The first method used in this thesis to distinguish plume and depleted sources is the Nb/Y vs. Zr/Y diagram originally developed by Fitton et al. (1997) for Icelandic basalts (Fig. 5.1c). A set of tramlines defines an 'Iceland array' which encompasses the higher Nb/Y ratios of plume-related Icelandic basaltic rocks compared to those derived from depleted mantle sources. The arc rocks in this study can also be plotted on this diagram if conservative behaviour of Nb and Zr can be demonstrated (e.g. Hastie et al., 2009, 2010c). Because the tramlines were defined for Icelandic basalts, the diagram may not be applicable to other localities, but can nevertheless give a good indication of source composition, particularly in the Caribbean region (e.g. Thompson et al., 2003; Kerr et al., 2009a).

Another test to investigate source depletion or enrichment is the absolute Zr/Nb ratio which varies as a function of the source composition. In the mantle, Zr is slightly more compatible with peridotite than Nb (Salters et al., 2002) and so very low degrees of partial melting (<5 %) can result in low Zr/Nb ratios. However, MORB, oceanic plateaus (e.g. Ontong Java and the Caribbean Oceanic Plateau) and tholeiitic-calc-alkaline arc rocks are the result of reasonably high degrees of partial melting (~10-30 %) (e.g. Pearce & Parkinson, 1993; Pearce & Peate, 1995; Kerr et al., 1996; Kushiro, 2001; Herzberg, 2004; Pearce & Stern, 2006). Low Zr/Nb ratios therefore relate directly to the source, not the melting process. In island arc rocks and in back-arcs, the Zr/Nb ratio varies systematically depending on whether or not the mantle source was plume-related or more MORB-like (Wendt et al., 1997; Hastie et al., 2010c; Neill et al., 2010, 2011). A study of the Tongan arc system by Wendt et al. (1997) showed that, where MORB-like sources are present, Zr/Nb ranges from 40-120 depending upon the degree of non-conservative Zr behaviour, however, where plume sources are present Zr/Nb ratios are less than 40 (Wendt et al. 1997). In this study, a value of Zr/Nb = 32 for average N-MORB (Sun & McDonough, 1995) is used as a boundary between MORB-like and plume-like sources. Mafic rocks with Zr/Nb consistently <32 are considered to be derived from plume-related mantle, assuming: (a) these rocks also have high Nb/Y on the diagram of Fitton et al. (1997) and (b) Zr has behaved conservatively. Those rocks with Zr/Nb consistently >32, with no high Nb/Y component and conservative Zr behaviour, may be derived from depleted mantle.

5.1.3. Identification of the slab-fluid component

LILE, LREE, and the HFSE Th in a subducting basaltic slab and its sedimentary veneer behave non-conservatively and are mobilised into the slab-flux thus contaminating the overlying mantle wedge (e.g. McCulloch & Gamble, 1991; Pearce & Parkinson, 1993; Pearce & Peate, 1995; Elliott, 2003; Plank, 2005). In the studied Caribbean rocks, some LILE such as Ba and Sr have been mobilised during sub-solidus hydrothermal and metamorphic alteration, leaving the immobile LREE (La, Ce, Pr, etc) and Th as the most suitable elements to use for assessment of the subduction component in the Caribbean samples. (e.g. Hastie, 2009). In this study, the sedimentary portion of the subduction component is investigated using Th and the LREE – be that either subducted terrigenous or (oxidised) pelagic sediments or a combination of the

two. The results may give qualitative clues as to whether or not the arc system in question was young or mature, situated in the open ocean or close to a continental landmass.

In modern arcs the Th/La ratio of arc basalts mirrors the Th/La ratio of the subducting fore-arc sediment (Plank, 2005). Th and La are significantly enriched in sediments derived from terrigenous sources (Th/La >0.3) relative to N-MORB (Th/La <0.1) (Plank, 2005). Some arcs therefore trend from low absolute Th/La ratios (<0.1) to high Th/La (>0.1), indicating input, at least in part, from fluid released by subducting terrigenous sediment (Plank, 2005).

Negative Ce anomalies on N-MORB-normalised plots of mafic island arc rocks are thought to be derived from mantle wedge fluids related to the subduction of oxidised pelagic sediment (Hole et al., 1984; McCulloch & Gamble, 1991). Pelagic sedimentation in oxidising environments can result in large negative Ce anomalies in phosphate-rich phases. In the subduction zone, oxidised Ce^{4+} is less soluble in the fluid phase than La^{3+}, so resulting in a deficiency of Ce in the resultant island arc magma (Hole et al., 1984; Toyoda et al., 1990; McCulloch & Gamble, 1991). The Ce anomaly in this thesis and in the work of Hastie et al. (2009) is expressed as a ratio of the N-MORB-normalised observed Ce concentration (Ce_{NMN}) to the expected Ce concentration given by the average of La and Pr concentrations (Ce^*_{NMN}), thus: $Ce/Ce^* = Ce_{NMN}/((La_{NMN}-Pr_{NMN})/2)+Pr_{NMM}$. Ce/Ce* consistently <1 confirms that the slab-flux may, at least in part, be derived from an oxidised pelagic sedimentary source.

In this project, the Th/La vs. Ce/Ce* plot, first used by Hastie et al. (2009), is updated to compare sedimentary slab-fluid sources for different units (Fig. 5.1d). In the sections that follow, samples are compared with mafic arc rocks from the Lesser Antilles and from the Marianas Arc which represent end-member compositions. Data is taken from the GEOROC database (2009, http://georoc.mpch-mainz.gwdg.de/georoc). In the case of the Lesser Antilles, the bulk of the sediment-related fluid component is derived from subducted terrigenous sediments originating from the Orinoco River system. On Fig. 5.1, these arc rocks have high Th/La ratios ranging from 0.1-0.6 (e.g. Fig. 5.1d) at Ce/Ce* ratios of ~0.9-1.0. The Marianas Arc is isolated from continental sedimentary sources and receives mostly pelagic sedimentary input. In contrast to the

Lesser Antilles, these rocks have low Th/La ratios (<0.2) but extend to Ce/Ce* ratios of 0.75 on Figure 5.1d. The worldwide distribution of oxidised pelagic sedimentary material with Ce anomalies is variable (Toyoda et al., 1990), but nonetheless, the Th/La vs. Ce/Ce* plot is an effective method of showing contributions in arc volcanic rocks from the addition of fluids related to the subduction of different sediment types.

5.2. Petrogenesis of La Désirade Island

5.2.1. Subduction-related origin of the La Désirade complexes

The new geochemical data demonstrates that many of the volcanic and plutonic rocks contain variable enrichments in Th relative to the HFSEs and negative Ce, Nb-Ta and Ti anomalies on N-MORB-normalised multi-element plots (Figs. 4.3, 4.4). These features are characteristic of supra-subduction zone settings and not mid-ocean spreading centres (e.g. Pearce & Peate, 1995; Pearce & Stern, 2006). Nevertheless, negative Nb-Ta anomalies could be formed by: (1) crustal contamination as the La Désirade magmas ascended and/or (2) slab-related fluids which enrich a mantle wedge in LILEs and LREEs and not Nb and Ta, the latter remaining in rutile in the subducting oceanic slab (e.g. Saunders et al., 1980; Pearce & Peate, 1995; Elliot, 2003). Fieldwork and Nd isotope data suggest that the basement below La Désirade is not composed of continental crust (Gauchat, 2004). Also, zircons separated for U-Pb dating show no evidence of inheritance from older continental basement (Mattinson et al., 2008). As a consequence, the geochemical character of the La Désirade lavas (e.g. negative Nb-Ta anomalies) is related to subduction zone processes and not continental contamination.

The Th/Yb vs. Ta/Yb diagram of Pearce (1983) (Fig. 5.1a) shows that Units 1 and 3, which do not have strong Nb-Ta anomalies (Fig. 4.3), plot in or close to the MORB array similar to some MORB-like back arc basin lavas (e.g. Pearce & Peate, 1995; Pearce & Stern, 2006). Unit 2 lavas, which have marked negative Nb-Ta and Ti anomalies, have much higher Th/Yb ratios (0.08 to 0.95) than Units 1 and 3. The Unit 2 lavas also plot above the MORB array on Figure 5.1a, similar to other Caribbean arc lavas, such as those found on Jamaica (Hastie et al., 2009, 2010b).

The felsic volcanic and plutonic rocks and intermediate-felsic dykes also plot within the tholeiitic island arc field on Fig. 5.1a. This diagram therefore shows that many of the rocks on the island have compositions compatible with a supra-subduction zone origin, but there are also N-MORB-like compositions present in Unit 1 of the NE mafic complex.

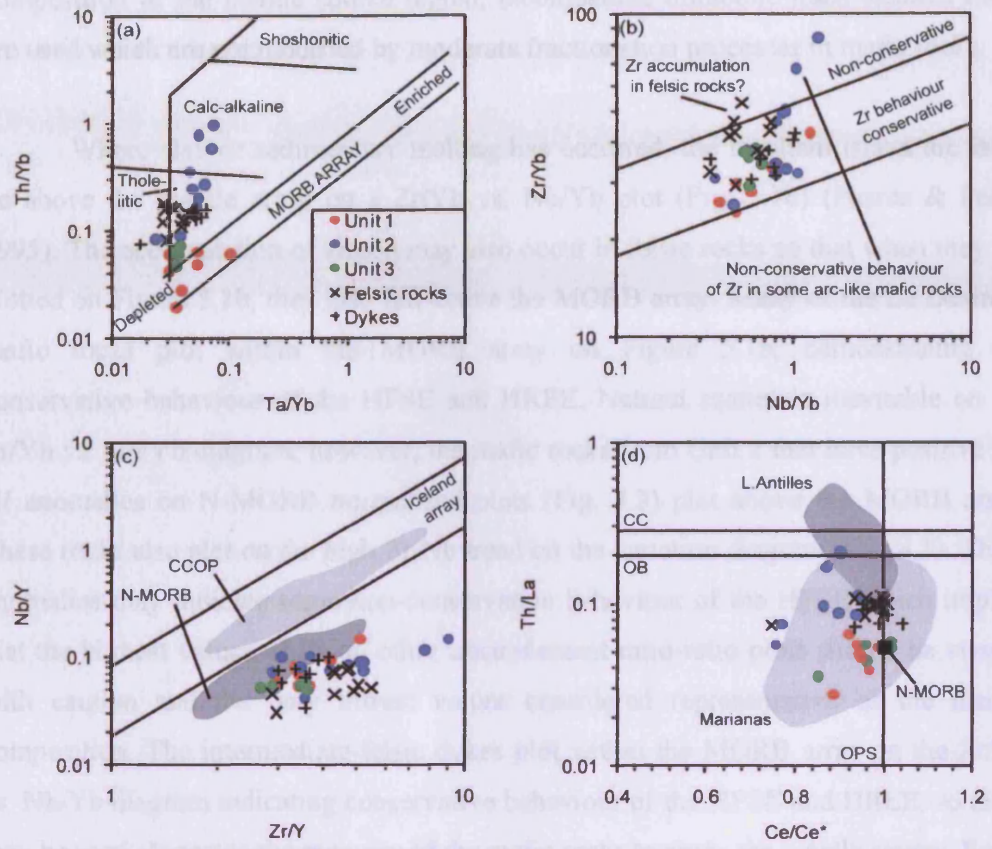

Figure 5.1. Block of four ratio-ratio plots to define the mantle and crustal sources of La Désirade magmatism. (a) Th/Yb vs. Ta/Yb diagram (Pearce, 1983) showing the tholeiitic-calc-alkaline arc affinity of the majority of the rocks, with the exception of Unit 1 which is MORB-like. (b) Zr/Yb vs. Nb/Yb diagram (Pearce & Peate, 1995) indicating slight non-conservative behaviour of Zr in some felsic rocks and Unit 2. (c) Nb/Y vs. Zr/Y diagram (Fitton et al., 1997) showing the MORB-like mantle affinity of the complexes of La Désirade. N-MORB from Fitton et al., 1997, CCOP from Hastie et al., 2008. (d) Th/La vs. Ce/Ce* diagram (Hastie et al., 2009; Neill et al., 2010, 2011) showing that the subducted sediment in the mantle beneath La Désirade was largely pelagic. CC = continental crust plots above this line. OB = oceanic basalts plot below this line. OPS = arc rocks involved with oxidised pelagic sediments plot to the left of this line. N-MORB from McDonough & Sun (1995), Marianas and Antilles data from GEOROC at http://georoc.mpch-mainz.gwdg.de/georoc (2009). References for these diagrams apply to their future use in this thesis.

5.2.2. Nature of the mantle wedge

The presence of mafic rocks with high concentrations of Cr and Ni is consistent with derivation from a mantle source (e.g. Perfit et al., 1980). Flat HREE patterns for the mafic samples on N-MORB-normalised plots also suggest that the source was shallow and garnet-free. Low MgO contents (mostly <6 wt.%) indicate that the mafic rocks have undergone substantial fractional crystallisation. Therefore, to study the

composition of the mantle source region, incompatible immobile trace element ratios are used which are not modified by moderate fractionation processes in mafic rocks.

Where slab or sedimentary melting has occurred, the resultant island arc lavas lie above the mantle array on a Zr/Yb vs. Nb/Yb plot (Fig. 5.1b) (Pearce & Peate, 1995). The accumulation of zircon may also occur in felsic rocks so that when they are plotted on Figure 5.1b, they also fall above the MORB array. Many of the La Désirade mafic rocks plot within the MORB array on Figure 5.1b, demonstrating the conservative behaviour of the HFSE and HREE. Natural scatter is inevitable on the Zr/Yb vs. Nb/Yb diagram; however, the mafic rocks from Unit 2 that have positive Zr-Hf anomalies on N-MORB normalised plots (Fig. 4.3) plot above the MORB array. These rocks also plot on the high Zr/Nb trend on the variation diagram (Fig. 4.1). These anomalies may indicate some non-conservative behaviour of the HFSE which implies that the highest values of Zr on other trace element ratio-ratio plots should be viewed with caution and the only lowest values considered representative of the mantle composition. The intermediate-felsic dykes plot within the MORB array on the Zr/Yb vs. Nb/Yb diagram indicating conservative behaviour of the HFSE and HREE, so these may be used alongside the majority of the mafic rocks to study the mantle source. Some felsic volcanic and plutonic rocks do plot above the MORB array on the Zr/Yb vs. Nb/Yb plot, consistent with their marked positive Zr-Hf anomalies on the N-MORB normalised diagram (Fig. 4.4).

As described in Section 5.1, the nature of the mantle wedge composition (where there has been conservative behaviour of Zr) can now be investigated using the Nb/Y vs. Zr/Y diagram of Fitton et al. (1997) and the absolute Zr/Nb ratio of the rocks in question from La Désirade. On the Nb/Y vs. Zr/Y plot on Fig. 5.1c, the conservative values for the La Désirade rocks plot beneath the tramlines close to the N-MORB field, and are similar to Jamaican arc rocks derived from N-MORB-like sources (Hastie et al., 2009) but are unlike arc-like rocks derived from plume-like sources such as the Blue Mountains Inlier, Jamaica (Hastie et al., 2010c).

Ignoring the samples with positive Zr-Hf anomalies on normalised plots (Fig. 4.3), the La Désirade mafic rocks have Zr/Nb ratios of 30 to 85 (mean = 52). The low Zr/Nb trend on Fig. 4.1 has a Zr/Nb ratio ~41, whereas the high trend has a Zr/Nb ratio

~60. The latter may relate to non-conservative behaviour of Zr. Nevertheless, both the trends on the differentiation plot (Fig. 4.1) and the absolute Zr/Nb ratios of the mafic lavas are consistent with a largely non-plume-related, depleted mantle wedge source similar to DMM.

5.2.3. Nature of the subducted component

The mafic rocks of Unit 1 and 3 have Ce/Ce* ratios from 1-0.85 and Th/La <0.07, portrayed on the Th/La vs. Ce/Ce* plot (Fig. 5.1d) suggesting a limited oxidised pelagic sediment fluid input, with little evidence of fluid related to subducted terrigenous sediment in the mantle wedge. As has already been shown (Figs. 4.3, 5.1a), Unit 2, has the most marked island arc signature of the three units and has a trend from Ce/Ce* ~1-0.75 at relatively high Th/La (0.07-0.22). These data point to a significant slab-fluid flux, related to the input of both subducted terrigenous and pelagic sediments into the source of Unit 2 compared to Units 1 and 3. Units 1 and 3 'trend back' to Th/La ratios similar to those found in depleted MORB mantle. The felsic volcanic and plutonic rocks and intermediate dykes have also been plotted on Figure 5.1d as Ce/Ce* ratios are unlikely to have been affected by crystal fractionation. The felsic volcanic and plutonic rocks define a trend from Ce/Ce* ~1-0.75 at moderately high Th/La (0.07-0.1) which is a similar trend to some of the rocks of Unit 2, indicating a significant involvement of fluid related to subducted oxidised pelagic sediment. The dykes plot relatively close to Ce/Ce* = 1 with Th/La ~0.1 indicating the presence of some subducted terrigenous sediment.

5.2.4. Tectonic setting

Although the geochemical results indicate the presence of an intra-oceanic subduction zone, the subduction-related input into the mantle wedge source of the rocks of La Désirade varied considerably. In particular, the very weak supra-subduction zone signature of Units 1 and 3 of the NE mafic complex is not easily explained in an arc-axis setting. Variable or low slab-fluid input is however to be expected in a back-arc supra-subduction zone setting (Pearce & Stern, 2006). A back-arc setting incorporates aspects of both the proposed ocean ridge settings (pillow lavas, slow eruption rate, pelagic sedimentation) (Mattinson et al., 2008; Montgomery & Kerr, 2009) and

subduction-related chemistry. Furthermore, because (1) the faulted contact between the NE mafic and felsic complexes is a geologically minor feature since fragments of the mafic complex can be found within the felsic complex and (2) the felsic rocks also share a subduction-related chemistry broadly similar to Units 2 and 3, the entire Mesozoic suite is likely to have been erupted in a back-arc setting in a period of ~10 Ma (Late Kimmeridgian to Mid Berriasian).

The argument for a single tectonic setting for all the complexes can be explored geochemically because the evolution of the mantle source and subducted sediment-related fluid fluxes of the complexes can be identified in stratigraphic order (Fig. 5.2). Although the felsic complexes and intermediate-felsic dykes are more evolved than the mafic complex, Fig. 5.2 shows, using La/Yb_{NMN} ratios, that the samples in all the complexes on the island are mostly tholeiitic in character. Where Nb has behaved conservatively and represents the contribution from the mantle alone, Nb/Yb_{NMN} (~0.6-1) (Fig. 5.2) varies with no obvious trends towards increasing depletion or enrichment in the incompatible element composition of the mantle source through time. Th/La values (Fig. 5.2) show that mafic Unit 2, the felsic rocks, and dykes, all contain varying degrees of input from slab-fluids related to terrigenous sediments. Ce/Ce* ratios (Fig. 5.2) show that the pelagic sediment-related flux mostly mirrors that from terrigenous sediments in mafic Units 1 and 2, but that this association does not hold true for mafic Unit 3, the felsic rocks or the dykes. Therefore at various times throughout the eruptive and intrusive sequence, different types of sediment had been subducted and contributed to the mantle source, but again there is no identifiable stratigraphic pattern. The fact that the mantle source composition and sedimentary components show few trends is, in part, due to the relatively rapid formation (~10 Ma) of the suite of complexes in a stable tectonic setting.

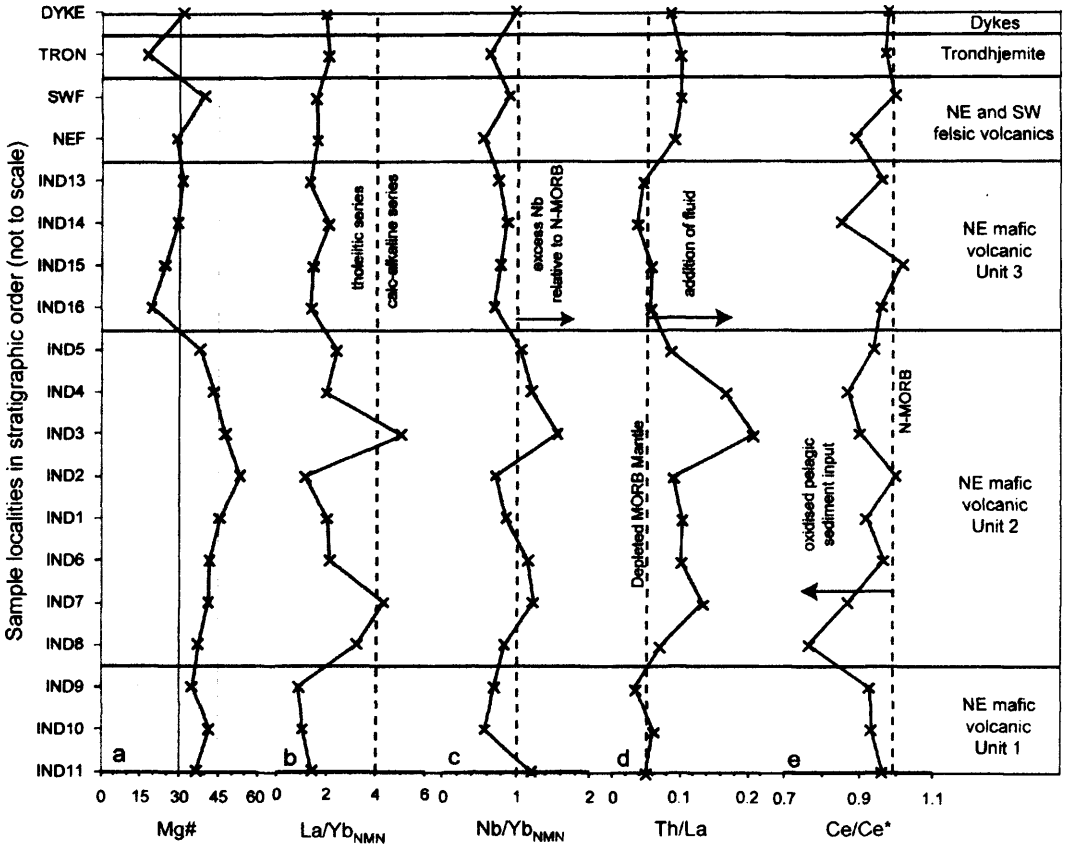

Figure 5.2. Chemostratigraphic column for the back-arc basin rocks of La Désirade Island.

5.2.5. Summary of investigation of La Désirade

La Désirade hosts the only Mesozoic rocks exposed in the Lesser Antilles. The entire suite was erupted in around ~10 Ma in the latest Jurassic to Early Cretaceous. Detailed investigation of the trace element content of the rocks of the NE mafic volcanic complex reveals that they originated in a back-arc supra-subduction setting by partial melting within a depleted mantle wedge. The mantle wedge was fluxed by fluids derived partly from variable quantities of subducted pelagic and terrigenous sediments along with a possible slab or subducted crust-related melt component which helped to modify immobile trace element ratios (Zr/Yb, Nb/Yb) in the NE mafic volcanic complex.

5.3. Petrogenesis of the rocks of Tobago

5.3.1. Petrogenesis of the North Coast Schist

Subduction-related origin of the North Coast Schist: In the Parlatuvier Formation, the presence of mafic rocks with relatively high levels of Cr and Ni clearly indicate a mantle source. Flat REE patterns and depleted isotope signatures suggest an intra-oceanic origin well away from the influence of continental crust. The Nb-Ta, Th, Ce and Ti anomalies on the N-MORB-normalised plots are quite small (Fig. 4.11), and on a Th/Yb vs. Ta/Yb diagram (Fig. 5.3a), the Parlatuvier Formation lies between tholeiitic arc compositions and the upper MORB tramline at relatively high Ta/Yb. These diagrams suggest that there is only a weak subduction zone influence on the chemistry of the Parlatuvier Formation. The high Ta/Yb, which shall be explored further below, suggests an incompatible trace-element enriched mantle source (e.g. Hastie et al., 2010c). Other rocks which plot between arc and MORB compositions on the Th/Yb vs. Ta/Yb diagram are of back-arc basin origin or relate to sediment-poor subduction systems (Pearce & Peate, 1995; Pearce & Stern, 2006). The presence of thick deposits of mafic and intermediate tuffs, tuff breccias and occasional lava flows indicates voluminous proximal explosive mafic volcanic activity, probably in relatively shallow water.

Moderate concentrations of Cr (up to 58 ppm) and Ni (up to 114 ppm) also indicate a mantle source for the felsic Mount Dillon Formation despite its more felsic character. Flat REE patterns (Fig. 4.10) and depleted isotopic signatures (Fig. 4.27) again point to an intra-oceanic origin. The Nb-Ta, Th, Ce and Ti anomalies on the N-MORB-normalised plots (Fig. 4.11) are very marked in the Mount Dillon Formation which clearly indicates a subduction-zone affinity. On the Th/Yb vs. Ta/Yb diagram (Fig. 5.3a) the Mount Dillon Formation has higher Th/Yb and slightly lower Ta/Yb than the Parlatuvier Formation, which may be related to the subduction of a greater proportion of crustal material and a more depleted mantle source. Inter-bedded meta-cherts in the Mount Dillon Formation (Snoke et al., 2001) along with the tuffaceous nature of the rocks suggest deposition occurred around or beneath sea level and not in the deep ocean where pillow basalts might be expected to form.

In 100 metre–long river section close to the Cameron Canal Fault in the centre of the island (Fig. 2.2), there are significant differences in the composition of the highly-deformed 'amphibolites' of Snoke et al. (2001a,b), from island-arc-like rocks to those with no obvious subduction component. This feature has already been partly described in Section 4.3.2. Most amphibolite samples lack negative Nb-Ta and Ti anomalies and have depleted Th in relation to the LREE on normalised plots (Figs 4.12). These MORB-like rocks plot within or slightly below the MORB array on the Th/Yb vs. Ta/Yb diagram (Fig. 5.3a). The one amphibolite sample which does have an island-arc-like signature (Fig. 4.12) plots within the calc-alkaline island arc field on the Th/Yb vs. Ta/Yb diagram, similar to the Mount Dillon Formation. One potential source of the low Th concentrations in these rocks is Th mobilisation due to the high grade of metamorphism these rocks have experienced. However, all amphibolites bar the calc-alkaline example have consistently low Th concentrations and LREE depletion on normalised plots (Fig. 4.12), coupled with reasonably straight trends for Th and La against Nb (Fig. 4.9). This consistency suggests that these elements have not mobilised and that the MORB-like character of much of the unit is primary.

The two lavas from the Karv Formation contain high quantities of Ni (171-190 ppm) and Cr (206-492 ppm) and also have flat REE patterns. These rocks also clearly have an intra-oceanic origin. The slight Ce, Zr-Hf and Ti anomalies and large Nb-Ta anomalies once more indicate a subduction-zone affinity (Fig. 4.12). These samples have intermediate Th/Yb ratios and low Ta/Yb, falling in the tholeiitic island arc field on Figure 5.3a, which is a similar pattern to the Mount Dillon Formation. Indeed on the element vs. Nb plots (Fig. 4.9), the scattered field of the Karv rocks is within the range of the rocks of the Mount Dillon Formation. These observations suggest that the meta-sedimentary and meta-igneous rocks of the Karv formation are probably not a separate part of the North Coast Schist, but merely a distinctive, sediment-rich facies of the Mount Dillon Formation.

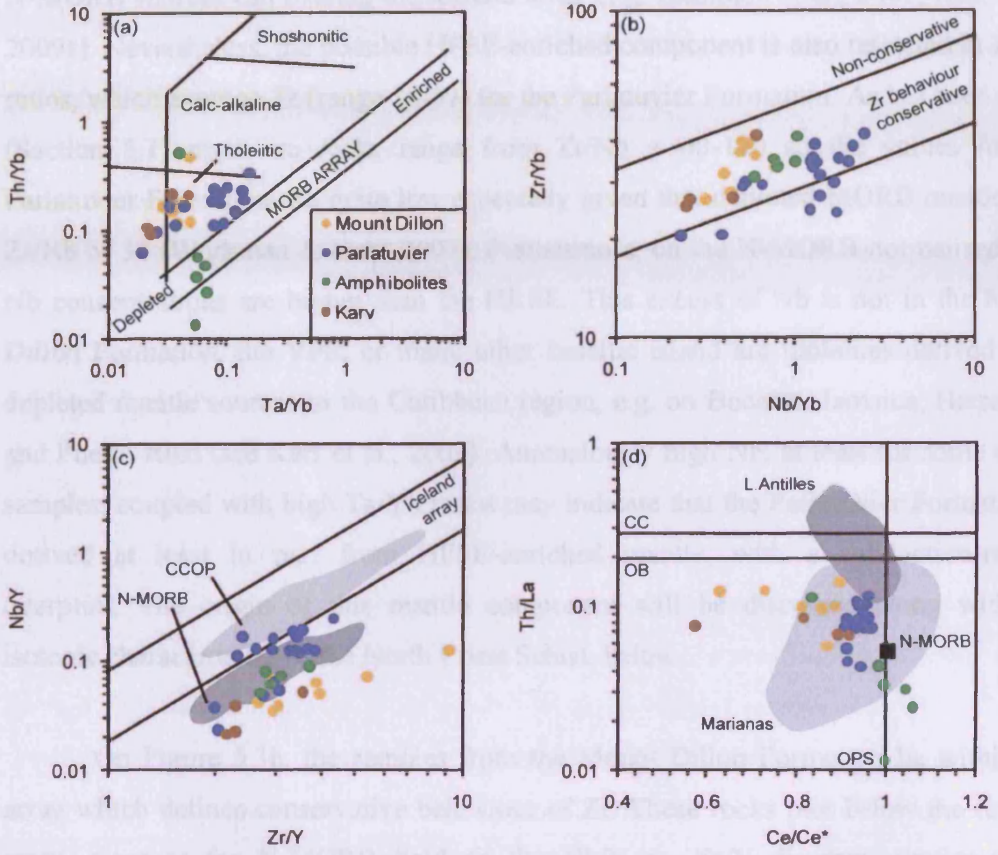

Figure 5.3. Block of four ratio-ratio plots to define the mantle and crustal sources of North Coast Schist magmatism. References as before. (a) Th/Yb vs. Ta/Yb diagram showing MORB-like characteristics of many of the amphibolites, arc-like character of the other formations and an enriched mantle source for the Parlatuvier Formation. (b) Zr/Yb vs. Nb/Yb diagram indicating conservative behaviour of Zr for all formations. (c) Nb/Y vs. Zr/Y diagram indicating a potential Nb-enriched (plume?) mantle source for the Parlatuvier Formation. (d) Th/La vs. Ce/Ce* diagram showing little terrigenous sediment involvement in any unit, and a clear MORB-like character for most of the amphibolites.

Nature of the mantle sources involved in the formation of the NCS: On the Zr/Yb vs. Nb/Yb diagram (Fig. 5.3b) all samples from the North Coast Schist fall within the MORB array, with the Parlatuvier Formation extending into the field of enriched sources. This indicates that there has been conservative behaviour of the HFSE and HREE and so they not been introduced to the mantle source in a melt phase. By extension the HFSE and REE may be used to show the affinity of the mantle source region.

The Parlatuvier Formation overlaps both N-MORB and the Iceland field on the Nb/Y vs. Zr/Y diagram (Fig. 5.3c) suggesting that the formation may contain a HFSE-enriched (plume?) component. However, studies have shown that rocks derived from

N-MORB sources can overlap the Iceland array (e.g. Kempton et al., 2000; Kerr et al., 2009a). Nevertheless, the possible HFSE-enriched component is also reflected in Zr/Nb ratios, which average 32 (range 18-57) for the Parlatuvier Formation. As has been noted (Section 5.1) most arc rocks range from Zr/Nb = 40-120 so the values for the Parlatuvier Formation are quite low especially given that depleted MORB mantle has Zr/Nb of 34 (Workman & Hart, 2005). Furthermore, on the N-MORB-normalised plot, Nb concentrations are higher than the HREE. This excess of Nb is not in the Mount Dillon Formation, the VPS, or many other basaltic island arc tholeiites derived from depleted mantle sources in the Caribbean region, e.g. on Bonaire, Jamaica, Hispaniola and Puerto Rico (see Kerr et al., 2003). Anomalously high Nb, at least for some of the samples, coupled with high Ta/Yb ratios may indicate that the Parlatuvier Formation is derived at least in part from HFSE-enriched mantle, with a subduction-related overprint. The origin of this mantle component will be discussed along with the isotopic characteristics of the North Coast Schist, below.

On Figure 5.3b, the samples from the Mount Dillon Formation lie within the array which defines conservative behaviour of Zr. These rocks plot below the Iceland array, close to the N-MORB field on the Nb/Y vs. Zr/Y diagram, similar to La Désirade, the Tobago Volcanic Group and other Caribbean island arc rocks (Fig. 5.3c). Furthermore, Zr/Nb ratios average 69 for the Mount Dillon Formation. These results are very different from the high Nb/Y and low Zr/Nb ratios in the Parlatuvier Formation and clearly indicate that the Mount Dillon Formation has a DMM-type depleted mantle source.

The amphibolite-facies samples which do not contain a subduction-related component are assumed to show conservative Zr behaviour – this is the case on Fig. 5.3b. The subduction-related amphibolite also shows conservative Zr behaviour. On the Nb/Y vs. Zr/Y plot (Fig. 5.3c) the amphibolites all fall below the lower plume-related tramline indicating a depleted mantle source. This conclusion is backed up by the Zr/Nb ratios of these rocks which are 35-47 for the MORB-like rocks and 53 for the subduction-related rock. The two meta-igneous samples from the Karv Formation also fall beneath the Iceland array within the N-MORB field on Figure 5.3c, and Zr/Nb ratios are ~102 which clearly indicate a depleted island arc mantle wedge source.

Nature of the subduction-related components in the NCS: The presence in the Parlatuvier Formation of slight Th, Nb-Ta, Ce and Ti anomalies and LREE enrichment on the N-MORB-normalised plots suggests a slab-related fluid was present although perhaps not in large quantities (Fig. 4.11). The Th/La vs. Ce/Ce* plot (Fig. 5.3d), shows that the Parlatuvier Formation has Ce/Ce* ratios between 0.9 and 1.0 and Th/La generally <0.1. This mantle-like Ce/Ce* and relatively low Th/La indicates that little subducted oxidised pelagic sediment or terrigenous sediment contributed to the slab fluid. This observation is consistent with the low Th/Yb ratios in the formation (Fig. 5.3a). Either of three possibilities might explain the lack of a strong subduction component in the Parlatuvier Formation. One possibility is that there was a low sediment input to the subduction zone and so the de-watering crust did not contribute high Th/La or anomalously low Ce concentrations to the mantle wedge. Alternatively, as the subduction-related component diminishes with distance from the arc axis (Pearce & Stern, 2006), the Parlatuvier Formation may have been erupted in the back-arc region of an intra-oceanic arc system; much of the sediment-related slab flux having contributed to arc axis magmatism. A third possibility is that the apparent subduction signature of the Parlatuvier Formation does not relate to slab-fluid addition to the mantle, but perhaps to a form of crustal contamination. This idea is untenable as the Nd isotope ratios of the Parlatuvier Formation are very depleted (Section 4.3.9) which precludes the significant involvement of continental crust in its origin. A final suggestion is that the Parlatuvier Formation is at least in part derived from subduction-modified lithospheric mantle and was not directly affected by the slab fluid-flux which was apparently present during the petrogenesis of the Mount Dillon Formation (see below).

There is no correlation in the Mount Dillon Formation between Nb concentration, as a proxy for magmatic differentiation, and Ce/Ce* ratios. Therefore, despite the silicification of the formation, Ce/Ce* ratios can be used to investigate any sediment-related signatures present. The Mount Dillon Formation is displaced to low Ce/Ce* (<0.8) at moderate Th/La (0.05-0.14) on Figure 5.3d, indicating that there was likely to have been an oxidised pelagic sediment-related fluid flux to the mantle wedge and perhaps minor involvement of terrigenous sediments. These low Ce/Ce* ratios, coupled with the large Nb-Ta anomalies in the Mount Dillon Formation, indicate that the formation is probably related to an intra-oceanic subduction zone which was distant

from the continental margins and with subducted sediment that was mostly of pelagic origin.

Karv has an intermediate geochemical signature between the Parlatuvier and Mount Dillon formations on Figure 5.3d. It has Ce/Ce* of ~0.9 at Th/La of 0.07 which suggests only a small involvement of subducted oxidised pelagic sediments and terrigenous sediments in its origin. However, only two samples were analysed and Karv overlaps both the other formations so it is difficult to accurately judge the nature of the subducted sedimentary component. Predictably, given their lack of subduction-related geochemical signatures, the majority of the MORB-like amphibolites have Ce/Ce* of ~1.0-1.1 and Th/La of 0.01 indicating no contribution from terrigenous or oxidised pelagic sedimentary material (Fig. 5.3d). The island-arc-like amphibolite plots in a similar location to the Karv and Mount Dillon formations (Fig. 5.3d).

Source of the isotopic signatures in the North Coast Schist: As introduced (Section 4.3.9), the isotopic signatures present within the North Coast Schist vary as a function of the different formations similar to the trace element geochemical results discussed above. Both the depleted MORB-like amphibolites and the enriched back-arc-like Parlatuvier Formation have more radiogenic Hf isotope ratios than the Mount Dillon Formation (Fig. 4.27) and the amphibolite and Parlatuvier Formation isotope data overlap. The different mantle trace element compositions of the amphibolite and Parlatuvier Formation require that, although isotopically similar, the mantle sources of these units were distinct. In contrast, the Mount Dillon Formation is isotopically variable and distinct from the other two units (Fig. 4.27) and does not appear to contain decoupled Hf-Nd isotope ratios. However, similar to the amphibolites, the Mount Dillon Formation appears to have a HFSE-depleted mantle source. Therefore it seems that at least three chemically or isotopically distinct mantle sources are required to generate the rocks of the North Coast Schist.

Of particular interest is the Parlatuvier Formation, which with the exception of the Arnos Vale-Mason Hall tonalite, contains the highest εHf_i yet analysed in the offshore Caribbean region (Section 4.3.9). There are several different tectonic settings in which high, radiogenic Hf isotope ratios may be generated and transferred to a subsequent melt. Mantle sources such as plumes entraining small proportions of

subducted pelagic sediments which have high Hf isotope ratios may be a candidate setting (e.g. Ingle et al., 2002). Potentially then, the Hf isotope signature of the Parlatuvier Formation was generated during plume activity, leaving a HFSE-enriched, high εHf_i residual mantle source which then partially melting due to fluid flux from a later subduction event. Another location in which high, decoupled Hf isotope ratios are found is in the sub-continental lithospheric mantle (e.g. Schmidberger et al., 2002; Choi et al., 2007). Therefore, it is also possible that the Parlatuvier Formation is related to partial melting of HFSE-enriched lithospheric mantle, perhaps during a back-arc extension event close to the arc with which the Mount Dillon Formation was related.

What does the North Coast Schist represent geologically, and when did deformation occur? Structural data from the studies of Snoke et al. (2001a,b and references therein) indicate that the North Coast Schist was deformed and metamorphosed at lower greenschist facies in an environment of largely dextral wrench shearing, causing the formation of several generations of folds, foliations, and lineations. Most studies assume that the North Coast Schist was a single island-arc-related unit deformed during intra-arc tectonic activity (Frost & Snoke, 1989; Snoke et al., 2001a). However, the occurrence of MORB-like, island-arc-like and back-arc like rocks, with isotopically and elementally different mantle sources, in an uncertain structural-stratigraphic order, is not easily explained by an origin in a single location within an intra-oceanic island arc. It appears that fragments of the North Coast Schist have been amalgamated from separate magmatic sources and brought together during deformation in fault-bounded slivers. Such a geodynamic history points towards a tectonic evolution either: (a) within an accretionary complex above a subduction zone, or (b) within a large transform fault system, perhaps at the termination of a subduction zone, where fragments of arc, back-arc and MORB-like material may be scraped from their respective positions into a single unit (see Pindell et al., 2011, for a Caribbean example).

Some further discussion of the boundary between the NCS and the VPS is necessary to confirm the timing of deformation. Firstly, an upper age limit on deformation is placed by the new U-Pb zircon age of 130.4±4.5 Ma from the Parlatuvier Formation. If the amphibolite-facies rocks are indeed a metamorphic aureole developed in the NCS in response to the emplacement of mafic and ultramafic

magmas of the TPS, then the latest age at which the NCS could have been deformed prior to intrusion is ~112 Ma, the oldest faunal age from the TVG (Snoke & Noble, 2001). However, if the amphibolite-facies rocks were somehow metamorphosed elsewhere during a different tectonic event, and are fortuitously structurally juxtaposed against the VPS today, it is possible that the NCS is allochthonous with respect to the VPS (e.g. Stephan et al., 1980 – these authors assumed that the boundary between the NCS and VPS was only a shear zone, not a contact aureole associated with dynamic emplacement of the VPS). This alternative hypothesis, if proven, would mean that there is essentially no lower limit on the timing of NCS deformation because the age of suturing of the two rock suites would be unknown. In such circumstances the deformation of the NCS cannot be definitively related to models of subduction polarity reversal (see Section 6.3.2). However, is there any evidence for suturing of the NCS and VPS after the two units had formed? Several factors suggest that this hypothesis is incorrect. Firstly to repeat, the metamorphic grade of the amphibolites decreases with distance from the contact with the VPS. Secondly, there is little evidence for deformation of the VPS at angles sub-parallel to the contact between the two suites, such as might be expected if they were brought together during later strike-slip faulting. Thirdly, zircon fission track dating of the TPS indicates cooling through 250-200°C at 103 Ma (Cerveny & Snoke). High strain features, such as mylonites, which are documented both in the amphibolite facies rocks and in the ultramafic rocks of the TPS, are unlikely to have formed at shallow crustal depths during a later suturing event, and are therefore most likely to have formed prior to 103 Ma during ductile deformation related to magmatic emplacement (Snoke et al., 2001a). Finally, Snoke et al. (2001a) and this study report the finding of mafic dykes with distinctive acicular hornblendes in both the NCS and the TPS, which, if part of the mafic dyke swarm, are likely to be ~103-91 Ma and therefore indicators that the NCS and VPS were together at this time. Therefore, the NCS is argued to have been 'in-situ' during VPS magmatism, and its deformation is most likely to have occurred between ~130 and ~112 Ma. A consideration of a possible location of this complex, and where the different elemental and isotopic mantle components may be derived from, is outlined in Section 6.3.

5.3.2. Petrogenesis of the Tobago Volcanic Group

Tectonic setting and mantle source of the TVG: The clear Th, Nb-Ta, Ce and Ti anomalies, coupled with largely tholeiitic-calc-alkaline compositions and depleted isotopic signatures indicate that the Tobago Volcanic Group is related to an intra-oceanic subduction zone. On a Th/Yb vs. Ta/Yb plot (Fig. 5.4a) most of the samples from each formation lie within the tholeiitic and calc-alkaline island arc fields well above the MORB array similar to many intra-oceanic island arcs. There are some samples which form a trend towards low Ta/Yb ratios outside of the normal island arc trend (Fig. 5.4a). There is no correlation between Ta/Yb ratios and SiO_2 or MgO content in the TVG indicating that Ta/Yb ratios are not due to fractionation of the main mafic mineral phases such as clinopyroxene. The most likely explanation for the low Ta/Yb ratios of some of the rocks from the TVG is that they are derived from a particularly depleted mantle source from which significant volumes of melt had been extracted.

The Zr/Yb vs. Nb/Yb diagram for the TVG (Fig. 5.4b), unlike the rocks of the North Coast Schist, also appears to show a trend running from low Zr/Yb and Nb/Yb, below the conservative Zr behaviour tramlines, to higher values of both ratios. One sample of undifferentiated, clinopyroxene-rich volcanogenic sediment lies alone at very low Zr/Yb. The sweep of Zr/Yb and Nb/Yb values is unusual and may again be a product of a particularly depleted mantle source (low Nb/Yb ratios) and the occasional introduction of Zr-rich fluids, perhaps from a sediment-related partial melt phase (high Zr/Yb ratios). It should be stressed that the bulk of analyses fall within the Zr conservative behaviour tramlines so the HFSE and REE have mostly behaved conservatively and can thus be used to study the nature of the mantle source region.

On the Nb/Y vs. Zr/Y diagram (Fig. 5.4c) almost all the samples from the TVG plot beneath the lower tramline indicating a depleted, non-plume-related source region similar to DMM. Zr/Nb ratios range from 40-114, within the range of island arcs derived from N-MORB-like mantle sources (Wendt et al., 1997).

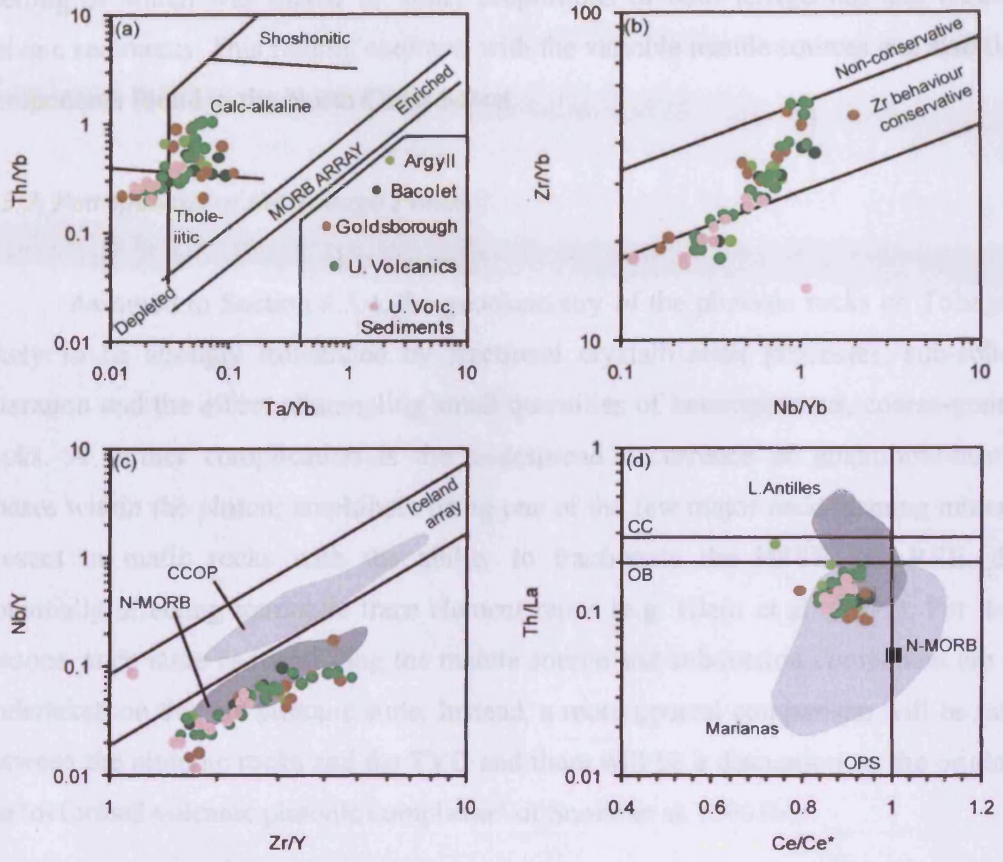

Figure 5.4. Block of four ratio-ratio plots to define the mantle and crustal sources of the Tobago Volcanic Group. (a) Th/Yb vs. Ta/Yb diagram showing that all formations fall into the tholeiitic-calc-alkaline island arc categories. (b) Zr/Yb vs. Nb/Yb diagram indicating largely conservative behaviour of Zr. (c) Nb/Y vs. Zr/Y diagram indicating a depleted MORB-like source for all formations of the TVG. (d) Th/La vs. Ce/Ce* diagram showing that all formations have been influenced by subducted terrigenous and oxidised pelagic sediments. References as per previous diagrams.

Nature of the subduction-related component: The Th/La vs. Ce/Ce* diagram is again employed to investigate the oxidised pelagic and terrigenous sedimentary input to the mantle wedge that formed the TVG (Fig. 5.4d). The studied formations almost completely overlap, which indicates that they are all derived from a mantle wedge into which similar compositions of slab flux were added. The trend shown is from relatively low Th/La (0.1) at quite high Ce/Ce* ratios (0.95) to higher Th/La (0.2) and lower Ce/Ce* (0.8) ratios, respectively, indicating a variation of sediment-related slab flux, but always with a contribution from high Th/La terrigenous sediments and low Ce/Ce* oxidised pelagic sediments. There is no correlation between Th/La and Ce/Ce* ratios against Nb concentrations indicating that fractional crystallisation is not responsible for the trends shown on Figure 5.4d. Therefore it is concluded that the Tobago Volcanic Group was formed at ~112-106 Ma from a depleted mantle wedge source, the partial

melting of which was fluxed by small proportions of both terrigenous and oxidised pelagic sediments. This finding contrasts with the variable mantle sources and slab fluid components found in the North Coast Schist.

5.3.3. Petrogenesis of the Tobago Pluton

As noted in Section 4.3.4, the geochemistry of the plutonic rocks on Tobago is likely to be strongly influenced by fractional crystallisation processes, sub-solidus alteration and the effect of sampling small quantities of heterogeneous, coarse-grained rocks. A further complication is the widespread occurrence of amphibole-bearing phases within the pluton; amphibole being one of the few major rock-forming minerals present in mafic rocks with the ability to fractionate the HFSE and REE, thus potentially affecting immobile trace element ratios (e.g. Klein et al., 1997). For those reasons, such tasks as identifying the mantle source and subduction component are not undertaken on this arc plutonic suite. Instead, a more general comparison will be made between the plutonic rocks and the TVG and there will be a discussion on the origin of the 'deformed volcanic plutonic complexes' of Snoke et al. (2001b).

Affinity of the TPS with the Tobago Volcanic Group: Previous chronological studies (e.g. Sharp & Snoke, 1988) have shown that the TVG and Tobago Plutonic Suite were essentially contemporaneous, with field studies indicating that the TPS intruded the lower reaches of the TVG shortly after the formation of the latter (Snoke et al., 2001a). The rocks of the TPS are plotted for comparison on the four diagrams used to define the mantle and crustal sources of the TVG (Fig. 5.5). On all four diagrams, the rocks of the pluton encompass the compositions of the TVG, but have a far wider spread of values, mostly towards much lower Th (e.g. Th/Yb vs. Ta/Yb diagram, Fig. 5.5a) or Zr concentrations (Figs 5.5b, c, d), with a few samples plotting at higher Th or Zr abundances. This feature appears to be most prevalent for the gabbro-diorite pluton and is interpreted as the result of accumulation or fractionation of HFSE-compatible phases such as zircon. In terms of Hf and Nd isotope ratios, the two analysed samples from the gabbro-diorite component of the TPS are identical to the composition of the TVG (Fig. 4.27). In summary it appears that the TPS and TVG are contemporaneous and derived from similar mantle sources.

Origin of the deformed mafic volcanic-plutonic complexes: The key features of the Anse Flamengo, Richmond River and Merchison River complexes are described in Sections 3.2.4 and 4.2.3. Snoke et al. (2001a) speculated that these complexes formed by dynamo-thermal metamorphism of pre-existing gabbroic and volcanic material during the intrusion of the ultramafic cumulate bodies, with metamorphism reaching pyroxene-hornfels facies in places. In terms of REE and HFSE concentrations (Figs. 4.18, 4.19) and the ratio-ratio plots (Fig. 5.5) there is significant overlap between the deformed complexes and the mafic and ultramafic components of the TPS. All have tholeiitic arc-like compositions with MORB-like mantle sources and slight inputs from fluid derived from terrigenous and oxidised pelagic sediments. Therefore the deformed complexes are almost certainly genetically related to the TPS and furthermore do not appear to bear any relationship to the amphibolites in the North Coast Schist.

Isotopic evidence for the origin of the TVG and pluton: On Figure 4.27, the rocks of the TVG and pluton fall on the mantle array in an almost identical location to the depleted island arc rocks of Bonaire, Dutch Antilles (Thompson et al., 2004). One sample in particular has high εHf_i, defining a short trend towards the radiogenic components of the Parlatuvier Formation and the Arnos Vale-Mason Hall tonalite. It is possible that these rocks have been derived from an eastern Pacific mantle source similar to Bonaire but that there has been some contamination by assimilation of high εHf_i rocks of the lower arc crust such as those in the Parlatuvier Formation.

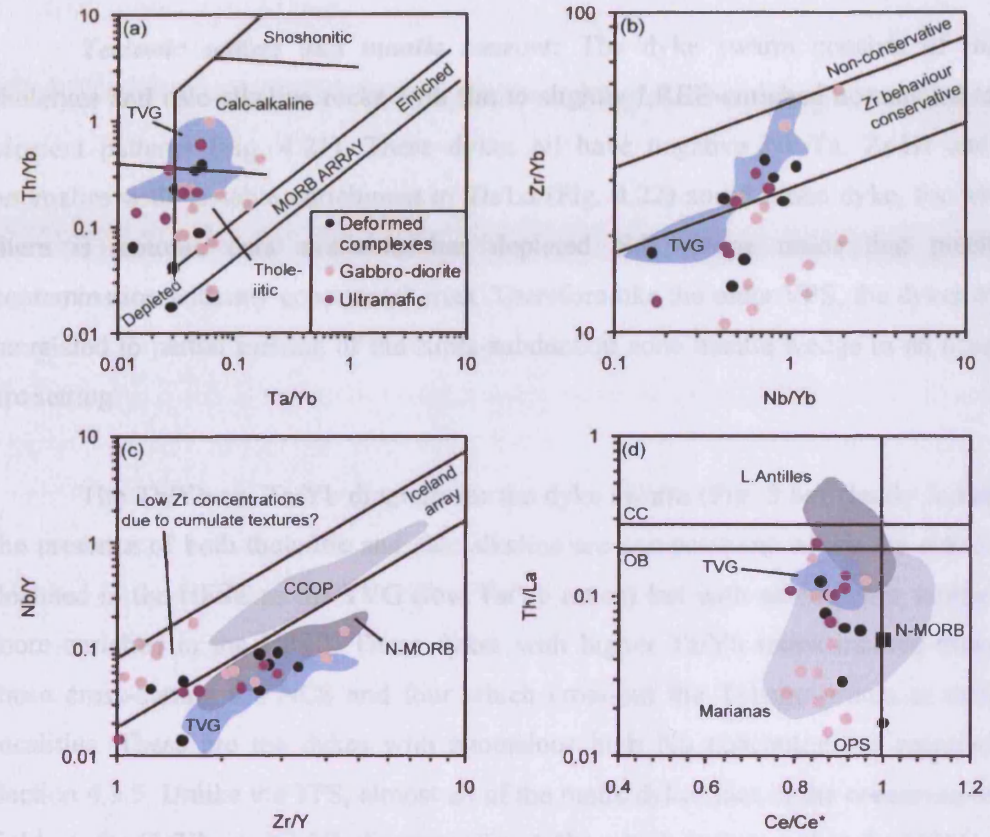

Figure 5.5. Block of four ratio-ratio plots to compare the Tobago Volcanic Group to the ultramafic-intermediate TPS. (a) The Th/Yb vs. Ta/Yb diagram shows that the pluton has quite a depleted island arc source but covers a wider range of compositions than the TVG. (b) Zr/Yb vs. Nb/Yb diagram indicating conservative behaviour of Zr, but values lower than the MORB array (tramlines) which may be due to the cumulate textures in these rocks and the collection of zircon-undersaturated samples. (c) Nb/Y vs. Zr/Y diagram indicating a similar problem to (b), a MORB-like source but with anomalously low Zr concentrations. (d) Th/La vs. Ce/Ce* diagram showing a wide spread of values similar to (a). The deformed complexes fall in the same areas as the ultramafic and some gabbroic components of the pluton, unlike the MORB-like amphibolites of the NCS. References as per previous diagrams.

5.3.4. Petrogenesis of the mafic dyke swarm

The results of dating (Section 2.2) and the major and trace element and isotopic analyses (Section 4.2) indicate that the mafic dyke swarm is variable in age, petrology and composition. The geochemical trends on Figure 5.6 indicate that there were probably subtle changes in mantle sources and the subduction component during their emplacement (up to 10-15 Ma from the time of formation of the TVG). Unfortunately it is difficult to quantify these changes because the age of all bar two dykes is unknown (Sharp & Snoke, 1988). Nevertheless, as with the other units on Tobago, this section represents an attempt to clarify the mantle sources and slab components in these rocks.

Tectonic setting and mantle sources: The dyke swarm consists of mafic tholeiites and calc-alkaline rocks with flat to slightly LREE-enriched normalised trace element patterns (Fig. 4.21). These dykes all have negative Nb-Ta, Zr-Hf and Ti anomalies with variable enrichment in Th/La (Fig. 4.22) and the one dyke, for which there is isotopic data available, has depleted Nd isotope ratios that preclude contamination with any continental crust. Therefore like the older VPS, the dykes must be related to partial melting of the supra-subduction zone mantle wedge in an oceanic arc setting.

The Th/Yb vs. Ta/Yb diagram for the dyke swarm (Fig. 5.6a) clearly indicates the presence of both tholeiitic and calc-alkaline arc compositions which are mostly as depleted in the HFSE as the TVG (low Ta/Yb ratios) but with some dykes somewhat more enriched in the HFSE. These dykes with higher Ta/Yb ratios include three of those cross-cutting the NCS and four which cross-cut the Tobago pluton at various localities. These are the dykes with anomalous high Nb concentrations reported in Section 4.3.5. Unlike the TPS, almost all of the mafic dykes plot in the conservative Zr field on the Zr/Yb vs. Nb/Yb diagram (Fig. 5.6b) which indicates that the HFSE and HREE can be used to study the petrogenesis of these rocks. The seven anomalous dykes on Figure 5.6a plot at systematically higher Nb/Yb ratios than the other mafic dykes on Figure 5.6b.

The Nb/Y vs. Zr/Y plot (Fig. 5.6c) shows that most of the samples plot close to or slightly below the lower tramline of the Iceland array, with the anomalous high Nb-Ta samples lying between the tramlines in the Iceland array. This implies that the mantle source of the majority of the dyke swarm was depleted, and similar to that which fed the Tobago Volcanic Group, which is consistent with the relatively low HREE abundances on the N-MORB-normalised plots (Fig. 4.22). Zr/Nb ratios from the dyke swarm are variable, ranging from 8-62. However, excluding the 7 samples with anomalous Nb-Ta concentrations, the range is 30-68. This indicates that the majority of the mafic dyke swarm is indeed derived from a depleted (DMM?) mantle. The dykes with the lowest Zr/Nb are not the lowest in MgO, nor are they high in LREE concentrations compared to the other members of the swarm. Therefore, their relatively high Nb concentrations (~4 ppm, the highest in the swarm) are not likely to be the

product of low degrees of partial melting and are instead a product of the mantle source composition.

The two dated dykes have ages of 103 and 91 Ma (Sharp & Snoke, 1988) and both are derived from depleted mantle sources. During this time, there was unlikely to have been plume-related mantle in the Caribbean region, because the bulk of the CCOP was generated rapidly at ~95-90 Ma (Kerr et al., 2003) and hitherto no clearly identified older fragments of oceanic plateau have been found in the region. Furthermore, if the dykes do represent a spread of intrusion ages between ~103 and 91 Ma, and the bulk of analyses suggest a MORB-like or more depleted mantle source, it is unlikely that the dykes containing unusually high Nb-Ta concentrations formed from a plume-related mantle. One suggestion is that these rocks formed by the hybridisation of tholeiitic island arc basalts (depleted mantle source) with a small amount of high-Nb basaltic melt (enriched mantle component), and thus overlap with a class of rock type known as Nb-enriched basalts (Reagan & Gill, 1989; Castillo et al., 2007; Castillo, 2008). Some dykes on Tobago have indeed been described separately (Section 4.3.8) as Nb-enriched basalts and the origin of these anomalous members of the mafic dyke swarm will be discussed in Section 5.3.6.

Nature of the subduction-related component: The subduction-related component of the dykes derived from depleted mantle is now investigated using Th/La and Ce/Ce* ratios. On the Th/La vs. Ce/Ce* diagram (Fig. 5.6d) the mafic dyke swarm falls in a single field which ranges from Ce/Ce* = 0.7-1.0 with a slope towards high Th/La from 0.05-0.15. Therefore, the mafic dykes are likely to have been influenced by the addition of fluid from both terrigenous and oxidised pelagic sediments. The field of the mafic dyke swarm covers the compositions of both the TVG and the Parlatuvier Formation, indicating that the dyke swarm records a range from high to low volumes of fluid related to subducting sediments. The ~103 Ma dyke dated by Sharp & Snoke (1988) has Th/La = 0.11 and Ce/Ce* = 0.92; the ~91 Ma dyke 2D-14 has Th/La = 0.06 and Ce/Ce* = 1.02, demonstrating that for the dated rocks, there may be a reduction in the subduction component derived from subducted sediments with time.

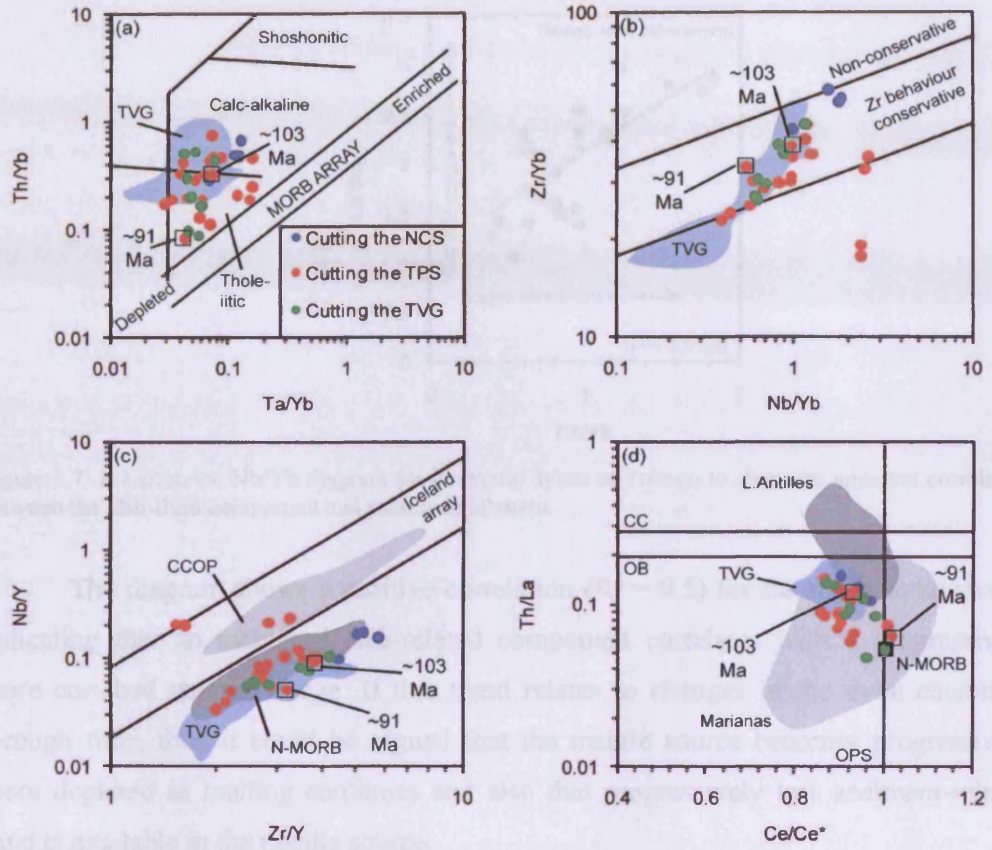

Figure 5.6. Block of four ratio-ratio plots to compare the mafic dyke swarm to the Tobago Volcanic Group. (a) The Th/Yb vs. Ta/Yb diagram shows a range of dyke compositions from almost MORB-like tholeiites to calc-alkaline island arc rocks. (b) Zr/Yb vs. Nb/Yb diagram indicating mostly conservative behaviour of Zr. Some values lower than the MORB array (tramlines) which may be due to elementally depleted samples. Note that these and some of the dykes cutting the NCS have relatively high Nb/Yb ratios suggesting an ultimately more enriched source than that for the TVG. (c) Nb/Y vs. Zr/Y diagram indicating that most dykes have an N-MORB-like source but some may come from sources with higher Nb concentrations (plume, or mixing with high-Nb basalts?). (d) Th/La vs. Ce/Ce* diagram that the dykes range from little input from subducted sediments to moderate input of both terrigenous and oxidised pelagic sediments. CC = continental crust plots above this line. OB = oceanic basalts plot below this line. OPS = arc rocks involved with oxidised pelagic sediments plot to the left of this line. References as per previous diagrams.

If this relationship holds true for the whole of the mafic dyke swarm, then a reduction in the sediment-related slab flux indicates a trend towards more mantle-dominated partial melting and mantle depletion. To this end, a plot of La/Sm vs. Nb/Yb is used as a proxy for the degree of slab-fluid input versus depletion of the mantle source (Fig. 5.7).

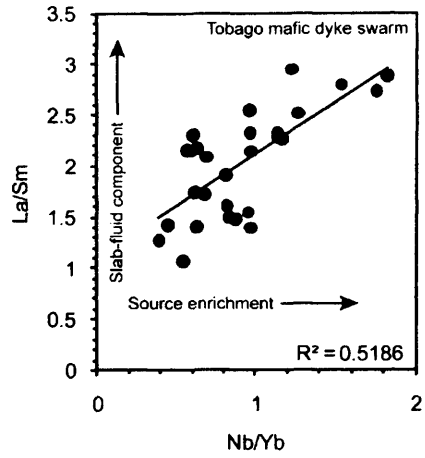

Figure 5.7. A La/Sm vs. Nb/Yb diagram for the mafic dykes of Tobago to show the apparent correlation between the slab-fluid component and source enrichment.

The diagram shows a positive correlation ($R^2 = 0.5$) for the mafic dyke swarm indicating that an increased slab-related component correlates with a progressively more enriched mantle wedge. If this trend relates to changes in the dyke chemistry through time, then it could be argued that the mantle source becomes progressively more depleted as melting continues and also that progressively less sediment-related fluid is available in the mantle source.

A plate tectonic explanation for the apparent depletion of the Tobago mantle source and reduction in the sediment-related component is more elusive. It is possible that subduction, and thus the sediment-flux, stalled and that some degree of inter-arc extension occurred along the arc axis allowing continued magmatism, albeit from an increasingly depleted mantle source. Isotopically, the analysed sample of the Tobago dyke swarm has a similar composition to EPR MORB and therefore contains a more depleted Nd isotope signature compared to the TVG (Fig. 4.27). However, many more analyses and dates would be needed to judge if the mafic dyke swarm is genuinely isotopically distinct from the other rocks of Tobago or if there are any time-integrated trends in isotopic composition.

5.3.5. Petrogenesis of the Arnos Vale-Mason Hall tonalite

Comparison with adakites: It has already been noted (Section 4.3.1) that the tonalite was emplaced only shortly after the TVG and TPS. Because of the geochemical

differences compared to the plutonic suite, and a lack of evidence for fractionation of the gabbro-diorite of the TPS (Section 4.3.4), the tonalite must have originated from a separate process and/or protolith within the same intra-oceanic subduction system compared to the rest of the Albian rocks. There appear to be geochemical similarities between the tonalite and high-silica adakites (Table 5.1) (e.g. Defant et al., 1992; Martin et al., 2005), which are considered to be formed by partial melting of an amphibolitic or eclogitic mafic protolith (e.g. Drummond & Defant, 1990; Rapp et al., 2003; Martin et al., 2005; Moyen, 2009). It should be noted that occurrences of Phanerozoic 'adakitic' plutons are relatively rare, and adakites are usually found as volcanic rocks (Drummond & Defant, 1990; Moyen, 2009). Because of these reasons, the Arnos Vale-Mason Hall tonalite will *not* be called an adakite.

Table 5.1. Comparison between Cenozoic adakites and the Arnos Vale-Mason Hall tonalite body.

Feature	Adakite (Drummond & Defant, 1990)	Arnos Vale tonalite (this study)
SiO_2	>56 wt.%	62-71 wt.%
Al_2O_3	>15 wt.%	16-20 wt.%
MgO	<3 wt.%	<2 wt.%
Sr (ppm)	>300 ppm (plagioclase-free source)	300-800 ppm
Sr/Y	>40 (plag-free source, residual garnet)	73-225
La/Yb	>20 (residual garnet)	5-30
Yb	<1.9 ppm (residual garnet)	<0.4 ppm
Y	<18 ppm (residual garnet)	<5 ppm
Nb	<10 ppm	<5 ppm

Whole rock geochemical constraints on the tonalite source: The SiO_2 content of 62-71 wt.% in the tonalite is too low to indicate melting of a quartz-bearing felsic protolith so it is most likely that the tonalite was formed by the partial melting of a metabasic protolith. High Na_2O/K_2O ratios of 6-10 indicate that the protolith was tholeiitic. Sr concentrations of 300-800 ppm and Al_2O_3 of 16-20 wt.% are both quite high, which, coupled with positive Eu anomalies on the chondrite-normalised plot (Fig. 4.23), demonstrate a largely plagioclase-free source and possibly the accumulation of plagioclase during crystallisation. High normalised Ce/Y, La/Yb and Gd/Yb ratios and low absolute Yb and Y contents indicate residual garnet in the source (Martin, 1999; Martin et al., 2005). Positive Zr-Hf anomalies on an N-MORB-normalised plot (Fig. 4.23) and slightly concave REE patterns (Fig. 4.23) can be ascribed to residual amphibole because amphibole is more compatible with the MREE compared to Zr, Hf and the HREE (Klein et al., 1997; Hastie et al., 2010a,b). A further constraint is provided by the low concentrations of TiO_2 in the tonalite which do not vary as a function of magmatic differentiation (Fig. 4.17). TiO_2 hosted in residual rutile during

partial melting would act as a buffer to TiO_2 concentrations in the tonalite magma. These constraints collectively demonstrate that the source of the tonalite was most likely to be a *plagioclase-free, tholeiitic garnet-rutile amphibolite.*

Depth and location of partial melting: Plagioclase stability is strongly temperature-and depth-dependent in high pressure metamorphic systems and may provide a clue to the depth of partial melting. The transition from blueschist to eclogite facies, defined by the breakdown of albite (plagioclase), occurs at around 50 km, so partial melting probably occurred at 50 km depth or greater where plagioclase is no longer a residual phase (Martin et al., 2005; Clemens et al., 2006). Also, rutile is stable at depths of ~50-80 km in the subduction zone again precluding a partial melting depth of <50 km (Xiong et al., 2005; Xiong, 2006). However, melting at significantly deeper than 50 km is also unlikely, because fluid-present conditions are necessary for the presence of residual amphibole, yet the formation of omphacite at the expense of glaucophane (amphibole) also occurs at around 50 km (Martin, 1999; Clemens et al., 2006). Therefore, it is suggested that the partial melting of the Arnos Vale-Mason Hall tonalite protolith occurred at ~50 km at the amphibolite-eclogite transition.

It should be noted that the depth of island arc crust rarely exceeds 50 km in the oldest most stable examples (Keary et al., 2009), so these mineralogical constraints strongly indicate that partial melting took place within the subducting slab.

Alternative models: One alternative to the slab-melting model is that island arc magmas generated in the same mantle wedge that formed the TVG underwent a very different crystallisation history, involving the high-pressure fractional crystallisation of garnet, and later amphibole to generate a tonalitic melt (e.g. Macpherson et al., 2006). However, the clearly different isotope signatures of the tonalite and the TVG/TPS preclude this model. As has already been discussed above, and in Sections 4.3.1, 4.3.6 and 4.3.9, the Arnos Vale-Mason Hall tonalite differs in REE and trace element patterns, incompatible trace element ratios (e.g. Nb/Yb), and Hf isotope ratios from the VPS. Therefore, low pressure fractional crystallisation, or re-melting of the VPS is also discounted as a model for tonalite genesis.

The problem of the mantle signature in the tonalite: In the absence of a mantle or a local crustal source for the tonalite, the melting of the down-going oceanic slab or crust delaminated from the arc will be considered as potential petrogenetic models. The tonalite was emplaced shortly after the TVG and is cut by island arc-related dykes, so partial melts were generated when there was already a partially molten metasomatised mantle wedge beneath the arc. A 'pristine' slab-derived partial melt should assimilate mantle peridotite within the wedge, producing a hybridised melt with >2.0 wt.% MgO, >40 ppm Ni and >50 ppm Cr despite the effects of fractional crystallisation (Rapp et al., 1999; Prouteau et al., 2001; Xu et al., 2002; Smithies et al., 2009). Although fractionation of mafic minerals and oxides might deplete some parts of the Arnos Vales tonalite in MgO, Ni and Cr, the concentrations of these elements within the 10 analysed samples (as low as 62.5 wt.% SiO_2) are always <1.7 wt.%, <35 ppm and <39 ppm, respectively. Because of the evidence that mantle wedge melting formed the TVG and mafic dyke swarm, any slab- or delamination-derived tonalite would therefore have to reach surface without assimilating significant volumes of mantle wedge peridotite.

Isotopic constraints on tonalite genesis: The strongly decoupled Hf-Nd isotopic signature of the tonalite body is more extreme even than that displayed by the MORB-like amphibolites and the Parlatuvier Formation of the North Coast Schist (Fig. 4.27). At ~106 Ma, the mantle sources of the TVG and TPS were not isotopically decoupled and logically the bulk island arc crust would have similar isotope ratios to the TVG and TPS. Therefore isotopically distinct subducting oceanic crust appears to be the most likely source of the tonalite. It is possible that the amphibolites, which do show a slightly decoupled Hf-Nd isotope signature, are representative of such oceanic crust, but they would have to be significantly more isotopically variable than the two analysed samples. It remains possible that partial melting of that crust could generate the tonalite body.

5.3.6. Petrogenesis of the Nb- and LREE-enriched mafic and felsic intrusions

In one common model applied to the Philippines island arc system, high-Nb basalts and Nb-enriched basalts are argued to be the indirect product of slab melting in an island arc system (Sajona et al., 1993, 1994, 1996; Aguillón-Robles et al., 2001). These authors suggest that partial melting of the down-going oceanic slab results in the formation of adakite magmas which metasomatise the mantle wedge, with melting of that enriched metasomatised mantle generating high-Nb basalts. High-Nb basalts may mix with tholeiitic arc magmas to generate Nb-enriched basalts (Castillo, 2008). However, it was later proposed (Castillo et al., 2002, 2007; Macpherson et al., 2006) that in the Philippines arc system, there was no slab melting event. These authors showed that the adakite magmas were isotopically similar to the erupted arc basalts and were geochemically unrelated to the subducting slab. The high-Nb basalts were also isotopically distinct from the adakites. Therefore, the high-Nb basalts were likely to be derived from a heterogeneous mantle containing pockets of HFSE-enriched material related to intra-plate magmatism (Castillo et al., 2007). The adakites were found to be related to high-pressure fractionation of island arc basalts (Macpherson et al., 2006). These studies have shown that the petrogenesis of high-Nb or Nb-enriched basalts does not fit a standard model and therefore any given occurrence requires careful geochemical and isotopic examination.

On Tobago, the Nb-enriched basalt has a lower εHf than the contemporaneous ~106 Ma Arnos Vale-Mason Hall tonalite (Fig. 4.27), and so these two rocks cannot be directly or indirectly related to each other. Therefore the genetic link between adakites and high-Nb basalts/Nb-enriched basalts proposed by Sajona et al. (1993, 1994, 1996) seems unlikely in this case. Likewise, the Nb-enriched basalt cannot be related directly to the island arc magmatism which formed the TVG as again it has a significantly lower Hf isotope ratio compared to the TVG (Fig. 4.27). Therefore the Nb-enriched basalt is likely to be derived from an isotopically distinct, HFSE-enriched mantle source, as appears to be the case in the Philippines (Castillo et al., 2007). It is clear that a much larger number of major, trace element and isotope analyses of the Arnos Vale-Mason Hall tonalite and the Nb-enriched mafic rocks are necessary to come to a definitive conclusion.

If slab melting occurred at ~106 Ma to form the Arnos Vale-Mason Hall tonalite, then it is possible that the slab melting led to the ingress of distinct, isotopically enriched, HFSE-enriched mantle which could partially melt to form high-Nb or Nb-enriched basalts. Ingress of isotopically distinct mantle could occur in many circumstances, for example subduction of a slab edge (e.g. Yogodzinski et al., 2001), or the subduction of a spreading ridge or ridge transform to form a slab window (e.g. Thorkelson & Breitsprecher, 2005). These are settings in which partial melting of the leading edge of the down-going oceanic slab might also occur, leading to the formation of isotopically distinct slab melts and high-Nb basalts. Some further suggestions for the formation of the VPS, mafic dyke swarm, tonalite and Nb-enriched rocks are given in Section 6.

The origin of the high-Nb granite body is difficult to explain because, although the plots of elements versus Nb for the granite and Nb-enriched basalts (Fig. 4.25) show an apparent geochemical trend linking the two rock types, the granite cannot be generated by fractional crystallisation of the Nb-enriched basalts. This is because the granite is isotopically distinct from the basalts (Fig. 4.27), having an isotopic composition almost identical to the TVG and TPS. Although the granite body is classed here alongside the Nb-enriched intrusions, the isotopic evidence suggests it has an entirely different petrogenesis. HFSE and LREE-enriched mantle melts could not be contaminated with TVG-like island arc rocks to form this granite body because the granite would develop negative Nb-Ta anomalies, which is not the case on the N-MORB-normalised plot (Fig. 4.26). One possible petrogenetic model permitted by the isotopic data, and in line with the ideas of Aguillón-Robles et al. (2001), relates to the continued emplacement of mafic material at the base of the arc following formation of the island arc pluton. Snoke et al. (2001a,b) record mafic pegmatites towards the NE of the pluton, including substantial quantities of hornblendite. If hornblendite bodies were present at depth beneath the current exposure level, their heating by the arrival of new mafic magmas (e.g. the mafic dyke swarm) might trigger partial melting and the formation of HFSE and LREE-enriched magma, due to the ability of amphiboles to retain the MREE and the HREE compared to the HFSE (Klein et al., 1997). It should however be noted that the granitoid body in question is volumetrically very small

(exposed outcrop of ~20 m^2) compared to the rest of the island so its origin does not necessarily affect the overall tectonic model for Tobago.

5.3.7. Summary of magmatic activity on Tobago

A summary of the magmatic and metamorphic history of the igneous rocks studied on Tobago is outlined in Table 5.2.

Table 5.2. Summary of the rock units found on Tobago Island, Trinidad and Tobago. References in the text.

Rock Unit	Age	Description	Likely origin
Mafic dyke swarm	~103-91 Ma (Ar-Ar) (The range of ages within the mafic dyke swarm is not widely known)	Mafic island arc dykes of varying Th/Yb, Th/La ratios; many chemically depleted. Quite depleted Nd isotope ratios similar to Atlantic and EPR MORB; unlike the more enriched Nd and more radiogenic Hf isotope ratios of the other units.	Many of the dykes may have been a continuation of arc magmatism in the form of feeders for later volcanism above the TVG. The remainder reflect the end of a sediment-related subduction component and the melting of a progressively more depleted mantle source
Arnos Vale-Mason Hall tonalite	105.83±0.17 Ma (U-Pb TIMS)	Major and trace element geochemistry consistent with Cenozoic adakitic volcanics; strongly radiogenic Hf isotope signature	Partial melting of the down-going oceanic slab. May be a link between the high Hf isotope ratios of this body and the high Hf isotope ratios of the Parlatuvier Formation (?)
Nb-enriched intrusions	~106 Ma (A felsic intrusion is dated to 106.24±0.16 Ma – U-Pb TIMS)	Four mafic dykes with enrichment in HFSE and LREE; isotopically depleted. One felsic dyke with similar trace element characteristics to the mafic rocks but isotopically similar to the TVG	Uncertain; the mafic rocks probably relate to the ingress of a HFSE-enriched, isotopically distinct mantle source, perhaps during slab tearing at ~106 Ma; the felsic rock is probably a low-degree partial melt of hornblendites at the base of the arc
Tobago Plutonic Suite (TPS)	>106 Ma	Ultramafic cumulates, gabbro-diorites; similar isotopically to the TVG	Cross-section of a island arc pluton
Tobago Volcanic Group (TVG)	112-106 (ammonites, radiolarians)	Mafic to intermediate tuffs, tuff breccias and lavas; depleted island arc source with slightly radiogenic Hf isotope ratios	Part of a depleted island arc sequence with a depleted mantle source
Greenschist-facies metamorphism and deformation of the NCS, dynamothermal metamorphism of the NCS by intruding island arc magmas			
Karv, Mount Dillon Formations, island-arc-like amphibolites, North Coast Schist (NCS)	Uncertain, presumed ~112-130 Ma	Mostly felsic tuffs with some more mafic compositions; lower greenschist to amphibolite-facies metamorphism; depleted island arc source	Part of an intra-oceanic island arc with a depleted mantle source
Parlatuvier Formation, NCS	130.4±4.5 Ma (U-Pb TIMS)	Mafic to intermediate tuffs, tuff breccias and lavas; lower greenschist-facies metamorphism; island arc or back-arc rocks but chemically enriched in the HFSE, with radiogenic Hf isotope ratios	Possibly a back-arc basin. The HFSE enrichment and radiogenic Hf isotopes may relate to a South American continental lithospheric mantle component
MORB-like amphibolites, NCS	Uncertain, presumed at least as old as the Parlatuvier Formation	Mafic plagioclase-phyric lavas with amphibolite-facies metamorphic overprint; chemically similar to N-MORB	Pre-existing oceanic crust upon which later arc sequences built; later thermally metamorphosed by nearby emplacement of the TPS

5.4. Petrogenesis of the San Souci Volcanic Formation

5.4.1. Tectonic setting

Field evidence and the detrital zircon signature from the Toco Formation (Algar et al., 1997), indicate the San Souci Formation was erupted through a passive margin sedimentary sequence during the early Late Cretaceous, probably to the SE of the postulated Greater Antilles arc and NW of the South American continent. The host turbidites may have received their clastic component from both continental and arc sources (Algar et al., 1997). On multi-element normalised plots, neither systematic depletion of the HFSE, such as Nb and Ta, nor depletion of Ti and enrichment in Th and the LREE are seen (Fig. 4.29). A Th/Yb vs. Ta/Yb plot (Pearce, 1983) (Fig. 5.8a) shows all mafic samples fall just slightly above the MORB array and extend towards enriched MORB compositions. The moderately depleted Nd-Hf isotopic composition of the mafic rocks (εNd_i = +8.4-9.0, εHf_i = +13.4-14.2) indicates little or no input from old continental crust. Therefore the mafic rocks of the San Souci Formation formed in a non-collisional oceanic setting and were not contaminated with a South American crustal component, nor were they contaminated by any material with a decoupled Nd-Hf isotope signature (c.f. Parlatuvier Formation, Tobago). The mafic rocks are thus likely to be of an enriched MORB or within-plate composition.

The two analysed felsic rocks are an integral part of the San Souci Formation as far as can be seen in the field, but as shown in Section 4.4.2, they have very different major and trace element characteristics to the mafic rocks. The felsic rocks contain more enriched isotopic signatures (εNd_i = +5.4-5.7, εHf_i = +8.0), LREE enrichment, high Th/La (0.17-0.19), slight negative Nb-Ta and positive Zr-Hf anomalies (Fig. 4.29) compared to the mafic rocks which could not have originated by fractional crystallisation of these mafic mantle-derived melts. Because the mafic rocks do not have any sign of subduction zone contamination, it is highly improbable that the felsic rocks formed in a subduction setting.

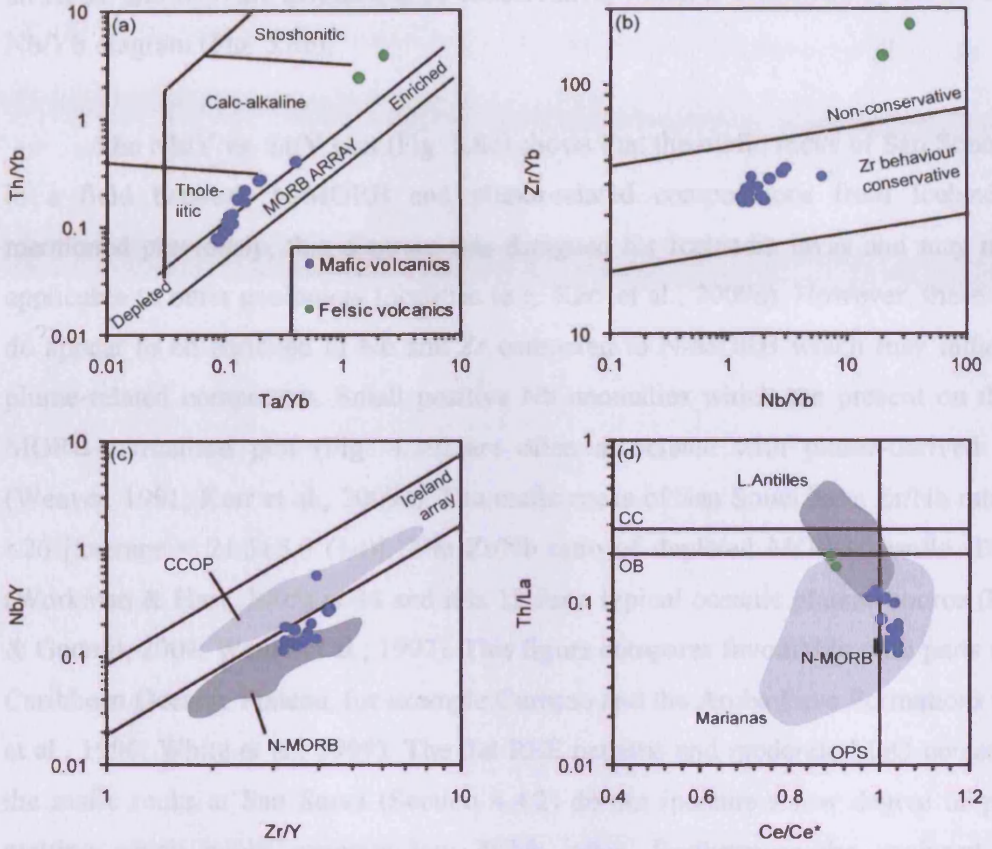

Figure 5.8. Block of four ratio-ratio plots to investigate the mantle source(s) of the San Souci Formation.. (a) The Th/Yb vs. Ta/Yb diagram shows that the tholeiitic mafic volcanics have a relatively enriched composition lying on the MORB array. The calc-alkaline to shoshonitic felsic volcanics plot towards the much enriched end of the MORB array. There is no evidence of a subduction zone input into these rocks. (b) Zr/Yb vs. Nb/Yb diagram indicates conservative behaviour of Zr for the mafic rocks, but not the felsic rocks, suggesting accumulation of zircon or very low degrees of partial melting. (c) Nb/Y vs. Zr/Y diagram indicating that the mafic rocks have slightly higher Nb/Y ratios than N-MORB (plume-related source?). (d) Th/La vs. Ce/Ce* diagram shows that the mafic volcanics have no input from either terrigenous or oxidised pelagic sediments. The felsic rocks may have some minor input from both. CC = continental crust plots above this line. OB = oceanic basalts plot below this line. OPS = arc rocks involved with oxidised pelagic sediments plot to the left of this line. References as per previous diagrams.

5.4.2. Mantle source of the mafic components of the San Souci Formation

The mafic rocks, with their moderate to high levels of MgO (up to 8.2 wt.%), Ni (up to 100 ppm) and Cr (up to 350 ppm), are clearly derived from a mantle source. The flat HREE patterns (Fig. 4.29) and moderate levels of Y and Yb indicate that partial melting occurred at shallow depths in the mantle where spinel, not garnet, was stable. Incompatible trace element ratios are now used to investigate the nature of this mantle source. As there is no evidence of a subduction zone or continental crust contribution,

all HFSE and REE are assumed to be conservative, which is confirmed by the Zr/Yb vs. Nb/Yb diagram (Fig. 5.8b).

The Nb/Y vs. Zr/Y plot (Fig. 5.8c) shows that the mafic rocks of San Souci plot in a field between N-MORB and plume-related compositions from Iceland. As mentioned previously, this diagram was designed for Icelandic lavas and may not be applicable to other geological localities (e.g. Kerr et al., 2009a). However, these rocks do appear to be enriched in Nb and Zr compared to N-MORB which may indicate a plume-related component. Small positive Nb anomalies which are present on the N-MORB-normalised plot (Fig. 4.29) are often associated with plume-derived lavas (Weaver, 1991; Kerr et al., 2009a). The mafic rocks of San Souci have Zr/Nb ratios of <26 [average = 21.5±5.6 (1σ)]. The Zr/Nb ratio of depleted MORB mantle (DMM) (Workman & Hart, 2005) is 34 and it is 12 for a typical oceanic plateau source (Fitton & Godard, 2004; Wendt et al., 1997). This figure compares favourably with parts of the Caribbean Oceanic Plateau, for example Curaçao and the Aruba Lava Formations (Kerr et al., 1996; White et al., 1999). The flat REE patterns and moderate MgO contents of the mafic rocks at San Souci (Section 4.4.2) do not indicate a low degree of partial melting which might generate low Zr/Nb ratios. Furthermore the analysed local sedimentary rock has a Zr/Nb ratio of 44, so assimilation of any proportion of such sediment cannot generate the low Zr/Nb ratios of the mafic rocks, therefore low Zr/Nb is a feature of the mantle source of the San Souci mafic rocks. These rocks are therefore dissimilar to N-MORB and are, at least in part, derived from partial melting of a mantle plume.

Isotopically, the mafic rocks are quite similar to both N-MORB and plume-related rocks from the Caribbean region and nearby. On a εHf_i vs. εNd_i plot (Fig. 4.27) they plot within the very wide field of plume-related rocks from the Galapagos Islands, the CCOP, and N-MORB from the East Pacific Rise. This diagram does not separate plume and MORB sources particularly well. On a related note, a very small amount of crustal contamination could also hide a depleted plume component. It is therefore difficult to judge whether or not the mafic rocks of the San Souci Formation were derived from an N-MORB-like or plume-related mantle source region using Nd and Hf isotopes.

5.4.3. Modelling mafic magmatism

There is no evidence for either subduction-related or crustal contamination in the mafic rocks of San Souci so there is an opportunity to model trace element behaviour during partial melting. Modelling may show if the studied rocks can be reproduced from an appropriate starting material. Firstly, it is clear that these rocks, which contain ~4-8 wt.% MgO and no olivine, do not represent primary magmas. Kerr et al. (1996) and Hastie et al. (2007) showed that some 25-30 % fractional crystallisation of olivine and Cr-spinel occurred in similar rocks (~8 wt.% MgO) of the Curaçao Lava Formation in the Dutch Antilles and the Bath-Dunrobin Formation in Jamaica. Here, an attempt is made to model primary melt compositions and adjust them for those same fractional crystallisation effects to produce the compositions of the least evolved mafic rocks of San Souci.

In order to keep the model relatively simple, non-modal batch (equilibrium) partial melting is used (models and equations from Shaw, 2006). This model assumes that mantle mineralogy and the melt mode differ and partial melts pond in contact with the residuum until extraction from the mantle at the end of the partial melting episode. Modelling is undertaken for relevant immobile trace elements (Zr, Nb and the REE) for which partition coefficients are well known. The governing equation is...

$$c_L = \frac{c_0}{D_0 + [F(1-P)]}$$

...where c_L represents the concentration of a given element in the liquid phase, c_0 is the concentration of that element in the starting material, D_0 is the bulk distribution coefficient of that element in the starting material, F is the degree of partial melting and P is the bulk distribution coefficient of that element in the melt. Table 5.3 shows the list of mineral proportions, melt modes, partition coefficients, starting materials used, and results of modelling of different degrees of partial melting.

Fractional crystallisation effects were then modelled on these results using only olivine and spinel fractional crystallisation governed by the equation...

$$\frac{C_1}{C_0} = F^{(D-1)}$$

...with the definitions as used above except that F is the fraction of residual liquid. Table 5.3 shows the list of minerals, partition coefficients and results partial melt modelling.

The results of modelling are presented on Figure 5.9, where the N-MORB-normalised compositions of the mafic volcanic rocks are plotted along with the results of modelling using two end member starting materials. The first starting material considered is the hypothetical source of the Ontong Java oceanic plateau (after Fitton & Godard, 2004) which is more enriched in HFSE and LREE compared to DMM, and represents an attempt at characterising the trace element composition of a plateau source. In the case of San Souci, only a high degree of partial melting was modelled (25%), and the effects of 30% fractional crystallisation were then modelled using the resulting element concentrations (Fig. 5.9). This modelling reproduces the positive Zr anomalies and HREE patterns of the San Souci volcanics almost exactly, but also slightly more LREE enrichment and larger positive Nb anomalies than many of the mafic lavas. This model does however replicate a trace element pattern running exactly parallel to the single sample with the largest positive Nb anomaly of the San Souci volcanics.

The second starting material considered was depleted MORB mantle (DMM) after Workman & Hart (2005). In this case, two melting models were considered. Firstly a high degree of partial melting was modelled (25%), and the results used as the starting compositions upon which to model 30% fractional crystallisation (Fig. 5.9). The resulting melt is depleted, with negative Nb and Zr anomalies and LREE depletion. Therefore high-degree melting of DMM is not a suitable source of the San Souci magmatism. A low-degree partial melt was also modelled (5% melting), which, without the effects of further crystallisation, reproduced quite reasonably the composition of the most depleted of the mafic San Souci lavas, albeit with a slightly negative Nb anomaly and no evidence of a positive Zr anomaly. Therefore, although low degrees of partial melting of a DMM source mirror the REE patterns of the San Souci volcanics, they cannot explain the positive Nb and Zr anomalies of some of the lavas.

This modelling suggests that neither starting material is able to model exactly the trace element patterns present at San Souci. The positive Nb and Zr anomalies of the San Souci volcanics appear to require a plume-related source, however modelling of the partial melting of such a source results in excessive LREE enrichment and Nb anomalies in the resulting melt. The range of Zr/Nb ratios at San Souci (6-27, average 21) is also not reproduced entirely by the modelling. A DMM source generates Zr/Nb = 23-33 in the range 5 to 25% partial melting whereas the plume source generates Zr/Nb = 11-12 at 25% partial melting. The most likely option for the origin of the San Souci mafic volcanics is therefore that they formed by the partial melting of a slightly more depleted plume source than that suggested by Fitton & Godard (2004) for the Ontong Java Plateau.

Table 5.3. Parameters and results for the partial melt modelling of the San Souci mafic volcanics. Page et al. (2009) was used as the source for partition coefficients as it was one of the few studies to contain the entire suite of required trace elements. Fractional crystallisation modelling results used the same partition coefficients for olivine and spinel as for the partial melting modelling.

Mineral proportions*		**Melt modes****	
Olivine	0.55	0.10	*Johnson et al. (1990)
Orthopyroxene	0.15	0.20	**Révillon et al. (2000)
Clinopyroxene	0.25	0.68	
Spinel	0.05	0.02	

Source compositions (ppm) *Fitton & Godard (2004); **Workman & Hart (2005)

	Nb	*La*	*Ce*	*Nd*	*Sm*	*Zr*	*Eu*	*Gd*	*Dy*	*Er*	*Yb*
*Plateau**	1	0.65	1.7	1.2	0.4	12	0.143	0.513	0.645	0.42	0.45
*DMM***	0.1485	0.192	0.55	0.581	0.239	5.082	0.096	0.358	0.505	0.348	0.365

Distribution coefficients from Page et al. (2009) for the Thetford Mines ophiolite

	Nb	*La*	*Ce*	*Nd*	*Sm*	*Zr*	*Eu*	*Gd*	*Dy*	*Er*	*Yb*
Olivine	0.00147	0.000237	0.000491	0.001836	0.005074	0.013898	0.007419	0.011012	0.021738	0.036771	0.053899
Opx	0.012	0.001929	0.003365	0.009216	0.020023	0.01514	0.016109	0.036139	0.060631	0.090376	0.120758
Cpx	0.009805	0.084237	0.127118	0.245971	0.370564	0.132709	0.42717	0.466742	0.526621	0.536847	0.514037
Spinel	0.0148	0.002445	0.002569	0.002735	0.00278	0.0503	0.00278	0.002742	0.002639	0.002503	0.002364

Bulk distribution coefficients *bulk in starting material; **bulk in melt phase

	Nb	*La*	*Ce*	*Nd*	*Sm*	*Zr*	*Eu*	*Gd*	*Dy*	*Er*	*Yb*
D_0*	0.005692	0.015824	0.024044	0.047643	0.074554	0.036323	0.085054	0.099160	0.121958	0.139501	0.152408
*P***	0.009478	0.057740	0.087214	0.169342	0.256551	0.095666	0.294495	0.325768	0.372455	0.386858	0.379134

Non-modal batch partial melting: oceanic plateau source *F = degree of partial melting **ppm

F*	*Nb***	*La*	*Ce*	*Nd*	*Sm*	*Zr*	*Eu*	*Gd*	*Dy*	*Er*	*Yb*
0.01	64.12	25.75	51.25	21.45	4.88	264.52	1.55	4.84	5.03	2.88	2.84
0.05	18.11	10.33	24.40	13.46	3.58	147.17	1.19	3.86	4.21	2.47	2.45
0.10	9.55	5.91	14.74	9.18	2.69	94.67	0.92	3.08	3.49	2.09	2.10
0.15	6.48	4.14	10.56	6.97	2.15	69.78	0.75	2.56	2.98	1.81	1.83
0.20	4.91	3.18	8.23	5.61	1.79	55.25	0.63	2.19	2.61	1.60	1.63
0.25	3.95	2.59	6.74	4.70	1.54	45.73	0.55	1.92	2.31	1.43	1.46
0.30	3.30	2.18	5.71	4.04	1.34	39.01	0.48	1.70	2.08	1.30	1.33

Non-modal batch partial melting: DMM source

F	*Nb*	*La*	*Ce*	*Nd*	*Sm*	*Zr*	*Eu*	*Gd*	*Dy*	*Er*	*Yb*
0.01	9.52	7.60	16.58	10.38	2.92	112.02	1.04	3.38	3.94	2.39	2.30
0.05	2.69	3.05	7.89	6.52	2.14	62.33	0.80	2.69	3.29	2.05	1.99
0.10	1.42	1.74	4.77	4.44	1.61	40.09	0.62	2.15	2.73	1.73	1.70
0.15	0.96	1.22	3.42	3.37	1.28	29.55	0.50	1.79	2.34	1.50	1.49
0.20	0.73	0.94	2.66	2.72	1.07	23.40	0.42	1.53	2.04	1.33	1.32
0.25	0.59	0.76	2.18	2.28	0.92	19.37	0.37	1.34	1.81	1.19	1.19
0.30	0.49	0.64	1.85	1.96	0.80	16.52	0.32	1.19	1.63	1.08	1.08

Zr/Nb ratios for different degrees of partial melting of plateau and DMM sources

	F	*0.01*	*0.05*	*0.10*	*0.15*	*0.20*	*0.25*	*0.30*
Plateau source		4.13	8.13	9.92	10.76	11.26	11.58	11.81
DMM source		11.77	23.18	28.28	30.70	31.11	33.04	33.69

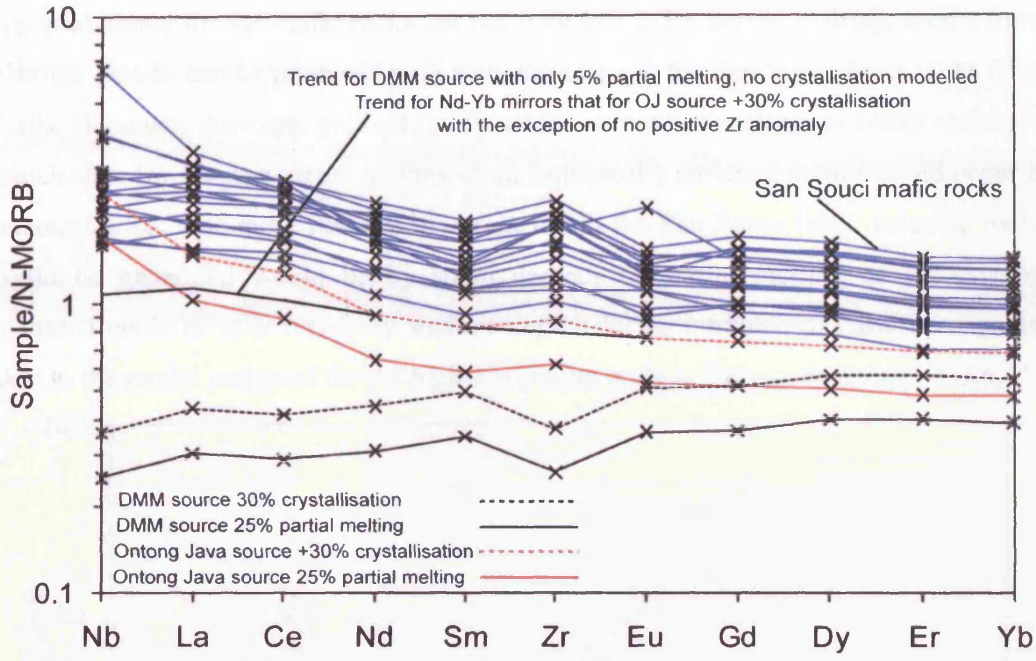

Figure 5.9. Plot of selected, N-MORB-normalised, trace element compositions from the mafic component of the San Souci Volcanic Formation. Non-modal batch partial melts are marked. High degrees of partial melting of a DMM source do not yield LREE, Nb or Zr enrichment over the HREE. Low degrees of partial melting of a DMM source (5%) do yield slight LREE enrichment and slight positive Zr anomalies. High degrees of partial melting of a theoretical oceanic plateau source do yield positive Nb and Zr anomalies along with LREE enrichment. See Table 5.3 for references.

5.4.4. Origin of the felsic magmatism

It has already been explained above that the felsic rocks cannot be modelled by the addition of an upper crustal component to the magma that fed the mafic volcanics of San Souci, because continental crustal contamination would cause a negative Nb-Ta anomaly in the felsic rocks, which is not the case.

Only one other rock sample from the Southern Caribbean is geochemically similar to the felsic rocks, the granitoid (INT/1-3/4) from Tobago which is classified with the high-Nb and Nb-enriched mafic intrusions on Tobago (Section 4.3.8). However, the felsic rocks of San Souci are more enriched isotopically than that felsic intrusion. It is unlikely that the two outcrops are linked, especially as the Tobago rocks formed in an island arc setting while the San Souci rocks formed in an open oceanic/passive margin setting. The felsic rocks of San Souci are quite dissimilar to OIBs, which do not usually have normalised positive Nb and Zr anomalies or flat HREE patterns (White, 2010). One interesting point is that if the melting models as

reported above for the mafic rocks are run with just 1-5% partial melting, then a trace element pattern can be produced with a similar slope to the San Souci felsic rocks (Fig. 5.10). However, the exact product (mafic or felsic rock) of melting or likely setting in which such low-degree partial melting of an isotopically enriched mantle could occur is unconstrained. One more realistic model in which the San Souci felsic volcanic rocks could be generated would be by small degrees of partial melting of pre-existing hydrated mafic crust at relatively shallow depths during intrusion of basaltic magmas, akin to the model proposed for the high-Nb granite body of Tobago in Section 5.3.6.

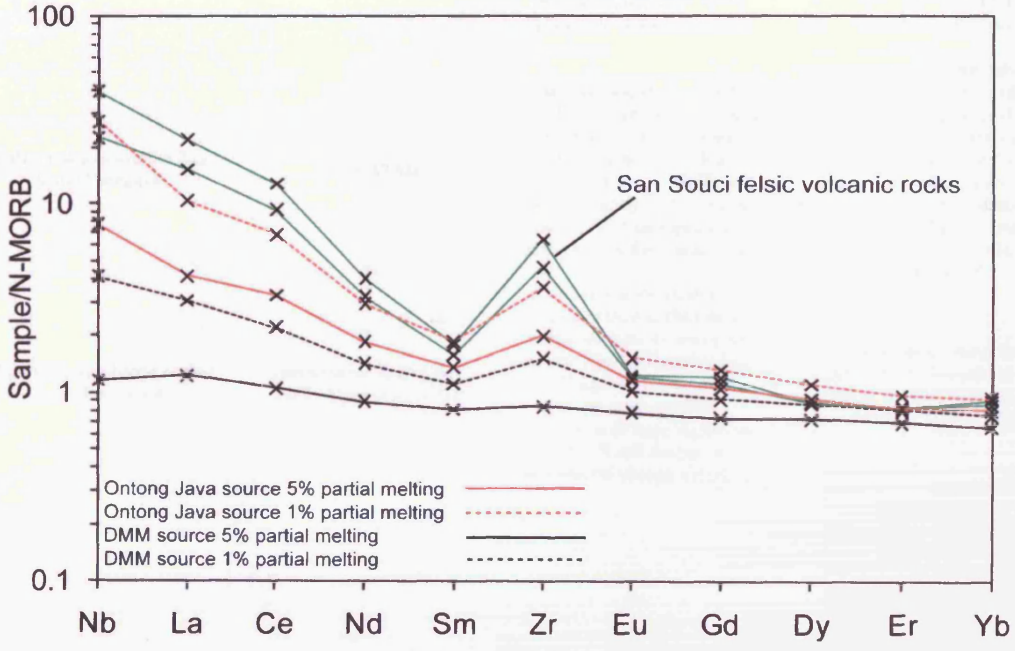

Figure 5.10. Summary of partial melt modelling to reproduce the felsic volcanic rocks of San Souci using the parameters outlined in Table 5.3. This model shows that ~5 % partial melting of a hypothetical plateau source, or ~1 % partial melting of a hypothetical DMM source, or a combination of the two, might yield similar trace element patterns to the felsic volcanics (subject to fractional crystallisation).

5.4.5. Summary of San Souci magmatism

A summary of the magmatic activity at San Souci is presented in Table 5.4.

Table 5.4. Summary of the rock units found at San Souci, Trinidad.

Rock Unit	Age	Description	Likely origin
Mafic volcanics of the San Souci Formation	~108-87 Ma	Tholeiitic basalts and basaltic andesites with flat chondrite- and N-MORB-normalised rare earth element patterns, slight positive Nb and Zr anomalies, depleted Nd-Hf radiogenic isotope signature	Oceanic setting with no obvious continental input. No subduction signature indicates MORB or within-plate origin. Lack of evidence for active rifting, trace element modelling and low Zr/Nb ratios suggests a within-plate setting
Felsic volcanics of the San Souci Formation	~108-87 Ma	Calc-alkaline to shoshonitic rhyolites genetically unrelated to mafic rocks. Extreme LREE-enrichment, high concentrations of Nb-Ta and Zr-Hf. Slightly more enriched Nd-Hf isotope signatures compared to the mafic rocks	No evidence of contamination of a mafic mantle-derived parental magma by local upper crust. May be derived by low-degree partial melting and fractionation of an isotopically enriched source, perhaps hydrated mafic crust through which the mafic magmas travelled
Turbiditic sandstone of the Toco Formation	Barremian-Albian (Barr, 1963; Algar et al., 1997)	Similar trace element composition to the felsic volcanics with the exception of low Nb-Ta concentrations and negative Eu anomaly. Some very enriched radiogenic isotope signatures (Nd, Hf) and moderately enriched Pb isotope signatures	Continental margin turbidites derived from Colombian margin or the Caribbean arc system (Algar et al., 1997)

5.5. Petrogenesis of the SE Aves Ridge

5.5.1. Are the granitoids and mafic rocks cogenetic?

The variation diagrams (Fig. 4.33) show that the mafic rocks define, in the case of the immobile and incompatible elements, clear intra-magmatic differentiation trends which may be related to crystal fractionation. The granitoid rocks plot in a distinct field at lower incompatible element concentrations than the most evolved mafic rocks (with the exception of Zr) and display no coherent liquid line of descent compatible with the mafic rocks. This shows that the mafic and felsic rocks are not related to each other by fractional crystallisation processes. The negative Zr-Hf anomalies on the multi-element plot for the mafic rocks (Fig. 4.34), indicated by $Zr/Sm_{NMN} < 1$, are likely to be related to subduction-related REE enrichment (Thirlwall et al., 1994). On the other hand, the positive Zr-Hf anomalies for the granitoids (Fig. 4.34) may indicate that these rocks have accumulated zircon, or that their source contained residual amphibole, because amphibole is more compatible with the MREE than Zr or Hf (Klein et al., 1997). These different Zr-Hf anomalies again point to distinct origins for the mafic and granitoid rocks. Most importantly, crystal fractionation cannot explain the different εNd_i and εHf_i isotopic ratios in Fig. 4.35, so although only two analyses are available it is concluded that the mafic and granitoid rocks of the Aves Ridge are not derived from the same source region. However, without field relationships, or drilling, with which to test the relative age of the mafic and felsic samples and without dateable mafic material, the age of the mafic rocks in this study remains uncertain.

5.5.2. Island arc origin of the SE Aves Ridge

The presence of negative Nb-Ta anomalies on N-MORB normalised plots (Fig. 4.34) is usually regarded as indicative of subduction zone processes as Nb and Ta are preferentially held in rutile in the down-going slab during aqueous fluid release (e.g. Saunders et al., 1980; Thirlwall et al., 1994). Furthermore, the Th/Yb vs. Ta/Yb diagram of Pearce (1983) (Fig. 5.11a) shows that the mafic rocks plot above the MORB array, which suggest they have a subduction zone affinity. The radiogenic isotope ratios of the mafic and granitoid rocks (Fig. 4.35) and zircons without rounded, inherited cores from the granitoids do not indicate contamination from old continental crustal

material. Therefore, geochemical evidence, confirmed by existing geophysical and geodynamic models shows the Aves Ridge represents the eroded products of an extinct subduction zone.

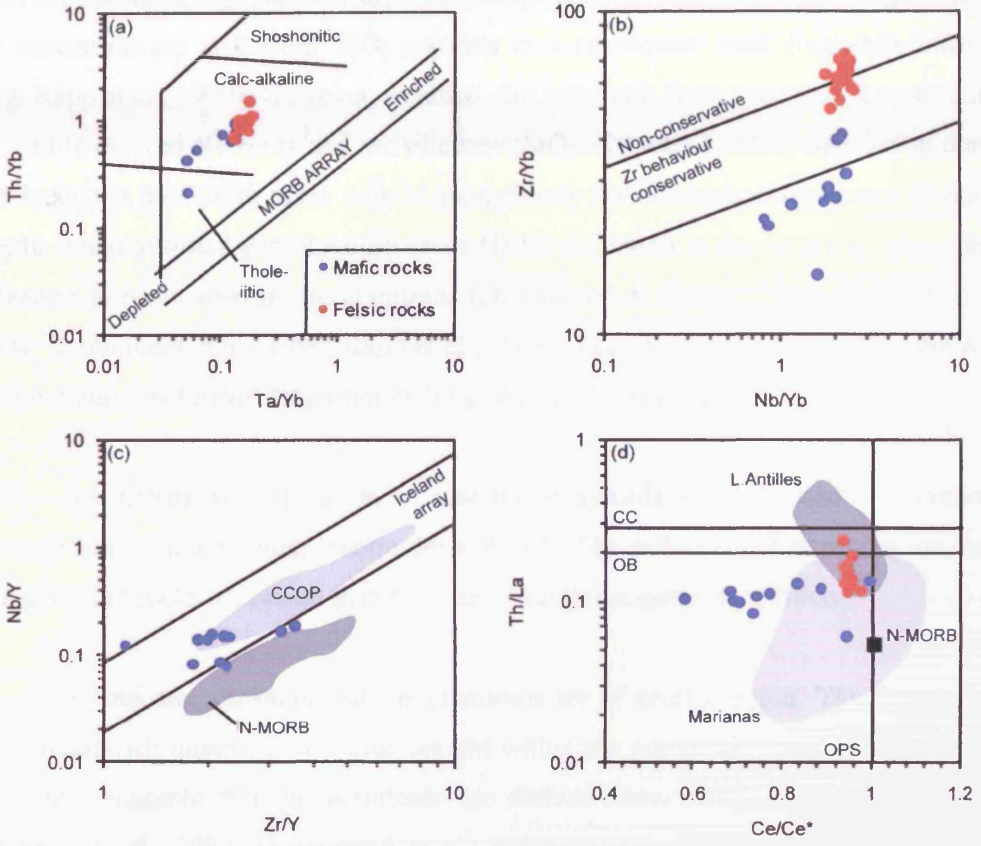

Figure 5.11. Block of four ratio-ratio plots to investigate the source(s) of the Aves Ridge rocks. (a) The Th/Yb vs. Ta/Yb diagram shows that both mafic and felsic rocks are calc-alkaline. Both rock suites are reasonably enriched. (b) Zr/Yb vs. Nb/Yb diagram indicates conservative behaviour of Zr for the mafic rocks, but not the felsic rocks, suggesting accumulation of zircon. The mafic rocks have particularly low Zr/Yb ratios. (c) Nb/Y vs. Zr/Y diagram indicates that the mafic rocks have higher Nb/Y ratios than N-MORB which points towards a plume-related source. Some caution should be applied as the low Zr/Yb ratios of the mafic rocks may have pushed the mafic rocks to the left in the Nb/Y vs. Zr/Y diagram. (d) Th/La vs. Ce/Ce* diagram shows that the mafic volcanics have considerable input from oxidised pelagic sediments but little from terrigenous sediments. The felsic rocks may have some input from terrigenous sediments. CC = continental crust plots above this line. OB = oceanic basalts plot below this line. OPS = arc rocks involved with oxidised pelagic sediments plot to the left of this line.

5.5.3. Source of the granitoid rocks

As the granitoid samples were sampled from only two outcrops, their lack of geochemical variation may be indicative of a sampling bias rather than a distinct petrogenetic feature. However, some petrological and geochemical constraints can be used to discuss their source region.

One possibility is partial melting of a subducting oceanic slab, which would generate an acidic melt (e.g. Drummond & Defant, 1990). Such a melt could interact with the mantle wedge beneath the Aves Ridge arc, and generate higher MgO, Ni and Cr concentrations and lower SiO_2 contents in a subsequent melt (high-Mg andesite) (e.g. Rapp et al., 1999). However, as noted, the granitoids have very low concentrations of mantle-derived elements and are siliceous (SiO_2 ~70 wt.%). Also, slab fusion during subduction is thought to occur only in anomalously hot subduction zones and largely at depths where residual garnet would cause HREE-depletion in the resulting felsic melts, a feature also not seen in the granitoids (Drummond & Defant, 1990; Peacock et al., 1994; Drummond et al., 1996; Rapp et al., 2003). Therefore it is unlikely that the Aves Ridge granitoids formed by partial melting of a subducting slab.

An alternative suggestion is that the granitoids were formed by fractional crystallisation from a mafic, mantle-derived melt. The earlier conclusion that the mafic and granitoid rocks are not co-genetic means that this scenario is unlikely.

A final suggestion is that the granitoids are of crustal origin. The fine-grained hornblende-rich intermediate facies present within the granitoids may be I-type restite. If so this suggests that the granitoids are derived from a mafic crustal source (cf. Chappell et al., 1987; Drummond et al., 1996; Stephens, 2001). Additionally, SiO_2 concentrations of 67 - 72 wt.% and a reasonably sodic character (Na_2O/K_2O = 1.65) are compatible with re-melting of a tholeiitic mafic source at moderate (10-20 %) degrees of partial melting (Rapp & Watson, 1995). The positive Zr-Hf anomalies (Fig. 4.34) and moderate Sr concentrations (up to 440 ppm) suggest that amphibole and plagioclase may have remained in the source residue of the granitoids. Moderate levels of Y (>16 ppm) and the HREE (Yb >1.7 ppm) and low La/Yb (~6.6) rule out residual garnet and constrain partial melting to <30 km depth (cf. Drummond & Defant, 1990; Rapp & Watson, 1995). If the granitoids are derived from a mafic protolith, their negative Nb-Ta anomalies (Fig. 4.34) might be attributed to re-melting of the lower Aves Ridge arc crust by advection due to the under-plating of hot basaltic arc magma (Petford et al., 2000; Petford & Gallagher, 2001).

5.5.4. Source of the mafic rocks

Mantle wedge component: Unlike the granitoids, the mafic rocks have high concentrations of Mg, Ni and Cr indicating derivation from a peridotite mantle source beneath the Aves Ridge. As the MREE and HREE are not depleted on the normalised plots (Fig. 4.34), garnet was not present in the source or completely melted out during partial melting. In the former case, the depth of partial melting is constrained to above the approximate spinel-garnet transition at <85 km within the mantle (Robinson & Wood, 1998).

To re-iterate, the HFSE and HREE are normally used to investigate the composition of the mantle wedge, but these elements can be mobilised from the slab if it partially melts (Pearce & Peate, 1995). Figure 5.11b (Zr/Yb vs. Nb/Yb) shows that the mafic samples plot below the Zr conservative behaviour array, suggesting that Zr has not been mobilised from the slab to the wedge, but that either Zr has been depleted or Nb enriched by some unknown process. Variations in the HFSEs and HREEs will nevertheless be investigated in terms of the composition of the mantle wedge alone, as with the rocks from La Désirade and Tobago.

The Nb/Y vs. Zr/Y plot (Fig. 5.11c) shows that the Aves Ridge rocks plot within and around the 'Iceland array', along with the plume-influenced Lau Basin lavas, suggesting that the mantle wedge beneath the Aves Ridge may have been of mantle plume composition. In terms of absolute Zr/Nb ratios, the Aves Ridge rocks have Zr/Nb = 9-38 (mean = 17.7), close to the values for the plume-influenced ~72 Ma Blue Mountains back-arc lavas in Jamaica (Hastie et al. 2010c) and northern Tonga (Wendt *et al.* 1997). It is therefore likely that the low Zr/Nb ratios of the Aves Ridge mafic rocks have been derived from partial melting of a mantle wedge composed of mantle plume material.

Slab-flux component: The Th/La vs. Ce/Ce* diagram (Fig. 5.11d) shows that the mafic rocks from the Aves Ridge have a clear trend from mantle-like Ce/Ce* values of ~1.0 to 0.58, indicating a significant involvement of pelagic sediment in the source region. The mafic rocks of the Aves Ridge therefore most likely formed in an intra-

oceanic setting away from terrigenous proto-Caribbean passive margin sedimentary sequences or continental masses.

5.5.6. Summary of magmatic activity on the Aves Ridge

A summary table is presented below (Table 5.5). Three dredge hauls originally collected from the SW corner of the Aves Ridge in the Caribbean Sea have been re-studied. Two hauls consist of calc-alkaline LREE-enriched granitoids with an apparent SHRIMP U-Pb zircon emplacement age of 75.9 ± 0.7 Ma. The third haul is genetically unrelated to the others and contains calk-alkaline island arc basaltic andesites of uncertain age. Petrological, trace element and isotopic constraints indicate that the granitoids have an oceanic crustal source which was itself formed in the recent geological past – possibly lower arc, oceanic or oceanic plateau material. The mafic rocks were formed by partial melting of an incompatible trace element-enriched mantle wedge above a subduction zone. The mantle wedge was probably plume-related and the subducted material consisted of hydrated oceanic crust and moderate quantities of pelagic sedimentary material. A geochemical signature derived from terrigenous sediment was not recognised.

Table 5.5. Summary of the rock units found at the Aves Ridge dredge sites, SE Caribbean Sea.

Rock Unit	Age		Likely origin
Hauls EA68 11317 and 9 (granitoids)	SHRIMP II – U-Pb zircon on single sample of haul 11317 – 75.9 ± 0.7 Ma	Calc-alkaline restite-bearing granitoids with enriched LREE, Nb-Ta anomalies, depleted Nd-Hf radiogenic isotope signature Calc-al grani LREE, Nb-Ta anomalies, depleted Nd-Hf radiogenic isotope signature	land arc setting. Presence of estite and lack of a genetic link to the mafic rocks ..idicates probably formation during partial melting of the lower oceanic or plateau crust, perhaps during ingress of the mafic rocks (see below)
Haul EA68 11318 (mafic rocks)	Undated – assumed to overlap in age with the granitoids or slightly pre-date (?)	Mostly calc-alkaline basalts or basaltic andesites with flat to slightly LREE-enriched trace element patterns, low Zr/Nb, high Nb/Y, slight normalised Ce anomalies, low Th/La, Nb-Ta anomalies, depleted Nd-Hf radiogenic isotope signature but distinct from the granitoids	Island arc. Formed by partial melting of supra-subduction zone mantle which was of mantle plume origin. Contribution of fluids (not melt) from the subducted slab related to the slab and a pelagic sedimentary veneer. No evidence of continental or terrigenous sedimentary input

CHAPTER SIX: DISCUSSION PART II – IMPLICATIONS OF THIS STUDY FOR THE TECTONIC EVOLUTION OF THE CARIBBEAN PLATE

The correlation of studied units to other nearby rocks of a similar age, the generation of tectonic models for their formation, and the implications of their collective origins for the tectonic evolution of the Caribbean Plate

6.1. Introduction

The purpose of this chapter is to generate a plate-tectonic framework for the origin of the four locations studied in this thesis. The first task will be to review the petrogenesis and tectonic setting of similar rocks from across the wider Caribbean region, and to identify models for their origin, evolution and preservation. For reference, Figure 6.1 shows a geographical map of the Caribbean region identifying the different locations mentioned throughout this chapter. The second task will be to evaluate which tectonic model of Caribbean Plate evolution, plateau collision vs. ~135-125 Ma subduction initiation, is most likely to have given rise to the studied rocks in each case. Palaeo-tectonic maps covering the Late Jurassic to Late Cretaceous will be presented, based on the preferred model of Caribbean tectonic evolution, showing where the studied locations might fit. The final section in this chapter is a short summary of the revised model of Caribbean tectono-magmatic evolution.

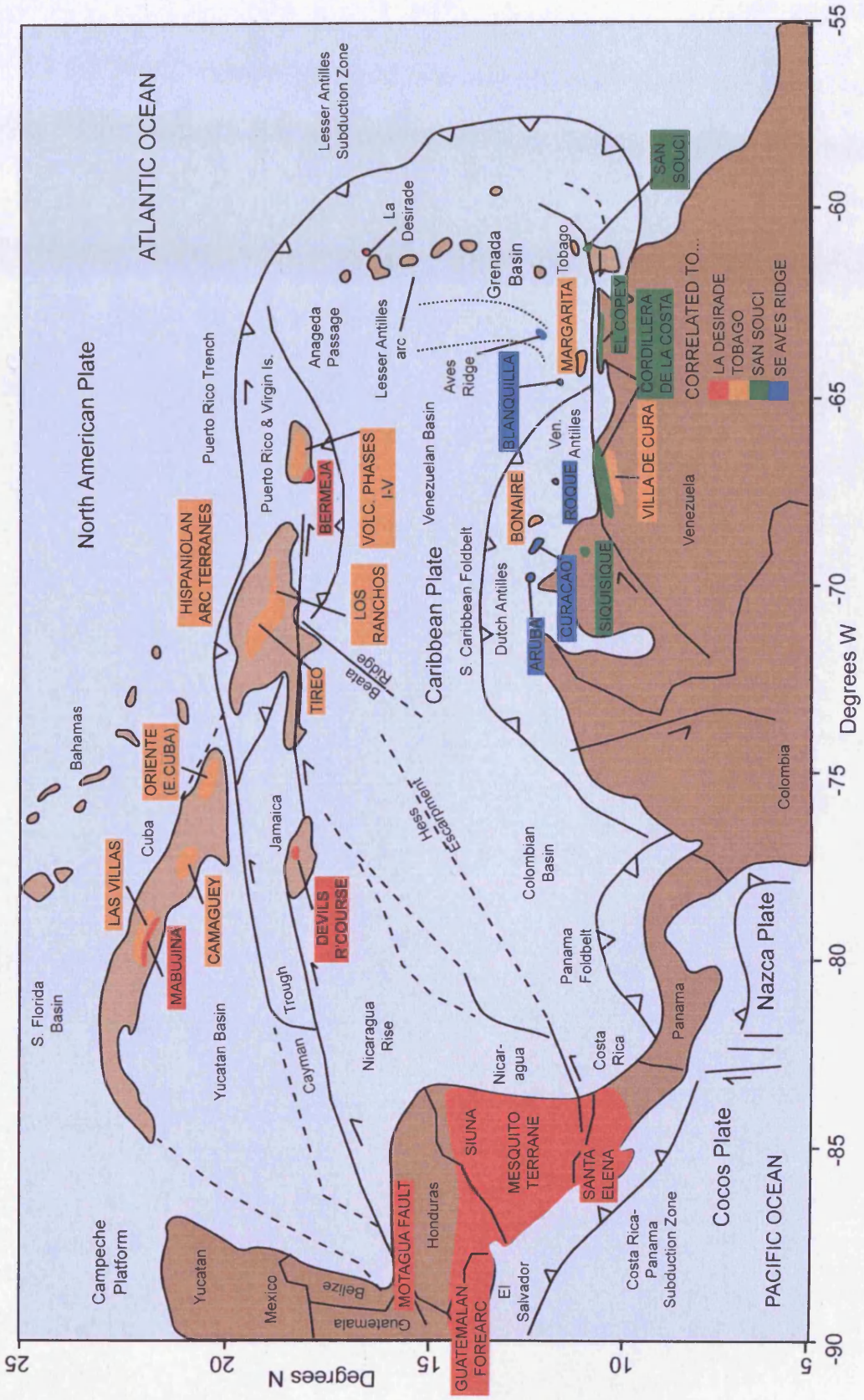

Figure 6.1. Location of rock units across the Caribbean region mentioned in this chapter.

6.2. Origin of La Désirade

6.2.1. Palaeo-latitudinal position of La Désirade

The Mid-Late Jurassic separation of the Americas left a complex region of intra-arc spreading, transverse motions and continued east-dipping subduction at the proto-Caribbean/Pacific boundary (e.g. Fig. 7 of Pindell & Kennan, 2009). The western proto-Caribbean has been called the Colombian Marginal Seaway by Pindell & Kennan (2009) (Fig. 6.2) and was in a back-arc position with respect to the Andean-Cordilleran subduction zone. This Colombian Marginal Seaway is a logical position in which La Désirade could have initially formed. Terrigenous input to the subduction system could be derived from the mature Andean/Cordilleran arc and the source of magmatism would be the moderately depleted back-arc mantle. La Désirade therefore formed in the proto-Caribbean realm, but would become an integral part of the Caribbean Plate during the inception of SW-dipping Greater Antilles subduction.

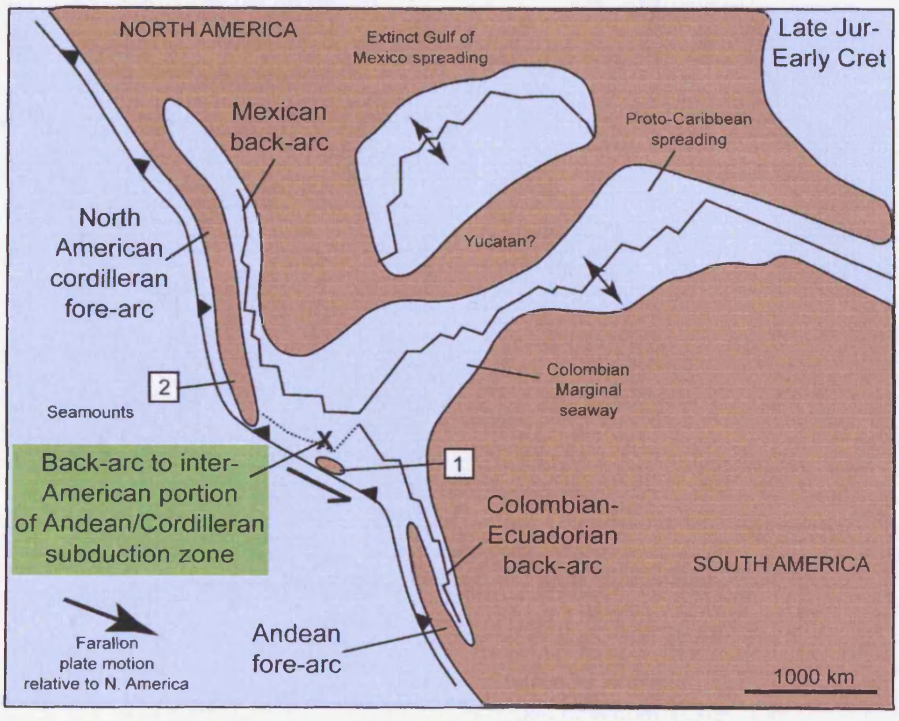

Figure 6.2. Possible positions of formation of La Désirade during the Late Jurassic, adapted from the map of Pindell et al. (2011). Andean fore-arc or Colombian back-arc locations are impossible due to relative Farallon plate motion. Back-arc-like chemistry probably precludes a North American fore-arc origin. As most arc-transform motion occurs within the fore-arc and arc, a Mexican back-arc basin origin is also unlikely. The most likely position for La Désirade is the back-arc to the rifted inter-American portion of the Andean/Cordilleran subduction system, i.e. the Colombian Marginal seaway of Pindell & Kennan (2009) (marked X). 1 = fragments of pre-existing Andean/Cordilleran island arc rocks (e.g. Devils Racecourse, Jamaica). 2 = Guatemalan fore-arc, Siuna high-pressure low temperature rocks.

Alternative locations of origin for La Désirade are set out in Figure 6.2. A Mexican back-arc basin did not open until the Early Cretaceous (Pindell & Kennan, 2009) and was supposedly closed by ~120 Ma along the Motagua-Polóchic suture by W-dipping subduction (Harlow et al., 2004; Geldmacher et al., 2008) perhaps linked to the Caribbean Great Arc to the south (Tardy et al., 1994; Dickinson & Lawton, 2001; Umhoefer, 2003). Because of this rapid Cretaceous basin opening and closure, the Jurassic rocks of La Désirade could not form in such a position. Nevertheless, is a more northerly location of origin than the Colombian Marginal seaway suitable for La Désirade?

Of the models which use the mantle reference frame, Duncan & Hargraves (1984) focus proto-Caribbean spreading on the palaeo-equator whilst Pindell & Kennan (2009) show the western edge of the Colombian Marginal Seaway centred on 10° N in the Late Jurassic. However, both Montgomery et al. (1994) and Mattinson et al. (2008) argue that Upper Jurassic radiolarian assemblages found on La Désirade, Puerto Rico, Hispaniola and Cuba all belong to the Northern or Southern Tethyan province of Pessagno et al. (1993). This implies an origin between 22 and 30° N or S of the equator. Jurassic radiolarian-bearing strata from the Blake Bahama Basin (Baumgartner, 1984) are assigned to the Central Tethyan Province (Pessagno et al., 1993) and should have been deposited at lower latitudes than the Caribbean occurrences.

The latitudinal findings contradict a near-equator origin for La Désirade and suggest that the radiolarian assemblages on La Désirade, Puerto Rico, Hispaniola and Cuba (Montgomery et al. 1994; Mattinson et al., 2008) could indeed have been derived from anything from ~1000-3000 km north of the Colombian Marginal Seaway. However, these outcrops would therefore have to migrate SE with respect to North America to be later incorporated in the Caribbean Plate. Studies of oblique convergence in modern and ancient arc systems and recent sandbox experiments show that the strike-slip component is largely taken up in the fore-arc and the arc, not the back-arc (e.g. Beck, 1983; ten Brink et al., 2009). Applied to the Andean/Cordilleran system, it would be difficult for the back-arc basin rocks of La Désirade to migrate SE significantly with respect to North America. Therefore, it is proposed that the original palaeo-latitudinal findings should be re-considered; a view shared by Pindell & Kennan

(2009), as they also place La Désirade close to the equator in the Colombian Marginal Seaway (Fig. 6.2).

6.2.2. Pre-Aptian subduction-related rocks preserved in the Caribbean and Central America

Although many pre-Aptian rocks are found at various locations around the Caribbean and in Central America, the focus here is on the fragments that formed during Andean/Cordilleran subduction which may be related to La Désirade. Baumgartner et al. (2008) have argued that such fragments exist in western Central America and on Cuba, Jamaica and Puerto Rico. This section uses their possible locations within the Andean/Cordilleran system to propose the regional 'pre-polarity reversal' plate tectonic reconstruction for the Late Jurassic shown in Fig. 6.2.

Central America: Rocks found in mélanges in Mexico, Nicaragua and Costa Rica belong the proposed Mesquito Composite Oceanic Terrane, the components of which were accreted to Central America as part of the Andean/Cordilleran arc system and lie north of the CCOP (Baumgartner et al., 2008) (Fig. 6.1). Tectonised gabbros and volcanic rocks, some with island arc chemistry, have been dredged from the fore-arc basement of Guatemala and Mexico. These ~180 to 100 Ma rocks record a long history of east-dipping Farallon Plate subduction (Geldmacher et al., 2008). At Santa Elena in Costa Rica (Fig. 6.1), three mafic volcanic island arc-related units have been identified with radiolarians in intercalated sediments ranging from 124-109 Ma (Hauff et al., 2000; Hoernle & Hauff, 2004). Beneath Santa Elena lies the Santa Rosa accretionary complex which has a more within-plate character (Hauff et al., 2000), but radiolarian ages from 190-93 Ma, which show that at least part of the complex was formed at a similar time to La Désirade (Baumgartner & Denyer, 2006). The Santa Elena and Santa Rosa complexes are possible equivalents to the Guatemalan forearc (Geldmacher et al., 2008). Finally, the Siuna complex in Nicaragua (Fig. 6.1) is a mélange of serpentinites, gabbros and metamorphosed sedimentary and mafic igneous rocks including Middle to Upper Jurassic radiolarian cherts (Baumgartner et al., 2008). A phengite ^{40}Ar-^{39}Ar cooling age of 139.2±0.4 Ma from the high-pressure parts of the Siuna mélange indicates Farallon east-dipping subduction-exhumation processes operating shortly after the formation of La Désirade (Flores et al., 2007).

Cuba: Cuba (Fig. 6.1) is built partly of allochthonous suites of Mesozoic subduction-accretion complexes thrust together during collision with the Bahama Platform in the early Tertiary (Stanek et al., 2009). At the base of the Las Villas Syncline in west-central Cuba (Stanek et al., 2009) the Mabujina complex (Somin & Millán, 1981), which pre-dates the other subduction-related units of Cuba, consists of amphibolites and gneissic granitoids of island arc origin (Kerr et al., 1999; Blein et al., 2003. The gneiss has been dated using U-Pb zircon methods to 133 Ma (Rojas-Agramonte et al., 2006). It is therefore possible that the amphibolites of the Mabujina complex formed at the same time as La Désirade and indeed the North Coast Schist of Tobago however the chronology is far from certain.

Jamaica: The Devils (sic) Racecourse Formation of the Benbow inlier (Fig. 6.1) (Burke et al., 1969) consists of a lower bimodal island arc tholeiite sequence and an upper suite of calc-alkaline basalt-basaltic andesite island arc rocks (Hastie et al., 2009). The Lower and Upper parts of the formation are separated by a sedimentary succession containing Hauterivian fossil assemblages at its base (Skelton & Masse, 1998). The >136 Ma Lower Devils Racecourse Formation arguably contains the oldest lavas convincingly formed at an island arc axis in the Caribbean. Although Hastie et al. (2009) and Pindell & Kennan (2009) argue the Lower and Upper sequences were erupted in one single tectonic setting, this is far from certain given: (1) 2600 m of sedimentary rocks, (2) faulting between the two Formations (Burke et al., 1969) and (3) the need for detailed mapping of the Benbow Inlier (Hastie et al., 2009). Nevertheless, Hastie et al. (2009) propose that the entire Devils Racecourse Formation was formed above an E-dipping Andean/Cordilleran subduction zone.

Puerto Rico: Much of Puerto Rico (Fig. 6.1) is made up of middle to Late Cretaceous island arc assemblages argued to relate to SW-dipping subduction of the proto-Caribbean crust (Jolly et al., 2001); however, to the southwest of these assemblages lies the Bermeja complex (Mattson, 1960) which consists of a tectonic melange of oceanic serpentinite, amphibolite, basalt and chert (Schellekens, 1998). The cherts have yielded a ~90 Ma history from the Early Jurassic to the Cretaceous including Kimmeridgian-Tithonian radiolarian- and Pantannelid-bearing tuffaceous cherts which overlap in age with La Désirade (Montgomery et al., 1992, 1994;

Schellekens et al., 1998). The tuffaceous nature of the chert may indicate deposition close to an island arc source, whilst the gabbros and greenstones apparently have a supra-subduction zone origin (Montgomery et al., 1994; Schellekens, 1998). Accretion of the Bermeja complex occurred during the Early Cretaceous before the deposition of Cenomanian sedimentary rocks (Schellekens, 1998). It is unlikely that the Bermeja complex was formed close to a SW-dipping subduction zone because of its age range and south-westerly position relative to the younger Greater Antilles arc assemblages. Hence, Bermeja may also represent part of the Andean/Cordilleran system.

6.2.3. Plate tectonic reconstruction of Middle America during the Late Jurassic

Figure 6.2 shows a model proposing that the arc rocks discussed above were related to the east-dipping Andean/Cordilleran subduction system. Some subduction-related rocks such as those found in Jamaica and Puerto Rico may have been close to, or part of, the original E-dipping arc axis from within the inter-American region. La Désirade formed as part of the back-arc of this inter-American portion of the arc. Further north, Late Jurassic to Early Cretaceous E-dipping subduction formed the island arc rocks of the Guatemalan fore-arc (Geldmacher et al., 2008) and the subduction of the Siuna high-pressure rocks (Flores et al., 2007; Baumgartner et al., 2008), which were later accreted to the Greater Antilles arc before final collision with North America (Pindell et al., 2011). Within-plate rocks also dredged from the Guatemalan fore-arc were erupted on the Pacific Plate and later accreted to the subduction mélange (Geldmacher et al., 2008). Any Cretaceous polarity reversal event analogous to the Caribbean models did not affect the western margin of Central America, so eastwards subduction and accretion of the fore-arc and seamounts continued through the Cretaceous (Fig. 6.2).

6.2.4. Which model of subduction polarity reversal is favoured for the preservation of La Désirade?

La Désirade formed at ~150-143 Ma in the back-arc of the Andean/Cordilleran system (Neill et al., 2010). It is assumed that, in the plateau-collision model (Chapter 1), La Désirade would remain in the back-arc region until ~90 Ma when collision of the CCOP with the inter-American portion of the Andean/Cordilleran arc system would

force a polarity reversal, with La Désirade accreting to the new NE-facing Greater Antilles arc. The implications of the ~135-125 Ma SW-dipping subduction initiation model of Pindell & Kennan (2009) and Pindell et al. (2006, 2011 and references therein) are similar to the plateau-collision model with the exception that La Désirade would be accreted to the Caribbean Plate during a much earlier polarity reversal at ~135-125 Ma. In both cases the new SW-dipping subduction zone would be located to the E of La Désirade. Likewise, the other suites of rocks which formed at a similar time to La Désirade, and are preserved today in the Caribbean (e.g. the Bermeja, Puerto Rico), would be part of the Andean/Cordilleran system until polarity reversal.

6.3. Origin of Tobago Island

6.3.1. Relationship of the North Coast Schist to other subduction-related rocks in the Caribbean

The new U-Pb zircon age for the North Coast Schist of 130.4±4.5 Ma (Hauterivian-Barremian) means that it is younger than the subduction-related rocks of La Désirade Island by approximately 10-20 Ma. Of the rock units described in Section 6.2.2., the two most similar in age to the North Coast Schist are the ~133 Ma granitoids of the granitoid- and amphibolite-bearing Mabujina complex of Cuba, and the ~Hauterivian-Aptian (~136-125 Ma) tholeiitic and calc-alkaline island arc rocks of the Devils Racecourse Formation, Jamaica (Fig. 6.1). In all three cases, these suites represent the oldest island arc rocks to be found on their respective islands. Of the remaining island arc rocks in the Greater Antilles, many are ~125 Ma or younger (Jolly et al., 2001; Escuder Viruete et al., 2006; Stanek et al., 2009). To date, the North Coast Schist is the oldest confirmed island-arc related unit in the offshore southern Caribbean.

6.3.2. Origin of the North Coast Schist in the context of the subduction polarity reversal models

Plateau collision model: In the plateau collision model for Caribbean tectonic evolution, the ages of the North Coast Schist and younger Tobago rocks (~130-91 Ma) indicate that Tobago formed entirely within an E-dipping island arc system. The NCS protoliths would form in the fore-arc of the Andean/Cordilleran subduction system and then were deformed in an environment of dextral wrench shearing. Following this deformation, island arc magmatism continued with the formation of the Volcano-Plutonic Suite.

It is pertinent to mention here that a model for plateau collision and subduction polarity reversal has been proposed for the Dutch Antilles island chain (van der Lelij et al., 2010). Van der Lelij et al. (2010) used zircon and apatite fission-track dating on Bonaire and Aruba (Fig. 6.1) to show that uplift of ~3 km or more of the Dutch Antilles at ~90-85 Ma was associated with plateau collision. In contrast, thermo-chronological work on the TPS of Tobago (Cerveny & Snoke, 1993) shows that Tobago cooled

through zircon closure (250-200°C) at ~103 Ma with no evidence for subsequent burial or uplift until cooling through the apatite annealing zone at ~45 Ma, the latter date concurrent with accretion of the Tobago terrane to northern South America (Speed & Smith-Horowitz, 1998). Therefore, the plateau-collision model is not substantiated by any thermo-chronological data from Tobago although more detailed work may be necessary. Furthermore, deformation of the NCS occurred between the formation of the 130.4±4.5 Ma Parlatuvier Formation and the first eruptions of the Tobago Volcanic Group (~112-106 Ma; Snoke & Noble, 2001) so collision of the 95-90 Ma CCOP cannot have played any role in deformation. Therefore an original explanation for that event must be sought; possibly that NCS deformation occurred during the oblique rifting of the E-dipping subduction system as proto-Caribbean spreading continued.

~135-125 Ma SW-dipping subduction initiation model: Figure 6.3, similar to that proposed by Pindell et al. (2011), shows that during the hypothesised ~135-125 Ma subduction initiation/polarity reversal event, fragments of the pre-existing Andean/Cordilleran arc system would be dragged along transform faults into the new Greater Antilles island arc axis. The structural observations of the NCS by Snoke et al. (2001) show that there was dextral wrench shear deformation of these greenschist-facies rocks. As Figure 6.3 shows, Pindell et al. (2011) propose that a series of transform systems should form at the interface between the old Andean/Cordilleran arc and the new SW-dipping Greater Antilles arc system during polarity reversal. Transform faulting would be dextral in nature at the southern end of the new subduction zone. Unfortunately, the relative ages of the Parlatuvier, Mount Dillon, Karv and MORB-like amphibolite units are unknown, so any model for the origin and deformation of the NCS is necessarily hypothetical. The geochemical results discussed in Section 5.3 showed that many of the amphibolites of the thermal aureole with the TPS were MORB-like and the other formations were subduction-related; with the Parlatuvier Formation derived from a HFSE-enriched mantle, and the other rocks derived from more a more depleted mantle source. Although it is possible to walk down-grade in continuous section from amphibolite-facies rocks of unknown chemistry to the Parlatuvier Formation of the NCS (Snoke et al., 2001b), all of the *chemical* boundaries between units may well be fault-bounded. The deformational environment of dextral wrench shear described above may be a convenient means of amalgamating

chemically-different parts of the NCS from slightly different parts of the Andean arc system.

As an aside; the DUPAL anomaly described from the Nd-Hf radiogenic isotope results for the Parlatuvier Formation and amphibolites in Chapter 5 might be explained by the mantle or mantle wedge source containing both South American sub-continental lithospheric mantle (SCLM) and more chemically depleted (isotopically enriched) components. This scenario is only possible with E-dipping subduction. In summary, unless an alternative explanation to the subduction polarity reversal is found for the ~130-112 Ma deformation and metamorphism of the NCS of Tobago, the work undertaken in this thesis supports the ~135-125 Ma SW-dipping subduction initiation model of the Caribbean.

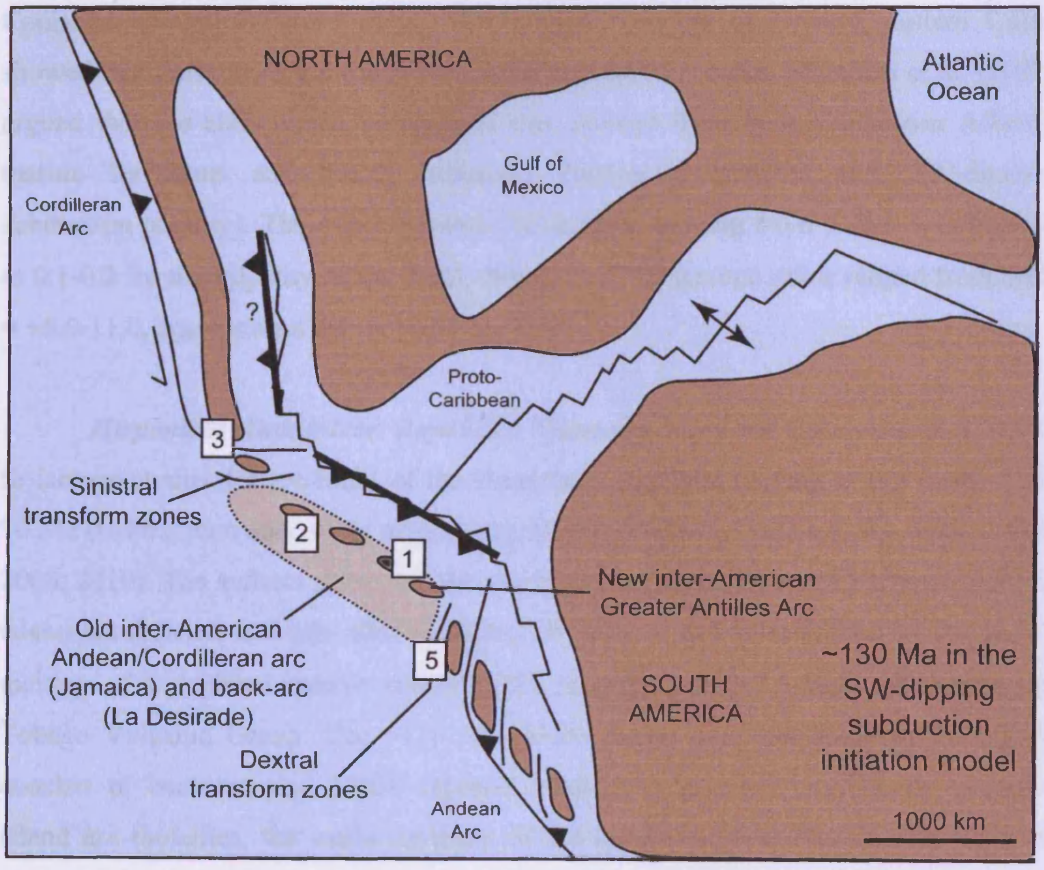

Figure 6.3. Diagram adapted and modified from Pindell et al. (2011) showing the model for ~135-125 Ma SW-dipping subduction initiation. In this model, La Désirade (point **1**) and any fragments of the older NE-dipping Andean/Cordilleran arc, e.g. Jamaica, Puerto Rico (point **2**) would lie in various positions with respect to the new Greater Antilles arc. Siuna would be trapped at the southern end of the Cordilleran arc system (point **3**). The North Coast Schist protoliths of Tobago (point **4**) would have formed in the E-dipping Andean fore-arc before dextral wrench-shear translation to the new Greater Antillean island arc axis. SW-dipping subduction of the proto-Caribbean crust would result in the formation of the TVG, TPS and younger tonalite, dykes and Nb-enriched rocks.

6.3.3. Correlation of the Volcano-Plutonic Suite with other Caribbean island arc rocks

Table 1.2 showed a selection of the island-arc fragments across the Caribbean region, the most pertinent of which are discussed here in relation to the ~112-106 Ma magmatism on Tobago. Unfortunately, Hf isotope ratios have not been calculated for any of these rocks with the exception of the Washikemba Group, Bonaire (Thompson et al., 2004).

Cuba: On the island of Cuba, island-arc rocks dating from ~125 Ma to ~75 Ma are preserved (summarised by Stanek et al., 2009). Geochemically relatively little is known about these rocks. A detailed study by Marchesi et al. (2007) on the Albian-Coniacian (Iturralde-Vinent et al., 2006) igneous suites of Oriente, eastern Cuba, showed that these were arc rocks with depleted mantle sources. Marchesi et al. (2007) argued that the slab-related component was derived from both Cretaceous Atlantic marine sediments and North American continental material (i.e. SW-dipping subduction polarity). Their data showed Th/La ratios ranging from 0.05-0.3, compared to 0.1-0.2 for the majority of the TVG. Whole-rock Nd isotope ratios ranged from εNd_i = +5.0-11.0, again within the range of the VPS.

Hispaniola (Dominican Republic): There are major and trace element and Nd-Sr isotope studies for arc rocks of the Dominican Republic ranging in age from ~125-90 Ma (U-Pb zircon and Ar-Ar plagioclase dating) (Escuder Viruete et al., 2006, 2007b, 2008, 2010). The authors show that the majority of these rocks are of back-arc basin to island-arc tholeiite and calc-alkaline island-arc affinity and were formed by the partial melting of a depleted mantle source (εNd_i ranging from +7.5-10.5), similar to the Tobago Volcanic Group. The >116 Ma (U-Pb zircon age) Los Ranchos Formation consists of boninites and LREE-depleted island arc tholeiites overlain by 'normal' island arc tholeiites, the mafic varieties of the lattermost with similar trace element patterns and Th/La ratios to the Tobago Volcanic Group (Escuder Viruete et al., 2006). One other unusual suite of rocks is the ~90 Ma Tireo Formation of Escuder Viruete et al. (2007b), dated by zircon U-Pb and hornblende Ar-Ar methods. Here, the Tireo Formation overlies island arc tholeiites, and consists of adakites, magnesian andesites

and Nb-enriched basalts. Escuder Viruete et al. (2007b) interpret these rocks to be the magmatic product of subduction of the proto-Caribbean spreading ridge and the partial melting of the resultant slab-window edges (e.g. Thorkelson & Breitsprecher, 2005). Hitherto this is the only location in the Cretaceous Caribbean arc system where this supposed genetically-related rock association has been recorded. Unfortunately, there is no isotopic data for these unusual rock types, a serious concern because: (a) the lack of isotope data precludes meaningful comparison with the Arnos Vale-Mason hall tonalite and Nb-enriched dykes of Tobago and (b) isotopic data is vital in proving a genetic link between slab melting and Nb-enriched basalt formation (e.g. Section 5.3.6; McPherson et al., 2006; Castillo, 2008).

Puerto Rico and the U.S. Virgin Islands: Puerto Rico contains Lower to Upper Cretaceous island arc assemblages which Jolly et al. (2001) separated into 5 volcanic phases, with phases I-III forming in the Late Aptian to Coniacian (~120-97 Ma), similar to the rocks of Tobago. Phase I comprises mafic to intermediate island arc tholeiites, with Th/La ratios of ~0.07-0.16 and εNd_i values of +7.2-8.5. Phase II is more calc-alkaline in composition, with Th/La ratios within the range of the phase I rocks (~0.10-0.14) and εNd_i values of +6.5-8.1. These results are comparable to Tobago and indicate a relatively depleted mantle wedge source with little contribution from subducted terrigenous sediments. The phase III rocks have Th/La ratios ranging from ~0.12 to 0.40, much higher than for Tobago. Jolly et al. (2001) interpreted the high Th/La as the product of fractional crystallisation processes (zircon accumulation?) because of the preponderance of more felsic rocks (up to 75 wt.% SiO_2) and a positive correlation between Th/La ratios and fractionation indices in phase III. Finally, Nb-Y concentrations at 8 wt.% MgO (Pearce & Parkinson, 1993) were used by Jolly et al. (2001) to show that mantle fertility increased throughout the growth of the arc system.

Jolly et al. (2001) interpreted the geochemistry of the mafic rocks as recording the build-up of an island arc system in the open ocean away from terrigenous sediment sources, with melt extraction in the back-arc basin reducing temporally to give a progressively more fertile mantle wedge. Jolly et al. (2008) later argued that the subduction of Atlantic biogenic clay and carbonates, and a smaller proportion of turbidites, was responsible for geochemical variations in the Puerto Rican lavas, as

opposed to Pacific pelagic chert; and that phases I to III were therefore formed above a SW-dipping Greater Antilles subduction zone. A more detailed study of the field relationships, isotope and trace element geochemistry of the arc rocks of Puerto may be required to prove SW-dipping or NE-dipping subduction through the Early to Late Cretaceous.

Finally, the Water Island Formation of the U.S. Virgin Islands consists of a bimodal suite of island arc basalts and dacites/rhyolites which have been loosely dated by radiolarian assemblages to ~115 Ma (Rankin, 2002). A major and trace element study by Jolly & Lidiak (2006) showed that the mafic rocks had flat to LREE-depleted normalised REE patterns, and negative Nb and Ce anomalies, the latter consistent with the subduction of oxidised pelagic sediments. However, the study also showed that the samples had relatively low analysed abundances of Th (<0.5 ppm), close to the limit of detection, so a clear assessment of the slab component related to subducted terrigenous sediment is impossible.

Bonaire, Dutch Antilles: The only Aptian-Albian island arc rocks of the southern Caribbean not to have not experienced HPLT metamorphism, are found on the Dutch Antilles island of Bonaire (Fig. 6.1). U-Pb and Ar-Ar dating has revealed that the Washikemba Group, consisting of felsic volcaniclastics intruded by felsic to intermediate dykes and sills, is ~98-94 Ma (Thompson et al., 2004; Wright & Wyld, 2011). The Matijs Group consists of argillites, cherts and conglomerates, with the argillites cut by doleritic stocks. A U-Pb baddeleyite age obtained from the dolerite was 111.6±5.1 Ma was reported by Wright & Wyld (2011). Chemically the igneous rocks of the island are of island arc origin, derived from a depleted mantle source with coupled Nd-Hf isotope ratios which overlap on Figure 4.27 with the VPS of Tobago (Thompson et al., 2004). The exact origin of the Bonaire island arc block is uncertain. Thompson et al. (2004) and van der Lelij et al. (2010) argue it formed in an E-dipping subduction setting (Andean arc?) whereas Wright & Wyld (2011) propose it formed at the southern end of the Greater Antilles arc and was dragged SW along a subduction-transform-edge-propagator fault (Govers & Wortel, 2005) between the SW-dipping Greater Antilles and E-dipping Andean trenches to its present location. To re-iterate, thermo-chronological data indicate >3 km of uplift on Bonaire at ~90-85 Ma which suggests the Bonaire arc block was part of an E-dipping subduction system with which the

CCOP collided (van der Lelij et al., 2010). Whatever the origin of Bonaire, it is important to understand that this arc-related fragment was probably located within an E-dipping Andean arc system by ~90 Ma. For a suggestion of the palaeo-locations of the Greater Antilles arc fragments, Tobago and Bonaire, see Figure 6.3 below.

Subduction-related rock units in Venezuela: Two rock units in Venezuela may have geological histories which can be correlated to the island arc activity on Tobago. The first of these is Margarita Island, offshore Venezuela (Fig. 6.1), which is part of the wider geological region of the Caribbean coast of Venezuela called the Cordillera de la Costa, consisting of fragments of oceanic, passive margin and continental rocks (Sisson et al., 1997). Margarita Island consists of a basement suite of HPLT rocks. Maresch (1971) defined continental rocks – dominated by metasedimentary schists and gneisses – as the Juan Griego Group, and oceanic rocks – mostly metabasalts – as the La Rinconada Group. Little geochemical work has been done on these rocks but structural investigations suggest these two units were amalgamated prior to peak subduction zone metamorphism (Stöckhert et al., 1995; Maresch et al., 2009). These authors conducted U-Pb dating of zircons from the two units and produced ages ranging from ~116-106 Ma to 85 Ma. The 85 Ma age comes from a post peak-metamorphic tonalite body. The significance of these results is difficult to assess because (a) it is not known for certain whether the older zircon ages are from the protoliths or if they represent metamorphic growth; (b) the origin of the igneous protoliths, particularly of the La Rinconada Group have not been assessed in detail geochemically and (c) there is a large error of ~10 Ma on the older U-Pb age which makes it difficult to interpret geologically. Nevertheless, Margarita was undergoing HPLT metamorphism in a subduction zone at the same time as the island arc rocks of Tobago were forming. Maresch et al. (2009, their Fig. 17) have argued that the opening of a back-arc basin between the Andean arc and South America during the Jurassic formed the La Rinconada Group; and that its W-directed closure during the Aptian-Late Cretaceous (coupled with a SW-dipping Greater Antilles arc), resulted in the subduction of fragments of South American continental margin (Juan Griego Group), as well as the La Rinconada Group.

The second Venezuelan unit of interest is the Villa de Cura, long reported as a large nappe-scale structure, and more recently sub-divided into four mafic volcanic and sedimentary formations metamorphosed in the pumpellyite-actinolite to barroisite

zones (blueschist facies) (Shagam, 1960; Smith et al., 1999; Unger et al., 2005). Limited major and trace element analyses of the volcanics indicate that the Villa de Cura was part of a tholeiitic island arc (Ostos & Sisson, 2005; Unger et al., 2005). The high-grade, more silicic barroisite sub-belt reached peak metamorphism at ~96 Ma (Ar-Ar dating of barrosite amphiboles), with the other belts experiencing peak metamorphism at ~80 Ma (Smith et al., 1999). Smith et al. (1999) and Unger et al. (2005) argued that these rocks formed in an E-dipping island arc setting and were deformed in a W-dipping subduction zone following polarity reversal. During the inception of W-dipping subduction the higher-grade rocks were argued to have been subducted earlier, and deeper, compared to the lower-grade rocks (Smith et al., 1999; Unger et al., 2005).

An untested alternative hypothesis was proposed by Ostos et al. (2005) - that the rocks of the Villa de Cura formed due to Cretaceous SE-sipping subduction beneath the rifted continental margin of NW South America. However, the correlation of this SE-dipping subduction zone to either Bonaire or the Greater Antilles arc has not been achieved. Both hypotheses for the origin of the Villa de Cura remain to be fully tested, particularly because of its unknown protolith age and lack of detailed geochemical information. Nevertheless, Mid-Cretaceous HPLT metamorphism took place in Venezuela at a similar time to the island arc rocks of Tobago.

6.3.4. Origin of the Volcano-Plutonic Suite in the southern portion of the Greater Antilles island arc

The comparison in Section 6.3.3 shows that the ~112-106 Ma VPS of Tobago is of a similar age to, and shares geochemical characteristics with, island arc rocks preserved in Eastern Cuba, Hispaniola, Puerto Rico, the U.S. Virgin Islands and potentially the Matjis Group of Bonaire. Reconstruction of the Caribbean region prior to the opening of the Grenada Basin at ~55 Ma would place Tobago close to the central-northern portion of the Aves Ridge arc (Pindell & Kennan, 2009). This palaeo-location and geochronological and chemical comparison strongly indicates that the rocks of the VPS formed above the same subduction zone as the rocks of the Greater Antilles and probably towards the southern end of the island arc system.

In the plateau collision model of the Caribbean, most of the locations listed in Section 6.3.3 would have formed above a NE-dipping subduction zone. In the ~135-125 Ma SW-dipping subduction initiation model, most of the formations would have been generated by partial melting above a SW-dipping subduction zone, with the possible exception of the rocks of Bonaire, discussed in Section 6.3.3. This model is set out in Figure 6.4. Aside from the contentions of Jolly et al. (2001), Jolly & Lidiak (2006) and Marchesi et al., (2007), based on the calculated composition of subducted sediments, there is little conclusive evidence taken from these rocks alone that favours either subduction polarity. However, as discussed in Section 6.3.2, the deformational history of the older NCS of Tobago implies that the VPS formed above a SW-dipping subduction zone following polarity reversal (Figs. 6.3, 6.4).

The relationship of the rocks of the Greater Antilles to those found on Margarita Island (Cordillera de la Costa) and in the Villa de Cura of Venezuela is, as noted in Section 6.3.3, extremely difficult to ascertain and will not be further discussed here.

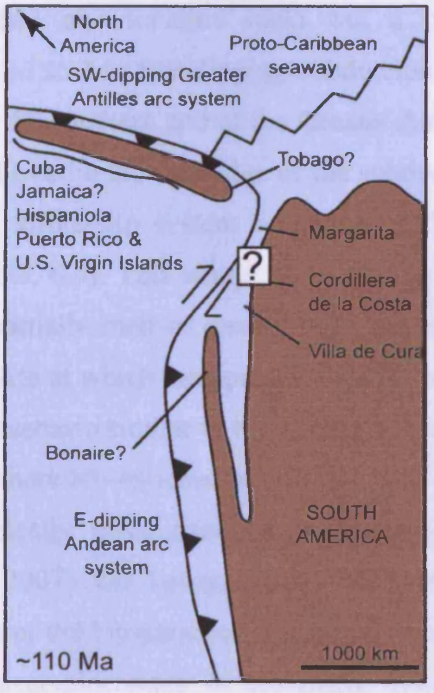

Figure 6.4. Possible origin of the VPS of Tobago in a SW-dipping subduction scenario, adapted from Pindell et al. (2011) and Wright & Wyld (2011). Tobago forms at the southern end of the Greater Antilles arc, while the island arc rocks of Bonaire form above the north end of the Andean subduction zone. The origin of Margarita, the Cordillera de la Costa and the Villa de Cura is uncertain.

6.3.5. Plate tectonic context for the dyke swarm, tonalite, and Nb-enriched mafic rocks

At the end of the main phase of volcanism on Tobago, at ~106 Ma, the VPS was intruded by the Arnos Vale-Mason Hall tonalite, followed by rare Nb-enriched mafic rocks. Contemporaneous with the final stages of formation of the VPS, and for ~15 Ma thereafter, a swarm of mafic dykes was emplaced with a waning subducted sediment-related component and increasingly depleted mantle signature, indicated by decreasing time-integrated Th/La, La/Sm and Nb/Yb ratios. Earlier in this thesis it was suggested that the tonalite was formed by partial melting of the subducting oceanic slab and that the Nb-enriched mafic rocks were probably formed by the partial melting of a HFSE- and isotopically-enriched source which was distinct from both the subducting oceanic crust and mantle source of the VPS.

In the plateau-collision model of the Caribbean, some local slab-melting and enriched mantle infiltration into the NE-dipping island arc system would have to occur to form these Nb-enriched and tonalitic rocks but a precise model is elusive. Alternatively, in the ~135-125 Ma SW-dipping subduction initiation model, Tobago would be situated near to the southern end of the Greater Antilles arc at ~106 Ma (Fig. 6.4). Here, the VPS could overlie the torn edge of the subducting proto-Caribbean slab where it met the dextral strike-slip system linking with the E-dipping Andean arc further to the SW (Figs. 6.3, 6.4). This would be an ideal location for the edge of the proto-Caribbean slab to partially melt in contact with hot, dry mantle. This slab-edge location would also be a site at which isotopically distinct sources could form the Nb-enriched dykes. This is a scenario similar to the northern termination of the Kamchatka arc (a slab-edge setting) where Nb-enriched basalts are erupted that are HFSE-enriched compared to, and isotopically more enriched than, the more southerly arc rocks (Portnyagin et al., 2005; 2007). On Tobago, any subsequent rifting of the island arc system after the formation of the Nb-enriched rocks and the tonalite could lead to upper crustal extension and the emplacement of the mafic dyke swarm, derived from a depleted, subduction-influenced mantle.

6.4. Origin of the mafic rocks of San Souci

6.4.1. Palaeo-location and correlations

The zircon fission track data discussed in Section 2.3.1 show peaks at ~108 Ma, ~200 Ma, ~245 Ma, ~336 Ma and ~435 Ma (Algar et al., 1998). The older ages are consistent with suitable protoliths found in the northern Andes (Barrett, 1986; Algar et al., 1998). The small cluster of ~108 Ma ages has been argued to tally with the San Souci Formation (Algar et al., 1998) which cannot be tested as there is, as yet, no reliable radiometric age from the San Souci Formation itself. It is almost certain that during the Middle to Late Cretaceous, the San Souci Formation was formed within a sedimentary basin that lay to the NW of continental South America and probably to the south and/or east of any island-arc-related units of the leading edge of the Caribbean Plate. There have also been several unpublished studies looking at outcrops of mafic rocks found in the Araya-Paria peninsula (Cordillera de la Costa) and the Los Algadones region south of the Falcon Basin, in Venezuela (McMahon, 2000; Kerr et al., 2009b; A.C. Kerr, unpublished data) (Fig. 6.1). These rocks, listed below, have been found to contain oceanic plateau geochemical signatures similar to those found at San Souci.

Cordillera de la Costa, Venezuela: The Cordillera de la Costa is a highly deformed belt running along the coastal regions of northern Venezuela (Fig. 6.1), consisting of 'oceanic and passive continental-margin rocks intermixed with Palaeozoic granites and granitic gneisses' (Sisson et al., 1997). The mixture of rocks, some of which have been metamorphosed to eclogite facies, have been interpreted as fragments of oceanic and continental material which were partly subducted near to the NW corner of South America before being transported eastwards with the Caribbean Plate (similar to Margarita Island and the Villa de Cura) (e.g. Sisson et al., 1997; Ellero et al., 2007). The Cordillera de la Costa strikes E-W discontinuously for over 600 km. Within the easternmost of the blocks on the Araya-Paria peninsula lies the poorly-studied El Copey Formation (Maxwell & Dengo, 1951) (Fig. 6.1). Little information is available, but A.C. Kerr has collected schistose tuffs and talc-schists (meta-serpentinites) and basaltic schist (Kerr et al., 2009b) and C. McMahon of Notre Dame University collected a suite of basalts (McMahon, 2000). The schistose tuffs and the basaltic schist

have flat normalised REE patterns with no Nb-Ta anomalies (Kerr et al., 2009b), similar to the basalts of McMahon (2000). Therefore, these rocks are not subduction-related. Zr/Nb ratios range from 8-23 (plume-like) (McMahon, 2000; Kerr et al., 2009b). Plotted on an Nb/Y vs. Zr/Y diagram (Fitton et al., 1997), the majority of the collected samples fall within the Iceland array close to the lower tramline (McMahon, 2000; Kerr et al., 2009b), again suggestive of a plume-related source (Fig. 6.5). Nd and Hf radiogenic isotope signatures, corrected to 90 Ma, are presented on Figure 6.5 (and Fig. 4.30) and are: εNd_i = +8.5-9.0 and εHf_i = +13.0 (Kerr et al., 2009b). These rocks are isotopically identical to the rocks of San Souci on the εHf_i vs. εNd_i plot.

Los Algadones, Venezuela: Siquisique (Fig. 6.1), in Los Algadones, Venezuela, lies to the NW of the Cordillera de la Costa belt and contains basalts and gabbros which are associated with, but not obviously intercalated between, Jurassic ammonite-bearing marine sedimentary rocks (Bartok, 1985; Kerr et al., 2009b). Because of the ammonite ages, it was assumed that the mafic rocks were the product of spreading between the Americas to form the proto-Caribbean Seaway (Bartok, 1985). However the basalts and gabbros may intrude the older sedimentary rocks or be in faulted contact. Gabbros and basalts were collected from Siquisique in 2004, and Ar-Ar dating of fresh plagioclases within these rocks indicates a likely intrusion age of 95-90 Ma (Kerr et al., 2009b). These rocks have flat REE patterns and have, like the rocks of San Souci and El Copey, no Nb-Ta or Ti anomalies (Kerr et al., 2009b). The Siquisique rocks have Zr/Nb ratios of 26-34 in the gabbros and 20-30 in the basalts, compared to the average Zr/Nb of San Souci of 21, and plot around the lower tramline of the Iceland array on the Zr/Y vs. Nb/Y diagram (Figure 6.5). Isotopically, the basalts are similar to El Copey and Siquisique, with εNd_i = +9.2 and εHf_i = +14.0. A single gabbro analysis was slightly more depleted with εNd_i = +10.1 and εHf_i = +15.5, similar to East Pacific Rise MORB and consistent with the more MORB-like Zr/Nb ratios of the gabbros (Figs. 6.5 and 4.30). Therefore, the basalts at least appear to be geochemically identical to the mafic rocks of El Copey and San Souci.

With the exception of the Siquisique gabbros, all of these units appear to be related to San Souci in that they are geochemically distinct from MORB, have plume-like trace element characteristics and isotopically are very similar to each other.

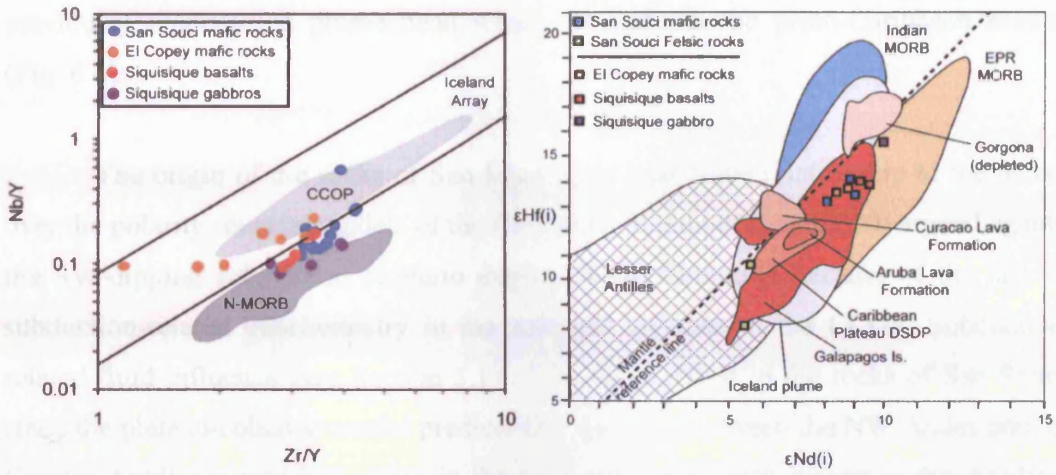

Figure 6.5. Left: Nb/Y vs. Zr/Y diagram. See Chapter 5 for an explanation. Sample references: San Souci – this study; El Copey mafic rocks – McMahon (2000), Kerr et al. (2009b); Siquisique basalts and gabbros – Kerr et al. (2009b). Right: Hf-Nd isotope diagram. San Souci – this study; El Copey and Siquisique – Kerr et al. (2009b).

6.4.2. Source of magmatism and location with respect to the Greater Antilles arc

There is no evidence for active rifting on the continental margin of NW South America at ~90 Ma (Wadge & Macdonald, 1985). All the units discussed above formed by moderate degrees of partial melting of a plume-like mantle source (Kerr et al., 2009b). Therefore it is concluded that these formations were derived from the partial melting of either: (a) a distinct proto-Caribbean plume source, or (b) part of the Galapagos plume head which formed the CCOP. There are 3 reasons which indicate that hypothesis (b) is unlikely to be correct. Firstly, the ages of the mafic rocks of San Souci and El Copey are unknown and could potentially pre-date the CCOP. The age of the Siquisique rocks is constrained only by Ar-Ar analyses and not by potentially more accurate U-Pb zircon dating (Kerr et al., 2009b). Secondly, if the Galapagos Plume head were to be responsible for this proto-Caribbean magmatism then plume activity at ~95-90 Ma would have to jump from the east to the west side of the Greater Antilles subduction system (either NE- or SW-dipping) almost certainly contaminating the mantle wedge source of the Caribbean arc system (see Hastie & Kerr, 2010). Thirdly, the Nb/Y vs. Zr/Y and Hf-Nd isotope plots presented in Figure 6.5 show no convincing evidence that the rocks of San Souci, Siquisique or El Copey were derived from a mantle source chemically and isotopically similar to the Galapagos Islands and the CCOP. Given the lack of chemical or geodynamic support for a Galapagos plume head origin, it is concluded that these rocks were formed by the partial melting of a distinct,

previously unidentified plume head which lay beneath the proto-Caribbean seaway (Fig. 6.6).

The origin of the rocks of San Souci does bear some relationship to the debate over the polarity reversal models of the Caribbean. Hastie & Kerr (2010) argued against the SW-dipping subduction scenario during CCOP formation because of the lack of subduction-related geochemistry in the analysed sections of the CCOP. Subduction-related fluid influence (see Section 5.1) might be expected in the rocks of San Souci, since the plateau-collision model predicts that the crust between the NW Andes and the Greater Antilles would have been in the back-arc region with respect to the Antillean arc. A pre-existing E-dipping subduction zone could potentially contaminate the mantle source of San Souci and the Venezuelan localities with a slab-related component unless it lay at a significant distance from the arc. A global study of back-arcs by Pearce & Stern (2006) showed that the size of the slab-fluid signature (traced by Ba/Nb ratios) in the back-arc was related to the distance between the back-arc spreading centre and the island arc. However, Pearce & Stern (2006) argue that the distance from the arc at which the slab-fluid signature is absent from back-arc rocks varies considerably between systems (usually over an order of 100's of km), and that complex tectonic histories or mantle flow patterns can affect the slab-signature/distance relationship. Therefore, although the lack of a subduction-related geochemical signature in the plateau rocks of this study implies no E-dipping subduction zone beneath the proto-Caribbean at ~100-90 Ma, the chemistry of these rocks is not definitive evidence against the plateau-collision model of Caribbean tectonic evolution.

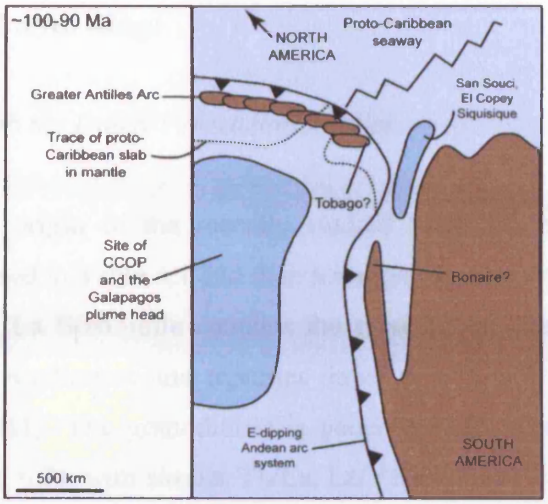

Figure 6.6. Hypothetical palaeo-tectonic scenario with the Galapagos plume head and CCOP lying to the SW of the Greater Antilles and W of the Andean arc system. San Souci, El Copey and Siquisique formed *within* the proto-Caribbean plate from a separate mantle plume head.

6.5. Origin of the SE Aves Ridge

6.5.1. Correlation with the Dutch-Venezuelan Antilles

The age and origin of the recently studied rocks of the Dutch-Venezuelan Antilles are summarised in Table 6.1 and their locations are shown on Figure 6.1. In the Venezuelan Antilles, La Blanquilla contains the closest exposure of igneous rocks to the Aves Ridge - granodiorites and tonalites dated at ~76 and ~59 Ma respectively (Wright & Wyld, 2011). The granodiorite is geochemically comparable to the Aves Ridge granitoids (Fig. 6.7), with similar Th/La, La/Yb and Nb/Yb ratios. Like the Aves Ridge, no CCOP mafic rocks are found on La Blanquilla. However, on Gran Roque of the Los Roques islands (Fig. 6.1), undated gabbros and dolerites of oceanic plateau affinity (likely the CCOP) are present (Giunta et al., 2002; A.C. Kerr, unpublished data). The mafic rocks are cut by quartz diorites, pegmatites and aplites with Ar-Ar biotite and hornblende ages of ~68 and ~59 Ma respectively (van der Lelij et al., 2010). Like La Blanquilla, the felsic rocks of Los Roques have almost identical trace element signatures to the granitoids of the Aves Ridge (Fig. 6.7) (data from Giunta et al., 2002; A.C. Kerr, unpublished data). All the Venezuelan Antilles arc rocks are considered to be formed by northwest or west-dipping subduction beneath the CCOP (Giunta et al., 2002; Wright & Wyld, 2011).

On Curaçao in the Dutch Antilles (Fig. 6.1), dykes of diorite and quartz diorite (~86 Ma; Wright & Wyld, 2011) intrude the CCOP-related Curaçao Lava Formation (~89 Ma; Sinton et al. 1998). These dykes also have very similar trace element signatures to the Aves Ridge granitoids (Fig. 6.7) (Wright & Wyld, 2011). Aruba, also part of the Dutch Antilles (Fig. 6.1), includes the mafic Aruba Lava Formation which is dated using the imprint of ammonite fossils to ~90 Ma (MacDonald, 1968), and is a part of the CCOP (White et al., 1999). The Aruba Lava Formation is cut by the dioritic to tonalitic Aruba Batholith, which has a weighted mean U-Pb zircon age of 88.6 ± 0.5 Ma (van der Lelij et al., 2010; Wright & Wyld 2011). White et al. (1999) showed that the batholith has low Nb, high Ba and Sr and flat to LREE-enriched REE patterns (Fig. 6.7). Although much more variable in major and trace element concentration, the Aruba batholith does resemble the Aves Ridge granitoids and is considered, like the Curaçao

dykes, to form by partial melting of CCOP crust during west-dipping subduction (White et al., 1999; van der Lelij et al., 2010; Wright & Wyld, 2011).

The only other mafic island arc rocks in Dutch-Venezuelan Antilles are found on Bonaire Island (Fig. 6.1) which have already been discussed in relation to the island arc rocks of Tobago (Thompson et al., 2004; Wright & Wyld, 2011). To re-iterate, poorly-studied mafic stocks of the Matijs Group intruded Aptian or older argillaceous rocks before deposition of a Coniacian conglomerate unit. The felsic volcanics, diorites and dacites of the Washikemba Group (Formation of Thompson et al., 2004) are ~96 Ma (Thompson et al., 2004; Wright & Wyld, 2010). These rocks were formed by subduction beneath a depleted mantle source (Thompson et al., 2004). There are no rocks of CCOP affinity or arc rocks derived from a plume-related mantle source on Bonaire.

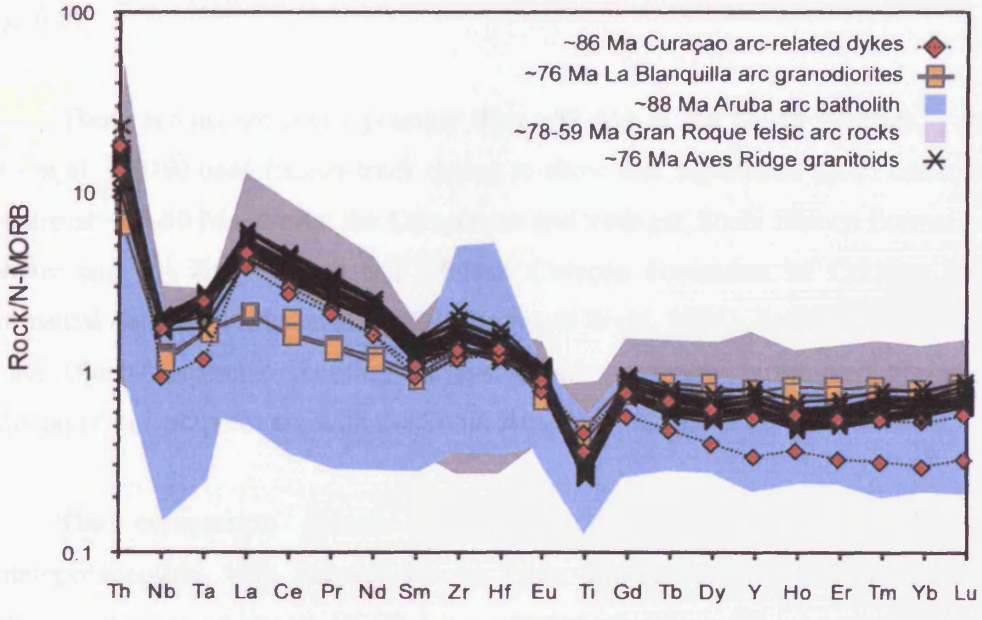

Figure 6.7. N-MORB-normalised trace element diagram comparing the characteristics of the Aves Ridge granitoids with subduction-related rocks of the Dutch and Venezuelan Antilles.

These results have profound implications for the tectonic evolution of the southern Caribbean (e.g. van der Lelij et al., 2010; Wright & Wyld, 2011). Because the CCOP rocks exposed on Aruba, Curaçao and Gran Roque show no sign of interaction with slab-fluids, Hastie & Kerr (2010) argue that there must have been no active subduction zone beneath this part of the CCOP during its formation. The island arc rocks of Bonaire form a parallel chain with the rocks of Aruba, Curaçao and Grand

Roque. As has been already discussed (Section 6.3.3), the ~96 Ma island arc rocks on Bonaire appear to represent E-dipping subduction in the region, or less likely, an allochthonous fragment of the SW-dipping Greater Antilles arc.

Following formation of the CCOP, arc-like rocks formed on Aruba and Curaçao within 1–3 Ma of plateau formation (Wright & Wyld, 2011). Studies of andesitic volcanoes using the U-Th decay series have shown that subduction-related fluids are generated and added to the mantle wedge just a few hundred ka before eruption (e.g. Turner et al., 2000). Partial melting to form the Aruba batholith and Curaçao dykes could therefore have occurred above a subduction zone that initiated along the edge of the CCOP (c.f., Niu et al., 2003; Stern, 2004; Wright & Wyld, 2011), most likely aided by collision of the CCOP with an east-dipping subduction zone shortly after its formation, triggering a rapid polarity reversal at ~89 Ma (van der Lelij et al., 2010) (Fig. 6.8).

There are no arc rocks younger than ~88 Ma in the Dutch Antilles. Van der Lelij et al. (2010) used fission track dating to show that significant uplift occurred on Bonaire at ~85-80 Ma, whilst the Campanian and younger Soebi Blanco Formation on Bonaire and the Knip Group and Midden Curaçao Formation of Curaçao contain continental detritus (Priem et al., 1986; Wright & Wyld, 2011). Subduction in this part of the Dutch-Venzuelan Antilles arc system was probably terminated abruptly by collision of the incipient arc with the South American margin (Fig. 6.8).

The comparison above shows that the Aves Ridge rocks formed contemporaneously with magmatism on Gran Roque and La Blanquilla. On La Blanquilla there is no known CCOP basement through which the arc rocks intruded, as may be the case for the Aves Ridge, because of the proximity of thin non-plateau-like crust in the SE corner of the Venezuelan Basin (see below). Therefore the subduction-related rocks of La Blanquilla appear to have formed in a similar setting to the Aves Ridge rocks and the island may indeed be a southerly extension of the Aves Ridge (Wright & Wyld, 2011). No subduction-related rocks have been found on the Aves Ridge or Venezuelan Antilles that are older or younger than ~76 Ma and ~59 Ma, respectively. It is possible that following cessation of magmatism on the Dutch Antilles

at ~88 Ma, subduction transferred eastwards to the Venezuelan Antilles and Aves Ridge, before stalling with inception of the Grenada Basin (Fig. 6.8).

Table 6.1. Summary of recent studies of igneous exposures from the Aves Ridge, Dutch-Venezuelan Antilles.

Location	Suite	Rock Types	Age(s) (Ma) *	Tectonic setting	References
SE Aves Ridge	n/a	Felsic intrusive	76 ± 1.4	Island arc	This thesis; Neill et al. (2011)
	n/a	Mafic extrusive and intrusive	n/a	Island arc (plume mantle source)	This theis; Neill et al. (2011)
La Blanquilla (Ven Antilles)	n/a	Felsic intrusive	75.5 ± 0.9	Island arc	Wright & Wyld (2011)
	n/a	Felsic intrusive	58.7 ± 0.5	Island arc	Wright & Wyld (2011)
Gran Roque (Ven Antilles)	n/a	Mafic intrusive	n/a	Oceanic plateau	Giunta *et al.* (2002); A.C. Kerr (*unpublished data*)
	n/a	Felsic intrusive	65.3 ± 1.4, 68.30 ± 0.76, 58.93 ± 1.22	Island arc	van der Lelij *et al.* (2010); Wright & Wyld (2011)
Curaçao (Dutch Antilles)	Lava Fm.	Mafic extrusive	88.9 ± 0.8	Oceanic plateau	Sinton *et al.* (1998)
	n/a	Intermediate intrusive	86.2 ± 1.1	Island arc	Wright & Wyld (2011)
Aruba (Dutch Antilles)	Lava Fm.	Mafic extrusive	Turonian (~90 Ma) †	Oceanic plateau	MacDonald (1968); White *et al.* (1999)
	Batholith	Mafic to felsic intrusive	88.6 ± 0.5‡	Island arc (plume mantle source)	van der Lelij *et al.* (2010); White *et al.* (1999); Wright & Wyld (2011)
Bonaire (Dutch Antilles)	Washikemba Group	Felsic extrusive, mafic intrusive	94.6 ± 1.4, 98.2 ± 0.6	Island arc (depleted mantle source)	Thompson *et al.* (2004); Wright & Wyld (2011)
	Matijs Group	Mafic intrusive	Albian (~112 Ma) §	Island arc	Wright & Wyld (2011)

* - Unmarked samples dated by U-Pb or Ar-Ar methods, see original references; † - Sample dated using ammonite imprints; ‡- Weighted mean of available ages; § - Relative dating from fieldwork

6.5.2. Petrogenesis of the Aves Ridge and La Blanquilla Island

The results presented above are consistent with a model in which the Aves Ridge and La Blanquilla were generated during west-dipping subduction beneath the CCOP between ~76 and ~59 Ma. However, as noted in Section 6.5.1, it appears that neither location is in immediate contact with the CCOP. Much of the Venezuelan Basin is made up of crust thickened by formation of the CCOP, reaching a maximum thickness of 20 km. However, in the far SE corner of the basin, some 40,000 km^2 of crust, minus sedimentary cover, is less than 5 km thick (Fig. 2.4) (Diebold et al., 1981). This thin crust is considered to pre-date the CCOP, based on interpretations of seismic patterns (Diebold et al., 1981; Mauffret & Leroy, 1997). Drilling has never been undertaken in this part of the Caribbean Sea. If this thin crust is not oceanic plateau material, then it is unlikely that the southern Aves Ridge was generated by subduction directly beneath the CCOP. Therefore, wedge convection is likely to have brought

plume mantle into the wedge above the Aves Ridge subduction zone. Also, there may be pre-existing plateau rocks or older arc fragments beneath the Aves Ridge, the former perhaps derived from the same plume that melted to form the CCOP, the latter perhaps related to the Greater Antilles arc system. Some authors have argued for the existence of an earlier Aptian-Albian phase of the CCOP which would lie to the east of the ~95-90 Ma rocks of the CCOP given eastward motion of the Farallon Plate (Mauffrey & Leroy, 1997), although there is no direct evidence for such an event.

The preferred petrogenetic model (Fig. 6.8) therefore shows the Aves Ridge arc overlying a plume-related mantle wedge and a subducting proto-Caribbean slab. The slab fluids ascend into the mantle wedge and promote partial melting to generate the Aves mafic lavas. The granitoids form by partial melting of tholeiitic amphibolite- and plagioclase-bearing rocks in the lower crust beneath the Aves Ridge arc. As mentioned above, it is likely that crustal partial melting was aided by the rise of hot mafic island arc magmas, perhaps even those which formed the mafic rocks in this study (Neill et al., 2011).

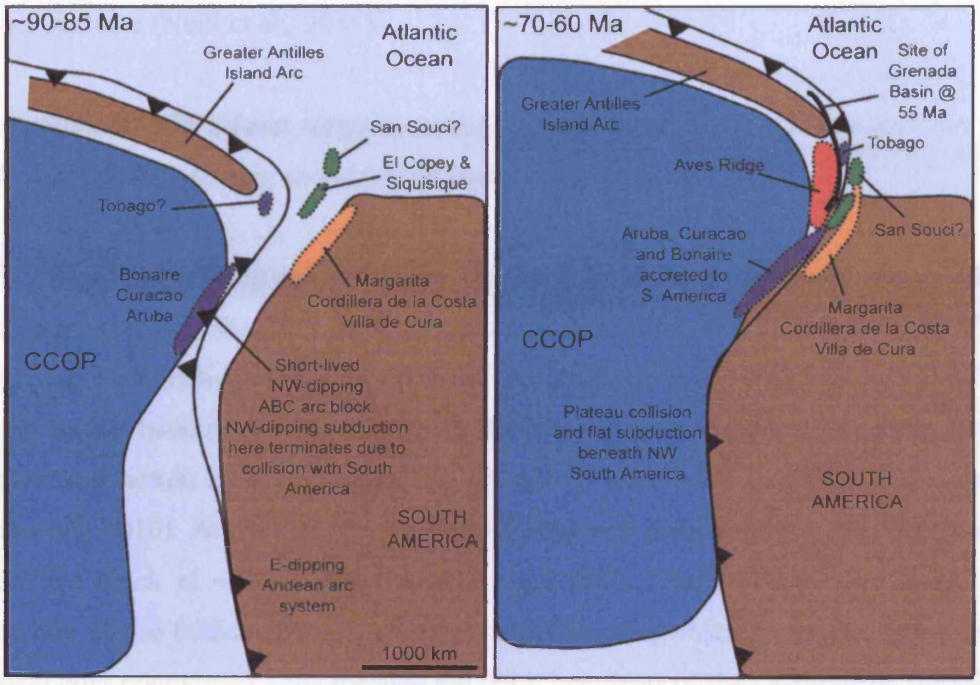

Figure 6.8. Speculative tectonic model for the evolution of the SE Caribbean, from ~90-60 Ma. Left: the reversal of subduction polarity in the Southern Caribbean has taken place following oceanic plateau collision. A short-lived NW-dipping arc system initiates beneath the CCOP. This arc system collides with NW S. America. Right: The Aves Ridge develops by W-dipping subduction close to the CCOP, effectively as part of the Greater Antilles island arc, trapping Tobago in the fore-arc. San Souci, El Copey, Siquisique, Margarita, the Cordillera de la Costa and the Villa de Cura in Venezuela are brought closer to the Greater Antilles during continued W-dipping proto-Caribbean subduction. Inception of the inter-arc Grenada Basin at ~55 Ma (Aitken et al. 2011), results in the splitting of the latter locations from the Aves Ridge and their diachronous accretion to South America as the Caribbean Plate moves eastwards.

It is unclear whether or not the crustal thickness of the Aves Ridge could be generated during a short ~20 Ma subduction history with a starting crustal thickness of just 5 km, the same as the thin crust of the SE Venezuelan Basin. Subduction rates, roll-back, sediment flux, slab dip and magma production vary from arc to arc hence it is difficult to quantify how quickly arc crust may be generated. The Lesser Antilles, which has a ~55 Ma history of ~2 cm/yr subduction, a similar rate to the Aves Ridge (Pindell & Kennan, 2009) has built up 30-35 km of crust (Christeson et al., 2008). It is possible that the 26 km-thick Aves crust was generated during its post-CCOP history, but, to repeat, the pre-existence of plateau-like crust or older island arc rocks should not be ruled out. It may be significant that the isotopic composition of the crustally-derived granitoid sample (Fig. 4.35) falls within the CCOP field and that this sample is

isotopically dissimilar to N-MORB or typical island arc rocks such as those of the Lesser Antilles (Neill et al., 2011).

6.5.3. Southern Caribbean tectonic model – relationship to the plateau-collision and ~135-125 Ma SW-dipping subduction initiation models

In Figure 6.8, a revised plate tectonic model is outlined for the southern Caribbean based on the findings from the Aves Ridge and a new consideration of the origins of the Dutch-Venezuelan Antilles (van der Lelij et al., 2010; Wright & Wyld, 2011). As has been previously discussed, Bonaire is shown as part of the northernmost Andean subduction zone with an E-dipping polarity at ~90 Ma (Section 6.3.3; van der Lelij et al., 2010). At ~95-90 Ma, the CCOP is formed and it collides with the Bonaire island arc block at ~90 Ma, triggering a rapid subduction polarity reversal and the formation of the felsic arc rocks of Aruba and Curaçao, which were intruded above a NW-dipping convergent zone through the thick basement of the CCOP (Fig. 6.8). This magmatism began at ~88 Ma and ended with collision of the Dutch Antilles arc with South America (RHS of Fig. 6.8). Between ~80 and 60 Ma, magmatism then moved eastward to the Venezuelan Antilles where the Gran Roque felsic rocks formed by crustal melting at ~68 to 59 Ma. Partial melting of plume mantle and lower crustal rocks contributed to formation of the subduction-related rocks of the Aves Ridge and La Blanquilla between ~76 and ~59 Ma, concurrent with continued W- and SW-dipping island arc magmatism in the Greater Antilles. Spreading in the Grenada Basin (Aitken et al., 2011) coincides with the cessation of magmatic activity on the Aves Ridge and Venezuelan Antilles.

6.6. Revision to models of Caribbean tectonic evolution

6.6.1. A summary of findings

In the first four sections of this chapter, the relationship between the study areas and nearby rocks of a similar age and composition was explored in order to better understand their petrogenesis and tectonic setting in relationship to Caribbean tectonic models. This discussion has shown that the origin and preservation of La Désirade is broadly consistent with either polarity reversal model for the Caribbean. The petrogenesis of the NCS of Tobago appears to be consistent with E-dipping subduction beneath an intra-oceanic portion of the Andean/Cordilleran subduction system. The amalgamation and deformation of the formations making up the NCS occurred in a dextral transform zone which may have formed due to the process of reversing Caribbean arc subduction polarity from E-dipping to SW-dipping at ~135-125 Ma. In contrast, the rocks studied from the Aves Ridge are argued to represent part of a much younger W- and NW-dipping island arc system (Dutch-Venezuelan Antilles-Aves Ridge) only partly related to the Greater Antilles arc. This arc system was generated following plateau-collision-induced polarity reversal on a mid-Cretaceous E-dipping subduction system (e.g. the island arc rocks of Bonaire). If the Greater Antilles Arc was formed by SW-dipping subduction from ~135-125 Ma to the Tertiary, then the rocks of Bonaire had to have formed on a separate E-dipping system which is likely to have been the northernmost portion of the Andean arc system which maintained an E-dipping subduction component throughout Caribbean tectonic history.

Therefore, the most important conclusion of this thesis is thus: if the bulk of the Greater Antilles island arc formed by SW-dipping subduction processes, then the evolution of the Caribbean Plate was dependent upon the formation of not one 'Great Arc' system with a polarity reversal during its history, but two. To re-iterate, the first would have been the E-dipping Triassic-Early Cretaceous Andean/Cordilleran subduction zone superseded by the SW-dipping Lower Cretaceous-Palaeogene Greater Antilles Arc (Fig. 6.3), and the second was the E-dipping Late Cretaceous northernmost portion of the Andean subduction zone superseded by a short phase of W- and NW-dipping Late Cretaceous subduction beneath the Dutch Antilles-Venezuelan Antilles-Aves island arc system (Figs. 6.4; 6.8).

Finally, it appears that the accreted material found at San Souci, El Copey and Siquisique were formed by melts derived from a mantle plume unrelated to the Galapagos plume head. These melts were erupted onto continent-derived turbidite sequences which lay to the E of the Greater Antilles arc and NW of South America within the proto-Caribbean seaway (Fig. 6.6).

6.6.2. Problems with the model for inception of SW-dipping subduction in the Greater Antilles at ~135-125 Ma

Cause of inception of SW-dipping subduction: The cause of inception of SW-dipping Antillean subduction, according to Pindell et al. (2005, 2006, 2011) and Pindell & Kennan (2009), was a westward acceleration of North America over the mantle compared to South America, which began at approximately 135 Ma (Pindell et al., 1988). These authors couple the acceleration with compression in the North American Cordillera and rifting of the Andean/Cordilleran arc system during the continued widening of the proto-Caribbean seaway, the latter resulting in the formation of a compressional intra-oceanic transform fault zone by ~135-125 Ma. The transform zone would then founder to generate a new SW-dipping subduction zone from which the Greater Antilles arc would originate.

One problem with this model is that the proto-Caribbean crust that would form the new subducting slab would be 0-35 Ma old at the proposed time of subduction initiation (Pindell & Kennan, 2009). The Farallon crust has not been conclusively dated, but is widely assumed to be at least of Jurassic to Late Triassic age (e.g. Baumgartner et al., 2008) and would therefore be tens of millions of years older than the proto-Caribbean crust. Models of spontaneous subduction initiation (Stern, 2004) indicate that without any other plate-tectonic drivers, the older plate will always be subducted beneath the younger, hotter, more buoyant plate. Furthermore, the proto-Caribbean plate would be coupled to the buoyant continental crust of North and South America. There is therefore no obvious reason why the proto-Caribbean crust should subduct in preference to the Farallon crust. It is possible that an E-dipping Andean/Cordilleran arc would become impossibly curved because of the relative motion of North America, meaning that the inception of SW-dipping subduction could

become geodynamically inevitable. Also, the directed pressure on the Andean/Cordilleran arc derived from the westward motion of North America could result in the down-bending of the proto-Caribbean crust beneath the arc, because, although younger and hotter, the proto-Caribbean lithosphere would be thinner and more ductile, and therefore more able to subduct, than the Farallon lithosphere.

Implications for the geochemistry of the CCOP: The recent models presented by Pindell et al. (2005, 2006, 2011) and Pindell & Kennan (2009) all state, implicitly or explicitly, that the CCOP was formed above a proto-Caribbean slab gap formed by the subduction of the proto-Caribbean spreading ridge; and that broadly speaking, the eastern edge of the CCOP was erupted in the back-arc region of the SW-dipping Greater Antilles subduction system. Workers such as Hastie & Kerr (2010) argue that there is no hint of a subduction-related geochemical signature in the rocks of the CCOP. CCOP rocks preserved within the present-day Caribbean region have all been shown to be derived from the melting of anhydrous peridotite without any subduction-related geochemical signatures such as those listed in Section 5.1 (Kerr et al., 2003; 2004; Kerr & Mahoney, 2007; Hastie et al., 2008; Kerr et al., 2009a; Hastie & Kerr, 2010). Nevertheless, if SW-dipping subduction initiated in the Greater Antilles at ~135-125 Ma, then it is surprising that no subduction-influenced geochemical signatures have been found in the CCOP.

These considerations indicate a serious geochemical problem for the ~135-125 Ma SW-dipping subduction initiation model of the Caribbean. This lack of subduction-related geochemistry in studied parts of the CCOP must be overcome before the model, which is based largely on the nature and timing of island arc magmatism and HPLT metamorphism in the Greater Antilles (Pindell & Kennan, 2009; Pindell et al., 2011), can gain widespread acceptance. Nevertheless, a large bulk of literature on the Greater Antilles finds support for, or is based on, the ~135-125 Ma SW-dipping subduction initiation hypothesis (e.g. Escuder Viruete et al., 2006, 2008, 2010; García-Casco et al., 2008; Jolly et al., 2008; Krebs et al., 2008). The record of SW-dipping subduction that these authors depict cannot be ignored or dismissed by those who believe that collision of the CCOP with an E-dipping island arc system can explain much of Caribbean tectonic evolution. The opinion expressed in this thesis (see Section 6.6.1) is that there were at least two separate island arc systems co-existing in the wider Caribbean region

during the Late Cretaceous when the CCOP was formed; and that the hitherto geochemically-studied CCOP locations were not derived from mantle that was close enough to the subducting proto-Caribbean slab to receive a significant slab-fluid component (see Pearce & Stern, 2006). It may be significant however, that there are no studies of CCOP rocks from the NE of the Venezuelan Basin which probably lay closest to the Greater Antilles arc during the late Cretaceous.

6.6.3. Late Jurassic to Early Cretaceous Caribbean tectonic history

Rifting apart of the Americas led to the generation of oceanic crust in the Gulf of Mexico, proto-Caribbean, and Colombian Marginal seaways from 160 Ma (Pindell & Kennan, 2009). The western seaboard of the Americas had been the site of E-dipping Andean/Cordilleran subduction since the Triassic (Dickinson & Lawton, 2001). As the Americas drifted apart during the Late Jurassic, subduction continued beneath SW North America, generating the rocks now preserved in Siuna, Santa Elena and Guatemalan fore-arc (Baumgartner et al., 2008). In the back-arc region to the expanding Andean/Cordilleran system, possibly at a Colombian Marginal seaway spreading centre, the basement of La Désirade was formed at 150-143 Ma (Pindell & Kennan, 2009; Neill et al., 2010). At ~143-130 Ma, the last island arc rocks were formed above an E-dipping Andean/Cordilleran subduction zone compatible with both models of Caribbean tectonics discussed in this thesis. These rocks are now found in the Devils Racecourse Formation of Jamaica, the Mabujina Complex of Cuba, the Bermeja complex of Puerto Rico, and, towards the S of the Caribbean region, the North Coast Schist of Tobago. See Figure 6.2 for a summary.

At this point in Caribbean tectonic history, the two models for the geological evolution of the region diverge. In the plateau-collision model, E-dipping Andean/Cordilleran subduction continues until ~90 Ma when collision of the CCOP with the island arc system results in a subduction polarity reversal. As described above, the single biggest concern with the plateau-collision model relating to rocks studied in this thesis, is the lack of a clear explanation for the igneous, structural and metamorphic history of the rocks of Tobago, which appear to be best explained by the ~135-125 Ma SW-dipping subduction initiation model. In the ~135-125 Ma SW-dipping subduction initiation model, the rocks of the NCS were generated above an E-dipping subduction

zone, metamorphosed, and then translated by dextral wrench shear (Snoke et al., 2001a) towards the NE into the southern portion of the Greater Antilles island arc (e.g. Pindell et al., 2011) where the rocks of the TVG and TPS would be formed above a SW-dipping subduction zone at ~112-106 Ma. See Figure 6.3 for a summary.

6.6.4. Late Early to Late Cretaceous Caribbean tectonics in the ~135-125 Ma SW-dipping subduction initiation model: two co-existing arcs of opposing polarity?

In the ~135-125 Ma SW-dipping subduction initiation model, from ~125 Ma onwards, the Greater Antilles arc built up on Cuba, Hispaniola, Jamaica, Puerto Rico, the U.S. Virgin Islands and Tobago. In some cases, such as Tobago, island arc rocks which were part of the older extinct Andean/Cordilleran system (NCS) were intruded by younger island arc rocks of Greater Antillean affinity (VPS). Intriguingly, in other locations such as La Désirade, the old pre-Greater Antilles basement was not later intruded, suggesting that these rocks may have been translated to a non-magmatic part of the Greater Antilles arc following subduction polarity reversal.

Some time after polarity reversal, at <130 Ma, the HPLT metamorphic belts and rare island arc rocks now preserved on Margarita Island, the Cordillera de la Costa and the Villa de Cura in Venezuela were formed although the polarity of subduction and relationship of these rocks to the processes ongoing in the Greater Antilles arc are uncertain. Meantime, the continuation of the E-dipping Andean subduction regime offshore from western S. America gave the island arc environment in which the rocks of the Matjis and Washikemba Groups of Bonaire may have been generated at ~112-94 Ma (Thompson et al., 2004; Wright & Wyld, 2011). See Figure 6.4 for a summary.

6.6.5. The SE Caribbean at ~90-55 Ma: The CCOP, Dutch-Venezuelan Antilles, Aves Ridge and opening of the Grenada Basin

Magmatism related to the building of the CCOP took place primarily at ~95-90 Ma (Kerr et al., 2003) and was located to the SW of the Greater Antilles arc and the W of the E-dipping Andean subduction zone. The plateau collided with the Andean arc, clogging the trench and forcing a subduction polarity reversal at ~90 Ma (van der Lelij et al., 2010). Re-melting of plateau material in a new environment of NW-dipping

subduction (still to the SW of the Greater Antilles arc) then formed the Aruba batholith at ~89-86 Ma (White et al., 1999; van der Lelij et al., 2010). On the islands of Aruba and Bonaire, there is a thermo-chronological record of uplift at ~90-85 Ma concurrent with the final docking of the plateau to the island arc system (van der Lelij et al., 2010). Following the subduction polarity reversal, NW-dipping subduction of oceanic crust between the arc and S. America led to the diachronous suturing of the Dutch-Venezuelan Antilles to S. America, W to E, from ~75-50 Ma (van der Lelij et al., 2010). Concurrent with the suturing was the generation of island arc rocks further north on the Aves Ridge and La Blanquilla, which formed by the partial melting of the existing crust and of the plume-related mantle wedge to the W of the arc (Neill et al., 2011; Wright & Wyld, 2011).

At ~60-50 Ma, rapid roll-back of the subducting proto-Caribbean plate took place, forming the Grenada Basin, and moving the subduction-related rocks of Tobago, Margarita, the Cordillera de la Costa and the Villa de Cura SE from their location close to the Aves Ridge, and establishing the presently active Lesser Antilles arc (Aitken et al., 2011). Accretion and eastwards translation of the allochthonous Caribbean units took place with respect to S. America (e.g. Speed, 1985; Robertson & Burke, 1989; Russo & Speed, 1992); and this process also resulted in the capture and accretion of fragments of the pre-existing proto-Caribbean seaway – e.g. the Jurassic Tinaquillo lherzolite of Venezuela (Choi et al., 2007), and the ~90 Ma plume-related rocks of San Souci, El Copey and Siquisique (Wadge & Macdonald, 1985; Kerr et al., 2009b; this study). See Figure 6.8 for a summary.

CHAPTER SEVEN: CONCLUDING REMARKS AND IDEAS FOR FURTHER RESEARCH

Conclusions from the geological research of the four chosen locations; comments on the future direction of research

7.1. Conclusions of this study

In this study the igneous petrogenesis of four SE Caribbean localities, ranging in age from the Late Jurassic to the Late Cretaceous, was re-evaluated using U-Pb geochronology, major and trace element and radiogenic isotope data. The new data and previous studies were used to place constraints on, and discuss the merits of, two subduction polarity reversal models used to explain the eastward migration of the Pacific-derived Caribbean Plate. One model invokes reversal following collision of the Caribbean Colombian Oceanic Plateau with a W-facing Andean/Cordilleran subduction zone at ~90 Ma. The second argues that an intra-oceanic transform zone rifted the Andean/Cordilleran arc between ~135-125 Ma. This transform zone would founder to form a long-lived SW-dipping Greater Antilles subduction zone with no significant role for the CCOP in its evolution.

On La Désirade Island (Guadeloupe), the ~150-143 Ma basement to the northern Lesser Antilles arc is exposed. A suite of pillow basalts, overlain by felsic volcanic rocks and intruded by a trondhjemite pluton and intermediate dykes, were generated in the back-arc region of an Andean/Cordilleran subduction zone, mostly likely in the Colombian Marginal seaway. The subduction polarity reversal event occurred somewhere to the east of the Colombian Marginal seaway in order to ensure its preservation in the central Caribbean today. The origin and preservation of these rocks have little bearing at present on subduction polarity reversal models as the location and longevity of the spreading ridge within the Colombian Marginal seaway is unknown.

Tobago has a multi-stage geological history. The North Coast Schist (~130 Ma) consists of an assemblage of mafic and felsic meta-tuffs and lavas amalgamated and deformed by dextral wrench shearing before the intrusion and eruption of younger rocks. The NCS protoliths were mostly subduction-related although some MORB-like mafic rocks are present. The MORB-like rocks have not been described geochemically before as they were assumed to be part of an amphibolite-facies aureole next to the younger rocks (Snoke et al., 2001a). A variety of mantle sources – depleted and HFSE-enriched, the latter characterised by unusually high Hf isotope ratios – are found in the different formations. These rocks are interpreted to be slivers of arc material formed by

the partial melting of different mantle- and slab-related sources possibly including South American sub-continental lithospheric mantle. In the two models of Caribbean plate evolution that have been discussed, the NCS protoliths could have formed above an E-dipping subduction zone. It is suggested in the ~135-125 Ma SW-dipping subduction initiation model that these rocks were wrenched in a series of dextral transform zones into the axis of the Greater Antilles arc, and suffered greenschist-facies metamorphism, before the formation of the younger rocks. The younger, mostly mafic rocks of Tobago (~112-91 Ma) include the Tobago Volcanic Group, Plutonic Suite, a dyke swarm, a dyke-like tonalite body and rare Nb-enriched rocks. The Volcanic Group and Pluton are interpreted to have formed by subduction beneath the Greater Antilles arc, with a depleted mantle wedge source and slab-flux derived in part from small proportions of terrigenous and pelagic sediments. The slightly younger tonalite and Nb-enriched rocks may have formed during partial melting of the southern edge of the proto-Caribbean slab and by ingress of an enriched mantle source, respectively, in the ~135-125 Ma SW-dipping subduction initiation model. Thereafter, mafic dyke emplacement continued, probably during island arc rifting, with an increasingly depleted mantle wedge source.

In Trinidad, the San Souci Volcanic Formation is assumed to be ~90 Ma, but U-Pb zircon age results were not available during the time of thesis submission. The formation cuts passive margin turbidites which detrital zircon and zircon fission track dating indicates lay between the NW coast of South America and the Caribbean island arc system. Other rocks in Venezuela have a similar origin and are likely to represent a suite formed between the Great Arc system of the Caribbean Plate and the South American continent. Geochemically these mostly mafic rocks appear to be of oceanic plateau origin, formed by moderate degrees of partial melting (~25 %). Isotope ratios and the western proto-Caribbean location of origin suggest that San Souci, and its related Venezuelan outcrops at El Copey and Siquisique, are not related to the Galapagos plume head and may be part of a separate proto-Caribbean plateau. There is no subduction-related component in these rocks which suggests that at there was no E-dipping subduction zone close to this part of the Caribbean. The lack of a subduction-related component lends some support to the ~135-125 Ma SW-dipping subduction initiation model of the Caribbean. However, the exact distance at which these plateau

outcrops were erupted from the Caribbean arc systems is unknown so the impact of the origin of these rocks on Caribbean tectonic models is difficult to assess.

Dredge hauls from the SE Aves Ridge contain calc-alkaline mafic and felsic island arc rocks. The mafic rocks contain a plume-related mantle wedge component and an oxidised pelagic sediment slab component, indicative of W-dipping subduction beneath the CCOP. The thermo-chronology of the Dutch and Venezuelan Antilles demonstrate that arc magmatism followed collision of the CCOP with a pre-existing island arc. If the long-lived SW-dipping subduction model of the Greater Antilles arc is correct, then the arc with which the CCOP collided lay above an E-dipping subduction zone which was situated offshore from western South America, to the SW of the Greater Antilles arc.

There are, to summarise, two main conclusion of this thesis. The first is that the Andean/Cordilleran E-dipping subduction zone in the Caribbean region *could* have been superseded during a polarity reversal event with a SW-dipping subduction zone (Greater Antilles arc) during the Lower, not Upper, Cretaceous, at ~135-125 Ma. The second main conclusion is that, if long-lived SW-dipping subduction in the Greater Antilles is correct, the history of the Caribbean Plate cannot be explained by the evolution of a single 'Great Arc of the Caribbean'. A SW-dipping Greater Antilles Arc system and an E-dipping subduction zone off the western coast NW South America may have co-existed at the end of the Lower Cretaceous (?-~90 Ma). Plateau collision with that E-dipping subduction system at ~90 Ma caused a second Caribbean polarity reversal event in the Upper Cretaceous, forming a new NW-dipping subduction zone coupled to the Greater Antilles to the NE, incorporating the rocks of the Dutch-Venezuelan Antilles and Aves Ridge as an integral part of the Caribbean Plate. This new, short-lived NW- and W-dipping arc system (~90-59 Ma), along with a fragment of NW S. America including accreted portions of the Greater Antilles system (Tobago, Margarita, Cordillera de la Costa, Villa de Cura), were dragged eastwards with the Caribbean Plate and accreted to northern S. America during the Tertiary.

7.2. Scope for further research

7.2.1. Future field and lab studies of Caribbean geology

Doubtless, studies will continue into the geodynamic, petrological, geochemical and metamorphic evolution of the Caribbean, not least because so many island arc and oceanic plateau rocks are uniquely exposed on land. These further studies will be in spite of significant Cenozoic tectonic activity, widely fragmented outcrop geology and the non-exposure of many rocks, particularly of the CCOP, beneath the Caribbean Sea. The high-resolution geochemical studies in this thesis have revealed significant new information about the tectonic evolution of the Caribbean Plate (e.g. Neill et al., 2010, 2011), following on from similar studies on Jamaica and the Dutch Antilles (e.g. White et al., 1999; Thompson et al., 2004; Hastie et al., 2008, 2009, 2010a,b,c). There are a number of locations in the Caribbean where such detailed work is yet to be undertaken, which could offer new insights and verification, or refutation, of tectonic models. For example, the Bermeja complex of Puerto Rico and the La Rinconada Group of Margarita Island, Venezuela are potential candidates for proto-Caribbean or eastern Pacific crust that remain to be studied in any significant detail. Their geochemical characteristics would help to understand the type of mantle sources present in the region prior to the formation of the Caribbean arc systems. It would be useful to know the detailed trace element and isotope geochemistry and protolith age(s) of the arc-related rocks of the Villa de Cura nappe in Venezuela; to compare with those of the Greater Antilles and Tobago. Likewise many island arc rocks of the Greater Antilles are only sparsely sampled and analysed in any detail. As has been made clear in this thesis, the Aves Ridge and the thin crust of the SE Venezuelan Basin are under-sampled and may yet reveal a more complex origin than that proposed here. However, drilling of the ridge and thin crust may be necessary and is unlikely to be undertaken given the present economic situation.

The Hf isotope study of this thesis has revealed the first evidence for an isotopically decoupled mantle component (the Dupal anomaly of Hart, 1984) in the Caribbean region. If this component is reflective of the composition of some of the proto-Caribbean (?) mantle sources then Hf isotopes could prove a very useful discriminatory tool in determining Pacific vs. proto-Caribbean mantle sources,

particularly for the Early Cretaceous rocks of the Caribbean region. As noted, only the Washikemba Group (Bonaire), the Devil's Racecourse Formation (Jamaica) and Tobago contain island arc rocks of Lower to Middle Cretaceous age for which there is Hf isotope data. A wider Hf isotope study of the allochthonous Caribbean arc units and slices of Pacific and proto-Caribbean oceanic crust should definitely be a future research topic, coupled with more detailed high-resolution trace element analyses.

7.2.2. Seismic tomography and plate motion histories

Finally, a recent innovation in geology is the refined use of high resolution seismic tomography to constrain the position of subducted slabs within the earth's mantle, assuming their near-vertical descent following slab breakoff (e.g., van der Meer et al., 2008). With respect to the Caribbean region, it has been interpreted that remnants of the Farallon, Atlantic and Greater Antilles arc (proto-Caribbean) slabs lie in the mantle beneath the Caribbean and present-day South America (van der Meer et al., 2010). However, the resolution is necessarily poor as often the models are run on a global scale. Furthermore, the implications of these findings for regional tectonic evolution are yet to be fully analysed for the Caribbean. Nevertheless, the ability to potentially trace slabs into the mantle may help assess the validity of interpretations of geological history and subduction polarity in complex regions such as the Caribbean which have a history of dispute and contentious subduction polarities through time (e.g. Hastie & Kerr, 2010 vs. Pindell et al., 2011).

REFERENCES CITED

Abbott, R.N., Draper, G. & Keshav, S. 2005. UHP magma paragenesis, garnet peridotite and garnet clinopyroxenite: An example from the Dominican Republic. *International Geology Review* **47**, 233-247.

Aguillón-Robles, A., Calmus, T., Benoit, M., Bellon, H., Maury, R.C., Cotten, J., Bourgois, J. & Michaud, F. 2001. Late Miocene adakites and Nb-enriched basalts from Vizcaino Peninsula, Mexico: indicators of East Pacific Rise subduction beneath southern Baja California? *Geology* **29**, 531-534.

Aitken, B.G., & Etcheverría, L.M. 1984. Petrology and geochemistry of komatiites and tholeiites from Gorgona Island, Colombia. *Contributions to Mineralogy and Petrology* **89**, 94-105.

Aitken, T., Mann, P., Escalona, A. & Christeson, G.L. 2011. Evolution of the Grenada and Tobago Basins and implications for arc migration. *Marine and Petroleum Geology*, **28**, 235-258.

Algar, S.T. & Pindell, J.L. 1991. Structural development of the Northern Range of Trinidad, and implications for the tectonic development of the southeastern Caribbean. In: Gillezeau, K.A. (Ed) *Transactions of the Second Geological Conference of the Geological Society of Trinidad and Tobago*, Pointe-a-Pierre, Trinidad, 6-22.

Algar, S.T. 1993. Structural, stratigraphic and thermo-chronological evolution of Trinidad. PhD Thesis, Dartmouth College, Hanover, New Hampshire, unpublished.

Algar, S.T. & Pindell, J.L. 1993. Structure and deformation history of the Northern Range of Trinidad and adjacent areas. *Tectonics* **12**, 814-829.

Algar, S.T., Heady, E.C. & Pindell, J.L. 1998. Fission track dating in Trinidad: Implications for provenance, depositional timing and tectonic uplift. In: Pindell, J.L. & Drake, C.L. (Eds) *Palaeogeographic Evolution and Non-glacial Eustacy, Northern South America.* SEPM Special Publication **58**, 111-128.

Alvarado, G.E., Denyer, P & Sinton, C.W. 1997. The 89 Ma Tortugal komatiitic suite, Costa Rica: Implications for a common geological origin of the Caribbean and eastern Pacific region from a mantle plume. *Geology* **25**, 439-442.

Apted, M.J. & Liou, J.G. 1983. Phase relations among greenschist, epidote-amphibolite and amphibolite in a basaltic system. *American Journal of Science* **283**, 328-354.

Auzende, J., Pelletier, B. & Eissen, J. 1995. The North Fiji Basin: geology, structure and geodynamic evolution. In: Taylor, B. (Ed) *Back-arc basins: tectonics and magmatism.* Plenum, New York, 139-175.

Avé Lallemant, H.G. & Sisson, V.B. 2005. Exhumation of eclogites and blueschists in northern Venezuela: Constraints from kinematic analysis of deformation structures. In: Avé Lallemant, H.G. & Sisson, V.B. (Eds) *Caribbean-South American plate interactions, Venezuela.* Geological Society of America Special Papers **394**, 193-206.

Barr, K.W. 1963. Geology of the Toco district, Trinidad, West Indies, Pt.1. *Overseas Geology and Mineral Resources* **9**, 1-29.

Barrett, S.F. 1986. Paleoecology and stratigraphy of Devonian sediments in the northern Andes, Columbia: Paleogeographic implications. *PhD Thesis, University of Chicago, Chicago, 329 pages.*

Bartok, P.E., Renz, O. & Westermann, J.E.G. 1985. The Siquisique ophiolites, northern Lara State, Venezuela: A discussion on their Middle Jurassic ammonites and tectonic implications. *Bulletin of the Geological Society of America* **96**, 1050-1055.

Baumgartner, P.O. 1984. A Middle Jurassic-Early Cretaceous low latitude radiolarian zonation based on unitary association and age of Tethyan radiolarites. *Eclogae Geologicae Helvetiae* **77**, 729-837.

Baumgartner, P.O. & Denyer, P. 2006. Evidence for middle Cretaceous accretion at Santa Elena Peninsula (Santa Rosa Accretionary Complex), Costa Rica. *Geologica Acta* **4**, 179-191.

Baumgartner, P.O., Flores, K., Bandini, A.N., Girault, F. & Cruz, D. 2008. Upper Triassic to Cretaceous Radiolaria from Nicaragua and northern Costa Rica – the Mesquito Composite Oceanic Terrane. *Ofioliti* **33**, 1-19.

Baumgartner-Mora, C., Gauchat, K. & Baumgartner, P.O. 2004. Larger Foraminifera (Nummulitinae, Archaiasinids) in the Neogene shallow water limestone of the Désirade island, Guadeloupe (French Antilles). *Abstracts of the Second Swiss Geoscience Meeting*, Lausanne, 19th-20th November, 2004.

Beard, J.S. & Day, H.W. 1988. Origin of gabbro pegmatite in the Smartville intrusive complex, northern Sierra Nevada, California. *American Mineralogist* **71**, 1085-1099.

Beck, M.E., Jr. 1983. On the mechanism of tectonic transport in zones of oblique subduction. *Tectonophysics* **93**, 1-11.

Bird, D.E., Hall, S.A., Casey, J.F. & Millegan, P.S. 1999. Tectonic evolution of the Grenada Basin. *In:* Mann, P. (ed) *Caribbean Basins.* Elsevier Science, Amsterdam, Sedimentary Basins of the World, **4**, 389-416.

Black, L.P., Kamo, S.L., Allen, C.M., Aleinikoff, J.N., Davis, D.W., Korsch, R.J. & Foudoulis, C. 2003. TEMORA 1: a new zircon standard for U-Pb geochronology. *Chemical Geology* **200**, 155-170.

Blein, O., Guillot, S., Lapierre, H., Mercier de Lépinay, B., Lardeaux, J.-M., Millan Trujillo, G., Campos, M. & Garcia, A. 2003. Geochemistry of the Mabujina complex, central Cuba: Implications on the Cuban Cretaceous arc rocks. *Journal of Geology* **111**, 89-110.

Blichert-Toft, J. & Albarede, F. 1997. The Lu-Hf geochemistry of chondrites and the evolution of the mantle-crust system. *Earth and Planetary Science Letters* **148**, 243-258.

Blichert-Toft, J. 2001. On the Lu-Hf isotope geochemistry of silicate rocks. *Geostandards Newsletters – the Journal of Geostandards and Geoanalysis* **25**, 41-56.

Bouysse, P., Schmidt-Effing, R. & Westercamp, D. 1983. La Désirade Island (Lesser Antilles) revisited: Lower Cretaceous radiolarian cherts and arguments against an ophiolitic origin for the basal complex. *Geology* **11**, 244-247.

Bouysse, P. 1984. The Lesser Antilles island arc: structure and geodynamic evolution. *Initial Reports of the Deep Sea Drilling Project* **78A**, 83-103.

Brun, J.-P. & Faccenna, C. 2008. Exhumation of high-pressure rocks driven by slab rollback. *Earth and Planetary Science Letters* **272**, 1-7.

Burke, K., Coates, A.G. & Robinson, E. 1969. Geology of the Benbow Inlier and surrounding areas, Jamaica. In: Saunders, J.B. (Ed.) *Transactions of the Fourth Caribbean Geological Conference*, 229-307.

Burke, K., Fox, P.J. & Sengor, A.M.C. 1978. Buoyant ocean floor and the evolution of the Caribbean. *Journal of Geophysical Research* **83**, 3949-3954.

Burke, K. 1988. Tectonic evolution of the Caribbean. *Annual Reviews of Earth and Planetary Science* **16**, 201-230.

Campbell, I.H. 2007. Testing the plume theory. *Chemical Geology* **241**, 153-176.

Campbell, I.H. & Griffiths, R.W. 1990. Implications of mantle plume structure for the evolution of flood basalts. *Earth and Planetary Science Letters* **99**, 79-93.

Cann, J.R. 1970. Rb, Sr, Zr and Nb in some ocean floor basaltic rocks. *Earth and Planetary Science Letters* **10**, 7-11.

Carney, J.N. & Macfarlane, A. 1982. Geological evidence bearing on the Miocene to recent structural evolution of the New Hebridies arc. *Tectonophysics* **87**, 147-175.

Carpentier, M., Chauvel, C., Maury, R.C. & Matielli, N. 2009. The "zircon effect" as recorded by the chemical and Hf isotopic compositions of Lesser Antilles forearc sediments. *Earth and Planetary Science Letters* **287**, 86-99.

Case, J.E., Macdonald, W.D. & Fox, P.J. 1990. Caribbean crustal provinces: seismic and gravity evidence. In: Dengo, G. & Case, J.E. (Eds) *The Caribbean Region.* The geology of North America, Geological Society of America, Boulder, Colorado **H**, 15-36.

Castillo, P.R., Solidum, R.U. & Punongbayan, R.S. 2002. Origin of high field strength element enrichment in the Sulu Arc, southern Philippines, revisited. *Geology* **30**, 707-710.

Castillo, P.R., Rigby, S.J. & Solidum, R.U. 2007. Origin of high field strength element enrichment in volcanic arcs: Geochemical evidence from the Sulu Arc, southern Philippines. *Lithos* **97**, 271-288.

Castillo, P.R. 2008. Origin of the adakite-high-Nb basalt association and its implications for postsubduction magmatism in Baja California, Mexico. *Bulletin of the Geological Society of America* **120**, 451-462.

Cerveny, P.F. & Snoke, A.W. 1993. Thermochronological data from Tobago, West Indies: Constraints on the cooling and accretion history of Mesozoic oceanic-arc rocks in the Southern Caribbean. *Tectonics* **12**, 433-440.

Chauvel, C. & Blichert-Toft, J. 2001. A hafnium isotope and trace element perspective on melting of the depleted mantle. *Earth and Planetary Science Letters* **190**, 137-151.

Choi, S.H., Mukasa, S.B., Andronikov, A.V. & Marcano, M.C. 2007. Extreme Sr-Nd-Pb-Hf isotopic compositions exhibited by the Tinaquillo peridotite massif, Northern Venezuela: implications for geodynamic setting. *Contributions to Mineralogy and Petrology* **153**, 443-463.

Christeson, G.L., Mann, P., Escalona, A. & Aitken, T.J. 2008. Crustal structure of the Caribbean-northeastern South America arc-continent collision zone. *Journal of Geophysical Research* **113**, B08104, doi:10.1029/2007JB005373.

Church, R.E. & Allison, K.R. 2004. The petroleum potential of the Saba Bank area, Netherlands Antilles. *Search and Discovery Article* 10076, 58 pp.

Clarke, T.F., Korgen, B.J. & Best, D.M. 1978. Heat flow in the eastern Caribbean. *Journal of Geophysical Research* **83**, 5883-5891.

Clemens, J.D., Yearron, L.M., Stevens, G. 2006. Barberton (South Africa) TTG magmas: geochemical and experimental constraints on source-rock petrology, pressure of formation and tectonic setting. *Precambrian Research* **151**, 53-78.

Coffin, M.F. & Eldholm, O. 1994. Large igneous provinces: crustal structure, dimensions, and external consequences. *Reviews of Geophysics* **32**, 1-36.

Condie, K.C. 2005. TTGs and adakites: are they both slab melts? *Lithos* **80**, 33-44.

Cooper, P.A. & Taylor, B. 1985. Polarity reversal in the Solomon Islands arc. *Nature* **314**, 428-430.

Cordey, F. & Cornée, J.J. 2009. New radiolarian assemblages from La Désirade Island basement complex (Guadeloupe, Lesser Antilles arc) and Caribbean tectonic implications. *Bulletin of the Geological Society of France* **180**, 399-409.

Corfu, F. & Noble, S.R. 1992. Genesis of the southern Abitibi greenstone belt, Superior Province, Canada: evidence from zircon Hf isotopic analyses using a single filament technique. *Geochimica et Cosmochimica Acta* **56**, 2081-2097.

Crowley, J.L., Schoene, B. & Bowring, S.A. 2007. U-Pb dating of zircon in the Bishop tuff at the millennial scale. *Geology* **35**, 1123-1126.

Cunningham-Craig, E.H. 1907. Preliminary report by the government geologist on the island of Tobago. *Trinidad Council Paper* **9**.

Dalziel, I.W.D. 1985. Collision and cordilleran orogenesis: an Andean perspective. In: Coward, M.P., Ries, A.C. (Eds.) *Collision Tectonics.* Geological Society of London Special Publication **19**, 389-404.

Defant, M.J. & Drummond, M.S. 1990. Derivation of some modern arc magmas by melting of young subducted lithosphere. *Nature* **347**, 662-665.

Defant, M.J., Jackson, T.E., Drummond, M.S., De Boer, J.Z., Bellon, H., Feigenson, M.D., Maury, R.C. & Stewart, R.H. 1992. The geochemistry of young volcanism throughout western Panama and southeastern Costa Rica: an overview. *Journal of the Geological Society* **149**, 569-579.

de Laeter, J.R., Bohlke, J.K, de Bievre, P., Hikada, H., Peiser, H.S., Rosman, K.J.R. & Taylor, P.D.P. 2003. Atomic weights of the elements: review 2000. *Pure and Applied Chemistry* **75**, 683-800.

DePaolo, D.J. & Wasserburg, G.J. 1976. Nd isotopic variations and petrogenetic models. *Geophysical Research Letters* **3**, 249-252.

Dewey, J.F. 1980. Episodicity, sequence, and style at convergent plate boundaries. The continental crust and its mineral deposits. *Proceedings of a symposium held for J. Tuzo Wilson, Toronto, May 1979*, 553-573.

Dickinson, W.R. 2004. Evolution of the North American Cordillera. *Annual Reviews in Earth and Planetary Sciences* **32**, 13-45.

Dickinson, W.R. & Lawton, T.F. 2001. Carboniferous to Cretaceous assembly and fragmentation of Mexico. *Bulletin of the Geological Society of America* **113**, 1142-1160.

Diebold, J.B., Stoffa, P.L., Buhl, P. & Truchan, M. 1981. Venezuelan Basin crustal structure. *Journal of Geophysical Research* **86**, 7901-7923.

Donnelly, T.W., Rogers, J.J.W., Pushkar, P. & Armstrong, R.L. 1971. Chemical evolution of the igneous rocks of the eastern West Indies: An investigation of thorium, uranium, and potassium distributions, and lead and strontium isotope ratios. In: Donnelly, T.W. (Ed) *Caribbean geophysical, tectonic and petrologic studies.* Geological Society of America Memoir **130**, 181-224.

Donnelly, T.W., Melson, W., Kay, R. & Rogers, J.W. 1973. Basalts and dolerites of Late Cretaceous age from the central Caribbean. *Initial Reports of the Deep Sea Drilling Project* **15**, US Government Printing Office, Washington DC, 989-1004.

Donnelly, T.W., Beets, D., Carr, M.J., Jackson, T., Klaver, G., Lewis, J., Maury, R., Schellekens, H., Smith, A.L., Wadge, G. & Westercamp, D. 1990. History and tectonic setting of Caribbean magmatism. In: Dengo, G. & Case, J.E. (Eds) *The Caribbean Region.* The geology of North America, Geological Society of America, Boulder, Colorado **H**, 339-374.

Donnelly, T.W. 1994. The Caribbean Cretaceous basalt association: A vast igneous province that includes the Nicoya complex of Costa Rica. *Profil* (University of Stuttgart) **7**, 17-45.

Draper, G. 1986. Blueschists and associated rocks in eastern Jamaica and their significance for Cretaceous plate margin development in the northern Caribbean. *Geological Society of America Bulletin* **87**, 48-60.

Draper, G., Gutiérrez, G. & Lewis, J.F. 1996. Thrust emplacement of the Hispaniola peridotite belt: Orogenic expression of the mid-Cretaceous Caribbean arc polarity reversal? *Geology* **24**, 1143-1146.

Drummond, M.S. & Defant, M.J. 1990. A model for trondhjemite-tonalite-dacite genesis and crustal growth via slab melting: Archean to modern comparison. *Journal of Geophysical Research* **95**, 21503-21521.

Drummond, M.S., Defant, M.J. & Kepezhinskas, P.K. 1996. Petrogenesis of slab-derived trondjemite-tonalite-dacite/adakite magmas. *Transactions of the Royal Society of Edinburgh: Earth Sciences* **87**, 205-215.

Duncan, R.A. & Hargraves, R.B. 1984. Plate tectonic evolution of the Caribbean region in the mantle reference frame. In: Bonini, W.E., Hargraves, R.B., Shagam, R., *The Caribbean-South American Plate Boundary and Regional Tectonics.* Geological Society of America Memoir **162**, 81-93.

Edgar, N.T., Ewing, J.I. & Hennion, J. 1971. Seismic refraction and reflection in the Caribbean Sea. *American Association of Petroleum Geologists Bulletin* **162**, 81-93.

Ellero, A., Malasoma, A., Marroni, M., Pandolfi, L. & Urbani, F. 2007. Tectono-metamorphic history of the Tacagua ophiolitic unit (Cordillera de la Costa, northern Venezuela): Insights in the evolution of the southern margin of the Caribbean Plate. *Island Arc* **16**, 105-123.

Elliot, T. 2003. Tracers of the slab – inside the subduction factory. *Geophysical Monograph* **138**, 23-45.

Escuder Viruete, J., Díaz de Neira, A., Hernáiz Huerta, P.P., Monthel, J., García Senz, J., Joubert, M., Lopera, E., Ullrich, T., Friedman, R., Mortensen, J. & Pérez-Estaún, A. 2006. Magmatic relationships and ages of Caribbean island arc tholeiites, boninites and related felsic rocks, Dominican Republic. *Lithos* **90**, 161-186.

Escuder Viruete, J., Pérez-Estaún, A. & Weis, D. 2007a. Geochemical constraints on the origin of the late Jurassic proto-Caribbean oceanic crust in Hispaniola. *International Journal of Earth Sciences* **98**, 407-425.

Escuder Viruete, J., Contreras, F., Stein, G., Urien, P., Joubert, M., Pérez-Estaún, A., Friedman, R. & Ullrich, T. 2007b. Magmatic relationships and ages between adakites, magnesian andesites and Nb-enriched basalt-andesites from Hispaniola: Record of a major change in the Caribbean island arc magma sources. *Lithos* **99**, 151-177.

Escuder Viruete, J., Joubert, M., Urien, P., Friedman, R., Weis, D., Ullrich, T. & Pérez-Estaún, A. 2008. Caribbean island-arc rifting and back-arc basin development in the Late Cretaceous: geochemical isotopic and geochronological evidence from Central Hispaniola. *Lithos* **104**, 378-404.

Escuder Viruete, J., Pérez-Estaún, A, Weis, D. & Friedman, R. 2010. Geochemical characteristics of the Río Verde Complex, Central Hispaniola: Implications for the palaeotectonic reconstructions of the Lower Cretaceous Caribbean island arc. *Lithos* **114**, 168-185.

Farnetani, C.G. & Richards, M.A. 1994. Numerical investigations of the mantle plume initiation model for flood basalt events. *Journal of Geophysical Research* **99**, 13813-13833.

Farnetani, C.G. & Samuel, H. 2005. Beyond the thermal plume paradigm. *Geophysical Research Letters* **32**, L07311, doi:10.1029/2005GL022360.

Fink Jr., L.K. 1972. Bathymetric and geologic studies of the Guadeloupe region, Lesser Antilles island arc. *Journal of Marine Geology* **12**, 267-288.

Fitton, J.G., Saunders, A.D., Norry, M.J., Hardarson, B.S. & Taylor, R.N. 1997. Thermal and chemical structure of the Iceland plume. *Earth and Planetary Science Letters* **153**, 197-208.

Fitton, J.G. & Godard, M. 2004. Origin and evolution of magmas on the OJP. In: Fitton, J.G., Mahoney, J.J., Wallace, P.J. & Saunders, A.D. (Eds) *Origin and Evolution of the Ontong-Java Plateau.* Geological Society of London Special Publications **229**, 151-178.

Flores, K., Baumgartner P.O., Skora S., Baumgartner L., Müntener, O., Cosca M. & Cruz D. 2007. The Siuna Serpentinite Mélange: An Early Cretaceous Subduction/Accretion of a Jurassic Arc. *Eos, Transactions of the American Geophysical Union* **88**, Fall Meet. Supplement Abstract T-11D-03.

Fox, P.J., Shreiber, E. & Heezen, B.C. 1971. The geology of the Caribbean crust: Tertiary sediments, granitic and basic rocks from the Aves Ridge. *Tectonophysics* **12**, 89-109.

Frey, M., Saunders, J.B. & Schwander, H. 1988. The mineralogy and metamorphic geology of the low grade metasediments, Northern Range, Trinidad. *Journal of the Geological Society of London* **145**, 563-575.

Frost, C.D. & Snoke, A.W. 1989. Tobago, West Indies, a fragment of a Mesozoic oceanic island arc: Petrochemical evidence. *Journal of the Geological Society of London* **146**, 953-964.

Frost, C.D., Schellekens, J.H. & Smith, A.L. 1998. Nd, Sr and Pb isotope characterisation of Cretaceous and Palaeogene volcanic and plutonic island arc rocks from Puerto Rico. *Geological Society of America Special Paper* **322**, 123-132.

García-Casco, A., Lázaro, C., Rojas-Agramonte, Y., Kröner, A., Torres-Roldán, R.L., Núñez, K., Neubauer, F., Millán, G. & Blanco-Quintero, I. 2008. Partial melting and counterclockwise P-T path of subducted oceanic crust (Sierra del Convento Mélange, Cuba). *Journal of Petrology* **49**, 129-161.

Gauchat, K. 2004. Geochemistry of Désirade Island rocks (Guadeloupe, French Antilles). MS Thesis, University of Lausanne (unpublished).

Geldmacher, J., Hoernle, K., van den Bogaard, P., Hauff, F. & Klügel, A. 2008. Age and Geochemistry of the Central American Forearc Basement (DSDP Leg 67 and 84): Insights into Mesozoic Arc Volcanism and Seamount Accretion on the Fringe of the Caribbean LIP. *Journal of Petrology* **49**, 1781-1815.

Ghosh, N., Hall, S.A. & Casey, J.F. 1984. Seafloor spreading magnetic anomalies in the Venezuelan Basin. In: Bonini, W.E., Hargraves, R.B. & Shagam, R. (Eds) *The Caribbean-South American Plate Boundary and Regional Tectonics.* Geological Society of America Memoir **162**, 65-80.

Giunta, G., Beccaluva, L., Coltorti, M., Siena, F. & Vaccaro, C. 2002. The southern margin of the Caribbean Plate in Venezuela: tectono-magmatic setting of the ophiolitic units and kinematic evolution. *Lithos* **63**, 19-40.

Goodenough, K.M., Millar, I.L., Strachan, R.A., Krabbendam, M. & Evans, J.A. 2011. Timing of regional deformation and development of the Moine Thrust Zone in the Scottish Caledonides: constraints from the U-Pb geochronology of alkaline intrusions. *Journal of the Geological Society* **168**, 99-114.

Govers, M. & Wortel, M.J.R. 2005. Lithospheric tearing at STEP faults: Response to edges of subduction zones. *Earth and Planetary Science Letters* **236**, 505-523.

Hanan, B.B., Shervais, J.W. & Vetter, S.K. 2008. Yellowstone plume-continental lithosphere interaction beneath the Snake River Plain. *Geology* **36**, 51-54.

Harlow, G.E., Hemming, S.R., Avé Lallement, H.G., Sisson, V.B. & Sorensen, S.S. 2004. Two high-pressure low-temperature serpentinite-matrix mélange belts, Motagua fault zone, Guatemala: A record of Aptian and Maastrichtian collisions. *Geology* **32**, 17-20.

Hart, S.R. 1984. A large-scale isotope anomaly in the Southern Hemisphere mantle. *Nature* **309** 753-757.

Hastie, A.R., Kerr, A.C., Pearce, J.A. & Mitchell, S.F. 2007. Classification of altered island arc rocks using immobile trace elements: development of the Th-Co discrimination diagram. *Journal of Petrology* **48**, 2341-2357.

Hastie, A.R., Kerr, A.C., Mitchell, S.F. & Millar, I.L. 2008. Geochemistry and petrogenesis of Cretaceous oceanic plateau lavas in eastern Jamaica. *Lithos* **101**, 323-343.

Hastie, A.R., Kerr, A.C., Mitchell, S.F. & Millar, I.L. 2009. Geochemistry and tectonomagmatic significance of Lower Cretaceous island arc lavas from the Devils Racecourse Formation, eastern Jamaica. In: James, K.H., Lorente, M.A., Pindell, J.L. (Eds.) *The Origin and Evolution of the Caribbean Plate*. Geological Society of London Special Publication **328**, 339-360.

Hastie, A.R., 2009. Is the Cretaceous primitive island arc series in the circum-Caribbean region geochemically analogous to the modern island arc tholeiite series? In: James, K.H., Lorente, M.A., Pindell, J.L. (Eds.) *The Origin and Evolution of the Caribbean Plate*. Geological Society of London Special Publication **328**, 399-409.

Hastie, A.R., Kerr, A.C., McDonald, I., Mitchell, S.F., Pearce, J.A., Wolstencroft, M. & Millar, I.L. 2010a. Do Cenozoic analogues support a plate tectonic origin for Earth's earliest continental crust? *Geology* **38**, 495-498.

Hastie, A.R., Kerr, A.C., McDonald, I., Mitchell, S.F., Pearce, J.A., Millar, I.L., Barfod, D. & Mark, D.F. 2010b. Geochronology, geochemistry and petrogenesis of rhyodacite lavas in eastern Jamaica: A new adakite subgroup analogous to early Archaean continental crust? *Chemical Geology* **276**, 344-359.

Hastie, A.R., Ramsook, R., Mitchell, S.F., Kerr, A.C., Millar, I.L. & Mark, D.F. 2010c. Age and geochemistry of compositionally distinct back-arc basin lavas, implications for the tectonomagmatic evolution of the Caribbean plate. *The Journal of Geology* **118**, 655-676.

Hastie, A.R. & Kerr, A.C. 2010. Mantle plume or slab window? Physical and geochemical constraints on the origin of the Caribbean oceanic plateau. *Earth Science Reviews* **98**, 283-293.

Hauff F., Hoernle K.A., Van den Bogaard P., Alvarado G.E. & Garbe-Schönberg D. 2000. Age and geochemistry of basaltic complexes in western Costa Rica: Contributions to the geotectonic evolution of Central America. *Geochemistry, Geophysics, Geosystems* **1**, doi:0.1029/1999GC000020.

Hauff, F., Hoernle, K., Tilton, G., Graham, D.W. & Kerr, A.C. 2004. Large volume recycling of oceanic lithosphere over short time scales: geochemical constraints from the Caribbean Large Igneous Province. *Earth and Planetary Science Letters* **174**, 247-263.

Hawkesworth, C.J., Gallagher, K., Hergt, J.M. & McDermott, F. 1993. Mantle and slab contributions in arc magmas. *Annual Reviews in Earth and Planetary Sciences* **21**, 175-204.

Haxby, W.F., Melkonian, A.K., Coplan, J., Chan, S-M & Ryan, W.B.F. 2010. GeoMapApp freeware software, **v.2.3**, Lamont Doherty Earth Observatory.

Hay, D.C. & Dempster, T.J. 2009. Zircon behaviour during low-temperature metamorphism. *Journal of Petrology* **50**, 571-589.

Heaman, L.M. & LeCheminant, A.N. 1993. Paragenesis and U-Pb systematics of baddeleyite (ZrO_2). *Chemical Geology* **110**, 95-126.

Herzberg, C. 2004. Partial melting below the Ontong Java Plateau. In: Fitton, J.G., Mahoney, J.J., Wallace, P.J. & Saunders, A.D. (Eds) *Origin and Evolution of the Ontong Java Plateau.* Geological Society of London Special Publications **229**, 179-183.

Herzberg, C. & Gazel, E. 2009. Petrological evidence for secular cooling in mantle plumes. *Nature* **458**, 619-622.

Hodges, K.V. 1991. Pressure-temperature-time paths. *Annual Reviews in Earth and Planetary Sciences* **19**, 207-236.

Hoernle, K.A., Hauff, F. & van den Bogaard, P. 2004. A 70 m.y. history (139-69 Ma) for the Caribbean large igneous province. *Geology* **32**, 697-700.

Hole, M.J., Saunders, A.D., Marriner, G.F. & Tarney, J. 1984. Subduction of pelagic sediments: implications for the origin of Ce-anomalous basalts from the Mariana Islands. *Journal of the Geological Society of London* **141**, 453-472.

Houtz, R.E. & Ludwig, W.J. 1977. Structure of Colombia Basin, Caribbean Sea, from profiler-sonobouy measurements. *Journal of Geophysical Research* **82**, 4861-4867.

Hughes, G.W. & Turner, C.C. 1977. Upraised Pacific Ocean floor, southern Malaita, Solomon Islands. *Geological Society of America Bulletin* **88**, 412-424.

Ingle, S., Weis, D., Doucet, S. & Mattielli, N. 2002. Hf isotope constraints on mantle sources and shallow-level contaminants during Kerguelen hot spot activity since ~120 Ma. *Geochemistry, Geophysics, Geosystems* **4**, doi:10.1029/2002GC000482.

Iturralde-Vinent, M.A., Díaz-Otero, C., Rodríguez-Vega, A. & Díaz-Martínez, R. (2006) Tectonic implications of paleontologic dating of Cretaceous-Danian sections of Eastern Cuba. *Geologica Acta* **4**, 89-102.

Jaffey, A.H., Flynn, K.F., Glendenin, L.E., Bentley, W.C. & Essling, A.M. 1971. Precision measurement of half-lives and specific activities of ^{235}U and ^{238}U. *Physical Review C* **4**, 1889-1906.

James, K.H. 2006. Arguments for and against the Pacific origin of the Caribbean Plate: discussion, finding for an inter-American origin. *Geologica Acta* **4**, 279-302.

James, K.H. 2009. In situ origin of the Caribbean: discussion of data. In: James, K.H., Lorente, M.A. & Pindell, J.L. (eds) *The Origin and Evolution of the Caribbean Plate*. Geological Society of London Special Publications **328**, 77-125.

Johnson, K.T.M., Dick, H.J.B. & Shimizu, N. 1990. Melting in the oceanic upper mantle: an ion microprobe study of diopsides in abyssal peridotites. *Journal of Geophysical Research* **95**, 2661-2678.

Johnston, T.H., Schilling, G.J., Oji, Y. & Fink Jr. L.K. 1971. Dredged greenstones from the Lesser Antilles island arc. *Eos, Transactions of the American Geophysical Union* **52**, 246.

Jolly, W.T., Lidiak, E.G., Schellekens, H.S. & Santos, S. 1998. Volcanism, tectonics and stratigraphic correlations in Puerto Rico. *Geological Society of America Special Paper* **322**, 1-34.

Jolly, W.T., Lidiak, E.G., Dickin, A.P. & Wu., T.-W. 2001. Secular geochemistry of central Puerto Rican island arc lavas: Constraints on Mesozoic tectonism in the eastern Greater Antilles. *Journal of Petrology* **42**, 2197-2214.

Jolly, W.T., Lidiak, E.G. & Dickin, A.P. 2006. Cretaceous sediment budget in Puerto Rico and the Virgin Islands (northeast Antilles Island arc). *Geologica Acta* **4**, 35-62.

Jolly, W.T. & Lidiak, E.G. 2006. Role of crustal melting in petrogenesis of the Cretaceous Water Island Formation (Virgin Islands, northeast Antilles Island arc). *Geologica Acta* **4**, 7-33.

Jolly, W.T., Lidiak, E.G. & Dickin, A.P. 2008. Bimodal volcanism in northeast Puerto Rico and the Virgin Islands (Greater Antilles island arc): genetic links with Cretaceous subduction of the mid-Atlantic ridge Caribbean spur. *Lithos* **103**, 393-414.

Jolly, W.T., Lidiak, E.G. & Dickin, A.P. 2009. The case for persistent southwest-dipping Cretaceous convergence in the northeast Antilles: Geochemistry, melting models, and tectonic implications. *Bulletin of the Geological Society of America* **120**, 1036-1052.

Keary, P, Klepis, K.A. & Vine, F.J. 2009. *Global Tectonics*. Wiley-Blackwell, 496pp.

Kempton, P.D. 1995. Common Pb chemical procedures for silicate rocks and minerals, methods of data correction and an assessment of data quality at the NERC Isotope Geosciences Laboratory. *NIGL Report Series*, **78**.

Kempton, P.D., Fitton, J.G., Saunders, A.D., Nowell, G.M., Taylor, R.N., Hardarson, B.S. & Pearson, G. 2000. The Iceland plume in space and time: a Sr-Nd-Pb-Hf study of the North Atlantic rifted margin. *Earth and Planetary Science Letters* **177**, 255-271.

Kempton, P.D., Nowell, G.M. & Barry, T.L. 2001. Procedure for the high precision isotopic analysis of hafnium in silicate rocks and minerals by plasma ionisation multi-collector mass spectrometry (PIMMS) and an assessment of data quality at the NERC Isotope Geosciences Laboratory. *NIGL Report Series* **171**, 45pp.

Kempton, P.D. & McGill, R. 2002. Procedures for the analysis of common lead at the NERC Isotope Geosciences Laboratory and an assessment of data quality. *NIGL Report Series* **178**, 60pp.

Kempton, P.D., Pearce, J.A., Barry, T.L., Fitton, J.G., Langmuir, C. & Christie, D.M. 2002. Sr-Nd-Pb-Hf isotope results from ODP Leg 187: evidence for mantle dynamics of the Australian-Antarctic discordance and origin of the Indian MORB source. *Geochemistry, Geophysics, Geosystems* **3**, 2002GC00320.

Kennan, L. & Pindell, J.L. 2009. Dextral shear, terrane accretion and basin formation in the Northern Andes: best explained by interaction with a Pacific-derived Caribbean Plate? In: James, K.H., Lorente, M.A., Pindell, J.L. (Eds.) *The Origin and evolution of the Caribbean Plate*. Geological Society of London Special Publications **328**, 487-531.

Kerr, A.C., Tarney, J., Marriner, G.F., Klaver, G.T., Saunders, A.D. & Thirlwall, M.F. 1996. The geochemistry and petrogenesis of the late-Cretaceous picrites and basalts of Curaçao, Netherlands Antilles: a remnant of an oceanic plateau. *Contributions to Mineralogy and Petrology* **124**, 29-43.

Kerr, A.C., Iturralde-Vinent, M.A., Saunders, A.D., Babbs, T.L. & Tarney, J. 1999. A new plate tectonic model of the Caribbean: implications from a geochemical reconnaissance of Cuban Mesozoic volcanic rocks. Bulletin of the Geological Society of America 111, 1581-1599.

Kerr, A.C., White, R.V., Thompson, P.M.E., Tarney, J. & Saunders, A.D. 2003. No oceanic plateau – no Caribbean Plate? The seminal role of an oceanic plateau in Caribbean plate evolution. *In:* Bartonlini, C., Buffler, R.T. & Blickwede, J.F. (eds) *The circum-Gulf of Mexico and the Caribbean; hydrocarbon habitats, basin formation and plate tectonics.* Tulsa, American Association of Petroleum Geologists Memoir **79**, 126-168.

Kerr, A.C., Tarney, J., Kempton, P.D., Pringle, M. & Nivia, A. 2004. Mafic pegmatites intruding oceanic plateau gabbros and ultramafic pegmatites from Bolívar, Colombia: Evidence for a 'wet' mantle plume? *Journal of Petrology* **45**, 1877-1906.

Kerr, A.C. 2005. La Isla de Gorgona, Colombia: A petrological enigma? *Lithos* **84**, 77-101.

Kerr, A.C. & Tarney, J. 2005. Tectonic evolution of the Caribbean and northwestern South America: The case for accretion of two Late Cretaceous oceanic plateaus. *Geology* **33**, 269-272.

Kerr, A.C. & Mahoney, J.J. 2007. Oceanci plateaus: Problematical plumes, potential paradigms. *Chemical Geology* **241**, 332-353.

Kerr, A.C., Pearson, D.G. & Nowell, G.M. 2009a. Magma source evolution beneath the Caribbean oceanic plateau: new insights from elemental and Sr-Nd-Pb-Hf isotopic studies of ODP Leg 165 Site 1001 basalts. *In:* James, K.H., Lorente, M.A. & Pindell, J.L. (eds) *The Origin and Evolution of the Caribbean Plate.* Geological Society of London Special Publications **328**, 809-827.

Kerr, A.C., Neill, I., Urbani, F., Spikings, R., Barry, T. & Tarney, J. 2009b. The Siquisique basalts and gabbros, Los Algadones, Venezuela: late Cretaceous oceanic plateau formed within the proto-Caribbean Plate? *AGU Fall Meeting Abstracts* V41C-2193.

Kesler, S.E., Campbell, I.H. & Allen, C.M. 2005. Age of the Los Ranchos Formation, Dominican Republic: Timing and tectonic setting of primitive island arc volcanism in the Caribbean region. *Geological Society of America Bulletin* **117**, 987-995.

Klein, M., Stosch, H.-G. & Seck, H.A. 1997. Partitioning of high field-strength and rare-earth elements between amphibole and quartz-dioritic to tonalitic melts: an experimental study. *Chemical Geology* **138**, 257-271.

Krebs, M., Maresch, W.V., Shertl, H.-P., Münker, C., Baumann, A., Draper, G., Idleman, B. & Trapp, E. 2008. The dynamics of intra-oceanic subduction zones: a direct comparison between fossil petrological evidence (Rio San Juan Complex, Dominican Republic) and numerical simulation. *Lithos* **103**, 106-137.

Kushiro, I. 2001. Partial melting experiments on peridotite and origin of mid-ocean ridge basalt. *Annual Reviews in Earth and Planetary Sciences* **29**, 71-107.

Lapierre, H., Dupius, V., de Lépinay, B.M., Bosch, D., Monié, P., Tardy, M., Maury, R.C., Hernandez, J., Polvé, M., Yeghicheyan, D. & Cotten, J. 1999. Late Jurassic oceanic crust and Upper Cretaceous Caribbean plateau picritic basalts exposed in the Duarte igneous complex, Hispaniola. *The Journal of Geology* **107**, 193-207.

Lázaro, C. & Garía-Casco, A. 2008. Geochemical and Sr-Nd isotope signature of pristine slab melts and their residues (Sierra del Convento mélange, eastern Cuba). *Chemical Geology* **255**, 120-133.

Lebrón, M.C. & Perfit, M.R. 1993. Stratigraphic and petrochemical data support subduction polarity reversal of the Cretaceous Caribbean island arc. *The Journal of Geology* **101**, 389-396.

Lebrón, M.C. & Perfit, M.R. 1994. Petrochemistry and tectonic significance of Cretaceous island-arc rocks, Cordillera Oriental, Dominican Republic. *Tectonophysics* **229**, 69-100.

Liu, L., Spasojević, S. & Gurnis, M. 2008. Reconstructing Farallon plate subduction beneath North America back to the Late Cretaceous. *Science* **322**, 934-938.

Liu, L., Gurnis, M., Seton, M., Saleeby, J., Dietmar Müller, R. & Jackson, J.M. 2010. The role of oceanic plateau subduction in the Laramide orogeny. *Nature Geoscience* **3**, 353-357.

Ludwig, K.R. 1999. *User's manual for Isoplot/Ex, Version 2.10, a geochronological toolkit for Microsoft Excel.* Berkeley Geochronology Center Special Publication **1a**.

Ludwig, K.R. 2000. *SQUID 1.00, A User's Manual.* Berkeley Geochronology Center Special Publication **2**.

Ludwig, K.R. 2003. A geochronological toolkit for Microsoft Excel. Berkeley Geochronological Centre, Special Publication **4**.

Lugmair, G.W. & Marti, K. 1978. Lunar initial $^{143}Nd/^{144}Nd$: differential evolution of the lunar crust and mantle. *Earth and Planetary Science Letters* **39**, 349-357.

Luzieux, L. 2007. Origin and Late Cretaceous-Tertiary evolution of the Ecuadorian forearc. *PhD thesis, ETH, Zurich, unpublished.*

MacDonald, W.D. 1968. Communication. *In:* Status of geological research in the Caribbean, University of Puerto Rico Publication **14**.

Mann, P. & Taira, A. 2004. Global tectonic significance of the Solomon Islands and Ontong Java Plateau convergence zone. *Tectonophysics* **389**, 137-190.

Marchesi, C., Garrido, C.J., Bosch, D., Proenza, J.A., Gervilla, F., Monié, P. & Rodríguez-Vega, A. 2007. Geochemistry of Cretaceous magmatism in eastern Cuba: Recycling of North American continental sediments and implications for subduction polarity in the Greater Antilles palaeo-arc. *Journal of Petrology* **48**, 1813-1840.

Maresch, W.V. 1971. *The metamorphism of northeastern Margarita Island, Venezuela.* PhD Thesis, Princeton University, Princeton, NJ.

Maresch, W.V., Kluge, R. Baumann, A., Krückhans-Lueder, G., Pindell, J., Stanek, K. & Stöckhert, B. 2009. The occurrence and timing of high-pressure metamorphism on Margarita Island, Venezuela: a constraint on Caribbean-South America interaction. In: James, K.H., Lorente, M.A. & Pindell, J.L. (eds) *The Origin and Evolution of the Caribbean Plate.* Geological Society of London Special Publications **328**, 705-741.

Marlowe, J.I. 1968. Geological reconnaissance of parts of Aves Ridge. In: Manson (ed) *Abstracts of papers from the 5th Caribbean Geological Conference,* Queens College, City University of New York, 51-52.

Martin, H. 1999. Adakitic magmas: modern analogues of Archaean granitoids. *Lithos* **46**, 411-429.

Martin, H., Smithies, R.H., Rapp, R.P., Moyen, J.-F. & Champion, D.C. 2005. An overview of adakite, tonalite-trondhjemite-granodiorite (TTG) and sanukitoid; relationships and some implications for crustal evolution. *Lithos* **79**, 1-24.

Mattinson, J.M., Fink, L.K. & Hopson, C.A. 1980. Geochronologic and isotopic study of the La Désirade basement complex: Jurassic oceanic crust in the Lesser Antilles. *Contributions to Mineralogy and Petrology* **71**, 237-245.

Mattinson, J.M. 2005. Zircon U-Pb chemical abrasion ('CA-TIMS') method: combined annealing and multi-step partial dissolution analysis from improved precision and accuracy of zircon ages. *Chemical Geology* **220**, 47-66.

Mattinson, J.M., Pessagno Jr., E.A., Montgomery, H. & Hopson, C.A. 2008. Late Jurassic age of oceanic basement at La Désirade Island, Lesser Antilles arc. In: Wright, J.E., Shervais, J.W., (Eds.) *Ophiolites, Arcs and Batholiths: A Tribute to Cliff Hopson.* Geological Society of America Special Paper **438**, 175-190.

Mattson, P.H. 1960. Geology of the Mayagüez area, Puerto Rico. *Bulletin of the Geological Society of America* **71**, 319-362.

Mattson, P.H. 1979. Subduction, buoyant braking, flipping, and strike-slip faulting in the northern Caribbean. *The Journal of Geology* **87**, 293-304.

Mauffrey, A. & Leroy, S. 1997. Seismic stratigraphy and structure of the Caribbean igneous province. *Tectonophysics* **283**, 61-104.

Maxwell, J.C. 1948. Geology of Tobago, British West Indies. *Geological Society of America Bulletin* **59**, 801-854.

Maxwell, J.C. & Dengo, G. 1951. The Carúpano area and its relations to the tectonics of northeastern Venezuela. *Transactions of the American Geophysical Union* **32**, 259-267.

McCulloch, M.T., Gamble, J.A. 1991. Geochemical and geodynamical constraints on subduction zone magmatism. *Earth and Planetary Science Letters* **102**, 358-374.

McDonald, I. & Viljoen, K.S. 2006. Platinum-group element geochemistry of mantle eclogites: a reconnaissance study of xenoliths from the Orapa kimberlite, Botswana. *Applied Earth Science Transactions of the Institute of Mining and Metallurgy (B)* **115**, 81-93.

McDonough, W.F. & Sun, S.-S. 1995. The composition of the Earth. *Chemical Geology* **120**, 223-254.

McMahon, C.E. 2000. Evaluating the effects of oblique collision between the Caribbean and South American plates using geochemistry from igneous and metamorphic bodies in Northern Venezuela. *PhD Thesis, University of Notre Dame*, 227 pp.

McPherson, C.G., Dreher, S.T. & Thirlwall, M.F. 2006. Adakites without slab melting: High pressure differentiation of island arc magma, Mindanao, the Phillipines. *Earth and Planetary Science Letters* **243**, 581-593.

Meschede, M. & Frisch, M. 1995. A plate-tectonic model for the Mesozoic and early Cenozoic history of the Caribbean Plate. *Tectonophysics* **296**, 269-291.

Meschede, M. 1998. The impossible Galapagos connection: geometric constraints for a near-American origin of the Caribbean Plate. *Geologische Rundschau* **87**, 200-205.

Minifie, M.J. 2010. The nature and origin of the ~1880 Ma circum-Superior Large Igneous Province. *PhD Thesis, Cardiff University, 545 pages.*

Miura, S., Suyehiro, K., Shinohara, M., Takahashi, N., Araki, E. & Taira, A. 2004. Seismological structure and implications of collision between the Ontong Java Plateau and Solomon Island Arc from ocean bottom seismometer-airgun data. *Tectonophysics* **389**, 191-220.

Montgomery, H., Pessagno Jr., E.A. & Munoz, I. 1992. Jurassic (Tithonian) radiolaria from La Désirade (Lesser Antilles): Preliminary paleontological and tectonic implications. *Tectonics* **11**, 1426-1432.

Montgomery, H., Pessagno Jr., E.A. & Pindell, J.L. 1994. A 195 Ma terrane in a 165 Ma ocean: Pacific origin of the Caribbean Plate. *GSA Today* **4**, 1-6.

Montgomery, H. & Pessagno Jr., E.A. 1999. Cretaceous microfaunas of the Blue Mountains, Jamaica, and of the Northern and Central basement complexes of Hispaniola. In: Mann, P. (Ed) *Caribbean Basins.* Sedimentary Basins of the World **4**, Elsevier Science, Amsterdam 237-246.

Montgomery, H. & Kerr, A.C. 2009. Rethinking the origins of the red chert at La Désirade, French West Indies. In: James, K.H., Lorente, M.A., Pindell, J.L. (Eds.) *The Origin and Evolution of the Caribbean Plate.* Geological Society of London Special Publications **328**, 457-467.

Moores, E.M. & Vine, F.J. 1971. The Troodos massif, Cyprus and other ophiolites as oceanic crust: Evaluation and implications. *Philosophical Transactions of the Royal Society of London* **268A**, 443-466.

Moyen, J.-F. 2005. High Sr/Y and La/Yb ratios: the meaning of the "adakite signature". *Lithos* **112**, 556-574.

Müller, R.D., Royer, J.-Y., Cande, S.C., Roest, W.R. & Maschenkov, S. 1999. New constraints on the Late Cretaceous/Tertiary plate tectonic evolution of the Caribbean. In: Mann, P. (Ed.) *Caribbean Basins.* Sedimentary Basins of the World **4**, Elsevier Science, 33-59.

Münker, C., Weyer, S., Scherer, E. & Mezger, K. 2001. Separation of high field strength elements (Nb, Ta, Zr, Hf) and Lu from rock samples for MC-ICPMS measurements. *Geochemistry, Geophysics, Geosystems* **2**, 2001GC000183.

Neill, I., Gibbs, J.A., Hastie, A.R. & Kerr, A.C. 2010. Origin of the volcanic complexes of La Désirade, Lesser Antilles: implications for tectonic reconstruction of the Late Jurassic to Cretaceous Pacific-proto-Caribbean margin. *Lithos* **120**, 407-420.

Neill, I., Kerr, A.C., Hastie, A.R., Stanek, K-P. & Millar, I.L. 2011. Origin of the Aves Ridge and Dutch-Venezuelan Antilles: interaction of the Cretaceous 'Great Arc' and Caribbean-Colombian Oceanic Plateau? Journal of the Geological Society **168**, 333-347.

Niu, Y., O'Hara, M.J. & Pearce, J.A. 2003. Initiation of subduction zones as a consequence of lateral compositional buoyancy contrast within the lithosphere: a petrological perspective. *Journal of Petrology* **44**, 851-866.

Nowell, G.M. & Parrish, R.R. 2001. Simultaneous acquisition of isotope compositions and parent/daughter ratios by non-isotope dilution solution-mode plasma ionisation multi-collector mass spectrometry (PIMMS). *In:* Holland, G. & Tanner, S.D. (eds) *Plasma Source Mass Spectrometry – The New Millenium.* Royal Society of Chemistry, Cambridge, 298-310.

Officer, C., Ewing, J., Hennion, J., Harkinder, D & Miller, D. 1959. Geophysical investigations in the eastern Caribbean – summary of the 1955 and 1956 cruises. In: Ahrens, L.M. (Ed) *Physics and Chemistry of the Earth.* Pergammon Press, London, 17-109.

Ogg, J.G., Karl, S.M. & Behl, R.J. 1992. Jurassic through Early Cretaceous sedimentation history of the central equatorial Pacific and of ODP Sites 800 and 801. *Proceedings of the Ocean Drilling Program, Scientific Results* **129**, 571-613.

Ogg, J.G., Ogg, G. & Gradstein, F.M. 2008. The concise geologic time scale. Cambridge University Press, Cambridge.

Oldow, J.S., Bally, A.W., Avé Lallemant, H.G. & Leeman, W.P., 1989. Phanerozoic evolution of the North American Cordillera, United States and Canada. In: Bally, A.W., Palmer, A.R. (Eds.) *Geology of North America – an overview.* Geology of North America **A**, Geological Society of America, Boulder, Colorado, 139-232.

Ostos, M. & Sisson, V.B. 2005. Geochemistry and tectonic setting of igneous and metaigneous rocks of northern Venezuela. In: Avé Lallemant, H.G. & Sisson, V.B. (eds) *Caribbean-South American plate interactions, Venezuela.* Geological Society of America Special Paper **394**, 119-156.

Ostos, M., Yoris, F. & Avé Lallemant, H.G. 2005. Overview of the southeast Caribbean-South American plate boundary zone. In: Avé Lallemant, H.G. & Sisson, V.B. (eds) *Caribbean-South American plate interactions, Venezuela.* Geological Society of America Special Paper **394**, 53-90.

Page, P., Bédard, J.H. & Tremblay, A. 2009. Geochemical variations in a depleted fore-arc mantle: The Ordovician Thetford Mines Ophiolite. *Lithos* **113**, 21-47.

Parrish, R.R. 1987. An improved micro-capsule for zircon dissolution in U-Pb geochronology. *Chemical Geology* **66**, 99-102.

Parrish, R.R. & Krogh, T.E. 1987. Synthesis and purification of ^{205}Pb for U-Pb geochronology. *Chemical Geology* **66**, 103-110.

Parrish, R.R., Bowring, S.A., Condon, D.J., Schoene, B., Crowley, J.L. & Ramezani, J. 2006. EARTHTIME tracer for community use. *Geochimica et Cosmochimica Acta* **70**, A473.

Patchett, P.J. & Tatsumoto, M. 1980. Hf isotope variations in oceanic basalts. *Geophysical Research Letters* **7**, 1077-1080.

Peacock, S.M., Rushmer, T. & Thompson, A.B. 1994. Partial melting of subducting oceanic crust. *Earth and Planetary Science Letters* **121**, 227-244.

Pearce, J.A. 1983. Role of the sub-continental lithosphere in magma genesis at active continental margins. *In:* Hawkesworth, C.J. & Norry, M.J. *Continental batholiths and mantle xenoliths.* Shiva Geology Series, Nantwich, 230-249.

Pearce, J.A., Lippard, S.J. & Roberts, S. 1984. Characteristics and tectonic significant of supra-subduction zone ophiolites. In: Kokelaar, B.P., Howells, M.F. (Eds.) *Marginal basin geology: volcanic and associated sedimentary and tectonic processes in modern and ancient marginal basins.* Geological Society of London Special Publications **16**, 77-94.

Pearce, J.A. & Parkinson, I.J. 1993. Trace element models for mantle melting: application to volcanic arc petrogenesis. In: Pritchard, H.M., Alabaster, T., Harris, N.B.W. & Neary, C.R. *Magmatic Processes and Plate Tectonics.* Geological Society of London Special Publications **76**, 373-403.

Pearce, J.A. & Peate, D.W. 1995. Tectonic implications of the composition of volcanic arc magmas. *Annual Reviews in Earth and Planetary Sciences* **23**, 251-285.

Pearce, J.A., Kempton, P.D., Nowell, G.M. & Noble, S.R. 1999. Hf-Nd element and isotope perspective on the nature and provenance of mantle and subduction components in western Pacific arc-basin systems. *Journal of Petrology* **40**, 1579-1611.

Pearce, J.A. & Stern, R.J. 2006. Origin of back-arc basin magmas: trace element and isotopic perspectives. *In:* Christie, D.M., Fisher, C.R., Lee, S.-M. & Givens, S. (eds) *Back-arc spreading systems: geological, biological, chemical and physical interactions.* AGU Geophysical Monograph Series **166**, 63-86.

Peccarillo, A. & Taylor, S.R. 1976. Geochemistry of Eocene calc-alkaline volcanic rocks from the Kastamonu area, Northern Turkey. *Contributions to Mineralogy and Petrology* **58**, 63-81.

Perfit., M.R., Gust, D.A., Bence, A.E., Arculus, R.J. & Taylor, S.R., 1980. Chemical characteristics of island-arc basalts: implications for mantle sources. *Chemical Geology* **30**, 227-256.

Pessagno Jr., E.A., Blome, C.D., Hull, D. & Six Jr., W.M., 1993. Middle and Upper Jurassic Radiolaria from the western Klamath terrane, Smith River subterrane, northwestern California: Their biostratigraphic, chronostratigraphic, geochronologic, and paleolatitudinal significance. *Micropalaeontology* **39**, 93-166.

Petford, N., Cruden, A.R., McCaffrey, K.J.W. & Vigneresse, J.-L. 2000. Granite magma formation, transport and emplacement in the Earth's crust. *Nature* **408**, 669-673.

Petford, N. & Gallacher, K. 2001. Partial melting of mafic (amphibolitic) lower crust by periodic influx of basaltic magma. *Earth and Planetary Science Letters* **193**, 483-499.

Petterson, M.G., Neal, C.R., Mahoney, J.J., Kroenke, L.W., Saunders, A.D., Babbs, T.L., Duncan, R.A., Tolia, D. & McGrail, B. 1997. Structure and deformation of north and central Malaita, Solomon Islands: tectonic implications for the Ontong Java Plateau – Solomon arc collision, and the fate of oceanic plateaus. *Tectonophysics* **283**, 1-33.

Pindell, J.L. & Dewey, J.F. 1982. Permo-Triassic reconstruction of Western Pangea and the evolution of the Gulf of Mexico/Caribbean region. *Tectonics* **1**, 179-211.

Pindell, J.L. 1985. Alleghenian reconstruction and subsequent evolution of the Gulf of Mexico, Bahamas, and proto-Caribbean. *Tectonics* **4**, 1-39.

Pindell, J.L., Cande, S.C., Pitman, W.C., Rowley, D.B., Dewey, J.F., La Brecque, J.L. & Haxby, W.F., 1988. A plate kinematic framework for models of Caribbean evolution. *Tectonophysics* **151**, 121-138.

Pindell, J.L. & Barrett, S.F. 1990. Geological evolution of the Caribbean region: a plate tectonic perspective. *In:* Dengo, G. & Case, J.E. (eds) *The Caribbean Region.* Geological Society of America, The Geology of North America, **H**, 405-432.

Pindell, J.L. 1993. Regional synopsis of Gulf of Mexico and Caribbean evolution. In: Pindell, J.L. & Perkins, R. (eds) *Mesozoic and Early Cenozoic development of the Gulf of Mexico and Caribbean region*, GCSSEPM Foundation, 13th Annual Research Conference Proceedings, 251-274.

Pindell, J.L., Kennan, L., Maresch, W.V., Stanek, K.-P., Draper, G. & Higgs, R. 2005. Plate-kinematics and crustal dynamics of circum-Caribbean arc-continent interactions: Tectonic controls on basin development in proto-Caribbean margins. In: Avé Lallemant, H.G. & Sisson, V.B. (Eds) *Caribbean-South American plate interactions, Venezuela.* Geological Society of America Special Paper **394**, 7-52.

Pindell, J.L., Kennan, L., Stanek, K.P., Maresch, W.V. & Draper, G. 2006. Foundations of Gulf of Mexico and Caribbean evolution: eight controversies resolved. *Geologica Acta* **4**, 303-341.

Pindell, J.L. & Kennan, L. 2009. Tectonic evolution of the Gulf of Mexico, Caribbean and northern South America in the mantle reference frame: an update. *In:* James, K.H., Lorente, M.A. & Pindell, J.L. (eds) *The Origin and Evolution of the Caribbean Plate*. Geological Society of London Special Publications **328**, 1-55.

Pindell, J.L., Maresch, W.V., Martens, U. & Stanek, K.P. 2011. The Greater Antillean Arc: Early Cretaceous origin and proposed relationship to Central American subduction mélanges: implications for models of Caribbean evolution. *International Geology Review, in press*, doi:10.1080/00206814.2010.510008.

Plank, T. & Langmuir, C.H. 1988. An evaluation of the global variations in the major element chemistry of arc basalts. *Earth and Planetary Science Letters* **90**, 349-370.

Plank, T. 2005. Constraints from Thorium/Lanthanum on sediment recycling at subduction zones and the evolution of the continents. *Journal of Petrology* **46**, 921-944.

Portnyagin, M., Hoernle, K., Avdeiko, G., Hauff, F., Werner, R., Bindeman, I., Uspensky, V. & Garbe-Schönberg, D. 2005. Transition from arc to oceanic magmatism at the Kamchatka-Aleutian junction. *Geology* **33**, 25-28.

Portnyagin, M., Bindeman, I., Hoernle, K & Hauff, F. 2007. Geochemistry of primitive lavas of the Central Kamchatka Depression: magma generation at the edge of the Pacific plate. In: *Volcanism and Subduction: The Kamchatka Region.* Geophysical Monograph Series. American Geophysical Union, Washington D.C., 199-239.

Priem, H.N.A., Beets, D.J., Boelrijk, N.A.I.M., & Hebeda, E.H. 1986. On the age of the late Cretaceous tonalitic/gabbroic batholith on Aruba, Netherlands Antilles (southern Caribbean borderland). *Geology en Mijnbouw* **65**, 247-265.

Prouteau, G., Scaillet, B., Pichavant, M. & Maury, R. 2001. Evidence for mantle metasomatism by hydrous silicic melts derived from subducted oceanic crust. *Nature* **410**, 197-200.

Rankin, D. 2002. Geology of St. John, U.S. Virgin Islands. *United States Geological Survey Professional Paper* **1631**, 1-36.

Rapp, R.P. & Watson, E.B. 1995. Dehydration melting of metabasalt at 8-32 kbar: implications for continental growth and crust-mantle recycling. *Journal of Petrology* **36**, 891-931.

Rapp, R.P., Shimizu, N., Norman, M.D. & Applegate, G.S. 1999. Reaction between slab-derived melt and peridotite in the mantle wedge: experimental constraints at 3.8 GPa. *Chemical Geology* **160**, 335-356.

Rapp, R.P., Shimizu, N. & Norman, M.D. 2003. Growth of early continental crust by partial melting of eclogite. *Nature* **425**, 605-608.

Reagan, M.K. & Gill, J.B. 1989. Coexisting calcalkaline and high-niobium basalts from Turrialba volcano, Costa Rica: implications for residual titanites in arc magma sources. *Journal of Geophysical Research* **94**, 4619-4633.

Révillon, S., Hallot, E., Arndt, N.T., Chauvel, C. & Duncan, R.A. 2000. A complex history for the Caribbean Plateau: Petrology, geochemistry and geochronology of the Beata Ridge, South Hispaniola. *Journal of Geology* **108**, 641-661.

Robertson, P. & Burke, K. 1989. Evolution of the southern Caribbean plate boundary, vicinity of Trinidad and Tobago. *AAPG Bulletin* **73**, 490-509.

Robinson, J.A.C. & Wood, B.J. 1998. The depth of the spinel to garnet transition at the peridotite solidus. *Earth and Planetary Science Letters* **164**, 277-284.

Rojas-Agramonte, Y., Neubauer, F., Bojar, A.V., Hejl, E., Handler, R. & García-Delgado, D.E. 2006. Geology, age and tectonic evolution of the Sierra Maestra Mountains, southeastern Cuba. *Geologica Acta* **4**, 123-150.

Rosenfeld, J.H. 1993. Sedimentary rocks of the Santa Cruz Ophiolite, Guatemala – a proto-Caribbean history. In: Pindell, J.L. & Perkins, R.F. (eds) *Mesozoic and Early Cenozoic development of the Gulf of Mexico and Caribbean region.* GCSSEPM Foundation 13th Annual Research Conference Proceedings, 173-180.

Rosman, K.J.R. & Taylor, P.D.P. 1998. Isotopic compositions of the elements 1997. *Pure and Applied Chemistry* **70**, 217-235.

Royse, K.R., Kempton, P.D. & Darbyshire, F.D. 1998. Procedure for the analysis of rubidium-strontium and samarium-neodymium isotopes at the NERC Isotope Geosciences Laboratory. *NIGL Report Series*, **121**.

Rowe, D.W. 1987. Structural and petrological history of northeastern Tobago, West Indies: A partial cross-section through a composite oceanic arc complex. *MS Thesis*, University of Wyoming, Laramie, Wyoming, 165 pages, unpublished.

Rudashevsky, N.S., Burakov, B.E., Lupal, S.D., Thalhammer, O.A.R. & Saini-Edukat, B. 1995. Liberation of accessory minerals from various rock types by electric pulse disintegration – method and applications. *Transactions of the Institute of Mining and Metallurgy* **104**, C25-C29.

Russo, R.M. & Speed, R.C. 1992. Oblique collision and tectonic wedging of the South American continent and Caribbean terranes. *Geology* **20**, 447-450.

Sajona, F.G., Maury, R.C., Bellon, H., Cotten, J., Defant, M.J. & Pubellier, M. 1993. Initiation of subduction and the generation of slab melts in western and eastern Mindanao, Philippines. *Geology* **21**, 1007-1010.

Sajona, F.G., Bellon, H., Maury, R.C., Pubellier, M., Cotten, J. & Rangin, C. 1994. Magmatic response to abrupt changes in tectonic setting: Pliocene-Quaternary calc-alkaline lavas and Nb-enriched basalts of Leyte and Mindanao (Philippines). *Tectonophysics* **237**, 47-72.

Sajona, F.G., Maury, R.C., Bellon, H., Cotten, J. & Defant, M.J. 1996. High field strength element enrichment of Pliocene-Pleistocene island arc basalts, Zamboanga Peninsula, western Mindanao (Philippines). *Journal of Petrology* **37**, 693-726.

Salters, V.J.M., Longhi, J.E. & Bizimis, M. 2002. Near mantle solidus trace element partitioning at pressures up to 3.4 GPa. *Geochemistry, Geophysics, Geosystems*, **3**, doi:10.1029/2001GC000148.

Saunders, A.D., Tarney, J. & Weaver, S.D. 1980. Transverse geochemical variations across the Antarctic Peninsula: implications for the genesis of calc-alkaline magmas. *Earth and Planetary Science Letters* **46**, 344-360.

Saunders, A.D., Tarney, J., Kerr, A.C. & Kent, R.W. 1996. The formation and fate of large igneous provinces. *Lithos* **37**, 81-95.

Schellekens, J.H. 1998. Geochemical evolution and tectonic history of Puerto Rico. In: Lidiak, E.G., Larue, D.K. (Eds.) *Tectonics and geochemistry of the northeastern Caribbean.* Geological Society of America Special Paper **322**, 35-66.

Scherer, E., Munker, C. & Metzger, K. 2001. Calibration of the lutetium-hafnium clock. *Science* **293**, 683-687.

Schmitt, A.K., Chamberlain, K.R., Swapp, S.M. & Harrison, T.M. 2010. In situ U-Pb dating of micro-baddeleyite by secondary ion mass spectrometry. *Chemical Geology* **269**, 385-395.

Schmitz, M.D. & Schoene, B. 2007. Derivation of isotope ratios, errors, and error correlations for U-Pb geochronology using ^{205}Pb-^{235}U-(^{233}U)-spiked isotope dilution thermal ionisation mass spectrometric data. *Geochemistry, Geophysics, Geosystems* **8**, Q08006, doi:10.1029/2006GC001492.

Seewald, J.S. & Seyfried, W.E. 1990. The effect of temperature on metal mobility in subseafloor hydrothermal systems: constraints from basalt alteration experiments. *Earth and Planetary Science Letters* **101**, 388-403.

Shagam, R. 1960. Geology of central Aragua State, Venezuela. *Bulletin of the Geological Society of America* **71**, 249-302.

Sharp, W.D. & Snoke, A.W. 1988. Tobago, West Indies: Geochronological study of a fragment of a composite Mesozoic oceanic island arc. *Geological Society of America Abstracts with Programs* **20**, A60.

Shaw, D.M. 2006. *Trace elements in magmas: a theoretical approach.* Cambridge University Press, 243pp.

Sinton, C.W., Duncan, R.A., Storey, M., Lewis, J. & Estrada, J.J. 1998. An oceanic flood basalt province within the Caribbean plate. *Earth and Planetary Science Letters*, **155**, 221-235.

Sinton, C. W., Sigurdsson, H. & Duncan, R.A. 2000. Geochronology and petrology of the igneous basement at the lower Nicaraguan Rise, Site 1001: Proceedings of the Ocean Drilling Program, Scientific Results, Leg 165: College Station, Texas, Ocean Drilling Program, Texas A&M University, 233–236.

Sisson, V.B., Ertan, I.E. & Avé Lallemant, H.G. 1997. High-pressure (~2000 MPa) kyanite- and glaucophane-bearing pelitic schist and eclogite from Cordillera de la Costa belt, Venezuela. *Journal of Petrology* **38**, 65-83.

Skelton, P.W., Masse, J.P. 1998. Revision of the lower Cretaceous rudist genera *Pachytraga* Paquier and *Retha* Cox (Bivalvia: Hippuritacea) and the origins of the Caprinidae. *Geobios* **22**, 331-370.

Smith, C.A., Sisson, V.B., Avé Lallemant, H.G. & Copeland, P. 1999. Two contrasting pressure-temperature-time paths in the Villa de Cura blueschist belt, Venezuela: possible evidence for Late Cretaceous initiation of subduction in the Caribbean. *GSA Bulletin* **111**, 831-848.

Smithies, R.H. 2000. The Archaean tonalite-trondhjemite-granodiorite (TTG) series is not an analogue of Cenozoic adakite. *Earth and Planetary Science Letters* **182**, 115-125.

Smithies, R.H., Champion, D.C. & Van Kranendonk, M.J. 2009. Formation of Paleoarchean continental crust through infracrustal melting of enriched basalt. *Earth and Planetary Science Letters* **281**, 298-306.

Snoke, A.W., Rowe, D.W., Yule, J.D. & Wadge, G. 2001a. Petrological and structural history of Tobago, West Indies: A fragment of the accreted Mesozoic oceanic arc of the southern Caribbean. *Geological Society of America Special Paper* **354**, 54 pp.

Snoke, A.W., Rowe, D.W., Yule, J.D. & Wadge, G. 2001b. Geologic map of Tobago, West Indies with explanatory notes. *Geological Society of America Map and Chart Series* **087**, 1:25,000, 1 sheet.

Snoke, A.W. & Noble, P.J. 2001. Ammonite-radiolarian assemblage, Tobago Volcanic Group, Tobago, West Indies – Implications for the evolution of the Great Arc of the Caribbean. *Geological Society of America Bulletin* **113**, 256-264.

Somin, M.L., Millán, G. 1981. Geologija metamorficheskich kompleksoc Kuby. Isdat. Nauka, Moscow, 219 pp.

Sorenesen, S.S., Sisson, V.B. & Avé Lallemant, H.G. 2005. Geochemical evidence for possible trench provenance and fluid-rock histories, Cordillera de la Costa eclogite belt, Venezuela. In: Avé Lallemant, H.G. & Sisson, V.B. (Eds) *Caribbean-South American plate interactions, Venezuela.* Geological Society of America Special Paper **394**, 173-192.

Speed, R.C. 1985. Cenozoic collision of the Lesser Antilles arc and continental South America and the origin of the El Pilar Fault. *Tectonics* **4**, 41-69.

Speed, R.C. & Foland, K.A. 1991. Miocene metamorphism and Neogene tectonics of Northern Range rocks. In: Gillezeau, K.A. (Ed) *Transactions of the Second Geological Conference of the Geological Society of Trinidad and Tobago*, Pointe-a-Pierre, Trinidad, 19-20.

Speed, R.C. & Walker, B.M. 1991. Oceanic crust of the Grenada Basin in the southern Lesser Antilles arc platform. *Journal of Geophysical Research* **96**, 3835-3852.

Stanek, K.P., Maresch, W.V. & Pindell, J. 2009. The geotectonic story of the northwestern branch of the Caribbean arc: implications from structural and geochronological data of Cuba. *In:* James, K.H., Lorente, M.A. & Pindell, J.L. (eds) *The Origin and Evolution of the Caribbean Plate.* Geological Society of London Special Publications **328**, 361-398.

Stephan, J.-F., Beck, C., Bellizzia, A. & Blanchett, R., 1980. La chaine Caraibe da Pacifique á l' Atlantique. *Memoire du Bureau de Recherches Geologiques et Minieres* **115**, 38-59.

Stephens, W.E. 2001. Polycrystalline amphibole aggregates (clots) in granites as potential I-type restite: an ion microprobe study of rare-earth distributions. *Australian Journal of Earth Sciences* **48**, 591-601.

Stern, R.J. 2002. Subduction Zones. *Reviews of Geophysics* **40**, doi:10.1029/2001RG000108.

Stern, R.J. 2004. Subduction initiation: spontaneous and induced. *Earth and Planetary Science Letters* **226**, 275-292.

Stern, R.J. & Dickinson, W.R. 2011. The Gulf of Mexico is a Jurassic backarc basin. *Geosphere* **6**, 739-754.

Stöckhert, B., Maresch, W.V., Brix, M., Kaiser, C., Toetz, A., Kluge, R. & Kruckhans-leuder, G. 1995. Crustal history of Margarita Island (Venezuela) in detail: Constraint on the Caribbean plate-tectonic scenario. *Geology* **23**, 787-790.

Sun, S.-S. & McDonough, W.F. 1989. Chemical and isotopic systematics of oceanic basalts: implications for mantle composition and processes. In: Saunders, A.D. & Norry, M.J. (eds) *Magmatism in the Ocean Basins*, Geological Society of London Special Publications **42**, 313-345.

Tardy, M., Lapierre, H., Freydier, C., Coulon, C., Gill, J.,-B., Mercier de Lepinay, B., Beck, C., Mertinez, J., Talavera, O., Ortiz, E., Stein, G., Bourdier, J.-L. & Yta, M., 1994. The Guerrero suspect terrane (western Mexico) and coeval arc terranes (the Greater Antilles and the Western Cordillera of Colombia): A late Mesozoic intraoceanic arc accreted to cratonal America during the Cretaceous. *Tectonophysics* **320**, 49-73.

ten Brink, U.S., Marshak, S. & Granja Bruña, J.-S. 2009. Bivergent thrust wedges surrounding oceanic island arcs: Insights from observations and sandbox models of the northeastern Caribbean plate. *Bulletin of the Geological Society of America* **121**, 1522-1536.

Thirlwall, M.F., Smith, T.E., Graham, A.M., Theodorou, N., Hollings, P., Davidson, J.P. & Arculus, R.J. 1994. High field strength element anomalies in arc lavas: source or process? *Journal of Petrology* **35**, 819-838.

Thirlwall, M.F. & Anczkiewicz, R. 2004. Multidynamic isotope ratio analysis using MC-ICP-MS and the causes of secular drift in Hf, Nd and Pb isotope ratios. *International Journal of Spectrometry* **235**, 59-81.

Thompson, P.M.E., Kempton, P.D., White, R.V., Kerr, A.C., Tarney, J., Saunders, A.D., Fitton, J.G. & McBirney, A. 2003. Hf-Nd isotope constraints on the origin of the Cretaceous Caribbean plateau and its relationship to the Galapagos plume. *Earth and Planetary Science Letters* **217**, 59-75.

Thompson, P.M.E., Kempton, P.D., White, R.V., Saunders, A.D., Kerr, A.C., Tarney, J. & Pringle, M.S. 2004. Elemental, Hf-Nd isotopic and geochronological constraints on an island arc sequence associated with the Cretaceous Caribbean plateau: Bonaire, Dutch Antilles. *Lithos* **74**, 91-116.

Thorkelson, D.J. & Breitsprecher, K. 2005. Partial melting of slab window margins: genesis of adakitic and non-adakitic magmas. *Lithos* **79**, 25-41.

Toyoda, K., Nakamura, Y. & Masuda, A. 1990. Rare earth elements of Pacific pelagic sediments. *Geochimica et Cosmochimica Acta* **53**, 1093-1103.

Turner, S.P., George, R.M.M, Evans, P.J., Hawkesworth, C.J. & Zellmer, G.F. 2000. Time-scales of magma formation, ascent and storage beneath subduction-zone volcanoes. *Philosophical Transactions of the Royal Society of London A* **358**, 1443-1464.

Umhoefer, P.J. 2003. A model for the North American Cordillera in the Early Cretaceous: Tectonic escape related to arc collision of the Guerrero terrane and a change in North America plate motion. In: Johnson, S.E., Paterson, S.R., Fletcher, J.M., Girty, G.H., Kimbrough, D.L., Martín-Barajas, A. (Eds.) *Tectonic evolution of northwestern Mexico and the southwestern USA*. Geological Society of America Special Paper **374**, 117-134.

Unger, L.M., Sisson, V.B. & Avé Lallemant, H.G. 2005. Geochemical evidence for island-arc origin of the Villa de Cura blueschist belt, Venezuela. *Geological Society of America Special Paper* **394**, 223-249.

Vallejo, C., Spikings, R.A., Luziuex, L., Winkler, W., Chew, D. & Page, L. 2006. The early interaction between the Caribbean Plateau and the NW South American Plate. *Terra Nova* **18**, 264-269.

van der Hilst, R. 1990. Tomography with P, PP, pP delay-time data and the three-dimensional mantle structure below the Caribbean region. Doctoral Thesis, University of Utrecht, 250 pp.

van der Lelij, R., Spikings, R.A., Kerr, A.C., Kounov, A., Cosca, M., Chew, D. & Villagomez, D. 2010. Thermochronology and tectonics of the Leeward Antilles: evolution of the Southern Caribbean Plate Boundary Zone. *Tectonics* **29**, TC6003, doi:10.1029/2009TC002654.

van der Meer, D.G., Spakman, W., van Hinsbergen, D.J.J., Amaru, M.L. & Torsvik, T.H. 2010. Towards absolute plate motions constrained by lower-mantle slab remnants. *Nature Geoscience* **3**, 36-40.

Veizer, J. 1989. Strontium isotopes in seawater through time. *Annual Reviews in Earth and Planetary Sciences* **17**, 141-167.

Vervoort, J.D. & Blichert-Toft, J. 1999. Evolution of the depleted mantle: Hf isotope evidence from juvenile rocks through time. *Geochimica et Cosmochimica Acta* **63**, 533-556.

Wadge, G. & Macdonald, R. 1985. Cretaceous tholeiites of the northern continental margin of South America: the San Souci Formation of Trinidad. *Journal of the Geological Society of London* **142**, 297-308.

Wadge, G. & Snoke, A.W. 1991. Images of the edges of aeromagnetic anomalies as an aid to geological mapping: The case history of Tobago, West Indies. *Surveys in Geophysics* **12**, 515-530.

Walker, B.M., Vogel, T.A. & Ehrlich, R. 1972. Petrogenesis of oceanic granites from the Aves Ridge in the Caribbean Basin. *Earth and Planetary Science Letters* **15**, 133-139.

Wasserburg, G.J., Jacousen, S.B., DePaolo, D.J., McCulloch, M.T. & Wen, T. 1981. Precise determinations of Sm/Nd ratios, Sm and Nd isotopic abundances in standard solutions. *Geochimica et Cosmochimica Acta* **45**, 2311-2323.

Weber, J.C., Dixon, T.H., DeMets, C., Ambeh, W.B., Jansma, P., Mattioli, G., Saleh, J., Sella, G., Bilham, R. & Pérez, O. 2001. GPS estimate of relative plate motion between the Caribbean and South American plates, and geologic implications for Trinidad and Venezuela. *Geology* **29**, 75-78.

Wendt, J.I., Regelous, M., Collerson, K.D. & Ewert, A. 1997. Evidence for a contribution from two mantle plumes to island-arc lavas from northern Tonga. *Geology* **25**, 611-614.

White, W.M. & Patchett, J. 1984. Hf-Nd-Sr isotopes and incompatible element abundances in island arcs: implications for magma origins and crust-mantle evolution. *Earth and Planetary Science Letters* **67**, 167-185.

White, R.V., Tarney, J., Kerr, A.C., Saunders, A.D., Kempton, P.D., Pringle, M.S. & Klaver, G.T. 1999. Modification of an oceanic plateau, Aruba, Dutch Caribbean: implications for the generation of continental crust. *Lithos* **46**, 43-68.

White, W.M. 2010. Oceanic Island Basalts and Mantle Plumes: The Geochemical Perspective. *Annual Reviews in Earth and Planetary Sciences* **38**, 133-160.

Wieser, M.E. 2006. Atomic weights of the elements 2005. *Pure and Applied Chemistry* **78**, 2051-2066.

Williams, I.S. 1998. U-Th-Pb Geochronology by Ion Microprobe. *In:* McKibben, M.A., Shanks, W.C. & Ridley, W.I. (Eds) *Applications of microanalytical techniques to understanding mineralizing processes.* Reviews in Economic Geology **7**, 1-35.

Wilson, B.M. 1989. *Igneous Petrogenesis: A Global Tectonic Approach.* Springer Publications, 466 pages.

Wilson, J.T. 1966. Are the structures of the Caribbean and Scotia arc regions analogous to ice rafting? *Earth and Planetary Science Letters* **1**, 335-338.

Woodhead, J.D., Hergt, J.M., Davidson, J.P. & Eggins, S.M. 2001. Hafnium isotope evidence for 'conservative' element mobility during subduction zone processes. *Earth and Planetary Science Letters* **192**, 331-346.

Workman, R.K. & Hart, S.R. 2005. Major and trace element composition of the depleted MORB mantle (DMM). *Earth and Planetary Science Letters* **231**, 53-72.

Wright, J.E. & Wyld, S.J. 2011. Late cretaceous subduction initiation on the southern margin of the Caribbean plateau: one great arc of the Caribbean or three? *Geosphere* **7**, 468-493.

Xiong, X.L., Adam, J. & Green, T.H. 2005. Rutile stability and rutile/HFSE partitioning during partial melting of hydrous basalts: implications for TTG genesis. *Chemical Geology* **218**, 339-359.

Xiong, X.L. 2006. Trace element evidence for growth of early continental crust by melting of rutile-bearing hydrous eclogite. *Geology* **34**, 945-948.

Xu, J.-F., Shinjo, R., Defant, M.J., Wang, Q. & Rapp, R.P. 2002. Origin of Mesozoic adakitic intrusive rocks in the Nigzhen area of east China: partial melting of delaminated lower continental crust? *Geology* **30**, 1111-1114.

Yogodzinski, G.M., Kay, R.W., Volynets, O.N., Koloskov, A.N. & Kay, S.M. 1995. Magnesian andesite in the western Aleutian Komandorsky region: Implications for slab melting and processes in the mantle wedge. *Bulletin of the Geological Society of America* **107**, 505-519.

Yogodzinski, G.M., Lees, J.M., Turikova, T.G., Dorendorf, F., Wöerner, G. & Volynets, O.N. 2001. Geochemical evidence for the melting of subducting oceanic lithosphere at plate edges. *Nature* **409**, 500-504.

Yule, J.D. 1988. Petrology and structure of south-central Tobago, West Indies: Part of a displaced fragment of a Mesozoic oceanic island arc terrane. *MS Thesis*, University of Wyoming, Laramie, Wyoming, 226 pages, unpublished.

APPENDIX ONE: LOCATION OF STUDIED SAMPLES

Sample locations and geological maps for the three exposed localities of La Désirade, Tobago and San Souci

La Désirade Island, Guadeloupe (sample locations numbered)

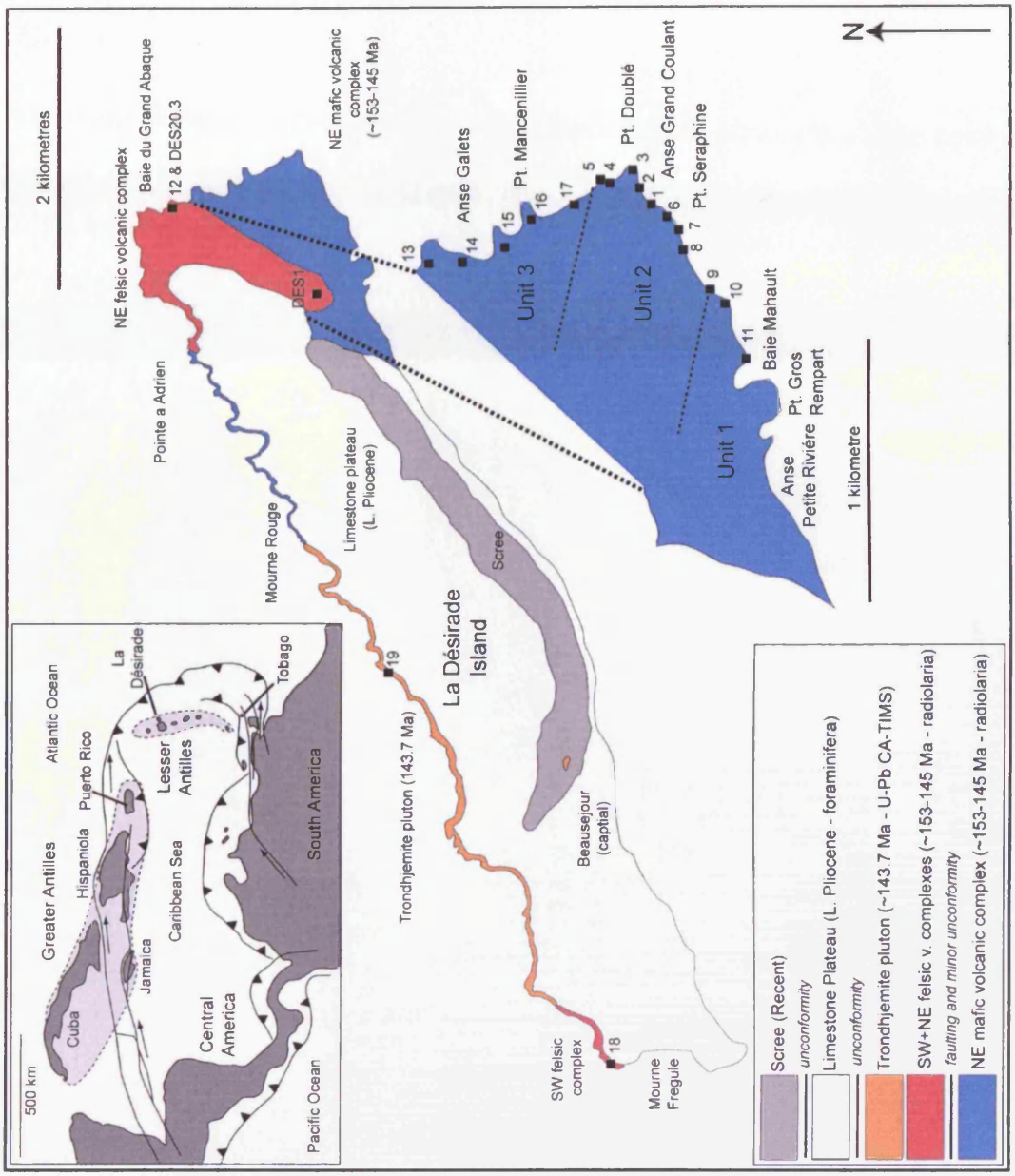

APPENDIX TWO: SAMPLE CHARTS BY LOCALITY AND UNIT

[ICP]Whole rock major and trace element analysis by ICP-OES/MS [ISO]Whole rock Nd-Hf radiometric isotope analysis undertaken [Date]Radiometric dating undertaken

A2.1. La Désirade Island Latest Jurassic complex, Guadeloupe, French West Indies

North-east mafic volcanic complex				
Number	*Location*	*Field/Hand Specimen*	*Thin Section*	*ICP/ISO/DATE*
IND1.1	West Anse Grand Coulant	Relatively vein-free ½ mm grain size autobrecciated blocky basaltic andesite with apple (epidote?), black, cloudy white crystals apparent (calcite). Red tinge from hydrothermal alteration.	n/a	Y/N/N
IND1.2	West Anse Grand Coulant/Point Seraphine	Similar to 1.1 above.	65% randomly orientated needle-like plagioclase to ½ mm. 30% twinned square-anhedral clinopyroxene. Calcite replacement. ~5% opaques including chrome spinel.	Y/N/N
IND2.1	Mid-east Anse Grand Coulant	Vesicular basalt from dykelet between pillow lavas with phrenite infill and little veining. Pyroxene and calcite visible.	n/a	N/N/N
IND2.2	Mid-east Anse Grand Coulant	Similar to 2.1 above with obvious black-green pyroxene.	n/a	Y/N/N
IND3.1	East Grand Coulant	½ mm grain size blocky flow basaltic andesite with bright green (pyroxene) phenocrysts. Possible brown copper or iron oxide.	n/a	Y/N/N
IND3.2	Pointe Doublé	½ mm grain size blocky flow basaltic andesite with more pyroxene phenocrysts. Somewhat vesicular.	¼ mm plagioclase. Occasional ½ mm glomeroporphyritic clots of clinopyroxene and rare up to 1 ½ mm relict phenocrysts. Opaques. Calcite replacement, prehnite, pumpellyite, chlorite replacing clinopyroxene.	Y/N/N
IND4.1	Station Meteo	< ½ mm grain size flow basalt with obvious calcite and pyroxene. Few vesicles and no veining.	n/a	Y/N/N
IND5.1	Station Meteo	Similar to 4.1 above.	50% ¼ mm plagioclase. 5% opaques to ½ mm. Rest clinopyroxene, square to anhedral to ½ mm with calcite growth and replacement of matrix/glass. Brown-green clays present in a rather strongly altered rock.	Y/N/N
IND6.1	Phare (Lighthouse)	Plain pillow basalt with little veining and few vesicles.	60% plagioclase to ½ mm, acicular and slightly aligned. Clinopyroxene mostly very small along with some to ½ mm. 10% opaques and clays. Some small-scale calcite veining.	
IND6.2	Phare	Basaltic andesite similar to 6.1 above.	60% plagioclase similar to 6.1 above. 25% clinopyroxene occasionally to 2 mm. Opaques and clays to 15%. Clays, calcite and rare pumpellyite.	Y/N/N
IND7.1	Phare	Calcified basaltic andesite porphyritic lava from flow banded sequence.	½ mm groundmass consisting of clinopyroxene replaced with calcite, prehnite and pumpellyite. Opaques including chrome spinel. Glomeroporphyritic with 1-2 mm patches of interlocked clinopyroxene > orthopyroxene. Little plagioclase if any.	Y/N/N
IND7.2	Phare	Basalt similar to 7.1 above.	n/a	Y/N/N
IND8.1	Phare	Basaltic pillow lava.	45-50% 1mm laths of plagioclase and 40-45% clinopyroxene. Stumpy clinopyroxene also present. 10% opaques. Quartz and prehnite cavity infill.	Y/N/N
IND8.2	Phare	Clinopyroxene-phyric basaltic andesite pillow lava.	Small stubby clinopyroxene and a lot of prehnite (possible) to 20:1 aspect ratio. Mostly quartz and opaques such as chrome spinel filling circular	Y/N/N

			cavities. Edges of cavities contain fine dark fibrous structures reminiscent of olivine replaced by serpentinite. No calcite and little plagioclase.	
IND9.1	Phare/Baie Mahault	Plagioclase and clinopyroxene-phyric pillow basalt with veining and vesicles.	Up to 60% acicular plagioclase. Rare stubby clinopyroxene. 10-20% calcite replacing groundmass. Opaques and clays present. Rare dendritic opaques indicating rapid quenching.	Y/N/N
IND9.2	Phare/Baie Mahault	Basalt similar to 9.1 above.	40% 1 mm elongate plagioclase. 35% 1 mm anhedral to elongate clinopyroxene. 10-20% olivine if present. 5% opaques. Black oxide dendrites to 1-2 mm indicating rapid quenching. Widespread calcite and clays replacing groundmass. Possible olivine replacement with clays.	Y/N/N
IND10.1	East Baie Mahault	Black, fine-grained pillow basalt.	¼ mm clinopyroxene and ultra-fine plagioclase needles. Badly altered with a lot of clay, calcite and chert.	Y/N/N
IND10.2	East Baie Mahault	Basalt similar to 10.1 above.	n/a	Y/N/N
IND11.1	Baie Mahault	Pillow basaltic andesite with buff yellow and red chert and limestone alteration. Phyric, poor-quality samples.	Coarse, almost doleritic sample with highly altered clinopyroxene and up to 60% plagioclase to 1 mm bladed or square to 2 mm. 5% oxides. Replacement with prehnite, pumpellyite, clays and chlorite.	Y/N/N
IND11.2	Baie Mahault	Basaltic andesite similar to 11.1 above.	Coarse, almost doleritic sample with 60% plagioclase to 1 mm and occasionally to 4 mm. Clinopyroxene up to 2 mm and badly altered. Black oxides. Veins filled with red oxide and common replacement with brown clays.	Y/N/N
IND11.3	Baie Mahault	Basalt similar to 11.1 above.	Medium-grained rock with very fine highly altered groundmass of plagioclase, clinopyroxene up to 3 mm, clays and oxides. Patchy replacement with calcite, vein calcite common.	Y/N/N
IND13.1	Anse Galet	Basaltic andesite from flow/breccia sequence, non-descript, fine-grained with some vesicles and no veining. Red weathering.	n/a	Y/N/N
IND14.1	Pt. Mancenillier	Basalt from blocky pillows.	Very fine elongate plagioclase to ¼ mm. Small agglomerations of clinopyroxene. Opaques present. Replacement with prehnite, pumpellyite and clays.	Y/N/N
IND15.1	Rubbish tip south side	Basaltic andesite with needle-like crystals. Quite altered.	Dominated by randomly-aligned plagioclase to 1 mm, needle-like. Altered with prehnite and calcite.	Y/N/N
IND15.2	Rubbish tip south side	Basaltic andesite similar to 15.1 above but more equigranular.	n/a	Y/N/N
IND16.1	Pt. Mancenillier	Altered vesicular basaltic andesite from above ignimbrite layers.	n/a	Y/N/N
North-east felsic volcanic complex				
Number	*Location*	*Field/Hand Specimen*	*Thin Section*	*ICP/ISO/DATE*
IND12.1	Anse Galet	Dacite lava from weathered flow outcrops.	~75% fine, altered elongate feldspar from 1mm to < ¼ mm. < 1% oxides and < 25% clinopyroxene, which is small and forms agglomerations. Clay and prehnite/pumpellyite mineralisation.	Y/N/N
DES1	Inland from Baie Mahault	Dacite sample collected by Jennifer Gibbs (2007). Fine-grained, plagioclase-rich lava.	n/a	Y/N/N
DES20.3	Grand Abaque	Dacite sample collected by Jennifer Gibbs (2007). Very fine-grained plagioclase-phyric flow-aligned lava.	n/a	Y/N/N
South-west felsic volcanic complex				

Number	*Location*	*Field/Hand Specimen*	*Thin Section*	*ICP/ISO/DATE*
IND18.1	Fregule	Dyke-like plagioclase-phyric dacite lava body.	Ultra-fine, dominated by plagioclase and perhaps K-feldspar, somewhat aligned with larger crystals up to 1 mm. Minor quartz. Mafic material < 5%. Epidote, clay and oxide replacement.	Y/N/N
IND18.2	Fregule	Similar to 18.1 above.	n/a	Y/N/N
IND18.3	Fregule	Similar to 18.1 above.	Very fine plagioclase and quartz with some plagioclase and K-feldspar up to 1-2 mm but badly eroded. Red oxide and epidote alteration.	Y/N/N
IND18.4	Fregule	Similar to 18.1 above.	n/a	Y/N/N
Trondhjemite pluton				
Number	*Location*	*Field/Hand Specimen*	*Thin Section*	*ICP/ISO/DATE*
IND19.5	L'Emballage	Microgranodiorite/trondhjemite.	~75 % plagioclase and quartz, ~5 % oxide and the rest clays and chlorite. Fine grained.	N/N/N
IND19.6	L'Emballage	Trondhjemite	n/a	N/N/N
IND19.7	L'Emballage	Trondhjemite	n/a	N/N/N
IND19.8	L'Emballage	Trondhjemite	80% plagioclase with interstitial 5% interstitial quartz. 5% oxides and 10% mafic material, mostly hornblende with trace biotite. Sericite and clay mineral alteration only.	Y/N/N
IND19.9	L'Emballage	Trondhjemite	70% plagioclase with 20% interstitial quartz. Also hornblende and oxide. Alteration to epidote, clays, sericite and chlorite.	Y/N/N
IND19.10	L'Emballage	Trondhjemite	2-3 mm grain size. Dominated by quartz and plagioclase. Minor muscovite (possible) replacing feldspars. Oxides present. Epidote a common replacement mineral.	Y/N/N
IND19.11	L'Emballage	Trondhjemite	60% plagioclase with quartz, hornblende, zircon and titanite. Chlorite and epidote as replacement minerals.	Y/N/N
IND19.12	L'Emballage	Trondhjemite	Quite badly altered. Inequigranular plagioclase, quartz, oxides and minor hornblende. Epidote and chlorite present with some calcite veining. Some evidence for relict clinopyroxene in the centre of the hornblendes.	N/N/N
IND19.13	L'Emballage	Trondhjemite, verging on more intermediate compositions.	n/a	Y/N/N
IND19.14	L'Emballage	Trondhjemite, verging on more intermediate compositions.	1-2 mm grain size. 65% tabular plagioclase which is broadly aligned, 20% hornblende, some interstitial quartz. Oxides present. Chlorite and epidote replacement.	Y/N/N
Intermediate dykes				
Number	*Location*	*Field/Hand Specimen*	*Thin Section*	*ICP/ISO/DATE*
IND19.1	L'Emballage	Basaltic andesite dyke cross-cutting the trondhjemite pluton.	n/a	Y/N/N
IND19.2	L'Emballage	Dacitic dyke cross-cutting the trondhjemite pluton.	n/a	Y/N/N
IND19.3	L'Emballage	Similar to 19.1 above.	Green-weathered with chlorite and clay alteration. Primary mineralogy of 60% ½ mm plagioclase, replaced hornblende to 30-40%. Minor quartz and oxides.	Y/N/N
IND19.4	L'Emballage	Similar to 19.1 above.	n/a	Y/N/N
5.14D3	Pointe Seraphine	Andesite dyke sample collected by Jennifer Gibbs (2007) cross-cutting the north-east mafic complex.	50% acicular plagioclase and minor quartz. 15% squat clinopyroxene, 20% chlorite, 10% pumpellyite and 5% oxides.	Y/N/N

4.10D	Pointe Doublé	Basaltic andesite dyke sample collected by Jennifer Gibbs (2007) cross-cutting the north-east mafic complex.	55% acicular plagioclase and minor quartz. 10% clinopyroxene phenocrysts. 25% chlorite and 10% opaques.	Y/N/N
6.25DC	Baie Mahault	Andesite dyke sample collected by Jennifer Gibbs (2007) cross-cutting the north-east mafic complex.	n/a	Y/N/N
20.13D	Grand Abaque	Dacitic dyke sample collected by Jennifer Gibbs (2007) cross-cutting the north-east felsic complex.	n/a	Y/N/N

A2.2. Tobago Island

Note: all occurrences of hornblende in the Tobago rocks are of green (replacement) hornblende, not brown, magmatic hornblende

North Coast Schist – Parlatuvier Formation				
Number	*Location*	*Field/Hand Specimen*	*Thin Section*	*ICP/ISO/DATE*
INT/13-2/1	Castara	Fine green mafic tuff collected from Castara Down River.	Mostly clays, oxides, quartz and chlorite; with needles of plagioclase and rarer shards of clinopyroxene. Grain size typically <0.25 mm.	N/N/N
INT/15-2/2	Castara	Grey-green metamorphosed intermediate rock from Castara Bay South End. Similar to samples collected from Englishman's Bay. Coarse, strongly foliated sample with 2-3 mm rotated quartz/plagioclases and mafic minerals (relict pyroxenes/hornblendes?) in a finer matrix.	Sample is quite badly altered with oxides, chlorite and epidote present. Plagioclase and clinopyroxene relict phenocrysts (probable), largely replaced by clays.	Y/N/N
INT/28-2/7	Castara	Collected from the road south of Castara. Grey-green foliated mafic tuff with plag, mafic minerals and oxides. Grain size ~1 mm.	n/a	Y/N/N
INT/28-2/8	Castara	Collected from the road south of Castara. Fine grey-green foliated mafic tuff with plag, mafic minerals and oxides. Grain size ~0.5 mm.	Sample is quite badly altered with iron oxides, clays and chlorite present. Patches of quartz crystals. Sharp plagioclase shards, possible relict clinopyroxene. Altered tuff.	Y/Y/N
INT/11-3/8	Castara	Fine green mafic metatuff from the road south of Castara. Grain size <0.5 mm.	Shards of clinopyroxene, with smaller crystals of plagioclase; clays, oxides, chlorite and patches of strained quartz run between the grains.	Y/N/N
INT/13-2/2	Englishman's Bay	Collected from Little Englishman's Bay River. Mafic tuff. Jumbled mess of coarse 1 mm rotated quartz/plagioclases and mafic minerals.	n/a	Y/N/N
INT/25-1/6	Englishman's Bay	Collected from Englishman's Bay. Coarse mafic tuff similar to 13-2/2 and 15-2/2 above.	n/a	Y/N/N
INT/29-2/7	Englishman's Bay	Collected from hill above N Englishman's Bay. Coarse mafic tuff similar to 13-3/2 and 15-2/2 above.	n/a	Y/N/N
INT/18-2/1	Anse Fourmi	Collected from block next to road at Anse Fourmi. Fine green mafic tuff. Grain size <0.25 mm.	Very fine with considerable chlorite alteration. Some relict clinopyroxene but also phrenite and quartz. Plagioclase needles common. Mafic tuff.	Y/N/N
3A-24	Anse Fourmi	Coarse andesitic green tuff breccia with obvious quartz crystals to 2 mm.	Crenulated sample which is quite felsic. Snoke et al. (2001) identified plagioclase, quartz, epidote, actinolite, white mica, oxides and titanite.	Y/N/Y
INT/29-2/3	Speyside	From Anse Bateau at Speyside. Fine-grained mafic tuff which contains relict hornblende fragments up to several cm in length.	Mostly contains patches of oxides, clays and chlorite. Relict hornblende has no obvious sense of shear; is cut across cleavage planes by chlorite.	Y/N/N
INT/29-2/4	Speyside	From the road north of Speyside (Anse Brisant). Badly altered and veined mafic tuff containing altered relict plagioclase (possible) in a brown grey-green matrix.	Mostly contains patches of oxides and clays. Prehnite/pumpellyite present. Relict plagioclase reaches 1-2 mm and shows sinistral sense of shear.	Y/Y/N
INT/29-2/5	Speyside	Coarse badly altered and veined tuff containing altered relict plagioclase similar to 29-2/4 above.	n/a	Y/N/N

INT/29-2/6	Speyside	Possible badly altered tuff breccias, patches of quartz and calcite present.	n/a	Y/N/N
INT/18-2/2	Charlotteville	From Pirate's Bay. Grey-green mafic tuff breccia containing up to 1 cm fragments of felsic minerals.	n/a	Y/N/N
INT/4-3/3	Charlotteville	From Charlotteville Bay South. Medium-grained foliated mafic tuff. Mineralogy not distinct. Grey-green colour.	n/a	Y/Y/N
INT/4-3/4	Charlotteville	From Charlotteville Bay South. Medium-grained foliated mafic tuff. Mineralogy not distinct. Grey-green colour.	n/a	Y/N/N
INT/2-3/1	Bloody Bay	Orange weathered rock with obvious quartz 'sweats'. Fragmental and highly altered texture – mostly likely a metamorphosed intermediate breccia.	n/a	Y/N/N
INT/2-3/3	Bloody Bay	Orange weathered rock with quartz sweats. Less fragmental than 2-3/1 above, grain size 1-2 mm but probably a metamorphosed mafic breccia.	Fine <0.25 mm groundmass with 1-2 mm grains of relict plagioclase (altered to sericite and clays). Groundmass consists of Fe Ti oxides, clays and chlorite, with quartz and plagioclase dominant. Hornblende, possible relict clinopyroxene, and titanite also present. No obvious metamorphic texture.	Y/N/N
INT/2-3/5	Bloody Bay	From roadside blastings. Fine-grained metamorphosed mafic tuff with glints of white mica and probable hornblende. Brown-grey-green colour.	n/a	Y/N/N
INT/2-3/6	Bloody Bay	Coarse green metamorphosed mafic tuff with a strong fabric. 1 mm relict plagioclases.	n/a	Y/N/N
North Coast Schist – Mount Dillon Formation				
Number	*Location*	*Field/Hand Specimen*	*Thin Section*	*ICP/ISO/DATE*
INT/28-2/1	Celery Bay	Quite dark sample, slaty grey in colour, ultra-fine grained probably silicified tuff with crenulations.	n/a	Y/Y/N
INT/28-2/2	Celery Bay	Dark sample similar to 28-2/2 above. Fine-grained, banded and probably quartz rich.	Ultra-fine-grained, dominated by small grains of interlocking quartz. Fe-Ti oxides appear in small veins and dendrites, larger veins of quartz and calcite cross-cut the sample, quartz is parallel to cleavage, calcite is later.	Y/N/N
INT/28-2/3	Celery Bay	Another dark, fine-grained sample similar to 29-2/2 above.	Sample almost identical to description of 28-2/2 above.	N/N/N
INT/29-2/8	Mount Dillon	Very silicic sample. Orange-grey weathered colour, with ultra-fine grain size and multiple veins. Probably silicified felsic tuff.	n/a	Y/N/N
INT/29-2/9	Mount Dillon	Silicic sample with orange-grey weathering. Fine-grained but mineralogy indistinct.	n/a	Y/N/N
INT/3-3/1	Mount Dillon	Fine grained brown-grey sample with prominent banding. Parallel quartz veins and cross-cutting calcite veins.	n/a	N/N/N
INT/3-3/2	Mount Dillon	Silicic sample with orange-grey weathering. Similar to 29-2/2 above.	n/a	Y/Y/N
INT/3-3/3	Mount Dillon	Similar to 29-2/2 above.	n/a	Y/N/N

INT/3-3/4	Mount Dillon	Ultra-fine grey rock with no distinct mineralogy except for oxides aligned to fabric. Probably a silicified tuff.	Sample consists entirely of interlocking quartz and oxides aligned to fabric. Veins of quartz cross-cut and parallel to fabric, all of which have strained quartz. <0.25 mm grain size.	Y/N/N
INT/11-3/9	Mount Dillon	Same as 3-3/4 above.	Identical to INT/3-3/2 above.	Y/N/N
INT/13-2/3	Little Englishman's Bay River	Same as 3-3/4 above.	n/a	Y/N/N
North Coast Schist - amphibolites				
Number	*Location*	*Field/Hand Specimen*	*Thin Section*	*ICP/ISO/DATE*
INT/8-3/3	N. of Cameron Canal Fault	Steel-grey very badly weathered sample. Very fine-grained and full of iron oxide weathering.	Oxides present but most alteration is related to chlorite. Small fragments of epidote. The bulk of the rock is made up of needles of a felsic mineral, approximately 0.5 mm long, which may be plagioclase.	Y/N/N
INT/8-3/4	N. of Cameron Canal Fault	Fine rock with green groundmass. Large white relict plagioclase to 4 mm across. Badly weathered and veined.	Groundmass consisting of <1 mm epidote and chlorite (not sure about amphiboles). Apparent plagioclase phenocrysts are almost completely replaced with clays, chlorites and micas.	Y/N/N
INT/8-3/5	N. of Cameron Canal Fault	Steel-grey, strongly foliated rock with grain size 0.5 mm. Mineralogy not certain but one mafic, one felsic mineral present. Amphibole + plagioclase?	Foliated hornblende and plagioclase to a maximum of 1 mm, mostly 0.5 mm. Some interstitial quartz veins. Chlorite alteration.	Y/Y/N
INT/8-3/6	N. of Cameron Canal Fault	Fine rock with grey-green groundmass. Large white relict plagioclase to 1 cm across.	Coarse relict plagioclases are almost completely replaced by clays, chlorite in veins and micas. The rest of the section contains abundant hornblende and oxides. Strong fabric.	Y/N/N
DY-3D-359	N. of Cameron Canal Fault	Metamorphosed plagioclase-phyric rock, grey coloured with flattened relict plagioclases up to 1 cm across.	n/a	Y/N/N
DY-3D-558	N. of Cameron Canal Fault	Metamorphosed plagioclase-phyric rock, grey coloured with a few strongly flattened relict plagioclases.	n/a	Y/Y/N
North Coast Schist - Karv				
Number	*Location*	*Field/Hand Specimen*	*Thin Section*	*ICP/ISO/DATE*
DR-693	Man O'War Hill	Dark slaty rock, fine-grained but with abundant pyrite.	Banded, ultra-fine-grained. Quartz and oxides <<0.25 mm. Other minerals indistinct. Probably a meta-sediment.	Y/N/N
DY-3D-448	Roxburgh to Bloody Bay Road	Dark crenulated sample with abundant pyrite.	Quartz and oxides, patches of oxides up to 1 mm. Other minerals indistinct. Probably a meta-sediment.	Y/N/N
DY-3D-447	Roxburgh to Bloody Bay Road	Ultra-fine dark sample with fabric. Probably metamorphosed lava.	Quartz and oxides <<0.25 mm. Other minerals indistinct.	N/N/N
DY-3D-304	Roxburgh to Bloody Bay Road	Deformed, plagioclase-phyric lava with plagioclase to 5 mm? Some patches of calcite?	Patches of calcite, riddled with oxide throughout the section. Hornblende, plagioclase and quartz present <0.5 mm. Suspect that the possible plagioclase is all calcite.	Y/N/N
DY-3D-305	Roxburgh to Bloody Bay Road	Dark, ultra-fine-grained rock with pyrite and a slaty cleavage.	n/a	Y/N/N
Tobago Volcanic Group – Argyle Formation				
Number	*Location*	*Field/Hand Specimen*	*Thin Section*	*ICP/ISO/DATE*
INT/1-3/3	Kendal Road	Dark grey lava with prominent 2-3 mm plagioclase phenocrysts. Moderately altered.	n/a	Y/Y/N
INT/16-2/2	Argyle River	Grey tuff breccia, quite silicic. Badly weathered on surface.	n/a	Y/N/N

INT/8-3/7	Argyle River/Inverawe	Grey lava with some light fawn alteration. Looks monomineralic with 1 mm grain size. Clinopyroxene?	n/a	Y/N/N
DY-3D-180	Inverawe River	Clinopyroxene-phyric tuff breccia	n/a	Y/N/N
DR-132	Louis D'Or	Clinopyroxene-plagioclase-phyric tuff breccia	Sample consists of fragments welded together of different grain size. Clinopyroxene and plagioclase to 1 mm with needle-like plagioclase in groundmass and stubby clinopyroxene. Oxides and a lot of clays also present.	Y/N/N
Tobago Volcanic Group – Bacolet Formation				
Number	*Location*	*Field/Hand Specimen*	*Thin Section*	*ICP/ISO/DATE*
INT/23-2/8	Bacolet	Clinopyroxene-phyric breccia. Moderately altered. Clinopyroxenes to 5 mm.	n/a	Y/N/N
INT/23-2/9	Bacolet	Clinopyroxene-phyric breccia with moderate alteration and clinopyroxenes to 5 mm and minor tabular plagioclase to 2 mm.	Ultra-fine groundmass, oxide-rich, with euhedral phenocrysts of plagioclase and clinopyroxene. Many of the phenocrysts have been replaced by chlorite, micas, epidote and some rare calcite patches. Rock quite badly altered.	Y/N/N
2G-1	Bacolet	Coarse volcanic breccia.	n/a	Y/N/N
2G-2	Bacolet	Coarse volcanic breccia.	Reported by Snoke et al. (2001) to contain plagioclase, clinopyroxene and oxides with replacement minerals chlorite, epidote, micas, prehnite and pumpellyite.	Y/N/N
INT/7-2/3	Hillsborough	Medium-grained volcanic breccia with 2-3 mm phenocrysts of plagioclase and clinopyroxene. Weakly altered.	n/a	Y/Y/N
DY-2H-282	Hillsborough	Clinopyroxene-phyric lava. Weakly altered.	Very large crystals of clinopyroxene up to 5 mm across, with smaller 1-2 mm phenocrysts of plagioclase. Groundmass fine-grained with mostly plagioclase and oxides. Plagioclases in good condition, pyroxenes are cracked and associated with vein infills and oxides.	Y/N/N
CF-2H-10	Hillsborough	Coarse clinopyroxene-phyric breccia, weakly altered.	n/a	Y/N/N
IJ-1C	Mount Pleasant Inlier	Volcaniclastic, weakly altered.	n/a	Y/N/N
Tobago Volcanic Group – Goldsborough Formation				
Number	*Location*	*Field/Hand Specimen*	*Thin Section*	*ICP/ISO/DATE*
INT/4-3/1	Granby	Quite badly altered, brown colour, veined. Looks like plagioclase-phyric tuff breccia.	n/a	Y/N/N
INT/4-3/2	Granby	Plagioclase-clinopyroxene tuff breccia. Veining with iron oxides and possible calcite.	n/a	Y/N/N
DY-2J-262	Granby	Clinopyroxene-phyric lava with possible amygdales.	Clinopyroxene to several mm. Mostly composed of fine groundmass of clinopyroxene, plagioclase and oxides. Not badly altered.	Y/N/N
DY-2J-N24	Granby	Clinopyroxene-phyric lava, weakly altered.	n/a	Y/N/N
DY-2J-18	Granby	Coarse, clinopyroxene-phyric lava, weakly altered.	n/a	Y/N/N
INT/8-3/1	Pembroke-Cardiff Road	Altered, veined and epidotised, chloritised sample also with some pyritisation; volcaniclastic breccia.	n/a	Y/N/N
INT/8-3/2	Pembroke-Cardiff Road	Clinopyroxene-phyric volcaniclastic breccia.	Sample consists almost entirely of relict clinopyroxene crystals which are	Y/Y/N

		Badly altered with veins (calcite) and epidote, chlorite.	cracked and replaced by chlorite and epidote. Veins of calcite.	
DY-3G-374	Richmond Island	Clinopyroxene-phyric lava.	n/a	Y/N/N
DY-2H-298	Studley Park	Phyric lava.	Sample weakly altered. Consists of a fine groundmass of plagioclase, minor clinopyroxene and abundant oxides. Plagioclase phenocrysts to 1 mm, lesser clinopyroxene phenocrysts to 1 mm. Clays and micas replacing plagioclase.	Y/N/N
DY-2J-11	Pinfold Bay	Equigranular lava with no obvious phenocryst phases, sample weakly altered	n/a	Y/N/N
INT/11-3/7	Pinfold Bay	Variably altered sample; probably lava. Plagioclase-phyric with phenocrysts tabular to 3 mm. Patches of calcite and epidote.	n/a	Y/N/N
DY-2J-27	Goodwood	Aphyric lava with patches of calcite growth up to 3 mm across.	n/a	Y/N/N
Tobago Volcanic Group – Undifferentiated lavas or good samples from volcaniclastic breccias				
Number	*Location*	*Field/Hand Specimen*	*Thin Section*	*ICP/ISO/DATE*
INT/3-2/1	Blackrock	Altered aphyric fine-grained lava, dark grey, with very fine patches of calcite and oxides.	Equigranular groundmass consisting of elongate plagioclase, oxides and interstitial clinopyroxene (all altered to a mineral with mustard birefringence?) to 0.25 mm. Rare altered phenocrysts of plagioclase and clinopyroxene to 1 mm.	Y/Y/N
IC-1B	Blackrock	Plagioclase and clinopyroxene-phyric lava, only weakly altered in hand specimen.	Groundmass consisting of equigranular plagioclase, oxides and clinopyroxene. Patches of unidentified alteration minerals present. 1 mm phenocrysts of plagioclase apparent in section (not seeing clinopyroxene); altered to clays and micas and are glomeroporphyritic.	Y/N/N
IC-11	Blackrock	Plagioclase-phyric lava, moderately altered in hand specimen.	Groundmass of plagioclase, oxides and clinopyroxene (altered to mineral with mustard birefringence), very fine. Plagioclase phenocrysts to 2 mm replaced by clays and micas.	Y/N/N
INT/7-3/6	Plymouth-Whim road	Coarse volcanic breccia, dark grey with clinopyroxene phenocrysts.	n/a	Y/N/N
INT/6-3/1	Hope-Adelphi Branch Road	Coarse plagioclase and clinopyroxene-phyric lava. Moderately altered.	Groundmass consists of oxides, chlorite and some very fine plagioclase needles. Phenocrysts were all clinopyroxenes, up to 3 mm, replaced by chlorite to varying extents, and by calcite.	Y/N/N
INT/6-3/2	Hope-Adelphi Branch Road	Clinopyroxene-phyric volcanic breccia, weakly altered.	n/a	Y/N/N
INT/6-3/3	Hope-Adelphi Branch Road	Possible lava, dark grey, moderately altered, with elongate crystals of a mafic mineral, possibly hornblende, to 3 mm.	n/a	Y/N/N
INT/7-2/1	Rocky Point	Medium-grey clinopyroxene-phyric lava with phenocrysts to 3 mm. Moderately altered with some calcite patches.	Very fine groundmass consists of plagioclase needles and oxides with patches of quartz and chlorite. The phenocryst phase is almost exclusively altered clinopyroxene to 3 mm with replacement by calcite, quartz and chlorite.	Y/N/N
INT/29-2/1	Merchison Road	Badly altered and veined lava (?) dominated by 1-2 mm clinopyroxene. Calcite and chlorite present.	n/a	Y/N/N
INT/28-2/6	Gordon Bay	Fine-grained lava with phenocrysts to 1 mm. Altered in patches (green).	Inequigranular. Almost glassy groundmass with needle-like plagioclase and oxides. Phenocrysts are plagioclase > clinopyroxene. Both, and the	Y/N/N

			groundmass are widely replaced by chlorite and epidote. Plagioclases replaced by clays and micas also.	
INT/23-2/2	Minster Point	Quite badly altered sample. Possible plagioclase and clinopyroxene-phyric lava. Fine-grained. Probable patches of chlorite.	n/a	Y/N/N
INT/23-2/3	Minster Point	Moderately altered clinopyroxene and plagioclase-phyric lava.	n/a	Y/Y/N
INT/23-2/5	Minster Point	Moderately altered clinopyroxene and plagioclase-phyric lava.	n/a	Y/N/N
INT/13-2/4	Stonehaven Bay	Badly altered lava, plagioclase-phyric. May be slightly calcified.	n/a	Y/N/N
INT/13-2/5	Stonehaven Bay	Badly altered aphyric lava with patches of calcite.	n/a	Y/N/N
IC-53	Stonehaven Bay	Clinpyroxene and plagioclase-phyric lava. Moderately altered.	Fine groundmass of plagioclase and oxides. Plagioclase phenocrysts to 2 mm with calcite and epidote common.	Y/N/N
INT/11-3/1	Speyside	Odd sample which looks slightly deformed and made up of distinct minerals, not clasts. Probably a crystal tuff. From Bishop's Bay at Speyside, Contains chlorite, calcite, oxides and clays (probably). Green/grey colouration.	n/a	Y/N/N
INT/19-2/2	Hillsborough West River	Badly altered plagioclase-phyric volcanic breccia. Patches of chlorite.	n/a	Y/N/N
IF-39	Patience Hill	Clinopyroxene and plagioclase-phyric lava. Weakly altered.	n/a	Y/N/N
Tobago Volcanic Group – Undifferentiated volcanogenic sediments (mostly crystal-bearing grits) and volcaniclastic breccias with obvious sedimentary reworking				
Number	*Location*	*Field/Hand Specimen*	*Thin Section*	*ICP/ISO/DATE*
INT/6-3/4	Hope-Adelphi Branch Road	Widespread chlorite in badly altered dark volcanogenic sediment. May be some calcite patches. No obvious clasts in hand specimen.	n/a	Y/N/N
INT/6-3/5	Hope-Adelphi Branch Road	Volcaniclastic sediment with cm-scale clasts. Possible clinopyroxene and plagioclase relict phenocrysts. Widespread alteration.	n/a	Y/N/N
INT/6-3/6	Hope-Adelphi Branch Road	Coarse volcaniclastic sediment with relict clinopyroxene and plagioclase phenocrysts. Looks quite badly altered with widespread chlorite.	Plagioclases aligned to current flow. Altered groundmass contains clays, oxides and chlorite. Relict phenocrysts are plagioclase to 2 mm and clinopyroxene (often zoned) to 5 mm. Plagioclase altered to clays and micas, clinopyroxene altered to chlorite.	Y/N/N
INT/6-3/7	Hope-Adelphi Branch Road	Moderately altered volcanogenic sediment with altered clinopyroxene relict phenocrysts to 3 mm.	n/a	Y/N/N
INT/6-3/8	Hope-Adelphi Branch Road	Similar to 6-3/7 above.	n/a	Y/N/N
INT/6-3/9	Hope-Adelphi Branch Road	Similar to 6-3/5 above.	Remarkably heterogeneous sample. Chlorite, epidote as distinct rounded grains up to 5 mm across partly replacing clinopyroxene. Oxides and clays also present. Individual clasts containing plagioclase altered to clays and micas, clinopyroxene altered to chlorite and chlorite patches <0.5 mm.	Y/N/N
INT/6-3/10	Hope-Adelphi Branch Road	Similar to 6-3/5 above.	n/a	Y/N/N

INT/23-2/1	Minster Point	Volcaniclastic sediments with cm-scale clasts, some red. Possible clinopyroxene relict phenocrysts. Widespread alteration. Patches and veins of calcite and red oxide.	Clasts, cm-scale, containing clinopyroxene to 1 mm, plagioclase (altered to micas and clays) to 0.5 mm. Patches of chlorite and epidote. Widespread calcite patches. The groundmass consists of clays, oxides, calcite, chlorite and epidote. Fragments of clinopyroxene in particular, to 2 mm, maybe altered in some cases to pumpellyite.	Y/N/N
INT/26-1/2	Minster Point	Green-red volcanic breccia with sharp-edged clinopyroxene phenocrysts to 5 mm. Clasts rounded, some reddened = sedimentary reworking.	Inequigranular. Groundmass consists of ultrafine material, some plagioclase altered to clays and micas, and oxides, widespread interstitial chlorite and clays. Oxides reach 2 mm, good clinopyroxene phenocrysts to 5 mm.	Y/N/N
INT/23-2/4	Minster Point	Sample almost identical to 26-1/2 above.	n/a	Y/N/N
INT/14-3/1	Little Tobago	Very heavy, very badly altered sample with a mixture of green patches (epidote and chlorite?) and dark blue patches (unknown).	n/a	Y/N/N
INT/19-2/1	Hillsborough West River	Moderately altered plagioclase-phyric reworked volcanic sediment.	Altered groundmass contains plagioclase crystals, chlorite and oxides. Plagioclase phenocrysts to 2 mm, weakly altered to clays and micas. Some clinopyroxene phenocrysts often altered to chlorite. Chlorite alteration widespread and interstitial. Plagioclases aligned to current flow.	Y/N/N
Tobago Plutonic Suite – Deformed Volcanic-Plutonic Complexes				
Number	*Location*	*Field/Hand Specimen*	*Thin Section*	*ICP/ISO/DATE*
INT/28-2/5	Gordon Bay	Sample is a deformed ultramafic rock which appears to be moderately altered and consists of clinopyroxene mostly. Grain size 3-4 mm.	n/a	Y/N/N
INT/4-2/4	King Peter's Bay	Deformed and strongly altered volcanic rock with 2-3 mm clinopyroxene phenocrysts, and a lot of rounded patches of calcite probably replacing plagioclase. Some calcite veins.	Sample has obvious fabric. Not too badly altered in thin section; consists of plagioclase (altered to clays and micas), hornblende and oxides.	Y/N/N
INT/6-3/11	Speyside	Badly altered, fractured and veined sample with blue-grey colouration may be deformed mafic plutonic rock. 1 mm grain size.	n/a	Y/N/N
INT/6-3/12	Speyside	Grey sample with some calcite veins. Groundmass 0.5 mm grain size probably plagioclase (needle-like) and clinopyroxene.	n/a	Y/N/N
INT/6-3/13	Speyside	Coarse-grained sample (2-3 mm) with equigranular hornblende and plagioclase, occasional large white patches to 2 cm. Deformed mafic plutonic.	White patches consist of chlorite, clays, quartz and oxides. Rest of the rock consists of plagioclase (replaced by clays), hornblende and oxides.	Y/N/N
INT/6-3/15	Merchison	Very fine-grained grey sample with some veining. Deformed mafic volcanic.	n/a	Y/N/N
INT/6-3/16	Merchison	Deformed mafic volcanic. 2-3 mm grain size with equigranular plagioclase? and hornblende.	Sample is equigranular and consists of hornblende, with some patches of unaltered clinopyroxene. The light-coloured mineral identified as plagioclase in hand spec appears to be altered clinopyroxene which has been replaced by small hornblende crystals and clays.	Y/N/N
INT/11-3/2	Merchison	Strongly deformed moderately altered sample with 1 mm grain size. May consist of hornblende, clinopyroxene and plagioclase. Deformed mafic	Roughly equal proportions of plagioclase and hornblende with lesser clinopyroxene (altering to hornblende) and oxides. Plagioclase altering to clays and oxides.	Y/N/N

		plutonic rock?		
Tobago Plutonic Suite – Ultramafic facies				
Number	*Location*	*Field/Hand Specimen*	*Thin Section*	*ICP/ISO/DATE*
INT/16-2/1	Argyle	Olivine clinopyroxenite, weakly altered.	n/a	Y/N/N
INT/21-2/2	Louis D'Or	Wehrlite. Grain size 4-5 mm (phenocrysts) in fine groundmass, moderately altered (green colouration).	Many large olivines in a groundmass containing clinopyroxene but also may be hornblende present (a lot of deep green colouration in ppl), possible epidote?	Y/N/N
INT/21-2/3	Louis D'Or	Dunite. Serpentinised; almost black colour, made up of many large (4-5 mm) olivines with a black mesh of groundmass.	n/a	Y/N/N
INT/21-2/4	Louis D'Or	Olivine clinopyroxenite, moderately altered, large clinopyroxenes to 5 mm in a steel-grey to black matrix.	Rock is dominated by large clinopyroxenes with the olivines making up <15% of the rock. Olivine is usually small and interstitial (unusual). Alteration minerals are in veins and interstitial; mostly chlorite and clays.	Y/N/N
INT/27-2/1	Culloden Bay	Hornblendite. Fine-grained (1 mm) badly altered with slight green colouration and white veins. Collected from Culloden Bay as an inclusion in gabbro-diorite – probably an altered clinopyroxenite.	Mostly altered hornblende with many good basal sections. Rest of the rock is made up of chlorite, clays and oxides.	Y/N/N
INT/8-2/1	King Peter's Bay	Olivine clinopyroxenite, moderately altered, similar to 21-2/4 above.	n/a	Y/N/N
INT/11-3/4	Delaford Bay	Clinopyroxenite with grain size up to 4 mm. Moderately altered.	Large clinopyroxenes but also hornblende present. Alteration minerals chlorite and clays.	Y/N/N
Tobago Plutonic Suite – gabbroic and dioritic facies				
Number	*Location*	*Field/Hand Specimen*	*Thin Section*	*ICP/ISO/DATE*
INT/1-3/5	Kendal Road	Weakly altered medium-grained gabbro (up to 2 mm) with equal proportions mafic and felsic minerals.	Hornblende replacing clinopyroxene (possible), with plagioclase interstitial. Only weakly altered otherwise with plagioclase to clays and micas.	Y/N/N
INT/20-2/1	Hillsborough West River	Moderately altered dolerite (up to 1 mm grain size) with equal proportions hornblende and plagioclase and some chlorite.	n/a	Y/Y/N
INT/21-2/1	Louis D'Or	Slightly deformed weakly altered coarse pegmatite with felsic and mafic minerals in equal proportions.	Rock dominated by bands rich in hornblende up to 4 mm across alternating with bands rich in very small micro-crystalline quartz and lesser plagioclase up to 1 cm long. Patches of clay alteration, also a few veins filled with clay alteration. The quartz may well be new growth and the rock as a whole a deformed dioritic pegmatite?	Y/N/N
INT/2-3/7	Courland River	Coarse (2-3 mm grain size) weakly altered diorite dominated by plagioclase with evenly distributed hornblendes.	Large hornblendes with integral small plagioclase crystals. Groundmass consists of plagioclase and lesser interstitial quartz. Alteration of plagioclase to clays and micas. Some patches of oxides present also.	Y/N/N
INT/4-2/2	Courland River	Medium (1-2 mm grain size) weakly altered diorite dominated by plagioclase with semi-aligned hornblende.	Equigranular plagioclase and hornblende with only weak alteration of the plagioclase to clays and micas.	Y/Y/N
INT/25-1/8	Culloden Bay	Coarse (2-3 mm grain size) weakly altered diorite with slightly aligned hornblende and plagioclase.	n/a	Y/N/N
INT/28-2/9	Culloden Bay	Moderately altered coarse (2-3 mm grain size) diorite with plagioclase, hornblende and some	n/a	Y/N/N

		quartz.		
INT/28-2/10	Culloden Bay	Weakly altered coarse inequigranular (1-5 mm grain size) gabbro-diorite with plagioclase and rounded hornblendes.	Rock is actually a norite with abundant orthopyroxene replaced by hornblende, and plagioclase, to a lesser extent, replaced by clays and micas.	Y/N/N
INT/28-2/4	Celery Bay	Weakly altered coarse gabbro-diorite with elongate hornblendes to 5 mm.	Hornblendes dominate with lesser plagioclase. Some patches of clay alteration. Clay, chlorite and oxides common particularly near possible relict clinopyroxene.	Y/N/N
INT/3-2/2	Arnos-Culloden Trail	Moderately altered coarse gabbro with grain size 3 mm. Abundant semi-aligned needle-like hornblende. Patches of chlorite.	Hornblendes dominate with lesser plagioclase, oxides and possible orthopyroxene? Only weakly altered in thin section.	Y/N/N
INT/3-2/3	Arnos-Culloden Trail	Badly altered hornblende diorite with veining and iron oxide staining. Otherwise coarse-grained (3 mm).	n/a	Y/N/N
INT/7-3/3	Arnos Bay	Coarse-grained (3-5 mm) inequigranular mafic rock with some large mafic crystals (hornblende?) in a finer groundmass consisting of equal proportions of plagioclase and a mafic mineral. Quite badly altered and green coloured.	n/a	Y/N/N
INT/11-3/3	Delaford Bay	Very coarse diorite, weakly altered, bearing elongate hornblendes (bottle green) up to 1.5 cm long and plagioclase.	n/a	Y/N/N
INT/11-3/6	Queen's Bay	Medium-grained diorite (2 mm grain size) with semi-aligned elongate hornblendes. Weakly veined with moderate alteration and a green tinge.	Abundant hornblende with plagioclase almost entirely replaced by clays, micas. Oxides also common.	Y/N/N
Tobago Mafic Dyke Swarm – dykes cutting the North Coast Schist				
Number	*Location*	*Field/Hand Specimen*	*Thin Section*	*ICP/ISO/DATE*
2Y-3D-432	Main Ridge	More likely a 'true' mafic dyke swarm dyke. Grey-medium grained microdiorite with 2-3 mm hornblende needles. Moderately altered.	n/a	Y/N/N
DR-780	Main Ridge	Identical to DR-509 below.	Large acicular hornblendes in a matrix comprising plagioclase, some opaques and small hornblendes.	Y/N/N
DR-430	Charlotteville	Grey hornblende diorite with 2-3 mm hornblende needles which have a slight alignment. Moderately altered with some calcite/quartz veining.	n/a	Y/N/N
DR-509	Flagstaff Hill	Grey hornblende diorite with 2-3 mm hornblende needles. Not particularly aligned. Significant quartz veining, otherwise not badly altered.	Strongly aligned acicular hornblende in a groundmass of plagioclase and quartz with few opaques. Prominent quartz-calcite vein.	Y/N/N
Tobago Mafic Dyke Swarm – dykes cutting the Plutonic Suite				
Number	*Location*	*Field/Hand Specimen*	*Thin Section*	*ICP/ISO/DATE*
INT/11-3/5	Delaford	Fine-grained aphyric mafic dyke with moderate alteration. Steel grey colouration.	n/a	Y/N/N
INT/7-3/1	Arnos Bay	Medium-grained (1 mm grain size) aphyric mafic dyke with moderate-weak alteration.	n/a	Y/N/N

INT/26-1/4	Arnos Bay	Badly altered brown-grey mafic dyke. Very fine-grained with some acicular hornblende.	n/a	Y/N/N
INT/7-3/2	Arnos Bay	Very fine-grained mostly aphyric mafic dyke with weak alteration.	Elongate hornblende to 0.5 mm, with plagioclase and cubic oxides. All in good condition. Rounded vesicles to 1 mm across filled with low relief, clear, high birefringence minerals (not calcite – may be zeolites).	Y/N/N
INT/26-1/6	Arnos Bay	Fine-grained moderately altered aphryic mafic dyke, similar to 7-3/2 above.	n/a	Y/N/N
INT/1-3/2	Kendal	Variable grain size with fine-grained matrix supporting coarser dioritic (1-2 mm grain size) fragments. Suspect the finer-grained areas are patches of alteration. Some veining.	n/a	Y/N/N
INT/1-3/6	Kendal	Mostly 1-2 mm grain size plagioclase and clinopyroxene- or hornblende-rich material with some fine-grained alteration patches. Grey colour.	n/a	Y/N/N
INT/1-3/7	Kendal	Dark grey coarse-grained (1-3 mm) mafic dyke with plagioclase and clinopyroxene. Few small green alteration patches but otherwise fresh.	n/a	Y/N/N
INT/25-1/4	Courland	Very coarse (2-4 mm) mafic dyke with a mottled texture containing hornblende and clinopyroxene. Weakly altered.	Green stubby hornblende in the groundmass from 0.25-0.5 mm, also glomeroporphyritic patches of hornblende crystals reaching 3 mm. Clinopyroxene reaching 4 mm, often altered to clays and oxides, surrounded by masses of hornblende and also altering to hornblende around the margins. Groundmass also contains plagioclase and abundant clays and lesser oxides.	Y/N/N
INT/25-1/2	Courland	Moderately altered medium-grained (1 mm grain size) microdiorite.	n/a	Y/N/N
INT/2-3/9	Courland	Grey hornblende microdiorite with acicular hornblende to 6 mm. Fine groundmass with some bottle-green patches (clinopyroxene?). Moderately altered.	n/a	Y/N/N
INT/2-3/10	Courland	Coarse (1-2 mm) hornblende diorite. Weakly altered.	n/a	Y/N/N
INT/2-3/11	Courland	Very fine grey micro-diorite with moderate alteration.	n/a	Y/N/N
INT/4-2/1	Courland	Fine mafic dyke with moderate alteration and occasional fine white veins. White, probably replacement minerals (1 mm) stand out from the groundmass.	n/a	Y/N/N
2D-14	Courland	Aphyric black microdiorite, moderately altered.	Very fine-grained microdiorite comprising hornblende and plagioclase with minor oxides and some calcite alteration patches.	Y/Y/Sharp and Snoke (1988) Ar-Ar hornblende – 91.4±2.2 Ma
INT/7-3/5	Back Bay	Moderately altered grey-green coarse (1-2 mm) microdiorite dyke.	n/a	Y/N/N
IC-29	Back Bay	Variable grain size rock similar to 25-1/4 above. Hornblende reaches 1 cm. Weakly altered.	Variable grain size with large hornblendes to 5 mm along with smaller more acicular varieties to 0.5 mm. Some relict square clinopyroxene, badly altered. Plagioclase in groundmass with some oxides. Clays and	Y/N/Sharp and Snoke (1988) Ar-Ar hornblende – 102.8±1.2 Ma

			oxides as replacement minerals.	
IC-32	Back Bay	Grey, medium-grained mafic dyke with 2-3 mm acicular hornblende along with plagioclase. Some veining but not badly altered.	Elongate clinopyroxene and hornblende to 2 mm with squat plagioclase and cubic oxides. Does not appear badly altered in section.	Y/N/N
IC-33b	Back Bay	Very coarse (3-5 mm) mafic dyke with occasional hornblende to 1 cm. Large patches of chlorite alteration giving a black-grey-green colouration.	Large clinopyroxenes to 5 mm breaking down to hornblende. Many patches of various alteration minerals including chlorite replacing entire phenocrysts. Groundmass consists of hornblende, plagioclase, clays and chlorite.	Y/N/N
Tobago Mafic Dyke Swarm – dykes cutting the Volcanic Suite				
Number	*Location*	*Field/Hand Specimen*	*Thin Section*	*ICP/ISO/DATE*
INT/23-2/6	Minster Point	Badly altered mafic dyke with green/orange colouration. May be a hornblende-phyric microdiorite with grain size 1-2 mm.	n/a	Y/N/N
2H-34	Minster Point	Moderately altered aphyric microdiorite. Grey colouration.	n/a	Y/N/N
INT/26-1/3	Mount St. George	Moderately altered clinopyroxene-phyric mafic dyke with a fine groundmass and occasional vesicles infilled with poss. quartz.	n/a	Y/N/N
INT/7-2/2	Mount St. George	Very fine-grained largely aphyric dark grey mafic dyke with little alteration and a few possible clinopyroxene phenocrysts.	n/a	Y/N/N
INT/23-2/7	Bacolet Bay	Moderately altered medium grained (1 mm grain size) mafic dyke, probably hornblende microdiorite.	n/a	Y/N/N
2G-43	Bacolet Bay	Identical to 23-2/7 above.	n/a	Y/N/N
2H-11a	Hillsborough West River	Very fine-grained dyke identical to 7-2/2 above.	n/a	Y/N/N
IC-15	Blackrock	Mottled grey microgabbro with clinopyroxene and plagioclase standing out. Moderately altered.	Patches of quartz, clays and oxides replacing some phenocrysts, otherwise a clinopyroxene and hornblende-phyric micro-gabbro with plagioclase and oxides. Alteration concentrated on the mafic minerals.	Y/N/N
Tobago other rocks – Arnos Vale – Mason Hall tonalite body				
Number	*Location*	*Field/Hand Specimen*	*Thin Section*	*ICP/ISO/DATE*
INT/2-3/12	Courland	Somewhat altered tonalite with quartz, plagioclase and biotite (5-10 %). 2mm grain size.	Veins infilled with clays. Plagioclase > quartz > biotite. Abundant clay and mica alteration of the plagioclase, chlorite replacing biotite.	Y/N/N
INT/2-3/8	Courland	Biotite tonalite only moderately altered with 5-10 % biotite. 2 mm grain size.	Plagioclase > quartz > biotite. Abundant clay replacing plagioclase. Plagioclase is optically concentrically zoned.	Y/N/N
INT/25-1/3	Courland	Somewhat altered tonalite with 10 % biotite. 2 mm grain size. Biotite looks quite 'rusty'.	n/a	Y/N/N
INT/4-2/3	Courland	Only moderately altered biotite tonalite with 2 mm grain size and biotite up to 4 mm.	Plagioclase > quartz > fresh biotite. Few possible grains of epidote. Widespread clay and mica replacing plagioclase.	Y/N/N
2D-70	Courland	Fine-grained (1 mm grain size) grey rock with plagioclase and quartz and very few mafic minerals. Not badly altered.	n/a	Y/N/N
2D-50	Courland	Only moderately altered biotite tonalite with 2 mm grain size and biotite 5-10 %.	n/a	Y/N/U-Pb zircon CA-ID-TIMS.
2D-56	Courland	Very fresh biotite tonalite with 2 mm grain size	n/a	Y/N/N

		and biotite 5-10 %.		
INT/26-1/5	Arnos Bay	Quite badly altered biotite tonalite with 2 mm grain size and biotite 5 %.	n/a	Y/Y/N
INT/7-3/4	Back Bay	Quite badly altered biotite tonalite with 2 mm grain size, also plagioclase-phyric, with very small weathered biotites 2-5 %.	n/a	Y/N/N
IC-8	Back Bay	Biotite tonalite, weakly altered, with biotite 10-15 %. 2mm grain size.	Plagioclase > quartz > fresh biotite. Plagioclase replaced by clay and micas.	Y/N/N
Tobago other rocks – Partial melts of the TVG at the contact with the TPS				
Number	*Location*	*Field/Hand Specimen*	*Thin Section*	*ICP/ISO/DATE*
INT/20-2/2	Hillsborough West River	Quartz and feldspar (variety?) in the groundmass, with 1-3 mm grain size. Large hornblendes, elongate to 4 mm. Hornblende 5-10 %.	1 mm grain size. Seems to be plagioclase > quartz > hornblende > oxides with lots of clay alteration to the plagioclases and chlorite with the hornblendes.	Y/Y/N
2D-7a	Hillsborough West River	Quartz and feldspar (variety? in the groundmass, with sub-aligned elongate hornblende to 7 mm. Hornblende 10 %.	n/a	Y/N/N
Tobago other rocks – HFSE and LREE-enriched intrusions from the NE end of the island				
Number	*Location*	*Field/Hand Specimen*	*Thin Section*	*ICP/ISO/DATE*
INT/29-2/2	Merchison	Aphyric basaltic dyke with some circular white alteration (vesicles?). Moderately altered with a grey-green colouration.	A groundmass of fine hornblende, plagioclase and oxides, with some 1 mm patches of coarser hornblende replacing clinopyroxene. A few intact clinopyroxene phenocrysts and some patches of glomeroporphyritic plagioclase. Not badly altered in thin section.	Y/Y/N
INT/6-3/14	Merchison	Aphyric medium-grained (1 mm grain size) mafic dyke, probably a hornblende dolerite.	A mesh of very fine hornblende and plagioclase with substantial clay and oxide alteration.	Y/N/N
DY-3D-103	Roxburgh	Coarse-grained (2-3 mm) clinopyroxene dolerite. Weakly altered.	n/a	Y/N/N
INT/1-3/4	Kendal Road	Granite with 2-3 mm grain size and dominated by quartz, feldspars and hornblende.	Alkali feldspars, plagioclase, quartz, hornblende and oxides in decreasing size and abundance. Minor minerals include zircon and apatite. Titanite not common. Alteration particularly of the feldspars to clay and mica.	Y/Y/U-Pb zircon CA-ID-TIMS.

A2.3. San Souci Volcanic Formation

Felsic rocks				
Number	*Location*	*Field/Hand Specimen*	*Thin Section*	*ICP/ISO/DATE*
INSS7.1	San Souci Point	Shoshonitic andesitic volcanic breccia.	Very fine-grained rock with elongate plagioclase and quartz and oxides. Autobrecciated into fragments. Cross-cut by some calcite veins and individual crystals.	Y/N/N
INSS7.3	San Souci Point	Shoshonitic andesitic volcanic breccia. Autobrecciated.	Occasional plagioclase to 1 mm. Otherwise plagioclase rich. Hornblende and oxides up to 30%. Plagioclase in good condition with some quartz and oxide veining in the whole rock.	Y/Y/Ar-Ar Plagioclase – dating not successful
INSS5.1	San Souci Point	Sandstone, slightly deformed.	n/a	Y/Y/N
Mafic rocks				
Number	*Location*	*Field/Hand Specimen*	*Thin Section*	*ICP/ISO/DATE*
INTr/28-1/1	San Souci Bay	Somewhat altered autobrecciated sample.	Dark ultra-fine rock with occasional plagioclase needles. Some patches of fine clinopyroxene. Some infill with calcite and pyrite veins, otherwise abundant prehnite and oxides.	Y/N/N
INSS3a1	Grand Riviere Road	Badly altered basaltic andesite coarse lava, calcite veining.	Altered plagioclase, badly altered clinopyroxene and abundant oxides.	Y/N/N
INSS3a2	Grand Riviere Road	Altered basaltic volcanic breccia. Autobrecciated.	Needle-like plagioclase and oxide. Mafic minerals all altered. Abundant calcite and brown oxide veining. Lithic fragments visible on a mm-scale.	Y/N/N
INSS3b1	Grand Riviere Road	Dolerite of basaltic andesite chemistry; badly altered.	Plagioclase to 2 mm. Uncertain of mafic mineralogy. Clays, orange oxides, calcite and prehnite visible.	Y/N/N
INSS3c brec	Grand Riviere Road	Very fine basaltic andesite breccia. Autobrecciated.	Needles of plagioclase alongside clinopyroxene, which sometimes reaches 1 mm. Very fine groundmass. A few oxides present. Clays and calcite in veins.	Y/Y/N
INSS3c dol	Grand Riviere Road	Basaltic andesite chemistry. Quite altered.	n/a	Y/N/N
INSS3d	Grand Riviere Road	Fine basaltic andesite lava.	Plagioclase to ¼ mm randomly aligned. Clinopyroxene present. Some calcite veining, plagioclase alteration in patches. Quartz in veins.	Y/N/Ar-Ar plagioclase – dating not successful
INSS3e	Grand Riviere Road	Basalt; may be part of a much coarser breccia.	Irregular, lath-like plagioclase to 1 mm. Good condition. Fine orange-purple (xpl) mineral – hornblende, has a green tinge (ppl). Oxides.	Y/N/N
INSS3f	Grand Riviere Road	Basalt lava.	Plagioclase in reasonable condition, some oxides, rounded, altered clinopyroxene. Veins infilled with pumpellyite and prehnite.	Y/N/N
INSS6.1	Grand Riviere Road	Basalt, somewhat brecciated.	Plagioclase to 1 mm, clinopyroxene. Sparse oxides. Clays, calcite replacement.	Y/N/N
INSS6.2	Grand Riviere Road	Dolerite with basaltic andesite chemistry.	Plagioclase laths with interstitial clinopyroxene both up to 2 mm. Plagioclase cloudy but inclusion free. Common oxides. Clinopyroxene may be replaced by hornblende. Fine zones of crushed amphibole, may be some pumpellyite in veins.	Y/N/N
INSS6.3	Grand Riviere Road	Dolerite with basaltic andesite chemistry.	Some crush zones with smaller crystals. Plagioclase to 2 mm with some inclusions. Pyroxenes altered on rims to amphibole, ranging ½ to 2 mm. Scattered oxides occasionally to 1 mm.	Y/N/Ar-Ar plagioclase – dating not successful/U-Pb zircon/baddeleyite in-situ SIMS dating – results not available in time for thesis
INSS6.4	Grand Riviere Road	Fine to medium basalt lava.	Needles of plagioclase. Clinopyroxene and oxides present. Clays largely	Y/N/N

			confined to veins. Occasional calcite.	
INSS6.5	Grand Riviere Road	Dolerite-gabbro.	Plagioclase, clinopyroxene (alteration to amphibole). Prehnite-pumpellyite, oxides, calcite present. Average grain size up to 3 mm.	Y/Y/U-Pb zircon/baddeleyite in-situ SIMS dating – results not available in time for thesis
INSS7.2	San Souci Point	Fine lava with basaltic andesite chemistry.	Fine, elongate plagioclase. Possible actinolite. Prehnite present along with calcite and quartz veining.	Y/Y/N

A2.4. SW Aves Ridge mafic and felsic suites

EA68 11317 – Felsic Dredge Hauls			
Number	*Hand Specimen*	*Thin Section*	*ICP/ISO/DATE*
11317UPb	Large blocks of leucocratic coarse-grained granitoid with quartz, feldspar and hornblende.	n/a	Y/N/U-Pb SHRIMP
11317a	Much of the sample was lost to crushing, milling and geochemical analysis, what remained of some samples was thin sectioned. The original description of the rubble blocks from which these samples were generated is thus: Briefly, hydrothermally altered I-type granite with abundant restite. Mostly medium-grained with plagioclase > alkali feldspar > quartz. The mafic phase is predominantly hornblende, which is occasionally acicular. Also present is a second facies occurring at a centimetre scale within the main body of the rock. This facies is more mafic than the granitoid and is composed of hornblende and plagioclase of a sub-mm grain size. Pale and more apple green colours suggest chlorite and epidote are common alteration phases. Overall the samples are coated with Mn-oxides from seafloor exposure but are internally not badly weathered.	n/a	Y/Y/N
11317b		n/a	Y/N/N
11317c		n/a	Y/N/N
11317d		n/a	Y/N/N
11317e		n/a	Y/N/N
11317f		n/a	Y/N/N
11317g		n/a	Y/N/N
11317h		As 319a below except a 0.5mm grain size facies containing only plagioclase, hornblende and oxides in a random alignment.	Y/N/N
11317i		n/a	Y/N/N
11317j		n/a	Y/N/N
11317k		As 319a below except large hornblende needles to 4mm, no biotite, some chlorite present.	Y/N/N
EA68 11319 – Felsic Dredge Hauls			
11319a	Samples very similar to those from dredge 11317. There is a lower proportion of the fine-grained more mafic facies compared to 11317 and a slightly greater proportion of hornblende.	Plagioclase, quartz and optically-zoned alkali feldspar. The feldspars are altered with sericite and some epidote. Rare stubby 1mm-long green amphibole. Sparse oxides and rare biotite, titanite and zircon.	Y/N/N
11319b		n/a	Y/N/N
11319c		n/a	Y/N/N
11319d		n/a	Y/N/N
11319e		n/a	Y/N/N
11319f		n/a	Y/N/N
11319g		n/a	Y/N/N
11319h		n/a	Y/N/N
11319i		n/a	Y/N/N
11319j		n/a	Y/N/N
EA68 11318 – Mafic Dredge Hauls			
11318a	The remaining material from this dredge haul fills one large sample bag only. Much of the material is very badly altered and few minerals can be clearly identified in hand specimen. Some pyroxenes and/or amphiboles may be present in coarser samples – suggesting at least some of the rocks were originally phyric dolerites or basalts. Other rocks appear to have been finer-grained.	n/a	Y/N/N
11318b		n/a	Y/N/N
11318c		n/a	Y/N/N
11318d		n/a	Y/N/N
11318e		n/a	Y/N/N
11318f		Altered feldspars to 2mm in a very badly altered groundmass of clays and oxides.	Y/N/N
11318g		n/a	Y/Y/N
11318h		As 318f above. Feldspars in this sample display a strong magmatic alignment.	Y/N/N
11318i		n/a	Y/N/N

11318j		n/a	Y/N/N
11318k		As 318f above plus amphiboles to 2mm and a single vein containing clays and possible foraminifera tests suggesting this is a sample from a near-surface weathered outcrop.	Y/N/N
11318l		n/a	Y/N/N

APPENDIX THREE: ANALYTICAL METHODS

A3.1. Introduction

In lieu of a methods chapter at the beginning of this thesis, this appendix covers the sample preparation and analysis techniques used to generate the U-Pb geochronological results, major element, trace element and radiogenic isotope results used in this thesis.

A3.2. Geochronology

A3.2.1. Sample selection and recovery of datable material

Five rock samples were identified for U-Pb geochronological studies and various methods were used to extract zircons for analysis and for the analysis itself because of financial constraints. These methods are summarised in Table A3.1 below.

Table A3.1. Samples selected for radiometric dating of zircons. UWyo = University of Wyoming, USA; Freiberg = Technical University of Freiburg; NIGL = Natural Environment Research Council Isotope Geoscience Laboratories, Nottingham, UK; VSEGEI = Centre for Isotopic Research, St. Petersburg, Russia; CA-ID-TIMS = chemical abrasion, isotope dilution thermal ionisation mass spectrometry; in-situ SIMS = dating of thin-sectioned zircons by secondary ionisation mass spectrometry; SHRIMP = sensitive high resolution ion microprobe. See text for further details.

Number	Location	Formation	Rock type	Separation method	Dating method
3A-24	Tobago	Parlatuvier Formation, North Coast Schist	basaltic andesite	crushing + electrodynamic (UWyo)	U-Pb CA-ID-TIMS (NIGL)
2D-50	Tobago	Arnos Vale tonalite	tonalite	selFrag + electrodynamic (Freiberg)	U-Pb CA-ID-TIMS (NIGL)
INT/1-3/4	Tobago	LREE- + Nb-enriched dykes	granite	selFrag + electrodynamic (Freiberg)	U-Pb CA-ID-TIMS (NIGL)
INSS6.3	San Souci, Trinidad	mafic rocks	dolerite	in-situ (thin sectioning) (UWyo)	U-Pb in-situ SIMS (UCLA)
INSS6.5	San Souci, Trinidad	mafic rocks	dolerite	in-situ (thin sectioning) (UWyo)	U-Pb in-situ SIMS (UCLA)
317UPb	Aves Ridge	granitoids	granitoid	selFrag + electrodynamic (Freiberg)	U-Pb SHRIMP (VSEGEI)

Tobago: Samples 2D-50 (tonalite) and INT/1-3/4 (high-Nb granite) were sent to Klaus-Peter Stanek at the Technical University of Freiberg. Zircons were extracted using an Ammann AG selFrag electronic disaggregator (e.g. Rudashevsky et al., 1995). This method applies a high-voltage pulse through a sample immersed in water. The pulse forms a short-lived plasma channel of 1-2 μm between grain boundaries which results in the sample shattering. Zircons were then separated from other grains using conventional electromagnetic separation in Freiberg. Zircon grains from these samples were partly hand-picked under ethanol in Freiburg by Klaus-Peter Stanek before being sent to Cardiff for final picking by the author. These samples were then sent to the NERC Isotope Geosciences Laboratories (NIGL), Nottingham, England for chemical abrasion-isotope dilution-thermal ionisation mass spectrometry (CA-ID-TIMS) dating. Sample 3A-24 was milled lightly and run through an electromagnetic separator in 1995

by Arthur Snoke and Kevin Chamberlain at the University of Wyoming. The separated zircons (<30, mostly <50 μm) were obtained by picking under ethanol but never analysed, so these remaining zircons were sent to Cardiff for final picking. This sample was also sent to NIGL for dating using CA-ID-TIMS.

San Souci: The samples from San Souci were too mafic and fine-grained to recover zircons by conventional means. A new technique for secondary ionisation mass spectrometric analysis (SIMS) of ng-mass zircon ($ZrSiO_4$) and baddeleyite (ZrO_2) crystals in-situ, in a thin sectioned sample, has recently been described by Schmitt et al. (2010). Like zircon, baddeleyite retains U and Th but cannot retain radiogenic Pb at magmatic temperatures, so is suitable for U-Pb dating of the crystallisation age and/or metamorphic overgrowths (Heaman and LeCheminant, 1993). Firstly, the whole rock sample was cut, thin sectioned and diamond polished at the University of Wyoming. Under a JEOL JXA-8900 electron microprobe at the University of Wyoming, high-Zr domains were identified which were then imaged and verified as zircon or baddeleyite using back-scattered electrons and energy-dispersive x-ray analysis on the same instrument. Domains rich in either mineral were trimmed off with a diamond corer or saw, and then mounted with their glass in epoxy resin. The mount was then ground, polished, cleaned in an ultrasound bath (in cleaning solution, hydrochloric acid, de-ionised water and methanol), dried and finally gold coated. Samples were then taken to the University of California, Los Angeles, for SIMS analysis.

Aves Ridge: Sample 317UPb was sent to the Technical University of Freiberg, where Klaus-Peter Stanek disaggregated the rock using the selFrag method as per the two Tobago samples. 200 grains from 317UPb were recovered by electromagnetic separation and picking under ethanol in Freiberg; and taken to the Centre for Isotopic Research (VSEGEI) in St. Petersburg, Russia, for sensitive high resolution ion microprobe analysis (SHRIMP) dating.

A3.2.2 U-Pb CA-ID-TIMS analysis at NIGL

For each sample, the following procedure was used (after Goodenough et al., 2011). Selected zircons were annealed and chemically abraded (Mattinson, 2005), a

technique designed to largely eliminate discordance caused by Pb loss. The grains were spiked with $^{205}Pb/^{235}U$ or $^{205}Pb/^{235}U/^{233}U$ tracers (Parrish & Krogh, 1987; Parrish et al., 2006) and then dissolved in Teflon microcapsules (Parrish, 1987). U and Pb fractions were then separated using the techniques outlined in Corfu & Noble (1992) before loading on to rhenium filaments using a silica gel. Measurement on a Thermo-Electron Triton thermal ionisation mass spectrometer (TIMS) was by peak-jumping using a secondary electron multiplier. Results were processed in MATLAB and the UPbR spreadsheet derived from Schmitz & Schoene (2007), and the final ages calculated using Isoplot 3.16 (Ludwig, 2003).

A3.2.3. U-Pb in-situ SIMS analysis at UCLA

Analysis was not undertaken in time for inclusion in this thesis.

A3.2.4. U-Pb SHRIMP analysis at VSEGEI

Fifty of the separated zircons from the Aves Ridge were mounted in epoxy resin alongside chips of TEMORA (Middledale gabbro-diorite of New South Wales) and 91500 (Geostandard) reference zircons. All grains were half-sectioned and polished. Reflected and transmitted light photomicrographs and cathodoluminscence images (CL) were prepared (Fig. 4.31). The CL images were used to decipher internal structures and to identify specific target areas.

The following description of the analysis technique is adapted from information supplied by Klaus-Peter Stanek and VSEGEI. U-Pb analyses were carried out by sensitive high-resolution ion microprobe (SHRIMP) using a SHRIMP-II produced by Australian Scientific Instruments. The method involves targeting an ion beam at the sample which sputters secondary electrons from the sample. These electrons are accelerated within the instrument where the respective isotopes of U, Pb and Th are measured and calibrated using known standards and calibration factors. Twelve sites on 8 selected zircons were analysed. Each analysis consisted of five scans through the mass range, with a beam spot diameter of ~25 μm and a primary beam intensity of ~10 nA. Data produced were reduced in a manner similar to that described by Williams

(1998 and references therein) using the SQUID Excel macro of Ludwig (2000). Pb/U ratios were normalised relative to a value of 0.0668 for the $^{206}Pb/^{238}U$ ratio of the TEMORA reference zircons, equivalent to an age of 416.75 Ma (Black et al., 2003). Uncertainties for single analyses (ratios and ages) are quoted at the 1σ level; however, uncertainties in calculated concordia ages are reported at the 2σ level. The inverse concordia plot used in the text (Fig. 4.32) was prepared using ISOPLOT/EX (Ludwig, 1999).

A3.3. Major and trace element analysis methods

Whole rock samples were prepared and analysed for their major and trace element contents at Cardiff University. Samples of around 2-fist size (where possible) were selected for analysis. Larger volumes of samples with large grain sizes were selected to ensure a homogenous sample. Each sample underwent the following procedure:

The sample was sawn into pieces up to 10 centimetres across, removing weathered or altered surfaces, obvious veining and patches of vesicles. It was washed, dried and then crushed in a steel jaw crusher to fine rubble (<5 mm grain size). Next, the sample was placed in an agate pot with five agate balls in a planetary ball mill and spun at ~300 r.p.m. for 30 minutes to produce a fine powder. The fine 'wet' powder was later used as the basis for radiogenic isotope analysis (see Section A3.4). Approximately 2 g of the sample was weighed into a porcelain pot and placed in an oven at 900°C for 2 hours to remove volatiles (H_2O and CO_2). In doing so, Fe^{2+} was oxidised to Fe^{3+}, hence all results are quoted as $Fe_2O_{3(total)}$. The sample was re-weighed in order to calculate the loss-on-ignition (LOI), which is used as a partial indicator of the degree of alteration of the samples (clay and calcite content).

0.1±0.0020 g of the dried sample was weighed into a platinum crucible, and 0.6±0.0050 g of lithium metaborate flux was added to aid fusion and dissolution of the sample. The crucibles rest in 50 % nitric acid during storage and are washed in de-ionised water (18.2 Ω) before use. Lithium iodide (3-4 drops) was added as a wetting agent to the sample in the crucible. The crucible was attached to a Claisse Fluxy-Fusion propane burner which roasted and rotated the crucibles in order to fuse the sample. Once molten, the sample was dropped into a Teflon beaker containing 20 ml of 10 % nitric acid and 30 ml de-ionised H_2O and stirred with a magnetic stirring rod for 5 minutes. The beaker, platinum crucible and sample were placed on a hotplate with a magnetic stirring rod until all traces of the sample had dissolved. At this stage, a 1 ml spike containing 1000 ppm Rh was added as an internal standard. The solution was then poured into a Teflon flask and made up to 100 ml with de-ionised H_2O before storing in a Nalgene sample container until use. Samples were run within 1-2 weeks in order to

prevent precipitation of any components from the solution. ICP-OES (inductively-coupled plasma optical emission spectrometry) analysis for major and some trace elements was undertaken by Dr. Ley Woolley using approximately 20 ml of the solution. 1 ml of the remaining solution was added to 1 ml of In-Tl solution and 8 ml of 2 % nitric acid to be run on the ICP-MS (mass spectrometry) system for trace elements by Dr. Iain McDonald. The systems used were a JY-Horiba Ultima 2 ICP-OES and a Thermo Elemental X7 series ICP-MS.

A3.4. Radiogenic isotopes

A3.4.1. Sample selection and prior preparation

There was a relatively limited allocation of analytical resources from NIGL, Nottingham, amounting to the analysis of Nd and Hf isotopes from 28 samples. Because of the degree of alteration discovered in these samples, it was decided that Pb or Sr isotope analysis would not add significantly to the interpretation of the origin of the rocks in question. Pb analysis was undertaken, affecting the methods used to extract Nd and Hf for analysis, but the results will not be reported here. The samples chosen were carefully selected to represent a broad cross-section of the rocks from Tobago and San Souci. Two samples were selected from the Aves Ridge and none from La Désirade as these were regarded as relatively minor components of the project. Samples were selected from those found to be as fresh as possible out of those already analysed and the fine 'wet' powders (see Appendix 3.3) were taken to the NERC Isotope Geosciences Laboratory (NIGL) at Keyworth, Nottingham.

A3.4.2. Preparation for isotopic analysis

Preparation methods are adapted from Minifie (2010) and incorporate the detailed analysis methods of Royse et al. (1998) and Kempton & McGill (2002) for Nd isotope analysis and Kempton et al. (2001) for Hf isotope analysis. Preparation was initially carried out by the author, with supervision from Dr. Neil Boulton and Dr. Ian Millar.

Initial preparation and dissolution of material: For each sample approximately 0.2 g of sample was measured into clean Savillex beakers. 1 ml of clean 16M nitric acid (HNO_3) and then 4 ml of 29M hydrofluoric acid (HF) was added to the beakers which were kept on a hotplate at ~60°C overnight. After cooling, the beakers were evaporated to dryness. The next cycle was the addition of 2 ml of 16M HNO_3 and evaporation to dryness. This was followed by the addition of 2 ml of 6M hydrochloric acid (HCl) and then the beakers were sealed and kept on the hotplate around 30 minutes before

evaporation to dryness. 1 ml of 1M hydrobromic acid (HBr) was added and the beakers sealed.

Nd separation: Samples were prepared for Pb isotope analysis first although the results are not reported here. The Pb fraction was separated from the samples using anion exchange columns. The columns are polypropylene tubes with a polyethylene tip. The columns are set up on a rotating holder with beakers for waste acids beneath. One column volume (CV) of 6M HCl was added to each column and drained through. Five drops of Dowex AG1-X8 resin was drained into the columns and washed with 1CV of 6M HCl followed by washing with 1CV of de-ionised water. This washing process was repeated. Finally, 1M HBr was run through the columns. The waste beakers were then replaced with clean Savillex beakers for the next part of the process.

The samples were transferred by clean pipette to the columns. 0.5CV of 1M HBr was added to the columns, followed by 0.75CV of 1M HBr. Once the acid had drained through, the Nd-bearing part of the sample solution should have passed into the Savillex beakers at the base of the columns. The Pb-bearing fractions remained in the columns, and were further processed for Pb collection.

In a separate processing area, quartz columns were set up which were part-filled with S-X8 biobeads coated in bis-diethylhexyl hydrogen phosphate (HDEHP). The Savillex beakers with the Nd fraction had 2 ml of 16M HNO3 added. These Nd-bearing solutions were evaporated to dryness on a hotplate followed by the addition of 2 ml of 2.5M HCl. The beakers were then left overnight cold. The next day, the beaker solutions were transferred to centrifuge tubes and centrifuged for 3 minutes at 3000 rpm, and 1.5 ml of the centrifuged solution was added to the quartz columns with the biobeads ready for the process of cleaning and Nd separation.

Firstly, 10 ml of 6M HCl was washed through the quartz columns and collected in a fresh set of Savillex beakers and evaporated to dryness. 1 ml of 0.25M HCl was added to these beakers. After dissolution had taken place, 0.5 ml of each solution was taken up by clean pipette, loaded into the quartz columns and allowed to drain through the resin, leaving behind the Nd-bearing fraction. Three sets of acids were then drained

through the columns. The first two contained 0.5 ml of 0.25M HCl and the third contained 6.4 ml of the same acid. In order to collect the Nd-bearing fraction, clean Savillex beakers were placed underneath the columns and 3.5 ml of 0.3M HCl was passed through the columns and collected. 2 µl of chlorophosphonazo III was added to each solution and the solutions were then evaporated to dryness.

Analysis of Nd isotopes was undertaken from this stage on by Dr. Ian Millar and the samples were run on a Thermo-Electron Triton I thermal ionisation mass spectrometer at NIGL.

Hf separation: In this instance, fresh samples were firstly placed in Savillex beakers. 2 ml of 16M HNO_3 was added, followed by 10 ml of 29M HF. Samples were left on a ~120°C hotplate overnight. After cooling, solutions were evaporated to dryness. 4 ml of 4M HF was and these were sealed, shaken and then placed in centrifuge tubes and centrifuged for 90 minutes at 4000 rpm, before repeating. Finally, 2 ml of 4N Hf was added to the residues and the centrifuge process was repeated.

Anion exchange columns, part-filled with BioRad anion exchange resin AG1-X8, were used to then separated the Hf. The samples were placed into the columns and unwanted elements washed using the following procedure. 6 ml of 4N HF, 200 ml of 4N HF and 30 ml of 4N HF were washed through in turn. Clean Savillex beakers were then placed under the columns and 60 ml of 1N HF/1N HCl was washed through each column. 30µl of 36.6N sulphuric acid (H_2SO_4) was added to each beaker and the solutions evaporated to dryness. Next, 1 ml of 0.52N H_2SO_4/5 % H_2O_2 was added to each sample and, on dissolution the solutions were added to a second set of columns. The Savillex beakers were washed in the same acid mix and placed beneath the new columns. The same acid solution was then washed through the columns followed by another 12 ml of the solution. In order to strip out the Hf fraction, 13 ml of 1N HF-2N HCl was washed through each column. The final Hf-bearing solutions were evaporated to dryness on a hotplate.

Analysis of Hf isotopes was undertaken from this stage on by Dr. Ian Millar and the samples were run initially on a VG Plasma P54 multi-collector ICP-MS at NIGL.

The final sample run (see results in Appendix 6) took place on a Thermo Neptune mass spectrometer.

A3.4.3. Correction of isotopic data

The igneous rocks analysed for their isotope ratios in this thesis are no older than ~130 Ma. It was discovered by Thompson et al. (2003) that time-integrated changes in Nd isotopes over approximately 90 Ma amount to <0.5 epsilon units. As noted by Patchett and Tatsumoto (1980), the variation in the Hf isotopic composition of rocks is nearly double that of Nd isotopes, partly because of the disparate partition coefficients of Lu and Hf and the relatively shorter half-like of ^{176}Lu compared to ^{147}Sm. Therefore, time-integrated changes in Nd isotopes would be expected to be <0.25 epsilon units. For those reasons, and because much of the work in this thesis is qualitative, it was decided that fields for present-day MORB would be plotted on isotopic diagrams without correction to the age of the analysed rocks.

Nevertheless, the data themselves are corrected to allow for radiometric decay since their time of formation and for comparison with rocks of a similar age from around the Caribbean, notably the Caribbean Oceanic Plateau for which age-corrected results are available from a variety of sources. The correction is achieved for Nd and Hf isotope systems by a series of steps conveniently summarised by Minifie (2010). Minifie (2010, Table D.1) gives the list of reference values used (Table A3.2 below), and the equations below.

Table A3.2. Values used in correcting the isotopic data (taken from Minifie, 2010).

Nd isotopes	Value	Reference
$(^{142}Nd/^{144}Nd)^{P}_{CHUR}$	1.141827	Wasserburg et al. (1981)
$(^{143}Nd/^{144}Nd)^{P}_{CHUR}$	0.512638	DePaolo & Wasserburg (1976)
$(^{145}Nd/^{144}Nd)^{P}_{CHUR}$	0.348417	Wasserburg et al. (1981)
$(^{146}Nd/^{144}Nd)^{P}_{CHUR}$	0.7219	Wasserburg et al. (1981)
$(^{148}Nd/^{144}Nd)^{P}_{CHUR}$	0.241578	Wasserburg et al. (1981)
$(^{150}Nd/^{144}Nd)^{P}_{CHUR}$	0.236418	Wasserburg et al. (1981)
$(^{147}Sm/^{144}Nd)^{P}_{CHUR}$	0.1967	DePaolo & Wasserburg (1976)
^{142}Nd (amu)	141.907719	de Laeter et al. (2003)
^{143}Nd (amu)	142.909810	de Laeter et al. (2003)

^{144}Nd (amu)	143.910083	de Laeter et al. (2003)
^{145}Nd (amu)	144.912569	de Laeter et al. (2003)
^{146}Nd (amu)	145.913113	de Laeter et al. (2003)
^{148}Nd (amu)	147.916889	de Laeter et al. (2003)
^{150}Nd (amu)	149.920887	de Laeter et al. (2003)
Sm (amu)	150.36	Wieser (2006)
^{147}Sm (% abundance)	14.99	Rosman & Taylor (1998)
$\lambda\ ^{147}$Sm (y^{-1})	6.54×10^{-12}	Lugmair & Marti (1978)
Hf isotopes		
$(^{174}Hf/^{177}Hf)^{P}_{CHUR}$	0.008659	Thirlwall & Anczkiewicz (2004)
$(^{176}Hf/^{177}Hf)^{P}_{CHUR}$	0.282772	Blichert-Toft & Albarede (1997)
$(^{178}Hf/^{177}Hf)^{P}_{CHUR}$	1.46734	Thirlwall & Anczkiewicz (2004)
$(^{179}Hf/^{177}Hf)^{P}_{CHUR}$	0.7325	Thirlwall & Anczkiewicz (2004)
$(^{180}Hf/^{177}Hf)^{P}_{CHUR}$	1.88676	Thirlwall & Anczkiewicz (2004)
$(^{176}Lu/^{177}Hf)^{P}_{CHUR}$	0.0332	Blichert-Toft & Albarede (1997)
^{174}Hf (amu)	173.940042	de Laeter et al. (2003)
^{176}Hf (amu)	175.941403	de Laeter et al. (2003)
^{177}Hf (amu)	176.9432204	de Laeter et al. (2003)
^{178}Hf (amu)	177.9436981	de Laeter et al. (2003)
^{179}Hf (amu)	178.9458154	de Laeter et al. (2003)
^{180}Hf (amu)	179.9465488	de Laeter et al. (2003)
Lu (amu)	174.9668	Wieser (2006)
^{176}Lu (% abundance)	2.59	Rosman & Taylor (1998)
$\lambda\ ^{176}$Lu (y^{-1})	1.865×10^{-11}	Scherer et al. (2001)

A3.4.4. Correction of Nd isotopes

For correction of Nd isotopes, the following equations are used. The sum of all Nd isotope ratios (with ^{144}Nd as the denominator) and the percentage of each isotope of Nd ($^{142\text{-}146,\ 148,\ 150}$Nd) are first calculated using equations A3.1-8 below. $\sum$ Nd is the sum of the Nd isotope ratios, $_{m}$ = a measured ratio, $_{CHUR}$ = ratio of the chondritic uniform reservoir, ^{P} = present day. $^{144}Nd/^{144}Nd = 1$.

Equation A3.1

$$\sum Nd = \left(\frac{^{142}Nd}{^{144}Nd}\right)^{P}_{CHUR} + \left(\frac{^{143}Nd}{^{144}Nd}\right)_{m} + \frac{^{144}Nd}{^{144}Nd} + \left(\frac{^{145}Nd}{^{144}Nd}\right)^{P}_{CHUR} + \left(\frac{^{146}Nd}{^{144}Nd}\right)^{P}_{CHUR} + \left(\frac{^{148}Nd}{^{144}Nd}\right)^{P}_{CHUR} + \left(\frac{^{150}Nd}{^{144}Nd}\right)^{P}_{CHUR}$$

Equation A3.2

$$\%^{142}Nd = \frac{100}{\sum Nd} \times \left(\frac{^{142}Nd}{^{144}Nd}\right)^{P}_{CHUR}$$

Equation A3.3

$$\%^{143}Nd = \frac{100}{\sum Nd} \times \left(\frac{^{143}Nd}{^{144}Nd} \right)_m$$

Equation A3.4

$$\%^{144}Nd = \frac{100}{\sum Nd} \times \frac{^{144}Nd}{^{144}Nd}$$

Equation A3.5

$$\%^{145}Nd = \frac{100}{\sum Nd} \times \left(\frac{^{145}Nd}{^{144}Nd} \right)^P_{CHUR}$$

Equation A3.6

$$\%^{146}Nd = \frac{100}{\sum Nd} \times \left(\frac{^{146}Nd}{^{144}Nd} \right)^P_{CHUR}$$

Equation A3.7

$$\%^{148}Nd = \frac{100}{\sum Nd} \times \left(\frac{^{148}Nd}{^{144}Nd} \right)^P_{CHUR}$$

Equation A3.8

$$\%^{150}Nd = \frac{100}{\sum Nd} \times \left(\frac{^{150}Nd}{^{144}Nd} \right)^P_{CHUR}$$

Using the percentages from the equations above, the atomic mass of Nd in atomic mass units (a.m.u.) for each sample is calculated using equation A3.9.

Equation A3.9

$$Nd\ (amu) = \left(\frac{\%^{142}Nd}{100} \times {}^{142}Nd\,(amu) \right) + \left(\frac{\%^{143}Nd}{100} \times {}^{143}Nd(amu) \right) +$$

$$\left(\frac{\%^{144}Nd}{100} \times {}^{144}Nd\,(amu) \right) + \left(\frac{\%^{145}Nd}{100} \times {}^{145}Nd(amu) \right) + \left(\frac{\%^{146}Nd}{100} \times {}^{146}Nd\,(amu) \right) +$$

$$\left(\frac{\%^{148}Nd}{100}\times{}^{148}Nd\,(amu)\right)+\left(\frac{\%^{150}Nd}{100}\times{}^{150}Nd(amu)\right)$$

The atomic mass of Nd is then used in equation A3.10 to calculate the $^{147}Sm/^{144}Nd$ ratio. Sm and Nd are measured concentrations from the ICP-MS analysis. The numbers 150.36 and 14.99 are the atomic mass of Sm and the percentage abundance of the ^{147}Sm isotope.

Equation A3.10

$$\frac{^{147}Sm}{^{144}Nd}=\frac{Sm}{Nd}\times\frac{Nd(amu)}{150.36}\times\frac{14.99}{\%^{144}Nd}$$

The initial Nd isotope ratio, Nd_i, is calculated using equation A3.11. t is the age of the rock in years, λ is the decay constant for ^{147}Sm.

Equation A3.11

$$\left(\frac{^{143}Nd}{^{144}Nd}\right)_i=\left(\frac{^{143}Nd}{^{144}Nd}\right)_m-\frac{^{147}Sm}{^{144}Nd}\left(e^{\lambda t}-1\right)$$

The last operation that can be done is to convert the initial Nd isotope ratio into epsilon units, which is achieved by equation A3.12. The $^{143}Nd/^{144}Nd$ isotope ratio of CHUR at the time t (years) is given using equation A3.11 with present day $^{143}Nd/^{144}Nd_{CHUR} = 0.512638$ and $^{147}Sm/^{144}Nd_{CHUR} = 0.1967$ (DePaolo and Wasserburg, 1976).

Equation 3.12

$$\varepsilon Nd_i=\left(\frac{\left(\frac{^{143}Nd}{^{144}Nd}\right)_i}{\left(\frac{^{143}Nd}{^{144}Nd}\right)^t_{CHUR}}-1\right)\times 10000$$

A3.4.5. Correction of Hf isotopes

For correction of Hf isotopes, the following equations are used. The sum of all Nd isotope ratios (with ^{177}Hf as the denominator) and the percentage of each isotope of Hf are first calculated using equations A3.13-19 below. $\sum$ Hf is the sum of the Hf

isotope ratios, $_m$ = a measured ratio, $_{CHUR}$ = ratio of the chondritic uniform reservoir, ^{P} = present day. $^{177}Hf/^{177}Hf = 1$.

Equation A3.13

$$\Sigma Hf = \left(\frac{^{174}Hf}{^{177}Hf}\right)^{P}_{CHUR} + \left(\frac{^{176}Hf}{^{177}Hf}\right)_{m} + \frac{^{177}Hf}{^{177}Hf} + \left(\frac{^{178}Hf}{^{177}Hf}\right)^{P}_{CHUR} + \left(\frac{^{179}Hf}{^{177}Hf}\right)^{P}_{CHUR} + \left(\frac{^{180}Hf}{^{177}Hf}\right)^{P}_{CHUR}$$

Equation A3.14

$$\%^{174}Hf = \frac{100}{\Sigma Hf} \times \left(\frac{^{174}Hf}{^{177}Hf}\right)^{P}_{CHUR}$$

Equation A3.15

$$\%^{176}Hf = \frac{100}{\Sigma Hf} \times \left(\frac{^{176}Hf}{^{177}Hf}\right)_{m}$$

Equation A3.16

$$\%^{177}Hf = \frac{100}{\Sigma Hf} \times \frac{^{177}Hf}{^{177}Hf}$$

Equation A3.17

$$\%^{178}Hf = \frac{100}{\Sigma Hf} \times \left(\frac{^{178}Hf}{^{177}Hf}\right)^{P}_{CHUR}$$

Equation A3.18

$$\%^{179}Hf = \frac{100}{\Sigma Hf} \times \left(\frac{^{179}Hf}{^{177}Hf}\right)^{P}_{CHUR}$$

Equation A3.19

$$\%^{180}Hf = \frac{100}{\Sigma Hf} \times \left(\frac{^{180}Hf}{^{177}Hf}\right)^{P}_{CHUR}$$

Using the percentages calculated from the equations above, the atomic mass of Hf in atomic mass units (a.m.u.) for each sample is calculated using equation A3.20.

Equation A3.20

$$Hf\ (amu) = \left(\frac{\%^{174}Hf}{100} \times {}^{174}Hf(amu)\right) + \left(\frac{\%^{176}Hf}{100} \times {}^{176}Hf(amu)\right) +$$

$$\left(\frac{\%^{177}Hf}{100} \times {}^{177}Hf(amu)\right) + \left(\frac{\%^{178}Hf}{100} \times {}^{178}Hf(amu)\right) + \left(\frac{\%^{179}Hf}{100} \times {}^{179}Hf(amu)\right) +$$

$$\left(\frac{\%^{180}Hf}{100} \times {}^{180}Hf(amu)\right)$$

The atomic mass of Hf is then used in equation A3.21 to calculate the $^{176}Lu/^{177}Hf$ ratio. Lu and Hf are measured concentrations from the ICP-MS analysis. The numbers 150.36 and 14.99 are the atomic mass of Lu and the percentage abundance of the ^{176}Lu isotope.

Equation A3.21

$$\frac{{}^{176}Lu}{{}^{177}Hf} = \frac{Lu}{Hf} \times \frac{Hf(amu)}{174.9668} \times \frac{2.59}{\%^{176}Hf}$$

The initial Hf isotope ratio, Hf_i, is calculated using equation A3.22. t is the age of the rock in years, λ is the decay constant for ^{176}Lu.

Equation A3.22

$$\left(\frac{{}^{176}Hf}{{}^{177}Hf}\right)_i = \left(\frac{{}^{176}Hf}{{}^{177}Hf}\right)_m - \frac{{}^{176}Lu}{{}^{177}Hf}\left(e^{\lambda t} - 1\right)$$

The last operation that can be done is to convert the initial Hf isotope ratio into epsilon units, which is achieved by equation A3.23. The $^{176}Hf/^{177}Hf$ isotope ratio of CHUR at the time t (years) is given using equation A3.21 with present day $^{176}Hf/^{177}Hf_{CHUR} = 0.282772$ and $^{176}Lu/^{177}Hf_{CHUR} = 0.0332$ (Blichert-Toft and Albarede, 1997).

Equation A3.23

$$\varepsilon Hf_i = \left(\frac{\left(\frac{^{176}Hf}{^{177}Hf} \right)_i}{\left(\frac{^{176}Hf}{^{177}Hf} \right)^t_{CHUR}} - 1 \right) \times 10000$$

APPENDIX FOUR: ANALYTICAL ERROR CALCULATIONS FOR ICP-OES/MS RESULTS

A consideration of the precision, accuracy and limit of detection for each analysed element, and a comment on errors resulting from the methodology

A4.1. Introduction

In this appendix, the results of repeat analyses of the major and trace element content of internationally certified standards are presented. These results are used to investigate the accuracy, precision and limits of elemental detection for each element.

Each sample batch included blank runs containing only flux, acids and Rh spike; the results of blank analysis were not presented but are reported by Iain McDonald to be satisfactory with the exception of Pb (see below). Also run were powders of internationally certified standard basalts JB-1A (7 runs) and BIR-1 (7 runs) and granite NIM-G (8 runs). JB-1A is basalt from Nagasaki, BIR-1 is Icelandic basalt and NIM-G is granite from the Bushveld Complex, South Africa. These rocks are supplied as 'wet' powders and were run through loss-on-ignition, fusion and analysis as per the methods in Appendix 3. Major and trace element results are presented in Tables A4.1, 4.3 and 4.5. Accuracy and precision information for each standard is analysed in Tables 4.2, 4.4 and 4.6. The precision and limit of detection to be applied to the Caribbean samples is summarised in Table 4.7.

A4.2. Analysis of errors

A4.2.1. Accuracy of the major and trace element data

The mean and standard deviation (σ) of the runs of each standard were taken for each analysed element (Tables 4.2, 4.4 and 4.6). The certified values for each element were taken from the GEO-REM database of the Max Plank Institute, Germany which is hosted at: http://*georem.mpch-mainz.gwdg.de*. Where the certified values lay outside of 2σ difference from the mean of the analyses, the accuracy of analysis of the element in question is considered suspect. It was found that the vast majority of results for each element fell within 2σ of the certified value. Those elements that did not fall within 2σ were: Cr (MS only), Ta, Th, Ho and Tm [in JB-1A]; Tb, Ho and Er [in NIM-G] and P_2O_5, Sr (OES only) and Zr (MS only) [in BIR-1]. In most cases these discrepancies are not systematic, except Ho, which was slightly under-analysed in both JB-1A and NIM-G. An alternative method to check the accuracy is a comparison of the percentage by which an individual analysis differs from the certified value. The average of these differences for each standard are recorded on the final column of tables 4.2, 4.4 and 4.6. By and large, the major and trace element data can be accepted as accurate in this thesis.

A4.2.2. Precision

One measure of precision is the relative standard deviation; is the ratio of the standard deviation to the mean expressed as a percentage. In this case, where the relative standard deviation is >5% then the precision of the results for that element is suspect. The relative standard deviations on Tables 4.2, 4.4 and 4.6 show that low concentrations of a given element in the standard results in high relative standard deviations. Nevertheless, where the element in question is present in concentrations significantly higher than the limit of detection, the relative standard deviation is typically <5 % and the results can therefore be considered precise. The lowest relative deviations for each element are presented in Table 4.7 and show that only P_2O_5, Ni, Cu, Rb and Pb have quite high deviations. In mafic rocks, P_2O_5 and Cu are not usually considered in analysis of the mantle source and crustal input. Rb and Pb are often

mobilised (Seewald & Seyfried, 1990), which leaves Ni, a good indicator of mantle provenance, as the only element where this relative deviation might be a slight concern.

The limit of detection is represented by 3σ; 99% of analyses of an element in a standard fall within 3 standard deviations of the mean; any analysis outside of that limit is not considered precise. The limits of detection presented in Table 4.7 are mostly very low and therefore present no problem for analysis of the Caribbean rocks, with the possible exception of ultramafic rocks generally, P_2O_5 in mafic rocks, Cr and Ni in crustally-derived rocks and Y and Yb in rocks with a residual garnet signature. Where analyses came out lower than the limit of detection in Appendix 5, those analyses were deleted and marked as below detection.

A4.2.3. Further findings regarding the accuracy of results

There are discrepancies between the trace element results for those elements analysed on both the ICP-OES and ICP-MS systems, which are V, Cr, Co, Ni, Cu, Sr, Y, Zr and Ba. V, Cr, Co, Cu, Y and Zr had higher relative standard deviations when analysed by ICP-OES compared to ICP-MS. Other elements had similar or slightly better results with the ICP-OES system. In Appendix 5, therefore, all trace elements results are those produced by the ICP-MS system with the exception of Sc, which was only analysed by ICP-OES.

Sc is analysed solely under ICP-OES because the ionised gases used in the ICP-MS facility can combine to form compounds with the same mass as Sc, resulting in a very high background count effect which cannot be quantified properly. Similarly, Y has been known to suffer this effect, resulting in significant positive Y anomalies on trace element plots. This does not appear to have happened, with analyses of Y under both the ICP-OES and ICP-MS being very similar.

Pb is relatively imprecise no matter which standard is run, with a minimum relative standard deviation of 20 %. This is an important consideration in this thesis because: (a) Pb is often used as a proxy for crustal input into mantle-derived rocks and (b) the total concentration of Pb is required in order to calculate initial (age-corrected) ratios for any Pb isotope work. Pb is known to also be mobile during alteration

processes (Seewald & Seyfried, 1990), so its use is limited for these Caribbean rocks in any case. It is not certain what causes the fluxy-fusion method to produce spurious Pb results. As the standards come ready-milled, contamination cannot be the result of sawing, crushing or milling processes at Cardiff University. The spurious Pb may be related to contamination within the lithium metaborate flux, suggested by high blank readings (I. McDonald, pers. comm.).

Consideration of errors would be improved by running an in-house standard in each batch; a homogeneous rock from the Caribbean sample collection which has undergone the same sawing, crushing and milling process as the other samples. Further improvement could be made by running at least one standard a statistically significant number of times (20) and considering further standards which are more chemically similar to the analysed Caribbean samples.

Table A4.1. Repeat analyses of JB-1A (basalt).

	JB-1A runs 1-7						
Majors by	ICP-OES						
SiO_2	52.32	52.68	52.10	52.61	52.31	53.18	52.74
TiO_2	1.28	1.29	1.25	1.29	1.30	1.29	1.29
Al_2O_3	14.01	14.56	14.34	14.50	14.84	14.63	14.49
Fe_2O_3	9.10	9.15	9.13	9.11	8.66	9.01	9.10
MnO	0.14	0.14	0.14	0.14	0.14	0.15	0.15
MgO	7.92	7.91	8.30	7.65	7.94	7.86	8.11
CaO	9.54	9.42	9.54	9.17	9.20	9.29	9.55
Na_2O	2.68	2.71	2.67	2.77	2.69	2.78	2.76
K_2O	1.32	1.33	1.39	1.42	1.42	1.40	1.26
P_2O_5	0.26	0.27	0.24	0.27	0.26	0.25	0.23
Traces by	ICP-OES						
Sc	27.6	27.9	27.8	27.7	26.1	24.9	27.7
V	206.3	199.0	221.3	206.4			252.5
Cr	422.6	416.8	422.7	411.3	401.7	389.7	420.4
Co	40.2	39.5	38.3	36.2	35.3	34.9	40.7
Ni	135.3	136.1	137.2	135.2	126.3	124.3	134.3
Cu	54.2	60.0	89.1	60.1	67.5	46.3	60.8
Sr	445.7	446.5	436.8	450.6	454.4	436.0	448.3
Y	24.0	24.0	24.3	24.0	23.4	24.4	23.4
Zr	140.7	147.6	143.9	142.8	151.8	149.0	140.6
Ba	492.4	508.1	502.4	501.0	493.2	484.9	493.8
Traces by	ICP-MS						
V	201.9	197.1	214.4	210.8	205.0	199.6	203.1
Cr	425.1	431.1	421.3	429.7	418.0	411.3	431.1
Co	38.9	38.8	36.6	38.7	36.8	37.3	38.0
Ni	197.2	140.9	145.2	137.1	138.9	129.3	133.1
Cu	57.6	58.7	60.7	56.4	56.7	53.3	57.9
Ga	17.6	18.3	17.6	18.0	17.9	17.2	18.6
Rb	43.5	40.3	39.9	36.9	41.5	33.9	41.3
Sr	441.4	452.0	439.6	447.9	441.3	436.5	442.9
Y	24.0	24.6	24.2	25.1	24.0	23.8	24.6
Zr	142.5	143.6	146.3	146.0	148.4	145.1	142.2
Nb	27.98	28.02	27.24	28.06	27.57	26.88	26.27
Ba	482.5	508.2	501.6	487.9	490.3	479.2	511.1
Hf	3.41	3.52	3.43	3.44	3.52	3.26	3.44
Ta	1.69	1.71	1.71	1.68	1.70	1.67	1.70
Pb	6.24	12.92	8.09	5.42	7.12	6.87	7.22
Th	8.94	9.04	8.84	8.77	8.67	8.67	8.95
U	1.59	1.72	1.67	1.68	1.68	1.59	1.62
REEs by	ICP-MS						
La	37.50	38.87	37.41	37.62	37.19	36.02	38.49
Ce	63.95	66.78	63.19	65.86	66.39	65.21	67.18
Pr	7.11	7.20	7.12	7.06	7.06	7.09	7.61
Nd	25.57	27.40	25.56	25.30	26.43	25.68	25.63
Sm	4.97	5.30	4.99	5.03	5.07	4.96	5.31
Eu	1.48	1.65	1.47	1.49	1.48	1.46	1.58
Gd	4.58	4.86	4.71	4.64	4.67	4.69	5.69
Tb	0.67	0.71	0.68	0.71	0.69	0.66	0.73
Dy	3.93	4.26	3.97	4.10	4.05	3.90	4.34
Ho	0.72	0.73	0.72	0.74	0.74	0.72	0.78
Er	2.07	2.20	2.08	2.08	2.10	2.03	2.26
Tm	0.32	0.33	0.32	0.33	0.32	0.31	0.34
Yb	2.07	2.12	2.06	2.07	2.10	1.98	2.22
Lu	0.32	0.33	0.32	0.32	0.32	0.31	0.34

Table A4.2. Error analysis of repeat runs of JB-1A. See text for details. *Does the certified value lie within 2 standard deviations of the mean of the repeat runs? **What is the mean percentage difference between the repeat runs and the certified value?

JB-1A		Mean	σ	Relative σ	2σ	3σ	Certified	Within 2σ?	%
Majors by	OES	n = 7	± % or ppm	± % (precision)	± % or ppm (precision)	(detecti-on limit)	% or ppm	(accuracy)*	differ-ence**
SiO_2		52.58	0.33	0.63	0.66	0.99	52.41	Y	0.55
TiO_2		1.29	0.02	1.34	0.03	0.05	1.28	Y	1.13
Al_2O_3		14.44	0.26	1.81	0.52	0.78	14.45	Y	1.37
Fe_2O_3		9.03	0.16	1.76	0.32	0.48	9.05	Y	1.11
MnO		0.15	0.00	1.30	0.00	0.01	0.148	Y	1.74
MgO		7.92	0.22	2.74	0.43	0.65	7.83	Y	2.28
CaO		9.37	0.16	1.72	0.32	0.48	9.31	Y	1.51
Na_2O		2.73	0.05	1.67	0.09	0.14	2.73	Y	1.47
K_2O		1.36	0.05	3.97	0.11	0.16	1.4	Y	3.39
P_2O_5		0.26	0.01	5.80	0.03	0.04	0.26	Y	4.46
Traces by	OES								
Sc		27.16	1.08	3.99	2.17	3.25	29	Y	6.33
V		214.53	20.15	9.39	40.30	60.44	203	Y	6.56
Cr		406.17	20.52	5.05	41.05	61.57	392	Y	5.54
Co		38.28	2.50	6.54	5.01	7.51	38.1	Y	5.66
Ni		133.50	5.34	4.00	10.67	16.01	140	Y	4.64
Cu		62.19	12.44	20.00	24.88	37.32	56.7	Y	15.36
Sr		444.25	7.22	1.63	14.44	21.66	444	Y	1.38
Y		23.93	0.36	1.51	0.72	1.08	24	Y	1.04
Zr		145.23	4.01	2.76	8.03	12.04	142	Y	2.76
Ba		498.03	8.31	1.67	16.61	24.92	489	Y	2.06
Traces by	MS								
V		204.35	5.71	2.79	11.41	17.12	203	Y	1.95
Cr		421.89	9.05	2.14	18.10	27.15	392	N	7.62
Co		37.85	0.89	2.36	1.79	2.68	38.1	Y	2.01
Ni		144.67	21.75	15.03	43.50	65.25	140	Y	7.96
Cu		57.69	2.34	4.05	4.68	7.02	56.7	Y	3.37
Ga		17.93	0.44	2.46	0.88	1.32	18	Y	1.91
Rb		39.82	3.02	7.57	6.03	9.05	39	Y	6.70
Sr		444.12	5.66	1.27	11.32	16.98	444	Y	1.06
Y		24.33	0.43	1.75	0.85	1.28	24	Y	1.59
Zr		145.12	2.20	1.52	4.40	6.60	142	Y	2.19
Nb		27.45	0.63	2.29	1.26	1.89	28	Y	2.04
Ba		495.09	11.81	2.39	23.62	35.44	489	Y	2.13
Hf		3.44	0.09	2.50	0.17	0.26	3.5	Y	2.01
Ta		1.69	0.03	1.49	0.05	0.08	1.8	N	6.32
Pb		7.67	2.27	29.59	4.54	6.81	6.3	Y	25.44
Th		8.86	0.15	1.66	0.29	0.44	9.2	N	3.68
U		1.64	0.05	2.94	0.10	0.14	1.6	Y	2.97
REEs by	MS								
La		37.73	0.95	2.51	1.90	2.84	38	Y	2.10
Ce		65.85	1.67	2.54	3.35	5.02	66	Y	1.96
Pr		7.20	0.20	2.75	0.40	0.59	7.2	Y	2.06
Nd		25.98	0.69	2.64	1.37	2.06	26.3	Y	2.40
Sm		5.09	0.14	2.76	0.28	0.42	5.1	Y	2.22
Eu		1.51	0.07	4.41	0.13	0.20	1.46	Y	3.33
Gd		4.84	0.36	7.43	0.72	1.08	4.7	Y	4.05
Tb		0.69	0.03	3.69	0.05	0.08	0.72	Y	4.66
Dy		4.08	0.16	3.81	0.31	0.47	4.1	Y	3.01
Ho		0.74	0.02	2.87	0.04	0.06	0.83	N	11.03
Er		2.11	0.08	3.57	0.15	0.23	2.2	Y	4.70
Tm		0.33	0.01	2.87	0.02	0.03	0.3	Y	8.57
Yb		2.08	0.07	3.41	0.14	0.21	2.16	Y	4.37
Lu		0.32	0.01	3.42	0.02	0.03	0.31	Y	3.74

Table A4.3. Repeat analyses of NIM-G (granite).

	NIM-G runs 1-8							
Majors by	ICP-OES							
SiO_2	76.47	76.27	75.43	76.24	76.79	76.73	75.60	76.21
TiO_2	0.09	0.09	0.09	0.09	0.08	0.08	0.09	0.09
Al_2O_3	11.93	11.84	11.85	11.98	12.30	11.98	12.22	12.01
Fe_2O_3	2.01	1.98	2.06	2.00	1.99	1.98	1.97	2.03
MnO	0.02	0.02	0.02	0.02	0.02	0.02	0.02	0.02
MgO	0.02	0.02	0.17	0.08	0.04	0.04	0.07	0.04
CaO	0.77	0.77	0.82	0.69	0.71	0.70	0.80	0.78
Na_2O	3.24	3.29	3.31	3.38	3.39	3.46	3.47	3.37
K_2O	4.97	4.80	4.95	5.20	5.06	4.88	4.95	4.91
P_2O_5	0.00	0.00	0.02	0.01	0.00	0.00	0.00	0.01
Traces by	ICP-OES							
Sc	0.1	0.4	0.9	0.1	0.2	0.2	0.2	0.2
V	4.1	3.0	2.3	9.2			5.0	0.8
Cr	11.8	22.3	3.7	11.3	7.5	8.8	14.4	14.2
Co	0.5	2.5	0.1	4.5	0.5	1.1	1.2	2.3
Ni	19.6	15.0	7.3	13.9	12.0	5.7	11.1	11.4
Cu	13.4	17.1	16.7	6.2	22.7	13.1	16.9	11.6
Sr	9.0	9.8	11.8	4.5	4.6	4.8	12.8	11.4
Y	145.5	144.8	139.9	147.7	148.5	143.3	144.0	150.8
Zr	324.0	283.2	289.6	313.6	309.4	356.6	296.1	301.1
Ba	109.0	114.3	122.6	117.0	105.4	100.0	106.8	115.3
Traces by	ICP-MS							
V	4.3	2.6	5.2	0.4	3.6	3.7	2.2	0.8
Cr	13.5	11.8	7.5	10.0	7.4	6.5	19.7	9.9
Co	3.8	3.4	1.2	0.7	0.4	0.4	0.5	2.6
Ni	29.1	15.1	8.9	6.0	8.7	6.0	16.6	8.3
Cu	15.8	19.6	30.9	17.6	37.8	37.3	17.3	16.2
Ga	29.5	27.5	27.7	26.7	26.7	26.2	28.1	29.5
Rb	400.3	324.6	308.9	302.4	297.1	276.0	313.7	317.2
Sr	12.8	8.8	8.5	5.8	7.6	7.1	9.0	12.1
Y	145.0	141.9	142.4	138.8	139.4	142.5	140.7	141.5
Zr	310.9	289.0	283.9	307.4	295.3	310.1	297.3	295.6
Nb	51.91	52.82	54.07	43.66	51.52	51.10	52.01	52.34
Ba	114.7	128.1	122.6	108.3	109.7	109.1	115.2	118.3
Hf	12.08	11.60	9.97	11.66	11.54	11.64	11.18	11.85
Ta	4.56	4.33	4.38	4.03	4.21	4.17	3.98	4.30
Pb	35.17	27.84	31.29	20.42	27.82	22.02	37.84	29.53
Th	50.52	48.71	45.44	48.40	41.69	43.82	47.09	48.29
U	17.08	16.04	16.72	15.56	15.50	14.97	15.72	16.13
REEs by	ICP-MS							
La	114.38	106.48	106.45	107.09	104.28	103.80	99.33	109.68
Ce	206.47	186.46	189.12	193.05	195.44	189.47	190.25	208.11
Pr	22.01	19.53	20.74	18.87	19.10	17.99	20.15	21.85
Nd	71.24	69.74	67.20	71.54	64.81	61.72	61.41	68.70
Sm	14.57	14.98	13.80	14.83	12.96	12.43	13.67	14.10
Eu	0.33	0.34	0.32	0.33	0.30	0.29	0.41	0.61
Gd	14.34	14.14	13.90	13.30	13.29	13.59	15.30	14.03
Tb	2.59	2.69	2.46	2.48	2.37	2.31	2.39	2.48
Dy	18.03	17.28	17.04	15.98	16.20	16.32	16.75	17.15
Ho	3.77	3.64	3.47	3.36	3.43	3.25	3.49	3.54
Er	12.45	11.73	11.59	10.82	11.01	10.95	11.25	11.24
Tm	2.13	2.02	2.01	1.92	1.88	1.88	1.93	1.96
Yb	14.33	13.79	13.31	13.53	12.82	12.89	12.94	12.57
Lu	2.14	2.14	2.03	1.95	1.94	1.92	1.98	1.95

Table A4.4. Error analysis of repeat runs of NIM-G. See text for details.

NIM-G		Mean	σ	Relative σ	2σ	3σ	Certified	Within 2σ?	%
Majors by	OES	n = 8	± % or ppm	± % (precision)	± % or ppm (precision)	(limit of detection)	% or ppm	(accuracy)	difference
SiO_2		76.22	0.49	0.64	0.97	1.46	75.88	Y	0.68
TiO_2		0.09	0.00	4.24	0.01	0.01	0.09	Y	3.29
Al_2O_3		12.01	0.16	1.36	0.33	0.49	12.08	Y	1.28
Fe_2O_3		2.00	0.03	1.47	0.06	0.09	2.02	Y	1.47
MnO		0.02	0.00	10.64	0.00	0.01	0.021	Y	17.63
MgO		0.06	0.05	80.68	0.10	0.15	0.06	Y	58.90
CaO		0.76	0.05	6.19	0.09	0.14	0.78	Y	4.94
Na_2O		3.36	0.08	2.40	0.16	0.24	3.36	Y	1.92
K_2O		4.96	0.12	2.42	0.24	0.36	4.93	Y	1.73
P_2O_5		0.01	0.01	134.89	0.02	0.02	0.01	Y	77.52
Traces by	OES								
Sc		0.29	0.27	92.68	0.54	0.80	0.451	Y	61.82
V		4.08	2.90	71.07	5.80	8.69	2	Y	117.59
Cr		11.76	5.55	47.24	11.11	16.66	11.4	Y	34.43
Co		1.59	1.44	90.69	2.88	4.32	4	Y	63.27
Ni		12.00	4.35	36.29	8.71	13.06	8	Y	59.10
Cu		14.70	4.85	32.99	9.70	14.55	11	Y	44.48
Sr		8.60	3.48	40.50	6.96	10.45	10	Y	29.10
Y		145.55	3.40	2.33	6.79	10.19	143	Y	2.32
Zr		309.22	23.25	7.52	46.51	69.76	300	Y	5.67
Ba		111.29	7.32	6.58	14.64	21.96	120	Y	7.81
Traces by	MS								
V		2.86	1.68	58.67	3.35	5.03	2	Y	77.50
Cr		10.80	4.28	39.68	8.57	12.85	11.4	Y	28.83
Co		1.62	1.43	88.21	2.86	4.29	4	Y	59.47
Ni		12.34	7.82	63.39	15.64	23.46	8	Y	66.83
Cu		24.06	9.61	39.96	19.23	28.84	11	Y	118.74
Ga		27.73	1.25	4.50	2.49	3.74	27	Y	4.08
Rb		317.53	36.58	11.52	73.15	109.73	320	Y	7.41
Sr		8.97	2.40	26.72	4.79	7.19	10	Y	22.69
Y		141.52	1.96	1.38	3.91	5.87	143	Y	1.38
Zr		298.68	9.93	3.32	19.85	29.78	300	Y	2.80
Nb		51.18	3.17	6.19	6.34	9.50	53	Y	3.94
Ba		115.77	6.99	6.04	13.99	20.98	120	Y	5.75
Hf		11.44	0.65	5.65	1.29	1.94	12	Y	4.84
Ta		4.24	0.19	4.47	0.38	0.57	4.5	Y	6.02
Pb		28.99	5.94	20.48	11.88	17.82	40	Y	27.52
Th		46.74	2.91	6.22	5.82	8.72	51	Y	8.34
U		15.97	0.68	4.27	1.36	2.05	15	Y	6.48
REEs by	MS								
La		106.44	4.41	4.14	8.82	13.23	109	Y	3.74
Ce		194.80	8.17	4.20	16.35	24.52	195	Y	3.31
Pr		20.03	1.43	7.15	2.86	4.30	20	Y	5.78
Nd		67.04	4.02	5.99	8.03	12.05	72	Y	6.88
Sm		13.92	0.90	6.44	1.79	2.69	15.8	Y	11.91
Eu		0.37	0.11	28.85	0.21	0.32	0.35	Y	18.51
Gd		13.99	0.65	4.67	1.31	1.96	14	Y	3.32
Tb		2.47	0.12	4.92	0.24	0.36	3	N	17.63
Dy		16.84	0.67	4.00	1.35	2.02	17	Y	3.12
Ho		3.49	0.16	4.64	0.32	0.49	4.13	N	15.39
Er		11.38	0.53	4.67	1.06	1.59	13	N	12.47
Tm		1.97	0.08	4.23	0.17	0.25	2	Y	3.65
Yb		13.27	0.59	4.44	1.18	1.77	14.2	Y	6.78
Lu		2.01	0.09	4.32	0.17	0.26	2	Y	3.45

Table 4.5. Repeat analyses of BIR-1 (basalt).

	BIR-1 runs 1-7						
Majors by	ICP-OES						
SiO_2	47.67	46.13	47.51	47.99	48.28	47.26	48.52
TiO_2	0.94	0.96	0.95	0.95	0.95	0.97	0.99
Al_2O_3	15.41	14.97	15.11	15.07	15.20	14.77	15.20
Fe_2O_3	11.17	11.36	11.67	11.05	11.04	11.39	11.65
MnO	0.17	0.17	0.17	0.17	0.17	0.17	0.18
MgO	9.64	9.69	9.48	9.40	9.40	9.86	8.79
CaO	13.24	13.90	13.03	12.71	12.78	13.12	13.26
Na_2O	1.72	2.25	1.77	1.80	1.89	1.77	1.81
K_2O	0.02	0.03	0.04	0.02	0.02	0.03	0.02
P_2O_5	0.02	0.12	0.04	0.02	0.01	0.02	0.01
Traces by	ICP-OES						
Sc	44.4	46.4	41.5	39.7	39.9	43.0	42.9
V	302.0	326.6	315.5			319.8	316.3
Cr	381.3	367.8	389.6	370.1	380.1	398.6	377.0
Co	50.4	51.3	45.7	49.2	44.3	51.2	51.1
Ni	177.5	161.8	168.1	183.8	148.2	160.3	168.5
Cu	113.7	150.8	111.0	118.8	91.4	122.8	128.6
Sr	104.6	108.0	100.3	100.9	100.9	103.3	104.3
Y	15.7	17.5	16.2	15.1	15.9	16.1	16.4
Zr	6.1	14.6	14.2	14.7	12.4	17.1	16.4
Ba	12.1	5.5	5.6	8.2	5.5	8.9	9.7
Traces by	ICP-MS						
V	320.5	306.3	330.6	312.9	312.1	307.7	316.6
Cr	399.3	397.5	388.0	375.8	376.0	394.1	397.2
Co	52.9	50.2	50.6	49.6	47.7	49.8	48.8
Ni	173.4	167.6	160.7	180.3	157.8	160.5	159.2
Cu	119.3	125.5	99.3	127.9	124.6	122.2	137.9
Ga	15.2	15.3	14.6	15.1	15.8	15.6	15.5
Rb	0.3	0.3	0.2	0.2	0.1	0.4	0.3
Sr	105.1	109.6	105.3	100.9	98.4	97.2	114.1
Y	15.7	16.5	15.8	15.6	15.5	15.5	16.2
Zr	16.2	15.6	15.3	16.7	15.8	15.0	15.7
Nb	0.59	0.61	0.46	0.58	0.51	0.50	0.61
Ba	14.5	57.6	2.4	7.8	9.0	7.9	3.6
Hf	0.54	0.58	0.55	0.53	0.54	0.53	0.59
Ta	0.04	0.04	0.03	0.04	0.04	0.04	0.04
Pb	3.11	2.47	1.70	5.60	6.50	4.76	2.83
Th	0.05	0.09	0.08	0.06	0.10	0.03	0.05
U	0.02	0.02	0.01	0.02	0.01	0.01	0.01
REEs by	ICP-MS						
La	0.63	0.67	0.48	0.64	0.66	0.53	0.56
Ce	1.89	1.88	1.96	1.97	2.00	1.93	1.84
Pr	0.35	0.37	0.34	0.38	0.37	0.34	0.37
Nd	2.50	2.35	2.08	2.38	2.33	1.97	2.20
Sm	1.08	1.09	0.98	1.06	1.04	1.04	1.04
Eu	0.54	0.52	0.52	0.49	0.48	0.57	0.48
Gd	1.79	1.69	1.75	1.64	1.60	1.58	1.60
Tb	0.36	0.33	0.33	0.33	0.31	0.31	0.32
Dy	2.54	2.46	2.46	2.42	2.34	2.33	2.43
Ho	0.57	0.51	0.54	0.51	0.49	0.54	0.50
Er	1.68	1.55	1.64	1.55	1.58	1.54	1.48
Tm	0.26	0.25	0.24	0.25	0.24	0.23	0.24
Yb	1.64	1.63	1.63	1.62	1.54	1.59	1.53
Lu	0.27	0.26	0.26	0.26	0.24	0.24	0.24

Table A4.6. Error analysis of repeat runs of BIR-1. See text for details.

BIR-1		Mean	σ	Relative σ	2σ	3σ	Certified	Within 2σ?	%
Majors by	OES	n = 7	± % or ppm	± % (precision)	± % or ppm (precision)	(detecti-on limit)	% or ppm	(accuracy)	difference
SiO_2		47.62	0.79	1.66	1.58	2.37	47.7	Y	1.18
TiO_2		0.96	0.02	1.85	0.04	0.05	0.97	Y	1.87
Al_2O_3		15.10	0.20	1.35	0.41	0.61	15.4	Y	1.95
Fe_2O_3		11.34	0.26	2.31	0.52	0.78	11.3	Y	1.91
MnO		0.17	0.00	2.41	0.01	0.01	0.176	Y	3.48
MgO		9.47	0.34	3.60	0.68	1.02	9.7	Y	2.87
CaO		13.15	0.39	2.97	0.78	1.17	13.4	Y	2.92
Na_2O		1.86	0.18	9.60	0.36	0.54	1.81	Y	5.43
K_2O		0.03	0.01	31.23	0.02	0.02	0.03	Y	25.48
P_2O_5		0.03	0.04	113.08	0.08	0.12	0.027	N	82.75
Traces by	OES								
Sc		42.55	2.42	5.68	4.83	7.25	43	Y	4.27
V		316.05	8.98	2.84	17.95	26.93	319	Y	1.98
Cr		380.65	10.74	2.82	21.48	32.22	391	Y	3.20
Co		49.04	2.85	5.82	5.71	8.56	52	Y	5.69
Ni		166.88	11.70	7.01	23.40	35.11	166	Y	5.31
Cu		119.57	18.13	15.16	36.25	54.38	119	Y	10.37
Sr		103.17	2.74	2.66	5.49	8.23	109	N	5.35
Y		16.12	0.74	4.57	1.47	2.21	15.6	Y	4.32
Zr		13.62	3.67	26.91	7.33	11.00	14	Y	16.83
Ba		7.94	2.55	32.17	5.11	7.66	7.14	Y	30.45
Traces by	MS								
V		315.24	8.35	2.65	16.71	25.06	319	Y	2.35
Cr		389.68	10.09	2.59	20.18	30.27	391	Y	2.09
Co		49.96	1.61	3.22	3.22	4.82	52	Y	4.41
Ni		165.63	8.50	5.13	17.00	25.50	166	Y	4.23
Cu		122.36	11.76	9.61	23.52	35.27	119	Y	7.56
Ga		15.30	0.38	2.47	0.76	1.14	15.3	Y	1.87
Rb		0.26	0.08	31.67	0.17	0.25	0.2	Y	42.49
Sr		104.38	6.08	5.82	12.15	18.23	109	Y	5.74
Y		15.81	0.41	2.57	0.81	1.22	15.6	Y	1.88
Zr		15.73	0.55	3.52	1.11	1.66	14	N	12.36
Nb		0.55	0.06	11.18	0.12	0.18	0.55	Y	9.65
Ba		14.70	19.34	131.57	38.67	58.01	7.14	Y	139.23
Hf		0.55	0.02	3.98	0.04	0.07	0.582	Y	5.37
Ta		0.04	0.01	14.70	0.01	0.02	0.0357	Y	16.29
Pb		3.85	1.78	46.21	3.56	5.34	3.1	Y	45.53
Th		0.07	0.02	36.53	0.05	0.07	0.032	Y	106.57
U		0.01	0.00	22.07	0.01	0.01	0.01	Y	37.82
REEs by	MS								
La		0.60	0.07	12.10	0.14	0.22	0.615	Y	9.61
Ce		1.93	0.06	2.94	0.11	0.17	1.92	Y	2.42
Pr		0.36	0.02	4.41	0.03	0.05	0.37	Y	3.59
Nd		2.26	0.18	8.15	0.37	0.55	2.38	Y	6.55
Sm		1.05	0.04	3.41	0.07	0.11	1.12	Y	6.45
Eu		0.51	0.03	6.51	0.07	0.10	0.53	Y	5.48
Gd		1.66	0.08	4.97	0.17	0.25	1.87	Y	11.05
Tb		0.33	0.02	6.03	0.04	0.06	0.36	Y	9.37
Dy		2.42	0.07	2.93	0.14	0.21	2.51	Y	3.68
Ho		0.52	0.03	5.25	0.05	0.08	0.56	Y	7.04
Er		1.57	0.07	4.29	0.13	0.20	1.66	Y	5.63
Tm		0.24	0.01	4.20	0.02	0.03	0.25	Y	3.75
Yb		1.60	0.05	2.88	0.09	0.14	1.65	Y	3.31
Lu		0.25	0.01	4.38	0.02	0.03	0.25	Y	3.95

Table A4.7. Summary: best relative standard deviations of standard analyses, percentage differences between standard analyses and certified values, and limits of detection.

Majors by OES	Relative σ (± %)	Difference (%)	LOD (wt.% or ppm)	Comments Detection Limit = LOD
SiO_2	0.63	0.55	0.99	
TiO_2	1.34	1.13	0.01	
Al_2O_3	1.35	1.28	0.49	
Fe_2O_3	1.47	1.11	0.09	
MnO	1.30	1.74	0.01	
MgO	2.70	2.28	0.15	
CaO	1.72	1.51	0.14	
Na_2O	1.67	1.47	0.14	
K_2O	2.42	1.73	0.02	
P_2O_5	5.80	4.46	0.02	Beware high LOD; poor precision.
Traces by OES				
Sc	3.99	4.27	0.80	
V	2.84	1.98	8.69	Poorer than ICP-MS.
Cr	2.82	3.20	16.66	Poorer than ICP-MS.
Co	5.82	5.66	4.32	Poorer than ICP-MS.
Ni	4.00	4.64	13.06	Marginally better than ICP-MS.
Cu	15.16	10.37	14.55	Poorer than ICP-MS.
Sr	1.63	1.38	8.23	Poorer than ICP-MS.
Y	1.51	1.04	1.08	Similar to ICP-MS.
Zr	2.76	2.76	11.00	Poorer than ICP-MS.
Ba	1.67	2.06	7.66	Marginally better than ICP-MS.
Traces by MS				
V	2.65	1.95	5.03	
Cr	2.14	2.09	12.85	Beware high LOD working with granitoids.
Co	2.36	2.01	2.68	LOD fine for Th-Co diagram.
Ni	5.13	4.23	23.46	Beware high LOD with granitoids; poor precision.
Cu	4.05	3.37	7.02	
Ga	2.46	1.87	1.14	
Rb	7.57	6.70	0.25	Quite poor precision and accuracy.
Sr	1.27	1.06	7.19	
Y	1.38	1.38	1.22	Be cautious of LOD with residual garnet signature.
Zr	1.52	2.19	1.66	
Nb	2.29	2.04	0.18	Be cautious of LOD with depleted samples.
Ba	2.39	2.13	20.98	High LOD.
Hf	2.50	2.01	0.07	
Ta	1.49	6.02	0.02	Not particularly accurate.
Pb	20.48	25.44	5.34	Not precise, or accurate, and very high LOD.
Th	1.66	3.68	0.07	LOD fine for most samples on Th-Co diagram.
U	2.94	2.97	0.01	
REEs by MS				
La	2.51	2.10	0.22	
Ce	2.54	1.96	0.17	
Pr	2.75	2.06	0.05	
Nd	2.64	2.40	0.55	
Sm	2.76	2.22	0.11	
Eu	4.11	3.33	0.10	Relatively poor precision compared to other REEs.
Gd	4.67	3.32	0.25	Relatively poor precision compared to other REEs.
Tb	3.69	4.66	0.06	
Dy	2.93	3.01	0.21	
Ho	2.87	7.04	0.06	Relatively poor accuracy compared to other REEs.
Er	3.57	4.70	0.20	
Tm	2.87	3.65	0.03	
Yb	2.88	3.31	0.14	Be cautious of LOD with residual garnet signature.
Lu	3.42	3.45	0.03	

APPENDIX FIVE: MAJOR AND TRACE ELEMENT DATA BY LOCALITY AND UNIT

Major elements are quoted in wt.% (weight per cent). Trace elements are quoted in ppm (parts per million). Analyses marked bd are those where the analysis was below the limit of detection quoted in Appendix 4.

Abbreviations:

CA – calc-alkaline
CAA – calc-alkaline arc
IAT – island arc tholeiite-like or back-arc tholeiite-like
MORB or MOR – mid-ocean ridge basalt-like
SH – shoshonitic
TH – tholeiitic

AM – amphibolite
AND - andesite
BA – basaltic andesite
BAS - basalt
DAC - dacite
RHY – rhyolite
TROND – trondhjemite

SED – volcanogenic sediment

REEs – Rare Earth Elements

A5.1. La Désirade Island, French West Indies

North-east mafic volcanic complex

	IND/1.1	IND/1.2	IND/2.2	IND/3.1	IND/3.2	IND/4.1	IND/5.1	IND/6.1	IND/6.2
Location	Coulant			Doublé		Meteo		Seraphine	
Type	IAT/BA	IAT/BA	IAT/BAS	IAT/BA	IAT/BA	IAT/BAS	IAT/BA	IAT/BAS	IAT/BA
Majors									
SiO_2	55.27	54.06	55.39	57.79	57.99	56.66	55.68	47.88	55.60
TiO_2	0.77	0.75	0.55	0.41	0.41	0.71	0.71	0.78	0.72
Al_2O_3	16.15	16.07	15.51	15.56	15.02	14.76	14.63	15.20	15.54
Fe_2O_3	6.97	6.76	6.43	5.57	5.47	5.98	6.27	7.12	7.05
MnO	0.08	0.08	0.10	0.06	0.06	0.09	0.09	0.10	0.06
MgO	5.49	4.77	6.56	5.09	3.88	4.05	3.44	5.67	3.39
CaO	4.81	6.12	4.63	6.64	6.96	5.75	7.96	9.70	7.03
Na_2O	7.43	7.09	6.52	6.69	7.18	7.29	7.08	4.75	6.61
K_2O	0.33	0.33	0.42	0.03	0.07	0.21	0.09	0.38	0.19
P_2O_5	0.12	0.12	0.05	0.11	0.08	0.09	0.11	0.11	0.10
LOI	3.69	5.14	4.65	2.87	2.95	4.50	4.64	9.16	2.81
Total	101.09	101.30	100.83	100.83	100.07	100.07	100.69	100.84	99.10
Traces									
Sc	25.3	23.9	30.6	20.8	19.9	23.0	22.7	24.0	22.2
V	220.1	252.0	244.4	193.1	207.3	226.2	251.6	221.4	256.8
Cr	228.0	244.2	242.7	350.4	330.0	212.6	189.9	204.2	196.6
Co	31.6	28.7	35.2	26.5	21.6	35.0	23.8	37.1	30.1
Ni	104.5	205.1	113.1	151.0	103.7	82.2	77.4	133.8	101.3
Cu	19.2	33.2	38.9	20.5	59.4	27.9	46.2	47.0	301.4
Ga	16.9	18.8	14.3	16.1	15.9	17.2	18.7	18.3	19.8
Rb	4.6	4.6	5.9	0.4	1.3	4.6	1.2	1.7	2.3
Sr	95.5	91.7	168.8	56.1	35.5	72.4	55.3	58.1	54.0
Y	16.1	11.8	10.8	8.7	7.9	18.3	15.5	17.1	15.3
Zr	75.8	49.3	56.6	67.1	71.4	67.3	78.9	86.9	80.0
Nb	1.37	0.89	0.82	1.02	1.17	1.87	1.37	1.54	1.40
Ba	829.0	60.6	103.6	28.9	33.7	50.6	46.6	35.0	31.6
Hf	2.01	1.39	1.49	1.69	1.73	1.87	1.99	2.08	2.05
Ta	0.10	0.07	0.04	0.05	0.06	0.12	0.09	0.09	0.08
Pb	bd	bd	bd	bd	bd	bd	bd	bd	bd
Th	0.41	0.17	0.12	0.77	0.81	0.55	0.28	0.35	0.24
U	0.27	0.14	0.11	0.22	0.25	0.34	0.17	0.17	0.18
REEs									
La	3.68	1.98	1.37	3.76	3.79	3.26	3.31	3.41	2.33
Ce	9.22	5.61	4.23	9.08	9.15	7.97	8.50	8.80	6.80
Pr	1.51	1.15	0.77	1.55	1.57	1.51	1.44	1.43	1.24
Nd	6.69	5.78	3.69	6.65	6.56	7.29	6.48	6.43	5.95
Sm	2.21	2.26	1.31	1.65	1.71	2.42	2.18	2.14	2.11
Eu	0.87	0.90	0.56	0.58	0.57	0.86	0.74	0.76	0.74
Gd	2.68	4.16	2.08	2.21	2.31	3.86	2.67	2.62	2.78
Tb	0.41	0.47	0.30	0.27	0.26	0.52	0.41	0.43	0.42
Dy	2.77	2.60	2.12	1.62	1.60	3.26	2.70	2.80	2.68
Ho	0.53	0.52	0.41	0.30	0.29	0.63	0.51	0.54	0.51
Er	1.53	1.59	1.31	0.94	0.89	1.86	1.54	1.59	1.52
Tm	0.24	0.23	0.21	0.14	0.13	0.29	0.24	0.25	0.24
Yb	1.53	1.93	1.50	0.99	0.85	2.04	1.71	1.71	1.63
Lu	0.24	0.24	0.22	0.15	0.13	0.29	0.27	0.27	0.24

La Désirade, continued

North-east mafic volcanic complex, continued

	IND/7.1	IND/7.2	IND/8.1	IND/8.2	IND/9.1	IND/9.2	IND/10.1	IND/10.2	IND/11.1
Location	Seraphine				Mahault				
Type	IAT/BA	IAT/BAS	IAT/BAS	IAT/BA	MORB/BAS	MORB/BAS	MORB/BAS	MORB/BAS	MORB/BA
Majors									
SiO_2	42.87	50.48	54.30	67.31	50.73	45.01	55.61	52.28	52.10
TiO_2	0.68	0.74	0.86	0.37	1.52	1.75	0.71	0.73	0.76
Al_2O_3	15.21	14.16	13.42	12.66	13.28	12.70	15.45	15.65	18.12
Fe_2O_3	7.22	8.59	9.11	6.42	7.55	7.31	8.11	7.96	6.92
MnO	0.09	0.11	0.11	0.07	0.09	0.13	0.10	0.11	0.09
MgO	3.91	5.96	5.15	3.14	3.66	3.48	4.64	5.54	3.16
CaO	24.57	9.45	10.74	3.16	10.60	14.98	4.59	6.69	10.98
Na_2O	0.42	5.63	4.56	6.79	5.36	5.10	6.95	5.07	5.23
K_2O	0.03	0.13	0.04	0.10	0.21	0.16	0.12	0.25	0.06
P_2O_5	0.10	0.12	0.13	0.03	0.18	0.18	0.05	0.06	0.10
LOI	5.82	5.27	2.42	1.13	5.55	8.58	3.04	5.96	4.00
Total	100.92	100.63	100.86	101.18	98.74	99.37	99.34	100.31	101.51
Traces									
Sc	27.9	31.4	32.3	23.3	31.4	28.8	28.5	29.4	33.3
V	317.3	339.2	321.3	243.0	298.0	310.7	266.1	232.5	275.9
Cr	400.6	457.9	987.9	518.8	343.9	38.9	422.4	496.1	321.2
Co	29.6	41.3	38.5	33.4	32.8	40.8	36.5	42.8	33.8
Ni	150.5	130.6	137.6	120.0	80.5	38.0	87.4	110.5	79.4
Cu	267.4	32.3	76.2	586.9	71.2	104.8	83.1	79.6	33.6
Ga	43.5	18.8	17.0	8.0	13.1	16.3	14.7	18.4	20.5
Rb	0.3	2.7	1.0	1.0	1.3	3.1	0.9	1.5	1.3
Sr	34.9	62.8	30.3	39.8	59.7	122.1	90.3	89.3	130.9
Y	15.6	18.3	20.1	9.1	33.1	42.6	18.1	26.8	11.4
Zr	53.9	55.8	57.7	32.5	98.0	145.1	66.4	91.1	47.9
Nb	1.24	1.84	1.44	0.38	1.93	2.98	0.98	1.46	1.07
Ba	bd	31.7	146.3	33.4	bd	55.3	bd	bd	23.7
Hf	1.41	1.55	1.53	0.78	2.40	3.56	1.71	2.41	1.12
Ta	0.07	0.12	0.09	0.02	0.14	0.21	0.08	0.10	0.08
Pb	bd	bd	bd	bd	bd	bd	bd	bd	bd
Th	0.55	1.00	0.44	0.09	0.08	0.14	0.11	0.19	0.07
U	0.16	0.29	0.11	0.05	0.12	0.61	0.04	0.05	0.07
REEs									
La	5.70	5.94	5.94	1.57	2.86	3.74	1.89	2.89	1.43
Ce	12.64	13.41	11.91	3.56	8.91	13.08	5.97	8.35	4.31
Pr	2.13	2.27	2.29	0.82	2.03	2.78	1.24	1.66	0.85
Nd	9.19	9.96	10.15	4.11	10.54	14.90	6.12	8.19	4.19
Sm	2.57	2.73	2.96	1.46	4.08	5.58	2.45	3.00	1.50
Eu	0.87	0.86	0.96	0.52	1.43	1.99	0.88	0.98	0.79
Gd	3.16	3.61	3.51	2.04	5.99	8.26	3.89	4.33	2.27
Tb	0.43	0.48	0.51	0.29	0.92	1.20	0.56	0.67	0.33
Dy	2.70	2.92	3.16	1.84	6.06	8.13	3.69	4.56	2.14
Ho	0.52	0.56	0.63	0.37	1.23	1.67	0.74	0.93	0.43
Er	1.48	1.73	1.80	1.02	3.69	4.83	2.19	2.72	1.29
Tm	0.23	0.25	0.28	0.15	0.57	0.75	0.35	0.44	0.21
Yb	1.56	1.75	1.82	1.05	4.03	5.18	2.55	3.06	1.43
Lu	0.22	0.25	0.27	0.16	0.57	0.76	0.36	0.45	0.20

La Désirade, continued

North-east mafic volcanic complex, continued

	IND/11.2	IND/11.3	IND/13.1	IND/14.1	IND/15.1	IND/15.2	IND/16.1
Location	Mahault		Galets				
Type	MORB/BA	MORB/BAS	IAT/BA	IAT/BAS	IAT/BA	IAT/BA	IAT/BA
Majors							
SiO_2	52.41	44.11	61.42	54.99	47.13	51.05	51.27
TiO_2	0.81	0.61	1.47	1.44	1.30	1.02	1.21
Al_2O_3	16.57	14.05	13.65	14.48	13.81	15.17	14.15
Fe_2O_3	9.33	7.22	8.86	11.61	9.28	9.35	10.18
MnO	0.07	0.10	0.16	0.15	0.09	0.10	0.08
MgO	3.19	5.73	3.59	4.34	1.65	3.78	2.22
CaO	8.30	20.26	2.39	4.69	13.01	10.17	6.34
Na_2O	5.69	1.83	4.96	3.23	5.42	5.10	6.09
K_2O	0.12	0.05	0.08	0.05	0.05	0.06	0.06
P_2O_5	0.10	0.09	0.69	0.15	0.14	0.16	0.13
LOI	3.41	6.67	3.44	4.06	7.55	3.98	7.40
Total	100.00	100.71	100.70	99.19	99.43	99.94	99.13
Traces							
Sc	31.3	27.0	19.1	25.9	31.1	31.2	29.7
V	301.9	283.4	134.8	356.7	435.9	331.3	498.8
Cr	278.8	446.7	17.0	18.3	22.5	129.4	bd
Co	33.5	42.5	13.9	32.8	30.0	32.4	31.0
Ni	69.2	136.5	bd	bd	bd	67.3	bd
Cu	68.3	41.1	62.4	54.9	79.6	55.2	44.2
Ga	21.3	25.7	20.9	23.6	26.2	23.9	28.5
Rb	2.4	0.7	1.2	0.7	0.6	1.4	0.5
Sr	115.1	48.5	57.8	186.7	63.4	126.9	31.8
Y	14.7	10.2	58.4	38.5	26.2	19.6	29.3
Zr	48.9	51.7	155.7	110.4	93.5	67.8	105.7
Nb	1.18	1.50	3.03	2.12	1.50	1.06	1.49
Ba	2894.5	bd	50.4	bd	33.4	43.1	31.4
Hf	1.08	1.31	3.83	2.74	2.13	1.50	2.65
Ta	0.08	0.12	0.19	0.12	0.09	0.07	0.10
Pb	5.52	bd	bd	bd	bd	bd	bd
Th	0.09	0.07	0.25	0.19	0.18	0.11	0.18
U	0.10	0.07	0.22	0.13	0.29	0.10	0.74
REEs							
La	1.96	1.38	5.54	5.40	3.00	2.10	3.15
Ce	5.44	4.14	18.43	13.43	8.97	6.46	8.87
Pr	0.99	0.75	3.83	2.70	1.52	1.12	1.60
Nd	4.80	3.77	19.84	13.36	7.38	5.44	8.07
Sm	1.72	1.32	7.12	4.41	2.67	1.95	2.96
Eu	1.44	0.70	2.48	1.73	1.08	0.87	1.12
Gd	2.16	1.99	9.33	5.92	3.53	2.62	3.81
Tb	0.36	0.29	1.45	0.88	0.58	0.46	0.67
Dy	2.46	1.86	9.45	5.92	4.11	3.04	4.64
Ho	0.48	0.37	1.83	1.13	0.81	0.61	0.93
Er	1.42	1.12	5.31	3.28	2.41	1.78	2.71
Tm	0.21	0.17	0.79	0.49	0.38	0.28	0.44
Yb	1.44	1.21	5.31	3.21	2.45	1.90	2.83
Lu	0.23	0.18	0.81	0.50	0.39	0.29	0.45

La Désirade, continued

North-east felsic volcanic complex

*BM = Baie Mahault

	IND/12.1	DES1	DES20.3
Location	Abaque	Inland BM	Abaque
Type	DAC	DAC	DAC
Majors			
SiO_2	62.21	78.98	77.27
TiO_2	0.93	0.26	0.46
Al_2O_3	14.88	10.15	10.44
Fe_2O_3	8.48	1.92	2.18
MnO	0.17	0.02	0.03
MgO	3.55	0.66	0.34
CaO	1.13	0.46	0.28
Na_2O	5.81	5.47	6.19
K_2O	0.07	0.08	0.15
P_2O_5	0.45	0.11	0.17
LOI	3.07	0.73	1.92
Total	100.74	98.84	99.43
Traces			
Sc	19.4	8.8	9.1
V	36.0	13.3	30.1
Cr	19.6	25.5	16.5
Co	10.6	3.8	3.1
Ni	bd	bd	bd
Cu	20.3	9.6	19.2
Ga	23.5	9.0	10.4
Rb	1.2	1.8	2.1
Sr	52.5	37.6	34.6
Y	42.2	30.7	48.0
Zr	121.0	132.4	141.4
Nb	1.95	1.38	1.47
Ba	1160.4	26.6	23.0
Hf	3.15	3.46	3.36
Ta	0.12	0.11	0.12
Pb	6.85	bd	bd
Th	0.34	0.51	0.52
U	0.17	0.28	0.47
REEs			
La	3.33	4.68	7.09
Ce	11.19	12.34	15.33
Pr	2.25	2.18	3.46
Nd	11.91	10.81	17.43
Sm	4.55	3.44	5.43
Eu	1.79	0.95	1.43
Gd	6.09	4.02	6.28
Tb	1.02	0.71	1.04
Dy	6.75	4.85	6.95
Ho	1.36	0.97	1.35
Er	3.98	2.97	4.13
Tm	0.63	0.49	0.67
Yb	4.11	3.17	4.36
Lu	0.65	0.50	0.69

La Désirade, continued

South-west felsic volcanic complex

	IND/18.1	IND/18.2	IND/18.3	IND/18.4
Location	Fregule			
Type	DAC	DAC	DAC	DAC
Majors				
SiO_2	71.94	71.86	71.58	71.67
TiO_2	0.57	0.55	0.58	0.45
Al_2O_3	13.36	13.25	13.60	12.52
Fe_2O_3	4.25	3.89	4.21	4.13
MnO	0.05	0.06	0.07	0.06
MgO	2.26	2.42	2.42	2.52
CaO	0.40	0.20	0.14	0.19
Na_2O	5.64	6.23	6.22	5.30
K_2O	0.31	0.07	0.11	0.17
P_2O_5	0.15	0.15	0.16	0.12
LOI	0.34	1.50	1.68	1.82
Total	99.26	100.18	100.77	98.95
Traces				
Sc	14.7	15.7	15.8	17.1
V	46.8	29.6	29.0	23.6
Cr	20.8	34.6	63.0	17.7
Co	5.2	3.8	4.3	3.5
Ni	bd	bd	49.0	bd
Cu	44.5	25.1	76.0	24.6
Ga	14.2	15.7	15.8	17.6
Rb	5.1	1.0	1.9	5.0
Sr	127.5	79.5	31.8	77.5
Y	22.9	28.9	27.9	30.4
Zr	108.3	123.1	120.2	142.4
Nb	1.83	2.18	1.97	2.28
Ba	62.0	bd	24.5	21.2
Hf	2.74	3.18	3.02	3.41
Ta	0.12	0.13	0.13	0.13
Pb	bd	bd	bd	bd
Th	0.34	0.37	0.40	0.46
U	0.22	0.30	0.26	0.23
REEs				
La	3.50	3.72	4.06	4.31
Ce	10.09	11.29	11.61	12.11
Pr	1.74	1.98	2.01	1.98
Nd	8.17	9.21	9.40	8.75
Sm	2.77	3.19	3.11	3.13
Eu	0.70	0.91	0.92	0.98
Gd	3.42	4.37	4.22	4.06
Tb	0.55	0.69	0.68	0.68
Dy	3.77	4.72	4.59	4.69
Ho	0.78	0.95	0.91	0.95
Er	2.29	2.95	2.80	2.90
Tm	0.38	0.48	0.45	0.47
Yb	2.50	3.31	3.19	3.08
Lu	0.39	0.53	0.50	0.50

La Désirade continued

Trondhjemite pluton

	IND/19.8	IND/19.9	IND/19.10	IND/19.11	IND/19.13	IND/19.14
Location	Emballage					
Type	Trond	Trond	Trond	Trond	Trond	Trond
Majors						
SiO_2	53.07	74.72	75.41	74.58	56.00	53.40
TiO_2	1.07	0.30	0.31	0.28	1.64	1.21
Al_2O_3	16.58	12.70	12.70	12.80	15.98	13.85
Fe_2O_3	12.09	3.55	3.66	3.32	10.12	14.37
MnO	0.29	0.10	0.10	0.09	0.34	0.26
MgO	4.88	0.68	0.72	0.62	2.75	4.73
CaO	6.60	1.94	1.60	1.95	5.67	4.74
Na_2O	3.55	5.37	5.11	5.26	4.38	4.27
K_2O	0.34	0.12	0.14	0.16	0.21	0.38
P_2O_5	0.05	0.06	0.06	0.07	0.69	0.10
LOI	1.77	1.24	1.32	1.24	1.99	2.05
Total	100.29	100.79	101.13	100.36	99.77	99.35
Traces						
Sc	30.1	11.3	11.7	11.2	24.6	40.4
V	230.1	20.4	14.5	12.7	16.8	375.7
Cr	bd	14.4	35.7	30.9	15.1	bd
Co	19.9	bd	bd	bd	6.1	23.5
Ni	bd	140.2	bd	bd	bd	bd
Cu	32.5	31.2	32.9	22.3	42.6	65.7
Ga	19.4	18.5	15.6	14.5	17.5	16.1
Rb	7.4	1.5	1.6	1.5	2.0	6.1
Sr	259.7	99.3	74.3	118.8	239.0	166.9
Y	9.2	26.8	24.2	23.2	21.1	11.6
Zr	36.0	146.8	122.1	113.1	42.6	35.5
Nb	0.32	1.41	1.33	1.12	0.82	1.41
Ba	130.9	66.9	50.2	50.5	57.6	72.7
Hf	0.81	3.48	3.35	2.88	0.97	1.20
Ta	0.02	0.08	0.09	0.07	0.06	0.08
Pb	bd	bd	bd	bd	bd	bd
Th	0.08	0.44	0.48	0.44	0.13	0.12
U	0.03	0.19	0.20	0.18	0.09	0.05
REEs						
La	1.36	5.18	4.27	4.12	2.84	1.09
Ce	3.67	12.68	11.14	10.37	8.26	3.35
Pr	0.54	1.93	1.69	1.63	1.39	0.55
Nd	2.47	8.34	7.82	7.02	6.97	2.72
Sm	1.02	2.63	2.71	2.35	2.52	1.08
Eu	0.55	0.74	0.75	0.67	1.10	0.51
Gd	1.27	3.49	3.56	3.04	3.50	1.47
Tb	0.22	0.57	0.60	0.52	0.53	0.27
Dy	1.48	3.89	4.17	3.59	3.51	1.90
Ho	0.29	0.79	0.85	0.72	0.69	0.38
Er	0.91	2.39	2.53	2.27	1.94	1.10
Tm	0.15	0.40	0.42	0.36	0.29	0.18
Yb	0.97	2.77	2.84	2.44	1.78	1.19
Lu	0.15	0.42	0.46	0.40	0.28	0.19

La Désirade continued

Intermediate-felsic dykes cutting the trondhjemite and north-east complexes

	IND/19.1	IND/19.2	IND/19.3	IND/19.4	5.14D3	4.10D	6.25DC	20.13D
Location	Emballage				Seraphine		Mahault	Abaque
Type	BA	DAC	BA	BA	AND	BA	AND	DAC
Majors								
SiO_2	58.57	57.57	54.41	49.53	54.13	53.97	53.97	52.81
TiO_2	1.10	1.14	1.29	0.53	1.00	1.00	0.87	0.90
Al_2O_3	14.35	14.58	14.20	16.13	16.08	16.65	16.81	12.57
Fe_2O_3	10.28	12.21	11.89	7.97	10.47	10.59	9.77	5.69
MnO	0.59	0.37	0.33	0.20	0.16	0.15	0.14	0.10
MgO	3.31	3.18	3.93	7.49	4.08	4.51	4.48	1.41
CaO	2.63	2.79	7.14	10.36	4.88	5.52	5.53	1.95
Na_2O	5.64	5.17	3.85	2.30	8.30	7.25	7.25	7.47
K_2O	0.05	0.35	0.06	0.38	0.07	0.16	0.34	0.12
P_2O_5	0.13	0.16	0.13	0.05	0.40	0.22	0.30	0.93
LOI	3.25	2.64	3.37	3.72	0.78	0.84	0.77	16.26
Total	99.91	100.17	100.61	98.66	100.35	100.85	100.22	100.20
Traces								
Sc	35.3	30.0	35.0	32.1	34.3	37.5	35.0	19.1
V	260.7	219.1	344.8	231.3	329.1	332.4	286.3	26.7
Cr	13.4	bd	bd	143.1	bd	bd	39.0	bd
Co	18.7	12.9	23.4	33.6	24.9	28.3	24.1	8.3
Ni	bd	bd	bd	49.0	145.4	bd	30.1	bd
Cu	70.8	119.0	347.0	56.5	20.5	94.6	105.0	38.8
Ga	22.0	18.9	20.6	18.1	20.5	17.9	17.3	15.4
Rb	bd	3.3	0.3	7.9	1.5	1.0	2.7	1.1
Sr	48.6	72.7	48.2	199.7	39.8	91.2	165.6	23.5
Y	28.3	28.8	24.1	16.3	27.7	25.7	23.4	29.6
Zr	104.1	111.0	100.0	58.2	98.8	78.4	78.1	88.6
Nb	2.01	2.71	2.39	0.56	1.83	1.48	1.80	2.22
Ba	26.0	91.9	22.2	254.5	21.2	72.8	36.6	bd
Hf	2.45	2.51	2.29	1.31	2.53	1.89	1.99	2.25
Ta	0.12	0.16	0.15	0.03	0.15	0.12	0.12	0.15
Pb	bd	bd	bd	bd	bd	bd	bd	bd
Th	0.33	0.36	0.37	0.12	0.44	0.39	0.36	0.36
U	0.18	0.15	0.16	0.07	0.23	0.21	0.18	0.23
REEs								
La	3.88	4.84	4.20	1.64	4.46	4.28	3.75	5.05
Ce	11.32	13.39	11.37	5.14	11.81	11.24	10.06	12.94
Pr	1.91	2.21	1.82	0.87	2.01	1.90	1.70	2.21
Nd	8.96	10.11	8.17	4.22	9.97	9.51	8.47	11.13
Sm	3.09	3.30	2.77	1.51	3.19	2.93	2.69	3.47
Eu	1.15	1.01	1.05	0.58	1.11	1.06	0.93	1.31
Gd	3.91	4.14	3.36	1.96	3.70	3.42	3.21	4.09
Tb	0.64	0.66	0.55	0.36	0.63	0.58	0.53	0.67
Dy	4.33	4.38	3.82	2.48	4.19	3.86	3.60	4.43
Ho	0.86	0.86	0.75	0.49	0.84	0.77	0.70	0.88
Er	2.59	2.55	2.23	1.47	2.56	2.34	2.15	2.63
Tm	0.42	0.41	0.36	0.24	0.42	0.39	0.36	0.42
Yb	2.76	2.74	2.36	1.65	2.79	2.55	2.34	2.81
Lu	0.45	0.42	0.38	0.25	0.44	0.40	0.37	0.44

5.2. Tobago Island

Parlatuvier Formation, North Coast Schist

	INT/2-3/1	INT/2-3/3	INT/2-3/5	INT/2-3/6	INT/13-2/1	INT/15-2/2	INT/28-2/7	INT/28-2/8
Location	Bloody Bay				Castara			
Type	CA-BA	CA-BA	IAT-BA	CA-BAS	CA-BA	CA-BA	CA-BA	CA-BA
Majors								
SiO_2	68.52	55.17	43.95	45.25	56.97	60.25	52.88	61.52
TiO_2	0.60	1.06	1.30	0.97	0.83	0.84	1.27	0.84
Al_2O_3	12.66	17.33	19.00	16.03	15.62	15.40	17.43	14.33
Fe_2O_3	4.50	7.37	12.39	9.32	8.20	7.44	9.53	6.97
MnO	0.08	0.09	0.16	0.15	0.10	0.09	0.11	0.08
MgO	1.21	4.89	7.42	7.09	6.46	3.27	7.13	5.38
CaO	3.91	4.24	7.07	13.51	6.19	2.90	4.13	4.09
Na_2O	3.61	6.31	2.19	1.92	1.84	6.30	4.73	2.45
K_2O	0.63	0.13	1.27	0.59	1.27	0.16	0.37	0.67
P_2O_5	0.14	0.22	0.13	0.14	0.14	0.14	0.16	0.18
LOI	1.17	2.23	4.37	6.24	3.17	1.88	3.23	3.06
Total	97.02	99.05	99.23	101.20	100.80	98.67	100.97	99.57
Traces								
Sc	16.5	25.6	40.6	35.1	30.1	26.5	29.5	23.5
V	75.5	218.9	321.6	288.8	232.4	155.3	265.7	192.9
Cr	13.3	92.9	15.9	146.6	109.3	21.8	61.7	101.2
Co	19.3	19.1	34.2	34.7	25.5	12.6	27.8	19.2
Ni	bd	36.7	92.3	89.1	37.1	33.7	102.8	73.0
Cu	39.4	55.9	126.5	76.1	47.9	59.7	56.8	52.4
Ga	12.4	16.0	17.9	14.6	13.4	13.9	16.4	11.6
Rb	6.8	2.7	15.5	8.3	19.8	2.3	5.1	10.0
Sr	193.9	289.5	258.4	328.2	249.2	104.4	232.4	143.1
Y	29.3	27.9	23.4	18.6	19.2	29.5	25.3	18.4
Zr	89.9	93.5	54.3	54.2	67.9	87.4	85.3	79.7
Nb	1.59	5.28	2.64	2.37	3.69	1.95	3.20	4.52
Ba	69.1	24.6	173.7	62.3	226.5	25.2	39.7	85.8
Hf	2.30	2.25	1.47	1.25	1.64	2.20	2.05	1.86
Ta	0.10	0.38	0.17	0.13	0.24	0.13	0.21	0.29
Pb	bd	bd	bd	bd	bd	bd	bd	bd
Th	0.50	0.51	0.25	0.32	0.41	0.49	0.48	0.64
U	0.34	0.35	0.12	0.11	0.19	0.49	0.27	0.27
REEs								
La	4.69	7.06	5.78	4.34	5.08	4.92	5.63	5.53
Ce	11.92	17.91	14.36	10.90	12.23	12.29	14.24	13.54
Pr	2.01	2.81	2.30	1.73	1.92	2.00	2.23	2.04
Nd	10.67	13.28	11.83	8.97	9.02	10.37	11.47	10.05
Sm	3.32	3.78	3.23	2.49	2.60	3.12	3.25	2.76
Eu	1.02	1.20	1.28	0.89	0.94	1.06	1.14	1.02
Gd	3.65	3.88	3.44	2.60	2.73	3.50	3.47	2.82
Tb	0.69	0.67	0.64	0.47	0.46	0.70	0.64	0.51
Dy	4.38	4.37	3.85	2.97	3.02	4.48	4.08	3.19
Ho	0.91	0.85	0.76	0.58	0.58	0.91	0.80	0.60
Er	2.75	2.57	2.22	1.70	1.75	2.74	2.38	1.83
Tm	0.44	0.42	0.34	0.26	0.28	0.45	0.37	0.29
Yb	3.00	2.69	2.19	1.72	1.76	2.98	2.55	1.89
Lu	0.49	0.42	0.34	0.27	0.28	0.48	0.40	0.30

5.2. Tobago Island, continued

Parlatuvier Formation, North Coast Schist, continued

	INT/11-3/8	INT/13-2/2	INT/29-2/7	INT/18-2/1	3A-24	INT/18-2/2	INT/29-2/3	INT/29-2/4
Location	Castara	Englishman's Bay		Anse Fourmi		Pirate Bay	Speyside	
Type	CA-BA	IAT-BA	CA-BA	IAT-BAS	CA-BA	IAT-BA	CA-BAS	IAT-BA
Majors								
SiO_2	54.47	51.49	48.16	49.68	56.54	57.47	48.90	58.53
TiO_2	0.89	1.39	0.95	0.76	1.03	0.91	0.88	0.86
Al_2O_3	16.99	18.25	18.45	16.31	16.35	15.93	18.43	14.68
Fe_2O_3	8.82	10.11	9.70	8.77	8.79	10.22	9.30	10.14
MnO	0.13	0.13	0.13	0.13	0.15	0.17	0.12	0.14
MgO	5.10	5.21	5.76	9.88	4.83	3.65	6.52	3.83
CaO	7.01	6.64	9.03	10.02	6.90	5.62	8.55	5.02
Na_2O	3.67	4.92	4.19	3.24	2.51	5.03	3.36	3.03
K_2O	0.32	0.13	0.38	0.04	1.40	0.18	0.21	0.35
P_2O_5	0.15	0.22	0.11	0.16	0.20	0.13	0.16	0.07
LOI	2.34	2.79	2.21	2.39	2.09	2.04	4.02	3.04
Total	99.88	101.27	99.07	101.39	100.80	101.35	100.44	99.69
Traces								
Sc	28.3	34.1	35.1	37.2	25.9	35.2	28.2	36.7
V	229.2	288.6	274.9	221.4	176.6	247.9	260.3	226.6
Cr	29.4	58.9	29.5	375.7	145.0	14.2	105.2	14.5
Co	26.1	23.3	29.9	35.9	25.6	23.4	42.1	22.9
Ni	31.9	34.7	41.5	185.2	187.9	bd	49.2	bd
Cu	70.1	60.2	72.7	57.7	52.4	66.7	35.3	94.6
Ga	15.4	17.1	15.3	12.9	17.3	17.8	17.3	15.9
Rb	4.5	1.7	6.2	bd	11.2	2.3	2.4	7.2
Sr	212.5	318.5	332.1	469.5	132.5	73.0	358.7	241.1
Y	21.0	31.3	18.7	17.2	31.6	26.3	20.7	26.4
Zr	72.9	91.9	48.9	41.3	121.6	52.8	76.5	54.3
Nb	2.56	5.02	2.44	2.90	4.83	1.00	2.92	0.62
Ba	69.8	bd	bd	bd	9365.1	48.3	53.6	56.8
Hf	1.79	2.19	1.26	1.03	2.75	1.48	1.96	1.57
Ta	0.18	0.29	0.15	0.20	0.31	0.07	0.21	0.05
Pb	bd	bd	bd	bd	bd	bd	bd	bd
Th	0.47	0.35	0.38	0.26	0.53	0.25	0.44	0.17
U	0.20	0.21	0.19	0.15	0.32	0.23	0.21	0.14
REEs								
La	5.34	7.71	3.89	4.62	7.09	3.01	6.18	2.28
Ce	13.06	18.37	9.57	10.54	19.50	7.84	16.52	6.41
Pr	2.02	2.99	1.49	1.63	3.08	1.43	2.57	1.22
Nd	10.36	15.11	7.90	8.43	14.12	7.52	12.70	6.60
Sm	2.93	4.22	2.33	2.39	3.90	2.61	3.32	2.42
Eu	1.01	1.43	0.84	0.83	1.48	0.95	1.16	0.84
Gd	3.03	4.59	2.56	2.52	4.25	3.12	3.40	2.95
Tb	0.56	0.85	0.49	0.45	0.71	0.58	0.56	0.57
Dy	3.48	5.12	3.09	2.86	4.74	3.98	3.47	3.95
Ho	0.69	0.99	0.61	0.55	0.94	0.80	0.68	0.80
Er	2.03	2.98	1.77	1.61	2.71	2.43	2.00	2.47
Tm	0.31	0.46	0.27	0.26	0.44	0.40	0.32	0.40
Yb	2.11	3.07	1.80	1.71	2.80	2.55	2.06	2.65
Lu	0.34	0.49	0.29	0.27	0.45	0.40	0.33	0.41

5.2. Tobago Island, continued

Parlatuvier Formation, North Coast Schist, continued

	INT/29-2/5	INT/29-2/6	INT/4-3/3	INT/4-3/4
Location	Speyside		Charlotteville	
Type	CA-BA	CA-BA	CA-BAS	CA-BAS
Majors				
SiO_2	62.06	49.27	49.14	48.57
TiO_2	0.95	0.98	0.98	0.93
Al_2O_3	15.19	18.29	15.78	16.58
Fe_2O_3	7.39	10.79	9.13	9.12
MnO	0.16	0.15	0.13	0.13
MgO	2.60	5.29	8.74	8.58
CaO	3.20	8.78	9.77	8.58
Na_2O	4.70	3.64	3.13	3.12
K_2O	0.56	0.62	0.23	0.58
P_2O_5	0.19	0.17	0.13	0.14
LOI	3.10	3.37	2.24	2.64
Total	100.10	101.36	99.41	98.97
Traces				
Sc	25.6	23.5	33.8	35.4
V	148.1	284.9	250.7	245.7
Cr	15.9	31.1	445.8	334.1
Co	16.0	26.3	38.1	34.8
Ni	bd	51.3	221.7	122.9
Cu	47.6	63.6	41.8	47.5
Ga	15.0	19.8	15.0	13.5
Rb	10.0	14.8	3.3	6.5
Sr	69.9	450.5	312.6	274.8
Y	42.8	24.5	19.1	19.5
Zr	117.8	83.7	72.9	63.4
Nb	2.06	4.10	2.38	2.42
Ba	99.7	154.6	30.2	895.3
Hf	3.10	2.18	1.58	1.48
Ta	0.15	0.24	0.14	0.14
Pb	6.39	bd	bd	bd
Th	0.45	0.59	0.45	0.35
U	0.58	0.24	0.17	0.14
REEs				
La	6.06	7.38	4.35	4.20
Ce	15.39	18.25	10.85	10.40
Pr	2.76	3.02	1.70	1.64
Nd	13.78	14.18	8.77	8.54
Sm	4.42	3.80	2.41	2.49
Eu	1.35	1.27	0.85	1.13
Gd	4.91	3.71	2.72	2.64
Tb	0.90	0.61	0.50	0.50
Dy	6.06	3.92	3.11	3.08
Ho	1.22	0.75	0.62	0.62
Er	3.81	2.26	1.82	1.78
Tm	0.63	0.37	0.28	0.28
Yb	4.04	2.37	1.86	1.84
Lu	0.63	0.37	0.29	0.30

5.2. Tobago Island, continued

Mount Dillon Formation, North Coast Schist

	INT/28-2/1	INT/28-2/2	INT/29-2/8	INT/29-2/9	INT/3-3/2	INT/3-3/3	INT/3-3/4	INT/11-3/9
Location	Celery Bay		Mount Dillon					
Type	CA-RHY	IAT-RHY	CA-BAS	CA-RHY	CA-RHY	CA-RHY	IAT-RHY	IAT-RHY
Majors								
SiO_2	75.01	79.14	84.61	78.84	80.54	73.65	86.49	88.29
TiO_2	0.35	0.42	0.15	0.37	0.45	0.36	0.14	0.15
Al_2O_3	12.62	9.49	8.50	10.85	10.37	13.17	6.96	5.99
Fe_2O_3	2.68	2.49	0.41	2.06	1.38	2.37	0.51	0.39
MnO	0.07	0.13	bd	0.02	0.02	0.03	bd	0.03
MgO	0.90	0.94	bd	0.44	0.38	0.55	0.19	bd
CaO	0.38	0.71	0.15	bd	0.26	0.16	0.25	bd
Na_2O	6.10	4.41	4.52	4.80	4.88	6.19	3.04	2.99
K_2O	0.38	0.67	0.12	0.65	0.70	0.96	0.49	0.12
P_2O_5	0.06	0.09	bd	0.03	0.06	0.04	bd	bd
LOI	1.06	1.02	0.14	1.24	0.86	1.23	0.48	0.40
Total	99.62	99.51	98.74	99.38	99.87	98.70	98.58	98.44
Traces								
Sc	12.4	9.6	3.8	10.1	10.2	10.6	3.9	4.1
V	29.2	43.9	328.4	25.1	17.8	48.7	9.4	5.7
Cr	35.2	20.7	58.2	bd	bd	45.1	29.2	bd
Co	bd	4.5	36.9	3.6	bd	4.0	bd	bd
Ni	31.0	27.7	91.1	bd	bd	113.5	52.1	bd
Cu	31.3	36.2	149.3	15.7	23.5	37.0	10.5	10.2
Ga	13.5	9.0	17.2	10.5	10.3	12.5	5.4	3.8
Rb	3.3	7.2	76.4	10.0	5.8	5.4	4.5	1.6
Sr	43.0	34.8	487.9	49.4	16.3	23.6	23.8	11.7
Y	52.7	32.6	23.7	20.2	46.6	47.4	18.2	6.1
Zr	154.2	86.9	70.3	109.1	141.7	187.8	70.1	56.1
Nb	1.86	1.38	1.64	1.45	1.80	2.38	1.16	0.77
Ba	71.9	316.7	1285.9	160.2	82.9	112.2	92.8	36.9
Hf	3.85	2.04	1.81	3.09	3.79	4.90	1.78	1.46
Ta	0.17	0.12	0.10	0.13	0.15	0.18	0.10	0.07
Pb	5.64	10.23	bd	bd	bd	bd	bd	7.76
Th	0.96	0.36	1.00	0.53	0.67	0.78	0.23	0.24
U	0.78	0.44	0.42	0.40	0.53	0.65	0.31	0.30
REEs								
La	9.72	6.35	10.26	3.12	4.72	6.33	2.32	1.96
Ce	20.20	14.08	22.19	11.83	12.92	10.81	5.79	3.08
Pr	3.62	2.34	3.68	1.57	2.57	2.71	1.07	0.45
Nd	18.41	11.78	16.89	7.73	13.75	13.00	5.39	1.98
Sm	5.51	3.27	4.38	2.31	4.28	4.10	1.63	0.53
Eu	1.23	0.91	1.62	0.56	0.79	0.75	0.33	0.13
Gd	6.14	3.76	3.99	2.24	4.83	4.57	1.74	0.41
Tb	1.20	0.73	0.61	0.40	0.98	0.85	0.37	0.10
Dy	7.77	4.60	3.74	2.86	6.15	6.02	2.50	0.88
Ho	1.59	0.96	0.71	0.61	1.31	1.28	0.53	0.22
Er	5.11	2.93	2.07	2.17	3.95	4.20	1.66	0.88
Tm	0.85	0.46	0.32	0.40	0.65	0.70	0.28	0.17
Yb	5.81	3.13	2.10	2.95	4.44	4.72	1.94	1.44
Lu	0.93	0.52	0.32	0.51	0.73	0.75	0.32	0.28

5.2. Tobago Island, continued

Mount Dillon Formation, North Coast Schist, continued

	INT/13-2/3
Location	Mt. Dillon
Type	CA-RHY
Majors	
SiO_2	74.85
TiO_2	0.30
Al_2O_3	12.38
Fe_2O_3	2.05
MnO	0.04
MgO	0.95
CaO	3.15
Na_2O	2.40
K_2O	1.38
P_2O_5	0.04
LOI	1.23
Total	98.76
Traces	
Sc	10.7
V	21.5
Cr	bd
Co	bd
Ni	bd
Cu	15.6
Ga	10.0
Rb	12.3
Sr	74.0
Y	46.5
Zr	204.4
Nb	2.56
Ba	68.3
Hf	4.99
Ta	0.23
Pb	bd
Th	0.75
U	0.53
REEs	
La	7.28
Ce	21.46
Pr	3.29
Nd	15.55
Sm	4.43
Eu	0.70
Gd	5.06
Tb	0.95
Dy	6.48
Ho	1.36
Er	4.32
Tm	0.74
Yb	5.01
Lu	0.86

5.2. Tobago Island, continued

Amphibolites, North Coast Schist

*Geochemically, this sample is similar to the Karv or Mount Dillon Formation of the NCS, but is identical in the field to the distinct relict-plagioclase-phyric amphibolites. See text for details.

	INT/8-3/4*	INT/8-3/3	INT/8-3/5	INT/8-3/6	DY3D359	DY3D558
Location	Inverawe River					
Type	CA-AM	MOR-AM	MOR-AM	MOR-AM	MOR-AM	MOR-AM
Majors						
SiO_2	48.34	51.58	49.13	48.65	50.91	49.71
TiO_2	0.91	1.88	2.14	1.13	1.22	1.27
Al_2O_3	19.85	15.72	15.99	20.19	20.05	16.57
Fe_2O_3	11.73	10.20	10.80	8.08	7.57	9.44
MnO	0.18	0.16	0.24	0.14	0.15	0.16
MgO	4.04	5.82	6.07	5.32	4.23	6.13
CaO	8.61	7.99	11.09	13.54	12.17	12.59
Na_2O	2.83	5.03	4.46	2.09	1.84	3.06
K_2O	0.99	0.12	0.18	0.07	0.08	0.28
P_2O_5	0.18	0.19	0.23	0.11	0.16	0.14
LOI	2.79	1.09	1.19	1.98	1.78	1.38
Total	100.45	99.78	101.52	101.30	100.16	100.71
Traces						
Sc	33.0	38.8	43.9	27.3	28.3	36.8
V	369.5	260.5	330.8	192.0	197.7	226.5
Cr	43.4	209.0	209.0	225.7	321.6	294.6
Co	20.2	42.0	51.1	34.0	37.0	39.3
Ni	119.0	133.5	73.1	66.5	96.8	138.2
Cu	129.2	74.0	77.5	80.2	72.6	105.3
Ga	17.1	16.3	19.0	15.6	16.7	16.8
Rb	19.0	1.6	2.7	0.6	0.5	4.2
Sr	370.8	130.3	57.6	192.9	183.8	177.7
Y	18.7	36.6	47.0	24.9	27.1	28.6
Zr	50.6	112.4	173.7	77.2	75.6	82.5
Nb	0.96	2.69	4.26	1.85	2.18	1.77
Ba	409.7	50.6	74.8	32.2	26.2	44.8
Hf	1.38	2.43	3.79	1.85	1.69	1.97
Ta	0.06	0.19	0.28	0.13	0.12	0.16
Pb	bd	6.15	bd	bd	bd	bd
Th	0.85	0.19	0.20	0.03	0.08	0.06
U	0.32	0.11	0.09	0.04	0.04	0.03
REEs						
La	7.55	4.43	6.06	2.69	2.66	2.63
Ce	15.46	12.64	17.77	8.14	8.80	9.06
Pr	2.52	2.18	3.08	1.45	1.56	1.62
Nd	11.50	12.00	15.53	7.67	7.81	8.37
Sm	3.01	3.97	5.22	2.62	2.75	2.90
Eu	1.01	1.25	1.64	0.91	0.97	1.07
Gd	2.92	4.67	5.91	3.13	3.28	3.48
Tb	0.46	0.91	1.08	0.56	0.58	0.62
Dy	2.89	5.72	7.25	3.86	3.98	4.31
Ho	0.55	1.11	1.40	0.76	0.78	0.84
Er	1.65	3.27	4.28	2.25	2.30	2.45
Tm	0.25	0.51	0.67	0.36	0.36	0.39
Yb	1.63	3.37	4.21	2.29	2.18	2.34
Lu	0.25	0.51	0.63	0.34	0.36	0.39

5.2. Tobago Island, continued

Karv (Cretaceous Argillite), North Coast Schist

*Man O' War Hill

	DY3D304	DY3D305	DY3D448	DY3D693
Location	Main Ridge			M'O' War*
Type	IAT-BAS	IAT-BAS	SED	SED
Majors				
SiO_2	45.73	51.69	59.87	63.45
TiO_2	0.76	0.87	0.78	0.62
Al_2O_3	19.69	16.19	15.05	14.66
Fe_2O_3	9.43	8.72	7.22	5.40
MnO	0.21	0.26	0.17	0.14
MgO	8.30	7.21	3.11	3.74
CaO	8.89	4.33	0.76	2.59
Na_2O	0.57	4.47	6.92	2.75
K_2O	2.35	1.66	0.43	1.64
P_2O_5	0.07	0.23	0.10	0.13
LOI	3.82	3.49	6.64	4.05
Total	99.83	99.11	101.05	99.16
Traces				
Sc	42.0	38.8	29.0	20.9
V	284.2	310.5	375.1	154.2
Cr	492.2	205.8	166.8	77.8
Co	43.0	47.3	23.6	23.3
Ni	171.0	190.1	83.2	41.3
Cu	107.2	156.3	171.8	75.3
Ga	22.3	15.7	16.6	19.7
Rb	23.4	19.0	7.1	33.1
Sr	174.4	83.4	56.1	128.6
Y	26.2	26.9	31.1	43.1
Zr	56.8	62.0	71.4	153.4
Nb	0.56	0.61	1.21	2.24
Ba	857.8	695.7	94.6	535.8
Hf	1.33	1.51	1.88	4.20
Ta	0.05	0.05	0.09	0.18
Pb	bd	bd	bd	bd
Th	0.21	0.25	0.57	0.78
U	0.29	0.24	1.54	1.06
REEs				
La	3.18	3.70	7.59	9.24
Ce	8.23	9.37	10.83	19.86
Pr	1.47	1.74	2.62	3.68
Nd	7.54	8.71	11.69	16.56
Sm	2.55	2.84	3.27	4.66
Eu	0.98	1.01	1.01	1.28
Gd	2.93	3.18	3.73	5.11
Tb	0.51	0.57	0.65	0.89
Dy	3.62	3.92	4.29	5.89
Ho	0.73	0.78	0.86	1.17
Er	2.17	2.31	2.61	3.51
Tm	0.36	0.37	0.42	0.60
Yb	2.24	2.33	2.65	3.68
Lu	0.37	0.38	0.42	0.60

5.2. Tobago Island, continued

Argyle Formation, Tobago Volcanic Group

	INT/1-3/3	DY3D180	INT/16-2/2	INT/8-3/7	DR132
Location	Kendal Road		Argyle River/Inverawe		Roxburgh
Type	CA-BA	CA-BAS	CA-BA	IAT-BAS	CA-BA
Majors					
SiO_2	51.45	51.20	59.28	50.44	51.21
TiO_2	0.93	0.87	0.63	0.12	0.94
Al_2O_3	19.07	16.09	14.79	1.24	18.56
Fe_2O_3	10.45	9.75	7.51	4.62	10.40
MnO	0.17	0.18	0.14	0.09	0.17
MgO	2.93	5.50	3.01	20.99	4.26
CaO	10.21	9.28	7.86	18.60	7.94
Na_2O	3.36	3.33	2.95	0.19	4.01
K_2O	0.62	1.73	1.17	0.04	1.01
P_2O_5	0.23	0.20	0.19	0.00	0.18
LOI	0.47	1.29	1.64	2.53	1.92
Total	99.89	99.44	99.18	98.86	100.60
Traces					
Sc	30.8	35.0	19.9	60.8	28.0
V	385.0	300.8	189.8	56.9	264.6
Cr	bd	121.2	27.0	2334.3	91.1
Co	25.3	32.9	19.4	43.2	30.3
Ni	bd	106.7	bd	260.7	800.0
Cu	110.0	149.4	54.7	13.0	29.1
Ga	17.5	17.9	14.1	2.3	20.0
Rb	6.9	34.7	23.0	0.3	20.9
Sr	457.1	408.8	368.3	22.1	360.3
Y	23.7	20.1	18.5	2.0	24.3
Zr	73.1	53.2	57.7	3.4	70.6
Nb	1.51	1.34	0.91	bd	1.48
Ba	298.3	675.0	842.9	27.1	355.0
Hf	1.97	1.32	1.50	0.12	1.95
Ta	0.11	0.10	0.07	bd	0.13
Pb	bd	bd	bd	bd	bd
Th	1.64	0.80	1.19	0.11	0.84
U	0.72	0.31	0.70	0.03	0.42
REEs					
La	8.50	7.49	8.35	0.44	6.51
Ce	17.67	17.66	16.49	0.86	16.09
Pr	2.70	2.77	2.46	0.18	2.59
Nd	12.11	12.15	10.78	1.00	11.52
Sm	3.32	3.18	2.78	0.36	3.18
Eu	1.08	1.14	0.98	0.13	1.05
Gd	3.44	3.25	2.72	0.31	3.47
Tb	0.59	0.50	0.45	0.05	0.54
Dy	3.54	3.19	2.75	0.35	3.74
Ho	0.70	0.61	0.53	0.07	0.72
Er	2.04	1.73	1.59	0.19	2.18
Tm	0.34	0.28	0.26	0.03	0.35
Yb	2.19	1.71	1.71	0.17	2.07
Lu	0.35	0.27	0.28	0.03	0.35

5.2. Tobago Island, continued

Bacolet Formation, Tobago Volcanic Group

*Mount Pleasant, Hillsborough East River and Mount St. George, in turn.

	INT/23-2/8	INT/23-2/9	2G-1	2G-2	IG-1C	DY2H282	CF2H10	INT/7-2/3
Location	Bacolet Bay				Pleasant*	Hillsb'*		Mt. St. G*
Type	CA-BA	CA-BA	CA-BAS	CA-BAS	CA-BAS	CA-BA	CA-BAS	CA-BA
Majors								
SiO_2	50.04	53.13	49.02	51.26	50.58	47.79	49.02	50.34
TiO_2	0.71	0.61	0.81	0.72	0.76	0.83	0.81	0.80
Al_2O_3	14.12	14.38	16.73	16.38	14.06	18.83	16.73	18.02
Fe_2O_3	8.81	7.36	11.13	9.09	9.32	9.98	11.13	9.98
MnO	0.16	0.16	0.18	0.15	0.18	0.19	0.18	0.14
MgO	8.89	6.94	7.23	6.80	7.56	5.17	7.23	4.69
CaO	11.79	12.87	10.41	10.60	9.57	10.80	10.41	7.74
Na_2O	1.91	1.70	1.80	2.70	2.19	2.74	1.80	3.70
K_2O	0.47	0.45	0.29	0.48	1.39	0.95	0.29	1.45
P_2O_5	0.10	0.14	0.11	0.10	0.22	0.12	0.11	0.19
LOI	2.58	2.34	3.17	3.09	3.38	2.16	3.17	2.56
Total	99.59	100.06	100.87	101.37	99.21	99.56	100.87	99.62
Traces								
Sc	50.8	51.7	45.2	38.8	32.9	36.3	45.2	31.8
V	307.5	271.7	324.7	259.4	231.3	315.5	324.7	287.7
Cr	203.0	264.5	179.7	241.3	370.9	64.0	179.7	31.3
Co	33.0	29.4	38.6	43.4	36.1	29.3	38.6	31.6
Ni	39.0	64.6	56.1	319.3	138.0	bd	56.1	bd
Cu	133.2	105.3	129.7	110.5	99.7	95.1	129.7	98.5
Ga	14.6	13.1	18.1	16.2	15.7	19.5	18.1	16.8
Rb	9.7	6.3	3.9	8.7	23.2	17.9	3.9	25.6
Sr	268.0	249.6	301.3	292.9	360.0	348.8	301.3	459.1
Y	17.2	15.0	16.5	17.3	20.1	19.5	16.5	19.3
Zr	38.8	25.3	45.5	47.0	66.1	44.2	45.5	46.2
Nb	0.77	0.45	0.86	1.16	1.74	0.87	0.86	1.10
Ba	326.7	274.7	189.3	347.9	353.9	405.5	189.3	623.6
Hf	1.17	0.81	1.16	1.24	1.76	1.10	1.16	1.39
Ta	0.05	0.03	0.07	0.10	0.14	0.05	0.07	0.08
Pb	6.50	bd	bd	bd	bd	bd	bd	bd
Th	0.58	0.35	0.54	0.51	0.84	0.52	0.54	0.90
U	0.29	0.18	0.18	0.22	0.33	0.20	0.18	0.28
REEs								
La	4.49	3.13	4.19	4.25	7.03	4.62	4.19	6.75
Ce	10.13	7.07	10.94	10.48	17.19	11.21	10.94	14.39
Pr	1.74	1.20	1.85	1.71	2.67	1.87	1.85	2.28
Nd	8.39	5.88	8.70	8.04	11.89	8.81	8.70	10.46
Sm	2.47	1.80	2.50	2.32	3.14	2.49	2.50	2.86
Eu	0.82	0.67	0.85	0.86	1.03	0.90	0.85	1.01
Gd	2.48	2.04	2.59	2.49	3.20	2.80	2.59	2.86
Tb	0.41	0.36	0.41	0.40	0.50	0.45	0.41	0.49
Dy	2.70	2.19	2.72	2.75	3.16	3.10	2.72	2.88
Ho	0.52	0.44	0.51	0.52	0.60	0.59	0.51	0.56
Er	1.55	1.28	1.49	1.53	1.83	1.79	1.49	1.66
Tm	0.24	0.20	0.24	0.24	0.29	0.28	0.24	0.27
Yb	1.53	1.26	1.45	1.48	1.71	1.74	1.45	1.71
Lu	0.24	0.21	0.23	0.24	0.28	0.28	0.23	0.27

5.2. Tobago Island, continued

Goldsborough Formation, Tobago Volcanic Group

	INT/8-3/2	INT/8-3/1	DY2F275	INT/4-3/2	INT/4-3/1	INT/11-3/7	DY-2J-27	DY-2J-11
Location	Inland from Pembroke			Studley Park, Granby Point and towards Goodwood				
Type	IAT-BAS	CA-BA	CA-BA	CA-BA	CA-DAC	CA-BA	CA-BA	CA-BAS
Majors								
SiO_2	50.16	48.00	60.13	59.98	56.77	57.64	52.03	49.28
TiO_2	0.51	0.85	0.51	0.86	0.85	0.80	0.84	0.79
Al_2O_3	7.18	17.75	17.32	15.80	16.48	15.65	17.21	14.12
Fe_2O_3	8.76	11.27	5.38	7.98	8.66	8.52	9.05	10.54
MnO	0.19	0.12	0.15	0.14	0.13	0.18	0.26	0.21
MgO	13.82	1.40	2.41	2.04	1.31	2.43	3.04	9.25
CaO	17.99	17.82	5.38	2.96	10.84	6.87	10.22	10.57
Na_2O	0.37	0.47	5.74	6.19	2.40	2.60	4.04	2.21
K_2O	0.17	0.04	0.71	1.84	0.06	2.22	0.86	1.33
P_2O_5	0.05	0.27	0.20	0.34	0.35	0.28	0.14	0.10
LOI	1.69	1.64	2.13	1.73	2.74	1.89	3.00	2.11
Total	100.90	99.64	100.07	99.86	100.59	99.07	100.69	100.50
Traces								
Sc	98.7	22.6	10.2	20.5	20.1	19.9	32.1	38.5
V	346.8	302.8	156.1	140.1	157.2	187.4	310.2	289.0
Cr	852.5	24.9	47.5	bd	bd	bd	59.6	399.6
Co	43.4	39.2	15.4	14.4	11.7	15.7	31.7	48.1
Ni	124.2	bd	bd	bd	bd	bd	35.8	151.1
Cu	38.2	371.4	92.6	70.6	41.2	70.8	173.3	98.0
Ga	8.0	22.1	22.4	16.4	23.7	15.2	21.0	16.2
Rb	0.7	bd	8.7	25.9	0.9	48.9	19.2	23.1
Sr	59.2	1002.2	506.6	196.7	767.7	301.8	430.4	285.5
Y	10.8	21.0	16.8	40.3	53.1	33.5	21.6	16.1
Zr	18.1	58.1	71.7	126.8	171.5	148.3	64.6	37.4
Nb	0.16	1.14	2.91	1.75	2.71	2.51	1.30	0.83
Ba	bd	bd	494.6	650.8	25.1	676.3	247.5	605.3
Hf	0.58	1.53	1.58	3.22	4.21	3.61	1.57	0.86
Ta	bd	0.07	0.16	0.13	0.18	0.14	0.11	0.07
Pb	bd	bd	bd	bd	6.76	bd	bd	bd
Th	0.21	0.58	0.52	3.25	3.31	2.65	0.63	0.25
U	0.08	0.42	0.32	1.36	1.47	0.94	0.49	0.12
REEs								
La	2.15	6.34	5.83	19.43	24.75	15.74	5.27	2.79
Ce	5.37	14.67	13.47	41.65	46.62	33.96	12.40	6.95
Pr	0.94	2.37	1.97	6.06	7.54	4.95	2.07	1.11
Nd	4.78	11.17	8.47	26.08	31.53	21.37	9.45	5.55
Sm	1.49	3.04	2.12	6.44	8.22	5.30	2.59	1.83
Eu	0.50	0.94	0.75	1.73	2.11	1.51	0.90	0.72
Gd	1.56	3.08	2.15	6.15	7.89	5.16	2.84	2.04
Tb	0.27	0.52	0.34	1.01	1.40	0.84	0.46	0.34
Dy	1.68	3.09	2.22	5.87	8.56	4.89	3.14	2.41
Ho	0.34	0.61	0.45	1.14	1.61	0.95	0.60	0.45
Er	0.96	1.80	1.36	3.37	4.79	2.81	1.75	1.26
Tm	0.15	0.29	0.23	0.56	0.80	0.46	0.29	0.21
Yb	0.95	1.89	1.48	3.66	5.32	2.99	1.76	1.19
Lu	0.15	0.30	0.26	0.60	0.82	0.50	0.29	0.19

5.2. Tobago Island, continued

Goldsborough Formation, Tobago Volcanic Group, continued

	DY2J262	DY2H298	DY2JN24	INT/8-3/2
Location	Studley Park, Granby Point and towards Goodwood			
Type	CA-BAS	CA-BA	CA-BAS	IAT-BAS
Majors				
SiO_2	48.94	57.14	51.97	49.77
TiO_2	0.84	0.91	0.91	0.51
Al_2O_3	17.03	17.12	16.57	6.72
Fe_2O_3	11.18	7.87	10.78	8.86
MnO	0.22	0.19	0.18	0.19
MgO	4.84	2.92	4.09	13.83
CaO	9.84	6.52	8.16	17.81
Na_2O	3.15	4.04	3.40	0.36
K_2O	1.78	1.62	1.26	0.17
P_2O_5	0.12	0.24	0.23	0.06
LOI	3.36	1.52	2.17	1.69
Total	101.28	100.09	99.72	99.97
Traces				
Sc	41.2	17.6	30.2	96.5
V	332.4	218.0	326.3	329.7
Cr	73.5	85.5	49.4	890.5
Co	45.8	22.2	33.7	44.7
Ni	34.2	254.7	26.4	93.6
Cu	131.4	144.6	153.8	23.2
Ga	22.5	20.4	19.1	8.2
Rb	37.5	32.3	26.4	0.7
Sr	347.1	516.3	314.9	63.9
Y	20.1	24.0	23.5	11.5
Zr	55.5	88.5	73.3	20.6
Nb	1.17	1.97	1.57	0.19
Ba	647.9	1002.2	516.3	bd
Hf	1.32	2.24	1.79	0.67
Ta	0.09	0.17	0.10	bd
Pb	bd	bd	bd	bd
Th	0.53	1.22	0.96	0.22
U	0.20	0.46	0.39	0.08
REEs				
La	4.99	9.50	7.39	2.30
Ce	11.73	20.40	17.78	5.77
Pr	1.91	3.25	2.74	1.01
Nd	8.75	13.77	12.31	5.12
Sm	2.52	3.60	3.35	1.57
Eu	0.92	1.18	1.08	0.53
Gd	2.64	3.51	3.48	1.70
Tb	0.44	0.53	0.55	0.29
Dy	2.87	3.57	3.59	1.83
Ho	0.55	0.66	0.67	0.36
Er	1.58	1.93	1.99	1.02
Tm	0.26	0.32	0.32	0.16
Yb	1.55	1.95	1.95	1.01
Lu	0.25	0.32	0.31	0.16

5.2. Tobago Island, continued

Undifferentiated Units, Tobago Volcanic Group

*Patience Hill

	INT/3-2/1	INT/7-2/1	INT/13-2/5	INT/13-2/4	IC-1B	IC-53	IC-11	IF-39
Location	Blackrock							Pat' Hill*
Type	CA-BAS	CA-BA	CA-BA	CA-DAC	CA-DAC	CA-DAC	CA-DAC	CA-BA
Majors								
SiO_2	54.57	56.98	50.15	65.69	65.77	64.26	72.84	57.41
TiO_2	1.30	0.68	0.96	0.74	0.69	0.70	0.66	0.80
Al_2O_3	15.53	15.30	17.58	14.80	12.34	13.41	12.43	16.20
Fe_2O_3	12.13	7.31	11.32	6.51	6.23	6.15	5.24	7.47
MnO	0.17	0.18	0.18	0.14	0.15	0.15	0.14	0.15
MgO	4.05	3.23	4.48	1.55	1.10	1.32	0.92	2.61
CaO	4.17	8.22	6.70	2.48	2.41	2.50	2.33	6.45
Na_2O	4.74	3.57	4.03	4.99	8.54	10.37	2.57	5.54
K_2O	2.25	1.19	1.68	2.03	1.24	0.20	3.26	1.45
P_2O_5	0.27	0.15	0.22	0.32	0.28	0.29	0.26	0.24
LOI	1.29	3.91	2.15	1.42	0.33	0.97	0.43	1.59
Total	100.47	100.70	99.44	100.67	99.09	100.32	101.08	99.90
Traces								
Sc	34.3	31.0	25.5	15.0	12.7	13.2	12.8	14.4
V	344.2	303.4	342.2	63.3	60.7	65.4	103.0	165.8
Cr	65.9	64.3	bd	bd	117.4	83.4	79.8	22.8
Co	35.0	21.5	31.6	9.6	11.7	11.6	10.2	20.5
Ni	62.1	bd	bd	68.4	891.7	bd	41.9	bd
Cu	178.8	73.1	118.1	37.7	67.0	62.0	51.7	40.9
Ga	15.9	14.3	18.4	17.5	17.1	17.8	15.3	20.3
Rb	14.4	22.8	25.4	24.0	24.9	2.7	51.6	41.7
Sr	407.8	308.1	501.6	221.5	93.8	121.2	128.3	610.9
Y	20.8	20.3	24.7	46.8	46.2	44.9	39.2	25.3
Zr	52.0	74.9	68.6	223.5	189.2	196.0	170.5	82.9
Nb	1.13	1.61	1.37	3.74	4.02	4.09	3.35	2.25
Ba	505.6	295.5	514.2	864.8	398.4	48.0	825.9	1037.4
Hf	1.46	1.98	1.77	5.26	4.78	5.12	4.28	1.87
Ta	0.07	0.09	0.09	0.21	0.22	0.27	0.19	0.13
Pb	bd	bd	bd	bd	bd	bd	bd	bd
Th	0.57	1.18	0.68	3.95	3.85	3.84	3.35	1.25
U	0.31	0.52	0.36	1.66	1.27	1.41	1.12	0.50
REEs								
La	5.25	7.94	6.40	22.96	23.34	21.24	19.64	9.83
Ce	12.16	16.81	14.74	48.25	51.80	48.01	42.81	21.10
Pr	2.09	2.48	2.42	6.91	7.28	6.92	6.12	3.24
Nd	10.02	11.13	11.52	29.50	30.31	29.08	25.77	14.09
Sm	2.93	2.98	3.34	7.18	7.23	6.96	6.19	3.58
Eu	1.02	0.93	1.17	1.88	1.76	1.89	1.58	1.19
Gd	2.97	2.95	3.48	6.92	6.73	6.67	5.94	3.59
Tb	0.50	0.51	0.60	1.13	1.05	1.01	0.87	0.57
Dy	3.22	3.06	3.65	6.60	6.60	6.32	5.58	3.60
Ho	0.62	0.60	0.72	1.29	1.27	1.24	1.09	0.69
Er	1.91	1.76	2.13	3.90	3.78	3.64	3.18	2.03
Tm	0.30	0.29	0.35	0.65	0.63	0.59	0.52	0.34
Yb	1.91	1.87	2.20	4.26	3.87	3.71	3.22	2.09
Lu	0.29	0.30	0.36	0.70	0.64	0.62	0.54	0.34

5.2. Tobago Island, continued

Undifferentiated Units, Tobago Volcanic Group, continued

	INT/23-2/5	INT/23-2/4	INT/26-1/2	INT/23-2/2	INT/23-2/3	INT/28-2/6a	INT/28-2/6b	INT/29-2/1
Location	Minster Point					Gordon Bay		Merchison
Type	CA-BAS	CA-BA	CA-BAS	CA-BA	CA-BA	CA-BAS	CA-BAS	CA-BAS
Majors								
SiO_2	49.32	50.53	49.69	49.50	50.80	48.25	47.99	48.45
TiO_2	0.99	0.76	1.02	0.91	0.98	0.86	0.90	0.66
Al_2O_3	17.09	16.80	16.96	17.34	18.57	18.41	18.94	9.04
Fe_2O_3	10.66	9.63	11.55	11.14	9.78	10.91	10.94	10.76
MnO	0.17	0.13	0.17	0.19	0.15	0.15	0.14	0.17
MgO	5.84	6.99	7.09	4.19	3.80	6.14	6.45	16.76
CaO	10.63	9.79	10.00	8.49	8.47	11.41	11.80	12.60
Na_2O	2.99	2.43	3.88	3.57	2.85	1.82	1.80	1.56
K_2O	0.83	0.49	0.64	1.76	1.63	0.36	0.36	0.38
P_2O_5	0.17	0.10	0.12	0.22	0.30	0.08	0.07	0.12
LOI	1.58	2.56	2.97	1.81	1.61	0.88	0.88	0.84
Total	100.27	100.21	104.09	99.11	98.92	99.27	100.28	101.34
Traces								
Sc	41.2	37.5	45.0	32.1	25.6	40.1	40.2	66.8
V	380.2	380.2	289.7	339.8	390.9	412.4	338.7	256.5
Cr	76.3	19.3	129.2	13.7	42.6	93.4	46.7	962.8
Co	36.8	29.4	36.8	27.8	25.5	32.0	33.6	43.6
Ni	25.2	bd	54.6	375.7	95.4	439.6	30.2	214.0
Cu	122.2	248.5	91.1	56.6	205.2	108.0	113.6	80.9
Ga	15.6	18.3	15.7	19.1	19.1	16.8	17.3	10.4
Rb	14.5	45.5	11.5	10.0	19.0	4.6	4.5	0.9
Sr	455.0	233.2	289.3	427.8	606.2	309.6	321.4	92.6
Y	20.5	30.6	17.2	21.2	25.1	18.2	18.5	12.6
Zr	57.8	90.6	47.1	50.1	86.8	30.1	32.1	25.6
Nb	1.24	1.91	0.87	0.78	1.73	0.61	0.44	0.45
Ba	640.6	1755.4	333.5	423.4	1377.3	210.4	217.0	58.2
Hf	1.56	2.41	1.29	1.43	2.32	0.97	1.05	0.82
Ta	0.08	0.13	0.06	0.06	0.12	0.05	0.04	0.03
Pb	bd	5.56	bd	bd	bd	bd	bd	bd
Th	0.69	1.40	0.47	0.68	1.60	0.44	0.33	0.43
U	0.23	0.58	0.29	0.27	0.70	0.21	0.18	0.14
REEs								
La	6.33	11.23	4.78	5.72	10.66	2.92	2.71	3.78
Ce	13.87	23.29	10.64	12.47	22.49	6.97	6.60	8.09
Pr	2.33	3.84	1.77	2.03	3.51	1.18	1.15	1.40
Nd	10.82	17.79	8.39	9.74	15.78	5.98	5.91	6.67
Sm	3.07	4.80	2.43	2.75	4.04	2.02	2.02	1.96
Eu	1.11	1.79	0.88	0.93	1.37	0.75	0.75	0.63
Gd	3.04	4.61	2.41	2.92	3.95	2.29	2.33	2.00
Tb	0.51	0.75	0.41	0.48	0.63	0.43	0.44	0.33
Dy	3.26	4.73	2.71	3.28	3.74	2.75	2.81	1.97
Ho	0.63	0.91	0.52	0.63	0.73	0.55	0.55	0.38
Er	1.89	2.73	1.58	1.93	2.15	1.62	1.65	1.07
Tm	0.30	0.43	0.25	0.31	0.35	0.26	0.27	0.17
Yb	1.91	2.85	1.65	2.07	2.23	1.69	1.70	1.06
Lu	0.29	0.43	0.25	0.33	0.36	0.27	0.27	0.17

5.2. Tobago Island, continued

Undifferentiated Units, Tobago Volcanic Group, continued

	INT/19-2/1	INT/6-3/3	INT/6-3/1	INT/19-2/2	INT/6-3/2	INT/7-3/6
Location	Hillsborough West River					Plymouth
Type						
Majors						
SiO_2	47.92	46.34	51.03	46.39	48.88	51.00
TiO_2	0.85	0.82	0.80	0.86	0.87	0.74
Al_2O_3	19.90	16.09	18.68	19.22	18.16	17.85
Fe_2O_3	10.62	10.05	8.81	10.49	10.21	9.22
MnO	0.18	0.18	0.15	0.20	0.18	0.15
MgO	5.28	7.38	3.95	5.94	6.40	5.93
CaO	11.52	9.42	9.53	10.28	10.21	10.52
Na_2O	2.45	3.12	2.34	2.34	1.99	2.34
K_2O	0.48	1.20	0.62	1.12	0.59	0.26
P_2O_5	0.14	0.21	0.16	0.12	0.15	0.17
LOI	1.68	4.61	2.70	2.10	2.66	0.80
Total	101.03	99.43	98.77	99.05	100.30	98.97
Traces						
Sc	34.7	37.0	33.8	41.8	38.7	40.6
V	354.8	320.5	285.6	353.2	429.1	294.1
Cr	109.5	204.0	bd	20.9	43.0	37.5
Co	29.5	36.4	24.8	24.9	29.9	29.3
Ni	45.6	71.6	bd	21.3	29.8	33.1
Cu	142.7	111.5	81.6	63.5	73.6	93.8
Ga	17.3	18.7	18.3	19.2	17.4	16.4
Rb	33.0	22.8	10.0	22.6	8.8	3.2
Sr	574.1	422.2	361.2	432.5	362.7	248.6
Y	22.2	21.2	19.0	20.8	20.4	21.8
Zr	65.1	56.6	41.4	40.4	37.2	34.6
Nb	1.48	1.41	0.56	0.51	0.50	0.52
Ba	882.3	601.5	359.4	363.3	301.5	176.6
Hf	1.79	1.58	1.30	1.28	1.21	1.12
Ta	0.10	0.09	0.04	0.03	0.04	0.04
Pb	bd	bd	bd	bd	bd	bd
Th	1.11	0.97	0.41	0.49	0.46	0.38
U	0.47	0.39	0.21	0.20	0.21	0.18
REEs						
La	8.83	8.18	3.56	3.88	4.02	3.86
Ce	18.30	17.73	8.66	9.11	9.50	8.79
Pr	2.91	2.75	1.47	1.55	1.63	1.49
Nd	13.14	12.59	7.25	7.70	8.12	7.41
Sm	3.53	3.40	2.26	2.48	2.50	2.34
Eu	1.24	1.17	0.84	0.87	0.91	0.82
Gd	3.34	3.33	2.49	2.71	2.77	2.73
Tb	0.54	0.55	0.45	0.49	0.49	0.48
Dy	3.44	3.22	2.82	3.10	3.03	3.06
Ho	0.66	0.62	0.56	0.62	0.60	0.61
Er	1.99	1.81	1.69	1.83	1.79	1.81
Tm	0.32	0.29	0.27	0.30	0.28	0.28
Yb	2.03	1.93	1.78	1.94	1.86	1.84
Lu	0.31	0.31	0.29	0.30	0.29	0.29

5.2. Tobago Island, continued

Undifferentiated volcanogenic sediments, Tobago Volcanic Group

*Th is below the limit of detection so this rock cannot be defined using the Th-Co diagram. Due to the high MgO, low SiO_2 and low REE, this is a tholeiitic basalt.

	INT/6-3/8	INT/6-3/5	INT/6-3/10a	INT/6-3/9	INT/6-3/9	INT/6-3/4	INT/6-3/6	INT/6-3/10b
Location	Hillsborough West River							
Type	CA-BA	n/a*	CA-BA	CA-BA	CA-BAS	CA-BA	CA-BA	CA-BA
Majors								
SiO_2	49.83	45.91	49.32	47.23	46.61	46.77	48.36	48.41
TiO_2	0.82	0.80	0.93	0.92	0.91	0.92	0.80	0.90
Al_2O_3	18.18	18.57	20.01	17.93	17.72	19.53	18.82	19.55
Fe_2O_3	10.22	10.28	10.18	10.70	11.04	10.93	10.11	10.09
MnO	0.18	0.19	0.15	0.18	0.18	0.17	0.17	0.15
MgO	6.09	7.19	4.54	6.65	6.52	6.15	5.35	4.60
CaO	11.56	10.86	8.46	10.74	11.13	9.98	10.49	8.08
Na_2O	2.12	2.32	2.69	2.50	2.15	1.62	2.10	2.68
K_2O	0.28	1.28	1.33	0.52	0.52	0.47	0.52	1.33
P_2O_5	0.12	0.12	0.17	0.11	0.10	0.12	0.13	0.16
LOI	1.27	2.56	2.84	2.77	2.77	2.99	2.15	2.84
Total	100.68	100.08	100.61	100.26	99.65	99.67	98.99	98.76
Traces								
Sc	37.9	40.1	31.9	52.8	54.8	35.0	34.5	31.1
V	333.0	465.2	306.4	419.3	520.7	407.4	380.6	283.3
Cr	67.6	35.3	13.5	22.2	22.5	29.2	17.5	15.2
Co	33.5	41.2	29.3	31.2	34.3	29.4	27.8	26.4
Ni	28.8	30.5	bd	21.1	26.2	21.9	bd	bd
Cu	194.1	103.2	92.0	82.8	73.7	71.9	45.5	100.9
Ga	16.1	19.1	18.7	17.1	17.5	17.9	18.4	16.7
Rb	16.3	3.2	26.3	6.9	6.9	7.0	7.4	23.8
Sr	401.7	579.9	408.7	318.1	307.4	364.9	355.1	403.1
Y	20.2	20.5	24.2	20.2	20.1	21.9	19.7	21.5
Zr	48.2	23.9	59.6	31.0	31.7	39.7	37.7	50.4
Nb	1.12	1.80	1.11	0.41	0.41	0.66	0.53	1.02
Ba	442.3	149.1	566.0	272.1	269.8	353.8	341.2	515.5
Hf	1.36	0.89	1.74	1.06	1.03	1.29	1.21	1.45
Ta	0.07	0.09	0.08	0.03	0.03	0.04	0.04	0.07
Pb	bd	bd	bd	bd	bd	bd	bd	bd
Th	0.74	bd	0.79	0.47	0.46	0.54	0.55	0.81
U	0.35	0.02	0.32	0.19	0.18	0.20	0.25	0.32
REEs								
La	7.14	2.77	5.75	4.00	4.05	4.22	4.06	5.20
Ce	15.19	7.73	13.41	9.01	9.16	9.82	9.32	12.06
Pr	2.49	1.53	2.23	1.54	1.56	1.69	1.58	1.98
Nd	11.35	8.63	10.58	7.60	7.69	8.46	7.67	9.30
Sm	3.09	3.01	3.14	2.39	2.37	2.68	2.33	2.73
Eu	1.05	1.02	1.08	0.87	0.87	0.95	0.86	0.97
Gd	3.07	3.22	3.33	2.69	2.68	2.96	2.64	2.96
Tb	0.49	0.54	0.59	0.48	0.49	0.52	0.46	0.52
Dy	3.09	3.45	3.62	3.03	3.03	3.25	2.91	3.23
Ho	0.59	0.64	0.72	0.60	0.61	0.65	0.59	0.64
Er	1.80	1.83	2.13	1.77	1.79	1.92	1.73	1.89
Tm	0.28	0.28	0.35	0.28	0.28	0.31	0.28	0.31
Yb	1.82	1.66	2.20	1.81	1.79	1.98	1.85	1.97
Lu	0.28	0.25	0.36	0.28	0.28	0.31	0.29	0.32

5.2. Tobago Island, continued

Undifferentiated volcanogenic sediments, Tobago Volcanic Group, continued

*Minster Point, Little Tobago Island and Speyside Bay South in turn.

	INT/23-2/1	INT/14-3/1	INT/11-3/1
Location	Minster P*	Little Tob*	Speys'*
Type	CA-BA	CA-BA	CA-BA
Majors			
SiO_2	48.56	41.57	50.62
TiO_2	0.84	1.29	0.69
Al_2O_3	17.07	18.15	16.72
Fe_2O_3	10.17	13.32	9.77
MnO	0.15	0.16	0.09
MgO	5.81	7.60	8.29
CaO	11.15	13.31	8.06
Na_2O	2.79	1.73	1.46
K_2O	0.80	0.31	0.24
P_2O_5	0.17	0.04	0.06
LOI	2.91	3.51	4.79
Total	100.42	101.00	100.80
Traces			
Sc	38.7	41.1	48.3
V	319.9	304.1	306.6
Cr	20.2	61.9	199.9
Co	29.4	31.7	32.6
Ni	24.0	59.4	84.9
Cu	60.9	73.4	85.3
Ga	18.0	17.7	14.5
Rb	6.2	24.7	2.4
Sr	356.1	383.1	161.8
Y	21.6	20.1	18.8
Zr	49.0	43.1	33.1
Nb	0.80	0.65	0.22
Ba	318.8	535.9	69.4
Hf	1.42	1.22	1.07
Ta	0.05	0.04	bd
Pb	bd	bd	bd
Th	0.58	0.40	0.31
U	0.23	0.16	0.15
REEs			
La	4.85	3.73	2.28
Ce	10.59	8.53	5.77
Pr	1.83	1.51	1.03
Nd	8.92	7.56	5.31
Sm	2.74	2.43	1.84
Eu	0.96	0.95	0.63
Gd	2.85	2.64	2.19
Tb	0.49	0.45	0.42
Dy	3.23	3.04	2.76
Ho	0.64	0.60	0.58
Er	1.97	1.85	1.72
Tm	0.32	0.30	0.29
Yb	2.10	1.95	1.86
Lu	0.33	0.30	0.30

5.2. Tobago Island, continued

Deformed mafic volcanic-plutonic complexes, Tobago Pluton

	INT/28-2/5	INT/4-2/4	INT/11-3/2	INT/6-3/11	INT/6-3/13	INT/6-3/15	INT/6-3/16	INT6-3/12
Location	Anse Flamengo Complex		Richmond River Complex					
Type	Deformed ultramafic	Deformed gabbro	Deformed gabbro	Deformed volcanic	Deformed gabbro	Deformed gabbro	Deformed gabbro	Deformed gabbro
Majors								
SiO_2	48.83	52.17	46.21	44.63	47.41	48.37	46.42	48.55
TiO_2	0.38	0.74	1.11	0.58	1.85	0.82	1.01	0.72
Al_2O_3	3.32	19.18	15.57	15.19	16.81	15.47	14.14	16.23
Fe_2O_3	7.22	9.10	14.61	6.55	11.53	11.43	9.72	8.42
MnO	0.13	0.17	0.23	0.10	0.20	0.18	0.17	0.14
MgO	17.21	4.69	7.09	7.24	7.51	7.69	11.18	5.23
CaO	21.60	8.33	9.61	8.11	10.28	11.33	13.58	9.86
Na_2O	0.42	3.90	3.38	3.73	3.85	2.82	1.66	5.21
K_2O	0.04	0.86	0.39	0.68	0.25	0.54	0.40	0.77
P_2O_5	bd	0.13	0.22	0.10	0.21	0.20	0.03	0.49
LOI	0.96	1.41	1.07	12.55	1.40	0.75	2.43	3.77
Total	100.13	100.69	99.51	99.46	101.30	99.61	100.73	99.40
Traces								
Sc	103.8	24.7	44.5	18.2	35.0	40.5	110.5	29.4
V	170.8	239.2	408.3	181.4	249.8	275.9	401.4	256.9
Cr	787.8	32.5	80.7	322.3	209.7	226.6	317.2	57.2
Co	43.4	24.2	38.4	31.0	42.9	36.0	37.2	22.8
Ni	111.5	bd	24.4	89.6	55.0	43.9	83.1	24.6
Cu	14.6	57.6	189.1	723.1	210.3	239.2	21.4	94.0
Ga	5.0	18.1	16.3	11.8	14.5	14.1	14.3	15.0
Rb	0.4	14.2	2.4	9.3	3.4	5.3	3.2	12.0
Sr	40.1	420.6	461.9	340.5	284.6	434.0	281.9	236.7
Y	8.6	22.0	25.7	15.2	39.2	19.7	19.6	20.3
Zr	13.3	56.5	40.0	39.0	113.7	53.9	24.5	67.5
Nb	0.12	0.91	1.30	1.38	3.70	1.42	0.83	1.39
Ba	43.1	430.7	280.5	382.2	147.0	195.1	160.2	313.6
Hf	0.39	1.55	1.41	1.00	2.62	1.38	0.92	1.74
Ta	bd	0.07	0.07	0.08	0.23	0.09	0.05	0.09
Pb	bd	bd	bd	bd	bd	bd	bd	bd
Th	bd	0.49	bd	0.13	0.08	0.69	bd	0.67
U	0.02	0.25	0.01	0.10	0.03	0.26	0.03	0.76
REEs								
La	0.76	4.82	5.15	2.20	4.81	8.85	2.50	5.42
Ce	2.39	11.07	13.56	5.78	14.81	19.75	6.84	11.60
Pr	0.52	1.89	2.52	0.98	2.67	3.32	1.33	1.89
Nd	3.07	9.05	12.89	4.92	13.56	15.26	7.12	8.83
Sm	1.19	2.67	3.75	1.56	4.34	3.58	2.48	2.45
Eu	0.41	0.98	1.22	0.61	1.50	1.12	0.87	0.86
Gd	1.39	2.82	4.08	1.88	5.14	3.41	2.92	2.67
Tb	0.23	0.49	0.65	0.33	0.88	0.51	0.50	0.44
Dy	1.51	3.26	4.18	2.26	5.94	3.15	3.31	2.95
Ho	0.27	0.64	0.79	0.44	1.14	0.59	0.62	0.58
Er	0.80	1.99	2.36	1.40	3.45	1.76	1.81	1.79
Tm	0.12	0.33	0.38	0.23	0.53	0.28	0.27	0.29
Yb	0.74	2.16	2.36	1.52	3.43	1.77	1.75	1.94
Lu	0.11	0.34	0.37	0.24	0.53	0.28	0.27	0.31

5.2. Tobago Island, continued

Ultramafic rocks, Tobago pluton

*King Peter's Bay **Hornblende clinopyroxenite ***Olivine clinopyroxenite

Some of these samples are serpentinised, some may contain amphibole.

	INT/11-3/4	INT/16-2/1	INT/21-2/2	INT/21-2/3	INT/21-2/4	INT/27-2/1	INT/8-2/1
Location	Delaford	Argyle	Louis D'Or River			Culloden	KP Bay*
Type	Hbl Cpx**	Ol Cpx***	Wehrlite	Dunite	Ol Cpx***	Hornblendite	Ol Cpx***
Majors							
SiO_2	48.72	47.37	49.49	40.45	49.33	46.20	49.38
TiO_2	0.58	0.33	0.43	0.03	0.16	0.62	0.53
Al_2O_3	4.64	6.08	7.00	bd	1.29	11.51	5.24
Fe_2O_3	8.73	9.39	8.16	13.55	7.05	10.39	8.76
MnO	0.14	0.13	0.14	0.22	0.12	0.19	0.17
MgO	15.02	24.33	14.66	42.66	24.23	16.59	15.86
CaO	20.12	10.87	17.05	0.46	16.60	9.74	18.48
Na_2O	0.43	1.51	1.59	0.27	bd	2.15	0.66
K_2O	0.07	0.06	0.19	bd	bd	1.01	0.12
P_2O_5	bd	0.27	0.13	0.03	bd	0.28	bd
LOI	0.73	0.68	1.29	1.80	2.43	0.41	0.99
Total	99.17	101.03	100.12	99.87	101.31	99.09	100.20
Traces							
Sc	114.9	45.4	86.4	8.3	71.6	39.7	99.3
V	253.3	186.0	183.9	18.9	73.6	232.5	219.8
Cr	377.2	1794.3	613.2	1273.5	1386.1	1559.4	415.7
Co	41.1	71.0	44.7	140.2	70.7	54.6	48.1
Ni	74.2	370.5	95.6	666.3	249.1	369.5	105.0
Cu	11.4	50.9	66.1	18.1	12.4	25.4	13.2
Ga	7.3	6.8	7.3	1.6	2.4	12.2	7.5
Rb	0.6	bd	1.5	bd	bd	21.8	0.8
Sr	63.0	32.4	134.7	bd	28.5	106.9	74.9
Y	9.7	7.1	9.8	bd	3.0	14.2	11.9
Zr	9.9	16.2	16.9	bd	bd	37.5	18.5
Nb	bd	0.31	0.39	bd	bd	1.01	0.48
Ba	265.5	37.4	119.9	37.0	bd	343.5	55.0
Hf	0.40	0.42	0.52	bd	bd	1.05	0.69
Ta	bd	bd	0.03	bd	bd	0.06	0.03
Pb	bd	bd	bd	bd	bd	bd	bd
Th	0.11	0.13	0.32	bd	bd	0.28	0.13
U	0.05	0.07	0.13	0.02	bd	0.09	0.06
REEs							
La	1.07	0.98	2.93	bd	bd	2.52	1.86
Ce	3.13	2.63	5.72	0.26	0.62	6.26	4.59
Pr	0.67	0.50	0.99	bd	0.15	1.08	0.85
Nd	4.05	2.60	4.82	bd	0.93	5.41	4.67
Sm	1.56	0.87	1.50	bd	0.39	1.71	1.70
Eu	0.55	0.31	0.51	bd	0.13	0.63	0.58
Gd	1.77	1.04	1.61	bd	0.41	2.02	1.94
Tb	0.28	0.17	0.26	bd	bd	0.34	0.32
Dy	1.78	1.16	1.67	bd	0.44	2.24	2.05
Ho	0.32	0.22	0.30	bd	0.08	0.43	0.38
Er	0.88	0.63	0.90	bd	0.21	1.28	1.09
Tm	0.13	0.10	0.14	bd	bd	0.21	0.16
Yb	0.79	0.63	0.91	bd	0.17	1.32	1.05
Lu	0.12	0.10	0.14	bd	bd	0.21	0.16

5.2. Tobago Island, continued

Gabbro-dioritic rocks, Tobago pluton

	INT/11-3/3	INT/11-3/6	INT/1-3/5	INT/21-2/1	INT/20-2/1	INT/28-2/4	INT/7-3/3
Location	Delaford	Queen's B*	Kendal*	Louis D'Or	Hills W*	Celery Bay	Arnos Bay
Type	diorite	gabbro	gabbro	diorite	gabbro	gabbro	gabbro
Majors							
SiO_2	45.78	43.17	48.63	54.85	51.64	42.39	45.72
TiO_2	0.44	1.10	0.77	0.72	0.64	1.26	1.25
Al_2O_3	26.79	19.91	14.48	18.45	13.20	20.49	15.58
Fe_2O_3	7.03	13.22	10.36	5.78	9.24	13.40	11.21
MnO	0.10	0.18	0.17	0.09	0.17	0.13	0.21
MgO	2.91	6.18	8.48	5.07	8.72	6.89	7.80
CaO	13.65	11.22	10.36	8.47	10.07	13.18	11.05
Na_2O	2.06	2.16	4.20	5.14	3.05	2.02	2.23
K_2O	0.39	1.54	0.50	0.48	1.58	0.40	0.50
P_2O_5	bd	0.47	0.46	bd	0.19	0.05	0.16
LOI	1.47	1.88	1.04	0.41	1.17	0.73	3.18
Total	100.62	101.03	99.44	99.47	99.68	100.96	98.89
Traces							
Sc	6.6	31.1	50.4	17.1	43.4	35.9	45.0
V	145.7	415.5	335.4	168.4	247.1	480.9	348.8
Cr	bd	21.3	239.8	bd	291.3	bd	95.1
Co	14.0	38.9	35.6	18.2	34.8	41.0	33.9
Ni	30.7	bd	56.1	bd	47.0	34.4	31.6
Cu	35.5	138.4	126.1	14.9	23.5	237.0	34.4
Ga	25.1	19.4	15.9	18.7	13.0	17.4	16.1
Rb	7.4	16.2	5.1	3.9	26.4	3.7	7.2
Sr	747.1	647.2	478.2	461.9	317.6	475.8	328.7
Y	9.6	22.9	14.8	16.8	14.3	15.7	22.9
Zr	7.1	19.7	32.2	12.4	57.4	18.5	47.5
Nb	0.21	0.79	0.94	1.16	1.20	0.77	1.36
Ba	173.9	593.9	913.7	563.5	535.3	171.8	267.7
Hf	0.32	0.74	1.01	0.54	1.45	0.66	1.35
Ta	bd	0.04	0.06	0.09	0.08	0.04	0.09
Pb	bd	bd	bd	bd	bd	bd	bd
Th	bd	bd	0.20	bd	1.28	0.11	0.47
U	bd	0.02	0.11	0.44	0.56	0.04	0.22
REEs							
La	1.23	6.10	5.71	2.05	7.46	2.16	4.69
Ce	2.98	15.57	11.12	5.23	14.76	5.60	10.56
Pr	0.55	2.89	1.78	0.93	2.24	1.08	1.89
Nd	3.13	14.97	8.32	5.05	10.27	5.98	9.67
Sm	1.08	4.30	2.41	1.81	2.79	2.10	3.04
Eu	0.57	1.42	0.92	0.73	0.92	0.82	1.05
Gd	1.21	4.09	2.52	2.21	2.73	2.52	3.46
Tb	0.21	0.63	0.39	0.38	0.40	0.41	0.56
Dy	1.41	3.85	2.48	2.47	2.40	2.68	3.65
Ho	0.27	0.71	0.46	0.48	0.43	0.50	0.70
Er	0.81	2.05	1.33	1.43	1.27	1.42	2.11
Tm	0.13	0.30	0.20	0.22	0.20	0.21	0.33
Yb	0.83	1.84	1.31	1.41	1.29	1.31	2.10
Lu	0.13	0.27	0.20	0.21	0.21	0.20	0.33

5.2. Tobago Island, continued

Gabbro-dioritic rocks, Tobago pluton, continued

	INT/4-2/2	INT/2-3/7	INT/25-1/8	INT/28-2/10	INT/28-2/9	INT/3-2/2	INT/3-2/3
Location	Courland River		Culloden Bay				
Type	diorite	diorite	gabbro	norite	diorite	gabbro	gabbro
Majors							
SiO_2	53.70	57.53	45.14	46.44	47.12	49.89	44.60
TiO_2	0.27	0.67	0.81	1.01	0.40	0.77	0.81
Al_2O_3	20.66	15.50	20.44	16.52	27.01	16.68	17.56
Fe_2O_3	6.20	7.07	11.21	10.53	4.11	10.10	10.76
MnO	0.12	0.13	0.14	0.19	0.05	0.14	0.19
MgO	4.10	4.95	5.46	8.05	2.12	9.17	7.08
CaO	9.37	7.09	12.20	12.71	12.76	11.45	14.25
Na_2O	4.47	5.01	2.64	2.51	3.97	1.32	2.20
K_2O	0.45	0.85	0.40	0.28	0.25	0.32	0.20
P_2O_5	0.17	0.37	0.60	0.13	0.53	0.07	0.09
LOI	0.82	1.00	0.47	0.94	1.14	1.24	1.30
Total	100.32	100.16	99.51	99.33	99.46	101.15	99.04
Traces							
Sc	9.6	30.1	24.0	41.9	11.9	49.5	38.4
V	147.0	241.0	309.5	350.9	143.0	314.4	321.1
Cr	20.3	91.5	bd	116.9	16.4	203.7	126.7
Co	18.7	22.1	28.2	35.4	11.6	41.3	33.9
Ni	35.2	25.6	bd	48.9	27.7	61.8	53.7
Cu	18.6	36.1	153.7	116.3	155.0	96.0	172.2
Ga	19.1	17.8	20.9	16.7	19.9	16.4	17.0
Rb	5.9	10.3	5.7	2.0	1.5	5.5	1.5
Sr	908.0	465.7	895.3	511.1	793.0	242.8	622.9
Y	4.3	15.8	23.5	18.5	7.7	17.1	13.7
Zr	19.5	26.3	27.4	24.1	10.1	42.9	14.4
Nb	0.64	2.72	2.62	1.66	0.80	0.84	0.75
Ba	346.7	325.6	2949.8	211.9	275.3	216.9	189.4
Hf	0.53	1.02	0.99	0.88	0.31	1.23	0.47
Ta	0.05	0.23	0.14	0.09	0.05	0.06	0.05
Pb	bd	bd	bd	bd	bd	bd	bd
Th	bd	0.60	0.15	0.10	0.13	0.37	0.10
U	0.06	0.28	0.07	0.04	0.06	0.71	0.04
REEs							
La	2.50	4.83	10.44	4.07	5.17	3.66	3.07
Ce	4.88	13.37	23.08	9.78	8.75	8.59	6.93
Pr	0.69	2.34	3.76	1.75	1.20	1.50	1.24
Nd	2.99	10.77	16.89	8.84	5.19	7.34	6.39
Sm	0.69	2.82	4.18	2.69	1.29	2.29	1.98
Eu	0.43	0.83	1.41	0.96	0.66	0.79	0.82
Gd	0.64	2.67	4.09	3.01	1.38	2.36	2.24
Tb	0.09	0.42	0.61	0.48	0.21	0.41	0.36
Dy	0.61	2.64	3.75	3.07	1.26	2.75	2.31
Ho	0.11	0.47	0.70	0.57	0.23	0.53	0.43
Er	0.33	1.41	2.06	1.67	0.66	1.61	1.26
Tm	0.05	0.22	0.33	0.26	0.10	0.26	0.19
Yb	0.34	1.36	2.08	1.65	0.62	1.62	1.22
Lu	0.05	0.21	0.34	0.26	0.09	0.26	0.19

5.2. Tobago Island, continued

Mafic dykes cross-cutting the North Coast Schist

*Charlotteville and Flagstaff Hill, in turn.

**Hornblende microdiorite

	INT 2-3/4	DR780	DR430	DR509
Location	Bloody Bay	Main Ridge	Charlotte'*	Flagstaff*
Type	CA-BA Hbl MD**	CA-DAC Hbl MD	CA-BA Hbl MD	CA-BA Hbl MD
Majors				
SiO_2	53.93	64.29	63.04	61.31
TiO_2	1.09	0.65	0.69	0.73
Al_2O_3	16.42	13.79	12.04	14.67
Fe_2O_3	8.34	5.68	6.79	6.33
MnO	0.11	0.13	0.15	0.13
MgO	6.27	2.40	6.34	3.37
CaO	3.63	4.39	5.61	4.52
Na_2O	5.09	4.20	3.58	4.42
K_2O	0.06	1.42	1.35	1.81
P_2O_5	0.20	0.36	0.31	0.35
LOI	3.47	1.52	1.56	1.65
Total	98.61	98.82	101.45	99.28
Traces				
Sc	bd	13.9	16.9	13.8
V	234.3	131.2	137.4	141.0
Cr	40.2	bd	349.1	61.7
Co	21.6	11.1	22.4	16.9
Ni	38.7	bd	123.1	46.2
Cu	64.3	47.1	45.6	44.3
Ga	15.5	15.8	13.9	17.8
Rb	1.1	24.0	25.9	30.6
Sr	286.3	415.8	286.4	371.3
Y	25.1	29.0	23.5	28.0
Zr	81.0	128.5	117.6	146.3
Nb	4.32	2.86	3.96	4.87
Ba	bd	195.7	133.8	226.0
Hf	1.89	2.94	2.57	3.30
Ta	0.28	0.20	0.28	0.34
Pb	bd	6.05	bd	bd
Th	0.41	0.84	1.45	1.32
U	0.23	0.43	0.60	0.57
REEs				
La	6.50	7.99	9.73	11.12
Ce	16.30	19.98	21.02	25.19
Pr	2.56	3.04	3.04	3.69
Nd	12.19	14.41	13.71	16.66
Sm	3.54	3.74	3.39	4.07
Eu	1.08	1.16	1.01	1.23
Gd	3.62	4.03	3.60	4.22
Tb	0.61	0.67	0.57	0.68
Dy	3.94	4.42	3.70	4.35
Ho	0.78	0.89	0.71	0.85
Er	2.28	2.65	2.09	2.54
Tm	0.36	0.44	0.33	0.41
Yb	2.30	2.93	2.17	2.77
Lu	0.36	0.48	0.35	0.45

5.2. Tobago Island, continued

Mafic dykes cutting the Volcano-Plutonic Suite and Arnos Vale tonalite

*Microdiorite **Hornblende dolerite ***Hornblende microdiorite

	INT 11-3/5	INT 7-3/1	INT/26-1/4	INT/7-3/2	INT/26-1/6	INT/1-3/2	INT/1-3/6	INT/1-3/7
Location	Delaford	Arnos Bay				Kendal Road		
Type	CA-BA MD*	IAT-BAS dolerite	CA-BAS Hbl D**	CA-BA MD	CA-BA MD	CA-BA Hbl MD***	CA-BA Hbl MD	CA-BA dolerite
Majors								
SiO_2	49.90	46.22	50.21	48.50	49.80	53.78	54.74	48.84
TiO_2	0.90	0.74	0.92	1.00	0.85	0.80	0.91	1.08
Al_2O_3	17.83	13.33	16.41	17.46	18.84	17.96	15.72	18.47
Fe_2O_3	10.32	9.87	10.12	11.33	10.24	9.43	9.16	10.76
MnO	0.16	0.16	0.19	0.16	0.12	0.17	0.13	0.15
MgO	5.83	15.71	7.14	5.16	4.02	3.72	5.07	5.85
CaO	9.30	9.59	7.56	9.11	7.61	8.99	8.87	10.64
Na_2O	3.94	1.66	3.20	3.09	3.52	3.84	2.95	3.53
K_2O	0.52	0.84	1.84	1.42	2.16	0.86	0.36	0.43
P_2O_5	0.13	0.08	0.20	0.24	0.20	0.20	0.30	0.35
LOI	1.57	2.50	2.14	1.32	1.65	0.80	0.77	0.77
Total	100.41	100.70	99.94	98.80	99.01	100.54	98.99	100.87
Traces								
Sc	bd	bd	37.4	35.0	21.2	27.7	20.3	24.2
V	309.5	243.3	361.2	306.6	267.3	265.4	325.7	375.7
Cr	21.1	1348.6	221.1	28.4	bd	18.1	116.9	132.5
Co	31.4	52.8	41.3	33.1	24.1	21.2	24.8	29.2
Ni	bd	328.0	70.5	41.6	30.0	bd	51.5	62.1
Cu	87.9	98.7	105.9	60.7	145.6	162.7	77.4	92.5
Ga	16.7	12.4	17.0	17.3	17.5	18.0	17.4	20.0
Rb	6.0	23.3	50.9	25.9	35.9	9.9	1.7	2.0
Sr	482.2	166.9	400.7	389.9	511.7	419.4	489.5	550.0
Y	19.8	15.3	19.1	24.8	21.3	24.1	21.9	25.1
Zr	53.1	41.6	61.7	65.5	59.9	68.4	35.7	38.7
Nb	1.26	1.16	4.44	1.77	1.84	1.33	4.38	5.14
Ba	367.0	399.3	1073.2	675.0	1077.6	439.8	373.5	440.7
Hf	1.44	1.06	1.62	1.69	1.58	1.86	1.18	1.29
Ta	0.08	0.08	0.27	0.12	0.12	0.09	0.28	0.26
Pb	bd	bd	bd	bd	bd	bd	bd	bd
Th	0.36	0.18	0.80	0.64	0.63	0.94	0.35	0.45
U	0.19	0.14	0.50	0.25	0.30	0.57	0.15	0.16
REEs								
La	4.15	2.55	6.50	5.98	7.38	6.56	5.97	6.77
Ce	9.71	6.15	14.15	14.06	15.00	14.27	14.44	16.64
Pr	1.61	1.07	2.08	2.18	2.19	2.33	2.35	2.70
Nd	7.79	5.29	9.48	10.35	10.18	10.81	11.33	13.04
Sm	2.41	1.71	2.71	3.15	2.90	3.07	3.23	3.78
Eu	0.90	0.70	1.09	1.19	1.13	1.04	1.08	1.27
Gd	2.58	1.93	2.85	3.45	3.06	3.23	3.37	3.90
Tb	0.45	0.34	0.49	0.60	0.53	0.57	0.58	0.67
Dy	3.01	2.33	2.96	3.72	3.22	3.54	3.38	3.91
Ho	0.59	0.45	0.58	0.73	0.63	0.69	0.65	0.75
Er	1.79	1.37	1.67	2.13	1.86	2.09	1.87	2.16
Tm	0.29	0.21	0.27	0.34	0.30	0.34	0.30	0.34
Yb	1.85	1.40	1.72	2.19	1.92	2.25	1.86	2.18
Lu	0.29	0.21	0.27	0.35	0.31	0.37	0.29	0.33

5.2. Tobago Island, continued

Mafic dykes cutting the Volcano-Plutonic Suite and Arnos Vale tonalite, continued

*Clinopyroxene dolerite **Hornblende microdiorite ***Hornblende dolerite

	INT 25-1/4	INT/25-1/2	INT/2-3/9	INT/2-3/10	INT/25-1/2	INT/2-3/11	INT/4-2/1	2D-14
Location	Courland River							
Type	CA-BAS Cpx D*	CA-BAS dolerite	CA-BA Hbl MD**	IAT-BAS dolerite	CA-BAS dolerite	CA-BAS dolerite	CA-BA diorite	IAT-BAS Hbl D***
Majors								
SiO_2	46.96	50.57	53.37	48.44	49.22	49.32	49.72	47.79
TiO_2	0.99	1.41	0.70	0.65	1.46	0.77	0.91	0.67
Al_2O_3	15.52	15.75	16.50	13.25	16.87	14.26	17.07	13.75
Fe_2O_3	11.39	12.51	9.04	10.69	12.29	11.03	10.78	8.82
MnO	0.18	0.22	0.14	0.17	0.21	0.18	0.20	0.20
MgO	7.11	4.34	5.00	9.65	4.43	7.68	6.59	9.42
CaO	10.24	8.69	7.10	11.79	9.17	11.87	8.69	9.89
Na_2O	2.42	2.78	3.40	1.75	2.83	2.49	3.33	1.72
K_2O	0.45	1.08	1.88	0.75	1.11	0.14	1.21	1.14
P_2O_5	0.13	0.52	0.18	0.10	0.51	0.11	0.26	0.08
LOI	5.78	2.14	1.38	2.03	2.14	1.83	1.76	6.19
Total	101.18	100.01	98.68	99.26	100.25	99.69	100.50	99.67
Traces								
Sc	bd	30.7	30.4	50.1	30.8	40.2	33.0	34.9
V	338.5	254.4	232.2	247.6	273.9	275.4	294.5	231.9
Cr	355.3	26.7	93.1	596.5	22.0	208.1	132.6	469.0
Co	45.5	31.3	25.1	49.5	31.2	43.2	28.7	37.9
Ni	82.4	bd	30.1	101.4	bd	192.5	86.1	129.4
Cu	131.6	194.3	56.8	106.4	198.1	133.4	23.5	75.9
Ga	14.4	19.2	16.5	13.5	19.5	16.9	18.8	14.9
Rb	25.9	21.5	27.6	10.9	20.9	0.8	23.2	22.0
Sr	359.2	391.6	418.9	250.9	464.1	519.7	598.1	270.0
Y	16.5	40.0	17.2	15.7	40.3	17.6	21.1	13.6
Zr	36.5	141.5	58.8	31.4	155.8	37.7	65.9	43.1
Nb	0.81	3.97	2.02	0.53	4.02	0.70	2.20	0.70
Ba	568.2	669.5	1078.2	661.8	664.5	77.0	475.4	560.9
Hf	1.10	3.44	1.61	0.97	3.64	1.11	1.75	1.14
Ta	0.06	0.26	0.14	0.04	0.24	0.05	0.13	0.06
Pb	bd	bd	bd	bd	bd	bd	bd	bd
Th	0.47	1.65	0.75	0.24	1.51	0.30	1.35	0.11
U	0.21	0.76	0.42	0.11	0.72	0.14	0.50	0.09
REEs								
La	5.26	13.76	6.18	2.19	13.68	2.79	10.44	1.68
Ce	11.31	32.55	13.45	5.58	32.37	7.03	22.09	5.04
Pr	1.85	5.00	1.97	0.95	5.04	1.19	3.23	0.85
Nd	8.68	22.58	8.83	4.96	22.90	5.97	14.14	4.74
Sm	2.45	6.03	2.46	1.73	6.04	1.97	3.55	1.58
Eu	0.92	1.77	0.97	0.73	1.77	0.73	1.16	0.68
Gd	2.49	6.18	2.55	2.03	6.19	2.33	3.50	1.93
Tb	0.40	1.02	0.43	0.38	1.03	0.42	0.57	0.32
Dy	2.56	6.03	2.65	2.40	6.00	2.67	3.24	2.19
Ho	0.49	1.15	0.51	0.47	1.15	0.53	0.61	0.43
Er	1.44	3.38	1.51	1.37	3.37	1.53	1.78	1.26
Tm	0.22	0.54	0.25	0.22	0.54	0.25	0.28	0.20
Yb	1.44	3.49	1.60	1.37	3.46	1.57	1.80	1.29
Lu	0.22	0.56	0.26	0.22	0.55	0.25	0.28	0.20

5.2. Tobago Island, continued

Mafic dykes cutting the Volcano-Plutonic Suite and Arnos Vale tonalite, continued

*Hornblende microdiorite **Hornblende gabbro ***Hornblende granodiorite ****Clinopyroxene microdiorite

	INT 7-3/5	IC-29	IC-32	IC-33b	INT/23-2/6	2H-34	INT/26-1/3	INT/7-2/2
Location	Back Bay				Minster Point		Mount St. George	
Type	CA-BAS	CA-BA	CA-BA	CA-BAS	CA-A	CA-BAS	CA-BA	CA-BAS
	dolerite	Hbl MD*	Hbl MD	Hbl G**	Hbl GD***	dolerite	Cpx MD****	dolerite
Majors								
SiO_2	49.81	53.90	55.81	47.74	55.39	49.57	49.31	51.29
TiO_2	0.79	0.85	0.76	1.00	0.85	1.65	1.02	0.89
Al_2O_3	13.87	16.60	17.06	11.04	18.29	14.68	17.57	17.41
Fe_2O_3	10.68	8.12	8.96	11.93	7.84	13.46	11.06	11.19
MnO	0.22	0.11	0.11	0.28	0.15	0.23	0.16	0.14
MgO	10.16	4.43	3.58	10.36	2.56	5.24	6.75	4.64
CaO	11.23	8.68	8.15	12.00	8.28	9.11	5.75	9.36
Na_2O	1.91	3.08	3.06	1.29	4.03	2.48	3.33	2.80
K_2O	1.17	1.68	0.95	1.27	0.55	1.41	1.59	1.00
P_2O_5	0.13	0.20	0.19	0.10	0.17	0.58	0.19	0.19
LOI	1.36	1.49	1.09	1.99	2.38	2.41	4.38	1.96
Total	101.33	99.15	99.73	99.00	100.51	100.82	101.11	100.86
Traces								
Sc	bd	23.9	13.3	61.2	16.9	33.3	32.9	32.1
V	320.6	236.6	202.5	341.1	192.8	297.3	404.0	303.6
Cr	114.8	17.1	bd	345.8	bd	50.1	138.5	13.8
Co	42.5	21.4	16.3	44.8	13.0	34.1	29.3	31.4
Ni	51.2	bd	bd	174.1	bd	33.5	76.6	bd
Cu	76.7	24.3	332.5	233.2	9.6	326.2	45.4	226.4
Ga	16.2	16.7	18.4	13.8	18.1	17.9	18.7	18.4
Rb	12.3	24.1	17.9	31.5	5.3	23.7	36.1	14.9
Sr	348.3	435.5	423.8	294.1	373.3	333.5	478.1	450.2
Y	20.6	20.0	25.1	15.1	30.1	38.2	20.1	20.8
Zr	54.6	75.9	93.3	42.5	110.5	159.5	51.1	50.9
Nb	1.72	1.88	2.53	3.18	2.30	4.01	1.19	1.14
Ba	334.9	619.0	500.2	435.1	236.1	802.7	867.4	681.2
Hf	1.43	1.75	2.16	1.09	2.58	3.67	1.50	1.50
Ta	0.11	0.14	0.18	0.21	0.17	0.27	0.09	0.08
Pb	5.99	bd	bd	bd	bd	bd	bd	bd
Th	0.34	0.64	0.29	0.32	0.47	1.55	0.91	0.96
U	0.22	0.33	0.21	0.17	0.31	0.75	0.40	0.43
REEs								
La	3.87	5.76	3.96	4.08	5.56	14.22	6.95	7.04
Ce	9.23	12.71	11.25	8.98	14.97	34.05	15.73	15.15
Pr	1.52	1.83	1.84	1.34	2.44	5.07	2.56	2.41
Nd	7.63	8.94	9.58	6.80	11.61	24.23	12.00	11.17
Sm	2.51	2.48	2.85	2.04	3.46	6.12	3.34	3.07
Eu	0.94	0.96	1.06	0.78	1.13	1.80	1.14	1.09
Gd	2.76	2.89	3.31	2.39	3.81	6.40	3.34	3.13
Tb	0.48	0.47	0.58	0.38	0.69	0.98	0.56	0.52
Dy	3.21	3.13	3.92	2.53	4.35	6.19	3.22	3.16
Ho	0.62	0.63	0.79	0.49	0.86	1.20	0.60	0.62
Er	1.85	1.85	2.36	1.38	2.62	3.47	1.70	1.80
Tm	0.28	0.29	0.38	0.21	0.43	0.55	0.27	0.30
Yb	1.81	1.95	2.60	1.28	2.81	3.53	1.72	1.88
Lu	0.28	0.31	0.42	0.20	0.45	0.55	0.27	0.30

5.2. Tobago Island, continued

Mafic dykes cutting the Volcano-Plutonic Suite and Arnos Vale tonalite, continued

*Hillsborough West River **Microdiorite ***Plagioclase + clinopyroxene microdiorite

	INT 23-2/7	2G-43	2H-11A	IC-15
Location	Bacolet		Hills W*	Blackrock
Type	IAT-BA MD**	IAT-BA MD	CA-BAS dolerite	IAT-BA PCpMD***
Majors				
SiO_2	50.95	51.25	48.38	50.40
TiO_2	1.54	0.78	1.03	0.87
Al_2O_3	14.45	17.72	15.87	15.67
Fe_2O_3	9.04	10.16	11.27	9.63
MnO	0.17	0.21	0.20	0.19
MgO	7.72	3.59	5.98	5.32
CaO	11.51	11.43	10.08	10.77
Na_2O	3.27	2.08	2.86	2.42
K_2O	0.67	0.05	0.94	1.26
P_2O_5	0.33	0.25	0.20	0.13
LOI	0.80	2.94	2.53	3.13
Total	100.46	100.45	99.35	99.78
Traces				
Sc	bd	16.2	36.4	31.9
V	270.5	192.1	335.9	313.6
Cr	bd	12.9	36.3	96.5
Co	25.6	20.2	34.7	29.3
Ni	bd	bd	41.6	313.5
Cu	65.6	41.9	139.5	125.1
Ga	18.2	17.1	17.9	16.3
Rb	2.3	0.4	16.9	32.3
Sr	596.4	353.0	403.2	335.4
Y	26.3	17.5	22.5	19.0
Zr	91.2	44.8	63.3	49.0
Nb	2.16	1.06	1.29	1.12
Ba	36.6	24.2	324.3	361.5
Hf	2.22	1.12	1.63	1.32
Ta	0.14	0.08	0.09	0.09
Pb	7.99	bd	bd	bd
Th	0.22	0.17	0.62	0.37
U	0.21	0.11	0.27	0.20
REEs				
La	4.66	3.12	7.15	3.89
Ce	12.48	8.74	16.64	9.24
Pr	2.11	1.42	2.63	1.46
Nd	10.48	7.46	12.95	7.49
Sm	3.15	2.23	3.31	2.25
Eu	1.06	0.91	1.18	0.86
Gd	3.50	2.58	3.59	2.67
Tb	0.60	0.43	0.57	0.46
Dy	4.07	2.86	3.68	3.08
Ho	0.79	0.56	0.71	0.61
Er	2.39	1.64	2.06	1.77
Tm	0.38	0.26	0.32	0.27
Yb	2.49	1.69	2.06	1.82
Lu	0.39	0.27	0.32	0.29

5.2. Tobago Island, continued

Arnos Vale tonalite

	2D-70	2D-56	2D-50	INT/2-3/12	INT/2-3/8	INT/25-1/3	INT/4-2/3	INT/26-1/5
Location	Courland River							Arnos Bay
Type	tonalite	tonalite	tonalite	tonalite	tonalite	tonalite	tonalite	tonalite
Majors								
SiO_2	64.31	68.20	66.12	66.43	64.96	63.80	62.49	63.71
TiO_2	0.31	0.33	0.20	0.28	0.34	0.34	0.37	0.31
Al_2O_3	17.29	17.79	16.79	17.57	18.25	19.63	18.41	17.40
Fe_2O_3	2.47	2.42	1.37	2.01	2.85	2.71	3.00	2.28
MnO	0.05	0.04	0.02	0.03	0.07	0.05	0.06	0.04
MgO	1.30	1.11	0.84	1.25	1.46	1.47	1.74	1.33
CaO	3.02	3.17	2.68	3.63	3.21	3.57	4.46	4.79
Na_2O	8.69	4.67	11.20	5.76	6.24	6.80	5.47	6.60
K_2O	1.12	1.13	0.78	0.85	0.93	0.70	0.89	0.92
P_2O_5	0.14	0.18	0.19	0.22	0.26	0.19	0.16	0.18
LOI	1.24	1.23	0.72	1.14	1.25	0.40	1.56	1.26
Total	99.93	100.27	100.91	99.16	99.80	99.66	98.60	98.82
Traces								
Sc	3.9	2.9	2.1	2.5	2.7	3.3	4.4	3.1
V	99.9	98.1	62.3	52.8	74.3	94.3	81.1	64.7
Cr	16.4	38.7	17.5	bd	bd	bd	18.4	12.9
Co	7.3	6.2	4.9	6.2	7.2	6.5	7.1	4.9
Ni	35.3	bd	bd	bd	bd	25.5	bd	bd
Cu	24.2	10.4	22.3	10.7	12.7	42.8	13.3	12.8
Ga	21.9	23.5	21.4	21.3	22.2	22.8	19.4	19.6
Rb	15.1	14.8	13.2	15.0	17.1	8.8	12.4	14.6
Sr	751.7	639.2	685.8	693.0	762.2	811.3	699.3	302.4
Y	4.9	4.0	4.3	4.5	4.4	3.6	5.2	4.2
Zr	57.5	90.7	68.9	104.2	91.8	88.5	72.7	87.8
Nb	0.85	2.40	1.87	4.76	3.39	1.10	1.93	2.20
Ba	886.6	802.2	971.6	732.9	938.2	740.2	856.0	307.1
Hf	1.50	2.32	1.65	2.73	2.32	2.20	1.92	2.24
Ta	0.07	0.18	0.15	0.23	0.17	0.06	0.13	0.14
Pb	5.59	bd	5.42	bd	5.63	bd	bd	bd
Th	0.21	0.77	0.42	0.80	0.32	0.29	0.69	0.90
U	0.24	0.31	0.34	0.30	0.31	0.14	0.32	0.41
REEs								
La	2.08	5.26	4.31	8.97	8.09	4.25	5.45	7.34
Ce	5.31	12.09	9.25	17.54	15.92	8.38	10.69	14.18
Pr	0.80	1.66	1.21	2.31	2.16	1.17	1.50	1.93
Nd	3.42	6.39	4.41	8.73	8.63	4.86	6.09	7.50
Sm	0.94	1.30	0.83	1.65	1.62	1.01	1.28	1.46
Eu	0.41	0.52	0.38	0.64	0.70	0.43	0.46	0.45
Gd	0.82	1.05	0.72	1.20	1.24	0.85	1.11	1.13
Tb	0.11	0.13	0.09	0.13	0.14	0.11	0.15	0.14
Dy	0.79	0.66	0.59	0.65	0.69	0.60	0.86	0.71
Ho	0.14	0.11	0.11	0.10	0.11	0.11	0.14	0.11
Er	0.41	0.31	0.33	0.30	0.30	0.31	0.43	0.33
Tm	0.07	0.05	0.06	0.05	0.04	0.05	0.07	0.05
Yb	0.44	0.31	0.43	0.33	0.28	0.33	0.44	0.35
Lu	0.07	0.05	0.07	0.05	0.05	0.06	0.07	0.06

5.2. Tobago Island, continued

Arnos Vale tonalite, continued; tonalitic partial melts of the TVG

	IC-8	INT/7-3/4	INT/20-2/2	2D-7A
Location	Back Bay		Hillsborough West River	
Type	tonalite	tonalite	tonalite	tonalite
			partial melt of the TVG	
Majors				
SiO_2	67.67	70.52	68.34	69.87
TiO_2	0.24	0.17	0.28	0.32
Al_2O_3	17.20	16.21	15.20	15.70
Fe_2O_3	1.91	1.13	2.79	3.35
MnO	0.05	0.02	0.07	0.05
MgO	0.95	0.82	1.08	1.26
CaO	3.04	2.27	2.84	3.49
Na_2O	6.30	6.10	5.23	4.30
K_2O	1.45	1.48	2.00	2.01
P_2O_5	0.20	0.19	0.10	0.10
LOI	0.66	2.10	1.11	1.10
Total	99.68	100.99	99.04	101.55
Traces				
Sc	2.0	1.6	4.1	6.1
V	35.8	28.4	66.5	116.6
Cr	24.3	bd	23.0	49.5
Co	5.2	2.7	5.3	11.4
Ni	bd	bd	108.6	134.7
Cu	10.1	15.0	17.3	71.9
Ga	21.9	15.7	15.7	20.1
Rb	29.8	24.7	22.5	35.3
Sr	739.1	381.8	294.7	389.9
Y	4.0	3.4	7.5	9.9
Zr	81.8	83.4	132.3	93.2
Nb	4.45	3.76	1.49	1.91
Ba	874.1	496.8	1214.3	890.9
Hf	1.79	2.08	2.84	2.37
Ta	0.24	0.31	0.12	0.16
Pb	5.45	7.87	bd	bd
Th	1.03	1.95	0.72	0.82
U	0.57	0.44	0.50	0.67
REEs				
La	7.69	11.06	6.07	4.46
Ce	15.83	19.35	11.40	9.71
Pr	1.96	2.32	1.56	1.31
Nd	6.82	7.81	5.53	4.97
Sm	1.17	1.20	1.08	1.15
Eu	0.47	0.32	0.43	0.53
Gd	0.93	0.89	1.07	1.16
Tb	0.10	0.10	0.16	0.18
Dy	0.58	0.51	1.04	1.27
Ho	0.10	0.09	0.21	0.26
Er	0.31	0.29	0.69	0.82
Tm	0.05	0.05	0.13	0.15
Yb	0.35	0.37	0.97	1.02
Lu	0.06	0.07	0.19	0.19

5.2. Tobago Island, continued

LREE- and Nb-enriched minor intrusions

*Clinopyroxene dolerite

	INT29-2/2	INT/6-3/14	DY-3D-103	INT/1-3/4
Location	Merchison		Roxburgh	Kendal
Type	CA-BAS dolerite	CA-BAS dolerite	IAT-BAS Cpx D*	granitoid
Majors				
SiO_2	46.92	47.54	49.72	61.73
TiO_2	0.91	1.24	1.06	0.54
Al_2O_3	17.60	14.26	17.09	18.69
Fe_2O_3	11.17	9.47	8.96	4.45
MnO	0.18	0.15	0.19	0.09
MgO	5.82	11.24	6.79	0.83
CaO	6.95	9.56	10.56	4.06
Na_2O	3.12	1.98	3.75	5.20
K_2O	3.40	1.58	0.27	3.82
P_2O_5	0.25	0.21	0.20	0.16
LOI	3.97	2.07	1.69	0.37
Total	100.29	99.30	100.29	99.93
Traces				
Sc	bd	36.8	28.0	1.1
V	285.3	252.2	267.3	64.1
Cr	271.6	538.0	381.0	bd
Co	35.0	43.3	37.6	6.9
Ni	94.6	217.6	89.2	bd
Cu	36.7	18.8	97.5	174.6
Ga	17.0	14.9	20.4	20.1
Rb	4.8	22.3	1.5	32.3
Sr	530.8	318.7	543.2	647.7
Y	26.4	17.5	18.1	26.4
Zr	128.3	78.3	58.8	264.4
Nb	27.85	15.40	7.30	48.70
Ba	623.9	473.7	157.4	850.4
Hf	2.80	1.85	1.28	4.90
Ta	1.66	0.97	0.39	2.89
Pb	bd	bd	bd	bd
Th	1.90	0.86	0.22	3.83
U	0.81	0.42	0.14	1.12
REEs				
La	17.31	8.55	5.72	36.97
Ce	33.20	17.59	14.08	67.06
Pr	4.58	2.40	2.14	7.80
Nd	18.97	10.31	9.54	27.90
Sm	4.65	2.74	2.51	5.31
Eu	1.56	1.01	0.91	1.72
Gd	4.43	2.87	2.67	4.59
Tb	0.70	0.48	0.43	0.67
Dy	4.15	2.81	2.78	3.97
Ho	0.75	0.53	0.52	0.77
Er	2.15	1.48	1.45	2.35
Tm	0.33	0.23	0.22	0.40
Yb	1.97	1.42	1.39	2.63
Lu	0.29	0.22	0.23	0.44

5.3. San Souci Formation, San Souci Group, Trinidad

Felsic Rocks; sediment from Toco Formation

*SS = San Souci **Grand Riviere Road

	INSS7.1	INSS7.3	INSS5.1
Location	SS* Point		GR Rd**
Type	SH-AND	SH-AND	sediment
Majors			
SiO_2	65.21	64.45	81.28
TiO_2	0.56	0.51	0.62
Al_2O_3	14.73	16.98	8.80
Fe_2O_3	5.61	4.37	2.35
MnO	0.08	0.10	bd
MgO	2.38	1.95	0.31
CaO	2.54	2.54	0.43
Na_2O	6.43	7.45	0.57
K_2O	0.08	0.12	1.25
P_2O_5	0.25	0.29	0.04
LOI	2.26	1.66	3.77
Total	100.12	100.44	99.44
Traces			
Sc	8.0	7.2	7.1
V	63.67	52.69	42.47
Cr	45.20	25.67	34.57
Co	13.39	7.44	5.60
Ni	bd	bd	bd
Cu	25.08	55.30	12.58
Ga	14.29	16.20	10.59
Rb	0.94	1.18	55.06
Sr	127.99	270.85	70.47
Y	26.50	26.70	29.94
Zr	340.37	476.28	659.87
Nb	52.57	92.24	14.69
Ba	22.89	65.53	160.86
Hf	6.31	8.45	14.49
Ta	3.57	6.18	1.14
Pb	3.00	1.65	18.46
Th	6.37	10.57	12.42
U	1.87	3.07	3.59
REEs			
La	38.04	54.49	31.82
Ce	69.10	95.94	70.15
Pr	6.83	9.08	7.73
Nd	23.46	29.24	28.65
Sm	4.14	4.69	5.25
Eu	1.22	1.26	0.82
Gd	4.10	4.40	4.47
Tb	0.64	0.66	0.70
Dy	4.03	4.04	4.45
Ho	0.79	0.80	0.90
Er	2.45	2.48	2.81
Tm	0.39	0.41	0.47
Yb	2.63	2.76	3.33
Lu	0.43	0.47	0.56

5.3. San Souci Formation, San Souci Group, Trinidad, continued

Mafic rocks

*dol = dolerite, SS = San Souci

	28-1/1	INSS3a1	INSS3a2	INSS3b1	INSS3b2	INSS3cdol	INSS3cbrec	INSS3d	INSS3e
Location	SS Bay	Grand Riviere Road							
Type	TH-BA	TH-BA	TH-BAS	TH-BA	CA-BA	CA-BA	CA-BA	TH-BA	TH-BAS
Majors									
SiO_2	50.86	45.60	47.47	50.11	47.86	49.34	52.89	50.66	48.15
TiO_2	1.84	1.47	1.69	1.31	1.54	1.63	1.30	0.99	1.92
Al_2O_3	14.19	14.77	14.35	15.53	14.30	14.46	13.96	13.92	14.43
Fe_2O_3	10.05	9.48	10.57	9.02	8.60	9.06	8.12	7.93	11.65
MnO	0.14	0.17	0.14	0.16	0.14	0.15	0.12	0.12	0.18
MgO	6.40	6.69	7.62	7.30	5.84	6.05	7.83	7.80	7.20
CaO	6.54	8.16	6.26	8.26	7.98	6.46	7.91	9.83	9.02
Na_2O	5.29	4.32	3.63	4.27	4.54	4.37	4.70	4.71	3.50
K_2O	0.16	0.19	0.13	0.15	0.09	0.13	0.34	0.39	0.09
P_2O_5	0.24	0.16	0.16	0.12	0.17	0.16	0.19	0.10	0.21
LOI	3.01	9.88	9.10	3.56	9.66	8.85	2.69	3.97	3.42
Total	98.71	100.90	101.12	99.79	100.72	100.65	100.05	100.42	99.78
Traces									
Sc	33.3	32.4	37.0	35.0	31.0	31.3	33.2	28.6	40.4
V	260.27	276.62	318.68	253.88	274.88	289.61	256.15	208.06	341.07
Cr	208.82	180.30	217.95	294.65	167.80	182.07	238.13	283.30	106.36
Co	31.14	34.84	36.20	34.57	31.64	32.74	31.17	32.55	37.26
Ni	101.59	81.78	59.93	81.77	72.94	69.18	82.15	96.80	51.69
Cu	61.78	68.37	40.87	84.08	61.24	68.06	14.22	31.00	41.70
Ga	14.74	15.42	17.17	12.98	15.34	15.17	13.29	12.21	17.15
Rb	1.75	2.16	1.53	1.64	0.86	1.49	2.15	3.36	0.47
Sr	131.62	274.21	158.62	164.10	199.61	182.10	181.09	113.67	86.64
Y	43.09	31.91	38.48	27.34	32.38	32.90	26.81	22.08	41.48
Zr	144.92	121.73	133.40	87.68	139.32	139.91	105.78	75.49	146.76
Nb	5.73	6.50	5.05	3.86	9.06	8.86	15.15	4.00	5.60
Ba	75.70	265.74	87.99	367.79	134.35	153.43	73.86	61.01	47.39
Hf	3.48	2.68	2.98	2.05	2.99	3.16	2.29	1.72	3.41
Ta	0.37	0.44	0.35	0.28	0.61	0.61	0.99	0.27	0.39
Pb	bd	bd	bd	bd	bd	bd	bd	bd	bd
Th	0.33	0.50	0.32	0.24	0.83	0.85	0.99	0.38	0.34
U	0.18	0.18	0.18	0.09	0.30	0.30	0.30	0.12	0.13
REEs									
La	5.61	6.22	5.93	3.91	7.55	7.62	8.42	3.82	6.12
Ce	16.46	16.00	16.49	11.29	18.19	18.81	20.01	10.49	17.74
Pr	2.75	2.32	2.59	1.78	2.54	2.63	2.65	1.55	2.76
Nd	15.17	11.67	13.48	9.34	12.28	12.91	12.19	7.88	14.58
Sm	4.85	3.53	4.27	2.97	3.59	3.77	3.24	2.43	4.55
Eu	1.28	1.25	2.18	0.99	1.30	1.33	1.14	0.89	1.46
Gd	5.68	4.23	5.19	3.65	4.31	4.58	3.72	2.96	5.66
Tb	1.12	0.75	0.92	0.65	0.76	0.80	0.64	0.52	0.99
Dy	6.92	4.96	6.03	4.43	5.05	5.41	4.27	3.57	6.72
Ho	1.36	1.00	1.21	0.88	1.02	1.06	0.84	0.71	1.34
Er	4.10	2.94	3.55	2.53	3.03	3.11	2.49	2.06	3.96
Tm	0.63	0.45	0.55	0.40	0.47	0.49	0.38	0.33	0.62
Yb	4.25	2.92	3.52	2.59	3.01	3.14	2.48	2.11	4.02
Lu	0.67	0.46	0.56	0.40	0.47	0.49	0.39	0.33	0.62

5.3. San Souci Formation, San Souci Group, Trinidad, continued

Mafic rocks, continued

*SS = San Souci

	INSS3f	INSS6.1	INSS6.2	INSS6.3	INSS6.4	INSS6.5	INSS7.2
Location	Grand Riviere Road						SS Point
Type	TH-BAS	TH-BAS	TH-BA	TH-BA	TH-BAS	TH-BA	TH-BA
Majors							
SiO_2	48.64	51.01	49.92	50.90	48.79	56.21	51.07
TiO_2	1.69	1.91	1.20	1.55	1.97	1.18	1.24
Al_2O_3	14.21	12.98	13.95	14.11	13.88	14.09	15.08
Fe_2O_3	11.77	10.56	9.02	9.44	11.00	6.48	8.78
MnO	0.18	0.14	0.16	0.16	0.18	0.12	0.17
MgO	8.18	6.20	7.00	6.68	6.76	4.22	7.85
CaO	8.86	9.49	11.26	9.57	9.96	8.91	10.74
Na_2O	3.13	3.29	3.35	4.38	3.77	5.13	3.66
K_2O	0.09	0.03	0.16	0.14	0.04	0.13	0.12
P_2O_5	0.16	0.23	0.14	0.15	0.21	0.17	0.13
LOI	3.76	3.04	2.77	2.46	2.89	2.47	2.82
Total	100.68	98.89	98.93	99.55	99.44	99.13	101.65
Traces							
Sc	38.3	37.4	35.5	34.1	37.5	32.1	34.1
V	310.02	306.04	237.52	264.49	323.80	201.20	238.20
Cr	156.65	98.33	174.71	149.93	155.38	129.78	343.80
Co	39.43	35.80	31.79	31.77	37.85	20.11	33.85
Ni	65.87	47.97	65.79	86.62	54.01	37.43	86.54
Cu	105.50	30.52	23.16	19.36	24.04	14.38	173.89
Ga	15.86	16.82	13.68	14.44	17.30	13.26	14.70
Rb	0.77	0.13	1.53	0.96	0.18	1.10	1.61
Sr	83.82	106.26	137.65	124.13	122.89	161.35	85.56
Y	37.26	42.68	27.55	30.70	45.89	39.27	25.32
Zr	118.13	156.04	93.25	114.32	168.18	154.89	81.96
Nb	4.35	6.29	3.75	5.17	6.67	5.76	4.82
Ba	42.01	30.33	47.22	52.36	29.19	57.12	22.39
Hf	2.79	3.36	2.11	2.56	3.81	3.38	1.96
Ta	0.30	0.47	0.27	0.35	0.46	0.40	0.36
Pb	bd	bd	bd	bd	bd	bd	bd
Th	0.26	0.53	0.25	0.32	0.49	0.46	0.52
U	0.10	0.17	0.08	0.11	0.16	0.15	0.19
REEs							
La	5.15	7.14	4.49	4.73	7.00	6.64	4.85
Ce	15.02	20.14	12.46	13.54	20.17	18.41	12.75
Pr	2.35	3.03	1.93	2.07	3.14	2.79	1.87
Nd	12.49	15.51	9.78	10.87	16.43	14.09	9.38
Sm	3.98	4.73	2.97	3.37	5.10	4.33	2.87
Eu	1.37	1.39	0.93	1.19	1.58	1.50	1.13
Gd	4.90	5.72	3.65	4.19	6.24	5.30	3.46
Tb	0.87	1.00	0.65	0.74	1.10	0.93	0.62
Dy	5.85	6.77	4.35	5.01	7.42	6.21	4.11
Ho	1.16	1.35	0.87	0.99	1.47	1.24	0.82
Er	3.41	3.98	2.57	2.88	4.30	3.66	2.41
Tm	0.52	0.62	0.39	0.46	0.68	0.57	0.37
Yb	3.37	4.00	2.53	2.95	4.37	3.67	2.39
Lu	0.53	0.63	0.40	0.46	0.68	0.58	0.38

5.4. SW Aves Ridge

Felsic dredge hauls

	EA68 317a	EA68 317b	EA68 317c	EA68 317d	EA68 317e	EA68 317f	EA68 317g	EA68 317h	EA68 317i
Type	CAA-granite	CAA-granite	CAA-granite	CAA-granite	CAA-granite	CAA-granite	CAA-granite	CAA-granite	CAA-granite
Majors									
SiO_2	68.13	69.56	69.58	69.98	69.61	68.65	69.95	67.30	68.01
TiO_2	0.43	0.41	0.43	0.39	0.39	0.42	0.37	0.42	0.44
Al_2O3	15.23	14.59	14.85	14.74	14.09	14.37	14.28	15.40	15.36
Fe_2O_3	3.92	3.85	3.50	3.45	3.69	3.80	3.63	3.56	3.43
MnO	0.08	0.09	0.07	0.08	0.07	0.12	0.11	0.09	0.08
MgO	1.29	1.26	1.22	1.27	1.20	1.23	1.23	1.17	1.26
CaO	3.61	2.48	3.51	2.92	2.61	2.78	1.95	3.15	2.81
Na_2O	3.84	4.27	3.85	4.28	4.01	4.01	4.37	4.12	4.28
K_2O	2.35	2.63	2.53	2.32	2.36	2.49	2.89	2.53	2.59
P_2O_5	0.17	0.18	0.17	0.16	0.15	0.16	0.15	0.15	0.15
LOI	0.99	1.47	1.04	1.16	1.23	1.43	1.83	1.06	1.07
Total	100.05	100.80	100.75	100.75	99.41	99.45	100.75	98.96	99.47
Traces									
Sc	9.9	9.9	9.7	10.0	8.8	10.1	9.2	10.0	8.9
V	78.0	77.4	67.2	75.5	70.5	70.8	71.0	70.1	71.4
Cr	bd	bd	bd	bd	17.2	bd	20.4	bd	bd
Co	6.7	6.8	6.5	6.1	5.9	6.4	5.7	5.8	6.0
Ni	bd	bd	bd	bd	bd	bd	bd	41.2	bd
Cu	16.6	12.9	13.6	11.8	11.4	9.6	19.4	14.7	12.1
Ga	12.6	13.2	13.4	12.9	12.3	12.5	12.3	12.9	12.6
Rb	26.4	32.8	30.2	24.4	24.9	31.3	31.1	30.5	29.3
Sr	405.4	367.6	424.0	404.5	384.5	382.7	444.3	402.1	413.3
Y	19.8	21.2	21.2	21.0	19.3	20.1	19.1	18.4	17.5
Zr	127.2	143.4	160.2	138.0	137.1	128.5	128.5	114.7	118.8
Nb	4.13	3.93	4.69	4.67	4.50	4.39	4.33	4.07	4.20
Ba	697.9	742.9	782.8	823.1	882.8	788.9	904.0	790.5	833.2
Hf	2.94	3.22	3.57	3.13	3.14	2.94	2.94	2.68	2.66
Ta	0.29	0.33	0.36	0.33	0.31	0.31	0.30	0.33	0.27
Pb	bd	bd	bd	bd	bd	bd	bd	bd	bd
Th	1.86	1.92	2.01	1.82	1.85	2.18	1.89	1.94	1.60
U	0.81	0.91	0.95	0.94	0.82	0.84	0.81	0.83	0.66
REEs									
La	13.91	15.07	15.35	14.77	15.56	13.25	12.63	11.97	12.35
Ce	30.79	33.14	33.93	32.67	34.24	29.37	27.94	26.33	27.19
Pr	4.11	4.39	4.46	4.30	4.48	3.94	3.70	3.55	3.64
Nd	17.47	18.72	18.77	18.37	18.76	16.76	15.78	15.29	15.52
Sm	3.74	3.98	3.95	3.92	3.90	3.57	3.41	3.27	3.30
Eu	1.05	1.11	1.10	1.09	1.06	1.05	0.98	1.05	1.03
Gd	3.31	3.52	3.50	3.46	3.32	3.26	3.08	2.94	2.93
Tb	0.48	0.51	0.52	0.51	0.48	0.49	0.46	0.44	0.43
Dy	2.97	3.18	3.19	3.15	2.96	3.06	2.88	2.79	2.69
Ho	0.59	0.63	0.62	0.62	0.58	0.60	0.57	0.55	0.53
Er	1.80	1.94	1.95	1.91	1.75	1.87	1.75	1.70	1.62
Tm	0.31	0.33	0.33	0.32	0.30	0.31	0.30	0.29	0.27
Yb	2.04	2.25	2.25	2.17	2.04	2.16	2.04	2.01	1.87
Lu	0.34	0.38	0.38	0.36	0.34	0.36	0.34	0.33	0.30

5.4 SW Aves Ridge, continued

Felsic dredge hauls, continued

	EA68 317j	EA68 319a	EA68 319b	EA68 319c	EA68 319d	EA68 319e	EA68 319f	EA68 319g	EA68 319h
Type	CAA-granite	CAA-granite	CAA-granite	CAA-granite	CAA-granite	CAA-granite	CAA-granite	CAA-granite	CAA-granite
Majors									
SiO_2	67.37	70.32	72.26	71.06	70.64	70.95	69.86	72.06	71.70
TiO_2	0.42	0.37	0.38	0.38	0.40	0.39	0.38	0.41	0.37
Al_2O3	15.34	13.28	13.62	12.59	13.50	14.12	12.90	13.63	12.91
Fe_2O_3	3.79	3.53	3.46	3.42	3.50	4.27	4.02	3.44	3.22
MnO	0.10	0.11	0.12	0.10	0.11	0.14	0.11	0.11	0.12
MgO	1.26	0.97	1.06	1.06	1.09	1.35	1.34	1.06	1.02
CaO	2.99	3.04	2.82	1.59	3.12	1.63	1.60	3.35	2.54
Na_2O	4.21	3.27	3.94	4.20	3.38	4.68	3.78	3.28	3.27
K_2O	2.60	2.72	1.93	2.58	2.72	1.12	2.70	2.61	3.08
P_2O_5	0.15	0.17	0.17	0.17	0.18	0.19	0.19	0.17	0.17
LOI	1.17	1.11	1.25	1.55	1.14	1.69	1.97	1.04	1.10
Total	99.40	98.88	101.00	98.70	99.79	100.53	98.86	101.15	99.50
Traces									
Sc	10.3	7.8	8.4	8.3	9.0	8.7	8.4	8.2	7.9
V	73.7	65.8	58.4	64.1	67.4	67.0	71.3	66.7	62.3
Cr	13.4	22.6	bd	bd	bd	bd	bd	bd	bd
Co	6.1	4.7	5.0	5.2	6.0	6.2	6.2	6.4	5.6
Ni	bd	bd	bd	bd	bd	bd	bd	bd	bd
Cu	12.2	40.0	16.0	13.2	12.7	19.7	23.6	22.9	18.4
Ga	12.6	12.4	11.4	10.5	12.1	11.9	11.4	12.5	11.6
Rb	30.1	34.6	22.9	23.4	32.6	16.9	27.4	31.3	32.7
Sr	391.2	379.1	348.8	261.6	387.1	327.4	320.6	401.3	356.6
Y	22.8	16.9	16.8	17.4	18.2	16.9	19.6	16.8	17.0
Zr	122.3	124.3	118.7	113.3	138.2	120.3	127.6	98.6	112.9
Nb	4.65	4.35	4.11	3.92	4.78	4.37	4.85	4.45	3.98
Ba	806.9	803.8	469.1	889.8	772.1	197.1	1094.9	789.4	1029.3
Hf	2.83	2.93	2.75	2.64	3.24	2.91	2.93	2.34	2.60
Ta	0.33	0.32	0.32	0.30	0.36	0.33	0.35	0.31	0.33
Pb	bd	bd	bd	bd	bd	bd	bd	bd	bd
Th	1.61	2.75	1.83	1.91	2.10	1.99	1.83	1.72	1.48
U	0.75	0.77	0.65	0.66	0.73	0.62	0.72	0.66	0.73
REEs									
La	12.35	11.59	12.57	13.62	12.64	10.54	13.47	13.26	12.62
Ce	27.71	25.29	27.48	29.99	27.73	23.92	30.03	28.91	28.79
Pr	3.82	3.36	3.58	3.91	3.69	3.22	3.92	3.75	3.72
Nd	16.70	14.28	14.89	16.17	15.54	13.82	16.69	15.77	15.68
Sm	3.80	2.98	3.06	3.25	3.29	3.05	3.44	3.14	3.18
Eu	1.08	0.93	0.86	0.95	0.96	0.87	0.99	0.96	0.97
Gd	3.56	2.76	2.72	2.93	2.93	2.75	3.20	2.82	2.84
Tb	0.54	0.41	0.40	0.42	0.44	0.42	0.46	0.40	0.41
Dy	3.49	2.59	2.54	2.68	2.74	2.62	2.91	2.53	2.62
Ho	0.69	0.52	0.50	0.52	0.55	0.52	0.58	0.49	0.51
Er	2.11	1.57	1.56	1.61	1.69	1.57	1.76	1.51	1.58
Tm	0.36	0.26	0.26	0.27	0.28	0.26	0.30	0.25	0.26
Yb	2.46	1.83	1.84	1.88	1.97	1.84	2.10	1.74	1.88
Lu	0.41	0.31	0.31	0.32	0.34	0.31	0.35	0.29	0.31

5.4. SW Aves Ridge, continued

Felsic dredge hauls, continued

	EA68 319i	EA68 319j	EA68 318j (317k?)
Type	CAA-granite	CAA-granite	CAA-granite
Majors			
SiO_2	70.68	71.90	70.49
TiO_2	0.36	0.34	0.44
Al_2O3	13.17	13.37	13.29
Fe_2O_3	3.23	3.21	3.91
MnO	0.09	0.09	0.07
MgO	0.98	0.87	1.28
CaO	2.89	2.78	3.17
Na_2O	3.45	3.47	3.47
K_2O	2.59	2.18	2.36
P_2O_5	0.17	0.14	0.22
LOI	1.09	0.98	0.99
Total	98.71	99.32	99.69
Traces			
Sc	8.8	7.8	10.2
V	65.3	58.8	74.2
Cr	15.0	21.1	bd
Co	5.4	5.0	6.7
Ni	bd	bd	bd
Cu	24.7	18.1	32.7
Ga	12.1	11.2	11.9
Rb	33.0	31.3	21.9
Sr	390.8	324.7	407.2
Y	18.2	16.4	17.0
Zr	102.7	102.3	129.3
Nb	4.12	4.40	3.96
Ba	780.8	686.7	803.7
Hf	2.50	2.46	2.81
Ta	0.32	0.33	0.23
Pb	bd	10.04	bd
Th	1.71	1.93	1.21
U	0.72	0.62	0.60
REEs			
La	13.66	11.80	10.63
Ce	30.29	25.81	24.02
Pr	3.95	3.37	3.31
Nd	16.64	14.20	14.49
Sm	3.34	2.90	3.13
Eu	0.95	0.85	1.06
Gd	2.99	2.66	2.88
Tb	0.43	0.38	0.43
Dy	2.67	2.44	2.61
Ho	0.53	0.48	0.52
Er	1.66	1.49	1.57
Tm	0.27	0.25	0.26
Yb	1.93	1.77	1.75
Lu	0.32	0.29	0.30

5.4. SW Aves Ridge, continued

Mafic dredge hauls

	EA68 318a	EA68 318b	EA68 318c	EA68 318d	EA68 318e	EA68 318f	EA68 318g	EA68 318h	EA68 318i
Type	CAA-BA	CAA-BA	CAA-BA	CAA-DAC	CAA-BA	CAA-BAS	CAA-BA	CAA-BA	CAA-BA
Majors									
SiO_2	43.41	44.99	49.75	52.88	49.32	44.18	54.02	55.83	34.39
TiO_2	0.63	0.59	0.74	0.68	0.79	0.52	0.68	0.70	0.57
Al_2O3	20.49	22.43	16.79	13.98	17.06	11.17	14.73	16.45	11.15
Fe_2O_3	10.04	8.72	12.14	9.53	9.85	7.03	8.58	7.59	9.63
MnO	0.21	0.15	0.50	0.49	0.44	1.11	0.41	0.38	0.88
MgO	5.52	4.58	2.56	1.11	2.47	1.92	1.35	2.13	5.07
CaO	7.42	7.19	2.05	4.76	3.18	13.13	3.69	1.57	17.30
Na_2O	3.85	3.68	0.17	0.19	0.16	0.32	0.26	0.25	1.33
K_2O	1.28	1.44	10.14	10.09	10.06	7.31	10.56	10.36	2.06
P_2O_5	0.20	0.24	1.09	1.73	0.86	2.97	1.80	0.78	1.24
LOI	7.09	5.29	3.54	4.77	5.24	10.20	3.45	2.99	15.21
Total	100.12	99.30	99.47	100.19	99.43	99.86	99.54	99.03	98.84
Traces									
Sc	22.4	21.9	36.5	33.6	41.2	26.5	33.0	36.4	24.4
V	251.4	200.0	359.6	303.1	385.8	253.5	288.3	268.2	275.9
Cr	bd	bd	94.4	58.5	68.2	66.5	71.4	71.3	21.8
Co	30.7	22.6	30.1	16.7	23.3	44.5	19.9	19.8	33.5
Ni	48.9	34.4	102.7	137.0	89.8	256.0	84.9	85.6	146.6
Cu	107.9	115.2	101.6	115.2	135.7	94.6	103.7	128.9	147.7
Ga	15.2	16.0	14.6	7.8	18.2	9.3	9.7	11.6	12.5
Rb	20.5	18.0	99.0	82.1	106.1	75.8	90.5	90.3	19.5
Sr	619.2	903.0	106.3	152.1	123.7	335.9	143.9	89.2	289.3
Y	13.6	14.1	34.4	25.5	33.7	30.3	25.4	26.5	23.8
Zr	29.5	31.8	64.7	58.5	74.9	35.1	52.0	85.5	42.9
Nb	1.16	1.12	4.75	3.78	5.08	3.70	3.99	4.41	1.96
Ba	229.5	423.5	6192.6	5698.9	5868.3	5130.6	5929.7	6259.6	977.6
Hf	0.76	0.83	1.62	1.39	1.83	0.69	1.17	2.05	1.01
Ta	0.07	0.07	0.33	0.28	0.36	0.24	0.29	0.30	0.11
Pb	bd	bd	30.07	30.80	13.95	31.09	20.53	22.01	18.29
Th	0.58	0.30	1.78	1.55	1.88	1.67	1.60	1.72	0.90
U	0.32	0.24	2.65	4.12	1.80	34.88	2.44	3.62	0.87
REEs									
La	4.29	4.81	14.93	15.64	18.72	16.08	14.91	15.26	10.68
Ce	10.83	11.69	33.69	23.73	28.07	19.88	24.76	27.37	18.19
Pr	1.56	1.81	5.48	3.57	4.36	3.51	3.85	4.40	3.04
Nd	7.69	8.94	25.77	16.21	20.05	15.74	17.04	19.93	14.41
Sm	2.06	2.33	5.97	3.77	4.86	3.46	3.76	4.37	3.38
Eu	0.72	0.83	2.93	1.43	1.71	1.34	1.51	1.68	1.12
Gd	2.07	2.33	5.76	3.63	4.77	3.55	3.60	4.08	3.41
Tb	0.33	0.36	0.76	0.54	0.72	0.51	0.52	0.57	0.50
Dy	2.17	2.32	4.33	3.44	4.62	3.24	3.28	3.51	3.08
Ho	0.43	0.45	0.80	0.69	0.94	0.68	0.67	0.70	0.60
Er	1.28	1.32	2.20	2.07	2.84	2.10	1.97	2.06	1.72
Tm	0.20	0.21	0.33	0.32	0.45	0.34	0.31	0.32	0.26
Yb	1.36	1.39	2.06	2.06	2.91	2.29	1.95	2.14	1.70
Lu	0.22	0.22	0.32	0.34	0.47	0.40	0.32	0.35	0.27

5.4. SW Aves Ridge, continued

Mafic dredge hauls, continued

	EA68 318k	EA68 318l
Type	CAA-BA	CAA-BA
Majors		
SiO_2	57.12	53.15
TiO_2	0.65	0.58
Al_2O3	14.21	13.07
Fe_2O_3	5.19	10.36
MnO	0.40	0.37
MgO	1.54	1.47
CaO	4.04	4.60
Na_2O	0.17	0.24
K_2O	10.73	8.74
P_2O_5	0.73	1.61
LOI	5.37	4.86
Total	100.14	99.06
Traces		
Sc	34.3	28.2
V	243.7	302.0
Cr	103.7	59.2
Co	21.8	14.1
Ni	174.2	95.6
Cu	97.1	91.2
Ga	11.0	9.2
Rb	94.7	78.1
Sr	117.1	141.8
Y	26.4	26.7
Zr	93.5	53.4
Nb	4.88	3.74
Ba	6755.1	5314.7
Hf	2.23	1.17
Ta	0.31	0.26
Pb	14.14	17.37
Th	2.07	1.86
U	3.16	3.46
REEs		
La	16.03	16.04
Ce	31.12	24.26
Pr	4.65	4.00
Nd	20.87	17.72
Sm	4.64	3.95
Eu	1.79	1.57
Gd	4.40	3.80
Tb	0.63	0.56
Dy	3.84	3.50
Ho	0.75	0.69
Er	2.21	1.99
Tm	0.35	0.31
Yb	2.24	1.98
Lu	0.36	0.32

APPENDIX SIX: RADIOGENIC ISOTOPE RESULTS FROM TOBAGO, THE SAN SOUCI VOLCANIC FORMATION, AND THE AVES RIDGE

A6.1. Analysis details

The measured ratios of isotopes of Nd and Hf from the NERC Isotope Geosciences Laboratory, Nottingham, are presented in Tables A6.1 and A6.2, respectively. Age-corrected isotope ratios are also displayed, along with Sm, Nd, Lu and Hf concentrations determined using the ICP-MS at Cardiff University (see Appendix 3).

For Nd isotope analysis (Table A6.1), $^{143}Nd/^{144}Nd$ is reported normalised to a preferred value of 0.511860 for the La Jolla standard. The measured $^{143}Nd/^{144}Nd$ ratios for one run of the La Jolla standard were $^{143}Nd/^{144}Nd = 0.511846 \pm 0.000003$ (1σ, n = 6), which accounts for the samples run during December 2009 (majority of those on Table A6.1). The values for INT/20-2/1, INT/4-2/2, INSS7.1 and INSS5.1 were obtained during a separate run in October 2010 during which the measured $^{143}Nd/^{144}Nd$ ratios for the La Jolla standard were $^{143}Nd/^{144}Nd = 0.511847 \pm 0.000003$ (1σ, n = 10). Finally, the values for INT/8-3/5, DY-3D-558 were obtained during a run in January-February 2011 during which the measured $^{143}Nd/^{144}Nd$ ratios for the La Jolla standard were 0.511853 ± 0.000008 (1σ, n = 3).

For Hf isotope analysis (Table A6.2), replicate analysis of the JMC475 standard during the December 2009 run for the majority of samples, gave $^{176}Hf/^{177}Hf$ ratios of 0.282161 ± 0.000006 (1σ, n = 45). This value is comparable to a preferred value of 0.282160 (Nowell & Parrish, 2001), and similar to previously reported values from the same lab of 0.282879 ± 0.000008 (Blichert-Toft, 2001) so no further corrections were made. The values for INT/20-2/1 and INT/4-2/2 were obtained during a separate run in October 2010 during which time the analysis of the JMC475 standard returned results of $^{176}Hf/^{177}Hf$ 0.282199 ± 0.000011 (1σ, n = 10). INT/8-3/5, DY-3D-558, INSS7.1 and INSS5.1 were run during January-February 2011 during which time the $^{176}Hf/^{177}Hf$ ratios of JMC475 were 0.282151 ± 0.000003 (1σ, n = 35). Blank values for Hf reported at the time of analysis were consistently <100 pg (I.L. Millar, 2009, pers. comm.).

Table A6.1. Nd isotope results for the rocks of Tobago, San Souci and the Aves Ridge.

Sample	Unit	Age (Ma)	$^{143}Nd/^{144}Nd_m$	± (2σ)	Sm (ppm)	Nd (ppm)	$^{147}Sm/^{144}Nd$	$^{143}Nd/^{144}Nd_i$	εNd_i
INT/29-2/4	Parlatuvier, NCS	130	0.513119	0.000009	2.42	6.60	0.221621	0.512930	+8.97
INT/28-2/8			0.513054	0.000007	2.76	10.05	0.165988	0.512913	+8.62
INT/4-3/3			0.513075	0.000007	2.41	8.77	0.166094	0.512934	+9.04
INT/3-3/2	Mt. Dillon, NCS	130	0.513109	0.000006	4.28	13.75	0.188139	0.512949	+9.34
INT/28-2/1			0.513002	0.000005	5.51	18.41	0.180895	0.512848	+7.36
INT/8-3/5	Amphibolite, NCS	130	0.513138	0.000007	2.90	8.37	0.209418	0.512960	+9.55
DY-3D-558			0.513139	0.000006	5.22	15.53	0.203161	0.512966	+9.67
INT/7-2/3	Tobago Volcanic Gp.	110	0.512979	0.000008	2.86	10.46	0.165259	0.512860	+7.09
INT/1-3/3			0.512991	0.000006	3.32	12.11	0.165699	0.512872	+7.32
INT/8-3/2			0.513022	0.000014	1.49	4.78	0.188403	0.512887	+7.62
INT/23-2/3			0.512957	0.000007	4.04	15.78	0.154738	0.512846	+6.82
INT/3-2/1			0.512978	0.000007	2.93	10.02	0.176736	0.512850	+6.91
INT/20-2/2	Tonalite vein	106	0.513047	0.000009	1.08	5.53	0.118040	0.512965	+9.04
INT/26-1/5	Arnos Vale Tonalite	106	0.513007	0.000007	1.46	7.50	0.117658	0.512925	+8.27
INT/1-3/4	High-Nb granite	106	0.512953	0.000007	5.31	29.70	0.108059	0.512878	+7.34
INT/29-2/2	Nb-enriched basalt	106	0.512997	0.000010	4.56	18.97	0.148154	0.512894	+7.67
2D-14	Mafic dyke	91	0.513124	0.000007	1.58	4.74	0.201474	0.513004	+9.43
INT/20-2/1	Gabbro-diorite	106	0.512967	0.000002	2.79	10.27	0.164194	0.512853	+6.85
INT/4-2/2			0.513009	0.000003	0.69	2.99	0.139078	0.512913	+8.02
INSS3c	San Souci mafic	90*	0.513088	0.000006	3.77	12.91	0.176503	0.512984	+9.01
INSS6.5			0.513089	0.000005	4.33	14.09	0.185743	0.512979	+8.92
INSS7.2			0.513065	0.000012	2.87	9.38	0.184932	0.512956	+8.46
INSS7.3	San Souci felsic		0.512856	0.000002	4.69	29.24	0.096941	0.512799	+5.40
INSS7.1			0.512878	0.000006	4.14	23.46	0.106657	0.512815	+5.72
INSS5.1	San Souci sediment		0.511782	0.000003	2.25	28.65	0.047453	0.511754	-14.99
EA68 11318g	Aves Ridge mafic	76	0.512843	0.000006	3.74	17.47	0.129387	0.512779	+4.65
EA68 11317a	Aves Ridge granitoid		0.513000	0.000007	3.76	17.04	0.133366	0.512934	+7.78

m = measured ratio, i = initial Nd, NCS = North Coast Schist, * = assumed age of the formation as U-Pb geochronology results not available

Table A6.2. Hf isotope results for the rocks of Tobago, San Souci and the Aves Ridge.

Sample	Unit	Age (Ma)	$^{176}Hf/^{177}Hf_m$	± (2σ)	Lu (ppm)	Hf (ppm)	$^{176}Lu/^{177}Hf$	$^{176}Hf/^{177}Hf_i$	εHf_i
INT/29-2/4	Parlatuvier, NCS	130	0.283300	0.000012	0.41	1.57	0.037110	0.283210	+18.34
INT/28-2/8			0.283277	0.000013	0.30	1.86	0.022920	0.283221	+18.75
INT/4-3/3			0.283229	0.000011	0.29	1.58	0.026082	0.283166	+16.79
INT/3-3/2	Mt. Dillon, NCS	130	0.283184	0.000007	0.73	3.79	0.027371	0.283118	+15.09
INT/28-2/1			0.283184	0.000006	0.93	3.85	0.034326	0.283101	+14.48
INT/8-3/5	Amphibolite, NCS	130	0.283249	0.000010	0.39	1.97	0.028132	0.282181	+17.31
DY-3D-558			0.283237	0.000008	0.63	3.79	0.023622	0.283180	+17.27
INT/7-2/3	Tobago Volcanic Gp.	110	0.283160	0.000005	0.27	1.39	0.027603	0.283103	+14.12
INT/1-3/3			0.283221	0.000008	0.35	1.97	0.025247	0.283170	+16.48
INT/8-3/2			0.283176	0.000010	0.15	0.58	0.036751	0.283100	+14.02
INT/23-2/3			0.283139	0.000005	0.36	2.32	0.022050	0.283093	+13.78
INT/3-2/1			0.283183	0.000005	0.29	1.46	0.028226	0.283125	+14.89
INT/20-2/2	Tonalite vein	106	0.283167	0.000008	0.19	2.84	0.009507	0.283148	+15.63
INT/26-1/5	Arnos Vale Tonalite	106	0.283292	0.000030	0.06	2.24	0.003806	0.283285	+20.45
INT/1-3/4	High-Nb granite	106	0.283154	0.000005	0.44	4.90	0.012760	0.283129	+14.93
INT/29-2/2	Nb-enriched basalt	106	0.283041	0.000006	0.29	2.80	0.014717	0.283012	+10.80
2D-14	Mafic dyke	91	0.283123	0.000006	0.20	1.14	0.024930	0.283080	+12.91
INT/20-2/1	Gabbro-diorite	106	0.283155	0.000005	0.21	1.45	0.020580	0.283114	+14.42
INT/4-2/2			0.283126	0.000015	0.05	0.53	0.013406	0.283100	+13.91
INSS3c	San Souci mafic	90*	0.283139	0.000005	0.49	3.16	0.022035	0.283102	+13.66
INSS6.5			0.283156	0.000007	0.58	3.34	0.024676	0.283114	+14.07
INSS7.2			0.283140	0.000006	0.38	1.96	0.027550	0.283093	+13.34
INSS7.3	San Souci felsic		0.282956	0.000006	0.47	8.45	0.007904	0.282943	+8.02
INSS7.1			0.283013	0.000008	0.43	6.31	0.009683	0.282997	+9.92
INSS5.1	San Souci sediment		0.282066	0.000004	0.56	14.49	0.005491	0.282057	-23.33
EA68 11318g	Aves Ridge mafic	76	0.283112	0.000005	0.32	1.17	0.038865	0.283057	+11.76
EA68 11317a	Aves Ridge granitoid		0.283178	0.000005	0.34	2.94	0.016434	0.283154	+15.19

m = measured ratio, i = initial Hf, NCS = North Coast Schist, * = assumed age of the formation as U-Pb geochronology results not available

APPENDIX SEVEN: REPRINTS OF PUBLISHED WORK RELATED TO THE THESIS

Online *Debate*

Pacific rise

In answer to the criticisms of James and Lorente (Geoscientist 19.9), Iain Neill sets out the stall for the widely-accepted "Pacific Origin Paradigm" model for the origin of the Caribbean Plate.*

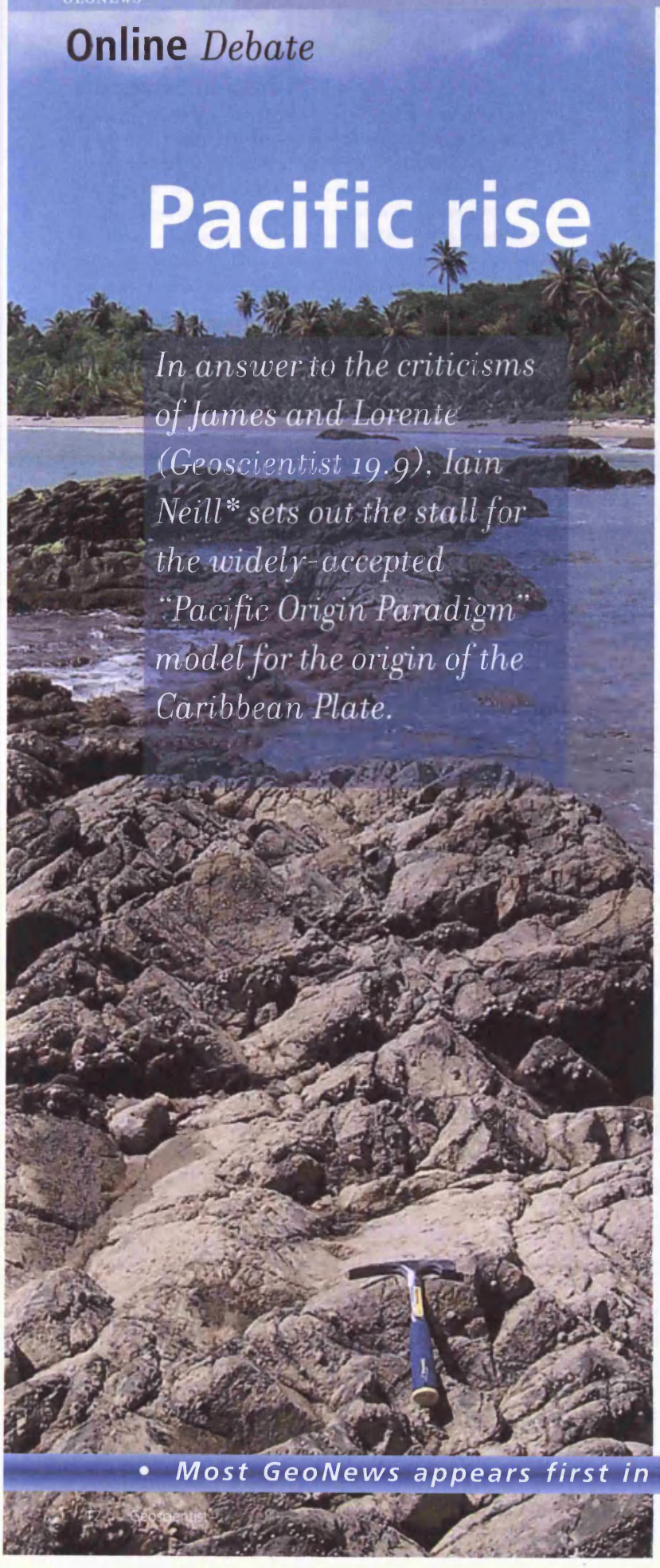

Pro-POP – some of the fundamental concepts[1,2,3]

- Andean/Cordilleran arc history due to Pacific subduction and the presence of passive Atlantic margins indicate that the Americas have moved westwards in the mantle reference frame during the Atlantic opening history. Lesser Antillean subduction can only be explained by the *relative* eastward movement of the Caribbean plate with respect to the Americas. Arc magmatism has been more or less continuous with a westward-dipping subduction zone, for the last ~85 Ma[4] ~125 Ma[3,5], even ~130+ Ma. Assuming 125 Ma of westwards subduction at a reasonably slow rate (say 2 cm/yr) the leading edge of the Caribbean plate will have originated 2500 km westward of its present location – that is, in the Pacific.
- Plate motion determinations for the Caribbean and North and South America indicate the Americas did not split until ~160 Ma and the present day Caribbean plate does not fit into the space available geometrically during the Jurassic-Cretaceous.[3,5]
- Most sedimentary successions in in-situ Caribbean margins do not show any evidence of island arc-related tuffs deposited during the Early Cretaceous, when the Caribbean island arc system was very much active. So the arc was hundreds, nay thousands of kilometres distant - in the Pacific.
- Pacific and Tethyan faunal successions merged only during the late Cretaceous, indicating that the two seaways were previously separate. We should expect to find Tethyan fauna in the older marine sediments of the Caribbean had it been formed "in situ".
- Seismic tomography actually images the Atlantic slab descending beneath the Caribbean plate - confirming at least 1500km of subduction, and therefore eastward displacement, of the Caribbean plate through time[6].

The "Origin of the Caribbean Plate" meeting at Sigüenza in 2006 should have been the final resting place of the "in situ" model of the Caribbean. The POP is over two decades old. It is a well established, tested model with more arguments in favour than space allows. I have outlined just five general pro-POP arguments in the box, and will respond in summary to James and Lorente's article by challenging first their reading of the POP, and second their "in situ" interpretation of existing data.

Understanding the POP

In their provocative piece *POP goes the paradigm?* (*Geoscientist 19.9 pp 12-14*: see their Figure 2) James and Lorente argue that the "Great Arc" of the Caribbean bends and lengthens "impossibly" in Pacific Origin models. We know that the arc has a long and complex history passing through oblique extension, collision, obduction, rotation, even polarity reversal. At a glance, what James and Lorente mark as "the Arc" is not telling the full story and their objection does not consider the numerous geological processes capable of occurring to change the surface shape of the arc.

On their Figure 3, magnetic lineations are marked in the Venezuelan basin. This basin is largely covered by the Caribbean Oceanic Plateau, and these lineations do not exist in anyone else's model, POP or otherwise. Occam's razor suggests that James misinterprets, or over-interprets the data.

The authors' description (p 13) of the POP is factually incorrect in places and seems to rely upon the "traditional" view of Burke, (1988)[7]. Many recent models (e.g. Pindell et al., in [3-5]) do not necessarily accept that the oceanic plateau collided with an arc, causing polarity reversal. So here it would seem that James and Lorente choose to ignore half the literature. It is vital, in proposing an alternative model to any theory, that the protagonists are up to date, in detail, with what they are fighting. Furthermore, it is now becoming established that the Caribbean Oceanic Plateau cannot be formed above a slab gap.[8]

The "in situ" model's interpretations of seismic lines (page 14 of the printed article) prompt me to ask how a salt diapir can possibly protrude a substantial distance above the sea floor when it would surely either dissolve or spread out. Such structures are more likely seamounts. In erroneously suggesting the presence of salt in the Venezuelan basin, the conclusion they then make, that much of the basin represents continental crust, is no longer valid.

Interpretations of existing data

As for James and Lorente's alternative interpretations of the known geology, I would make the following points.

1. Crust of 45km thickness does not necessarily indicate continental material. Data suggest the presence of arc roots, but not necessarily continental crust, in the Caribbean plate. Average continental crust is intermediate in composition, so are mature oceanic arcs. Gravity cannot distinguish the two. Understanding geochemistry is vital in this respect. High silica does not indicate continental rocks. Crystal fractionation from a basaltic melt and crustal re-melting generate high silica contents in an intra-oceanic setting and are extremely common processes. The trace element and isotopic record from the Oceanic Plateau and arcs, through dozens upon dozens of publications, shows that there is little continental material beneath the Caribbean Plate. Salt diapirs are not present.

2. The authors appear to argue for punctuated phases of extension from the Triassic through to the Oligocene. Broadly extensional tectonics lasting up to 170 Ma seems geologically unfeasible and certainly cannot account for the formation of the Oceanic Plateau. Accepting that renders much of the discussion that follows irrelevant.

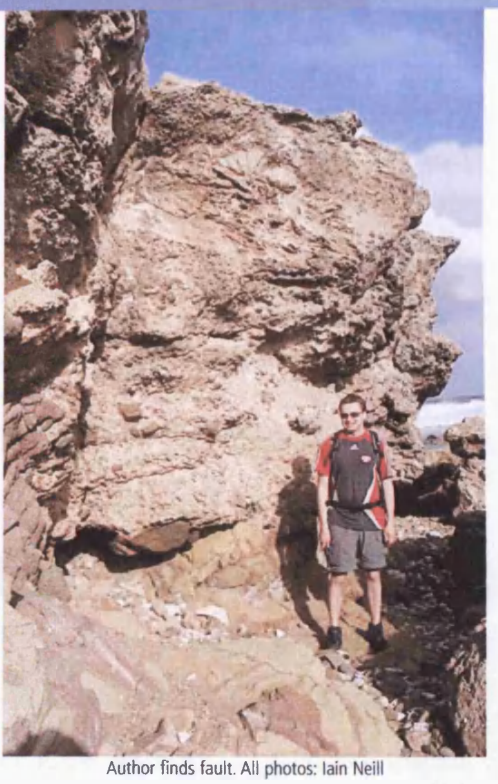

Author finds fault. All photos: Iain Neill

3. In paragraph 4 (page 14) the authors argue that the Caribbean Plateau formed by "serpentinization of the mantle". However, in reality, we know - from geochemical and isotopic investigations of extensive land and a number of offshore samples - that it could *only* have formed in a short space of time by the impingement of a hot mantle plume beneath the Caribbean lithosphere. James and Lorente may argue that little of the Plateau has been drilled to work out exactly what it is. I hold my hand up; I would love to see more samples, but everything we have today fails to counter a Pacific origin model.

4. James and Lorente suggest that mid, late Cretaceous and mid Eocene unconformities are present in the Caribbean. Convergent events are not correlated across the region and I suspect their contention is a generalisation. A pause in volcanic events certainly doesn't ring true for the Cretaceous period; the Caribbean arc successions were active throughout.

5. There is no evidence in the geochemical or isotopic record for significant continental input into the Caribbean arc(s) during their early history. Why then should continental input appear at an arbitrary point during the middle of the history of the arc, if continental material was always present in the Caribbean region? The change from island arc tholeiite to calc-alkaline compositions reflects changing sediment input and arc maturity.

6. The authors speak of back-arc spreading occurring along the Aves Ridge. The Aves Ridge is an extinct island arc - I have the geochemical data to prove it. Geophysical surveys point to thicker, arc-like crust. Hence I presume this is a mistake on the authors' part.

James and Lorente suggest that our chemical and isotopic data need to be completely re-examined and "statistically tested". It is over this point that I take particular umbrage. Geochemists are examining and re-interpreting their data all the time, whatever model is presumed. I cannot accept the trashing of over four decades of good geological practice in the Caribbean.

I would readily admit that the Caribbean community has faced challenges regarding the exact details of the POP, challenges that are being ironed out as new information becomes available. Any model is allowed to evolve. However, James and Lorente suggest that the POP model invokes processes that are difficult to explain or test. We *are* explaining, we *are* testing. I simply do not recognise their argument, especially as the "in situ" model in itself breaks so many fundamental geological and especially geochemical concepts.

The positive upshot from the Sigüenza meeting is that there are a number of cracking articles which will appear in Special Publication 328. Research in the Caribbean has moved far beyond the objections raised by James and Lorente. Let the "in situ" model rest in peace.

References

1. Pindell, J.L., 1990, in Larue, D.K., Draper, G. (eds), Trans 12th Caribbean Geological Conference, Miami Geological Society, 1-4.
2. Pindell, J.L., 1993, in Pindell, J.L., Perkins, R.F. (eds), GCSSEPM Foundation 13th annual research conference, Gulf Coast Section, papers, 251-274.
3. Pindell, J.L., 2006, Geologica Acta, 4(1-2), 303-341.
4. Kerr, A.C. et al., 2003, AAPG Memoir, 79, 126-168.
5. Pindell, J.L. et al., 2009, Geological Society Special Publication 328, GSL.
6. van der Hilst, R., 1990. Doctoral thesis, University of Utrecht, unpublished.
7. Burke,K., 1988. Annual Reviews in Earth & Planetary Sciences, 201-230.
8. Hastie, A.R., Kerr, A.C., in final review, Earth Science Reviews.

** Iain Neill BSc FGS, Postgraduate Student, School of Earth & Ocean Sciences, Cardiff University, Main Building, Park Place, Cardiff, CF10 3YE, Wales. Co-convener of "Circum-Caribbean and North Andean tectonomagmatic evolution," a workshop in Cardiff, 2-4 September, 2009.*

Lithos 120 (2010) 407–420

Contents lists available at ScienceDirect

Lithos

journal homepage: www.elsevier.com/locate/lithos

Origin of the volcanic complexes of La Désirade, Lesser Antilles: Implications for tectonic reconstruction of the Late Jurassic to Cretaceous Pacific-proto Caribbean margin

Iain Neill [a,*], Jennifer A. Gibbs [b], Alan R. Hastie [c], Andrew C. Kerr [a]

[a] School of Earth and Ocean Sciences, Cardiff University, Park Place, Cardiff, CF10 3YE, UK
[b] Department of Earth Sciences, The University of St. Andrews, North Street, St. Andrews, KY16 9AL, UK
[c] School of Geography, Geology and the Environment, Kingston University, Penrhyn Road, Kingston upon Thames, Surrey, KT1 2EE, UK

ARTICLE INFO

Article history:
Received 2 June 2010
Accepted 24 August 2010
Available online 17 September 2010

Keywords:
La Désirade
Caribbean
Geochemistry
Tectonics
Subduction

ABSTRACT

La Désirade Island is located on the hanging wall of the present-day Lesser Antilles subduction zone and consists of a suite of Mesozoic igneous rocks capped by Neogene limestone. The basement suite contains Kimmeridgian to Tithonian (~153–145 Ma) mafic lava flows and pillow basalts overlain by felsic flows and breccias and intruded by a Mid-Berriasian (~144 Ma) trondhjemite pluton and intermediate to felsic dykes. The mafic rocks form a ~300 m thick sequence which trace element geochemistry reveals to contain, in stratigraphic order: (1) tholeiites with a very weak subduction signature; (2) calc-alkaline and tholeiitic arc rocks containing pelagic and terrigenous sediment slab-related components and (3) arc tholeiites with a minor subduction signature. The mantle wedge source was depleted and did not contain a significant plume-related component. The overlying felsic rocks show similar trace element patterns and incompatible trace element ratios to the mafic units. Factors such as pelagic sedimentary deposition and re-working, low eruption rates and the presence of MORB-like and felsic rocks are best explained by an origin at a back-arc spreading ridge. This back-arc was most likely in the proto-Caribbean (Colombian Marginal) seaway and was related to east-dipping Andean/Cordilleran subduction. Other sites in the Greater Antilles and Central America older than the ~135 Ma westward acceleration of North America appear to corroborate a latest Jurassic–Early Cretaceous east-dipping arc system. The preservation of La Désirade in the fore-arc of the present Antilles arc is consistent with Mid-to-Late Cretaceous inception of west-dipping subduction along the former back-arc axis which had previously given rise to La Désirade.

1. Introduction

The Caribbean plate (Fig. 1) is widely considered to have originated in the Pacific region and subsequently tectonically emplaced between North and South America (e.g. Kerr et al., 2003; Pindell and Kennan, 2009). Plate reconstructions show that the Americas separated during the break-up of Pangaea to form oceanic crust by ~160 Ma in the Gulf of Mexico, proto-Caribbean and Colombian Marginal seaways (Pindell and Kennan, 2009). Divergence between the Americas focussed on the proto-Caribbean seaway until the late Campanian (Pindell et al., 1988; Müller et al., 1999; Pindell and Kennan, 2009). From the Early Triassic onwards, oceanic crust of the Farallon (proto-Pacific) plate subducted beneath North and South America and island arc sequences were accreted to the American continental margins (the Andean/Cordilleran arc) (e.g. Oldow et al., 1989).

Subduction at the proto-Caribbean–Pacific boundary during much of the Cretaceous also generated the "Great Arc" of the Caribbean (sensu Burke et al., 1978; Burke, 1988), including the extinct Greater Antilles arc. However it is unclear whether the earliest stages of the Greater Antilles arc were related to east-dipping or to southwest-dipping subduction. At ~94–89 Ma, to the southwest of the Greater Antilles, the mantle plume-derived Caribbean–Colombian Oceanic Plateau (CCOP) formed on the Farallon Plate (Sinton et al., 1998; Kerr et al., 2003). The CCOP crust is up to 20 km thick, much thicker than "normal" oceanic crust (Edgar et al., 1971; Mauffrey and Leroy, 1997). East-dipping subduction initiated at the western margin of the CCOP during the Campanian which isolated the Caribbean Plate and formed the Costa Rica–Panama arc (e.g. Pindell and Dewey, 1982). By this time, subduction on the Greater Antilles system had become southwest-directed, allowing the Americas to move westwards past the Caribbean Plate (e.g. Mattson, 1979). The Caribbean Plate partially collided with North and South America during the Campanian and moved east along transpressional boundaries into its present location (e.g. Pindell and Dewey, 1982; Kennan and Pindell, 2009; Hastie et al., 2010).

* Corresponding author. Tel.: +44 2920 876420 (Office).
E-mail address: neilli@cf.ac.uk (I. Neill).

0024-4937/$ – see front matter © 2010 Elsevier B.V. All rights reserved.
doi:10.1016/j.lithos.2010.08.026

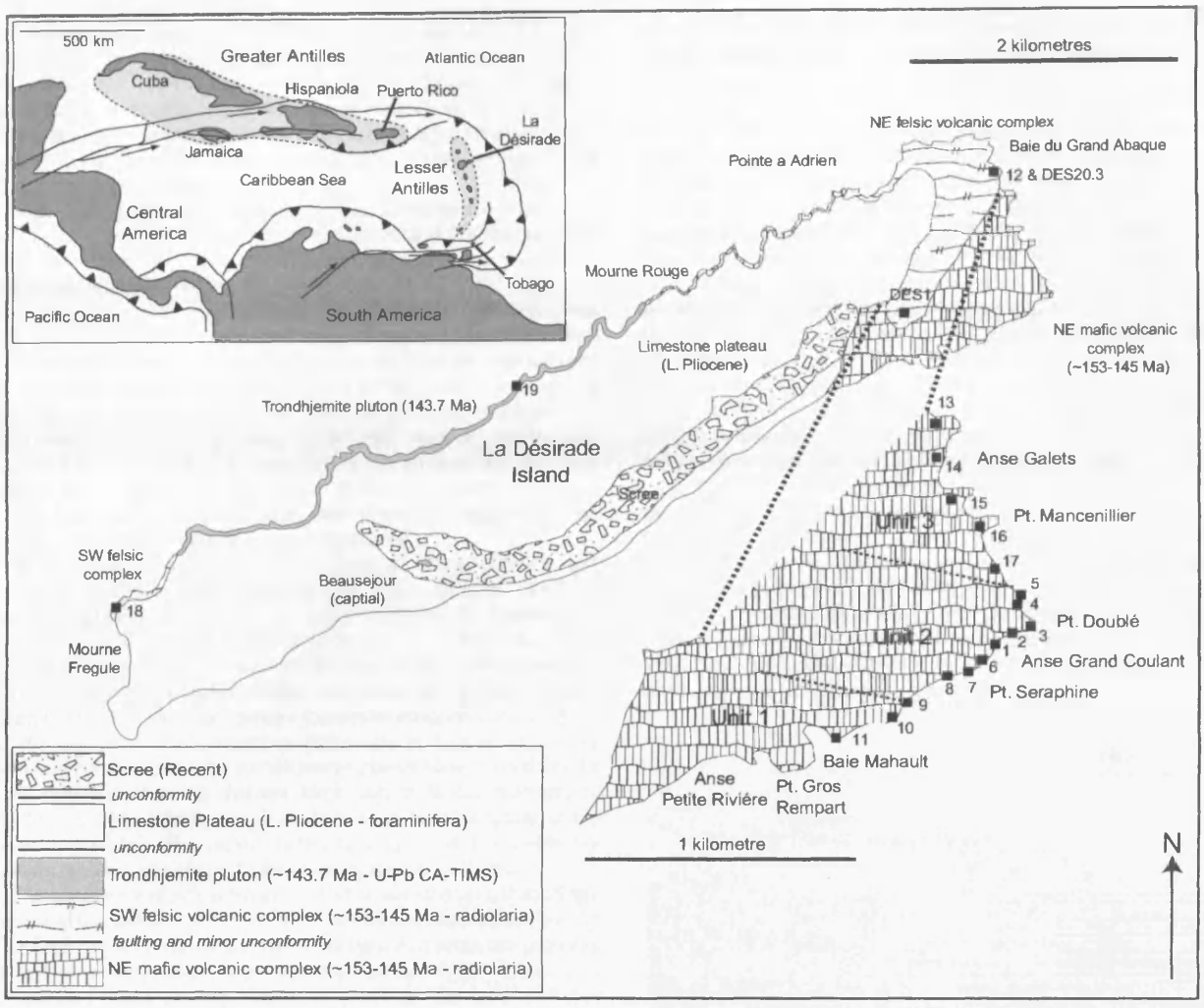

Fig. 1. Simplified geological and location map of La Désirade with insets showing the Caribbean Plate and a stratigraphic column for the island. Intermediate-felsic dykes are scattered throughout the trondhjemite and NE volcanic complexes. Numbers indicate sample locations. For geochronological references, see text.

The cause and timing of the polarity reversal are arguably the most contentious aspects of Caribbean geology (e.g. Hastie et al., 2009; Hastie and Kerr, 2010; Pindell and Kennan, 2009). Atlantic spreading rates increased during the Early Cretaceous (~135–125 Ma) so North America travelled westwards over the mantle faster than South America (Pindell et al., 1988). Some suggest that the effect of this acceleration was to turn the proto-Caribbean–Pacific boundary into a sinistral transform zone which would 'flip' to become a southwest-dipping subduction zone (Greater Antilles arc) during the Aptian–Albian (e.g. Pindell et al., 2006; Pindell and Kennan, 2009). A second model is that the thickened crust of the CCOP collided with the Great Arc of the Caribbean (80–90 Ma), which at that time was east-dipping and still part of the Andean/Cordilleran system. The plateau was too hot, thick and buoyant to subduct, thus, blocking the trench and initiating polarity reversal (e.g. Duncan and Hargraves, 1984; Burke, 1988; White et al., 1999; Kerr et al., 2003; Hastie and Kerr, 2010).

There are also subduction-related rocks in the Caribbean region today which pre-date the westward acceleration of North America and whose origin is the result of Andean/Cordilleran subduction. The preservation of these rocks is due in part to the nature of the 'flip' or subduction polarity reversal in the Greater Antilles region. However, although these rocks are likely to be highly significant in understanding the origin and evolution of the Caribbean Plate, little is known of their distribution and tectonomagmatic setting. In this paper we investigate the Late Jurassic to Early Cretaceous (Mattinson et al., 2008) igneous rocks of the island of La Désirade in the Lesser Antilles (Fig. 1). Previous studies disagree on La Désirade's tectonomagmatic setting, with suggestions ranging from mid-ocean ridge (e.g. Mattinson et al., 1980, 2008) to island arc (e.g. Bouysse et al., 1983; Baumgartner et al., 2008; Cordey and Cornée, 2009). In this paper we use trace element geochemistry to determine the tectonic setting of the rocks, and to identify mantle and crustal inputs into their magmas. Using this new data and published data from Late Jurassic to Early Cretaceous subduction-related fragments from around the Caribbean region, we propose a tectonic reconstruction for the Late Jurassic period and a framework for the preservation of La Désirade following the onset of southwest-dipping subduction in the Greater Antilles.

2. Geological outline of La Désirade

La Désirade (22 km^2) lies 10 km east of Grande Terre, Guadeloupe, on the hanging wall of the active Lesser Antilles subduction zone (Fig. 1). The island is capped by Neogene limestone (Baumgartner-Mora et al., 2004) and has been uplifted on a fault scarp revealing the only suite of Mesozoic volcanic and plutonic rocks in the Lesser Antilles. Trondhjemites and basalts similar to those found on La Désirade have

also been dredged from the Falmouth Spur between La Désirade and Antigua and from the Désirade sea trough (Johnston et al., 1971; Fink, 1972; Bouysse, 1984). The presence of Late Jurassic radiolarian assemblages of Pacific origin which pre-date much of the proto-Caribbean seaway demonstrate that La Désirade has travelled eastwards relative to the Americas at the leading edge of the Caribbean Plate (Montgomery et al., 1992, 1994) (Fig. 1).

Approximately 10 km^2 of Mesozoic igneous rocks are exposed on the island, chiefly around the coasts and particularly in the northeast from Baie Mahault to Baie du Grand Abaque (Fig. 1). Recent geochronology and fieldwork (Mattinson et al., 2008) reveal a subaqueous eruptive and intrusive sequence. The first event was eruption of mafic pillow lavas and massive flows, inter-bedded with chert and subordinate limestone. In this paper these are referred to as the *NE mafic volcanic complex*, and are the main focus of our investigation. Magmatism then evolved to felsic compositions (Mattinson et al., 2008) forming the *NE felsic volcanic complex* near Grand Abaque, the central *trondhjemite pluton* and the *SW felsic complex* which consists of dykes and flows around Morne Frégule. Finally, a suite of *intermediate-felsic dykes* which cuts both the pluton and the northeastern complexes was emplaced.

Radiolarians in inter-lava flow chert at Pointe Doublé (NE mafic complex) and Pointe Frégule (SW felsic complex) are from bio-chronostratigraphic zone 4, upper subzone 4β [mid-Upper Tithonian (~150–145 Ma)] (Montgomery et al., 1992; Mattinson et al., 2008). Work by Cordey and Cornée (2009) on the northeast mafic complex has revealed radiolarians dating to the Late Kimmeridgian (~153–150 Ma), indicating a maximum eruption time of ~8 Ma for the northeast mafic complex (timescale of Ogg et al., 2008). Zircons separated from the trondhjemite pluton have been dated by U–Pb chemical abrasion–thermal ionisation mass spectrometry to 143.74 ± 0.33 Ma (Mattinson et al., 2008), i.e. mid-Berriasian of the Lower Cretaceous. The oldest radiolarian age and the U–Pb age indicate igneous activity on La Désirade lasted up to 10 Ma.

The occurrence of pillow basalts and what was interpreted as pelagic chert, lead Mattinson et al. (1980, 2008) to conclude that the mafic rocks of La Désirade were the upper part of an ophiolitic sequence probably formed at a mid-ocean ridge. Bouysse et al. (1983) favoured a subduction-related setting based, in part, on the lack of lower components of an ophiolite such as sheeted dykes, gabbros and ultramafic rocks. There has been a recent re-investigation of the chert of the northeast mafic volcanic complex by Montgomery and Kerr (2009) and Cordey and Cornée (2009) indicating that radiolarites are sparse and that the chert has high levels of MgO and Fe_2O_3, inferring rapid formation in a hydrothermal regime. However there were periods of quiescence during which time pelagic chert and limestone deposition occurred. The subordinate limestones found between the pillows are low in Fe_2O_3 and high in SiO_2 and contain radiolarians and planktonic foraminifera indicating a pelagic origin suggestive of a spreading centre (Montgomery and Kerr, 2009). Because pillow basalts and pelagic sediments are components of both subaqueous arcs and spreading centres and many ophiolites are not analogues for mid-ocean ridges (e.g. Moores and Vine, 1971), but integral parts of supra-subduction zone settings (Pearce et al., 1984), the outcrop geology of the island is not equivocal in resolving a subduction-related or mid-ocean origin. Perhaps the only indicator comes from the predominance of felsic volcanic rocks on La Désirade which is more common to island arcs than mid ocean ridges. Therefore, trace element geochemistry is required to resolve the tectonic setting of these rocks.

3. Rock types and petrography

3.1. NE mafic volcanic complex

The NE mafic volcanic complex outcrops from Baie Mahault to Anse Galets where it is overlain by the northeast felsic volcanic complex. The dominant rock type is a vesicular black to grey-green, often reddened, basalt–basaltic andesite lava, which typically forms pillows up to 1 m across (Fig. 2). Voluminous red cherts (jasper) and minor limestone pinch-ups occur between the pillows (Montgomery and Kerr, 2009), which exhibit right-way-up 'teardrop' structures and glassy rinds. Individual packages of pillow lavas define a crude layering which dips at 10° or more to the north exposing ~300 m of volcanic rocks in stratigraphic order. Additionally, volumetrically rare massive mafic lava flows and 1–2 m thick banded hyaloclastites of <1–3 mm grain size are also found. Some minor faulting occurs with displacements of only a few centimetres to several metres, which may be related to emplacement of the intermediate dyke suite; however, the entire mafic complex is continuous with no recognisable unconformities. The contact with the overlying northeast felsic volcanic complex is faulted (Fig. 2), but chert and basalt clasts are found within the felsic breccias of the overlying unit indicating eruption through the pre-existing mafic complex and an unconformity between the two complexes of unknown length.

In the lower part of the mafic complex, (Loc. 10–11; Fig. 1) the lavas can be divided into two petrographic facies. The first type is fine-grained with 0.5 to 1 mm clinopyroxene phenocrysts set in a groundmass consisting of randomly aligned acicular plagioclase, squat clinopyroxene and Fe–Ti oxides. There are brown/green clays, oxides/haematite patches and in some cases, abundant calcite replacing the original textures. The second type of lava has a grain size of up to 2 mm with plagioclase phenocrysts up to 4 mm. Interstitial plagioclase is more tabular, with clinopyroxene and Fe–Ti oxides that

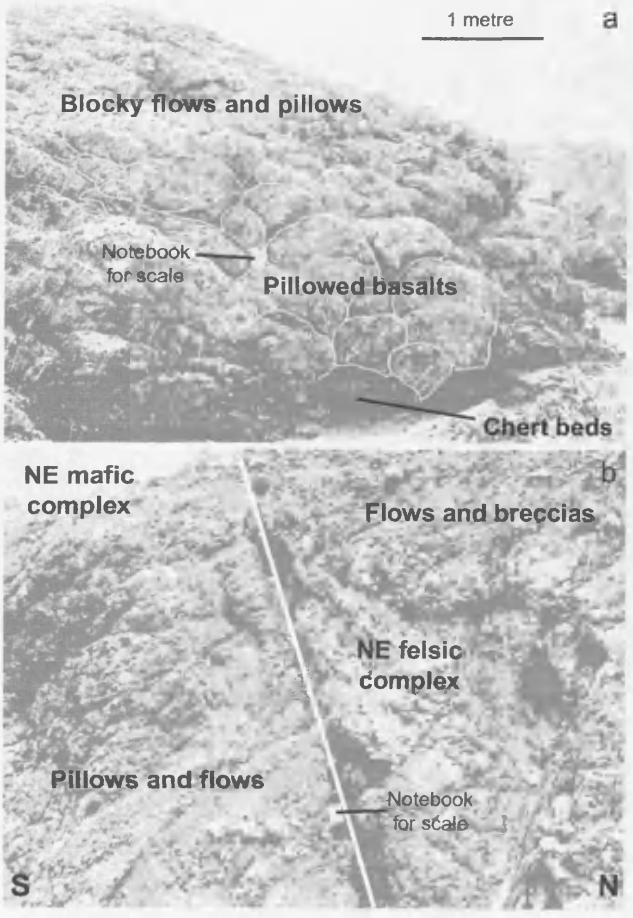

Fig. 2. (a) Pillowed mafic lavas inter-bedded with thin cherts. (b) Faulted contact between the northeast mafic volcanic complex and the northeast felsic volcanic complex.

have needle-like patterns. Replacement minerals in this second type are brown/green clays, oxides/haematite, chlorite, prehnite and pumpellyite.

Overlying these rocks, some of the pillows at Locality 8 (Fig. 1) are quite distinct, consisting of 1 mm grains of hopper-shaped or acicular to elongate splays of clinopyroxene and lesser acicular plagioclase which might indicate rapid quenching of the lava. Replacement minerals are quartz, prehnite, pumpellyite and oxides. Vesicles are infilled by quartz and Fe–Ti oxides. The remaining samples from Localities 8 and 9 (Fig. 1) are largely aphyric, ranging from 0.25 mm to 1 mm grain sizes and consisting of acicular plagioclase, squat clinopyroxene, and Fe–Ti oxides, sometimes comb-like or acicular. Replacement minerals include calcite patches and veins, prehnite and oxides including haematite.

The youngest lavas in the complex (Localities 1–7 and 14–17; Fig. 1) vary in grain size from <0.25 mm to 0.5 mm. Acicular plagioclase dominates the groundmass with elongate to squat clinopyroxene present. Some samples are clinopyroxene-phyric, often with glomeroporphyritic blebs reaching 1 mm whilst others appear glassy with abundant calcite replacement. Other replacement minerals include chlorite, prehnite, pumpellyite, green/brown clays and oxides. The replacement minerals found across the complex are diagnostic of a low-grade prehnite–pumpellyite facies metamorphic assemblage.

3.2. Felsic volcanics and the trondhjemite pluton

The NE felsic volcanic complex outcrops around Grand Abaque and contains orange-weathered massive rhyolitic flows, volcanic breccia and scoria. Breccias are darker in colour than the flows and are vesicular with abundant geodes containing quartz and epidote. Other breccias look similar to basalts and cherts of the NE mafic volcanic complex. The rhyolitic flows and breccias consist mostly of plagioclase and quartz with minor haematite crystals and veins. Some chlorite, clays and epidote are present replacement minerals.

The SW felsic complex occurs at the coast near Mourne Frégule and is regarded as temporally equivalent to the NE felsic complex (Bouysse et al., 1983; Mattinson et al., 2008), containing similar rhyolitic flows. These flows contain plagioclase and quartz phenocrysts up to 1 mm across, with a fine groundmass dominated by plagioclase with minor quartz and oxides. Clays, haematite and epidote are replacement minerals.

A trondhjemite pluton is exposed for 4 km along the north coast of the island. There are a variety of igneous facies, with the majority comprising plagioclase-rich trondhjemite with minor amounts of diorite and albite granite, which are cut by abundant intermediate dykes. The trondhjemite is characterised by 2–3 mm sized grains of tabular plagioclase (~60%), hornblende, quartz, Fe–Ti oxides, titanite and zircon. Alkali feldspar and biotite are absent. The most common replacement minerals are chlorite and epidote.

Although not yet dated by U–Pb methods, the felsic complexes appear of similar age to the pluton (Mattinson et al., 2008). Mattinson et al. (2008) proposed that the pluton intruded the lavas of its own volcanic carapace. These lavas were of the same composition and age as those which formed the NE and SW felsic complexes.

3.3. Intermediate-felsic dykes

Clinopyroxene dolerite, microdiorite, granodiorite and granophyre dykes cut the trondhjemite and NE mafic and felsic complexes (Mattinson et al., 1980). Mattinson et al. (2008) contend that the less evolved dykes are the last magmatism on the island whilst the most felsic dykes are related to the earlier felsic magmatism. The more mafic dykes are yellow-green tinged, 2–3 m thick, trend roughly NE–SW within the NE mafic volcanic complex and show chilled margins with the surrounding pillow basalts. Minor faults within the NE mafic complex occur at angles parallel or sub-parallel to the dykes suggesting a structural control upon dyke emplacement. These dykes have a grain size of around 0.25 mm and contain clinopyroxene phenocrysts (~10%) in a groundmass of elongate plagioclase and minor clinopyroxene and quartz with alteration to chlorite and pumpellyite. Epidote, albite and prehnite have also been reported (Mattinson et al., 1980). Dykes cutting the trondhjemite pluton are dark green, up to 1 m across and have a grain size of 0.25 to 0.5 mm. They are dominated by a groundmass of elongate plagioclase, clinopyroxene and Fe–Ti oxides with rare clinopyroxene phenocrysts. Replacement of the clinopyroxenes by clays and chlorite is very common.

4. Geochemistry

4.1. Analytical methods

Forty-three samples were collected from across the complexes with emphasis on the northeast mafic volcanic complex due to good exposure and the suitability of mafic rocks for petrogenetic study. Fresh material was difficult to obtain because of the vesicular nature and hydrothermal/metamorphic alteration of some of the rocks. The freshest samples were obtained from the centre of pillows or from coeval dyke-lets between the pillows. Each sample was trimmed by rotary saw to remove weathered surfaces, calcite veining and vesicular patches and ground in a steel jaw crusher before powdering in an agate ball mill. Analysis was undertaken at Cardiff University, UK. Loss-on-ignition values were calculated after heating 2 g of each sample at 900 °C for 2 hours. Samples were dissolved using the fluxy-fusion method outlined in McDonald and Viljoen (2006). Major element and Sc abundances were determined by using a JY Horiba Ultima 2 Inductively Coupled Plasma Optical Emission Spectrometer (ICP-OES). Trace elements were analysed by a Thermo X7 Series Inductively Coupled Plasma Mass Spectrometer (ICP-MS). Silicate rock standards JB-1A, NIM-G and BIR-1 were run through repeated sample batches. Relative standard deviations show precision of 1–5% for most major and trace elements for JB-1A. 2σ values encompass certified values for the vast majority of elements. Representative analyses from the different complexes are shown in Table 1. Full analytical results including repeat runs of standard basalt JB-1A can be found in the Supplementary Information.

4.2. Element mobility

High loss-on-ignition values (Table 1) are likely to be due to sub-solidus alteration processes. Mobilisation of many major and trace elements such as Si, Mg, Na, K, Ba and Sr is therefore to be expected, as has been noted for other Cretaceous Caribbean igneous rocks (e.g. Hastie et al., 2007). Elements considered to be relatively immobile under low-grade metamorphism (up to greenschist grade) and hydrothermal alteration processes are the rare Earth elements (REE), high field strength elements (HFSE) along with Co, Cr, Ni, Sc, V, Y and P (e.g. Pearce, 1983; Seewald and Seyfried, 1990). Nb (a HFSE) is considered immobile, hence elements for samples within a given magmatic suite that are also immobile should show clear trends related to intra-magmatic differentiation processes when plotted against Nb (c.f. Cann, 1970).

The NE mafic volcanic complex can be split into three units based on their geochemistry (Section 5.1). Unit 1 consists of the lowermost clinopyroxene and plagioclase-phyric lavas (Localities 10 and 11) whereas Unit 2 covers Localities 1 to 9 and Unit 3 is found at Localities 14 to 17 (Fig. 1). Representative major and trace elements in the three units are plotted against Nb in Fig. 3 to demonstrate elemental mobility. None of the recognised units display coherent intra-magmatic differentiation trends for the major elements (except Al_2O_3 and TiO_2) or large ion lithophile elements (LILE). Conversely,

Table 1
Representative data for the La Désirade mafic volcanic units and felsic complexes.

Number	IND/10.2	IND/11.2	IND/4.1	IND/5.1	IND/15.2	IND/16.1	DES20.3	IND/18.2	IND/19.9	IND/19.11	IND/19.2	5.14D3
Class	BAS	BA	BAS	BA	BA	BA	DAC	DAC	TROND	TROND	DAC	AND
Type	TH/MOR	TH/MOR	CA/IA	TH/IA	TH/BAB	CA/BAB	TH/IA	TH/IA	TH/IA	TH/IA	TH/IA	TH/IA
Unit	1	1	2	2	3	3	NE FEL	SW FEL	TROND	TROND	DYKE	DYKE
SiO_2	52.28	52.41	56.66	55.68	51.05	51.27	77.27	71.86	74.72	74.58	57.57	54.13
TiO_2	0.73	0.81	0.71	0.71	1.02	1.21	0.46	0.55	0.30	0.28	1.14	1.00
Al_2O_3	15.65	16.57	14.76	14.63	15.17	14.15	10.44	13.25	12.70	12.80	14.58	16.08
Fe_2O_3(T)	7.96	9.33	5.98	6.27	9.35	10.18	2.18	3.89	3.55	3.32	12.21	10.47
MnO	0.11	0.07	0.09	0.09	0.10	0.08	0.03	0.06	0.10	0.09	0.37	0.16
MgO	5.54	3.19	4.05	3.44	3.78	2.22	0.34	2.42	0.68	0.62	3.18	4.08
CaO	6.69	8.30	5.75	7.96	10.17	6.34	0.28	0.20	1.94	1.95	2.79	4.88
Na_2O	5.07	5.69	7.29	7.08	5.10	6.09	6.19	6.23	5.37	5.26	5.17	8.30
K_2O	0.25	0.12	0.21	0.09	0.06	0.06	0.15	0.07	0.12	0.16	0.35	0.07
P_2O_5	0.06	0.10	0.09	0.11	0.16	0.13	0.17	0.15	0.06	0.07	0.16	0.40
LOI	5.96	3.41	4.50	4.64	3.98	7.40	1.92	1.50	1.24	1.24	2.64	0.78
Total	100.31	100.00	100.07	100.69	99.94	99.13	99.43	100.18	100.79	100.36	100.17	100.35
Sc	29.4	31.3	23.0	22.7	31.2	29.7	9.1	15.7	11.3	11.2	30.0	34.3
V	232.5	301.9	226.2	251.6	331.3	498.8	30.1	29.6	20.4	12.7	219.1	329.1
Cr	496.1	278.8	212.6	189.9	129.4	5.5	16.5	34.6	14.4	30.9	11.1	3.7
Co	42.8	33.5	35.0	23.8	32.4	31.0	3.1	3.8	2.5	1.8	12.9	24.9
Ni	110.5	69.2	82.2	77.4	67.3	3.7	2.8	3.2	140.2	5.3	10.1	145.4
Ga	18.4	21.3	17.2	18.7	23.9	28.5	10.4	15.7	18.5	14.5	18.9	20.5
Rb	1.5	2.4	4.6	1.2	1.4	0.5	2.1	1.0	1.5	1.5	3.3	1.5
Sr	89.3	115.1	72.4	55.3	126.9	31.8	34.6	79.5	99.3	118.8	72.7	39.8
Y	26.8	14.7	18.3	15.5	19.6	29.3	48.0	28.9	26.8	23.2	28.8	27.7
Zr	91.1	48.9	67.3	78.9	67.8	105.7	141.4	123.1	146.8	113.1	111.0	98.8
Nb	1.46	1.18	1.87	1.37	1.06	1.49	1.47	2.18	1.41	1.12	2.71	1.83
Ba	19.9	2894.5	50.6	46.6	43.1	31.4	23.0	18.5	66.9	50.5	91.9	21.2
Hf	2.41	1.08	1.87	1.99	1.50	2.65	3.36	3.18	3.48	2.88	2.51	2.53
Ta	0.10	0.08	0.12	0.09	0.11	0.18	0.12	0.13	0.08	0.07	0.16	0.15
Th	1.35	0.08	0.55	0.28	0.10	0.74	0.52	0.37	0.44	0.44	0.36	0.44
La	2.89	1.96	3.26	3.31	2.10	3.15	7.09	3.72	5.18	4.12	4.84	4.46
Ce	8.35	5.44	7.97	8.50	6.46	8.87	15.33	11.29	12.68	10.37	13.39	11.81
Pr	1.66	0.99	1.51	1.44	1.12	1.60	3.46	1.98	1.93	1.63	2.21	2.01
Nd	8.19	4.80	7.29	6.48	5.44	8.07	17.43	9.21	8.34	7.02	10.11	9.97
Sm	3.00	1.72	2.42	2.18	1.95	2.96	5.43	3.19	2.63	2.35	3.30	3.19
Eu	0.98	1.44	0.86	0.74	0.87	1.12	1.43	0.91	0.74	0.67	1.01	1.11
Gd	4.33	2.16	3.86	2.67	2.62	3.81	6.28	4.37	3.49	3.04	4.14	3.70
Tb	0.67	0.36	0.52	0.41	0.46	0.67	1.04	0.69	0.57	0.52	0.66	0.63
Dy	4.56	2.46	3.26	2.70	3.04	4.64	6.95	4.72	3.89	3.59	4.38	4.19
Ho	0.93	0.48	0.63	0.51	0.61	0.93	1.35	0.95	0.79	0.72	0.86	0.84
Er	2.72	1.42	1.86	1.54	1.78	2.71	4.13	2.95	2.39	2.27	2.55	2.56
Tm	0.44	0.21	0.29	0.24	0.28	0.44	0.67	0.48	0.40	0.36	0.41	0.42
Yb	3.06	1.44	2.04	1.71	1.90	2.83	4.36	3.31	2.77	2.44	2.74	2.79
Lu	0.45	0.23	0.29	0.27	0.29	0.45	0.69	0.53	0.42	0.40	0.42	0.44

BAS = basalt, BA = basaltic andesite, AND = andesite, DAC = dacite, TH = tholeiitic, CA = calc-alkaline, MORB = MORB-like, IA = island arc-like, BAB = back-arc basin-like, LOI = loss on ignition. The complete data set can be found in the Supplementary Information.

immobile trace elements (e.g. Zr, Th and Yb) display coherent intra-magmatic differentiation trends against Nb within each unit. On this basis, Al_2O_3, TiO_2, the REE, HFSE and Co, Cr, Ni, Sc, V and Y have not been significantly mobilised and may be used in petrogenetic interpretation. Interestingly, on the Zr vs. Nb diagram, two sub-groups can be seen which both display divergent trends against Nb, with 8 samples from Units 1 and 2 following a lower Zr/Nb trend.

Major element classification diagrams such as SiO_2 vs. K_2O (Peccarillo and Taylor, 1976) cannot be used on La Désirade due to sub-solidus alteration processes so the Th vs. Co diagram of Hastie et al. (2007) for island arc volcanic rocks is used (Fig. 4). The diagram is an immobile element proxy for SiO_2 and K_2O and is able to classify lavas on the basis of rock suite and type. Fig. 4 shows that the majority of La Désirade lavas range from tholeiitic basalts to rhyolites.

4.3. Geochemical results from the northeast mafic complex

4.3.1. Unit 1

The lavas contain ~45–56 wt.% SiO_2, 0.6–1.75 wt.% TiO_2, 13–18 wt.% Al_2O_3 and 3–6 wt.% MgO and can be classified as tholeiitic basalts (Fig. 4). Vanadium ranges from 230 to 310 ppm, Cr from 280 to 450 ppm and Ni from 40 to 140 ppm. Chondrite-normalised REE patterns (8–30 times chondrite) are flat to slightly light (L)REE depleted with some positive Eu anomalies (Fig. 5). The N-MORB-normalised multi-element plots show a wide spread of values but many samples are slightly depleted with respect to N-MORB (Fig. 5). They have small negative Nb–Ta anomalies, relatively flat to slightly negative Zr–Hf profiles and a slight depletion in Ti. Some samples are slightly enriched in Th/La whilst others are depleted. All samples show a small negative Ce anomaly (Fig. 5).

4.3.2. Unit 2

These rocks have 43–58 wt.% SiO_2, 0.4–0.8 wt.% TiO_2, 13–16 wt.% Al_2O_3 and 3.4–6.6 wt.% MgO and are mostly tholeiitic and calc-alkaline basaltic andesites (Fig. 4). Compared to Unit 1, Unit 2 lavas are more siliceous and have lower TiO_2 concentrations. They contain high abundances of V, Cr and Ni—190–340, 190–990 and 80–210 ppm respectively. The chondrite-normalised REE patterns for Unit 2 vary from flat to slightly LREE enriched and are generally more depleted in the middle (M)REE and heavy (H)REE than the rocks of Unit 1 (Fig. 5). Overall the HREE are 5–15 times chondrite with some small positive Eu anomalies. The N-MORB-normalised multi-element plot shows

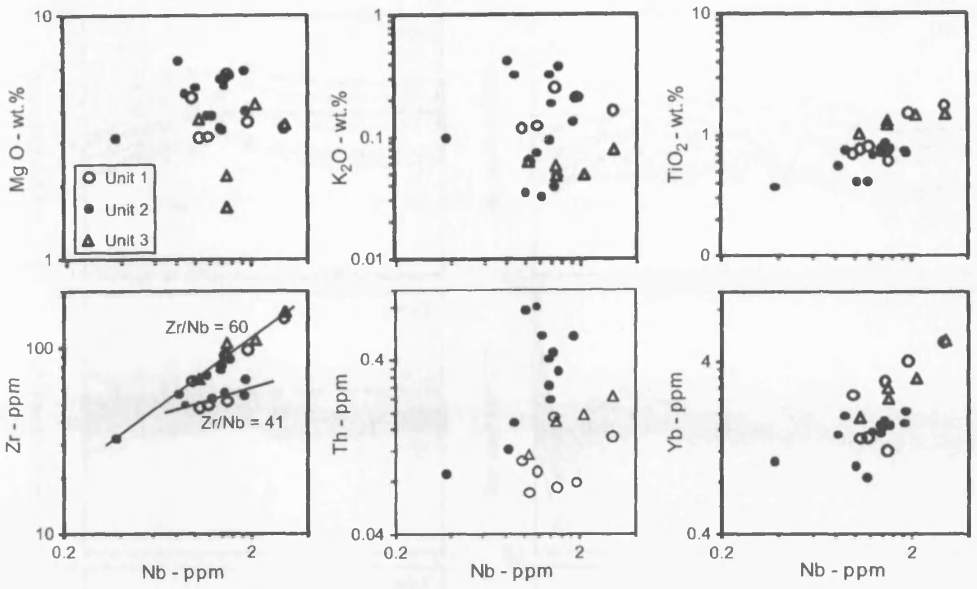

Fig. 3. Differentiation plots to assess element mobility within the NE mafic volcanic unit.

that Unit 2 lavas are quite depleted in the MREE and HREE relative to N-MORB. Unit 2 lavas also have negative Nb–Ta anomalies (Fig. 5) along with both positive and negative Zr–Hf anomalies. Ti is also depleted relative to the MREE. Th is strongly enriched over the LREE in all samples compared to the depletion in Unit 1 and all samples possess negative Ce anomalies (Fig. 5).

4.3.3. Unit 3

The lavas are mostly tholeiitic basaltic andesites (Fig. 4). SiO_2 varies from 47 to 61 wt.% and MgO from 1.7 to 3.8 wt% whilst TiO_2 is consistently above 1 wt.%, much higher than in Unit 2. These rocks contain similar levels of V (130–500 ppm) to the other Units, but much less Cr (10–130 ppm) and Ni (5–65 ppm). The chondrite-normalised REE patterns of Unit 3 are flat to slightly LREE-depleted which is similar to the rocks of Unit 1 (Fig. 5), however on the N-MORB-normalised plot (Fig. 5), Nb–Ta depletions are present, unlike Unit 1. Zr–Hf is only very slightly enriched or depleted relative to the REE, Ti is depleted relative to the REE and there are some marked Ce depletions relative to La and Pr, more like Unit 2 (Fig. 5).

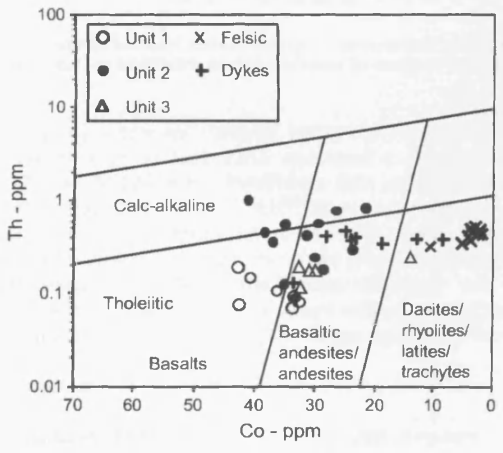

Fig. 4. Th–Co plot (Hastie et al., 2007) showing the tholeiitic to calc-alkaline affinity of the NE mafic volcanic complex and the tholeiitic affinity of the felsic complexes of La Désirade. Felsic = NE and SW felsic volcanic complexes and trondhjemite pluton, Dykes = intermediate-felsic dykes.

4.4. Felsic volcanic and plutonic rocks

SiO_2 ranges from 62 to 79 wt.%, Al_2O_3 from 10 to 15 wt.%, MgO from 0.3 to 3.6 wt.% and TiO_2 from 0.3 to 0.9 wt.%. Ni, Cr and V are considerably lower than in the NE mafic complex. The felsic rocks have nearly identical chondrite-normalised REE patterns to each other (Fig. 5), which fall completely within the range of the NE mafic complex. These patterns are flat to very slightly LREE- and HREE-enriched with negative Eu anomalies. The N-MORB-normalised plot (Fig. 5) shows that the felsic complexes all have pronounced positive Th and Zr–Hf and negative Nb–Ta, Ce and Ti anomalies, characteristics which are similar to Unit 2 of the NE mafic complex.

4.5. Intermediate-felsic dykes

The dykes range from basaltic andesites to rhyolites (Fig. 4) and have a spread of SiO_2 contents from 50 to 58 wt.%. Al_2O_3 ranges from 13 to 16 wt.%, MgO from 3.2 to 7.5 wt.% and TiO_2 from 0.5 to 1.3 wt.%. Contents of V (30–340 ppm), Cr (5–145 ppm) and Ni (5–145 ppm) fall between those of the mafic and felsic complexes. These dykes overlap almost completely with both the felsic and mafic rocks on the chondrite-normalised plot (Fig. 5), with the exception that the dykes do not have negative Eu anomalies but many of the felsic rocks do. On the N-MORB normalised plot (Fig. 5), the dykes are again similar to the felsic rocks but do not have positive Zr–Hf anomalies or such pronounced negative Ti anomalies.

4.6. Radiogenic isotopes

Mattinson et al. (1980) reported Pb and Sr radiogenic isotope ratios from the trondhjemite pluton (Fig. 1) and Gauchat (2004) analysed Pb, Nd and Sr isotopic ratios from all magmatic complexes on the island. Given the level of alteration present, it is unlikely that the Sr and Pb isotopic values can be used to assess petrogenetic processes or mantle sources (e.g. Thompson et al., 2003; Hastie, 2009). $^{144}Nd/^{143}Nd$ ratios are more resistant to sub-solidus alteration processes and so are likely to represent the primary composition of

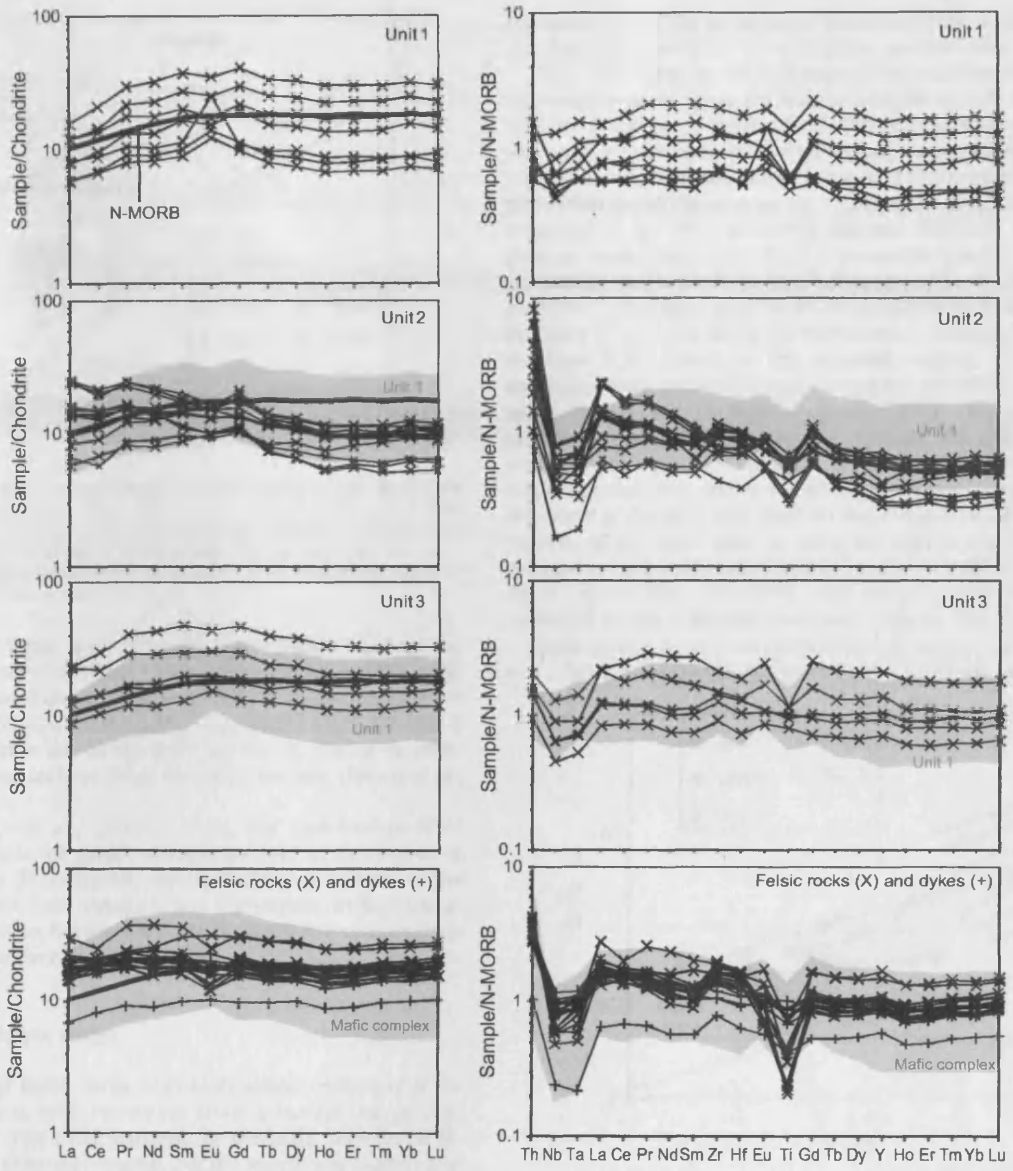

Fig. 5. REE patterns and multi-element plots for (1) each volcanic unit of the mafic complex and (2) the rocks of the NE and SW felsic volcanic complexes, trondhjemite pluton and the intermediate to felsic dykes. Normalising values for chondrite are from McDonough and Sun (1995) and for N-MORB from Sun and McDonough (1989).

the lavas (e.g. White and Patchett, 1984). The $^{144}Nd/^{143}Nd$ ratios are depleted relative to bulk earth and span a narrow range from 0.512786 to 0.512914 but insufficient data are available for each sample to calculate initial $^{144}Nd/^{143}Nd$ ratios or compare isotopic values with trace element ratios. However, these ratios overlap between the different complexes on the island, suggesting that the mantle source region for all the igneous complexes was relatively homogeneous whilst the depleted values indicate that old continental crustal material was not involved in the petrogenesis of these rocks.

5. Discussion

5.1. Subduction-related origin of the La Désirade complexes

The new geochemical data demonstrates that many of the volcanic and plutonic rocks contain variable enrichments in Th relative to the HFSEs and negative Ce, Nb–Ta and Ti anomalies on N-MORB-normalised multi-element plots (Fig. 5). These features are characteristic of supra-subduction zone settings and not mid-ocean spreading centres (e.g. Pearce and Peate, 1995; Pearce and Stern, 2006).

Nevertheless, negative Nb–Ta anomalies could be formed by: (1) crustal contamination as the La Désirade magmas ascended and/or (2) slab-related fluids which enrich a mantle wedge in LILEs and LREEs and not Nb and Ta, the latter remaining in rutile in the subducting oceanic slab (e.g., Saunders et al., 1980; Pearce and Peate, 1995; Elliot, 2003). Fieldwork and Nd isotope data suggest that the basement below La Désirade is not composed of continental crust (Gauchat, 2004). Also, zircons separated for U–Pb dating show no evidence of inheritance from older continental basement (Mattinson et al., 2008). As a consequence, the geochemical character of the La Désirade lavas (e.g. negative Nb–Ta anomalies) is related to subduction zone processes and not continental contamination.

The Th/Yb vs. Ta/Yb diagram of Pearce (1983) (Fig. 6) shows that Units 1 and 3, which do not have strong Nb–Ta anomalies (Fig. 5), plot

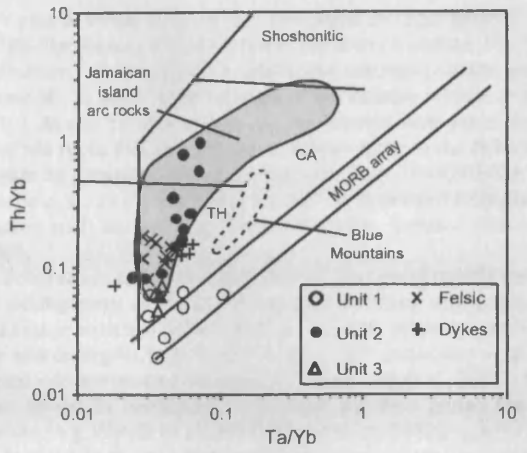

Fig. 6. Th/Yb vs. Ta/Yb plot (Pearce, 1983) showing the subduction zone affinity of the La Désirade Mesozoic complexes. TH = tholeiitic, CA = calc-alkaline. Jamaican island arc data are from Hastie (2009, in press), Jamaican Blue Mountains back-arc rocks from (Hastie et al., in press) plot at higher Ta/Yb than the Désirade rocks due to a plume component in the mantle source, but demonstrate their intermediate character between MORB and island arc rocks.

in or close to the MORB array similar to some MORB-like back arc basin lavas (e.g. Pearce and Peate, 1995; Pearce and Stern, 2006). Unit 2 lavas, which have marked negative Nb–Ta and Ti anomalies, have much higher Th/Yb ratios (0.08 to 0.95) than Units 1 and 3. The Unit 2 lavas also plot above the MORB array on Fig. 6, similar to other Caribbean arc lavas, such as those found on Jamaica (Hastie et al., 2009, 2010).

The felsic volcanic and plutonic rocks and intermediate-felsic dykes also plot within the Jamaican island arc field on Fig. 6, albeit at lower Th/Yb ratios. This diagram therefore shows that many of the rocks on the island have compositions compatible with a supra-subduction zone origin, but there are also N-MORB-like compositions present in Unit 1 of the NE mafic complex.

5.2. Nature of the mantle wedge

The presence of mafic rocks with high concentrations of V, Cr and Ni is consistent with derivation from a mantle source (e.g. Perfit et al., 1980). Flat HREE patterns for the mafic samples on N-MORB-normalised plots also suggest that the source was shallow and garnet-free. Low MgO contents (mostly <6 wt.%) indicate that the mafic rocks have undergone substantial fractional crystallisation. Therefore, to study the composition of the mantle source region, immobile trace element ratios are used which are not modified by moderate fractionation processes in mafic rocks. These trace elements also have to be absent from fluids derived from the downgoing slab. Zirconium, Nb and Yb are not mobilised from the subducting slab in aqueous fluids and are thus described as 'conservative.' elements. However, when the slab and/or its sedimentary veneer undergo partial melting these elements contribute to the slab-flux, and are termed 'non-conservative' elements (Pearce and Peate, 1995).

Adakites are formed when siliceous slab-related melts, (with LREE, La/Yb and Sr/Y enrichment), erupt without interaction with the mantle wedge (e.g. Defant and Drummond, 1990). Conversely, when assimilation occurs, high-Mg andesites or low-silica adakites are formed (e.g. Yogodzinski et al., 1995; Martin et al., 2005). Plutonic trondhjemite–tonalite–granodiorite suites (TTGs) are common components of Archean and Paleoproterozoic terranes and are compositionally similar to adakites (Smithies, 2000; Condie, 2005). However none of these rock types have been identified on La Désirade and furthermore the La Désirade trondhjemite has a markedly different composition to TTGs or adakites. Therefore, there is not an obvious slab melt component in the La Désirade igneous rocks.

As a result of Nb, Zr and Yb being variably mobilised in a slab-melt, slab-melt lavas lie above the mantle array on a Zr/Yb vs. Nb/Yb plot (Fig. 7a) (Pearce and Peate, 1995). The accumulation of zircon may also occur in felsic rocks so that when they are plotted on Fig. 7a, they too plot above the MORB array. Many of the La Désirade mafic rocks plot within the MORB array on Fig. 7a, demonstrating the conservative behaviour of the HFSE and HREE. Because the fields on ratio–ratio plots are constructed on the basis of percentile contours, some scatter is inevitable on the Zr/Yb vs. Nb/Yb diagram; however, the mafic rocks from Unit 2 that have positive Zr–Hf anomalies on N-MORB normalised plots (Fig. 5) plot above the MORB array. These rocks also plot on the high Zr/Nb trend on the variation diagram (Fig. 3). These anomalies may indicate non-conservative behaviour of the HFSE which implies that the highest values of Zr on trace element ratio–ratio plots should be viewed with caution and the only lowest values considered representative of the mantle composition. The intermediate-felsic dykes plot within the MORB array indicating conservative behaviour of the HFSE and HREE, so these may be used alongside the majority of the mafic rocks to study the mantle source. Some felsic volcanic and plutonic rocks do plot above the MORB array on the Zr/Yb vs. Nb/Yb plot, consistent with their marked positive Zr–Hf anomalies on the N-MORB normalised diagram (Fig. 5).

Mafic plume lavas from Iceland and elsewhere (e.g. Thompson et al., 2003), consistently fall between the tramlines on the Nb/Y vs.

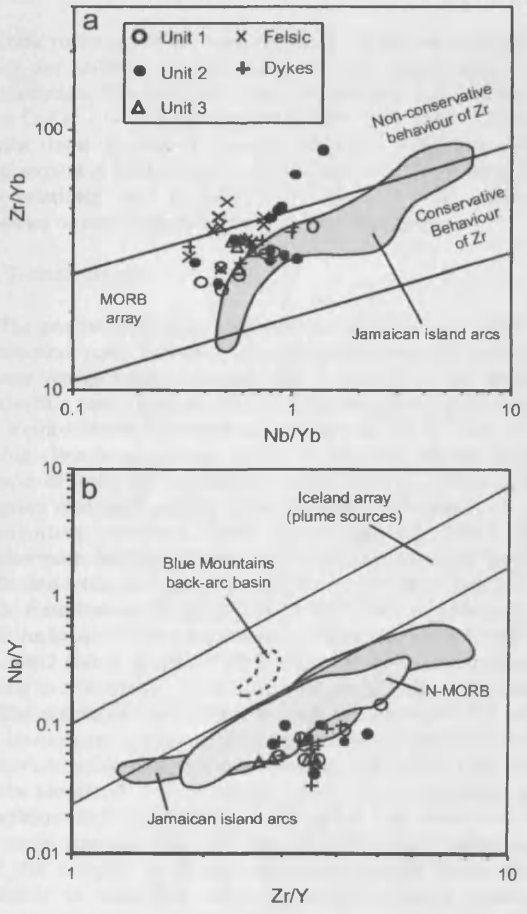

Fig. 7. (a) Zr/Yb vs. Nb/Yb diagram (Pearce and Peate, 1995) which tests for conservative behaviour of Zr during subduction processes. (b) Nb/Y vs. Zr/Y plot comparing plume and N-MORB sources. Sources: N-MORB—Fitton et al. (1997); Jamaican island arc rocks—Hastie et al. (2009, in press).

Zr/Y plot of Fitton et al. (1997) compared to rocks derived from N-MORB-like sources which lie below the lower tramline (Fig. 7b). This distinction can be applied in subduction settings (e.g. the Lau Basin) where Nb, Zr and Y have behaved conservatively (Hastie et al., 2009, 2010). As can be seen on Fig. 7b, the conservative values for the La Désirade rocks plot beneath the tramlines close to the N-MORB field, similar to Jamaican arc rocks derived from N-MORB-like sources (Hastie et al., 2010) and unlike arc-like rocks derived from plume-like sources such as the Blue Mountains Inlier, Jamaica (Hastie et al., 2010).

Zr/Nb ratios are also used to indicate the type of mantle involved in the petrogenesis of the La Désirade rocks. Many subduction-related rocks have enriched Zr/Nb ratios of ~40–120, related to an N-MORB-like source region (e.g. Wendt et al., 1997; Carpentier et al., 2009). Values <40 are much less common (Carpentier et al., 2009), but have been linked to derivation from more enriched plume-like mantle sources (e.g. Wendt et al., 1997; Hastie et al., 2010).

As most back-arc and arc magmas are generated by >10% partial melting (e.g. Pearce and Parkinson, 1993; Pearce and Stern, 2006) Zr/Nb ratios in mafic arc lavas should reflect the composition of the source and will not be affected by low degrees of partial melting. Hence, island arc suites with Zr/Nb significantly lower than the value of ~40 may indicate a mantle–plume related source region. Ignoring the samples with positive Zr–Hf anomalies, the La Désirade mafic rocks have Zr/Nb ratios of 30 to 85 (mean = 52). The low Zr/Nb trend on Fig. 3 has a Zr/Nb ratio ~41, whereas the high trend has a Zr/Nb ~60. Both the trends on the differentiation plot (Fig. 3) and the absolute Zr/Nb ratios of the mafic lavas are therefore consistent with a largely non-plume-related, depleted mantle wedge source.

5.3. Nature of the subducted component

The LILE, LREE and Th in a subducting basaltic slab and its sedimentary veneer behave non-conservatively and mobilise into the slab-flux to contaminate the overlying mantle wedge (e.g. McCulloch and Gamble, 1991; Pearce and Parkinson, 1993; Pearce and Peate, 1995; Elliot, 2003; Plank, 2005). Some LILE such as Ba and Sr have been mobilised during sub-solidus hydrothermal and metamorphic alteration, leaving the immobile LREE and Th as the most suitable elements to use for assessment of the subduction component in the La Desirade samples.

In modern arcs the Th/La ratio of arc basalts mirrors the Th/La ratio of the forearc sediment (Plank, 2005) with Th and La significantly enriched in sediments derived from terrigenous sources (Th/La >0.3) relative to N-MORB (Plank, 2005). Many arcs trend from low absolute Th/La ratios (<0.1) to high Th/La (>0.1), indicating input, in part, from fluid released by subducting terrigenous sediment (Plank, 2005). Furthermore, negative Ce anomalies on N-MORB-normalised plots are related to incorporation of fluids from oxidised subducted pelagic sediment in the mantle wedge (Hole et al., 1984; McCulloch and Gamble, 1991). The Ce anomaly is expressed as a ratio of the N-MORB-normalised observed Ce concentration (Ce_{NMN}) to the expected Ce concentration (Ce^*_{NMN}), thus: $Ce/Ce^* = Ce_{NMN}/((La_{NMN} - Pr_{NMN})/2) + Pr_{MNM}$. A Ce/Ce* ratio consistently <1 confirms that the slab-flux is, at least in part, derived from an oxidised pelagic sedimentary source.

The mafic rocks of Unit 1 and 3 have Ce/Ce* ratios from 1 to 0.85 and Th/La <0.07 (Fig. 8) suggesting a limited oxidised pelagic sediment fluid input with no evidence of fluid related to subducted terrigenous sediment in the mantle wedge. Unit 2, as has already been shown, (Figs. 5 and 6) has the most marked arc signature of the three units and has a trend from Ce/Ce* ~1–0.75 at relatively high Th/La (0.07–0.22). These data point to a significant slab fluid flux related to both subducted terrigenous and pelagic sediments into the source of Unit 2 compared to Units 1 and 3. Units 1 and 3 'trend back' to Th/La ratios similar to those found in DMM, the calculated source for mid-ocean ridge basalts (Workman and Hart, 2005). The felsic volcanic and plutonic rocks and dykes have also been plotted on Figure 8 as Ce/Ce* ratios are unlikely to have been affected significantly by crystal fractionation. The felsic volcanic and plutonic rocks define a trend from Ce/Ce* ~1–0.75 at moderately high Th/La (0.07–0.1) which is a similar trend to some of the rocks of Unit 2, indicating a significant involvement of fluid related to subducted pelagic sediment. The dykes plot relatively close to Ce/Ce* = 1 with Th/La ~0.1 indicating the presence of some subducted terrigenous sediment.

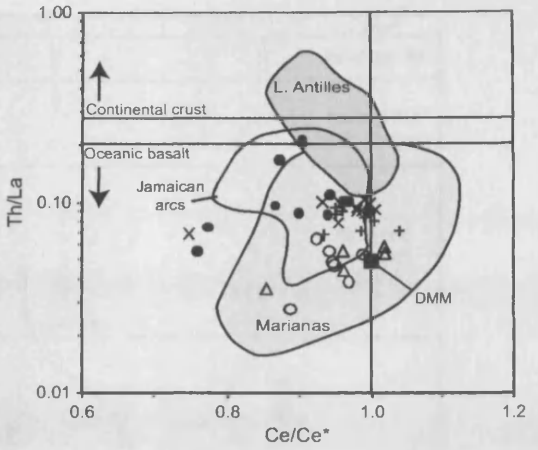

Fig. 8. Th/La vs. Ce/Ce* diagram (after Hastie et al., 2009, in press). Continental crust plots above Th/La = 0.29 and oceanic crust plots below Th/La = 0.2. Arc lavas involving slab-flux from pelagic oxidised sediments plot to the left of Ce/Ce* = 1 and arc lavas involving slab-flux from terrigenous sediments plot towards high values of Th/La similar to the continental crust. Examples of arc rocks involving slab-flux from dominantly pelagic oxidised (Marianas) and terrigenous (Lesser Antilles) sediments are shown. Cretaceous Jamaican island arc rocks show both pelagic and terrigenous sediment-related slab fluxes. The majority of La Désirade arc and back-arc rocks show fluid flux related to pelagic sediment, with Unit 2 of the NE mafic volcanic complex showing terrigenous sedimentary input. Symbols as for previous figures.

5.4. Tectonic setting

The geochemical results indicate the presence of an intra-oceanic subduction zone, however, the subduction-related input into the mantle wedge varied considerably. For example, the weak supra-subduction zone signature of Units 1 and 3 is best explained by a back-arc supra-subduction origin as opposed to an arc axis or fore-arc setting (Pearce and Stern, 2006). A back-arc setting incorporates aspects of both the argued-for ridge settings (pillow lavas, slow eruption rate, and pelagic sedimentation) (Mattinson et al., 2008; Montgomery and Kerr, 2009) and subduction-related chemistry. Furthermore, because (1) the faulted contact between the northeast mafic and felsic complexes is a minor feature since fragments of the mafic complex can be found within the felsic complex and (2) the felsic rocks also share a subduction-related chemistry broadly similar to Units 2 and 3, the entire Mesozoic suite was erupted in a back-arc setting in a period of ~10 Ma (Late Kimmeridgian to Mid Berriasian).

The argument for a single tectonic setting for all the complexes can be explored geochemically because the evolution of the mantle source and subducted sediment-related fluid fluxes of the complexes can be identified in stratigraphic order (Fig. 9). Although the felsic complexes and intermediate-felsic dykes are more evolved than the mafic complex (Fig. 9a), Fig. 9b shows, using La/Yb_{NMN} ratios, that the samples in all the complexes on the island are mostly tholeiitic in character. Where Nb has behaved conservatively and represents the contribution from the mantle alone, Nb/Yb_{NMN} (~0.6–1) (Fig. 9c) varies with no obvious trends towards increasing depletion or enrichment in the incompatible element composition of the mantle source through time. Th/La values (Fig. 9d) show that

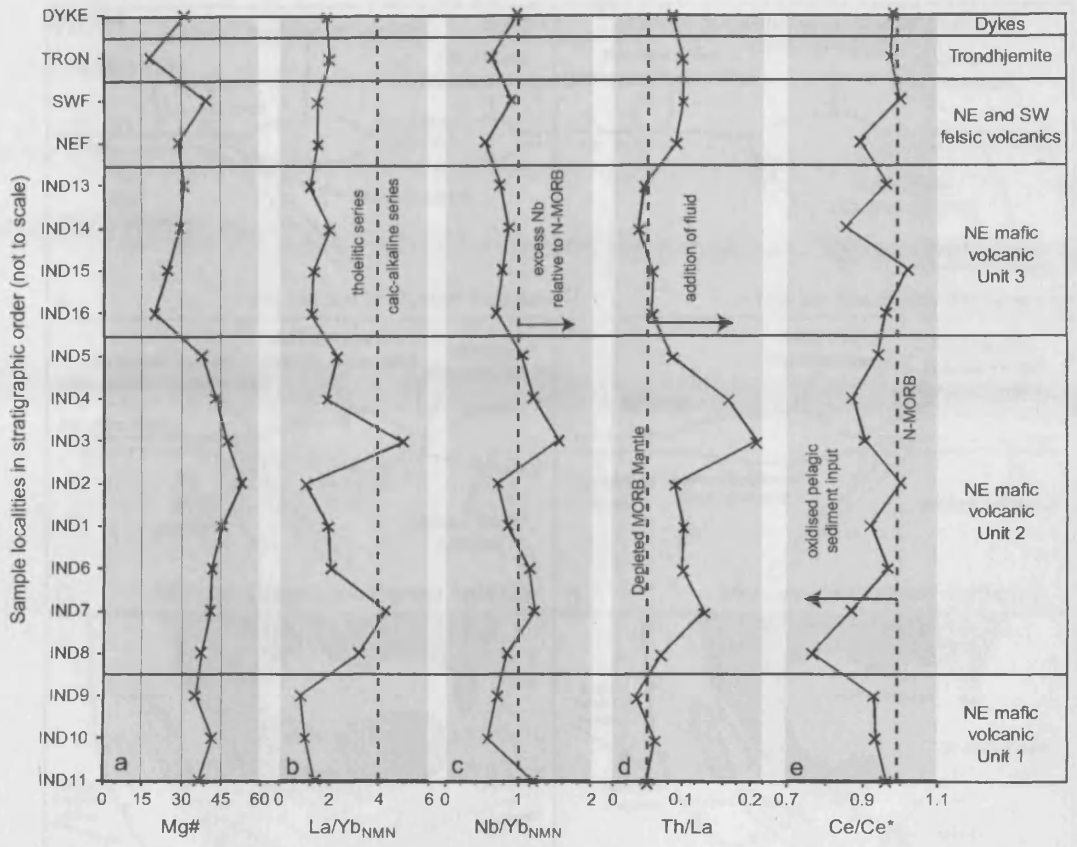

Fig. 9. Chemostratigraphic column for La Désirade. (a) Magnesium number. (b) La/Yb$_{NMN}$ ratios showing a pattern of LREE enrichment in mafic Unit 2, also the broadly tholeiitic character of magmatism on La Désirade. (c) Nb/Yb$_{NMN}$ ratios with the lowest ratio of ~0.6, similar to N-MORB. (d–e) Th/La and Ce/Ce* ratios showing the contribution of fluids related to subducted terrigenous sediment (high Th/La) and subducted oxidised pelagic sediment (causes Ce/Ce* <1 in arc lavas). See text for details.

mafic Unit 2, the felsic rocks, and dykes, all contain varying degrees of input from slab-fluids related to terrigenous sediments. Ce/Ce* ratios (Fig. 9e) show that the pelagic sediment-related flux mostly mirrors that from terrigenous sediments in mafic Units 1 and 2, but that this association does not hold true for mafic Unit 3, the felsic rocks or the dykes. Therefore at various times throughout the eruptive and intrusive sequence, different types of sediment had been subducted and contributed to the mantle source, but again there is no identifiable stratigraphic pattern. The fact that the mantle source composition and sedimentary components show few trends is, in part, due to the relatively rapid formation (~10 Ma) of the suite of complexes in a stable tectonic setting.

5.5. Palaeo-latitudinal position of La Désirade

The Mid-Late Jurassic separation of the Americas left a complex region of intra-arc spreading, transverse motions and continued east-dipping subduction at the proto-Caribbean/Pacific boundary (e.g. Fig. 7 of Pindell and Kennan, 2009). The western proto-Caribbean has been dubbed the Colombian Marginal Seaway by Pindell and Kennan (2009) (Fig. 10) and was in the back-arc with respect to the Andean–Cordilleran subduction zone. This Colombian Marginal Seaway is a logical position in which La Désirade could have initially formed. Terrigenous input to the subduction system could be derived from the mature Andean/Cordilleran arc and the source of magmatism would be the depleted back-arc mantle. La Désirade therefore formed in the proto-Caribbean realm, but would become an integral part of the Caribbean Plate during the inception of southwest-dipping Greater Antilles subduction.

A basin between Guerrero and Chortis and continental North America did not open until the Early Cretaceous (Pindell and Kennan, 2009) and was closed by ~120 Ma along the Motagua–Polóchic suture by west-dipping subduction (Harlow et al., 2004; Geldmacher et al., 2008) perhaps linked to the Caribbean Great Arc to the south (Tardy et al., 1994; Dickinson and Lawton, 2001; Umhoefer, 2003). Because of this rapid Cretaceous basin opening and closure, La Désirade could not form in such a position. The intra-oceanic east-dipping Andean/Cordilleran subduction zone in Central America (see Fig. 9 of Geldmacher et al., 2008) may have had its own back-arc between the arc and Guerrero and Chortis. This back-arc would be several degrees of latitude to the north of the Colombian Marginal Seaway but is a more northerly location of origin for La Désirade suitable?

Of the models which use the mantle reference frame, Duncan and Hargraves (1984) focus proto-Caribbean spreading on the palaeo-equator whilst Pindell and Kennan (2009) show the western edge of the Colombian Marginal Seaway centred on 10° N in the Late Jurassic. However, both Montgomery et al. (1994) and Mattinson et al. (2008) argue that Upper Jurassic radiolarian assemblages found on La Désirade, Puerto Rico, Hispaniola and Cuba all belong to the Northern or Southern Tethyan province of Pessagno et al. (1993). This implies an origin between 22 and 30° N or S of the equator. Jurassic radiolarian-bearing strata from the Blake Bahama Basin (Baumgartner, 1984) are assigned to the Central Tethyan Province (Pessagno et al., 1993) and should have been deposited at lower latitudes than the Caribbean occurrences.

The latitudinal findings contradict a near-equator origin for La Désirade and suggest that the radiolarian assemblages on La Désirade, Puerto Rico, Hispaniola and Cuba (Montgomery et al., 1994;

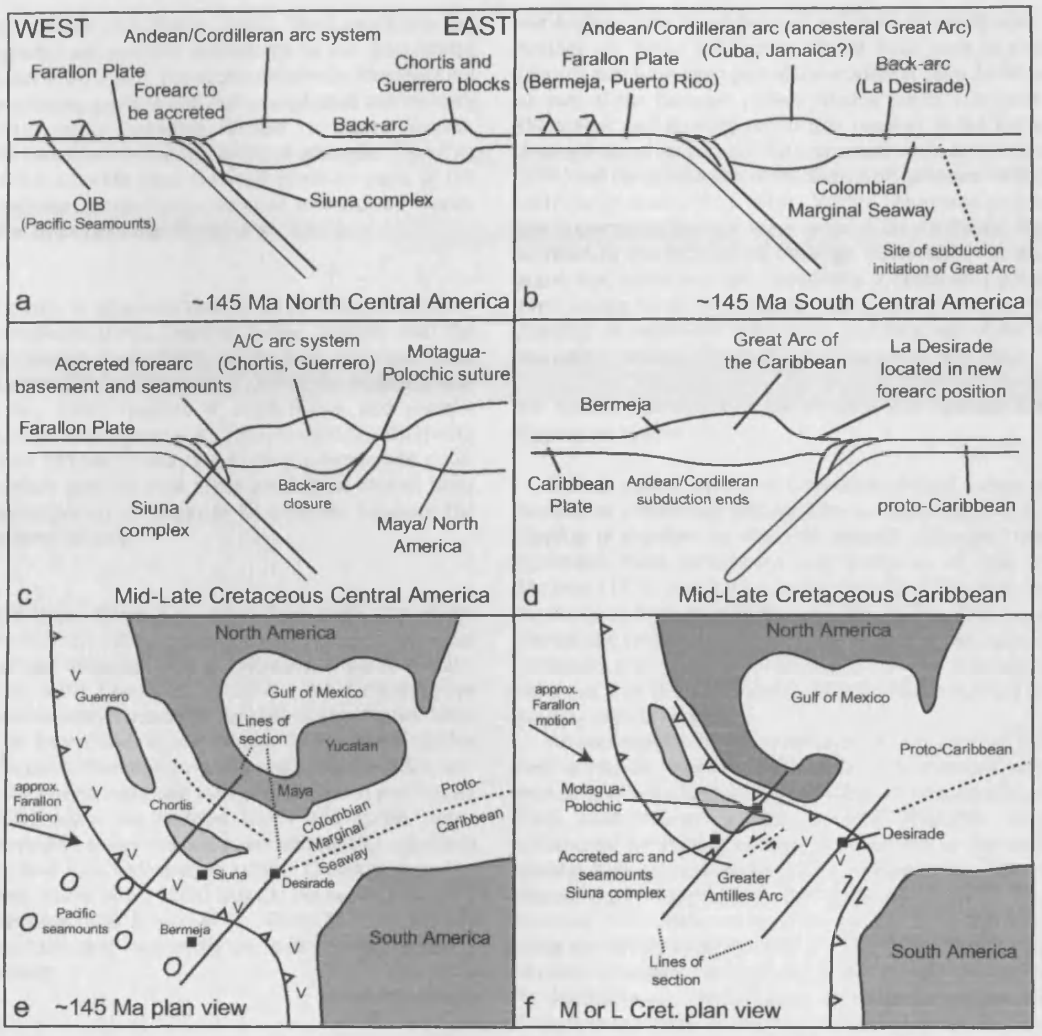

Fig. 10. Schematic tectonic model of the Caribbean and Central America (not to scale) with cross-section and plan views in Late Jurassic (145 Ma) and post-subduction polarity reversal Cretaceous times. Model adapted from Geldmacher et al. (2008) with plate motions taken from Pindell and Kennan (2009).

Mattinson et al., 2008) were derived from anything between ~1000 and ~3000 km north of the Colombian Marginal Seaway. An origin for these rocks south of the equator is unlikely because of southeast-directed subduction of Farallon crust in the Late Jurassic (Glazner, 1991; Pindell and Kennan, 2009). These outcrops would therefore have to migrate south-eastward with respect to North America to be later incorporated in the Caribbean Plate. Many studies of oblique convergence in modern and ancient arc systems and recent sandbox experiments show that the strike–slip component is largely taken up in the fore-arc and the arc, not the back-arc (e.g. Beck, 1983; ten Brink et al., 2009). Applied to the Andean/Cordilleran system it would be difficult to migrate La Désirade south-eastwards significantly with respect to North America. Therefore, we suggest that the original palaeo-latitudinal findings should be re-considered, a view shared by Pindell and Kennan (2009), as they place La Désirade close to the equator in the Colombian Marginal Seaway.

5.6. Pre-Aptian subduction-related rocks preserved in the Caribbean and Central America

Although there are many pre-Aptian rocks are found at various locations around the Caribbean and in Central America, we focus here on the fragments that formed during Andean/Cordilleran subduction. Baumgartner et al. (2008) have argued that such fragments exist in western Central America and on Cuba, Jamaica and Puerto Rico. This section uses their possible locations within the Andean/Cordilleran system to propose a regional plate tectonic reconstruction for the Late Jurassic.

5.6.1. Central America

Rocks found in melanges in Mexico, Nicaragua and Costa Rica belong to what has been called the Mesquito Composite Oceanic Terrane, the components of which were accreted to Central America as part of the Andean/Cordilleran arc system and lie north of the CCOP (Baumgartner et al., 2008). Tectonised gabbros and volcanic rocks, some with island arc chemistry and others of within-plate origin, have been dredged from the fore-arc basement of Guatemala and Mexico. These ~100 to 180 Ma rocks record a long history of east-dipping Farallon Plate subduction (Geldmacher et al., 2008). At Santa Elena in Costa Rica, three mafic volcanic island arc-related units have been identified with radiolarians ranging from 109 to 124 Ma (Hauff et al., 2000; Hoernle et al., 2004). Beneath Santa Elena is the Santa Rosa accretionary complex which has a more within-plate character (Hauff et al., 2000), but radiolarian ages from 93 to 190 Ma, contemporary to

La Désirade (Baumgartner and Denyer, 2006). The Santa Elena and Santa Rosa complexes are possible equivalents to the Guatemalan forearc (Geldmacher et al., 2008). The Siuna complex in Nicaragua is a mélange of serpentinites, gabbros and metamorphosed sedimentary and mafic igneous rocks including Middle to Upper Jurassic radiolarian cherts (Baumgartner et al., 2008). A phengite ^{40}Ar–^{39}Ar cooling age of 139.2 ± 0.4 Ma from the high-pressure parts of the Siuna mélange indicates active subduction and exhumation shortly after the formation of La Désirade (Flores et al., 2007).

5.6.2. Cuba

Cuba is built partly of allochthonous suites of Mesozoic subduction–accretion complexes thrust together during collision with the Bahama Platform (Stanek et al., 2009). At the base of the Las Villas Syncline in west-central Cuba (Stanek et al., 2009) the Mabujina unit (Somin and Millán, 1981) consists of amphibolites and gneissic granitoids of island arc origin (Kerr et al., 1999; Blein et al., 2003) with the gneiss dated to 133 Ma (U–Pb zircon) (Rojas-Agramonte et al., 2006). It is therefore possible that some subduction-related units on Cuba are contemporary in origin to La Désirade however the chronology is far from certain.

5.6.3. Jamaica

The Lower and Upper Devils Racecourse Formations (sic) of the Benbow inlier (Burke et al., 1969) consist of a lower bimodal island arc tholeiite sequence and an upper suite of calc-alkaline basalt–basaltic andesite island arc rocks (Hastie et al., 2009). The formations are separated by a sedimentary succession containing Hauterivian fossil assemblages at its base (Skelton and Masse, 1998). The >136 Ma Lower Devils Racecourse Formation arguably contains the oldest arc-axis lavas in the Caribbean. Although Hastie et al. (2009) and Pindell and Kennan (2009) argue the undated Lower and Aptian Upper Formations were erupted in one single tectonic setting, this is far from certain given: (1) 2600 m of sedimentary rocks, (2) faulting between the two Formations (Burke et al., 1969) and (3) the need for detailed mapping of the Benbow Inlier (Hastie et al., 2009). The Lower Devils Racecourse Formation may represent an east-dipping Andean/Cordilleran arc setting.

5.6.4. Puerto Rico

Much of Puerto Rico is made up of middle to Late Cretaceous island arc assemblages (Jolly et al., 2001); however, to the southwest of the Cretaceous rocks lies the Bermeja complex (Mattson, 1960) which consists of a tectonic melange of oceanic serpentinite, amphibolite, basalt and chert (Schellekens, 1998). The cherts have yielded a ~90 Ma history from the Early Jurassic to the Middle Cretaceous including Kimmeridgian–Tithonian radiolarian- and Pantannelid-bearing tuffaceous cherts which overlap in age with La Désirade (Montgomery et al., 1992, 1994; Schellekens, 1998). The tuffaceous nature of the chert may indicate deposition close to an island arc source, whilst the gabbros and greenstones apparently have a supra-subduction zone origin (Montgomery et al., 1994; Schellekens, 1998). Accretion of the Bermeja complex occurred during the Early Cretaceous before the deposition of Cenomanian sedimentary rocks (Schellekens, 1998). It is unlikely that the Bermeja complex was formed close to a west-dipping subduction zone because of its age range and south-westerly position relative to the younger Greater Antilles arc assemblages. Hence, Bermeja may also represent part of the Andean/Cordilleran system.

5.6.5. Plate tectonic reconstruction of Middle America during the Late Jurassic

In Figs. 10a, b and e we present a model which proposes that the arc rocks discussed previously were related to the east-dipping Andean/Cordilleran subduction system and were part of the Mesquito Terrane of Baumgartner et al. (2008). Complexes such as Bermeja formed near the Andean/Cordilleran fore-arc and were obducted onto the Greater Antilles arc. Some subduction-related rocks such as those found in Jamaica may have been part of the original arc axis. La Désirade formed as part of the back-arc region. Further north, Late Jurassic to Early Cretaceous east-dipping subduction resulted in the formation of the depleted island arc rocks of the Guatemalan fore-arc (Geldmacher et al., 2008) and the subduction of the Siuna high-pressure rocks (Flores et al., 2007; Baumgartner et al., 2008). Within-plate rocks also dredged from the Guatemalan fore-arc were erupted on the Pacific Plate and later accreted to the subduction mélange (Geldmacher et al., 2008). We argue that there was not necessarily a Cretaceous polarity reversal event analogous to the Caribbean along the western margin of Central America, so eastwards subduction and accretion of the fore-arc and seamounts continued through the Cretaceous (Fig. 10c).

5.7. Tectonic framework for preservation of La Désirade in a southwest-dipping arc system

In most interpretations of Caribbean geology, a reversal of Greater Antilles arc subduction polarity from northeast-dipping to southwest-dipping is required to facilitate relative eastwards motion of the Caribbean Plate in-between the Americas, as first proposed by Mattson (1979) and two possible timings of reversal were outlined in the introduction—120 Ma and 80–90 Ma. This paper will not discuss the relative merits of either model, as we have no new data pertaining to the timing of the polarity reversal however we highlight the point that the preservation of La Désirade is a key aspect of the polarity reversal event.

An analogue for the preservation of La Désirade is to be found in the back-arc region of the Scotia Sea during its Late Cretaceous to Paleogene evolution where a back-arc formed in relation to a Pacific arc which ran from South America to the Antarctic Peninsula. South America accelerated westwards relative to Antarctica in the mid-Cretaceous causing back-arc compression and eventually the subduction of the Atlantic plate beneath the former back-arc (Dalziel, 1985; Barker and Lonsdale, 1991; Barker et al., 1991; Barker, 2001). Subduction initiated along the former back-arc ridge (Barker, 2001, Fig. 5), meaning half of the original oceanic back-arc was preserved and lies today in the South Sandwich fore-arc. We have generated a similar model in Fig. 10c, d and f which could apply to the Mid Cretaceous (~125 Ma) in the case of Aptian–Albian subduction polarity reversal or to the Late Cretaceous (~85 Ma) in the case of a later reversal.

Aptian subduction initiation, probably in response to the westward acceleration of North America, occurred along a zone running from along the western margin of the basin between Guerrero/Chortis and the North American mainland. The Guerrero/Chortis basin then closed along the Motagua/Polóchic suture (Harlow et al., 2004; Geldmacher et al., 2008; Pindell and Kennan, 2009). In the Caribbean region, southwest-dipping subduction initiation (or polarity reversal) occurred to the east of La Désirade. The pre-existing Andean/Cordilleran arc was the approximate axis upon which the new Greater Antilles arc built up. To the southwest of the arc axis, the old Andean/Cordilleran forearc (e.g. Bermeja) was preserved. To the east of the arc axis, the new subduction zone began destruction of the proto-Caribbean seaway but the rate of slab roll-back must have equalled or exceeded the rate of westward motion of the Americas over the mantle through the Cretaceous to the present in order to prevent subduction erosion and the destruction of the crust containing La Désirade. The abundant high-pressure metamorphic belts present in the Greater Antilles may be the manifestation of a different regime further to the north.

6. Conclusions

La Désirade hosts the only Mesozoic rocks exposed in the Lesser Antilles. The entire suite was erupted in around ~10 Ma in the latest

Jurassic to Early Cretaceous. Detailed investigation of the trace element content of the rocks of the northeast mafic volcanic complex reveals that they originated in a back-arc supra-subduction setting by partial melting within a depleted mantle wedge. The mantle wedge was fluxed by fluids derived partly from variable quantities of subducted pelagic and terrigenous sediments along with a possible slab or subducted crust-related melt component which slightly altered the MORB-like immobile trace element ratios.

The back-arc lay to the east of the Andean/Cordilleran east-dipping subduction zone in the Colombian Marginal Seaway prior to the inception of a southwest-dipping Greater Antilles arc. Other Late Jurassic to Early Cretaceous Caribbean and Central American subduction-related rocks appear to corroborate the presence of an east-dipping Andean/Cordilleran arc. We suggest that in the Caribbean region, initiation of southwest-dipping subduction occurred to the east of La Désirade whereas in Central America a continual record of east-dipping subduction is present.

Supplementary data to this article can be found online at doi:10.1016/j.lithos.2010.08.026.

Acknowledgements

I.N. acknowledges NERC PhD studentship NE/F00219X/1. J.A.G. acknowledges the Irving Fund and the Norman Kemp travel scholarship of the University of St. Andrews. Laura Cotton assisted in the field. The Oualiri Beach Hotel, Beauséjour provided accommodation and transport. Karine Gauchat supplied the radiogenic isotope data, Iain McDonald ran the elemental analyses at Cardiff University and James Pindell has discussed many aspects of the origins and evolution of the Caribbean region with us. Helpful reviews by Javier Escuder-Viruete and Grenville Draper improved the manuscript.

References

Barker, P.F., 2001. Scotia Sea regional tectonic evolution: implications for mantle flow and palaeocirculation. Earth Science Reviews 55, 1–39.

Barker, P.F., Lonsdale, M.J., 1991. A multichannel seismic profile across the Weddell Sea margin of the Antarctic Peninsula: regional tectonic implications. In: Thomson, M.R.A., Crame, J.A., Thomson, J.W. (Eds.), Geological Evolution of Antarctica. Cambridge University Press, Cambridge, pp. 237–241.

Barker, P.F., Dalziel, I.W.D., Storey, B.C., 1991. Tectonic development of the Scotia Arc region. In: Tingey, R.J. (Ed.), Geology of Antarctica. Oxford University Press, Oxford, pp. 215–248.

Baumgartner, P.O., 1984. A Middle Jurassic–Early Cretaceous low latitude radiolarian zonation based on unitary association and age of Tethyan radiolarites. Eclogae Geologicase Helvetiae 77, 729–837.

Baumgartner, P.O., Denyer, P., 2006. Evidence for middle Cretaceous accretion at Santa Elena Peninsula (Santa Rosa Accretionary Complex), Costa Rica. Geologica Acta 4, 179–191.

Baumgartner, P.O., Flores, K., Bandini, A.N., Girault, F., Cruz, D., 2008. Upper Triassic to Cretaceous Radiolaria from Nicaragua and northern Costa Rica—the Mesquito Composite Oceanic Terrane. Ofioliti 33, 1–19.

Baumgartner-Mora, C., Gauchat, K., Baumgartner, P.O., 2004. Larger Foraminifera (Nummulitinae, Archaiasinids) in the Neogene shallow water limestone of the Désirade island, Guadeloupe (French Antilles). Abstracts of the Second Swiss Geoscience Meeting, Lausanne, 19th–20th November, 2004.

Beck Jr., M.E., 1983. On the mechanism of tectonic transport in zones of oblique subduction. Tectonophysics 93, 1–11.

Blein, O., Guillot, S., Lapierre, H., Mercier de Lépinay, B., Lardeaux, J.-M., Millan Trujillo, G., Campos, M., Garcia, A., 2003. Geochemistry of the Mabujina complex, central Cuba: implications on the Cuban Cretaceous arc rocks. Journal of Geology 111, 89–110.

Bouysse, P., 1984. The Lesser Antilles island arc: structure and geodynamic evolution. Initial Reports of the Deep Sea Drilling Project 78A, 83–103.

Bouysse, P., Schmidt-Effing, R., Westercamp, D., 1983. La Desirade Island (Lesser Antilles) revisited: Lower Cretaceous radiolarian cherts and arguments against an ophiolitic origin for the basal complex. Geology 11, 244–247.

Burke, K., 1988. Tectonic evolution of the Caribbean. Annual Reviews of Earth and Planetary Science 16, 201–230.

Burke, K., Coates, A.G., Robinson, E., 1969. Geology of the Benbow Inlier and surrounding areas, Jamaica. In: Saunders, J.B. (Ed.), Transactions of the Fourth Caribbean Geological Conference, pp. 229–307.

Burke, K., Fox, P.J., Sengor, A.M.C., 1978. Buoyant ocean floor and the evolution of the Caribbean. Journal of Geophysical Research 83 (B8), 3949–3954.

Cann, J.R., 1970. Rb, Sr, Zr and Nb in some ocean floor basaltic rocks. Earth and Planetary Science Letters 10, 7–11.

Carpentier, M., Chauvel, C., Maury, R.C., Matielli, N., 2009. The "zircon effect" as recorded by the chemical and Hf isotopic compositions of Lesser Antilles forearc sediments. Earth and Planetary Science Letters 287, 86–99.

Condie, K.C., 2005. TTGs and adakites: are they both slab melts? Lithos 80, 33–44.

Cordey, F., Cornée, J.J., 2009. New radiolarian assemblages from La Désirade Island basement complex (Guadeloupe, Lesser Antilles arc) and Caribbean tectonic implications. Bulletin of the Geological Society of France 180, 399–409.

Dalziel, I.W.D., 1985. Collision and cordilleran orogenesis: an Andean perspective. In: Coward, M.P., Ries, A.C. (Eds.), Collision Tectonics: Geological Society of London Special Publication, vol. 19, pp. 389–404.

Defant, M.J., Drummond, M.S., 1990. Derivation of some modern arc magmas by melting of young subducted lithosphere. Nature 347, 662–665.

Dickinson, W.R., Lawton, T.F., 2001. Carboniferous to Cretaceous assembly and fragmentation of Mexico. Bulletin of the Geological Society of America 113, 1142–1160.

Duncan, R.A., Hargraves, R.B., 1984. Plate tectonic evolution of the Caribbean region in the mantle reference frame. In: Bonini, W.E., Hargraves, R.B., Shagam, R. (Eds.), The Caribbean–South American Plate Boundary and Regional Tectonics: Geological Society of America Memoir, vol. 162, pp. 81–93.

Edgar, N.T., Ewing, J.I., Hennion, J., 1971. Seismic refraction and reflection in the Caribbean Sea. American Association of Petroleum Geologists Bulletin 162, 81–93.

Elliot, T., 2003. Tracers of the slab—inside the subduction factory. Geophysical Monograph 138, 23–45.

Fink Jr., L.K., 1972. Bathymetric and geologic studies of the Guadeloupe region, Lesser Antilles island arc. Journal of Marine Geology 12, 267–288.

Fitton, J.G., Saunders, A.D., Norry, M.J., Hardarson, B.S., Taylor, R.N., 1997. Thermal and chemical structure of the Iceland plume. Earth and Planetary Science Letters 153, 197–208.

Flores, K., Baumgartner, P.O., Skora, S., Baumgartner, L., Müntener, O., Cosca, M., Cruz, D., 2007. The Siuna Serpentinite Mélange: An Early Cretaceous Subduction/Accretion of a Jurassic Arc. Eos Transactions of the American Geophysical Union 88, Fall Meet. Supplement Abstract T-11D-03.

Gauchat, K., 2004. Geochemistry of Désirade Island rocks (Guadeloupe, French Antilles). MS Thesis, University of Lausanne (unpublished).

Geldmacher, J., Hoernle, K., van den Bogaard, P., Hauff, F., Klügel, A., 2008. Age and geochemistry of the Central American forearc basement (DSDP Leg 67 and 84): insights into Mesozoic arc volcanism and seamount accretion on the fringe of the Caribbean LIP. Journal of Petrology 49, 1781–1815.

Glazner, A.F., 1991. Plutonism, oblique subduction, and continental growth: an example from the Mesozoic of California. Geology 19, 784–786.

Harlow, G.E., Hemming, S.R., Avé Lallement, H.G., Sisson, V.B., Sorensen, S.S., 2004. Two high-pressure low-temperature serpentinite-matrix mélange belts, Motagua fault zone, Guatemala: a record of Aptian and Maastrichtian collisions. Geology 32, 17–20.

Hastie, A.R., 2009. Is the Cretaceous primitive island arc series in the circum-Caribbean region geochemically analogous to the modern island arc tholeiite series? In: James, K.H., Lorente, M.A., Pindell, J.L. (Eds.), The Origin and Evolution of the Caribbean Plate: Geological Society of London Special Publication, vol. 328, pp. 399–409.

Hastie, A.R., Kerr, A.C., 2010. Mantle plume or slab window?: Physical and geochemical constraints on the origin of the Caribbean oceanic plateau. Earth Science Reviews 98, 283–293.

Hastie, A.R., Kerr, A.C., Pearce, J.A., Mitchell, S.F., 2007. Classification of altered island arc rocks using immobile trace elements: development of the Th–Co discrimination diagram. Journal of Petrology 48, 2341–2357.

Hastie, A.R., Kerr, A.C., Mitchell, S.F., Millar, I.L., 2009. Geochemistry and tectonomagmatic significance of Lower Cretaceous island arc lavas from the Devils Racecourse Formation, eastern Jamaica. In: James, K.H., Lorente, M.A., Pindell, J.L. (Eds.), The Origin and Evolution of the Caribbean Plate: Geological Society of London Special Publication, vol. 328, pp. 339–360.

Hastie, A.R., Kerr, A.C., McDonald, I., Mitchell, S.F., Pearce, J.A., Wolstencroft, M., Millar, I.L., 2010. Do Cenozoic analogues support a plate tectonic origin for Earth's earliest continental crust? Geology 38 (6), 495–498.

Hastie, A.R., Ramsook, R., Mitchell, S.F., Kerr, A.C., Millar, I.L., Mark, D.F., 2010. Age and geochemistry of compositionally distinct back-arc basin lavas, implications for the tectonomagmatic evolution of the Caribbean plate. The Journal of Geology 118, 655–676.

Hauff, F., Hoernle, K.A., Van den Bogaard, P., Alvarado, G.E., Garbe-Schönberg, D., 2000. Age and geochemistry of basaltic complexes in western Costa Rica: contributions to the geotectonic evolution of Central America. Geochemistry, Geophysics, Geosystems. 1. doi:10.1029/1999GC000020.

Hoernle, K.A., Hauff, F., van den Bogaard, P., 2004. A 70 m.y. history (139–69 Ma) for the Caribbean large igneous province. Geology 32, 697–700.

Hole, M.J., Saunders, A.D., Marriner, G.F., Tarney, J., 1984. Subduction of pelagic sediments: implications for the origin of Ce-anomalous basalts from the Mariana Islands. Journal of the Geological Society of London 141, 453–472.

Johnston, T.H., Schilling, G.J., Oji, Y., Fink Jr., L.K., 1971. Dredged greenstones from the Lesser Antilles island arc. Eos (Transactions of the American Geophysical Union) 52, 246.

Jolly, W.T., Lidiak, E.G., Dickin, A.P., Wu, T.-W., 2001. Secular geochemistry of central Puerto Rican island arc lavas: constraints on Mesozoic tectonism in the eastern Greater Antilles. Journal of Petrology 42, 2197–2214.

Kennan, L., Pindell, J.L., 2009. Dextral shear, terrane accretion and basin formation in the Northern Andes: best explained by interaction with a Pacific-derived Caribbean Plate? In: James, K.H., Lorente, M.A., Pindell, J.L. (Eds.), The Origin and Evolution of the Caribbean Plate: Geological Society of London Special Publication, vol. 328, pp. 487–531.

Kerr, A.C., Iturralde-Vinent, M.A., Saunders, A.D., Babbs, T.L., Tarney, J., 1999. A new plate tectonic model of the Caribbean: implications from a geochemical reconnaissance of Cuban Mesozoic volcanic rocks. Bulletin of the Geological Society of America 111, 1581–1599.

Kerr, A.C., White, R.V., Thompson, P.M.E., Tarney, J., Saunders, A.D., 2003. No oceanic plateau—no Caribbean Plate? The seminal role of an oceanic plateau in Caribbean plate evolution. In: Bartolini, C., Buffler, R.T., Blickwede, J.F. (Eds.), The circum-Gulf of Mexico and the Caribbean: hydrocarbon habitats, basin formation and plate tectonics: American Association of Petroleum Geologists Memoir, vol. 79, pp. 126–168.

Martin, H., Smithies, R.H., Rapp, R.P., Moyen, J.-F., Champion, D.C., 2005. An overview of adakite, tonalite–trondhjemite–granodiorite (TTG) and sanukitoid: relationships and some implications for crustal evolution. Lithos 79, 1–24.

Mattinson, J.M., Fink, L.K., Hopson, C.A., 1980. Geochronologic and isotopic study of the La Desirade basement complex: Jurassic oceanic crust in the Lesser Antilles. Contributions to Mineralogy and Petrology 71, 237–245.

Mattinson, J.M., Pessagno Jr., E.A., Montgomery, H., Hopson, C.A., 2008. Late Jurassic age of oceanic basement at La Désirade Island, Lesser Antilles arc. In: Wright, J.E., Shervais, J.W. (Eds.), Ophiolites, Arcs and Batholiths: A Tribute to Cliff Hopson: Geological Society of America Special Paper, vol. 438, pp. 175–190.

Mattson, P.H., 1960. Geology of the Mayagüez area, Puerto Rico. Bulletin of the Geological Society of America 71, 319–362.

Mattson, P.H., 1979. Subduction, buoyant braking, flipping, and strike–slip faulting in the northern Caribbean. The Journal of Geology 87, 293–304.

Mauffrey, A., Leroy, S., 1997. Seismic stratigraphy and structure of the Caribbean igneous province. Tectonophysics 283, 61–104.

McCulloch, M.T., Gamble, J.A., 1991. Geochemical and geodynamical constraints on subduction zone magmatism. Earth and Planetary Science Letters 102, 358–374.

McDonald, I., Viljoen, K.S., 2006. Platinum-group element geochemistry of mantle eclogites: a reconnaissance study of xenoliths from the Orapa kimberlite, Botswana. Transactions of the Institutions of Mining and Metallurgy, Section B 115, 81–91.

McDonough, W.D., Sun, S.-S., 1995. The composition of the Earth. Chemical Geology 120, 223–254.

Montgomery, H., Kerr, A.C., 2009. Rethinking the origins of the red chert at La Désirade, French West Indies. In: James, K.H., Lorente, M.A., Pindell, J.L. (Eds.), The Origin and Evolution of the Caribbean Plate: Geological Society of London Special Publication, vol. 328, pp. 457–467.

Montgomery, H., Pessagno Jr., E.A., Munoz, I., 1992. Jurassic (Tithonian) radiolaria from La Désirade (Lesser Antilles): preliminary paleontological and tectonic implications. Tectonics 11, 1426–1432.

Montgomery, H., Pessagno Jr., E.A., Pindell, J.L., 1994. A 195 Ma terrane in a 165 Ma ocean: Pacific origin of the Caribbean Plate. GSA Today 4, 1–6.

Moores, E.M., Vine, F.J., 1971. The Troodos massif, Cyprus and other ophiolites as oceanic crust: evaluation and implications. Philosophical Transactions of the Royal Society of London 268A, 443–466.

Müller, R.D., Royer, J.-Y., Cande, S.C., Roest, W.R., Maschenkov, S., 1999. New constraints on the Late Cretaceous/Tertiary plate tectonic evolution of the Caribbean. In: Mann, P. (Ed.), Caribbean Basins. : Sedimentary Basins of the World, vol. 4. Elsevier Science, pp. 33–59.

Ogg, J.G., Ogg, G., Gradstein, F.M., 2008. The concise Geologic Time Scale. Cambridge University Press, Cambridge.

Oldow, J.S., Bally, A.W., Avé Lallemant, H.G., Leeman, W.P., 1989. Phanerozoic evolution of the North American Cordillera, United States and Canada. In: Bally, A.W., Palmer, A.R. (Eds.), Geology of North America—an overview. : Geology of North America, vol. A. Geological Society of America, Boulder, Colorado, pp. 139–232.

Pearce, J.A., 1983. Role of the sub-continental lithosphere in magma genesis at active continental margins. In: Hawkesworth, C.J., Norry, M.J. (Eds.), Continental Basalts and Mantle Xenoliths. Shiva, Nantwich, pp. 230–249.

Pearce, J.A., Parkinson, I.J., 1993. Trace element models for mantle melting: applications to volcanic arc petrogenesis. In: Prichard, H.M., Alabaster, T., Harris, N.B.W., Neary, C.R. (Eds.), Magmatic processes and Plate Tectonics: Geological Society of London Special Publication, vol. 76, pp. 373–403.

Pearce, J.A., Peate, D.W., 1995. Tectonic implications of the composition of volcanic arc magmas. Annual Reviews in Earth and Planetary Sciences 23, 251–285.

Pearce, J.A., Stern, R.J., 2006. Origin of back-arc basin magmas: trace element and isotopic perspectives. In: Christie, D.M., Fisher, C.R., Lee, S.-M., Givens, S. (Eds.), Back-arc spreading systems: geological, biological, chemical and physical interactions: AGU Geophysical Monograph Series, vol. 116, pp. 63–86.

Pearce, J.A., Lippard, S.J., Roberts, S., 1984. Characteristics and tectonic significant of supra-subduction zone ophiolites. In: Kokelaar, B.P., Howells, M.F. (Eds.), Marginal basin geology: volcanic and associated sedimentary and tectonic processes in modern and ancient marginal basins: Geological Society of London Special Publication, vol. 16, pp. 77–94.

Peccarillo, A., Taylor, S.R., 1976. Geochemistry of Eocene calc-alkaline volcanic rocks from the Kastamonu area, Northern Turkey. Contributions to Mineralogy and Petrology 58, 63–81.

Perfit, M.R., Gust, D.A., Bence, A.E., Arculus, R.J., Taylor, S.R., 1980. Chemical characteristics of island-arc basalts: implications for mantle sources. Chemical Geology 30, 227–256.

Pessagno Jr., E.A., Blome, C.D., Hull, D., Six Jr., W.M., 1993. Middle and Upper Jurassic Radiolaria from the western Klamath terrane, Smith River subterrane, northwestern California: their biostratigraphic, chronostratigraphic, geochronologic, and paleolatitudinal significance. Micropalaeontology 39, 93–166.

Pindell, J.L., Dewey, J.F., 1982. Permo-Triassic reconstruction of Western Pangea and the evolution of the Gulf of Mexico/Caribbean region. Tectonics 1, 179–211.

Pindell, J.L., Kennan, L., 2009. Tectonic evolution of the Gulf of Mexico, Caribbean and northern South America in the mantle reference frame: an update. In: James, K.H., Lorente, M.A., Pindell, J.L. (Eds.), The Origin and evolution of the Caribbean Plate: Geological Society of London Special Publication, vol. 328, pp. 1–55.

Pindell, J.L., Cande, S.C., Pitman, W.C., Rowley, D.B., Dewey, J.F., La Brecque, J.L., Haxby, W.F., 1988. A plate kinematic framework for models of Caribbean evolution. Tectonophysics 151, 121–138.

Pindell, J.L., Kennan, L., Stanek, K.P., Maresch, W.V., Draper, G., 2006. Foundations of Gulf of Mexico and Caribbean evolution: eight controversies resolved. Geologica Acta 4, 303–341.

Plank, T., 2005. Constraints from thorium/lanthanum on sediment recycling at subduction zones and the evolution of the continents. Journal of Petrology 46, 921–944.

Rojas-Agramonte, Y., Kröner, A., García-Casco, A., Iturralde-Vinent, M.A., Wingate, M.T.D., Liu, D.Y., 2006. Geodynamic implications of zircon ages from Cuba. Geophysical Research Abstracts 8, 04943. SRef-ID: 1607-7962/gra/EGU06-A-04943.

Saunders, A.D., Tarney, J., Weaver, S.D., 1980. Transverse geochemical variations across the Antarctic Peninsula: implications for the genesis of calc-alkaline magmas. Earth and Planetary Science Letters 46, 344–360.

Schellekens, J.H., 1998. Geochemical evolution and tectonic history of Puerto Rico. In: Lidiak, E.G., Larue, D.K. (Eds.), Tectonics and geochemistry of the northeastern Caribbean: Geological Society of America Special Paper, vol. 322, pp. 35–66.

Seewald, J.S., Seyfried, W.E., 1990. The effect of temperature on metal mobility in subseafloor hydrothermal systems: constraints from basalt alteration experiments. Earth and Planetary Science Letters 101, 388–403.

Sinton, C.W., Duncan, R.A., Storey, M., Lewis, J., Estrada, J.J., 1998. An oceanic flood basalt province within the Caribbean plate. Earth and Planetary Science Letters 155, 221–235.

Skelton, P.W., Masse, J.P., 1998. Revision of the lower Cretaceous rudist genera *Pachytraga* Paquier and *Retha* Cox (Bivalvia: Hippuritacea) and the origins of the Caprinidae. Geobios 22, 331–370.

Smithies, R.H., 2000. The Archaean tonalite–trondhjemite–granodiorite (TTG) series is not an analogue of Cenozoic adakite. Earth and Planetary Science Letters 182, 115–125.

Somin, M.L., Millán, G., 1981. Geologija metamorficheskich kompleksoc Kuby. Isdat. Nauka, Moscow. 219pp.

Stanek, K.P., Maresch, W.V., Pindell, J.L., 2009. The geotectonic story of the northwestern branch of the Caribbean Arc: implications from structural and geochronological data of Cuba. In: James, K.H., Lorente, M.A., Pindell, J.L. (Eds.), The Origin and Evolution of the Caribbean Plate: Geological Society of London Special Publication, vol. 328, pp. 361–398.

Sun, S.-S., McDonough, W.D., 1989. Chemical and isotopic systematics of oceanic basalts: implications for mantle composition and processes. In: Saunders, A.D., Norry, M.J. (Eds.), Magmatism in the Ocean Basins: Geological Society of London Special Publication, vol. 42, pp. 313–345.

Tardy, M., Lapierre, H., Freydier, C., Coulon, C., Gill, J.-B., Mercier de Lepinay, B., Beck, C., Mertinez, J., Talavera, O., Ortiz, E., Stein, G., Bourdier, J.-L., Yta, M., 1994. The Guerrero suspect terrane (western Mexico) and coeval arc terranes (the Greater Antilles and the Western Cordillera of Colombia): a late Mesozoic intraoceanic arc accreted to cratonal America during the Cretaceous. Tectonophysics 320, 49–73.

ten Brink, U.S., Marshak, S., Granja Bruña, J.-S., 2009. Bivergent thrust wedges surrounding oceanic island arcs: insights from observations and sandbox models of the northeastern Caribbean plate. Bulletin of the Geological Society of America 121, 1522–1536.

Thompson, P.M.E., Kempton, P.D., White, R.V., Kerr, A.C., Tarney, J., Saunders, A.D., Fitton, J.G., McBirney, A., 2003. Hf–Nd isotope constraints on the origin of the Cretaceous Caribbean plateau and its relationship to the Galapagos plume. Earth and Planetary Science Letters 217, 59–75.

Umhoefer, P.J., 2003. A model for the North American Cordillera in the Early Cretaceous: tectonic escape related to arc collision of the Guerrero terrane and a change in North America plate motion. In: Johnson, S.E., Paterson, S.R., Fletcher, J.M., Girty, G.H., Kimbrough, D.L., Martín-Barajas, A. (Eds.), Tectonic evolution of northwestern Mexico and the southwestern USA: Geological Society of America Special Paper, vol. 374, pp. 117–134.

Wendt, J.I., Regelous, M., Collerson, K.D., Ewart, A., 1997. Evidence for a contribution from two mantle plumes to island-arc lavas from northern Tonga. Geology 25, 611–614.

White, W.M., Patchett, J., 1984. Hf–Nd–Sr isotopes and incompatible element abundances in island arcs: implications for magma origins and crust–mantle evolution. Earth and Planetary Science Letters 67, 167–185.

White, R.V., Tarney, J., Kerr, A.C., Saunders, A.D., Kempton, P.D., Pringle, M.S., Klaver, G.T., 1999. Modification of an oceanic plateau, Aruba, Dutch Caribbean: implications for the generation of continental crust. Lithos 46, 43–68.

Workman, R.K., Hart, S.R., 2005. Major and trace element composition of the depleted MORB mantle (DMM). Earth and Planetary Science Letters 231, 53–72.

Yogodzinski, G.M., Kay, R.W., Volynets, O.N., Koloskov, A.N., Kay, S.M., 1995. Magnesian andesite in the western Aleutian Komandorsky region: implications for slab melting and processes in the mantle wedge. Bulletin of the Geological Society of America 107, 505–519.

KT1 2EE, UK
[3]Institut für Geologie, TU Bergakademie Freiberg, Bernhard-von-Cotta-Strasse 2, D-09596 Frei
[4]Natural Environment Research Council Isotope Geoscience Laboratories, Kingsley Dunham Ce
NG12 5GG, UK
*Corresponding author (e-mail: neilli@cardiff.ac.uk)

Abstract: In this paper we reassess the geochronology and geochemistry of three dredge hauls from th corner of the Aves Ridge (Caribbean Sea) originally sampled in 1968 by Duke University's R.V. *Eastv* Two hauls consist of light rare earth element-enriched granitoids with a U–Pb zircon emplacement ag 75.9 ± 0.7 Ma. A further haul contains mostly calc-alkaline island arc basaltic andesites of uncertain Petrological, trace element and isotopic constraints indicate that the granitoids have an oceanic crustal so and were formed by melting of the lower arc, oceanic or oceanic plateau crust. The mafic rocks forme partial melting of an incompatible trace element-enriched mantle wedge, which was probably compose mantle plume material. Both the dredged rocks and data from the Dutch–Venezuelan Antilles indica period of west-dipping underthrusting and subduction beneath, or close to, the Caribbean–Colombian Oce Plateau between *c.* 88 and *c.* 59 Ma, concurrent with collision of part of the plateau with northwestern S America. Constraints from the geochemistry and geochronology of offshore southern Caribbean arc plateau rocks suggest that in the southern Caribbean there was no pre-existing west-dipping subduction sy during formation of the Caribbean–Colombian Oceanic Plateau, whereas long-lived SW-dipping subducti the northern Greater Antilles is more probable.

Supplementary material: Sample details, major and trace element data (file 1), cathodoluminescence im of analysed zircons (file 2) and whole-rock standards (file 3) are available at http://www.geolsoc.or SUP18438.

The extant Caribbean Plate, bounded by subduction and transform margins, is considered to represent an allochthonous region of Pacific crust that has overridden proto-Caribbean oceanic crust and moved into the region between North and South America from the Cretaceous to the present day (Fig. 1; e.g. Kerr *et al.* 2003; Pindell *et al.* 2006; Pindell & Kennan 2009). During its relative eastwards motion, the Caribbean Plate was thickened by eruption of mantle plume-derived lavas mostly at *c.* 94–88 Ma (Sinton *et al.* 1998; Kerr *et al.* 2003) to form the Caribbean–Colombian Oceanic Plateau (e.g. Kerr *et al.* 2003).

North and South America rifted apart in the Jurassic during the break-up of Pangaea, intimately associated with sea-floor spreading in the central Atlantic. Separation resulted in the formation of oceanic crust between the Americas during the Late Jurassic in the Gulf of Mexico and the proto-Caribbean seaway (reviewed by Pindell & Kennan 2009). On the western margin of the proto-Caribbean, an island arc system initiated during the Early Cretaceous, termed the 'Great Arc of the Caribbean' (*sensu* Burke *et al.* 1978; Burke 1988). Burke *et al.* (1978) and Burke (1988) proposed that the rocks of the Greater Antilles, Aves Ridge, Lesser Antilles and Dutch–Venezuelan Antilles (Fig. 1) represent a history of subduction at the eastern edge of the Pacific and then the Caribbean Plate following its isolation from the Pacific. However, some workers treat these components of the Great Arc as separate entities becau distinct tectonic histories and initiated a different times during the Cretaceous to P & Wyld 2010). Most magmatism is thou the pre-Lesser Antilles subduction system to Early Eocene as the Grenada Basin ope 1990; Speed & Walker 1991; Bird *et al.* the west-dipping proto-Caribbean subduc initiated the currently active Lesser Anti 2010). The Cretaceous subduction system South America (Kerr *et al.* 2003) where subduction zone continues to facilitate th of the Caribbean Plate relative to the Am sive plate boundaries (Fig. 1).

The polarity of subduction, particularly arc system during the Early Cretaceous, much debate. It has been argued that the r long-lived high-pressure metamorphic hi blages in Cuba and Hispaniola suggest SW proto-Caribbean crust dating back to at lea subduction polarity reversal event (e.g. Pi Pindell & Kennan 2009; Stanek *et al.* 20 *al.* 2010). An alternative hypothesis is Colombian Oceanic Plateau choked an

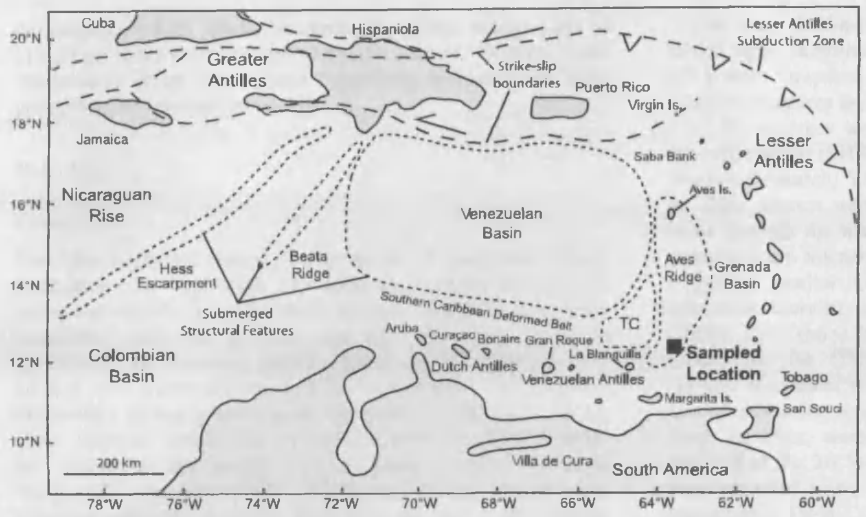

Fig. 1. Simplified map of the eastern Caribbean based on GEOMapApp (Haxby *et al.* 2010) showing the sampled location. Aruba, Curaçao and Bonaire make up the Dutch Antilles; Los Roques and La Blanquilla the Venezuelan Antilles; and Cuba, Jamaica, Hispaniola, Puerto Rico and the Virgin Isles the Greater Antilles. TC, thin crust of the southeastern Venezuelan Basin.

Antilles trench, forcing initiation of SW-dipping subduction during the Late Cretaceous (e.g. Burke 1988; Kerr *et al.* 2003; Thompson *et al.* 2003; Hastie & Kerr 2010).

In the southern Caribbean, the origin of the Dutch–Venezuelan Antilles (Fig. 1) is also contentious, as discussed by Wright & Wyld (2010) and van der Lelij *et al.* (2010). These workers showed that the Dutch–Venezuelan Antilles have a shorter geological history that is distinct from the Greater Antilles. In the Dutch–Venezuelan Antilles NW-dipping subduction began beneath the Caribbean–Colombian Oceanic Plateau at *c.* 88 Ma, and lasted until collision of the newly formed Dutch–Venezuelan Antilles arc with South America prior to the Campanian. Wright & Wyld (2010) argued that this subduction zone initiated at the southeastern margin of the Caribbean–Colombian Oceanic Plateau. In their model, island arc fragments that predate the Caribbean–Colombian Oceanic Plateau, such as those on Bonaire (Fig. 1), originated in a SW-dipping Greater Antilles arc and were transported southwards to their present locations by strike-slip motion. Alternatively, van der Lelij *et al.* (2010) proposed that the newly formed Caribbean–Colombian Oceanic Plateau collided with a pre-existing east-dipping subduction zone, causing a polarity reversal akin to the second model for the Greater Antilles outlined above.

The largely submerged Aves Ridge lies between the Dutch–Venezuelan Antilles and the Greater Antilles (Fig. 1). Most workers have argued that the Aves Ridge originated as a Late Cretaceous to early Palaeocene island arc (Bouysse 1984; Christeson *et al.* 2008; Pindell & Kennan 2009). However, the precise age, magmatic source(s) and subduction polarity of this arc are unclear. Given its significant spatial extent and because it is likely to represent some of the last island arc magmatism in the southeastern Caribbean prior to the opening of the Grenada Basin; a deeper understanding of the origin of the Aves Ridge could help to better constrain Caribbean Plate tectonic evolution.

In this paper we present new major and trace element and Nd and Hf isotopic analyses and new U–Pb zircon geochronological data from samples collected during dredging by R.V. *Eastward* in 1968. We use these results to determine the origin of the Aves Ridge. Data from the Aves Ridge and Dutch–Venezuelan Antilles are then combined to provide new constraints on models for the tectonic evolution of the southeastern Caribbean.

Geology of the Aves Ridge

Although the Aves Ridge is an extensive region of crust in the eastern Caribbean, the geochemistry of basement samples has not previously been studied in any detail. The ridge is a broadly north–south-trending arcuate structure *c.* 500 km in length, running between its sole emergent point at Aves Island in the Caribbean Sea and Margarita to the north of the Venezuelan coast (Fig. 1). The ridge has a topographic profile of up to 1500 m above the surrounding ocean basins and seismic studies reveal that the ridge has little sedimentary cover and a crustal thickness of *c.* 26 km (Christeson *et al.* 2008). Seismic velocities are $>6.0\ km\ s^{-1}$ in the mid-crust and *c.* $7.3\ km\ s^{-1}$ at the base of the crust, consistent with an interpretation as a remnant island arc of intermediate composition (Clark *et al.* 1978; Christeson *et al.* 2008).

Glassy, brecciated basalts and andesites dredged or drilled from the northern end of the ridge and the Saba Bank between Aves Island and the Greater Antilles (Fig. 1) also suggest a volcanic arc origin (Marlowe 1968; Church & Allison 2004; Fig. 1). Dredge samples collected in 1968 by Duke University's R.V. *Eastward* are the only samples collected from the southern part of the ridge. Three dredges from the eastern scarp of the ridge (Fig. 1) contained significant quantities of igneous rocks and were described and dated by K–Ar methods by Fox *et al.* (1971). Dredge 11317 (12.30°N) contained 1500 kg of granitic boulders and pebbles. Four whole-rock K–Ar ages ranged from 57 to 89 Ma. Dredge 11318 (12.25°N) consisted of 40 kg of mostly doleritic cobbles and pebbles with lesser amounts of porphyritic and/or metamorphosed basalt, with two K–Ar ages of 57 and 60 Ma. Dredge 11319 (12.35°N) contained 2000 kg of granitoid material seemingly identical to dredge 11317, but with four K–Ar ages ranging from 18.5 to 67 Ma. No methods or errors were given for these K–Ar dates by Fox *et al.* (1971); however, the ages are unlikely to be reliable because of alteration, and this is evidenced by the wide spread of ages obtained.

Walker *et al.* (1972) showed that the granitoids had some primitive $^{87}Sr/^{86}Sr$ ratios, which ranged from 0.7038 to 0.7080. None the less, these ratios are likely to have been increased by interaction with Cretaceous seawater of $^{87}Sr/^{86}Sr$ *c.* 0.7075 (Veizer 1989) and/or hydrothermal alteration. No mafic rocks were found in the granitic dredges and vice versa. For this study,

the largest, freshest blocks remaining from each dredge (tens of kilograms only) were selected from the Lamont–Doherty Earth Observatory Deep Sea Sample Repository in November 2008, generating 34 samples for analysis.

Petrology

Granitoids

The felsic rocks are coated in thick layers of manganese oxides, sometimes over 1 cm thick. The rocks are typically pink to pale green and slightly hydrothermally altered. Two facies have been identified within the granitoid samples. The dominant facies (*c.* 75%) is of a coarse, granitic nature and the other is fine-grained and more intermediate in composition. The primary mineralogy of the granitic rocks comprises plagioclase, quartz, alkali feldspar, hornblende and opaque minerals. The feldspars are sericitized and epidote is a common secondary mineral along with clays and chlorite. Zircon and titanite are the most common accessory minerals. Texturally, the rock is of a coarse interlocking nature, with grain sizes up to 2 mm and abundant interstitial quartz. Plagioclase is sometimes optically zoned and alkali feldspar is perthitic. Hornblende is squat or slightly elongate.

The intermediate facies occurs as isolated masses or clots distinct from the surrounding granitic material. The boundary between the two facies is, however, indistinct and gradational in thin section, suggesting that the darker clots may be restitic in nature. This second facies is dioritic and has a grain size ranging from 0.5 to 1 mm. The primary mineralogy is dominated by interlocking sericitized plagioclase, amphiboles, titanite and oxides. Only the dominant coarse granitic facies was selected for geochemical analysis, to avoid the generation of artificial mixtures of the two rock types.

Mafic rocks

The mafic rocks have undergone variable degrees of pervasive alteration. The freshest specimens from the small sample set were reserved for geochemical analysis so little solid rock remains. From the remaining rocks it can be seen that many have a fine-grained matrix that is composed of clay minerals with a small proportion of calcite. Outlines of aligned tabular sericitized plagioclase feldspar can be seen, which are up 2 mm across. Patches of green epidote and oxides up to 1 mm across are present and there are small regions of squat, altered clinopyroxene. The rocks with obvious plagioclase crystals may be porphyritic basalts or basaltic andesites of an extrusive or hypabyssal nature.

Analytical methods

U–Pb zircon geochronology

A single fresh granitoid (317UPb) from dredge EA6811317 was selected for U–Pb zircon dating. Approximately 200 zircons were recovered using the Ammann AG selFrag machine and electromagnetic separation at the Technical University of Freiberg. selFrag applies a high-voltage pulse that disaggregates samples by introducing a short-lived plasma channel of 1–2 μm between grain boundaries (Gnos *et al.* 2006). Fifty zircon grains of 100–150 μm were selected and mounted in epoxy resin with chips of TEMORA (Middledale gabbro–diorite of New South Wales, Australia) and 91500 (geostandard) reference zircons. Grains were half-sectioned and polished. Reflected and transmitted light photomicrographs and cathodoluminescence images (CL) were prepared. The CL images were used to decipher internal structures and to identify target specific areas.

U–Pb analyses were carried out by sensitive high-resolution ion microprobe (SHRIMP) using a SHRIMP-II at the Center for Isotopic Research, VSEGEI, St. Petersburg, Russia. Twelve sites on eight zircons were selected. Each analysis consisted of five scans through the mass range, with spot diameter *c.* 25 μm and primary beam intensity *c.* 10 nA. The data have been reduced in a manner similar to that described by Williams (1998, and references therein) using the SQUID Excel Macro of Ludwig (2000). Pb/U ratios have been normalized relative to a value of 0.0668 for the $^{206}Pb/^{238}U$ ratio of the TEMORA reference zircons, equivalent to an age of 416.75 Ma (Black *et al.* 2003). Uncertainties for single analyses (ratios and ages) are at the 1σ level; however, uncertainties in calculated concordia ages are reported at the 2σ level. The inverse concordia plot (Fig. 2) has been prepared using ISOPLOT/EX (Ludwig 1999). Results are presented in Table 1.

Major and trace elements

Whole-rock samples were prepared and analysed for major and trace elements at Cardiff University in accordance with the fluxy-fusion method outlined by McDonald & Viljoen (2006) and Hastie *et al.* (2009). Loss-on-ignition (LOI) values were calculated following heating at 900 °C for 2 h. Ignited samples were fused and dissolved in dilute nitric acid. Major elements and Sc were analysed by inductively coupled plasma optical emission spectrometry (ICP-OES) on a JY Horiba Ultima 2. All other trace elements were analysed by inductively coupled plasma mass spectrometry (ICP-MS) (Thermo X7 series). Silicate rock standards JB-1a, NIM-G and BIR-1 were run through repeated sample batches. Relative standard deviations show precision of 1–5% for most major and trace elements; 2σ values encompass certified values for the vast majority of elements. Representative analyses are shown in Table 2.

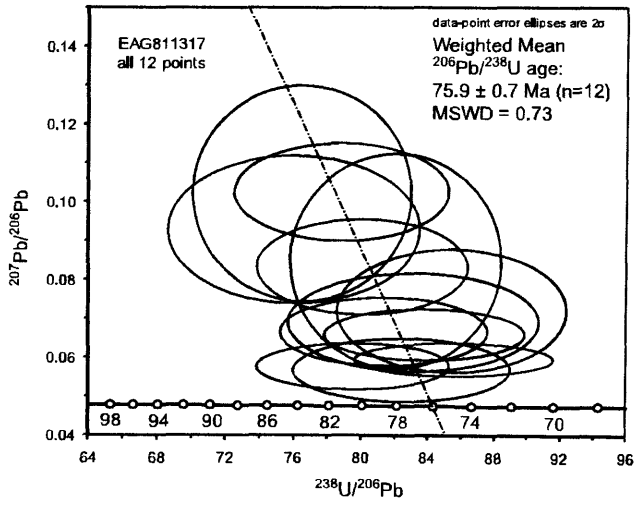

Fig. 2. Inverse concordia plot for zircon U–Pb analyses of granitoid sample 317UPb.

Table 1. *U–Pb zircon SHRIMP results for sample 317UPb*

Spot	$^{206}Pb^{*}$ (%)	U (ppm)	Th (ppm)	$^{232}Th/^{238}U$	$^{206}Pb\dagger$ (ppm)	Total $^{238}U/^{206}Pb$	±%	Total $^{207}Pb/^{206}Pb$	±%	$^{206}Pb/^{238}U$ age‡ (Ma)
EA6811317UPb.1.1	3.86	64	21	0.33	0.724	76	4	0.093	8.3	79.4 ± 3.2
EA6811317UPb.2.1	15.63	84	30	0.37	0.877	82.5	3.2	0.0568	5.9	76.8 ± 2.5
EA6811317UPb.4.1	5.96	106	35	0.35	1.11	82.1	3.1	0.085	13	74.4 ± 2.6
EA6811317UPb.4.2	13.71	73	27	0.38	0.794	78.9	3.3	0.1026	5	75.6 ± 2.5
EA6811317UPb.3.1	7.37	119	47	0.41	1.23	83.2	3.7	0.0692	7.5	74.9 ± 2.8
EA6811317UPb.5.1	6.99	123	47	0.40	1.3	81.4	3.1	0.0667	5.3	76.8 ± 2.4
EA6811317UPb.5.2	2.81	427	287	0.69	4.28	85.6	2.8	0.0595	3	73.8 ± 2.1
EA6811317UPb.7.1	14.03	79	29	0.38	0.79	85.4	3.3	0.0721	9	72.7 ± 2.5
EA6811317UPb.7.2	29.44	56	15	0.27	0.629	76.5	3.4	0.102	11	77.9 ± 2.9
EA6811317UPb.6.1	20.28	200	120	0.62	2.05	83.8	2.9	0.0659	4.1	74.7 ± 2.2
EA6811317UPb.8.1	15.69	94	40	0.44	1	80.1	3.2	0.0835	6	76.4 ± 2.5
EA6811317UPb.8.2	10.71	197	80	0.42	2.13	79.5	2.9	0.0578	4.3	79.5 ± 2.3

Errors in the age calculation are at 1σ. Error in standard calibration was 0.90% (not included in above errors but required when comparing data from different mounts).
*Common Pb proportion.
†Radiogenic Pb proportion.
‡Common Pb corrected assuming $^{206}Pb/^{238}U$–$^{207}Pb/^{235}U$ age-concordance.

Nd and Hf radiogenic isotopes

Nd and Hf isotope compositions were analysed at the NERC Isotope Geoscience Laboratories, Nottingham, UK. Full analytical details have been given by Hastie *et al.* (2009) and results are presented in Table 3. For Hf isotope analysis, the samples were prepared following the procedures of Münker *et al.* (2001), and analysed by ICP-MS using a Nu-Plasma multicollector ICP-MS system. Hf blanks were less than 100 pg. Replicate analysis of the JMC475 standard gave $^{176}Hf/^{177}Hf = 0.282161 \pm 0.000006$ (1σ, $n = 45$), directly comparable with the preferred value of 0.282160 (Nowell & Parrish 2001). Replicate analysis of BCR-2 gave $^{176}Hf/^{177}Hf = 0.282866 \pm 0.000006$ (1σ, $n = 7$), similar to the previously reported value of 0.282879 ± 0.000008 (Blichert-Toft 2001). Determinations of Nd isotopes followed the procedures of Kempton (1995) and Royse *et al.* (1998). Nd was run as the metal species using double Re–Ta filaments on a Finnigan Triton mass spectrometer. Replicate analysis of the La Jolla standard gave a value of $^{143}Nd/^{144}Nd = 0.511846 \pm 0.000003$ (1σ, $n = 6$) and results are normalized to a preferred value of 0.511860.

Results

U–Pb zircon age

The zircons imaged by CL are generally clear, with magmatic zoning throughout, and lack rounded (inherited) cores. Many are prismatic, euhedral crystals. All 12 analyses from eight zircon grains yield a concordant age with no sign of discordance or inheritance on the $^{207}Pb/^{206}Pb$ v. $^{238}U/^{206}Pb$ inverse concordia plot (Fig. 2). Assuming $^{206}Pb/^{238}U$–$^{207}Pb/^{235}U$ age-concordance, the weighted mean of $^{206}Pb/^{238}U$ ages (Table 1) is 75.9 ± 0.7 Ma (mean square weighted deviation (MSWD) = 0.73), which we interpret as the crystallization age of the granitoid.

Alteration and elemental mobility

Many geochemical studies have shown that most major elements and large ion lithophile elements (LILE) are mobilized by sub-solidus processes such as hydrothermal alteration, metamorphism and weathering (e.g. Seewald & Seyfried 1990; Hastie *et al.* 2007). To test element mobility, elements are plotted against a known incompatible immobile element, in this case Nb (Fig. 3). Within a given magmatic suite, samples should form coherent liquid lines of descent. For the Aves Ridge samples the high field strength elements (HFSE) and the rare earth elements (REE) in the mafic rocks display good correlations with Nb. These correlations indicate that (1) these elements have been relatively immobile during sub-solidus alteration, despite LOI values of *c.* 3–15%, and so may be used to investigate the origin of the mafic rocks, and (2) the mafic rocks are part of one cogenetic suite. As the granitoids are evolved and fairly uniform in composition they do not show liquid lines of descent in Figure 3. Nevertheless, the granitoids can be investigated using the immobile HFSE and REE as, despite some epidotization, the rocks are relatively fresh and not silicified or calcified, with LOI values of *c.* 1%. The Mn-oxide coating on many granitoid samples may have acted as a protective layer.

Granitoid major and trace element geochemistry

SiO_2 spans a narrow range from 67 to 72 wt%. The granitoids have low abundances of TiO_2 (0.4 wt%), Fe_2O_3 (3.5 wt%) and MgO (<1.5 wt%). These rocks have elevated Ba (up to 1095 ppm) and Sr (up to 444 ppm) contents and low Cr (<24 ppm), V (*c.* 70 ppm), Co (<7.5 ppm) and Ni (<46 ppm). Compared with the mafic rocks, the granitoids have lower contents of Sm and Sc and higher abundances of Sr and Zr (Fig. 3). There is no clear magmatic differentiation trend between the most evolved mafic rocks and the least evolved felsic rocks for any immobile elements shown. Both granitic dredges show identical, slightly concave-up, chondrite-normalized (CN) REE patterns (Fig. 4). The samples are light REE (LREE) enriched with an average La/Yb_{CN} of 4.5 consistent with a calc-alkaline affinity and there is slight heavy/middle REE (HREE/MREE) enrichment. On an normal mid-ocean ridge basalt (N-MORB)-normalized (NMN) plot (Fig. 4) the granitoids are LREE/HREE enriched and have positive Zr–Hf and Th anomalies along with negative Nb–Ta and Ti anomalies.

Mafic rock major and trace element geochemistry

SiO_2 ranges from 34 to 57 wt%, MgO from 1 to 6 wt%, Al_2O_3 from 11 to 22 wt% and $Na_2O + K_2O$ from 3 to 11 wt%. TiO_2 has a much narrower range of concentrations than other major

Table 2. *Representative elemental data for the Aves Ridge*

Dredge:	317a	319d	318a	318b	318c	318d	318e	318g
Type:	CAA–G	CAA–G	IAT–BA	IAT–BA	CAA–BAS	CAA–BA	CAA–BA	CAA–BA
Major elements (wt%)								
SiO_2	68.13	70.64	43.41	44.99	49.75	52.88	49.32	54.02
TiO_2	0.43	0.40	0.63	0.59	0.74	0.68	0.79	0.68
Al_2O_3	15.23	13.50	20.49	22.43	16.79	13.98	17.06	14.73
$Fe_2O_3^T$	3.92	3.50	10.04	8.72	12.14	9.53	9.85	8.58
MnO	0.08	0.11	0.21	0.15	0.50	0.49	0.44	0.41
MgO	1.29	1.09	5.52	4.58	2.56	1.11	2.47	1.35
CaO	3.61	3.12	7.42	7.19	2.05	4.76	3.18	3.69
Na_2O	3.84	3.38	3.85	3.68	0.17	0.19	0.16	0.26
K_2O	2.35	2.72	1.28	1.44	10.14	10.09	10.06	10.56
P_2O_5	0.17	0.18	0.20	0.24	1.09	1.73	0.86	1.80
LOI	0.99	1.14	7.09	5.29	3.54	4.77	5.24	3.45
Total	100.05	99.79	100.12	99.30	99.47	100.19	99.43	99.54
Trace elements (ppm)								
Sc	9.9	9.0	22.4	21.9	36.5	33.6	41.2	33.0
V	78.0	67.4	251.4	200.0	359.6	303.1	385.8	288.3
Cr	9.9	11.7	8.6	12.5	94.4	58.5	68.2	71.4
Co	6.7	6.0	30.7	22.6	30.1	16.7	23.3	19.9
Ni	8.1	1.3	48.9	34.4	102.7	137.0	89.8	84.9
Cu	16.6	12.7	107.9	115.2	101.6	115.2	135.7	103.7
Ga	12.6	12.1	15.2	16.0	14.6	7.8	18.2	9.7
Rb	26.4	32.6	20.5	18.0	99.0	82.1	106.1	90.5
Sr	405	387	619	903	106	152	124	144
Y	19.8	18.2	13.6	14.1	34.4	25.5	33.7	25.4
Zr	127.2	138.2	29.5	31.8	64.7	58.5	74.9	52.0
Nb	4.13	4.78	1.16	1.12	4.75	3.78	5.08	3.99
Ba	698	772	230	424	6193	5699	5868	5930
Hf	2.94	3.24	0.76	0.83	1.62	1.39	1.83	1.17
Ta	0.29	0.36	0.07	0.07	0.33	0.28	0.36	0.29
Pb	3.21	3.22	3.47	1.80	30.07	30.80	13.95	20.53
Th	1.86	2.10	0.58	0.30	1.78	1.55	1.88	1.60
U	0.81	0.73	0.32	0.24	2.65	4.12	1.80	2.44
La	13.91	12.64	4.29	4.81	14.93	15.64	18.72	14.91
Ce	30.79	27.73	10.83	11.69	33.69	23.73	28.07	24.76
Pr	4.11	3.69	1.56	1.81	5.48	3.57	4.36	3.85
Nd	17.47	15.54	7.69	8.94	25.77	16.21	20.05	17.04
Sm	3.74	3.29	2.06	2.33	5.97	3.77	4.86	3.76
Eu	1.05	0.96	0.72	0.83	2.93	1.43	1.71	1.51
Gd	3.31	2.93	2.07	2.33	5.76	3.63	4.77	3.60
Tb	0.48	0.44	0.33	0.36	0.76	0.54	0.72	0.52
Dy	2.97	2.74	2.17	2.32	4.33	3.44	4.62	3.28
Ho	0.59	0.55	0.43	0.45	0.80	0.69	0.94	0.67
Er	1.80	1.69	1.28	1.32	2.20	2.07	2.84	1.97
Tm	0.31	0.28	0.20	0.21	0.33	0.32	0.45	0.31
Yb	2.04	1.97	1.36	1.39	2.06	2.06	2.91	1.95
Lu	0.34	0.34	0.22	0.22	0.32	0.34	0.47	0.32

All dredges prefixed EA68-11. LOI, loss on ignition; CAA, calc-alkaline arc; IAT, island arc tholeiite; G, granite; BA, basaltic andesite; BAS, basalt.

Table 3. *Nd–Hf radiogenic isotope data from the Aves Ridge*

Sample	$^{147}Sm/^{144}Nd$	$^{143}Nd/^{144}Nd$	$^{143}Nd/^{144}Nd(i)$	εNd(i)	$^{176}Lu/^{177}Hf$	$^{176}Hf/^{177}Hf$	$^{176}Hf/^{177}Hf(i)$	εHf(i)
EA68 11317a	0.1333662	0.513000	0.512934	7.677	0.0164336	0.283178	0.283154	15.185
EA68 11318g	0.1293869	0.512843	0.512779	4.653	0.0388652	0.283112	0.283057	11.756

(i), values are age corrected to 76 Ma.

elements, from 0.5 to 0.8 wt%. When plotted against Nb, MgO and Al_2O_3 show a weak positive correlation (Fig. 3). As these samples are altered, classification based on major elements is impractical, so we use the Th–Co plot of Hastie *et al.* (2007) (Fig. 5). This diagram, based on a global arc dataset, uses Th and Co as immobile proxies for the SiO_2–K_2O discrimination diagram of Peccarillo & Taylor (1976). Figure 5 shows that the rocks mostly classify as basaltic andesites of calc-alkaline affinity, although two samples plot in the tholeiite field.

The mafic samples have LREE-enriched chondrite-normalized REE patterns (Fig. 4). Nine samples have La/Yb_{CN} ratios of about five (calc-alkaline), whereas two are less LREE-enriched and have La/Yb_{CN} values of about two (tholeiitic), in line with the Th–Co diagram (Fig. 5). The most enriched calc-alkaline

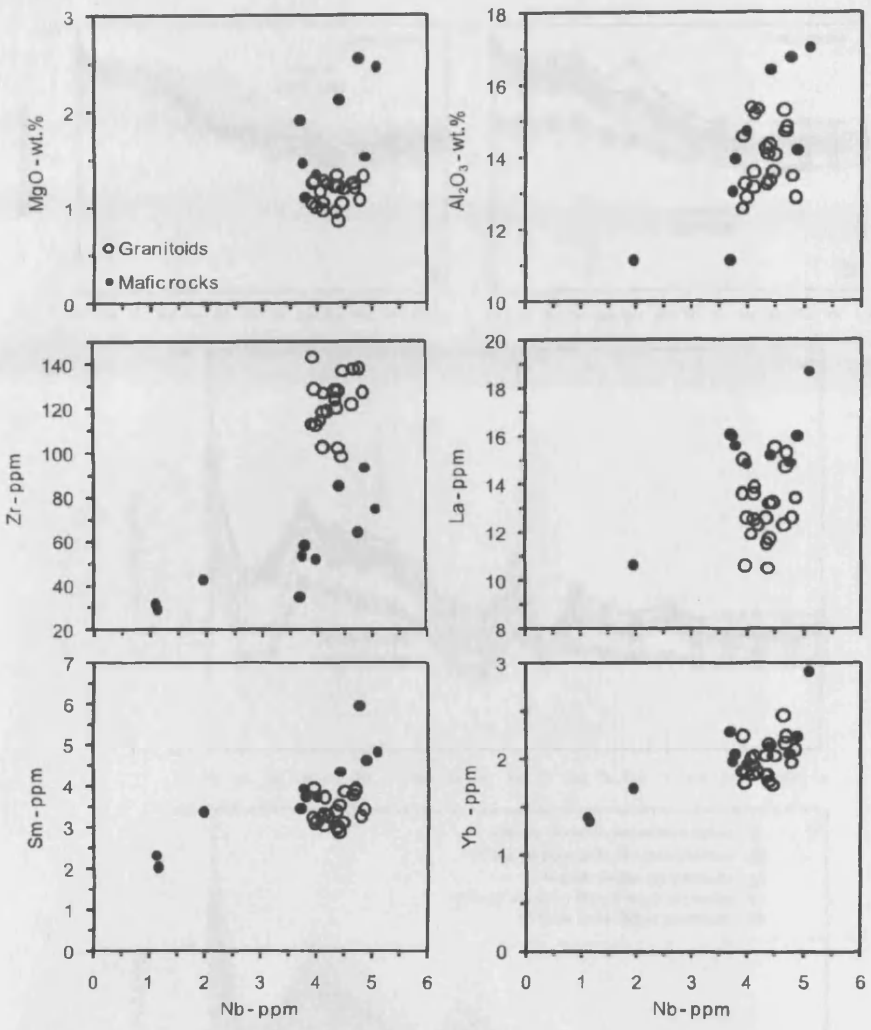

Fig. 3. Variation diagrams for selected elements for both granitoids and mafic rocks.

samples show a small positive Eu anomaly. The HREE and MREE in these mafic rocks are not depleted relative to N-MORB (Fig. 4). Negative Ce anomalies are also present in some of the mafic samples, which do not correlate with LOI values and are therefore unlikely to be related to sub-solidus alteration processes. On the N-MORB-normalized trace element plot (Fig. 4), all samples show significant Th enrichment and Nb–Ta and Ti depletions (e.g. $Nb/La_{NMN} = 0.20–0.33$). In contrast to the granitoid rocks, the mafic samples have negative Zr–Hf anomalies.

Nd and Hf radiogenic isotopes

Radiogenic Nd and Hf isotope data for granitoid and basaltic andesite samples are shown in Table 3 and Figure 6. The results have been age-corrected to 76 Ma and are markedly distinct from one another. The granitoid sample has a relatively depleted signature ($\varepsilon_{Ndi} = +7.68$ and $\varepsilon_{Hfi} = +15.19$), whereas the basaltic andesite is less depleted with $\varepsilon_{Ndi} = +4.65$ and $\varepsilon_{Hfi} = +11.76$. The granitoid plots well within the main Caribbean–Colombian Oceanic Plateau field (Hastie *et al.* 2009) on the ε_{Hfi} v. ε_{Ndi} diagram, but the basaltic andesite has a more enriched isotopic signature similar to the present-day Lesser Antilles arc (White & Patchett 1984). Both samples have higher ε_{Hfi} than Pacific MORB. The field for present-day Pacific MORB has not been age-corrected, as Thompson *et al.* (2003) demonstrated that present-day and Jurassic Pacific MORB were isotopically very similar and predicted that the Hf isotope composition within a uniform chondritic reservoir would change by <0.5 epsilon units in 90 Ma.

Discussion

Are the granitoids and mafic rocks cogenetic?

The variation diagrams (Fig. 3) show that the mafic rocks define, in the case of the immobile and incompatible elements, clear intra-magmatic differentiation trends, which may be related to crystal fractionation. The granitoid rocks plot in a distinct field at lower incompatible element concentrations than the most evolved mafic rocks with the exception of Zr, and display no coherent liquid line of descent compatible with the mafic rocks. This shows that the mafic and felsic rocks are not related to each other by fractional crystallization processes. The negative Zr–Hf

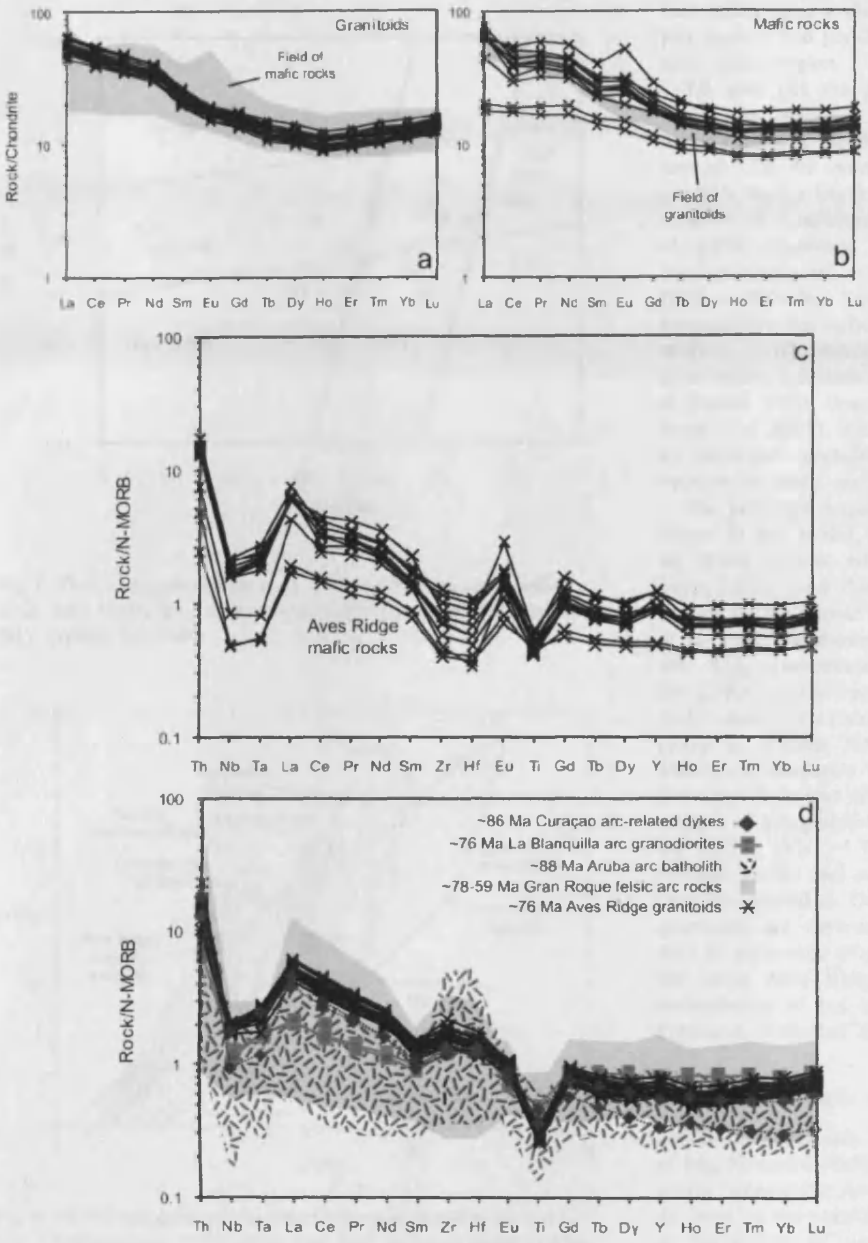

Fig. 4. Chondrite-normalized REE plots for: **(a)** Aves Ridge granitoids and **(b)** mafic rocks using normalizing values from Sun & McDonough (1989). Multi-element plots for **(c)** for the Aves Ridge mafic rocks and **(d)** the Aves Ridge granitoids compared with Gran Roque arc granodiorites (Wright & Wyld 2010; A. C. Kerr, unpublished data), Aruba batholith (White *et al.* 1999) and Curaçao–La Blanquilla arc intrusions (Wright & Wyld 2010). N-MORB-normalizing values from McDonough & Sun (1995).

anomalies on the multi-element plot for the mafic rocks (Fig. 4c), indicated by $Zr/Sm_{NMN} < 1$, are likely to be related to subduction-related REE enrichment (Thirlwall *et al.* 1994). On the other hand, the positive Zr–Hf anomalies for the granitoids (Fig. 4d) may indicate that these rocks have accumulated zircon, or that their source contained residual amphibole, because amphibole is more compatible with the MREE than Zr or Hf (Klein *et al.* 1997). These different Zr–Hf anomalies again point to distinct origins for the mafic and granitoid rocks. Most importantly, crystal fractionation cannot explain the different ε_{Ndi} and ε_{Hfi} isotopic ratios in Figure 6, so although only two analyses are available it is concluded that the mafic and granitoid rocks of the Aves Ridge are not derived from the same source region. However, without field relationships with which to test the relative age of the mafic and felsic samples and without dateable mafic material, the age of the mafic rocks in this study remains uncertain.

Island arc origin of the southeastern Aves Ridge

The presence of negative Nb–Ta anomalies on N-MORB-normalized plots (Fig. 4) is usually regarded as indicative of subduction zone processes, as Nb and Ta are preferentially held in rutile in the downgoing slab during aqueous fluid release (e.g. Saunders *et al.* 1980; Thirlwall *et al.* 1994). Furthermore, the Th/Yb v. Ta/Yb diagram of Pearce (1983) (Fig. 7a) shows that the mafic rocks plot above the MORB array, which suggests that they have a subduction zone affinity. The radiogenic isotope

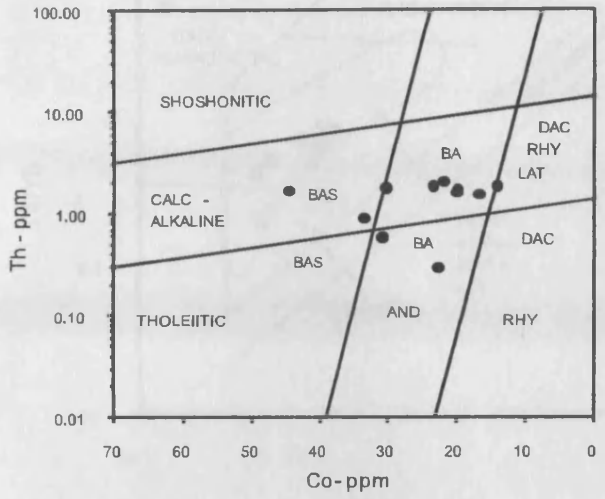

Fig. 5. Th–Co diagram (Hastie *et al.* 2007) for the Aves Ridge mafic rocks. BAS, basalt; BA, basaltic andesite; AND, andesite; DAC, dacite; RHY, rhyolite; LAT, latite.

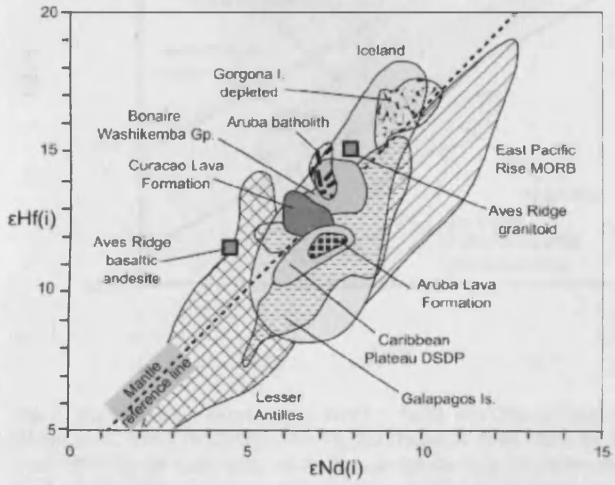

Fig. 6. Hf–Nd radiogenic isotope plot for the Aves Ridge rocks. Fields from Thompson *et al.* (2003, 2004) apart from the Lesser Antilles (White & Patchett 1984).

ratios of the mafic and granitoid rocks (Fig. 6) and zircons without rounded, inherited cores from the granitoids do not indicate contamination from old continental crustal material, an alternative source of negative Nb–Ta anomalies. Therefore, geochemical evidence, confirmed by existing geophysical and geodynamic models, shows that the Aves Ridge represents the eroded products of an extinct subduction zone.

Source of the granitoid rocks

As the granitoids were sampled from only two outcrops, their lack of geochemical variation may be indicative of a sampling bias rather than a distinct petrogenetic feature. However, some petrological and geochemical constraints can be used to discuss their source region.

We rule out the possibility that the granitoids formed by partial melting of a subducting oceanic slab, to generate an acidic melt (e.g. Drummond & Defant 1990). Such a melt could interact with the mantle wedge beneath the Aves Ridge arc, and generate higher MgO, Ni and Cr concentrations and lower SiO_2 contents in a subsequent melt (high-Mg andesite) (e.g. Rapp *et al.* 1999). However, as noted, the granitoids have very low concentrations of mantle-derived elements and are siliceous (SiO_2 *c.* 70 wt%). Slab fusion during subduction occurs only in anomalously hot subduction zones and largely at depths where residual garnet would cause HREE depletion in the resulting felsic melts, a feature also not seen in the granitoids (Drummond & Defant 1990; Peacock *et al.* 1994; Drummond *et al.* 1996; Rapp *et al.* 2003). We also argue that the granitoids did not form by fractional crystallization from a mafic, mantle-derived melt because the mafic and granitoid rocks are not cogenetic.

Our preferred hypothesis is that the granitoids are of crustal origin. In this model, the fine-grained hornblende-rich intermediate facies present within the granitoids are interpreted to be I-type restite and the granitoids are considered to have been formed by the partial melting of the mafic lower crust (Chappell *et al.* 1987; Drummond *et al.* 1996; Stephens 2001). Additionally, SiO_2 concentrations of 67–72 wt% and a sodic character ($Na_2O/K_2O = 1.65$) are compatible with re-melting of a tholeiitic mafic source at moderate (10–20%) degrees of partial melting (Rapp & Watson 1995). The positive Zr–Hf anomalies (see above) and moderate Sr concentrations (up to 440 ppm) suggest that amphibole and plagioclase may have remained in the source residue of the granitoids. Moderate levels of Y (>16 ppm) and the HREE (Yb >1.7 ppm) and low La/Yb (*c.* 6.6) rule out residual garnet and constrain partial melting to <30 km depth (see Drummond & Defant 1990; Rapp & Watson 1995). If the granitoids are derived from a mafic protolith, their negative Nb–Ta anomalies (Fig. 4) might be attributed to re-melting of the lower Aves Ridge arc crust by advection owing to the underplating of hot basaltic arc magma (Petford *et al.* 2000; Petford & Gallacher 2001).

Source of the mafic rocks: mantle wedge component

Unlike the granitoids, the mafic rocks have high concentrations of Mg, Ni and Cr indicating derivation from a peridotitic mantle source beneath the Aves Ridge. As the MREE and HREE are not depleted on the normalized plots (Fig. 4), garnet was not present in the source or was completely melted out during partial melting. In the former case, the depth of partial melting is constrained to above the approximate spinel–garnet transition at <55 km within the mantle (Su, 2008).

Of particular interest is the composition of the mantle wedge source, but any investigation must first assess whether the wedge was fluxed by slab- and sediment-related fluids alone, or also by slab-derived partial melts. The HFSE and HREE are normally used to investigate the composition of the mantle wedge, but these elements can be mobilized from the slab if it partially melts (Pearce & Peate 1995). Figure 7b (Zr/Yb v. Nb/Yb) shows that the mafic samples plot within the MORB array, suggesting that the HFSE and HREE have not been mobilized from the slab to the wedge. Therefore, variations in the HFSE and HREE can be explained by partial melting and fractional crystallization processes and the composition of the mantle wedge. We focus on Zr and Nb in particular because in mafic rocks, Zr and Nb behave

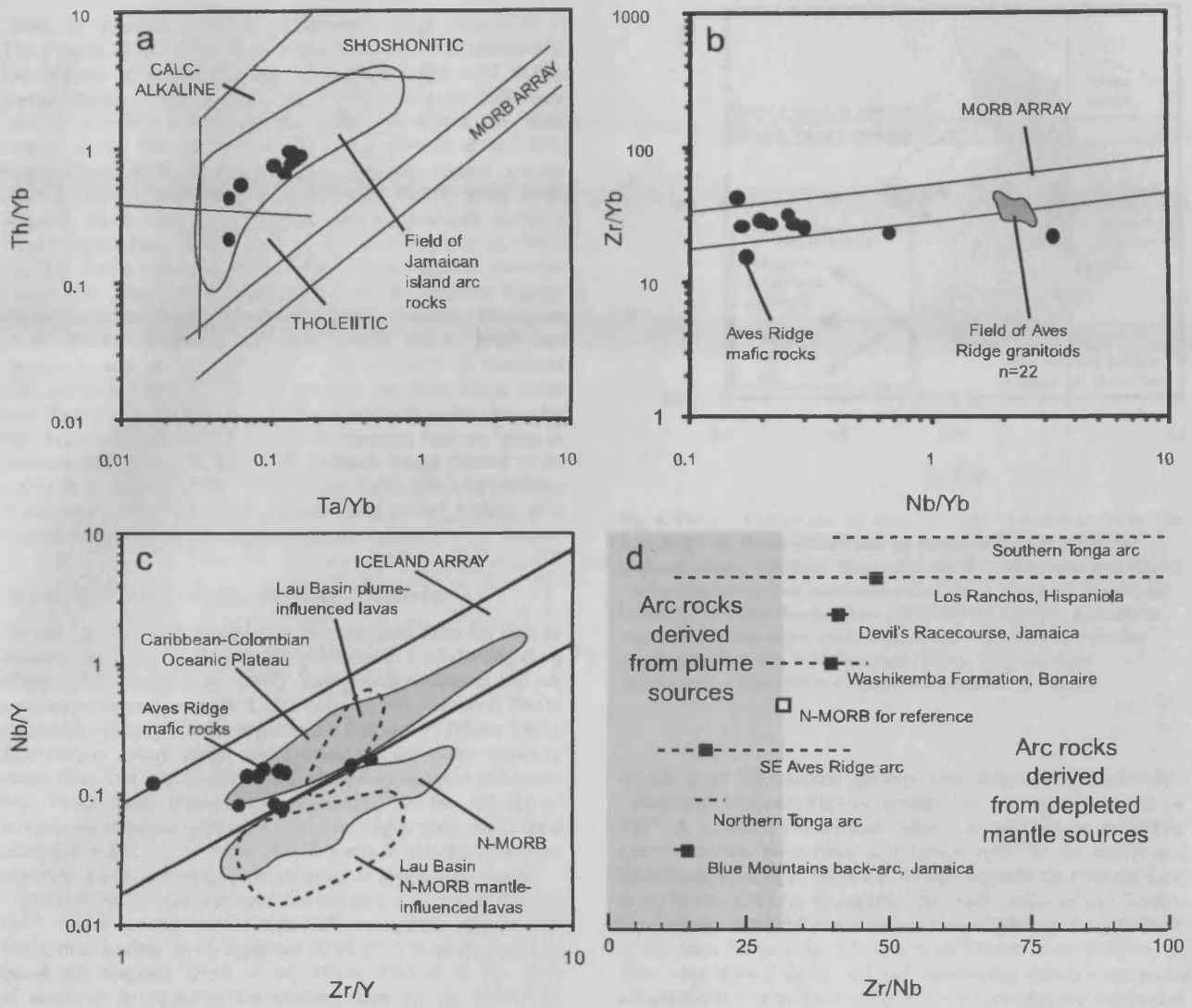

Fig. 7. Trace element ratio plots: (**a**) Th/Yb v. Ta/Yb plot (Pearce 1983) showing the Aves Ridge mafic rocks compared with arc rocks from Jamaica (Hastie *et al.* 2009); (**b**) Zr/Yb v. Nb/Yb plot (Pearce & Peate 1995) for the mafic and granitoid rocks of the Aves Ridge; (**c**) Nb/Y v. Zr/Y diagram (Fitton *et al.* 1997) for the mafic rocks of the Aves Ridge showing the Caribbean–Colombian Oceanic Plateau field of Hastie *et al.* (2008), N-MORB from Fitton *et al.* (1997) and the Lau Basin from Hastie *et al.* (2010); (**d**) Zr/Nb ratios with mean values (squares) and ranges (dotted lines) for selected mafic arc and oceanic plateau occurrences in the Caribbean region and Tonga arc. Sources: Blue Mountains back-arc basin, Jamaica, Hastie *et al.* (2010); Curacao Lava Formation, Kerr *et al.* (1996) and Hauff *et al.* (2000); Devil's Racecourse Formation, Jamaica, Hastie *et al.* (2009); Los Ranchos Formation, Hispaniola, Escuder Viruete *et al.* (2006); N-MORB, Sun & McDonough (1989); Tongan arc, Wendt *et al.* (1997); Washikemba Group, Bonaire, Thompson *et al.* (2004).

similarly during fractional crystallization of the major phases. Additionally, Zr and Nb behave incompatibly between the main mineral species of mantle peridotite and a coexisting partial melt (e.g. Salters *et al.* 2002). Therefore, unless the partial melt volume is extremely small, the Zr/Nb ratio will not vary significantly with the degree of partial melting. Island arc magmas are generated by 15–30% partial melting (Pearce & Parkinson 1993; Pearce & Stern 2006), therefore the Zr/Nb ratio of the mafic rocks of the Aves Ridge should represent the composition of the source region.

The Nb/Y v. Zr/Y plot (Fig. 7c) distinguishes mafic rocks derived from depleted MORB mantle (DMM) and mantle plume sources that are enriched in Nb relative to MORB (Fitton *et al.* 1997). The plot has been used to identify Caribbean–Colombian Oceanic Plateau lavas (e.g. Kerr *et al.* 2009), and to discriminate between island arc rocks derived from depleted mantle wedges and those derived from plume-enriched sources in the Caribbean region (Hastie *et al.* 2010; Neill *et al.* 2010). High Nb/Y in relation to N-MORB-like rocks may indicate a plume mantle wedge source, as shown by Hastie *et al.* (2010) for the Lau Basin. The Aves Ridge rocks plot within and around the 'Iceland array', along with the plume-influenced Lau Basin lavas (Fig. 7c), consistent with the idea that the mantle wedge beneath the Aves Ridge may have been of mantle plume composition.

In average N-MORB, Zr/Nb is *c.* 32 (Sun & McDonough

1989) but in mafic arc rocks, Zr/Nb ratios range from *c.* 40 to 120 (Wendt *et al.* 1997). It is difficult, except at unrealistically low degrees of partial melting, to produce Zr/Nb <32 during partial melting of DMM. Therefore, Zr/Nb <32 in arc rocks may indicate a plume-related mantle wedge as shown for lavas erupted in the Tongan arc and in Jamaica (Wendt *et al.* 1997; Hastie *et al.* 2010). Rocks from the southern Tongan arc are derived from a depleted source and have Zr/Nb ratios >40, whereas those from the Samoan plume-influenced northern Tonga region have Zr/Nb ratios of 16–21 (Wendt *et al.* 1997; Fig. 7d). Zr/Nb ratios for the Caribbean region are also shown in Figure 7d. Many pre-Caribbean–Colombian Oceanic Plateau Caribbean island arc lavas such as those on Bonaire (Thompson *et al.* 2004), Hispaniola (Escuder Viruete *et al.* 2006) and Jamaica (Hastie 2009), show high Zr/Nb ratios (>40) consistent with derivation from DMM. In contrast, the Aves Ridge rocks have Zr/Nb = 9–38 (mean = 17.7), much closer to the values for the plume-influenced *c.* 72 Ma Blue Mountains back-arc lavas in Jamaica (Hastie *et al.* 2010) and northern Tonga (Wendt *et al.* 1997). It is therefore likely that the low Zr/Nb ratios of the Aves Ridge mafic rocks have been derived from partial melting of a mantle wedge composed of mantle plume material.

Source of the mafic rocks: slab-flux component

Th and La are widely regarded to be mobilized from the slab by aqueous fluids during dehydration reactions in a subducting plate (Plank 2005; Hastie *et al.* 2007). Terrigenous sediments and the continental crust have high Th/La ratios of >0.2 whereas DMM and mantle plume sources range from 0.048 to 0.11 (Plank 2005). Accordingly, many island and continental arc rocks typically range from low mantle-like Th/La to high terrigenous sediment-like Th/La ratios (Plank 2005) depending on the volume of terrigenous sediment subducted. The Aves Ridge mafic rocks have consistently low Th/La ratios (<0.13), which indicate that there was little subducted terrigenous sediment in their source region.

In oxidizing pelagic sediment and red clay, Ce^{3+} is oxidized to Ce^{4+}, which is more soluble than La^{3+} in aqueous slab-derived fluids, thus leading to Ce depletion (Ce/Ce* <1) in the resultant island arc magmas (Hole *et al.* 1984). Ce/Ce* is the ratio of observed to expected Ce concentration on an N-MORB-normalized REE plot, with Ce* = ((La − Pr)/2) + Pr. The Th/La v. Ce/Ce* diagram (Fig. 8) discriminates between terrigenous and pelagic sedimentary sources in arc rocks (Hastie *et al.* 2009; Neill *et al.* 2010). The mafic rocks from the Aves Ridge show a clear trend from mantle-like Ce/Ce* values of *c.* 1.0–0.58, indicating a significant involvement of pelagic sediment in the source region. The mafic rocks of the Aves Ridge therefore most probably formed in an intra-oceanic setting away from terrigenous proto-Caribbean passive margin sedimentary sequences or continental masses.

Correlation with the Dutch–Venezuelan Antilles

The age and origin of the recently studied rocks of the Dutch–Venezuelan Antilles are summarized in Table 4. In the Venezuelan Antilles, La Blanquilla contains the closest exposure of igneous rocks to the Aves Ridge (Fig. 1), where granodiorites and tonalites dated at *c.* 76 and *c.* 59 Ma respectively are found (Wright & Wyld 2010). The granodiorite is geochemically comparable with the Aves Ridge granitoids (Fid. 4d), with similar Th/La, La/Yb and Nb/Yb ratios. Like the Aves Ridge, no Caribbean–Colombian Oceanic Plateau mafic rocks are found on La Blanquilla. However, on Gran Roque of the Los Roques

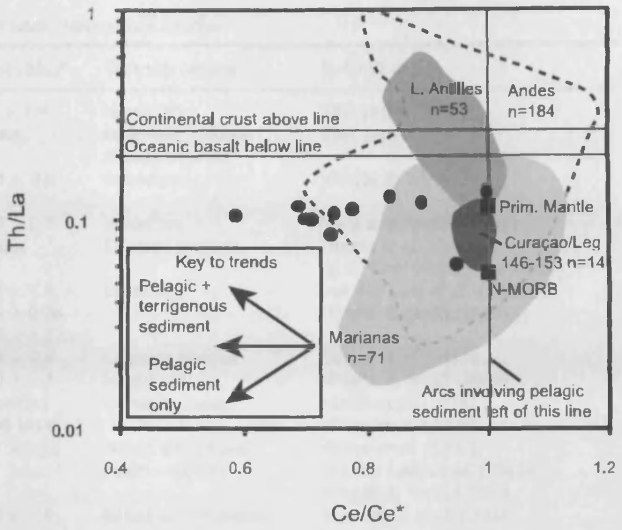

Fig. 8. Th/La v. Ce/Ce* plot for mafic arc rocks (Hastie *et al.* 2009). The Aves Ridge arc (filled circles) and the Marianas arc both subducted oxidized pelagic sediments. The Lesser Antilles and Andean arcs contain a subducted terrigenous sedimentary component. Marianas, Andean and Lesser Antilles arcs data are from the GEOROC database, available at http://georoc.mpch-mainz.gwdg.de/georoc (2009). Data for primitive mantle data from Sun & McDonough (1989), N-MORB from McDonough & Sun (1995), Curaçao from Hauff *et al.* (2000).

islands (Fig. 1), undated gabbros and dolerites of Caribbean–Colombian Oceanic Plateau affinity are present (Giunta *et al.* 2002; A. C. Kerr, unpublished data). The mafic rocks are cut by quartz diorites, pegmatites and aplites with Ar–Ar biotite and hornblende ages of *c.* 68 and *c.* 59 Ma respectively (van der Lelij *et al.* 2010). Like La Blanquilla, the felsic rocks of Los Roques have almost identical trace element signatures to the granitoids of the Aves Ridge (Fig. 4d; data from Giunta *et al.* 2002; A. C. Kerr, unpublished data). All the Venezuelan Antilles arc rocks are considered to be formed by NW- or west-dipping subduction beneath the Caribbean–Colombian Oceanic Plateau (Wright & Wyld 2010).

On Curaçao in the Dutch Antilles (Fig. 1), dykes of diorite and quartz diorite (*c.* 86 Ma; Wright & Wyld 2010) intrude the Caribbean–Colombian Oceanic Plateau-related Curaçao Lava Formation (*c.* 89 Ma; Sinton *et al.* 1998). These dykes also have very similar trace element signatures to the Aves Ridge granitoids (Fig. 4d; Wright & Wyld 2010). Aruba, also part of the Dutch Antilles (Fig. 1), includes the mafic Aruba Lava Formation, which is dated using the imprint of ammonite fossils to *c.* 90 Ma, and is a part of the Caribbean–Colombian Oceanic Plateau (MacDonald 1968; White *et al.* 1999). The Lava Formation is cut by the dioritic to tonalitic Aruba Batholith, which has a weighted mean U–Pb zircon age of 88.6 ± 0.5 Ma (van der Lelij *et al.* 2010; Wright & Wyld 2010). White *et al.* (1999) showed that the batholith has low Nb, high Ba and Sr, and flat to LREE-enriched REE patterns (Fig. 4d). Although much more variable in major and trace element concentration, the Aruba batholith does resemble the Aves Ridge granitoids and is considered, like the Curaçao dykes, to have formed by partial melting of Caribbean–Colombian Oceanic Plateau crust during west-dipping subduction (White *et al.*, 1999; van der Lelij *et al.* 2010; Wright & Wyld 2010).

Table 4. *Summary of recent studies of igneous exposures from the Aves Ridge, Dutch–Venezuelan Antilles*

Location	Suite	Rock types	Age(s) (Ma)*	Tectonic setting	References
SE Aves Ridge	n.a.	Felsic intrusive	76 ± 1.4	Island arc	This paper
	n.a.	Mafic extrusive and intrusive	n.a.	Island arc (plume mantle source)	This paper
La Blanquilla (Venezuelan Antilles)	n.a.	Felsic intrusive	75.5 ± 0.9	Island arc	Wright & Wyld (2010)
	n.a.	Felsic intrusive	58.7 ± 0.5	Island arc	Wright & Wyld (2010)
Gran Roque (Venezuelan Antilles)	n.a.	Mafic intrusive	n.a.	Oceanic plateau	Giunta *et al.* (2002), A. C. Kerr (unpublished data)
	n.a.	Felsic intrusive	65.3 ± 1.4, 68.30 ± 0.76, 58.93 ± 1.22	Island arc	van der Lelij *et al.* (2010), Wright & Wyld (2010)
Curaçao (Dutch Antilles)	Lava Fm.	Mafic extrusive	88.9 ± 0.8	Oceanic plateau	Sinton *et al.* (1998)
	n.a.	Intermediate intrusive	86.2 ± 1.1	Island arc	Wright & Wyld (2010)
Aruba (Dutch Antilles)	Lava Fm.	Mafic extrusive	Turonian (*c.* 90 Ma)†	Oceanic plateau	MacDonald (1968), White *et al.* (1999)
	Batholith	Mafic to felsic intrusive	88.6 ± 0.5‡	Island arc (plume mantle source)	White *et al.* (1999), van der Lelij *et al.* (2010), Wright & Wyld (2010)
Bonaire (Dutch Antilles)	Washikemba Group	Felsic extrusive, mafic intrusive	94.6 ± 1.4, 98.2 ± 0.6	Island arc (depleted mantle source)	Thompson *et al.* (2004) Wright & Wyld (2010)
	Matijs Group	Mafic intrusive	Albian (*c.* 112 Ma)§	Island arc	Wright & Wyld (2010)

*Unmarked samples dated by U–Pb or Ar–Ar methods (see original references).
†Sample dated using ammonite imprints.
‡Weighted mean of available ages.

The only other mafic island arc rocks in the Dutch–Venezuelan Antilles are found on Bonaire Island (Table 4; Fig. 1), which has two suites of Cretaceous igneous rocks (Thompson *et al.* 2004; Wright & Wyld, 2010). Poorly studied mafic stocks of the Matijs Group intruded Aptian or older argillites before deposition of a Coniacian conglomerate unit. The felsic volcanic rocks, diorites and dacites of the Washikemba Group (Washikemba Formation of Thompson *et al.* 2004) have an age of *c.* 96 Ma (Thompson *et al.* 2004; Wright & Wyld, 2010). These rocks were formed by subduction beneath a depleted mantle source (Fig. 7d; Thompson *et al.* 2004). There are no rocks of Caribbean–Colombian Oceanic Plateau affinity or rocks derived from a plume-related mantle source on Bonaire.

These results have profound implications for the tectonic evolution of the southern Caribbean (van der Lelij *et al.* 2010; Wright & Wyld 2010). Because the Caribbean–Colombian Oceanic Plateau rocks exposed on Aruba, Curaçao and Gran Roque show no sign of interaction with slab fluids (see the Curaçao field in Fig. 8), Hastie & Kerr (2010) stated that there must have been no active subduction zone beneath this part of the Caribbean–Colombian Oceanic Plateau during its formation. Therefore, the *c.* 96 Ma island arc rocks on Bonaire would represent east-dipping subduction in the region (van der Lelij *et al.* 2010), as a west-dipping subduction would result in contamination of the Caribbean–Colombian Oceanic Plateau mantle source with slab-related fluids. Wright & Wyld (2010) suggested that Bonaire is a slice of the Greater Antilles arc that moved into the southern Caribbean along strike-slip faults before the inception of the Aves Ridge, but because Bonaire is an integral part of the Dutch Antilles we prefer the interpretation of van der Lelij *et al.* (2010).

Following eruption of the Caribbean–Colombian Oceanic Plateau, subduction-related rocks formed on Aruba and Curaçao within only 1–3 Ma of plateau formation (Wright & Wyld 2010). Studies of andesitic volcanoes using the U–Th decay series have shown that subduction-related fluids are generated and added to the mantle wedge only a few hundred thousand years before eruption (e.g. Turner *et al.* 2000). Partial melting to form the Aruba batholith and Curaçao dykes could therefore have occurred above a subduction zone that initiated along the edge of the Caribbean–Colombian Oceanic Plateau almost immediately following its formation (see Niu *et al.* 2003; Wright & Wyld 2010), or by collision of the Caribbean–Colombian Oceanic Plateau with an east-dipping subduction zone, triggering a rapid polarity reversal at *c.* 89 Ma (van der Lelij *et al.* 2010).

There are no arc rocks younger than *c.* 88 Ma in the Dutch Antilles. van der Lelij *et al.* (2010) used fission-track dating to show that significant uplift occurred on Bonaire at *c.* 85–80 Ma, and the Campanian and younger Soebi Blanco Formation on Bonaire and the Knip Group and Midden Curaçao Formation of Curacao contain continental detritus (Priem *et al.* 1986; Wright & Wyld 2010). Subduction was probably terminated abruptly by collision of the South American margin with the incipient arc.

The comparison above shows that the Aves Ridge rocks formed contemporaneously with magmatism on Gran Roque and La Blanquilla. On La Blanquilla there is no Caribbean–Colombian Oceanic Plateau basement through which the arc rocks intruded, as may be the case for the Aves Ridge (see below). Therefore La Blanquilla appears to be a southern extension of the Aves Ridge. There are no rocks found on the small proportion of the Aves Ridge that has been studied, nor in the Venezuelan Antilles older or younger than *c.* 76 Ma and *c.* 59 Ma, respectively. It is possible that following cessation of magmatism in the Dutch Antilles, subduction transferred eastwards to the Venezuelan Antilles and Aves Ridge, before stalling with inception of the Grenada Basin.

Petrogenesis of the Aves Ridge and La Blanquilla Island

The results presented above are consistent with a model in which the Aves Ridge and La Blanquilla were generated during west-dipping subduction beneath the Caribbean–Colombian Oceanic Plateau between *c.* 76 and *c.* 59 Ma. However, it appears that neither location is in immediate contact with the Caribbean–

Colombian Oceanic Plateau. Much of the Venezuelan Basin has up to 20 km thick plateau crust but in the far SE corner of the basin, a region of some 40 000 km^2, the crustal thickness, minus sedimentary cover, is <5 km (Fig. 1; Diebold *et al.* 1981). This thin crust is considered to predate the Caribbean–Colombian Oceanic Plateau, based on seismic interpretation (Diebold *et al.* 1981; Mauffret & Leroy 1997), although drilling has never been undertaken in this part of the Caribbean Sea. If this thin crust turns out not to be oceanic plateau material, then it is unlikely that the southern Aves Ridge was generated by west-dipping subduction of the proto-Caribbean slab directly beneath the Caribbean–Colombian Oceanic Plateau. Therefore, mantle convection is likely to have brought plume mantle into the wedge above the Aves Ridge subduction zone. Also, we cannot rule out the possibility that there were pre-existing plateau or island arc fragments beneath the site of the Aves Ridge. Some workers have argued that the Caribbean–Colombian Oceanic Plateau dates back to *c.* 115 Ma (Mauffret & Leroy 1997) and in addition there are *c.* 90 Ma volcanic rocks with oceanic plateau-like chemistry cutting proto-Caribbean passive margin sediments at San Souci, Trinidad (Wadge & Macdonald 1985; I. Neill, unpublished data).

Our petrogenetic model (Fig. 9) therefore shows the Aves Ridge arc overlying a plume-related mantle wedge and a subducting proto-Caribbean slab. The slab fluids ascend into the mantle wedge and promote partial melting to generate the Aves mafic lavas. The granitoids form by partial melting of tholeiitic amphibole- and plagioclase-bearing rocks in the lower crust beneath the Aves Ridge arc. As mentioned above, it is possible that partial melting was aided by the rise of hot mafic island arc magmas, perhaps even those that formed the mafic rocks in this study.

It is unclear whether or not the crustal thickness of the Aves Ridge could be generated during a short *c.* 20 Ma post-Caribbean–Colombian Oceanic Plateau subduction history (see below) with a starting crustal thickness of only 5 km, the same as the thin crust of the SE Venezuelan Basin. Subduction rates, roll-back, sediment flux, slab dip and magma production vary from arc to arc, hence it is difficult to quantify how quickly arc crust may be generated. The Lesser Antilles, which has a *c.* 55 Ma history of *c.* 2 cm a^{-1} subduction, a similar rate to the Aves Ridge (Pindell & Kennan 2009) has built up 30–35 km of crust (Christeson *et al.* 2008). It is possible that the 26 km thick Aves crust was generated during its post-Caribbean–Colombian Oceanic Plateau history, but we repeat that the pre-existence of plateau-like crust or older island arc rocks should not be ruled out. It may be significant that the isotopic composition of the granitoid sample (Fig. 6) falls within the Caribbean–Colombian Oceanic Plateau field and that this sample is isotopically dissimilar to N-MORB or island arc rocks.

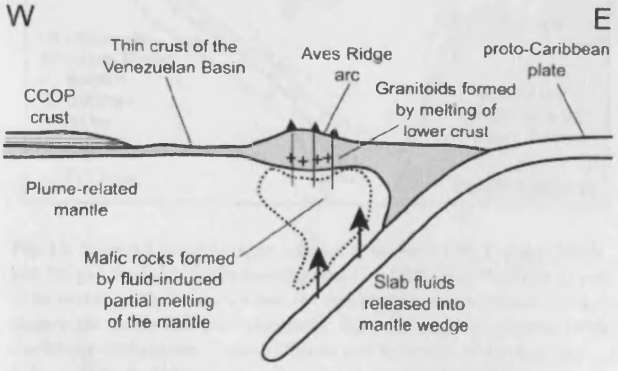

Fig. 9. Petrogenetic model (not to scale) for the Aves Ridge. CCOP, Caribbean–Colombian Oceanic Plateau.

Southern Caribbean tectonic model

In Figure 10, we outline a revised plate-tectonic model for the southern Caribbean based on the findings from the Aves Ridge and a new consideration of the origins of the Dutch–Venezuelan Antilles (van der Lelij *et al.* 2010; Wright & Wyld 2010). At *c.* 100 Ma (Fig. 10a), because Bonaire is an integral part of the Dutch Antilles, and its related mantle wedge did not contaminate the melts that formed the Caribbean–Colombian Oceanic Plateau, it is shown as part of an east-dipping subduction system in the southern Caribbean (van der Lelij *et al.* 2010). At a similar time, high-pressure rocks evolved on Margarita Island and in the Venezuelan interior in the Villa de Cura allochthon (Fig. 1). Margarita appears to have been affected by subduction zone magmatism during the Aptian–Coniacian (Maresch *et al.* 2009). The blueschist-facies Villa de Cura allochthon contains some subducted slivers of island arc material of unknown protolith age, metamorphosed under barroisite-stable conditions at *c.* 96 Ma (Smith *et al.* 1999; Unger *et al.* 2005). It seems likely that both locations represent the products of subduction zone activity relatively close to the South American continent but their precise origins are uncertain.

The next event to occur, as shown in the *c.* 88 Ma reconstruction (Fig. 10b), was the formation of the felsic arc rocks of Aruba and Curaçao, which were intruded above a convergent zone through the thick basement of the Caribbean–Colombian Oceanic Plateau. This magmatism began at *c.* 88 Ma and ended with collision of the arc with South America.

Our final reconstruction covers the period between *c.* 80 and 60 Ma (Fig. 10c). Magmatism moved eastward to the Venezuelan Antilles where the Gran Roque felsic rocks formed by crustal melting at *c.* 68 to 59 Ma. Further north and east where Caribbean–Colombian Oceanic Plateau crust was absent in the Venezuelan Basin, partial melting of plume mantle and the lower crust of unknown composition contributed to formation of the Aves Ridge and La Blanquilla between *c.* 76 and *c.* 59 Ma. Spreading in the Grenada Basin (Aitken *et al.* 2010) coincides with the cessation of magmatic activity on the Aves Ridge and in the Venezuelan Antilles.

Further work is required to refine models of southern Caribbean tectonic evolution including: (1) study of the geochemistry and geochronology of igneous rocks on Tobago; (2) re-sampling of the Aves Ridge including dating of the mafic rocks; (3) detailed geochemical study of the igneous rocks of Margarita Island; (4) identification of protolith ages for the Villa de Cura allochthon; (5) a study of the link between magmatism preserved in the Dutch–Venezuelan Antilles and Villa de Cura and the Cretaceous arc rocks that have been accreted to the South American margin in Colombia and Ecuador; (6) drilling of the thin crust of the far southeastern Venezuelan Basin.

Conclusions

Dredge hauls from the SE Aves Ridge consist of subduction-related granitoids and mafic rocks. U–Pb geochronology and regional constraints indicate that they were most probably formed at *c.* 80–75 Ma. Partial melting of a plume-related mantle wedge, which lay beneath, or close to, the Caribbean–Colombian Oceanic Plateau, is believed to be the trigger for generation of the ridge. The plume-related mantle generated

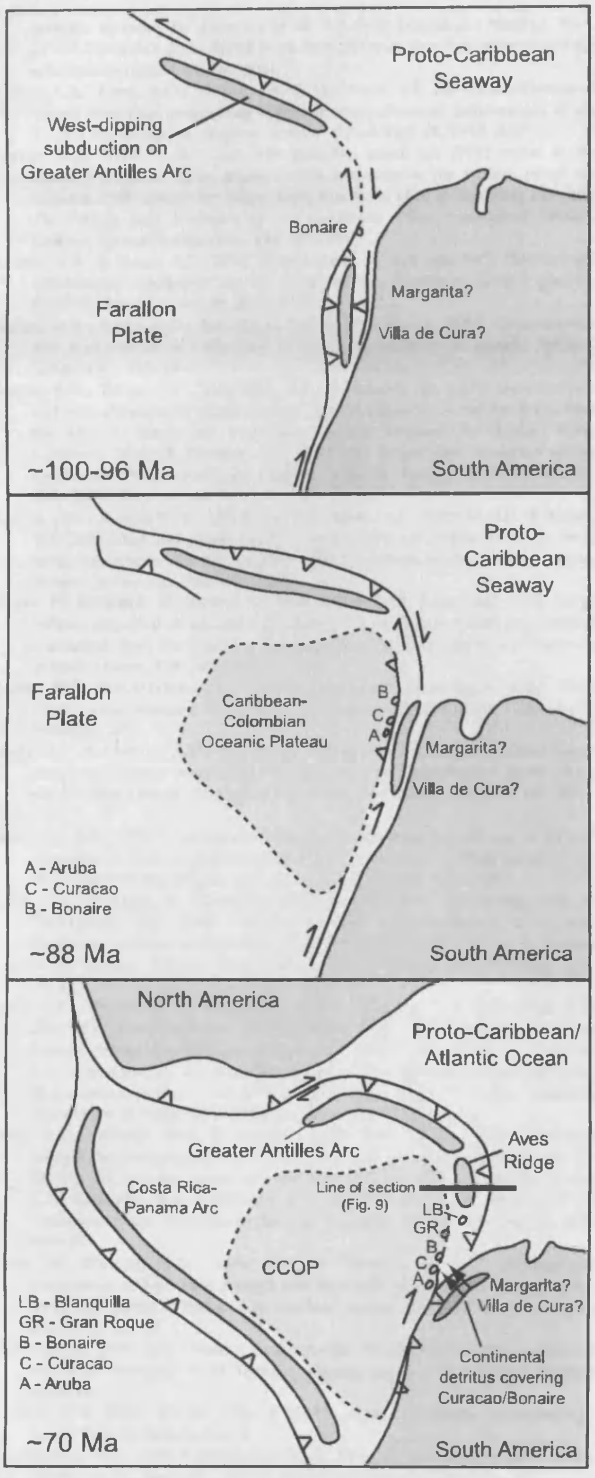

Fig. 10. Regional tectonic maps adapted from Pindell & Kennan (2009) and Wright & Wyld (2010) showing: (**a**) *c.* 100 Ma, with Bonaire as part of an east-dipping Dutch Antilles arc and Margarita and Villa de Cura close to the South American continent; (**b**) *c.* 88 Ma, with eruption of the Caribbean–Colombian Oceanic Plateau and formation of the Curaçao dykes and Aruba batholith by subduction beneath the Caribbean–Colombian Oceanic Plateau; (**c**) subduction under way beneath the Aves Ridge and Venezuelan Antilles at *c.* 75 Ma.

unusual trace element compositions identified in the mafic rocks. Island arc magmatism occurred above a subduction zone or zones separate from the SW-dipping subduction zone of the Greater Antilles arc from *c.* 88 to *c.* 59 Ma in the southern Caribbean and has been preserved as the Aves Ridge and the Dutch and Venezuelan Antilles.

I.N. acknowledges Natural Environment Research Council PhD studentship NE/F00219X/1 and NIGSFC isotope analysis grant-in-kind IP/1064/1108. R. L. Bond and G. Lozefski helped with sampling from the Lamont–Doherty Earth Observatory Deep Sea Sample Repository, supported by National Science Foundation Grant OCE00-02380/Office of Naval Research Grant N00014-02-1-0073. I. McDonald and L. Woolley assisted with major and trace element analyses. We have had valuable discussions on Caribbean tectonic evolution with J. Pindell and J. Wright. We thank J. Wright and C. Chauvel for their constructive reviews and D. Pyle for his editorial comments, which significantly improved the paper.

References

Aitken, T., Mann, P., Escalona, A. & Christeson, G.L. 2010. Evolution of the Grenada and Tobago Basins and implications for arc migration. *Marine and Petroleum Geology*, doi: 10.1016/j.marpetgeo.2009.10.003.

Bird, D.E., Hall, S.A., Casey, J.F. & Millegan, P.S. 1999. Tectonic evolution of the Grenada Basin. *In*: Mann, P. (ed.) *Caribbean Basins. Sedimentary Basins of the World, 4*. Elsevier, Amsterdam, 389–416.

Black, L.P., Kamo, S.L., Allen, C.M., Aleinikoff, J.N., Davis, D.W., Korsch, R.J. & Foudoulis, C. 2003. TEMORA 1: a new zircon standard for U–Pb geochronology. *Chemical Geology*, **200**, 155–170.

Blichert-Toft, J. 2001. On the Lu–Hf isotope geochemistry of silicate rocks. *Geostandards Newsletter*, **25**, 41–56.

Bouysse, P. 1984. The Lesser Antilles island arc: structure and geodynamic evolution. *In*: Orlofsky, S. (ed.) *Initial Reports of the Deep Sea Drilling Project, 78A*. US Government Printing Office, Washington, DC, 83–103.

Burke, K. 1988. Tectonic evolution of the Caribbean. *Annual Review of Earth and Planetary Sciences*, **16**, 210–230.

Burke, K., Fox, P.J. & Sengor, A.M.C. 1978. Buoyant ocean floor and the evolution of the Caribbean. *Journal of Geophysical Research*, **83**, 3949–3954.

Chappell, B.W., White, A.J.R. & Wyborn, D. 1987. The importance of residual source material (restite) in granite petrogenesis. *Journal of Petrology*, **28**, 1111–1138.

Christeson, G.L., Mann, P., Escalona, A. & Aitken, T.J. 2008. Crustal structure of the Caribbean–northeastern South America arc–continent collision zone. *Journal of Geophysical Research*, **113**, B08104, doi:10.1029/2007JB005373.

Church, R.E. & Allison, K.R. 2004. The petroleum potential of the Saba Bank area, Netherlands Antilles. *Search and Discovery*, Article 10076.

Clark, T.F., Korgen, B.J. & Best, D.M. 1978. Heat flow in the eastern Caribbean. *Journal of Geophysical Research*, **83**, 5883–5891.

Diebold, J.B., Stoffa, P.L., Buhl, P. & Truchan, M. 1981. Venezuelan Basin crustal structure. *Journal of Geophysical Research*, **86**, 7901–7923.

Drummond, M.S. & Defant, M.J. 1990. A model for trondhjemite–tonalite–dacite genesis and crustal growth via slab melting: Archean to modern comparison. *Journal of Geophysical Research*, **95**, 21503–21521.

Drummond, M.S., Defant, M.J. & Kepezhinskas, P.K. 1996. Petrogenesis of slab-derived trondjemite–tonalite–dacite/adakite magmas. *Transactions of the Royal Society of Edinburgh: Earth Sciences*, **87**, 205–215.

Escuder Viruete, J., Díaz de Neira, A., *et al.* 2006. Magmatic relationships and ages of Caribbean island arc tholeiites, boninites and related felsic rocks, Dominican Republic. *Lithos*, **90**, 161–186.

Escuder Viruete, J., Pérez-Estaún, A., Weis, D. & Friedman, R. 2010. Geochemical characteristics of the Río Verde Complex, Central Hispaniola: Implications for the palaeotectonic reconstructions of the Lower Cretaceous Caribbean island arc. *Lithos*, **114**, 168–185.

Fitton, J.G., Saunders, A.D., Norry, M.J., Hardarson, B.S. & Taylor, R.N. 1997. Thermal and chemical structure of the Iceland plume. *Earth and Planetary Science Letters*, **153**, 197–208.

Fox, P.J., Shreiber, E. & Heezen, B.C. 1971. The geology of the Caribbean crust: Tertiary sediments, granitic and basic rocks from the Aves Ridge. *Tectonophysics*, **12**, 89–109.

Giunta, G., Beccaluva, L., Coltorti, M., Siena, F. & Vaccaro, C. 2002. The southern margin of the Caribbean Plate in Venezuela: tectono-magmatic setting of the ophiolitic units and kinematic evolution. *Lithos*, **63**, 19–40.

Gnos, E., Kurz, D. & Eggenberger, U. 2006. Electrodynamic disaggregation of

geologic material. *In: Abstracts of the 4th Swiss Geoscience Meeting, Bern, 24–25 November, 2006*. World Wide Web Address: http://geoscience-meeting.scnatweb.ch/sgm2006/index.html.

HASTIE, A.R., KERR, A.C., PEARCE, J.A. & MITCHELL, S.F. 2007. Classification of altered island arc rocks using immobile trace elements: development of the Th–Co discrimination diagram. *Journal of Petrology*, **48**, 2341–2357.

HASTIE, A.R. 2009. Is the Cretaceous primitive island arc (PIA) series in the circum-Caribbean region geochemically analogous to the modern island arc tholeiite (IAT) series? *In:* JAMES, K.H., LORENTE, M.A. & PINDELL, J.L. (eds) *The Origin and Evolution of the Caribbean Plate*. Geological Society, London, Special Publications, **328**, 397–409.

HASTIE, A.R. & KERR, A.C. 2010. Mantle plume or slab window?: Physical and geochemical constraints on the origin of the Caribbean oceanic plateau. *Earth-Science Reviews*, **98**, 283–293.

HASTIE, A.R., KERR, A.C., MITCHELL, S.F. & MILLAR, I.L. 2008. Geochemistry and petrogenesis of Cretaceous oceanic plateau lavas in eastern Jamaica. *Lithos*, **101**, 323–343.

HASTIE, A.R., KERR, A.C., MITCHELL, S.F. & MILLAR, I.L. 2009. Geochemistry and tectonomagmatic significance of lower Cretaceous island arc lavas from the Devil's Racecourse Formation, eastern Jamaica. *In:* JAMES, K.H., LORENTE, M.A. & PINDELL, J.L. (eds) *The Origin and Evolution of the Caribbean Plate*. Geological Society, London, Special Publications, **328**, 337–359.

HASTIE, A.R., RAMSOOK, R., MITCHELL, S.F., KERR, A.C., MILLAR, I.L. & MARK, D.F. 2010. Age and geochemistry of compositionally distinct back-arc basin lavas, implications for the tectonomagmatic evolution of the Caribbean plate. *Journal of Geology*, **118**, 655–676.

HAUFF, F., HOERNLE, K., TILTON, G., GRAHAM, D.W. & KERR, A.C. 2000. Large volume recycling of oceanic lithosphere over short time scales: geochemical constraints from the Caribbean Large Igneous Province. *Earth and Planetary Science Letters*, **174**, 247–263.

HAXBY, W.F., MELKONIAN, A.K., COPLAN, J., CHAN, S.-M. & RYAN, W.B.F. 2010. *GeoMapApp freeware software, v.2.3*. Lamont–Doherty Earth Observatory, Palisades, NY.

HOLE, M.J., SAUNDERS, A.D., MARRINER, G.F. & TARNEY, J. 1984. Subduction of pelagic sediments: implications for the origin of Ce-anomalous basalts from the Mariana Islands. *Journal of the Geological Society, London*, **141**, 453–472.

KEMPTON, P.D. 1995. *Common Pb chemical procedures for silicate rocks and minerals, methods of data correction and an assessment of data quality at the NERC Isotope Geosciences Laboratory*. NIGL Report Series, **78**.

KERR, A.C., TARNEY, J., MARRINER, G.F., KLAVER, G.T., SAUNDERS, A.D. & THIRLWALL, M.F. 1996. The geochemistry and petrogenesis of the late-Cretaceous picrites and basalts of Curaçao, Netherlands Antilles: a remnant of an oceanic plateau. *Contributions to Mineralogy and Petrology*, **124**, 29–43.

KERR, A.C., WHITE, R.V., THOMPSON, P.M.E., TARNEY, J. & SAUNDERS, A.D. 2003. No oceanic plateau—no Caribbean Plate? The seminal role of an oceanic plateau in Caribbean plate evolution. *In:* BARTONLINI, C., BUFFLER, R.T. & BLICKWEDE, J.F. (eds) *The Circum-Gulf of Mexico and the Caribbean; Hydrocarbon Habitats, Basin Formation and Plate Tectonics*. American Association of Petroleum Geologists, Memoirs, **79**, 126–168.

KERR, A.C., PEARSON, D.G. & NOWELL, G.M. 2009. Magma source evolution beneath the Caribbean oceanic plateau: new insights from elemental and Sr–Nd–Pb–Hf isotopic studies of ODP Leg 165 Site 1001 basalts. *In:* JAMES, K.H., LORENTE, M.A. & PINDELL, J.L. (eds) *The Origin and Evolution of the Caribbean Plate*. Geological Society, London, Special Publications, **328**, 809–827.

KLEIN, M., STOSCH, H.-G., SECK, H.A. & SHIMIZU, N. 1997. Experimental partitioning of high field strength and rare earth elements between clinopyroxene and garnet in andesitic to tonalitic systems. *Geochimica et Cosmochimica Acta*, **64**, 99–115.

LUDWIG, K.R. 1999. *User's manual for Isoplot/Ex, Version 2.10, a geochronological toolkit for Microsoft Excel*. Berkeley Geochronology Center Special Publications, **1a**.

LUDWIG, K.R. 2000. *SQUID 1.00, A User's Manual*. Berkeley Geochronology Center Special Publications, **2**.

MACDONALD, W.D. 1968. Communication. *In: Status of geological research in the Caribbean 14: Mayaqüez, Puerto Rico, University of Puerto Rico*, **40**.

MARESCH, W.V., KLUGE, R., BAUMANN, A., KRÜCKHANS-LUEDER, G., PINDELL, J., STANEK, K. & STÖCKHERT, B. 2009. The occurrence and timing of high-pressure metamorphism on Margarita Island, Venezuela: a constraint on Caribbean–South America interaction. *In:* JAMES, K.H., LORENTE, M.A. & PINDELL, J.L. (eds) *The Origin and Evolution of the Caribbean Plate*. Geological Society, London, Special Publications, **328**, 705–741.

MARLOWE, J.I. 1968. Geological reconnaissance of parts of Aves Ridge. *In:* MANSON, P. (ed.) *Abstracts of Papers from the 5th Caribbean Geological Conference, Queens College, City University of New York*, 51–52.

MAUFFRET, A. & LEROY, S. 1997. Seismic stratigraphy and structure of the Caribbean igneous province. *Tectonophysics*, **283**, 61–104.

MCDONALD, I. & VILJOEN, K.S. 2006. Platinum-group element geochemistry of mantle eclogites: a reconnaissance study of xenoliths from the Orapa kimberlite, Botswana. *Applied Earth Science Transactions of the Institute of Mining and Metallurgy (B)*, **115**, 81–93.

MCDONOUGH, W.F. & SUN, S.-S. 1995. The composition of the Earth. *Chemical Geology*, **120**, 223–254.

MÜNKER, C., WEYER, S., SCHERER, E. & MEZGER, K. 2001. Separation of high field strength elements (Nb, Ta, Zr, Hf) and Lu from rock samples for MC-ICPMS measurements. *Geochemistry, Geophysics, Geosystems*, **2**, 2001GC000183.

NEILL, I., GIBBS, J.A., HASTIE, A.R. & KERR, A.C. 2010. Origin of the volcanic complexes of La Désirade, Lesser Antilles: implications for tectonic reconstruction of the Late Jurassic to Cretaceous Pacific–proto-Caribbean margin. *Lithos*, **120**, 407–420, doi:10.1016/j.lithos.2010.08.026.

NIU, Y., O'HARA, M.J. & PEARCE, J.A. 2003. Initiation of subduction zones as a consequence of lateral compositional buoyancy contrast within the lithosphere: a petrological perspective. *Journal of Petrology*, **44**, 851–866.

NOWELL, G.M. & PARRISH, R.R. 2001. Simultaneous acquisition of isotope compositions and parent/daughter ratios by non-isotope dilution solution-mode plasma ionisation multi-collector mass spectrometry (PIMMS). *In:* HOLLAND, G. & TANNER, S.D. (eds) *Plasma Source Mass Spectrometry—The New Millenium*. Royal Society of Chemistry, Cambridge, 298–310.

PEACOCK, S.M., RUSHMER, T. & THOMPSON, A.B. 1994. Partial melting of subducting oceanic crust. *Earth and Planetary Science Letters*, **121**, 227–244.

PEARCE, J.A. 1983. Role of the sub-continental lithosphere in magma genesis at active continental margins. *In:* HAWKESWORTH, C.J. & NORRY, M.J. (eds) *Continental Batholiths and Mantle Xenoliths*. Shiva, Nantwich, 230–249.

PEARCE, J.A. & PARKINSON, I.J. 1993. Trace element models for mantle melting: application to volcanic arc petrogenesis. *In:* PRITCHARD, H.M., ALABASTER, T., HARRIS, N.B.W. & NEARY, C.R. (eds) *Magmatic Processes and Plate Tectonics*. Geological Society, London, Special Publications, **76**, 373–403.

PEARCE, J.A. & PEATE, D.W. 1995. Tectonic implications of the composition of volcanic arc magmas. *Annual Review of Earth and Planetary Sciences*, **23**, 251–285.

PEARCE, J.A. & STERN, R.J. 2006. Origin of back-arc basin magmas: trace element and isotopic perspectives. *In:* CHRISTIE, D.M., FISHER, C.R., LEE, S.-M. & GIVENS, S. (eds) *Back-arc Spreading Systems: Geological, Biological, Chemical and Physical Interactions*. American Geophysical Union, Geophysical Monograph Series, **166**, 63–86.

PECCARILLO, A. & TAYLOR, S.R. 1976. Geochemistry of Eocene calc-alkaline volcanic rocks from the Kastamonu area, Northern Turkey. *Contributions to Mineralogy and Petrology*, **58**, 63–81.

PETFORD, N. & GALLACHER, K. 2001. Partial melting of mafic (amphibolitic) lower crust by periodic influx of basaltic magma. *Earth and Planetary Science Letters*, **193**, 483–499.

PETFORD, N., CRUDEN, A.R., MCCAFFREY, K.J.W. & VIGNERESSE, J.-L. 2000. Granite magma formation, transport and emplacement in the Earth's crust. *Nature*, **408**, 669–673.

PINDELL, J.L. & BARRETT, S.F. 1990. Geological evolution of the Caribbean region: a plate tectonic perspective. *In:* DENGO, G. & CASE, J.E. (eds) *The Caribbean Region*. Geological Society of America, The Geology of North America, **H**, 405–432.

PINDELL, J.L. & KENNAN, L. 2009. Tectonic evolution of the Gulf of Mexico, Caribbean and northern South America in the mantle reference frame: an update. *In:* JAMES, K.H., LORENTE, M.A. & PINDELL, J.L. (eds) *The Origin and Evolution of the Caribbean Plate*. Geological Society, London, Special Publications, **328**, 1–55.

PINDELL, J.L., KENNAN, L., STANEK, K.P., MARESCH, W.V. & DRAPER, G. 2006. Foundations of Gulf of Mexico and Caribbean evolution: eight controversies resolved. *Geologica Acta*, **4**, 303–341.

PLANK, T. 2005. Constraints from thorium/lanthanum on sediment recycling at subduction zones and the evolution of the continents. *Journal of Petrology*, **46**, 921–944.

PRIEM, H.N.A., BEETS, D.J., BOELRIJK, N.A.I.M. & HEBEDA, E.H. 1986. On the age of the late Cretaceous tonalitic/gabbroic batholith on Aruba, Netherlands Antilles (southern Caribbean borderland). *Geologie en Mijnbouw*, **65**, 247–265.

RAPP, R.P. & WATSON, E.B. 1995. Dehydration melting of metabasalt at 8–32 kbar: implications for continental growth and crust–mantle recycling. *Journal of Petrology*, **36**, 891–931.

RAPP, R.P., SHIMIZU, N., NORMAN, M.D. & APPLEGATE, G.S. 1999. Reaction between slab-derived melt and peridotite in the mantle wedge: experimental constraints at 3.8 GPa. *Chemical Geology*, **160**, 335–356.

RAPP, R.P., SHIMIZU, N. & NORMAN, M.D. 2003. Growth of early continental crust

by partial melting of eclogite. *Nature*, **425**, 605–608.

ROYSE, K.R., KEMPTON, P.D. & DARBYSHIRE, F.D. 1998. *Procedure for the analysis of rubidium–strontium and samarium–neodymium isotopes at the NERC Isotope Geosciences Laboratory*. NIGL Report Series, **121**.

SALTERS, V.J.M., LONGHI, J.E. & BIZIMIS, M. 2002. Near mantle solidus trace element partitioning at pressures up to 3.4 GPa. *Geochemistry, Geophysics, Geosystems*, **3**, doi:10.1029/2001GC000148.

SAUNDERS, A.D., TARNEY, J. & WEAVER, S.D. 1980. Transverse geochemical variations across the Antarctic Peninsula: implications for the genesis of calc-alkaline magmas. *Earth and Planetary Science Letters*, **46**, 344–360.

SEEWALD, J.S. & SEYFRIED, W.E. 1990. The effect of temperature on metal mobility in subseafloor hydrothermal systems: constraints from basalt alteration experiments. *Earth and Planetary Science Letters*, **101**, 388–403.

SINTON, C.W., DUNCAN, R.A., STOREY, M., LEWIS, J. & ESTRADA, J.J. 1998. An oceanic flood basalt province within the Caribbean plate. *Earth and Planetary Science Letters*, **155**, 221–235.

SMITH, C.A., SISSON, V.B., AVÉ LALLEMANT, H.G. & COPELAND, P. 1999. Two contrasting pressure–temperature–time paths in the Villa de Cura blueschist belt, Venezuela: possible evidence for Late Cretaceous initiation of subduction in the Caribbean. *Geological Society of America Bulletin*, **111**, 831–848.

SPEED, R.C. & WALKER, B.M. 1991. Oceanic crust of the Grenada Basin in the southern Lesser Antilles arc platform. *Journal of Geophysical Research*, **96**, 3835–3852.

STANEK, K.P., MARESCH, W.V. & PINDELL, J. 2009. The geotectonic story of the northwestern branch of the Caribbean arc: implications from structural and geochronological data of Cuba. *In:* JAMES, K.H., LORENTE, M.A. & PINDELL, J.L. (eds) *The Origin and Evolution of the Caribbean Plate*. Geological Society, London, Special Publications, **328**, 361–398.

STEPHENS, W.E. 2001. Polycrystalline amphibole aggregates (clots) in granites as potential I-type restite: an ion microprobe study of rare-earth distributions. *Australian Journal of Earth Sciences*, **48**, 591–601.

SU, B. 2008. Natural evidence for the garnet–spinel transition (GST) in the Earth's mantle. *Nature Proceedings*, doi:10.1038/npre.2008.1898.2.

SUN, S.-S. & MCDONOUGH, W.F. 1989. Chemical and isotopic systematics of oceanic basalts: implications for mantle composition and processes. *In:* SAUNDERS, A.D. & NORRY, M.J. (eds) *Magmatism in the Ocean Basins*. Geological Society, London, Special Publications, **42**, 313–345.

THIRLWALL, M.F., SMITH, T.E., GRAHAM, A.M., THEODOROU, N., HOLLINGS, P., DAVIDSON, J.P. & ARCULUS, R.J. 1994. High field strength element anomalies in arc lavas: source or process? *Journal of Petrology*, **35**, 819–838.

THOMPSON, P.M.E., KEMPTON, P.D., *ET AL.* 2003. Hf–Nd isotope constraints on the origin of the Cretaceous Caribbean plateau and its relationship to the Galapagos plume. *Earth and Planetary Science Letters*, **217**, 59–75.

THOMPSON, P.M.E., KEMPTON, P.D., WHITE, R.V., SAUNDERS, A.D., KERR, A.C., TARNEY, J. & PRINGLE, M.S. 2004. Elemental, Hf–Nd isotopic and geochronological constraints on an island arc sequence associated with the Cretaceous Caribbean plateau: Bonaire, Dutch Antilles. *Lithos*, **74**, 91–116.

TURNER, S.P., GEORGE, R.M.M., EVANS, P.J., HAWKESWORTH, C.J. & ZELLMER, G.F. 2000. Time-scales of magma formation, ascent and storage beneath subduction-zone volcanoes. *Philosophical Transactions of the Royal Society of London, Series A*, **358**, 1443–1464.

UNGER, L.M., SISSON, V.B. & AVÉ LALLEMANT, H.G. 2005. Geochemical evidence for island-arc origin of the Villa de Cura blueschist belt, Venezuela. *In:* AVÉ LALLEMANT, H.G. & SISSON, V.B. (eds) *Caribbean–South American Plate Interactions, Venezuela*. Geological Society of America, Special Papers, **394**, 223–249.

VAN DER LELIJ, R., SPIKINGS, R.A., KERR, A.C., KOUNOV, A., COSCA, M., CHEW, D. & VILLAGOMEZ, D. 2010. Thermochronology and tectonics of the Leeward Antilles: evolution of the Southern Caribbean Plate Boundary Zone. *Tectonics*, **29**, TC6003, doi:10.1029/2009TC002654.

VEIZER, J. 1989. Strontium isotopes in seawater through time. *Annual Review of Earth and Planetary Sciences*, **17**, 141–167.

WADGE, G. & MACDONALD, R. 1985. Cretaceous tholeiites of the northern continental margin of South America: the San Souci Formation of Trinidad. *Journal of the Geological Society, London*, **142**, 297–308.

WALKER, B.M., VOGEL, T.A. & EHRLICH, R. 1972. Petrogenesis of oceanic granites from the Aves Ridge in the Caribbean Basin. *Earth and Planetary Science Letters*, **15**, 133–139.

WENDT, J.I., REGELOUS, M., COLLERSON, K.D. & EWERT, A. 1997. Evidence for a contribution from two mantle plumes to island-arc lavas from northern Tonga. *Geology*, **25**, 611–614.

WHITE, W.M. & PATCHETT, J. 1984. Hf–Nd–Sr isotopes and incompatible element abundances in island arcs: implications for magma origins and crust–mantle evolution. *Earth and Planetary Science Letters*, **67**, 167–185.

WHITE, R.V., TARNEY, J., KERR, A.C., SAUNDERS, A.D., KEMPTON, P.D., PRINGLE, M.S. & KLAVER, G.T. 1999. Modification of an oceanic plateau, Aruba, Dutch Caribbean: implications for the generation of continental crust. *Lithos*, **46**, 43–68.

WILLIAMS, I.S. 1998. U–Th–Pb geochronology by ion microprobe. *In:* MCKIBBEN, M.A., SHANKS, W.C., III & RIDLEY, W.I. (eds) *Applications of Microanalytical Techniques to Understanding Mineralizing Processes*. Reviews in Economic Geology, **7**, 1–35.

WRIGHT, J.E. & WYLD, S.J. 2010. Late Cretaceous subduction initiation on the southern margin of the Caribbean plateau: one great arc of the Caribbean or three? *Geosphere* (in press).

Received 20 April 2010; revised typescript accepted 13 September 2010.
Scientific editing by David Pyle.